UNIVERSITÀ DEGLI STUDI DI CAMERINO

School of Advanced Studies

DOCTORAL COURSE IN
MOLECULAR BIOLOGY AND CELLULAR BIOTECHNOLOGY

LIFE AND HEALTH SCIENCES

XXXII CYCLE

PROGNOSTIC ROLE OF PD-L2 AND TRPV2 IN HUMAN ENDOMETRIAL CANCER AND NOVEL INTEGRATIVE THERAPIES

PhD Student

Dott. Marinelli Oliviero

Supervisor

Prof. Nabissi Massimo

INDEX

1. INTRODUCTION

1.1 The Controversial Role of PD-1 and Its Ligands in Gynecological Malignancies

1.1.1 PD-1 and Its Ligands, PD-L1 (B7-H1) and PD-L2 (B7-DC)

Programmed death-1 (PD-1, CD279) receptor and its ligands, programmed death ligand 1 (PD-L1, CD274, B7-H1) and programmed death ligand 2 (PD-L2, CD273, B7- DC), play crucial roles in one of the immune checkpoint pathways responsible for the inhibition of T-cell activation (1).

PD-1 receptor belongs to the CD28 family and is mainly expressed on the cellular surface of activated T and B cells, monocytes, natural killer (NK), and dendritic cells (DCs), with a role in the induction and maintenance of peripheral tolerance and for the maintenance of the stability and the integrity of T cells (2–5). PD-1 ligands are glycoproteins, members of the B7 family, with 40% homology in amino acids sequence, but have quite distinct expression patterns, being expressed by a wide variety of immune and non-immune cells (1, 3, 4).

PD-L1 is a type I transmembrane glycoprotein with a single N-terminal immunoglobulin variable (IgV)-like domain sharing 21–33% sequence identity with CTLA-4, CD28, and ICOS, about 20 amino acids that separate the IgV domain from the plasma membrane, a transmembrane domain and a cytoplasmic tail (4). It is constitutively expressed on activated T and B cells, DCs, macrophages, mesenchymal stem cells, and bone marrow-derived mast cells (4, 6). Additionally, it is expressed on a wide variety of non-hematopoietic cells including the vascular endothelium, fibroblastic reticular cells, keratinocytes, lung, non-parenchymal cells of the liver, mesenchymal stem cells, pancreatic islet cells, astrocytes, and neurons (4, 5, 7). PD-L1 expression on human T cells is induced by common γ chain cytokines (IL-2, IL-7, and IL-15), whereas PD-L1 expression on B cells is stimulated by IL-21 (4). In cancer cells, PD-L1 expression is regulated by the MAPK and PI3K/AKT pathways, as well as by HIF-1α, STAT-3, NF-κB and epigenetic mechanisms via microRNAs (8). PD-L1 also exists in a soluble form (sPD-L1) that originates from the cleavage of membrane-bound PD-L1 by matrix metalloproteinases. Such PD-L1 soluble isoform, mainly produced by myeloid-derived cells, retains the IgV-like domain, necessary for the interaction with PD-1, and it is able to suppress T-cell activation. However, its physiological role is still unknown. Interestingly, sPD-L1 has been found in several human

1

cancer cell lines, including H1299 non-small cell lung cancer cells, U-937 lymphoma cells, HO8910 ovarian carcinoma cells, SPCA-1 lung adenocarcinoma cells and U251 glioblastoma cells. In addition, high plasma levels of sPD-L1 have been associated with metastasis and poor prognosis in breast cancer and diffuse large B-cell lymphoma (8).

PD-L2 is a type I transmembrane protein containing an IgV-like domain and an immunoglobulin constant (IgC)-like domain in its extracellular region (9). PD-L2 expression is mainly restricted to antigen-presenting cells (APCs), including macrophages and myeloid DCs (6, 7), and non-hematopoietic tissues, such as the lung (10), human umbilical vein endothelial cells, and fibroblasts (1, 5). Three isoforms of PD-L2 have been described that might influence the outcome of the immune response (9). The most common splice variant contains all 6 exons. In humans, an alternative variant with a spliced-out exon 3, resulting in a protein lacks the IgC-like domain and with a shorter—extracellular region has been reported. A third isoform misses the transmembrane domain, because exon 3 is spliced out to an alternative acceptor site within exon 4, and the protein is secreted as a soluble form. This evidence underscores the importance of post-transcriptional regulation in the expression and function of PD-L2. He *et al.* suggested that isoforms II and III should be able to interact with PD-1, but further confirmation is needed (9).

Exposure to IL-4, Interferon-gamma (IFN-γ), IL-2, IL-7, IL-15, IL-21, and toll-like receptor ligands induces PD-L2 upregulation in DCs and macrophages (1). Additionally, IL-4, in the presence of respiratory syncytial virus infection, stimulates PD-L2 expression in alveolar epithelial cells (1, 10). Stimulation by tumor necrosis factor alpha (TNF-α) and IFN-γ enhances the constitutive expression of PD-L2 on endothelial cells from human umbilical vein in vitro (1). The NF-κB and the STAT-6 pathways are two major signaling reported to regulate PD-L2 expression (1).

Different molecular mechanisms dictate PD-Ls binding to PD-1, as demonstrated by the crystallographic structures of the complexes, showing that PD-Ls cross-compete and that the concurrent presence of both ligands might modify the functional outcome of the binding (11). Specifically, PD-L1 binding to PD-1 requires complex conformational changes of the ligand, while PD-L2 directly interacts with PD-1, explaining its reported 2 to 6-fold higher affinity for the receptor (1). Consequently, when both ligands are expressed at similar levels, PD-L2 would be expected to outcompete PD-L1 for binding to PD-1. However, PD-L2 is

generally expressed at lower levels in physiological conditions, such as during maturation of DCs by LPS, when PD-L1 acts as the main ligand of PD-1. A known exception is Th2 responses, where PD-L2 is predominant (1, 11).

Regarding the PD-1/PD-L1 and PD-1/PD-L2 pathways involved in T cell immune evasion, different reports have been published, mainly regarding the biochemical signaling regulated by the PD-1/PD-L1. It was reported that the binding of PD-L1 to PD-1 may cause T cell apoptosis, anergy, exhaustion, and interleukin-10 (IL-10) expression, suggesting that PD-L1 can act as a defender for PD-L1+ cancer cells from CD8+ T cell–mediated lysis (12, 13) (Figure 1).

Figure 1. *PD-1/PD-Ls pathways in cancer*. *PD-L1 is a type I transmembrane glycoprotein with a single N-terminal IgV-like domain and exists also in a soluble form sPD-L1 that retains the IgV-like domain. PD-L2 is a type I transmembrane protein containing an IgV- like domain and an IgC-like domain and three isoforms of PD-L2 have been described that might influence the outcome of the immune response. It is suggested that isoforms II and III should be able to interact with PD-1, but further confirmation is needed. During TCR cross-linking, PD-1 by interacting with its ligands, causes inhibition of PI3K/Akt/mTOR and Ras/MAPK/Erk pathways, leading to down-regulation of T cells metabolism, and exhausted T cells.*

Regarding the PD-L2/PD-1 signaling pathways, it may not be biologically identical, since Repulsive Guidance Molecule B (RGMb) is also a binding partner for PD-L2 (14). Thus, the PD-L2 blockade may evocate different cellular responses, depending on the binding partner interaction, which can lead to potential varied biological outcomes. Up to now, in human anti-tumor immunity, the relationship between PD-1, PD-L1, and PD-L2 in their cellular expression profile and regulation, potential interactions and biological is considered not completely defined.

1.1.2 PD-1 Ligands in the Tumor Microenvironment Influence the Anti-tumor Response

PD-L1 and PD-L2 are expressed in different cancer cells and in their microenvironment (4, 8), including infiltrating immune cells (15, 16). However, their prognostic value is still debated and the role they might play when expressed in the tumor microenvironment has not be fully elucidated yet (17).

Previous evidence shows that PD-L1 expression by cancer cells correlates with poor prognosis (18), while PD-L1 expression by tumor-infiltrating immune cells is associated with improved overall survival (OS) (16). Furthermore, it seems that PD-L1 expressed by APC, rather than cancer cells, is essential for the response to immune checkpoint blockade therapy (19). Specifically, survival analysis showed that the presence of PD-L1 on macrophages had a protective role and enhanced the prognosis of patients with hepatocellular carcinoma. Macrophages are involved in maintaining an active immune microenvironment, with high numbers of infiltrating CD8+ T cells and high immune-related gene expression levels (15). Sepesi *et al*. investigated PD-L1 expression in surgically resected stage I non-small cell lung cancer and, in contrast, demonstrated that lower PD-L1 expression in the tumor, but also in tumor-infiltrating macrophages, was associated with significantly better OS (20).

The existence of conflicting reports about PD-L1 and−2 prognostic value can be generally attributed to technical disparities (e.g., variations in staining protocols across individual laboratories and use of different primary antibody clones to identify PD-Ls in tumor tissue), as well as different clinical features of the analyzed samples (site and size of cancer, treatments, follow-up time, etc.). Moreover, PD-L1 and−2 are dynamic markers that can be up- or downregulated over time, making their evaluation complicated (17, 21).

Direct activation of the PD-1 axis by cancer cells leads to a potent inhibitory signal in T lymphocytes resulting in anti-tumor immunity impairment and tumor cells ability to escape immunosurveillance (4, 19). Specifically, it has been shown that PD-1 activation inhibits glucose consumption, cytokine production, proliferation and survival in T lymphocytes, thus preventing the expression of transcription factors associated with effector T cell functions, such as GATA-3, T-bet, and Eomesodermin (Eomes) (4). PD-1/PD-Ls binding attenuates TCR-mediated signaling, thus impairing PI3K/Akt and Ras/MEK/Erk pathways, both required for T-cell activation (4).

PD-Ls are expressed in several solid tumors (8, 22), and immune checkpoint inhibitors, such as anti-PD-1 and anti-PD-L1 antibodies, showed efficacy in cancers with high mutational load, including lung cancer, melanoma, and microsatellite instable (MSI) tumors (23). It was shown that this efficacy is linked to the presence of tumor specific neoantigens that induce a Th1/CTL response that is counterbalanced by overexpression of multiple immune checkpoints such as PD-1/PD-L1 (23). In addition, PD-1/PD-L1 axis blockade might activate tumor-specific T lymphocytes to kill tumor cells by inducing TNF-α and IFN-γ (22).

For gynaecologic malignancies, the expression of PD-1 ligands has been reported in ovarian (17, 21, 22, 24–31), uterine (5–7, 32–38), cervical (23, 32, 39–50), and vulvar (32, 51–54) cancers, which we describe in detail in the next section.

1.1.3 PD-1 and PD-Ls Expression in Endometrial Cancer

In normal endometrium the role of the immune system is extremely complex, since it must prevent sexually transmitted infections but should also be able to help the growth of an allogenic fetus during pregnancy (23). So far, few reports characterized PD-1 and its ligands' expression in gynecological cancer and data are quite controversial. The expression profile of these immune checkpoints has been analyzed predominantly by immunohistochemistry, in biopsies obtained from both healthy subjects and cancer patients.

1.1.3.1 PD-1 in Endometrial Cancer

The PD-1 receptor has been found almost exclusively in immune cells infiltrating the tumor (32, 37, 38), and not in normal endometrium (5). Additionally, a deep analysis performed on 183 patients showed that high expression of PD-1 within and at the margins of a tumor, with a high PD-1/CD8+ ratio in the center, was associated with favourable OS (35). Additional

reports found a correlation between PD-1 expression in intraepithelial and peri-tumoural lymphocytes with DNA polymerase ε (POLE) mutation and MSI status of the patients (32, 37, 38). Specifically, it has been reported that PD-1 expression in tumor-infiltrating immune cells was more frequently found in moderately, poorly differentiated endometrial cancers, non-endometrioid type II (serous, clear cell, mucinous) endometrial cancers (5, 35, 36), and POLE and MSI subgroups (32, 37, 38).

1.1.3.2 PD-L1 in Endometrial Cancer

Regarding PD-1 ligands, all data concordantly showed that PD-L1 is expressed in most of the analyzed specimens (5–7, 32–35, 37), predominantly located in the cytoplasm (5–7). Several studies showed that PD-L1 was expressed in a similarly high percentage of samples in both normal endometrium and endometrial tumors (5–7). PD-L1 expression in cancer cells correlates with post-menopausal status, high histological grade (grade 3), deep myometrial invasion ($\geq 1/2$), lymphovascular invasion, adjuvant therapy, and MSI status (35). High PD-L1 immuno-reactivity on immune cells, and not on tumor cells, is an independent predictor of adverse progression-free survival (PFS) in all patients, including the microsatellite stable (MSS) subgroup (35). In addition, some reports evidenced that PD-L1 expression in intraepithelial immune cells was significantly more frequent in POLE mutant and MSI tumors, compared to MSS tumors (32, 37, 38), while PD-L1 expression in tumor cells did not differ between POLE mutant, MSI and MSS patients (32). However, data regarding PD-L1 expression in cancer cells are controversial: one study showed that only 1 out of 116 tumors expressed PD-L1 on tumor cells, but this under-estimation could be linked with the use of tissue microarrays, since PD-L1 expression is known to be heterogenous (37). Another study regarding gynecological samples, in 47 uterine sarcoma samples, found that PD-L1 expression was upregulated in comparison with normal endometrium, suggesting that this protein is a potential target for immunotherapy (7), while Bregar *et al.*, using a smaller number of samples (10 patients), found that PD-L1 is expressed in only 30% of specimens (34).

1.1.3.3 PD-L2 in Endometrial Cancer

For PD-L2 very few data are available so far, and its expression seems to differ from PD-L1, with no significant difference between normal endometrium and tumor (5–7). High PD-L2 expression was shown in 30% of primary endometrial carcinoma patients and 16% of

uterine sarcoma patients, demonstrating the potential of PD-L2 blockade in a limited proportion of uterine cancer patients (7). It has been shown that PD-L1 and PD-L2 expression was more frequent in moderately, poorly differentiated, non-endometrioid endometrial cancer and seems to be correlated with POLE and MSI status (5, 33, 36). Type II endometrial cancer and poorly differentiated histological features are generally associated with worse prognosis and, in addition, PD-1 axis expression suggests that it may cause immunosuppression to favor tumor growth, thus negatively affecting patients' survival (5).

1.1.4 Expression of PD-1, PD-L1, and PD-L2 in Ovarian Cancer

Ovarian cancer is the most lethal disease among gynecological cancers (17, 22, 29–31) and is known to be an immunogenic tumor.

1.1.4.1 PD-1 and PD-L1 in Ovarian Cancers

Some reports showed that PD-L1 expression is found in epithelial ovarian cancers (EOC) (17, 20, 21, 24–26, 30), especially in serous ovarian cancers (SOC) (28, 29), ovarian clear cell carcinomas (OCCC) and in malignant ascites (31), a sign of peritoneal carcinomatosis derived from ovarian cancer (22). In a cohort of 122 patients with OCCC, Zhu *et al.* showed that 55 cases (44.7%), classified as having high PD-L1 expression (PD-L1high), were significantly associated with advanced stages (III–IV) (22). Cases with high PD-L1 and PD-1 expression showed significantly poorer PFS and OS, compared to those with low PD-L1/PD-1 expression (22, 24, 28, 29). In subgroup analysis, PD-L1high was associated with poorer prognosis compared to PD-L1low in platinum-resistant and advanced stages (III–IV) patients (22). Drake *et al.* analyzed 55 ovarian cancer biopsies and showed that PD-1 was detected in 87% of the tumors in both stroma and epithelium, while PD-L1 was only present in 33% of patients, exclusively in high-grade tumors (17). Additionally, they found that low density of PD-1 and PD-L1 expressing cells in tumor tissue was significantly associated with advanced disease, failing to show any significant association between survival and PD-1 or PD-L1 expression in ovarian cancer (17), while patients with recurrent tumors and increased infiltrating PD-1+ immune cells had longer OS (21). The correlation of PD-1 and PD-L1 expression with high-grade tumors and stage IV International Federation of Gynecology and Obstetrics (FIGO) disease has also been confirmed by other studies (28, 29). Wieser *et al.* showed that, in a cohort of 158 patients with high-grade serous ovarian cancers, BRCA1/2 mutated tumors were characterized by high PD-1 expression, and that PD-L1 was observed

mainly in BRCA1/2 and TP53 mutated cancers (29). Xiao *et al.* reported that PD-1 is expressed in tumor infiltrating lymphocytes and PD-L1 in tumor cells and in intratumoural immune cells, but there was no significant difference of PD-1+ intratumoural immune cells in tumors with different mismatch repair (MMR) status (30). MSI ovarian cancers exhibited a significantly higher number of PD-L1+ intratumoural immune cells compared to MSS ovarian cancers, while PD-L1 expression was not different in tumors, irrespectively from their MMR status (30). In addition, no significant difference regarding PD-L1 expression in tumor cells and tumor infiltrating lymphocytes, and PD-1 expression in infiltrating lymphocytes, has been found between primary and recurrent disease (21).

1.1.4.2 PD-L2 in Ovarian Cancers

So far, only few studies investigated the expression of PD-L2 in ovarian cancer. An analysis on 70 patients showed that PD-L2 expression was not related to patient prognosis or other clinical variables, but negatively correlated with the number of FOXP3+ T regulatory cells (Tregs) (24). Imai *et al.* analyzed the expression of PD-L1 and PD-L2 on tumor cells and APCs in malignant ascites from epithelial ovarian cancer patients (31), and found differential PD-L1 expression in tumor cells between patients with high or low PD-1-expressing CD4+ T cells (43.9 and 27.3%, respectively), while no difference in PD-L1 expression was observed between patients with high and low PD-1 expression on CD8+ T cells (34.1 and 27.3%, respectively). Between 2.3 and 3.2% of the patients with high or low PD-1 on CD4+ T cells and CD8+ T cells also expressed PD-L2. No correlation was found between PD-L1/2 expression and clinical variables or outcomes (31). To support a potential role of PD-1 and PD-L1/ PD-L2 axis as targets in ovarian cancer, it has been reported in syngeneic orthotopic mouse model of epithelial ovarian cancer, that treatment with anti-PD-1 or anti-PD-L1 antibodies resulted in tumor rejection in 75% of the treated-mice, while mice treated with anti-PD-L2 antibody did not reject tumors (25). These data can be explained considering the selected models that expressed lower levels of PD-L2 than PD-1 and PD-L1. Additionally, PD-1 and PD-L1 blockade significantly increased the CD8+ to Tregs and CD4+ to Tregs ratios within the tumor, while, on the contrary, there was no significant change in the CD8+ or CD4+ to Tregs ratios (25).

1.1.5 Expression of PD-1, PD-L1, and PD-L2 in Other Gynecological Cancers

Cervical cancer is the third most common gynecological malignancy in Europe (23). Little information is available, up to now, regarding the expression of PD-1 ligands (23, 32, 39, 43–47). A report from Howitt *et al.* showed that cervical cancer is a potential candidate for clinical trials testing PD-1 blockade (23, 32, 39). In fact, using FISH analysis on 48 Formalin-Fixed Paraffin-Embedded (FFPE) tissue specimens of cervical squamous cell carcinoma, they observed co-amplification or co-gain of PD-L1 and PD-L2 in 32 out of 48 cases (67%). Immunohistochemical staining for PD-L1 revealed high expression in 95% of the tumors with membranous staining pattern (32). Persistent infection with human papilloma virus (HPV) is an essential step in the development of most cervical cancers (40). Some studies hypothesized that HPV may activate PD-1/PD-L1 to evade host immune responses, resulting in persistence of the cervical intraepithelial neoplasia (41). The identification of HPV as an etiological factor leads to antigen production and presentation, thereby making cervical cancer immunogenic (42). Recently, the role of the PD-1/PD-L1 axis in HPV associated head and neck squamous cell cancer (HPV-HNSCC) creating an "immune-privileged" site for initial viral infection and subsequent adaptive immune resistance suggests a rationale for therapeutic blockade of this pathway in patients with HPV-associated tumors (43). Significant PD-L1 expression in cervical carcinoma has been confirmed in several studies (44–47). As a consequence, this immunogenic disease requires a highly immunosuppressive microenvironment to progress and metastasize (48, 49) which has been demonstrated in tumor-positive lymph nodes where high Treg levels, low CD8+ T cell/Treg ratio and high levels of PD-L1+ and HLA-DR+ myeloid cells were found (50). Regarding another gynecological malignancy, vulvar cancer, the clinical relevance of PD-L1 expression has not been completely studied so far (32). Although rare, incidence rates of vulvar cancer are increasing and, in locally advanced, metastatic or recurrent disease, prognosis is poor and new treatment modalities are needed (51). Screening of 23 vulvar squamous cell carcinomas revealed 6 cases (26%) with co-amplification of PD-1 ligands, 4 cases (17%) showed co-gain, 6 cases (26%) showed polysomy, and 7 cases (30%) showed disomy. Immunohistochemical staining for PD-L1 across all cases revealed the highest median PD-L1 protein expression in cases with co-amplification of PD-L1 and PD-L2 and decreasing values with decreasing genetic complexity (32). Previous studies showed that PD-L1 is expressed in the majority of vulvar squamous cell carcinoma samples (51–54), in

both cancer cells and peritumoural immune cells (52–54). Additionally, its expression was related with several components of immune system (CD3+, CD20+, and CD68+ intra-tumor immunocytes) (51, 54), while a significant correlation with immunosuppressive cell populations (FOxP3+ Treg cells) was reported only by Sznurkowski *et al.* (54). Data analyzing the clinical impact of PD-L1 expression in vulvar cancer reveal that it is not clear whether its expression correlates with clinicopathological parameters. In summary, no significant associations were observed between PD-L1 presence and typical clinicopathological factors (51), except for tumor stage as reported by Sznurkowski *et al.* (54), and PD-L1 expression occurs more often in high risk HPV-negative samples (51). Regarding survival analysis, it is reported that PD-L1 expression did not influence the OS (51, 53), but patients with primary tumors positive for immune cells-PD-L1 expression had improved OS compared to negative ones (54). The presence of PD-L1 also seems to be an independent prognostic factor for recurrence free survival (51).

1.1.6 Ongoing Immunotherapy Clinical Trials in Gynecological Malignancies

Several clinical trials are ongoing at the moment, according to the ClinicalTrials.gov database [accessed July 06, 2019], testing anti-PD-1/PD-L1 blockade alone or in combination in patients with endometrial, cervical, vulvar and ovarian cancer, while there are no ongoing clinical trials using anti-PD-L2 (Tables 1–3). Clinical trials data were collected from ClinicalTrials.gov database, selecting only completed trials or in "Active, not recruiting" status.

1.1.6.1 Endometrial Cancer

Regarding endometrial cancer, 6 clinical trials are ongoing (Table 1). Most of them are Phase I 0clinical trials and preliminary results, reported by the American Society of Clinical Oncology (asco.org), showed that atezolizumab (anti-PD-L1), and pembrolizumab (anti-PD-1) might be promising agents for endometrial cancer treatment. Most relevant results showed that in a phase I study, 15 patients eligible based on PD-L1 status (>5% of positivity in tumor-infiltrating immune cells) were treated with atezolizumab and evaluated for safety and efficacy. Results showed that atezolizumab had a favorable safety profile and 13% (2/15) of patients showed a reduction in tumor size. A trend for higher PFS and OS has been observed in patients with high levels of tumor-infiltrating immune cells. Clinical benefit appeared to increase with higher PD-L1 expression, suggesting a link between PD-L1 status

and response to atezolizumab. In addition, hypermutation, and/or high immune infiltration may be linked to response to PD-L1 blockade (Clinical trial information: NCT01375842) (55). In a different phase I clinical trial, pembrolizumab was administered in 24 patients with endometrial carcinoma (excluding sarcomas), failure of prior systemic therapy, and PD-L1 expression in ≥1% of tumor or stromal cells. A reduction in tumor size was confirmed in 13.0% of the patients, while 3 patients achieved stable disease. PFS and OS rates were 19.0 and 68.8%, respectively. In conclusion, Pembrolizumab demonstrated an acceptable safety profile and anti-tumor activity (Clinical trial information: NCT02054806) (56).

ClinicalTrials.gov identifier	Status	Interventions/alone or in combination	Phase
NCT02630823	Active, not recruiting	Pembrolizumab (anti-PD-1) + Paclitaxel/Carboplatin/Radiation (standard of care)	I
NCT02725489	Active, not recruiting	Durvalumab (anti-PD-L1)	II
NCT02728830	Active, not recruiting	Pembrolizumab (anti-PD-1)	Early I
NCT02646748	Active, not recruiting	Pembrolizumab (anti-PD-1) + itacitinib/INCB050465	I
NCT02914470	Active, not recruiting	Atezolizumab (anti-PD-L1) + cyclophosphamide/Carboplatin	I
NCT02521844	Active, not recruiting	Pembrolizumab (anti-PD-1) + ETC-1922159	I

Table 1. Ongoing immunotherapy clinical trials for patients with endometrial cancer.

1.1.6.2 Ovarian Cancer

For ovarian cancer 22 clinical trials are ongoing, 2 of which are completed (Table 2). Some of the early-phase clinical trials of anti-PD-1 or anti-PD-L1 antibodies have shown good safety profiles and durable anti-tumor response in certain patient population(s). However,

ClinicalTrials.gov identifier	Status	Interventions (alone or in combination)	Phase
NCT02608684	Active, not recruiting	Pembrolizumab (anti-PD-1) + Gemcitabine/Cisplatin	II
NCT02728830	Active, not recruiting	Pembrolizumab (anti-PD-1)	Early I
NCT03287674	Active, not recruiting	Nivolumab (anti-PD-1) + Cyclophosphamide/Fludarabine/TIL infusion/Interleukin-2/Ipilimumab	I/II
NCT03277352	Active, not recruiting	Pembrolizumab (anti-PD-1) + INCAGN01876/Epacadostat	I/II
NCT03312114	Active, not recruiting	Avelumab (anti-PD-L1)	II
NCT02674061	Active, not recruiting	Pembrolizumab (anti-PD-1)	II
NCT03029598	Active, not recruiting	Pembrolizumab (anti-PD-1) + Carboplatin	I/II
NCT02335918	Completed	Nivolumab (anti-PD-1) + varlilumab	I/II
NCT02915523	Active, not recruiting	Avelumab (anti-PD-L1) + entinostat	I/II
NCT02452424	Completed	Pembrolizumab (anti-PD-1) + PLX3397	I/II
NCT02644369	Active, not recruiting	Pembrolizumab (anti-PD-1)	II
NCT03073525	Active, not recruiting	Atezolizumab (anti-PD-L1)	II
NCT02526017	Active, not recruiting	Nivolumab (anti-PD-1) + FPA008	I
NCT02580058	Active, not recruiting	Avelumab (anti-PD-L1) + PLD	III
NCT03365791	Active, not recruiting	PDR001 (anti-PD-1) + LAG525	I
NCT02764333	Active, not recruiting	Durvalumab (anti-PD-L1) + TPIV200	II
NCT02431559	Active, not recruiting	Durvalumab (anti-PD-L1) + Pegylated Liposomal Doxorubicin	I/II
NCT02914470	Active, not recruiting	Atezolizumab (anti-PD-L1) + carboplatin, cyclophosphamide	I
NCT02725489	Active, not recruiting	Durvalumab (anti-PD-L1)	II
NCT01975831	Active, not recruiting	MEDI4736 (anti-PD-L1) + Tremelimumab	I
NCT03038100	Active, not recruiting	Atezolizumab (anti-PD-L1) + Carboplatin/Atezolizumab/Bevacizumab	III
NCT01772004	Active, not recruiting	Avelumab (anti-PD-L1)	I/II
NCT03574779	Active, not recruiting	TSR-042 (anti-PD-1) + Niraparib/Bevacizumab	II
NCT02521844	Active, not recruiting	Pembrolizumab (anti-PD-1) + ETC-1922159	I

Table 2. Ongoing immunotherapy clinical trials for patients with ovarian cancer.

their response rates remain between 10 and 15% (31, 57). Available interim reports from some of the trials show promising objective response rates (ORR) for the treatment of ovarian cancer with nivolumab (anti-PD-1) (ORR of 15%, n = 20 patients), pembrolizumab (ORR 11.5%, n = 49), or avelumab (anti-PD-L1) (ORR 10%, n = 124) (17, 58, 59). Preliminary data presented at the annual ASCO meeting in 2016 of a phase I trial evaluating durvalumab (anti-PD-L1) in combination with olaparib (PARP inhibitor), showed a disease control rate (DCR) of 67% for the doublet olaparib - durvalumab in a cohort including BRCA wild type triple negative breast cancer and EOC cases (23). In the KEYNOTE-28 trial, which explored the activity of pembrolizumab in several solid tumors, outcome of ovarian cancer was ORR of 11.5%, and only 23.1% showed tumor shrinkage from baseline (57).

1.1.6.3 Cervical Cancer

For cervical cancer, 6 clinical trials are ongoing (Table 3). Most relevant findings showed that in a phase Ib study with 24 patients affected by advanced cervical squamous cell cancer and PD-L1 expression in ≥1% of tumor or stromal cells, pembrolizumab was well-tolerated and showed promising anti-tumor activity (Clinical trial information: NCT02054806) (60), while its clinical benefit was investigated in the phase 2 KEYNOTE-158 trial. Pembrolizumab administration has been also investigated in a single cohort trial enrolling 98 patients with recurrent or metastatic cervical cancer, expressing PD-L1 with a positive ratio of the number of all PD-L1–expressing cells (tumor cells, lymphocytes, macrophages) to the number of all tumor cells, or a Combined Positive Score (CPS) ≥1. The ORR in 77 patients was 14.3% (95% CI: 7.4, 24.1), including 2.6% complete responses and 11.7% partial responses. No responses were observed in patients with tumors negative for PD-L1 expression (CPS <1). Serious adverse reactions occurred in 39% of patients (Clinical trial information: NCT02628067) (61). On June 12th 2018, pembrolizumab was approved by Food and Drug Administration (FDA), for treatment of patients with recurrent or metastatic

ClinicalTrials.gov Identifier	Status	Interventions	phase
NCT01975831	Active, not recruiting	MEDI4736 (anti-PD-L1) + Tremelimumab	I
NCT02914470	Active, not recruiting	Atezolizumab (anti-PD-L1) + Carboplatin/Cyclophosphamide	I
NCT02725489	Active, not recruiting	Durvalumab (anti-PD-L1)	II
NCT02921269	Active, not recruiting	Atezolizumab (anti-PD-L1) + Bevacizumab	II
NCT02257528	Active, not recruiting	Nivolumab (anti-PD-1)	II
NCT03073525	Active, not recruiting	Atezolizumab (anti-PD-L1)	II

Table 3. Ongoing immunotherapy clinical trials for patients with cervical cancer.

cervical cancer, expressing PD-L1 (CPS ≥1) as determined by an FDA-approved test, with disease progression on or after chemotherapy[1].

In conclusion, since in all gynecological cancers ORR is around 10–15%, this emphasizes the need for combination treatments to improve efficacy of immune checkpoint (Figure 2).

[1] Merck & Co. Press Release Details. https://investors.merck.com/news/pressrelease-details/2018/FDA-Approves-Mercks-KEYTRUDA-pembrolizumab-for-Previously-Treated-Patients-with-Recurrent-or-Metastatic-Cervical-Cancer-Whose-Tumors-Express-PD-L1-CPS-Greater-Than-or-Equal-to-1/default.aspx

Figure 2. Immunotherapy against PD-1/PD-Ls in gynecological cancers. *Blocking the PD-1/PD-L1 immune checkpoint pathway by anti-PD-1 or anti-PD-L1 antibodies suppresses cancer cell survival and enhances the antitumor responses of T cells, leading to tumor regression and rejection. Actually, several clinical trials are ongoing testing anti-PD-1/PD-L1 blockade alone or in combination, in patients with endometrial, cervical, vulvar, and ovarian cancer, while there are no ongoing clinical trials using anti- PD-L2. In all gynecological cancers ORR is around 10–15%, argues for combinatorial treatments are taken in consideration.*

1.1.7 Future Directions for Immune Checkpoint Inhibitors (ICIs) Combination Therapies

Albeit ICIs therapies have been shown to induce durable responses and long-term remission in several cancer types, many patients fail to respond, develop resistance over the time or show immune-related adverse effects (62–65). The unresponsiveness or the toxicity of ICIs represents a strong rationale for the combination of ICIs with other treatments to increase the response rate of non-immunological tumors. For example, therapeutic approaches that induce the release and presentation of tumor antigens could be able to foster a de novo anti-tumor T cell response. In this regard, candidates for a combination therapy with ICIs could be cancer vaccines, oncolytic viruses, radiation, or low-dose chemotherapy (66).

Another potential combination approach with ICIs could be with bispecific antibodies, which recruit patient's T cells or NK cells against cancer cells expressing tumor-associated

14

antigens. An example came from hematologic malignancies, wherein a bispecific antibody targeting both CD3 and CD123 (67, 68) was used but showed benefit in only a small fraction of patients. A major mechanism limiting the therapeutic efficacy was T cell anergy and exhaustion driven by ICIs pathways (mainly PD-L1/PD-1) (69). Inspired by this inhibitory role of ICIs pathway, combining ICIs with bispecific antibodies showed enhanced T cell proliferation and IFN-γ production (70).

One more possibility to improve ICI efficacy might be combination with cytokine therapy. The cytokine IL-2 has been approved for the treatment of metastatic renal cell carcinoma and advanced melanoma but is accompanied by severe side effects (71). However, modified IL-2 formulations such as bempegaldesleukin (NKTR-214) have an improved safety profile and have shown capabilities of enhancing the proliferation and activation of CD8+ T cells and NK cells without increasing the number of Tregs (72). Recently, the PIVOT-02 trial (combination of NKTR-214 and nivolumab) has shown that this combination is safe and efficacious (ORR 48% in 23 patients) in metastatic urothelial carcinoma (73).

In addition, a recent study has demonstrated that DC-derived IL-12 is necessary for successful anti-PD-1 cancer therapy, suggesting that IL-12 and ICIs could be rationally combined (74).

Finally, there is strong rationale to combine anti-angiogenic therapies with ICI's, since anti-angiogenic therapies induce a normalization of the tumor vasculature, which leads to enhanced infiltration of T lymphocytes in the tumor.

1.2 Endometrial cancer

1.2.1 Anatomical outlines and functions of endometrium

The wall of the uterus is stratified in three layers. The most superficial layer is the perimetrium, a serous membrane, which consists of epithelial tissue that covers the exterior portion of the uterus. The myometrium is the thick middle layer of smooth muscle responsible for uterine contractions. Most of the uterus is myometrial tissue, characterized by the muscle fibers running horizontally, vertically, and diagonally, allowing contractions during labor and the less powerful contractions that contribute to expel menstrual blood
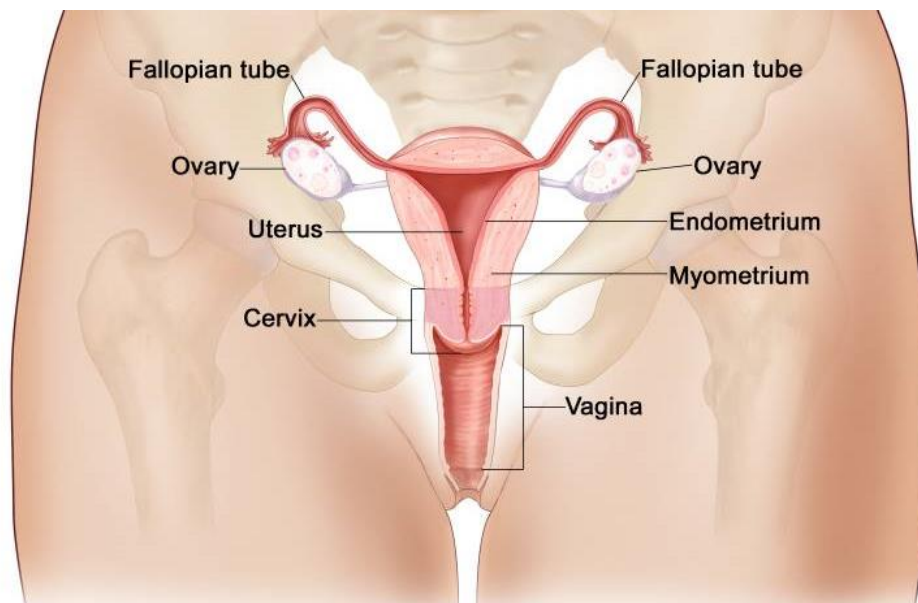
Figure 3. Anatomy of the female reproductive system. The organs in the female reproductive system include the uterus, ovaries, fallopian tubes, cervix, and vagina. The uterus has a muscular outer layer called the myometrium and an inner lining called the endometrium (76).

during a woman's period (75,76). The innermost layer of the uterus is the endometrium, a tiny internal mucous membrane that fills the cavity of the uterus and is dropped during the monthly menstrual period. This inner layer adheres to the myometrium without insertion of a submucosal layer and its thickness varying from 1 to 7 mm. It is a plastic tissue in which cells undergo a variety of adaptation reactions in response to the physiological changes that occur during the menstrual cycle and embryo implantation (77). The endometrium is composed of luminal and glandular epithelia, stromal fibroblasts, and vascular smooth muscle cells and it is divided in two tissue compartments: the upper transient functionalis is formed and shed during each menstrual cycle, whereas the deep germinal basalis persists from cycle to cycle and it is adjacent to the myometrium (78). The blood supply to the basal portion of the endometrium is via the straight basal arteries, and the spiral arterioles supply

the functionalis layer. During the early part of the cycle, before the releasing of an egg from ovaries (ovulation), the ovaries produce hormones called estrogens. Estrogens cause the thickening of endometrium in order to support an embryo if fertilization happens. The post-ovulatory increased in progesterone, which characterizes the luteal phase, maintaining a thick stratum functionalis. If there is no pregnancy, progesterone production ceases, ending the luteal phase. Without progesterone and increased levels of prostaglandin, the endometrium thins and the spiral arteries of the endometrium constrict and rupture, preventing oxygenated blood from reaching the endometrial tissue. As a result, endometrial tissue dies and blood, pieces of the endometrial tissue, and white blood cells are shed through the vagina during menstruation. This cycle repeats until the women go through menopause (78, 79). Endometrial cell migratory behaviour can be considered as a central feature of its plasticity and crucial for endometrial physiology. The stromal component starts to grow when the endometrial wound is completely re-epithelialized and endometrial cell movements are essential to repopulate the space created by tissue loss and to avoid excessive fibroplasia. These events are mainly regulated by steroid hormones, concentrations of which regulate the balance between endometrial growth and transformation. Primary function of endometrium is to create an immuno-privileged site for embryo implantation and its development (77).

1.2.2 Molecular biology and histological subtypes of endometrial cancer

Endometrial cancer is the most common gynaecological malignant disease, and the fourth most common cancer in European and North American women, accounting for about 6% of new cancer cases and 3% of cancer deaths per year (80,81). Approximately, 90% of cases of endometrial cancer are sporadic, whereas the remaining 10% of cases are hereditary (82). Tumours developed in the epithelial layer of endometrium are classified as endometrial carcinomas (98% of the endometrial tumours), while tumours developed in the muscle layer or stromal tissue are called sarcomas (2%) (83).

Endometrial cancers are classified into two clinicopathological types, the estrogen-dependent endometrioid type I and non-estrogen-dependent non-endometrioid type II (84).

Type I endometrial endometrioid cancers represent the majority of sporadic cases of endometrial cancer and occur in both menopausal than premenopausal women (85). Features

of the type I carcinomas include increased exposure to estrogens (nulliparity, early menarche, chronic anovulation, and unopposed exogenous estrogens), obesity, and responsiveness to progesterone therapy. They develop from a hypertrophic endometrium, commonly express estrogens and progesterone receptors and they are characterized by slow growth and a good prognosis (85). Almost of 83% of endometrioid carcinomas and 55% of precancerous lesions exhibit a loss of the oncosuppressor gene PTEN expression (83, 86, 87).

PTEN, located at chromosome 10q23, encodes a tyrosine with both lipid and protein phosphatase activity, with each serving different functions. The lipid phosphatase activity leads to a cell cycle arrest at the G1/S checkpoint. PTEN acts in opposition to phosphotidylinositol 3-kinase (PI3KCA) to control levels of phosphorylated AKT indeed, PTEN loss of function increases PI3KCA activation, leading to phosphorylation of AKT and then, cell growth and survival. PTEN is involved, also, in the inhibition of focal adhesion formation as well as migration. PTEN loss of function results in an uncontrolled cell growth and apoptotic escape (85).

Microsatellite instability (MSI) is a significant genetic alteration demonstrated in almost 45% of endometrial cancer lesions that results from impaired DNA mismatch repair. Mismatch repair gene MLH1 deficiency, caused by epigenetic hypermethylation in its promoter region, is most frequently observed in sporadic endometrial adenocarcinomas (88). Other genetic alterations in type I endometrial cancers include mutations in K-RAS and βcatenin (83, 87).

K-RAS mutations have been detected in 10% to 30% of cases with a higher frequency in MSI cancers. Gain of function mutations in the β-catenin gene at 3p21 is seen in 25% to 38% of cases (85).

Type II non-endometrioid carcinomas are less common, accounting for 10% to 20% of endometrial cancers (85, 87). They are frequently serous or clear cell adenocarcinomas (87) arising from atrophic endometrium and unrelated to estrogens exposure. Hormonal risk factors have not been implicated in their pathogenesis (85). These tumours occur predominantly in women after menopause, are very aggressive, with a propensity for early spread and poor prognosis (89).

TP53 mutations occur in ~90% of serous adenocarcinomas and they are almost always associated with aneuploidy (87). TP53 gene is located on chromosome 17 and it is important

in preventing damaged cells proliferation. After DNA damage, nuclear p53 accumulates and causes cell cycle arrest and promoting apoptosis (85).

Moreover, oncosuppressor p16 inactivation, oncogene HER2 overexpression, and reduced E-cadherin expression are observed in ~45, 70, and 80% of total cases of serous adenocarcinomas analyzed (87).
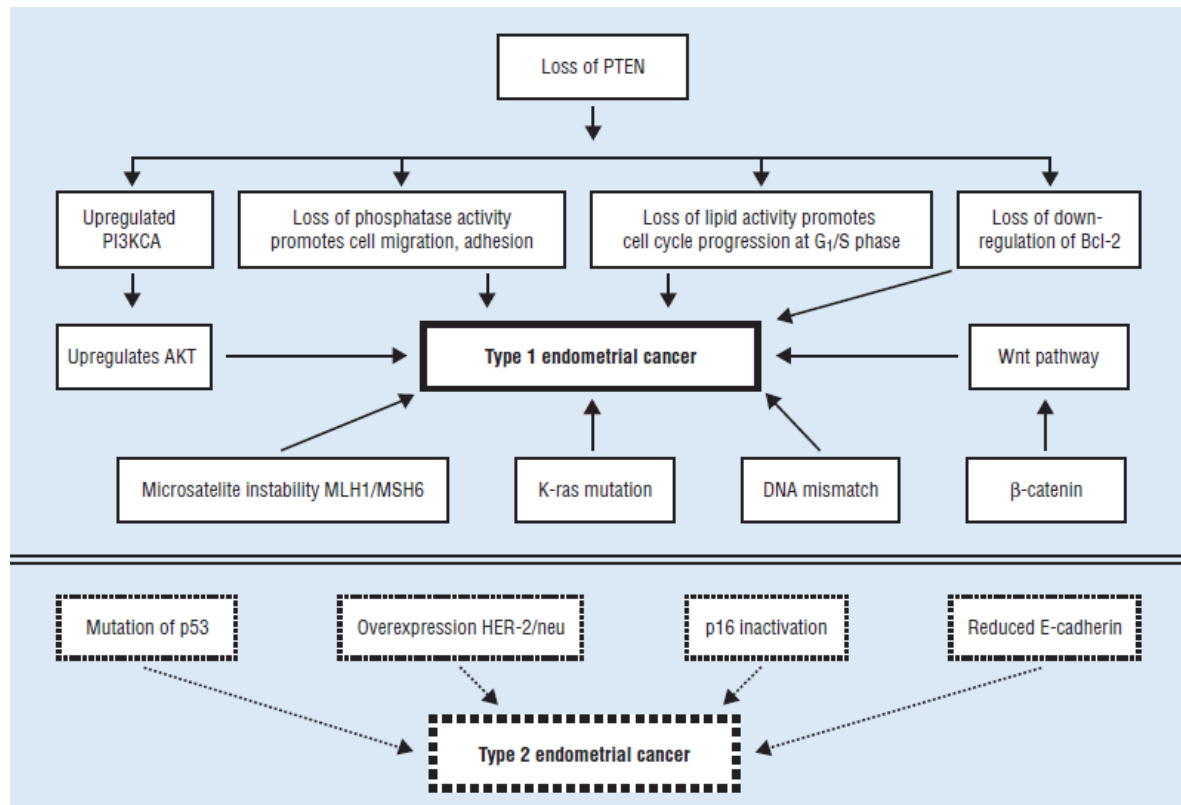
Figure 4. Molecular basis of type 1 and type 2 endometrial cancers. Solid lines indicate type 1 causes and dashed lines indicate causes for type 2 (85).

Endometrioid endometrial cancer is characterized by tubular glands, lined by stratified or pseudostratified columnar cells, showing a similarity with benign endometrial epithelium (90).

The most common histological types of non-endometrioid endometrial cancer include uterine papillary serous carcinoma (UPSC) and uterine clear cell carcinoma (UCCC). Other non-endometrioid subtypes include mucinous and squamous cell carcinoma (85, 90).

The UPSC subtype shows a complex papillary architecture, with broad fibrous stalks underlying a tufted stratification of the epithelial lining, profound tumor necrosis, unusually high amounts of vascular invasion and a significant peritoneal spread. Approximately, 5% to 10% of all endometrial cancers are classified as UPSC and it is the cause of almost 40%

of endometrial cancer-related deaths (85). The 5-year overall survival rate for all stages of UPSC is 53% compared with 83% for endometrioid carcinoma.

The second most aggressive non-endometrioid subtype UCCC is characterized by the clearing of cellular cytoplasm (glycogen) and display different shapes and patterns ranging from solid and glandular to papillary structures (90). The recurrence rate is approximately 50% at 3 years. The 5-year survival rate ranges from 79% for early disease to 21% for advanced disease. Although UCCC accounts for only 4% of uterine cancers, it accounts for approximately 8% of uterine cancer-related deaths (85).

Whereas the primary endometrial squamous cell carcinoma (PESCC) is uncommon, accounting 0.1%-0.5% of all uterine cancers, the endometrial carcinoma with mucinous histology comprises 0.6% to 5% of total cases. Rarely it is found as a pure cell type and mucinous areas have a micro glandular pattern with intraluminal and intracytoplasmic secretions and micropapillary formation (90).

The most common symptom of endometrial cancer is an abnormal uterine bleeding that occurs in 90% of patients. Other symptoms include thin white or clear vaginal discharge in postmenopausal women. In advanced disease, the uterus may become enlarged or cancer may spread, causing pelvic cramping painful sexual intercourse or painful urination (91).

1.2.3 Endometrial cancer stages

Endometrial cancer stages range from stage I to IV and the systems used for staging endometrial cancer are the FIGO (International Federation of Gynecology and Obstetrics) system and the American Joint Committee on Cancer TNM staging system (92).

Stage	Stage grouping	FIGO Stage	Stage description
I	T1, N0, M0	I	The cancer is growing inside the uterus. It may also be growing into the glands of the cervix, but not into the supporting connective tissue of the cervix (T1). It has not spread to nearby lymph nodes (N0) or to distant sites (M0).

IA	T1a, N0, M0	IA	The cancer is in the endometrium (inner lining of the uterus) and may have grown less than halfway through the underlying muscle layer of the uterus (the myometrium) (T1a). It has not spread to nearby lymph nodes (N0) or to distant sites (M0).
IB	T1b, N0, M0	IB	The cancer has grown from the endometrium into the myometrium. It has grown more than halfway through the myometrium but has not spread beyond the body of the uterus (T1b). It has not spread to nearby lymph nodes (N0) or to distant sites (M0).
II	T2, N0, M0	II	The cancer has spread from the body of the uterus and is growing into the supporting connective tissue of the cervix (called the cervical stroma). But it has not spread outside the uterus (T2). It has not spread to nearby lymph nodes (N0) or to distant sites (M0).
III	T3a, N0, M0	III	The cancer has spread outside the uterus but has not spread to the inner lining of the rectum or urinary bladder (T3). It has not spread to nearby lymph nodes (N0) or to distant sites (M0).
IIIA	T3a, N0, M0	IIIA	The cancer has spread to the outer surface of the uterus (called the serosa) and/or to the fallopian tubes or ovaries (the adnexa) (T3a). It has not spread to nearby lymph nodes (N0) or to distant sites (M0).
IIIB	T3b, N0, M0	IIIB	The cancer has spread to the vagina or to the tissues around the uterus (the parametrium) (T3b). It has not spread to nearby lymph nodes (N0) or to distant sites (M0).
IIIC1	T1-T3	IIIC1	The cancer is growing in the body of the uterus. It may have spread to some nearby tissues but is not

			growing into the inside of the bladder or rectum (T1 to T3). It has also spread to pelvic lymph nodes (N1, N1mi, or N1a), but not to lymph nodes around the aorta or distant sites (M0).
IIIC2	T1-T3 N2, N2mi or N2a M0	IIIC2	The cancer is growing in the body of the uterus. It may have spread to some nearby tissues but is not growing into the inside of the bladder or rectum (T1 to T3). It has also spread to lymph nodes around the aorta (para-aortic lymph nodes) (N2, N2mi, or N2a), but not to distant sites (M0).
IVA	T4, Any N, M0	IVA	The cancer has spread to the inner lining of the rectum or urinary bladder (called the mucosa) (T4). It may or may not have spread to nearby lymph nodes (Any N) but has not spread to distant sites (M0).
IVB	Any T, Any N, M1	IVB	The cancer has spread to inguinal (groin) lymph nodes, the upper abdomen, the omentum, or to organs away from the uterus, such as the lungs, liver, or bones (M1). The cancer can be any size (Any T) and it might or might not have spread to other lymph nodes (Any N).

Table 4. The system described is the most recent AJCC system. It went into effect January 2018 (92).

1.2.4 Risk factors

Type I endometrial cancer is mainly responsive to estrogen then, the most important risk factor for this malignancy is a long-term exposure to excess endogenous or exogenous estrogens without adequate progesterone balance. This imbalance causes proliferation of the endometrium leading to endometrial hyperplasia and eventually carcinoma (93). A long

estrogens exposure and hyperestrogenic state are caused by conditions of chronic anovulation, polycystic ovary syndrome, Stein-Leventhal Syndrome, early menarche and late menopause that can increase the risk of endometrial cancer. Obesity is a well-established risk factor for endometrial carcinoma, and it has been demonstrated a positive correlation between obesity and mortality with endometrial carcinoma (94). A recent meta-analysis documented a strong association of onset of endometrial cancer with an increase of BMI by 5 kg/m^2 (95). In obese women is demonstrated an endogenous conversion of adrenal precursors to estrone and estradiol by adipose cells leading to hyperestrogenic state. Additionally, some factors like nulliparity and hypertension, which invariably lead to excessive estrogens exposure, are almost always associated with the disease. Diets rich in carbohydrates, hyperinsulinemia and elevated levels of insulin-like growth factors can cause proliferation of endometrium and may lead to endometrial cancer, but the mechanism is not clear established. Systemic (oral, patch, or vaginal ring) estrogen therapy without an opposing progestin markedly increased risk of hyperplasia of the endometrium or cancer development. Tamoxifen is an anti-estrogen used in the treatment of breast cancer and it is a risk factor for endometrial cancer, but this is still not clear (93).

Other risk factors include long or irregular menstrual cycles, family history of endometrial cancer, age older than 50 years, Lynch syndrome, estrogen-secreting tumors, Cowden syndrome and Peutz-Jeghers syndrome.

Recently, a pooled analysis with a total of 14,069 endometrial cancer patients of both types revealed that the risk factor profiles for type II and type I tumors are quite similar, suggesting that they have some common etiologic pathways. The etiology of type II tumors may, therefore, not be completely estrogen independent suggesting might be better moving away from the traditional type I versus type II distinction (96).

1.2.5 Treatment of endometrial cancer

In addition to the previously described immunotherapy, the treatment options provided for endometrial cancer are surgery, radiation therapy, chemotherapy, hormone therapy and targeted therapy. The prognosis of patients with early stage disease is generally good and surgery is the main option treatment. It consists of a hysterectomy, salpingo-oophorectomy, and lymph nodes removal. Many women with endometrial cancer have comorbidities, such as diabetes and obesity that poses challenges to surgery as well as radiation and

chemotherapy delivery (97). Despite surgery, prognosis for patients with advanced disease at stage II or III is poor with increased risk of recurrence and therapeutic options beyond first-line chemotherapy are limited. For metastatic or recurrent endometrial cancer, adjuvant treatment options include chemotherapy and radiation with a sequential delivery or a sandwich approach (chemotherapy – radiation -chemotherapy). Chemo drugs used to treat endometrial cancer may include Paclitaxel, Carboplatin, Doxorubicin or liposomal Doxorubicin, Cisplatin and Docetaxel (98).

Recently, it is increased the interest towards targeted therapies but identifying and targeting mutations do not necessarily lead to high treatment response because tumour is characterized by high heterogeneity and complexity. Among many targeted agents investigated, antiangiogenic and mTOR/PI3K pathway inhibitor agents have demonstrated clinical activity and remain under further investigation (99).

Hormonal therapy is a treatment option in endometrial cancer, and it can include progestins, Tamoxifen, luteinizing hormone-releasing hormone agonists (LHRH agonists) or aromatase inhibitors (AIs). Actually, the predictive value of estrogen receptor/progesterone receptor status remains a little controversial and no one type of hormone treatment has been found to be the best for endometrial cancer treatment (100, 101).

1.3 Cannabidiol, its biological effects and receptors

1.3.1 Cannabis sativa and its constituents

Cannabis sativa is a plant belonging to Cannabaceae family diffused in different habitats and altitudes and it was used traditionally as source of food and textile fiber since ancient times, firstly in Egypt and Asia, then in Europe and South American and later in North America (102).

In 1990's, it was firstly described cannabinoid receptors and endogenous cannabinoid system and therefore, it was increased the interest for the Cannabis use in therapy. Therapeutic effects of its main constituents (Δ9-THC and CBD) were studied in patients with epilepsy, insomnia, vomit, pain, glaucoma, asthma, inappetence, anxiety, brain damage, inflammations, psychosis and others (103).

Cannabis sativa is a complex species because it produces an elevated number of natural secondary metabolites. It contains 545 known molecules and they are chemically classified as phytocannabinoids, alkenes, flavonoids, fatty acids, nitrogenous compounds, sugars, monoterpenes, triterpenes, sesquiterpenes and others. The most considerable are the phytocannabinoids, which are C21 terpeno-phenolic natural cannabinoids biosynthesized by the plant, with physiological and sometimes psychogenic effects. Their derivates and transformation products are also considered as cannabinoids (102-105). The main phytocannabinoids are Cannabigerol (CBG), Cannabichromene (CBC), Cannabidiol (CBD), Cannabinol (CBN) and Tetrahydrocannabinol (THC) (105).

1.3.2 Endogenous cannabinoid system in female reproductive system

The endocannabinoid system (ECS) is composed by cannabinoid receptors, endogenous cannabinoids and some enzymes involved in synthesis and degradation of endogenous endocannabinoids. Generally, the ECS is a neuromodulatory system which has activities in CNS development, synaptic activity and response to endogenous and external stimuli (106) but, it is also known to impact the female reproductive system where it affects folliculogenesis, oocyte maturation, and ovarian endocrine secretion (107).

The two most extensively studied endocannabinoids are N-arachidonoyl ethanolamine (anandamide AEA) and 2-arachy-donoylglycerol (2-AG) (107) but there are also other endogenous molecules. In several physiological conditions, 2-AG concentrations are much higher than that of AEA and, interestingly, these endocannabinoids are not stored within

cells, but are thought to be produced "ex-novo" from membrane phospholipid precursors. However, recent reports suggest that they may be stored intracellularly within lipid droplets known as adiposomes (106, 107). Anandamide is synthesized through the hydrolysis of a phospholipidic precursor N-arachidonoyl-phosphatidyl-ethanolamine (NAPE), reaction catalysed by phospholipase-D. 2-AG derives from the hydrolysis of phosphatidylinositol 4,5-bisphosphate (PIP2), catalysed by phospholipase C (105, 106, 108). The degradation process of anandamide is mediated by Fatty Acid Amide Hydro-lase (FAAH), but also it is involved in 2-AG degradation (108). The endocannabinoids are released after depolarization Ca^{+2} – dependent in the cell and, subsequently, they are inactivated after degradation or re-uptake (105, 106, 108).

AEA and 2-AG exert most of their biological effects by binding to the seven-transmembrane G-protein-coupled cannabinoid receptors CB1 and CB2, encoded by different genes and exhibiting 44% homology in their primary structure (77, 105, 106, 108). A new putative cannabinoid receptor, CB3 or GPR55, has been recently identified, but its biological significance has not been completely elucidated. GPR55 is expressed in neurons, immune system, vascular endothelial cells and it controls hypotension and anti-nociception (109). CB1 receptor is expressed in central nervous system neurons and it regulates different functions in different areas: ganglia and cerebellum for the motility, cortex and hippocampus for the memory, amygdala for the emotions, thalamus for sensory perceptions and hypothalamus for endocrine functions (109), but it is found also in peripheric nerves, spleen, heart, adrenal gland, endometrium, ovaries and testes (107). CB2 receptor is less expressed in SNC than CB1 while it is mainly expressed by immune cells as B cells, NK cells, neutrophils, $CD8^+$ and $CD4^+$ T cells. Its activation limits the cell migration and the release of pro-inflammatory elements (106, 109, 110). Additionally, CB2 receptors are involved in neuroinflammation, atherosclerosis and bone remodelling (111-113). Cannabinoids affinity is different for each type of receptors. THC has affinity for both types of receptors, acting as a partial agonist of both, yet it is more effective for CB1 type. CBD has also been found to be a negative allosteric modulator of the CB1 receptors and acts as inverse agonist of CB2 receptors, (112, 114) but it has low affinity (113, 115). The ligand binding of CB receptors activates several signalling intracellular pathways leading to reduced intracellular cAMP concentrations, activation of MAP kinases, regulation of ionic current and activation or inhibition of inducible nitric oxide synthase (77). The multiple signal transduction pathways activated by endocannabinoids underlie the different biological activities exerted within the

CNS and the peripheral tissues. Endocannabinoids are involved in modulating neurotransmitters release; they induce an inhibitory effect on pre-synaptic voltage-dependent Ca^{2+} channels blocking depolarization-induced release. The majority effects on nervous system are related with inhibitory activity, for example on the level of cerebellum endocannabinoids module and inhibit release of glutamate reducing motor coordination, on the hippocampus block cholinergic transmission with effect on memory and learning. On basal ganglia and substantia nigra with the inhibition of GABA re-uptake and dopamine synthesis, induce loss of locomotory activity and hypotension through the release inhibition of noradrenaline in sympathetic nervous system (108).

In the uterus, the endometrium is a significant source of endocannabinoids and, compared with other reproductive tissues, AEA levels are high (116-118). It has been reported that CB1 immunoreactivity is more intense in the glandular epithelium (118) compared with the stroma and its expression increase in the secretory phase likely due to progesterone modulation (119). Regarding CB2, its expression is found in both glands and stroma with an higher expression during the late proliferative phase (118).

The NAPE-hydrolysing phospholipase D (NAPE-PLD), the enzyme responsible for the cleavage of NAPE into AEA, is intensively expressed in the menstrual, early-proliferative and late secretory glands with its lowest levels in the early-secretory phase and also in the stroma (118). FAAH glandular expression increases during the menstrual cycle reaching a peak during menstruation and, similarly, it is also expressed in the stroma (118). Their expression suggests that AEA concentrations are modulated during the menstrual cycle and lower levels of AEA are beneficial for blastocyst development (120, 121).

Recently, data support the hypothesis that the ECS is involved in controlling endometrial plasticity by regulating endometrial cell motility (122).

Methanandamide, a synthetic stable chiral analog of AEA, in a dose-dependent manner, stimulates the endometrial stromal cell migration via CB1 receptor (123) and not via CB2 activation, through intracellular activation of ERK1/2 and PI3K/Akt pathways, that leads to a cytoskeleton rearrangement of endometrial stromal cells. Furthermore, it has been demonstrated that cannabinoids exert an antiproliferative effect on proliferation of endometrial cells. Indeed, the non-selective cannabinoid agonist WIN 55212-2 reduces endometrial cells proliferation through a reduction of reactive oxygen species production and inactivation of the Akt pathway (124). Additionally, high doses of methanandamide

influence endometrial stromal cells proliferation in a bimodal time-dependent manner. The first 24h stimulation increases cell proliferation, while prolonged treatments induce an apoptotic cell death (125). It was investigated the involvement of ECS in endometriosis, a
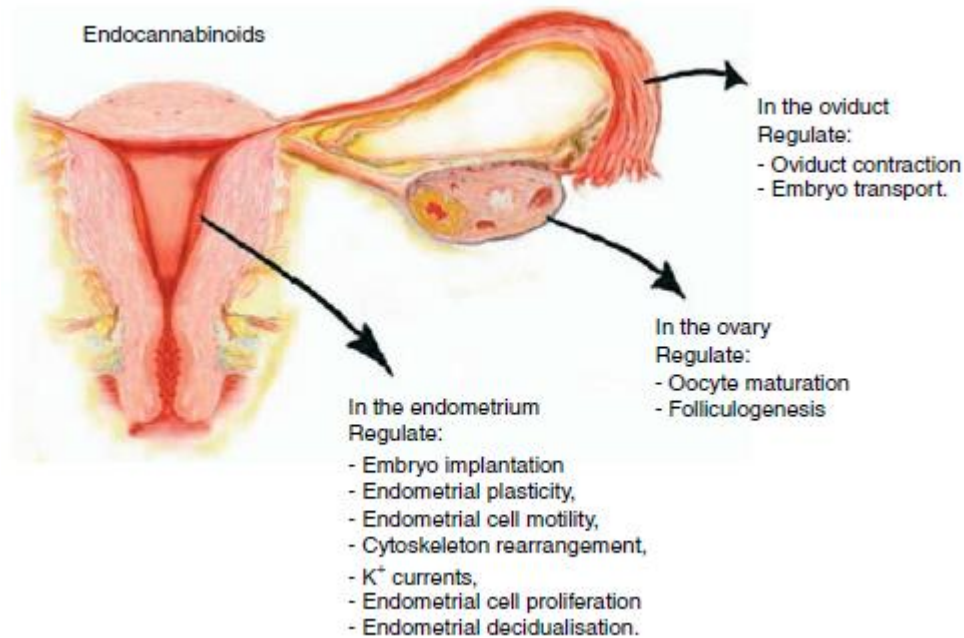
Figure 5. Overview of the most important biological activities of endocannabinoids in the female reproductive organs (77).

pathological condition characterised by deregulated endometrial cell proliferation and invasion, and CB1 receptor, at both mRNA and protein level, was lower in eutopic endometrium of patients with endometriosis compared with control from healthy patients. This down regulation has been attributed to a progesterone resistance phenotype in patients with endometriosis and this evidence might underlie the possible role of ECS in regulating endometrial proliferation (119).

1.3.3 TRPV2, member of TRP Channels, in female reproductive system

In addition to cannabinoid receptors, cannabinoids interact with some ions channels belonging to the family of Transient Receptor Potential (TRP). TRP channels are a superfamily of transmembrane ion channels involved in transduction in response to an overabundance of chemical and physical stimuli and, on the basis of amino acid sequence homology, TRP channels are grouped into different subfamily, called canonical (TRPC), melastatin (TRPM), vanilloid (TRPV), ankyrin (TRPA), mucolipin (TRPML), and

polycystin (TRPP) subfamily and cannabinoids interact with TRPV1, TRPV2, TRPV3, TRPV4, TRPM1, TRPM8, and TRPA1 (126, 127). Structurally, they have four subunits with six transmembrane spanning domains (S1–S6) with a pore domain between the fifth (S5) and sixth (S6) segment and, a cytoplasmic amino-terminus with three ankyrin-repeat domains, and a cytoplasmic carboxy terminus. TRP channels conduct cations, are weakly voltage-sensitive and non-selective for calcium, with a permeability ratio to Na (PCa/PNa) in a range between 0.3 and 10 (126).

At present, TRP channel ligands are only partially known, although they function as multimodal signal integrators for exogenous ligands. The G protein-coupled receptors (Gq/11; linked to PLCβ) and tyrosine kinase receptors (linked to PLCγ) potentiate the signaling and function of most TRP channels (11), elements of phosphatidylinositol signaling pathway, in particular, PIP2, can regulate TRP channels (126). These channels are active directly by ligands such as natural molecules (capsaicin, cannabinoids) and endogenous compounds like endocannabinoids and changing of environmentally conditions like pH (128). TRP channels have also been implicated as sensors of many physiological and pathological processes including itch, temperature sensation, cancers, genetic disorders, and pain (127).

The Vanilloid subtype of TRP family are divided in thermosensitive (TRPV1-TRPV4) and non-thermosensitive (TRPV5 and TRPV6) and they are located in most of nociceptors, contributing to the nociception, but at the same time, they can be found on non-neural tissue such as heart, lung, small intestine, pancreas, hair cell epithelial to induce nonneurogenic inflammation, basal insulin release and hearing factors (128).

TRPV2 is localized in the intracellular membranes and it is not stimulated by heat or in vivo by vanilloid exposure but it is activated by 2- aminoethoxydiphenyl borate (2-APB), Probenecid, CBD and inhibited by Ruthenium red (RR), Gadolinium (Gd) and Tranilast. TRPV2 is expressed not only in sensory neurons but also in motor neurons and in many non-neuronal tissues, displaying tissue-specific physiological functions (129). It is involved in perception of noxious stimuli, due to its stretch-dependent properties, and in the regulation of calcium homeostasis functioning as a mechanosensor, thermosensor, and lipid sensor.

Recently it has been investigated if members of the TRP channel superfamily are functionally expressed in the human endometrial stroma (130) and if they are implicated in progression of endometriosis (131).

De Clercq *et al*. analyzed the expression of TRP channels in 17 whole endometrium biopsies obtained from the menstrual (Days 1–5, n=3), follicular (Days 6–14, n=6), the early luteal
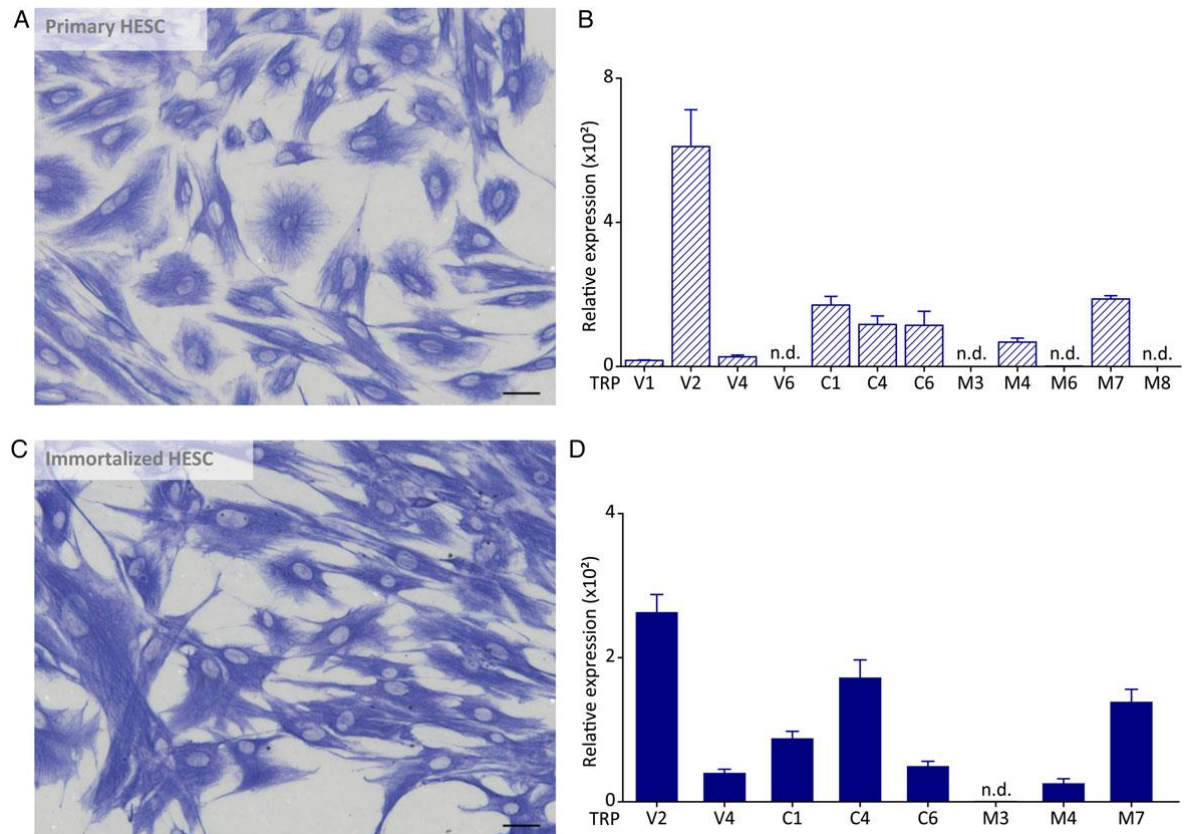
Figure 6. Quantitative RT–PCR of TRP channels in purified vimentin-positive human endometrial stromal cell cultures and immortalized stromal cell cultures. (A) Human endometrial stromal cells (hESC) stained positive for the intermediate filament vimentin (blue), a mesenchymal marker, whereas no cytokeratin positivity (red) could be observed, confirming their stromal nature. Scale bar ¼ 50 mm. (B) Quantitative RT–PCR on primary hESC cultures set up from freshly isolated endometrium obtained during the luteal phase (n ¼ 5). RNA levels are quantified relative to the geometric mean of housekeeping genes ACTB, and PGK-1. TRPV6, TRPM3, TRPM6 and TRPM8 were below the detection limit. n.d. ¼ not detectable. (C) Immortalized human endometrial stromal cells stained positive for vimentin. Scale bar ¼ 50 mm. (D) Quantitative RT–PCR on immortalized hESC. Data are presented as mean+SEM (130).

(Days 15–20, n=5) and the late luteal phase (Days 21–28, n=5) and studied their functional expression in primary human endometrial stromal cells (hESC) isolated from fresh endometrial biopsies (n=13) obtained from women during the luteal phase (menstrual cycle days 15–28). They found that TRPV2, TRPV4, TRPC1, TRPC4, TRPC6, TRPM4 and TRPM7 was detected at mRNA level in endometrial biopsies and hESC with a TRPV2, TRPV4, TRPC6 and TRPM7 localization in the plasma membrane and in the cytoplasm of hESC, confirmed by immunocytochemistry. TRPV2 RNA expression increased in stromal cells compared with the whole endometrium biopsies, indicating that the stroma is likely the

main site of TRPV2 expression. A significant increase of TRPV2, TRPC4 and TRPC6 mRNA level was detected in the late luteal phase suggesting that the specific up and down regulation of certain TRP channels around the time of implantation might be important to confer endometrial receptivity (130).

It has been well demonstrated that some of these TRP channels are involved in processes like cell migration (TRPC1/C4 and TRPV2) (132, 133), cell adhesion (TRPC4) (134), and cell proliferation (TRPV2, TRPM4, TRPM7) (135, 136) and endometriosis lesions are assumed to acquire additional capacities, such as migration, adhesion, proliferation, and neuroangiogenesis, in order for them to establish and flourish in the abdominal cavity. Then, Persoons *et al.* investigated the contribution of TRP channels in stromal cells in endometriosis, analysing human biopsies and the primary cell cultures of both endometriosis patients and controls. They found that mRNA expression of TRPV1, TRPV2, TRPV4, TRPM4, TRPM7, TRPC1, TRPC3, TRPC4, and TRPC6 in hESC of endometriosis patients but these levels were not significantly different from the TRP channel expression in hESC isolated from healthy patients. Additionally, they demonstrated that their functional expression did not affect significantly the proliferative and migratory capacity of endometriosis-derived eutopic stromal cells compared with control (131).

1.3.3.1 Prognostic role of TRPV2 in cancer

TRPV2-mediated signaling pathways have profound effects on a variety of pathological processes such as cardiomyopathies and muscular dystrophy, diabetes and obesity, fibromyalgia, infection diseases and cancer (129). Its stimulation by growth factors, cytokines, hormones, and endocannabinoids induces TRPV2 translocation from the endosome to the plasma membrane affecting, in normal cells, both cell proliferation and cell death (137). Indeed, previous evidences show that inactivation of TRPV2-mediated signals in cancer leads to an uncontrolled proliferation and cell death-resistance whereas TRPV2 activation increases migratory capability and invasiveness of cancer cells (135).

Regarding urogenital cancers, an increased TRPV2 expression was detected in high-grade and -stage urothelial cancer tissues and it is involved in enhancing migration process of prostate cancer cells through a TRPV2-mediated calcium influx, via Gq/Go and phosphatidylinositol-3,4 kinase (PI3,4K) signaling and translocation of TRPV2 from endosome to the plasma membrane (138). Furthermore, it was demonstrated that TRPV2

mRNA levels were higher in metastatic cancer patients compared with non-metastatic primary prostate cancer (139).

Recent studies have demonstrated an upregulation of the TRPV2 protein in triple-negative breast cancer tissues and its overexpression correlates with a higher recurrence-free survival in patients with triple negative and estrogen receptor β (ERβ) negative breast cancers, treated with chemotherapy. It has been demonstrated that TRPV2 overexpression or CBD treatment enhanced the uptake of Doxorubicin and apoptotic cell death *in vitro* and *in vivo* models. These studies suggest that TRPV2 is a good prognostic factor for triple negative breast cancer (140).

TRPV2, but also TRPV1 and TRPV4, are functional and up-regulated in esophageal squamous cell carcinoma and a high TRPV2 expression was observed in patients with advanced disease, high-stage and lymph node metastasis. Its high expression correlated with a worse 5-year disease-specific survival and disease-free survival compared with patients expressing low levels of TRPV2. Additionally, it has been shown that in patients surgical resected, TRPV2 mRNA overexpression represents a negative prognostic factor (141).

In hepatocellular carcinoma, an increased expression of TRPV2 was detected in 29% of cases, significantly associated with clinicopathologic features as portal vein invasion and histopathologic differentiation. These data suggest that TRPV2 might play a role in human hepatocarcinogenesis and might be a prognostic marker of patients with hepatocellular carcinoma (142).

Regarding the glioblastoma multiforme, Alptekin *et al*. have analyzed the relationship between TRP gene expressions and survival of the patients and they found that TRPC1, TRPC6, TRPM2, TRPM3, TRPM7, TRPM8, TRPV1, and TRPV2 were significantly higher in glioblastoma patients. Additionally, dividing patients into two subgroups according their survival time, they shown that patients who survived more than 12 months had a higher TRP gene expression levels, among which, TRPV2 channel (143).

Several data evidenced that TRP expression, including TRPV2, was altered in hematologic malignancies (129). A high percentage of patients with multiple myeloma present bone lesions, hypercalcemia, fractures or bone pain during the disease progression and Bai *et al*. findings show that TRPV2 correlates with shorter event free survival and overall survival and it is involved in osteoclastic activity. Indeed, TRPV2 overexpression supported osteoclastogenesis by activating Ca^{2+}-calcineurin-NFATc3 signaling pathway and

mediating the excessive secretion of inflammatory cytokines and RANKL, involved in the progression of osteoclastic differentiation (144).

Recently, it has been analyzed the expression of TRPV2 in gastric cancer and its mRNA and protein levels were detected higher in gastric cancer samples compared with normal stomach specimens. Furthermore, TRPV2 expression increased with increasing tumour stage, correlating with poor overall survival (145).

TRPV2 expression was also detected in melanoma, together with TRPV4, TRPA1, and TRPM8. TRPV2 activation induced a necrotic cell death in melanoma cell line suggesting that its expression might be considered as a potential marker for melanoma (146).

So far, no research findings are available about the TRPV2 expression and its potential role in endometrial cancer.

1.3.4 Overview of the Cannabidiol (CBD) pharmacological action

Cannabidiol (Figure 7) is the main non-psychotropic cannabinoid of Cannabis sativa (102). It is biosynthesized in the acid form named cannabidiolic acid (CBDA) and, with the heat and light exposition, it is decarboxylated in CBD (147).
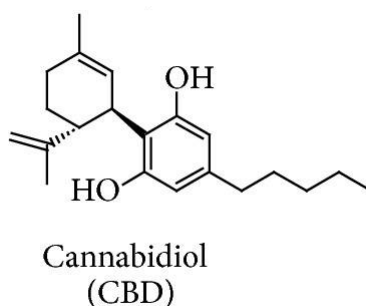
Figure 7. CBD structure (102)

CBD is a very interesting molecule providing several pharmacological effects in different pathologic conditions such as inflammation, neurodegeneration, epilepsy, multiple sclerosis, diabetes, arthritis and cancer (147). Moreover, administered with Δ9-THC, CBD antagonizes the CB1 receptor reducing THC adverse effects like tachycardia, anxiety, sedation and hunger. CBD interacts, also, with other important targets, among these, TRPs, PPAR-γ (Peroxisome Proliferator-Activated Receptor γ), GPR55, lipoxygenase (LO), cyclooxygenase-2 (COX-2) (147). Additionally, recent studies have demonstrated that CBD

is also a CB1 allosteric modulator with efficacy in treatment of central nervous system and peripheral disorders (148).

CBD is an inverse agonist of CB2 receptor, property that may support its anti-inflammatory activity. Indeed, investigations have shown inhibition of macrophages and neutrophils migration in a CB2-dependent mechanism (148).

Orphan receptor GPR55 is a G-protein involved in angiogenesis, neuropathic pain and gastrointestinal motility in a calcium-dependent manner; then it is involved also in inflammatory process, migration and cell adhesion and several pathways such as RhoA, ROCK, ERK and p38 mitogen-activated protein kinase (147, 149).

Regarding generalized social anxiety disorders, CBD shown a significant decrease of anxiety and this was associated with its effect on paralimbic and limbic areas. CBD exerts also an anti-convulsivant, neuroprotective and anti-nausea properties (148).

In the last decades, the potential effects of the efficacy of CBD in the management of epilepsy, as an adjunct to common anti-epileptic drugs, were investigated in some clinical trials. Results shown that most of combination tested assess the efficacy and safety of CBD especially in infants, children and teenagers (150).

Pharmacokinetics of CBD seems better defined respect to its pharmacodynamic. Once orally consumed, after a first-pass effect, CBD bioavailability is between 13% and 19%, suggesting that the intravenous administration as preferable. CBD is a molecule with lipophilic property, then it can diffuse and easily cross the blood–brain barrier, while in turn its elimination is prolonged (151). CBD is metabolized by several metabolic pathways. Indeed, it is subjected to hydroxylation, oxidation to carboxylic acids, conjugation, epoxidation and beta-oxidation (152). Finally, CBD is primarily excreted from urine and has a half-life of 9 h (153). Thus, CBD showed a very low toxicity in humans and in other species and did not show teratogenic or mutagenic activities (154).

1.3.4.1 Anti-inflammatory effects

It has been largely characterized CBD action on the immune compartment and its properties in treatment of different inflammatory conditions, for instance Crohn's and ulcerative colitis, neuronal diseases (Alzheimer and Parkinson) and skin diseases (atopic dermatitis and psoriasis) (147).

CBD has role in peripheral inflammation, indeed endocannabinoids, their metabolites and receptors has been discovered in immune system cells such as macrophages, monocytes, basophils, lymphocytes and dendritic cells, in order to regulate immune functions in an autocrine and paracrine way (147).

CBD exerts its anti-inflammatory effect through various other receptors in addition to the canonical CB1 and CB2 receptors, among them, TRPV1 and GPR55 (148). In a murine model of lipopolysaccharide (LPS)-induced acute lung injury, CBD reduced the inflammatory lung response in an adenosine A2A receptor-dependent manner (155). Additionally, CBD decreased neutrophils, macrophages and lymphocytes migration, myeloperoxidase activity and the production of pro-inflammatory cytokines tumor necrosis factor-α (TNF-α), interleukin-6 (IL-6) and chemokines monocyte chemoattractant protein-1 (MCP-1) and macrophage inflammatory protein-2 (MIP-2) (156).

Prolonged or excessive activation of microglial cells in response to pathogen infection or injury, may result in pathological forms of inflammations that contribute to the progression of neurodegenerative (Parkinson's and Alzheimer's diseases, multiple sclerosis and HIV-associated dementia) and neoplastic diseases (157). Previous *in vitro* and *in vivo* evidences showed that CBD strongly inhibit inflammatory cytokines production, including IL-1β, IL-6, and interferon-β (IFN-β), in LPS-stimulated murine microglial cells, decreasing the activity of the nuclear factor-k B (NF-kB) signaling pathway (158).

Moreover, controlling the neuroimmune axis, CBD is a promising molecule for the therapy of inflammatory bowel disease, especially Chrohn's disease. Indeed, CBD strongly inhibited mast cells and macrophages recruitment in the intestine in an *in vivo* inflammatory model and significant reduction of TNF-α secretion in *ex vivo* cultured human derived intestinal biopsies from patients with ulcerative colitis, achieving a reduction of intestinal damage principally mediated by peroxisome proliferator activated receptor-γ (PPAR-γ) receptor pathway (159).

CBD exerts an immunomodulatory action inducing a suppressive effect on T-cell functional activities through induction of CD11b^{+}Gr-11^{+} myeloid-derived suppressor cells (MDSC), apoptotic cell death caspase 8-dependent, anergy, a reduction of their proliferative potential and a reduction of cytokine secretion including IL-17 (160).

Interestingly, in a recent study *in vivo*, a repeated administration of CBD increased the total number of Natural Killer T cells that play a fundamental role in non-specific antiviral response and cancer immune surveillance (161, 162).

1.3.4.2 Anti-cancer effect

Initially, the use of cannabinoids in cancer therapy was limited to reduce symptoms associated with disease and chemotherapy like pain, vomiting and weight loss but, recently, it has been demonstrated that cannabinoids induce an antiproliferative and proapoptotic activities against cancer cells (147). Cannabinoids can interfere with different process of cancer cell growth, cell migration and survival and stimulate autophagy-mediated apoptotic cancer cell death (148). CBD was able to exert an anticancer effect in glioblastoma (163-166), lung (167-169), gastric (170), breast (171-173), melanoma (174) and colon (175, 176) cancers, neuroblastoma (177), myeloma (178, 179), leukaemia and lymphoma (180), pancreatic and endometrial cancers (181, 182). Its mechanism of action is via a both dependent and independent-receptors mechanisms (148).

Glioblastoma multiforme. It is the most aggressive primary tumour of the central nervous system. Massi *et al.* shown that CBD induced an anti-proliferative effect, CB2 receptor-dependent, on U87 and U373 human glioma cell lines (165). Furthermore, Vaccani *et al.* demonstrated that non-cytotoxic concentration of CBD inhibited, with a receptor-independent mechanism, the migration of U87 human glioma cells *in vitro* (166). These anti-cancer effects were better characterized. Indeed, CBD decreases proteins level involved in survival signaling pathway as ERK and Akt, decreases the hypoxia inducible factor HIF-α and modulates Id-1 transcriptional factor, which is involved in invasiveness and cancer cell growth. Moreover, CBD reduced the expression of markers associated with epithelial mesenchymal transition (EMT) (vimentin and snail) and invasion (membrane type 1-matrix metalloproteinase 1 (MT1-MMP)), matrix metalloproteinase-2 (MMP-2), and focal adhesion kinase (FAK). Apoptotic cell death CBD-induced in glioma cells is linked with an early production of ROS and a contemporary decrease of glutathione (GSH) leading to caspase-8 and -9 activation (148).

It has been demonstrated that glioblastoma cells express TRPV2 and CBD, increasing its expression and activity, increases drug uptake and synergized with cytotoxic agents to induce apoptosis of glioma cells, whereas no effects were observed in normal human astrocytes. Additionally, in glioma stem-like cells (GSCs), a cell subpopulation involved in glioblastoma onset and chemoresistance, CBD induced autophagy, in a TRPV2-dependent manner, and strongly increased ROS production with consequent inhibition of cell survival, phosphorylated AKT, self-renewal and inhibition of intracranial growth of primary GSC-

derived tumours *in vivo* (163). Previous data have demonstrated CBD can be used in combination with radiotherapy, this event underlines the importance of synergistic effect among different kind of anti-cancer therapies (164).

Lung cancer. It has been investigated the effect of CBD human lung cancer, both *in vitro* and *in vivo* (148). Its anti-cancer effect is mediated by CB1, CB2 and TRPV1 receptors, which are expressed in lung cancer cells (168). Apoptotic cell death is associated up-regulation of COX-2 that leads to PPAR-γ accumulation in the nucleus, activating a PPAR-γ-dependent apoptosis. Furthermore, cancer invasiveness is reduced, with a CB1-, CB2- and TRPV1- dependent mechanism, by induction of ICAM-1 and TIMP1 (Tissue Inhibitor of Metalloproteinase), associated with p38 and p42/44 MAPK phosphorylation (167, 168). Additionally, CBD decreased lung cancer invasiveness trough the decrease of plasminogen activator inhibitor (PAI-1) expression and release (169).

Breast cancer. It has been demonstrated that CBD is able to reduce cancer proliferation and metastases in the triple negative breast cancer but, it has demonstrated efficacy also in both estrogenic receptor-positive and estrogenic receptor-negative breast cancer type, inducing apoptosis in a concentration-dependent manner, whereas it shows little effect on non-tumorigenic mammary cells (148, 171). CBD causes breast cancer MDA MB-231 cells death in an autophagy-dependent manner increasing the endoplasmic reticulum (ER) stress, followed by LC3-II accumulation, a classical marker of autophagy. Additionally, it induces apoptosis in breast cancer cells by inhibiting AKT/mammalian target of rapamycin (mTOR) signaling and enhancing ROS generation. Then, CBD mediates a complex balance between mitochondria-mediated apoptosis and autophagy, independent from both CB1 and CB2 receptors, inducing translocate on of beclin-1 to the mitochondria leading to release of cytocrome C into cytosol (172). In triple-negative breast cancer, CBD reduced cell proliferation, migration and metastasis, through multi-target effects. It suppressed EGF/EGFR signaling transduction pathways repressing Nf-Kb activity, MMP2 and MMP9 secretion, and reduced Id-1 gene expression, which support the invasive and proliferative phenotype of cancer cells up-regulating the active isoform of ERK (173). Interestingly, CBD has been reported to induce TRPV2 overexpression in triple negative breast cancer cells enhancing the anti-tumor action of doxorubicin through its augmented uptake (140).

Colorectal cancer. CBD showed potential anticancer effects also in colorectal cancer. Previous data have demonstrated anti-inflammatory effects of CBD in the gut. Indeed, reducing oxidative stress through the inhibition of iNOS expression and modulation of IL-1β and IL-10. Additionally, CBD exerts a chemopreventive action by the increasement of caspase-3 and the decrease of PI3/Akt surviving pathway. Antiproliferative effects are linked with induction of poly (ADP ribose) polymerase (PARP) and caspase-3 cleavage in phosphatase-dependent and CB receptors-independent manner, inactivation of p42/44 MAPK, Akt, STAT3, c-Jun N-terminal kinase (JNK), ERBB2 and p38 MAPK involved in cancer progression. Furthermore, antagonizing GPR55, it reduced liver metastasis in *in vivo* model of colon cancer (175, 176).

Multiple myeloma. It has been reported that in patients with multiple myeloma (MM) exist two distinct CD138$^+$ subpopulations according to the expression of TRPV2 (CD138$^+$TRPV2$^+$ and CD138$^+$TRPV2$^-$). In order to mimic the *in vivo* MM phenotypes, Morelli *et al.* evaluated CBD effects on TRPV2 transfected MM cell lines U266 and RPMI. They found that TRPV2 expression increased CBD-induced cytotoxicity, synergizing with Bortezomib, a highly selective and reversible inhibitor of 26S proteasomes and ubiquitin-dependent proteolysis, currently used in MM treatment. Additionally, this combination induced cell cycle arrest at the G1 phase and mitochondrial and ROS-dependent necrosis, mainly in TRPV2+CD138+ MM cells. On TRPV2−MM cells, the action of CBD was independent of the CB1 and CB2 receptors, TRPs and PPARγ (178). Furthermore, Nabissi *et al.* shown that CBD and THC, mainly in combination, were able to reduce cell viability by inducing autophagic-dependent necrosis in MM cell lines and reduced cell migration by down-regulating expression of the chemokine receptor CXCR4 and of the CD147 plasma membrane glycoprotein. They confirmed the ability of CBD to synergize with other chemotherapeutic drugs, in this case the immuno-proteasome inhibitor carfilzomib (179).

Leukaemia and lymphoma. CBD treatment, interacting with CB2 receptors, has demonstrated to induce apoptosis, caspase 3-dependent, in human acute myeloid leukaemia HL-60 cell line, without affecting human monocytes from healthy individuals. Same results have been confirmed both in vitro and *in vivo*. In Jurkat cells, CBD induced the activation of caspase-8, -9, and -3, the cleavage of poly (ADPribose) polymerase, the decrease in full-length Bid, the release of cytochrome C and increase of ROS production, suggesting a possible cross-talk between the intrinsic and extrinsic apoptotic pathways (180).

Pancreatic cancer. It has been reported that CB1 and CB2 receptors are expressed in pancreatic cancer cells, while very low mRNA levels were detected in normal pancreatic cells. In *in vitro* model of pancreatic cancer, cytotoxic effects of cannabinoids are both receptor- dependent and receptor-independent. Furthermore, recent study has demonstrated orphan receptor GPR55 may has an interesting role in pancreatic cancer development via cell cycle regulation and MAPK signalling pathway and CBD, blocking its activity, induced a cell cycle arrest. Gemcitabine, a chemotherapeutic drug used in pancreatic cancer treatment, can increase the mRNAs of both CB1 and CB2 via an NF-κB-mediated mechanism and it enhances cannabinoid-induced autophagy through ROS-mediated mechanism. Moreover, the effect of combination of CBD and Gemcitabine in strongly reduce cell viability of HPAFII and PANC1 cell lines might be potentiated by inhibition of GPR55 (181).

Endometrial cancer. So far, only Fonseca *et al.* reported a potential anticancer effect of CBD in endometrial cancer. Firstly, they found that Ishikawa and Hec50co expressed all the endocannabinoid system machinery, among which CB1 and CB2 receptors, and TRPV1. Moreover, they shown that CBD, but not THC, reduced cell viability in a dose-dependent manner, inducing an apoptotic cell death in Ishikawa cell line partially TRPV1-dependent while, in Hec50co, cannabinoids did not cause any increase in the apoptotic markers (182).

Other tumours. CDB anticancer effects were analyzed in other several models of human cancers. In melanoma, CBD, combined with a low dose of THC, induced an increased anti-tumour effect *in vitro* and *in vivo* compared with THC alone, suggesting that they act with different intracellular mechanism in cooperation of cell death induction (148, 174). In bladder cancer and prostate cancer, CBD induced an apoptotic cell death, respectively, in a TRPV2- and TRPM8- dependent mechanism (148). In gastric cancer, it has been demonstrated that CBD significantly inhibited cell viability, inducing cell cycle arrest and apoptosis as demonstrated by up-regulation of ataxia telangiectasia-mutated gene (ATM) and p53 protein and increased levels of Bax, cleaved caspase -3 and -9 (170). CBD and THC were tested also in the most common solid paediatric cancer, neuroblastoma. Fisher *et al.*, shown that both compounds induced an anticancer effect *in vitro* and *in vivo*, and CBD was more active than THC in inducing apoptosis caspase-3 dependent (177).

1.3.4.3 Anti-angiogenetic effect

Growing tumors activate an angiogenetic process secreting high levels of pro-angiogenic factors which contribute to the creation of an abnormal vascular network characterized by disorganized, immature and permeable blood vessels. Most of angiogenetic events are mediated by vascular endothelial growth factor (VEGF), that is the most important pro angiogenetic protein, often overexpressed by cancer tissue. The angiostatic factors angiopoietin-1 (Ang1) and 2 (Ang2) are also involved in angiogenetic process and tumor tissue produces matrix metalloproteinases (MMPSs), which remodelling tissue, support the angiogenesis. Previous studies have investigated cannabinoids ability to inhibit vascular endothelial cell migration and survival in order to prevent blood vessels formation. Instead cannabinoids, by targeting tumor cells, induce apoptosis and supress proangiogenic factor and MMP production. This anti-angiogenetic effect might be related to CB receptors expression by vascular endothelial cells and, also, CBD might exert its angiogenic activity thanks to GPR55 receptors (147, 183).
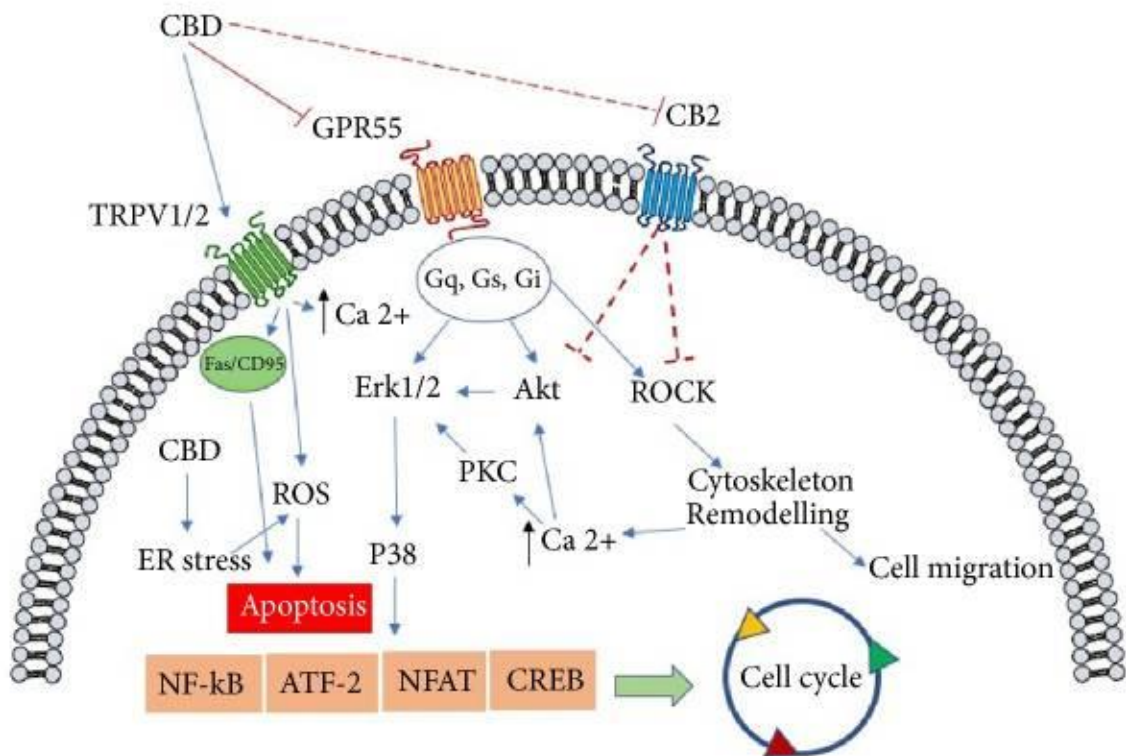
Figure 8. General anticancer pathway mediated by CBD. *Apoptotic process is induced by the stimulation of TRPV 1/2 channels and endoplasmic reticulum stress. CBD antagonises GPR55 receptor and interacts with CB2 receptor in order to inhibit cell migration by blocking ERK pathway, protein involved in cell cycle stimulation, and ROCK (Rho-associated protein kinase), which is liked to antimigratory events (147).*

2. AIM OF THE PROJECT

The relative lack of robust diagnostic/prognostic biomarkers for EC, compared with other tumours, and its often-late presentation, interferes with the amelioration of the morbidity and mortality rates associated with this type of cancer. Additionally, the non-endometrioid type II EC is responsible for most EC-related deaths because it is characterized by an aggressive behaviour, a late stage detection and high resistance to the common therapy. Furthermore, there are no targeted therapies for this subtype, and it is still treated in the same way as endometrioid type I EC, which is characterized by good prognosis and good response to therapy. Clinical trials using anti-PD-1 or anti-PD-L1 antibodies, but not anti-PD-L2, are currently ongoing, in all types of gynecological cancers. They have shown good safety profiles, but response rates remain low and many aspects remain controversial. Regarding PD-L2, it might be useful to better clarify its role in order to improve the efficiency of immunotherapy in female malignancies. The aim of the project was to investigate and characterize PD-1 ligands expression and CBD targets receptors in six endometrial cancer cell lines and, additionally, evaluate PD-L2 and TRPV2 expression in human Type II endometrial cancer biopsies, correlating their expression with Overall survival and Progression-Free survival. Furthermore, it was evaluated the biological effect of CBD as potential integrative therapy.

3. MATHERIALS AND METHODS

3.1 Endometrial cancer cell lines

Ishikawa and MFE-280 were purchased from Sigma Aldrich (Milan, Italy).

Ishikawa cells were grown in EMEM medium (Lonza, Milan, Italy), supplemented with 5% foetal bovine serum (FBS), 2 mM/L glutamine, 100 IU/ml penicillin, 100 mg streptomycin.

MFE-280 cells were grown in EMEM medium (Lonza, Milan, Italy), supplemented with 10% foetal bovine serum (FBS), 2 mM/L glutamine, 100 IU/ml penicillin, 100 mg streptomycin.

HEC-1A and the primary endometrial cancer cell lines PCEM002, PCEM004a, PCEM004b were kindly provided by Dr. Amant Frederic (Department of Oncology, KU Leuven, Leuven, Belgium).

HEC-1A cells were grown in Mc Coy's medium (Lonza, Milan, Italy), supplemented with 10% foetal bovine serum (FBS), 100 IU/ml penicillin, 100 mg streptomycin., while the primary cell lines were grown in RPMI1640, supplemented with 20% foetal bovine serum (FBS), 2 mM/L glutamine, 100 IU/ml penicillin, 100 mg streptomycin. Media were changed every 48 h until cells were 90% confluent. All cell lines were maintained at 37 °C with 5% CO_2 and 95% humidity.

3.2 Materials

RNAs and protein lysate from healthy donors (CU0000000015, CI0000009692) were purchased from OriGene. Pure CBD was supplied from ENECTA. CBD was dissolved in ethanol. Cisplatin, Doxorubicin and Paclitaxel were purchased from Sigma-Aldrich.

3.3 TCGA and cBioportal database analysis

The cBioPortal for Cancer Genomics is an open-access downloaded bio-database, providing visualization and analyzing tool for large-scale cancer genomics data sets (http://cbioportal.org). This portal collected records that were derived from 147 individual cancer studies, in which 31 types of cancer were analyzed, which included over 21000 samples. Analysis from of 506 sequenced endometrial cancer samples from this database (PanCancer Atlas) was performed in silico.

3.4 RNA Isolation, Reverse Transcription and Quantitative Real-Time PCR

Total RNA from cell lines was extracted with the RNeasy Mini Kit (Qiagen), and cDNA was synthesized using the iScript Advanced cDNA Synthesis Kit for RT-qPCR (Bio-Rad) according to the manufacturer's instructions. Quantitative real-time polymerase chain reactions (qRT-PCR) were performed with QuantiTect Primer Assays for Programmed Cell Death 1 Ligand 2 (CD273, PD-L2), Programmed Cell Death 1 Ligand 1 (CD274, PD-L1), Human Cannabinoid receptor 1 (CNR1, CB1), Human Cannabinoid receptor 2 (CNR2, CB2), Transient Receptor Potential Vanilloid receptor 1 cation channel (TRPV1) and Transient Receptor Potential Vanilloid receptor 2 cation channel (TRPV2) (Qiagen), using the iQ5 MulticolorvReal-Time PCR Detection System (Bio-Rad, Hercules, CA). The PCR parameters were 10 min at 95 °C followed by 40 cycles at 95°C for 15 s and 60 ° C for 40 s. The relative amount of target mRNA was calculated by the $2^{-\Delta\Delta Ct}$ method, using GAPDH as a housekeeping gene. All samples were assayed in triplicates in the same plate. Measurement of GAPDH levels was used to normalize mRNA contents and target genes levels were calculated by the $2^{-\Delta\Delta Ct}$ method.

3.5 Western blot analysis

20 ug of the lysates were separated on a SDS polyacrylamide gel, transferred onto Hybond-C extra membranes (GE Healthcare), blocked with 5% low-fat dry milk in PBS-Tween 20, immunoblotted with goat anti-CD274 (B7-H1, PD-L1, 0,5 µg/ml, R&D System, Minneapolis, MN), mouse anti-CD273 (B7-DC, PD-L2, 1 µg/ml, R&D System, Minneapolis, MN), rabbit anti-pAKT (1:1000, Cell Signaling, Danvers, MA, USA), rabbit anti-AKT (1:1000, Cell Signaling, Danvers, MA, USA), mouse anti-pERK (1:2,000) (Cell Signalling Technology, Danvers, MA), rabbit anti-ERK (1:1,000) (Cell Signalling Technology), mouse monoclonal anti-CB1 (1:300, Santa Cruz, Dallas, TX), anti-TRPV1 (1:100, Novus, Littleton, CO), anti-TRPV2 (2 1:300, Santa Cruz, Dallas, TX), anti-LC3 (2 µg/mL; Novus Biologicals), anti-p62 (1:1000, Cell Signaling Technology, CO, USA) and anti-glyceraldehydes-3-phosphate dehydrogenase (GAPDH, 1:8000, Origene, Rockville, MD) antibodies (Abs) for 1 h and then incubated with HRP-conjugated anti-mouse or anti-rabbit secondary Abs (1:2000, Cell Signaling Technology, Danvers, MA) and with HRP-conjugated anti-goat secondary Ab (1:1000, Cell Signaling Technology, Danvers, MA) for 1 h.

Peroxidase activity was visualized with the LiteAblot®PLUS or TURBO (EuroClone, Milan, Italy) kit and densitometric analysis was carried out by a Chemidoc using the Quantity One software (Bio- Rad).

3.6 Patient samples

After obtaining approval from the Medical Ethics Committee UZ/KU Leuven, 68 archived formalin-fixed, paraffin-embedded type II endometrial cancer samples, along with clinical data, and 15 normal tissues (5 of which are peritumoural tissues) were collected from UZ Leuven, Belgium. The sample set included 29 serous type tumours, 7 clear cell type tumours, 17 mixed type I and II, 5 peritumoural tissues from patients with type II endometrial cancer and 10 healthy endometrial samples. For clinical data collection, the International Federation of Gynecologic Oncology 2009 system was applied for staging of all samples.

3.7 Immunohistochemical stainings

Paraffin slides (4 μm) were heated for 3 to 4 hours at 55°C, deparaffinized in toluol, and rinsed in ethanol. Tissues were blocked for endogenous peroxidases by 30-minute incubation in 0.5% H_2O_2 (107209, Merck Millipore) in methanol. For PD-L2 staining, after washing in TBS, epitopes were retrieved for 2 h at 90°C in Tris-EDTA (pH=9). Tissues were cooled down slowly in TBS. Upon extensive washing, tissues were blocked with 1% milk powder, 2% BSA (A4503, Sigma-Aldrich), and 0.1% Tween-80 (822187, Merck Millipore) in TBS before antibody incubation. Blocking solutions were removed and tissues were incubated with mouse anti-CD273 (B7-DC, PD-L2, 1 μg/ml, R&D System, Minneapolis, MN) in TBS, overnight at 4°C. After washing, were incubated with anti-mouse–HRP (Dako) for 30 minutes and washed again. For TRPV2 staining, after washing in TBS, epitopes were retrieved for 1 h at 90°C in Tris-sodium citrate (pH=6). Tissues were cooled down slowly in TBS. Upon extensive washing, tissues were blocked with 1% milk powder, 2% BSA (A4503, Sigma-Aldrich), and 0.1% Tween-80 (822187, Merck Millipore) in TBS before antibody incubation. Blocking solutions were removed and tissues were incubated with rabbit anti-TRPV2 (VRL-1, 1:250, Thermofisher, Grand Island, NY) in TBS, overnight at 4°C. After washing, were incubated with anti-mouse–HRP or anti-rabbit-HRP (Dako) for 30 minutes and washed again. All antibodies were visualized by 10-minute incubation in 3,3′-diaminobenzidine (DAB, D5905, Sigma) + 0.015% H_2O_2 (107209, Merck Millipore) in the dark. Nuclei were stained with Mayer's hematoxylin, and tissues were dehydrated in

propanol, dipped in xylene, and mounted. To ensure no staining was caused by a specific binding of secondary/tertiary molecules, control slides without addition of primary antibody were used.

3.8 Evaluation and scoring of immunohistochemical stainings

All stainings were evaluated semiquantitatively, using a scoring system that takes into account both the staining intensity (0 = absent, 1 = weak, 2 = moderate, and 3 = strong) and the percentage of stained cells (0 = absent, 1 = less than 1%, 2 = 1%–10%, 3 = 11%–33%, 4 = 34%–66%, and 5 = 67%–100%). Both scores were added to obtain a maximum score of 8. Stainings were evaluated only in the cellular component where expression was expected. Tissues were considered with a high expression at a cut-off score of 6, corresponding to strong positivity in ≥11% of cells, moderate positivity in ≥34% of cells, or weak staining in ≥67% of cells. This cut-off was deemed clinically relevant for therapeutic applications, as a targeted therapy would most likely be effective when a sufficient number of cells express the target. Tissues with a value between 4 and 5, were classified as moderate. Photographs of representative cases were taken using the Axioskop microscope (MRc5, Zeiss) and the ZEN 2.0 software.

3.9 Confocal Laser Scanning Microscopy Analysis

Ishikawa cells were maintained on 8-well culture slide in fresh medium, fixed, and permeabilized using 2% and 4% of paraformaldehyde with 0.5% of Triton X-100 in PBS. After washes in PBS, cells were incubated with 10% of Foetal Bovine Serum (FBS) and 0.1% of Tween-20 in PBS for 1 h at room temperature and then stained with mouse anti-PD-L2 overnight at 4 °C. Then, slide was washed with 0.3% of Triton X-100 in PBS and incubated with Alexa Fluor 594-conjugated secondary Ab for 1 h at 37 °C. Nuclei were stained with DAPI. Slide was then analyzed with C2 Plus confocal laser scanning microscope (Nikon Instruments, Firenze, Italy). Optimized emission detection bandwidths were configured by Zeiss Zen control software. Images were processed using NIS Element Imaging Software (Nikon Instrumentes, Firenze, Italy).

3.10 Cell Transfection

PCEM004b and Ishikawa cells were plated at a density of 4×10^5 cells/ml and 1.5×10^5 cells/ml, respectively. After 12hs of incubation, transfection is achieved with 3 µl/ml of the

reagent TurboFectin Transfection Reagent (OriGene, Rockville, MD) and 1 μg/ml of pCMV empty (pCMV6), pCMV6-PDCD1LG2 or pCMV6-TRPV2 vectors (OriGene, Rockville, MD), according to the manufacturer's instructions. The cells were harvested at 72 hs post-transfection for analysis. The efficiency of transfection was evaluated by western blot analysis.

3.11 PD-L2 Silencing

Small interfering RNAs (siRNAs) targeted to PD-L2 (siPDCD1LG2) and a non-silencing siRNA (NC1) served as control were purchased from Riboxx GmbH (Radebeul, Germany). Ishikawa cells were plated at a density of 1×10^5 cells/ml. After overnight incubation, transfections were achieved with 80 μl/ml of the reagent riboxxFECT and 20 nM of siPDCD1LG2 or NC1 (negative control) according to the manufacturer's instructions. The cells were harvested at 72 hs post-transfection for analysis. The efficiency of silencing was evaluated by western blot analysis.

3.12 Wound-healing assay

PCEM004b and Ishikawa native cells and transfected/silenced cells were seeded onto a twenty-four well plate at density of $4x10^4$/ml and $1.5x10^5$/ml, respectively. Confluent cells were scratched using 10 μl sterile pipette tips and replace medium with low percentage of serum to minimize cell proliferation and prevent cell detachment. Images of wounded areas were taken at 0h, 24hs and 48hs. Images acquisition was carried out by a LeitzFluovert FU (Leica Microsystems) microscope. Remaining wound areas were determined using NIH Image J software for calculation of the percentage of wound closure. Analyses were performed in triplicate.

3.13 MTT assay

Endometrial cancer cell lines (3×10^4 cells/ml) were seeded in 96-well plates, in a final volume of 100 μl/well. After one day of incubation, treatments or vehicles were added in single and daily administration for 72hs. At least six replicates were used for each treatment. At the indicated time point, cell viability was assessed by adding 0.8 mg/ml of 3-[4,5-dimethylthiazol-2-yl]-2,5 diphenyl tetrazolium bromide (MTT) (Sigma Aldrich) to the media. After 3 h, the plates were centrifuged, the supernatant was removed, and the pellet was solubilized with 100 μl/well DMSO. The absorbance of the samples against a

background control (medium alone) was measured at 570 nm using an ELISA reader microliter plate (BioTek Instruments, Winooski, VT, USA).

3.14 Cell cycle analysis

Cells, at a density of $3x10^4$ cells/ml, were incubated with CBD for up to 48 hs, in single and daily administration. Cells were fixed by adding ice-cold 70% ethanol for 1 h and then washed with staining buffer (PBS, 2% FBS and 0.01% NaN3). Next, cells were treated with 100 µg/ml ribonuclease A solution (Sigma Aldrich), incubated for 30 min at 37°C, stained with 20 µg/ml propidium iodide (PI) (Sigma Aldrich) for 30 min at room temperature and finally analysed by flow cytometry using linear amplification.

3.15 Apoptosis assays and PI staining

Cell death was evaluated using Annexin V-FITC Apoptosis detection Kit (eBioscience) followed by biparametric FACS analysis. Cells, at a density of $3x10^4$ cells/ml, were treated with CBD for a maximum of 48 hs, in single and daily administration, and then incubated with Annexin V-FITC and PI, following the protocol provided. The percentage of positive cells determined over 10.000 events was analysed on a FACScan cytofluorimeter using the CellQuest software.

3.16 Acridine orange staining

To detect the development of acidic vesicular organelles, which are the hallmark of autophagy, the vital staining of PCEM004b cells with acridine orange (AO; Sigma- Aldrich; St. Louis, MO, USA) was performed. The cells were seeded in 12-well plates and were treated with CBD at 7.85 and 15.72 µg/ml for 24hs. Then, the cells were stained with medium containing 1 μg/ml AO for 15 min at 37 °C, washed twice in PBS and immediately examined with Nikon Eclipse E800 fluorescence microscope and NIS-Elements 4.0 software (all from Nikon; Tokyo, Japan). The cytoplasm and nucleus of AO-stained cells fluoresced bright green, whereas the acidic autophagic vacuoles fluoresced bright red.

3.17 Statistical analysis

The data presented represent the mean with standard deviation (SD) of at least 3 independent experiments. The statistical significance was determined by Student's t-test and by One Way-Anova and Two Way-Anova with Bonferroni's post-test; $*p < 0.05$. Patients were

divided in three groups according to high, moderate or low expression of protein target. The Kaplan-Meier (KM) method was also used for Overall Survival and Progression-free survival analysis. For Univariate analysis of significance (Graph Pad), the long-rank test or Cox analysis was used. *p < 0.05 was considered as statistically significant. The statistical analysis of IC_{50} levels was performed using Prism 5.0a (Graph Pad).

4. RESULTS

### 4.1 PD-1 ligands expression in EC EC samples from TCGA and EC cancer cell lines

PD-1 ligands gene expression was assessed in 506 EC data samples from TCGA, queried with cBioportal (TCGA, PanCancer Atlas). Samples were divided in endometrioid (397 samples) and serous type (109 samples) and the mRNA levels were expressed in log2. PD-L2 mRNA expression was higher than PD-L1 ($p < 0.0001$) but no significant differences were observed between Type I and II tumors (Figure 9A).

The expression of PD-L1 and PD-L2 in normal uterine tissue obtained from a healthy donor and in six EC cell lines, two of which, PCEM004a and PCEM004b, are classified as mixed Type I/II, was evaluated by RT-PCR (data not shown) and Western blot analysis. At the protein level, PD-L2 levels were significantly higher in most EC cell lines compared to normal uterus, while PD-L1 was expressed predominantly in both mixed Type cell lines but without significant difference respect to the control. Furthermore, in all Type I EC cell lines PD-L2 levels were higher than PD-L1 (Figure 9B). According data evidenced in patients, the expression profile of PD-L1 and PD-L2 was similar to that determined in our cell line models, suggesting that these cell lines can be a representative models for PD-1 ligands in in vitro study.
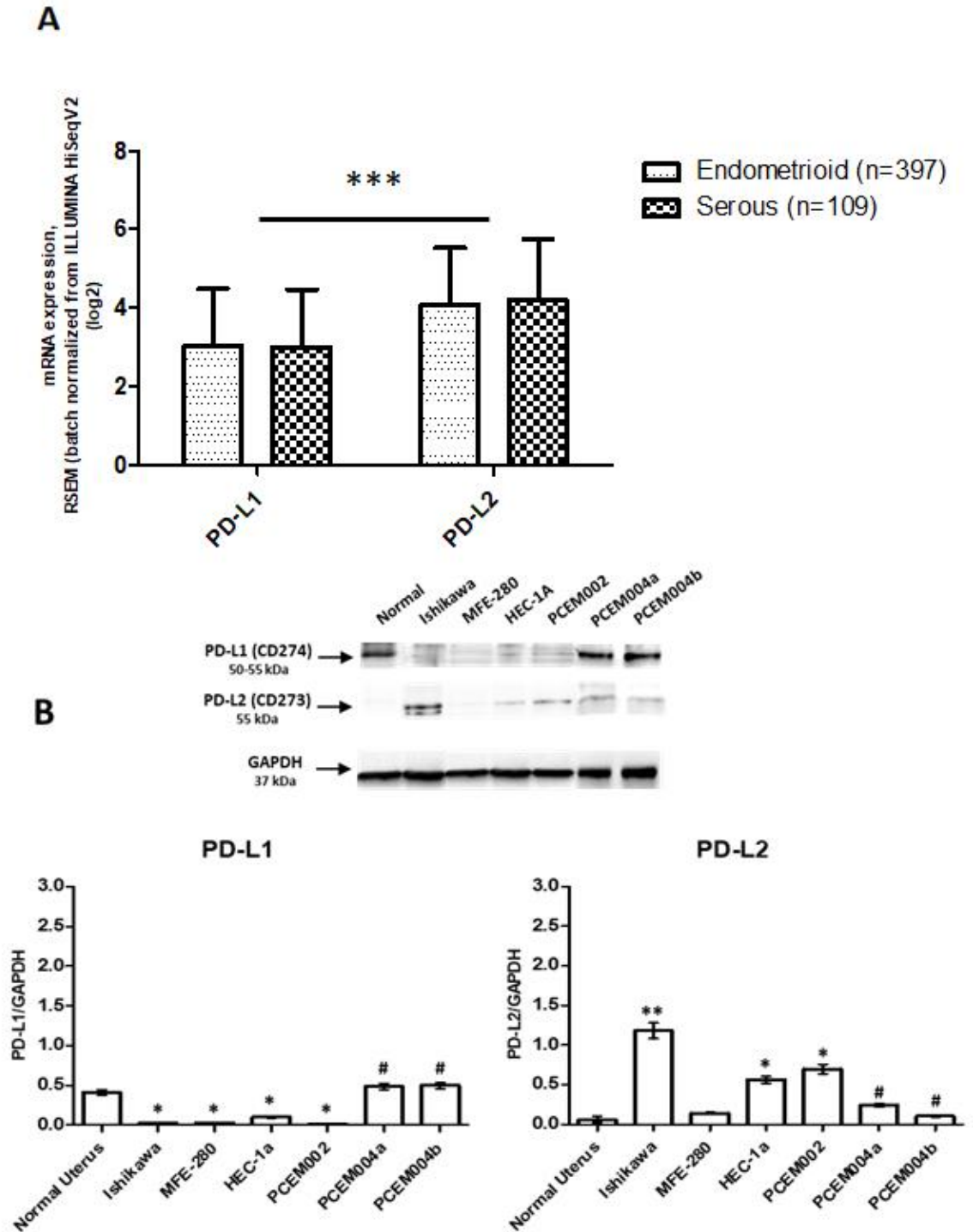
Figure 9. PD-L1 and PD-L2 expression in EC. *(A) The expression of PD-L1 and PD-L2 in EC patients. The mRNA expression (log2) of PD-L1 and PD-L2 in 506 EC samples, divided in 397 for Type I and 109 for Type II, from TCGA database. ***p < 0.0001 Type II vs Type I. (B) PD-L1 and PD-L2 protein expression was evaluated by western blot in normal human uterus and six EC cell lines. PD-L1 and PD-L2 densitometry values were normalized to GAPDH used as loading control. Densitometric values shown are the mean ± SE of three separate experiments. *p < 0.05 vs normal control, **p < 0.01 vs normal control, #p < 0.05 vs Type I primary EC cell line PCEM002.*

To determine the type of PD-L2 localization in the cells, Ishikawa cells, that express the highest amount of PD-L2, were analyzed by confocal laser scanning microscopy. Result shows that PD-L2 has a punctuate distribution localized mainly in the cytoplasm, as dot spots (Figure 10).
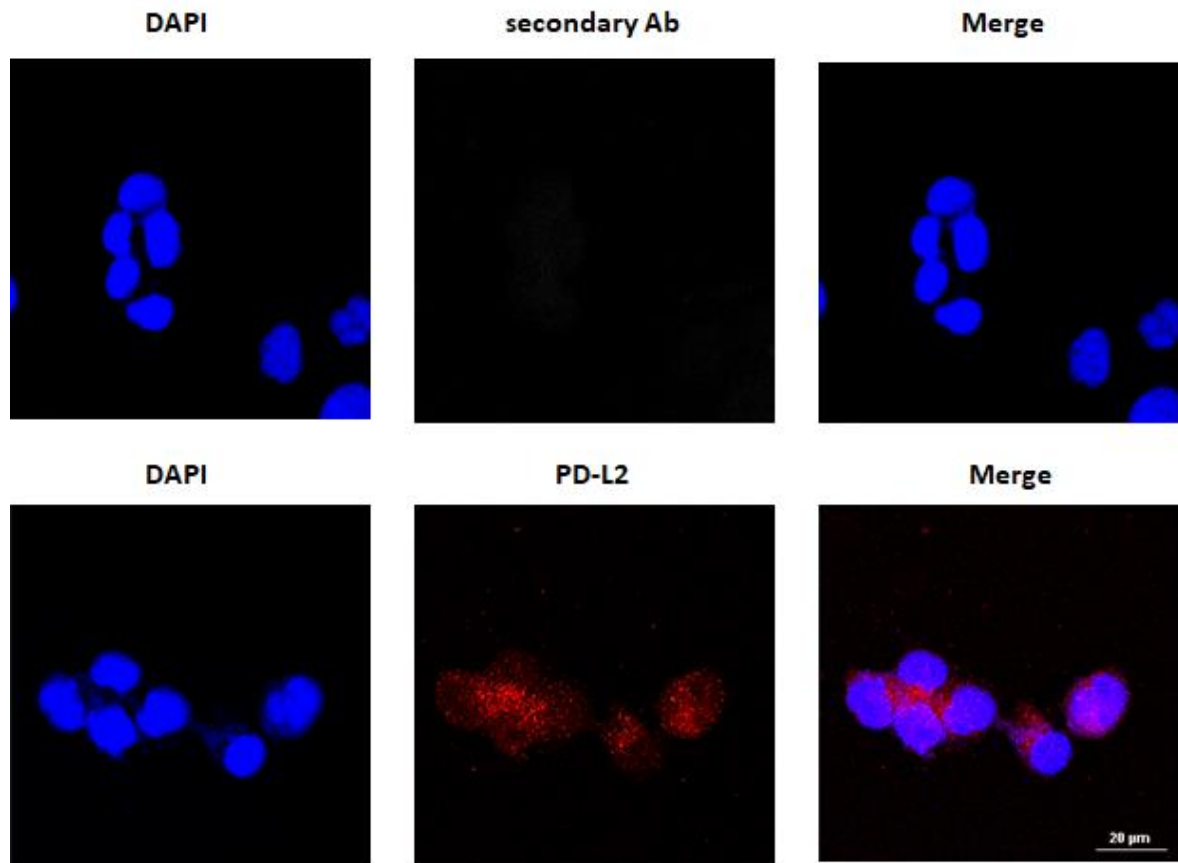
Figure 10. PD-L2 cytoplasmatic expression in Ishikawa cells. Cells were fixed, permeabilized, and stained with anti-human PD-L2 Ab followed by Alexa Fluor-594 secondary Ab. 4',6-diamidino-2-phenylindole (DAPI) was used to counterstain nuclei. Calibration bar: 20 µm.

4.2 PD-L2 expression in human biopsies of EC type II

On the basis of available literature and preliminary data obtained from our cell line models and database, we investigated PD-L2 expression in a cohort of human endometrial cancers type II. Its expression level was determined in a total of 51 samples, including serous, clear cell, mixed type, peritumoral tissues and normal endometrium. Expression data are summarized in Table 5, divided for histological subgroups, FIGO stage, age and localization.
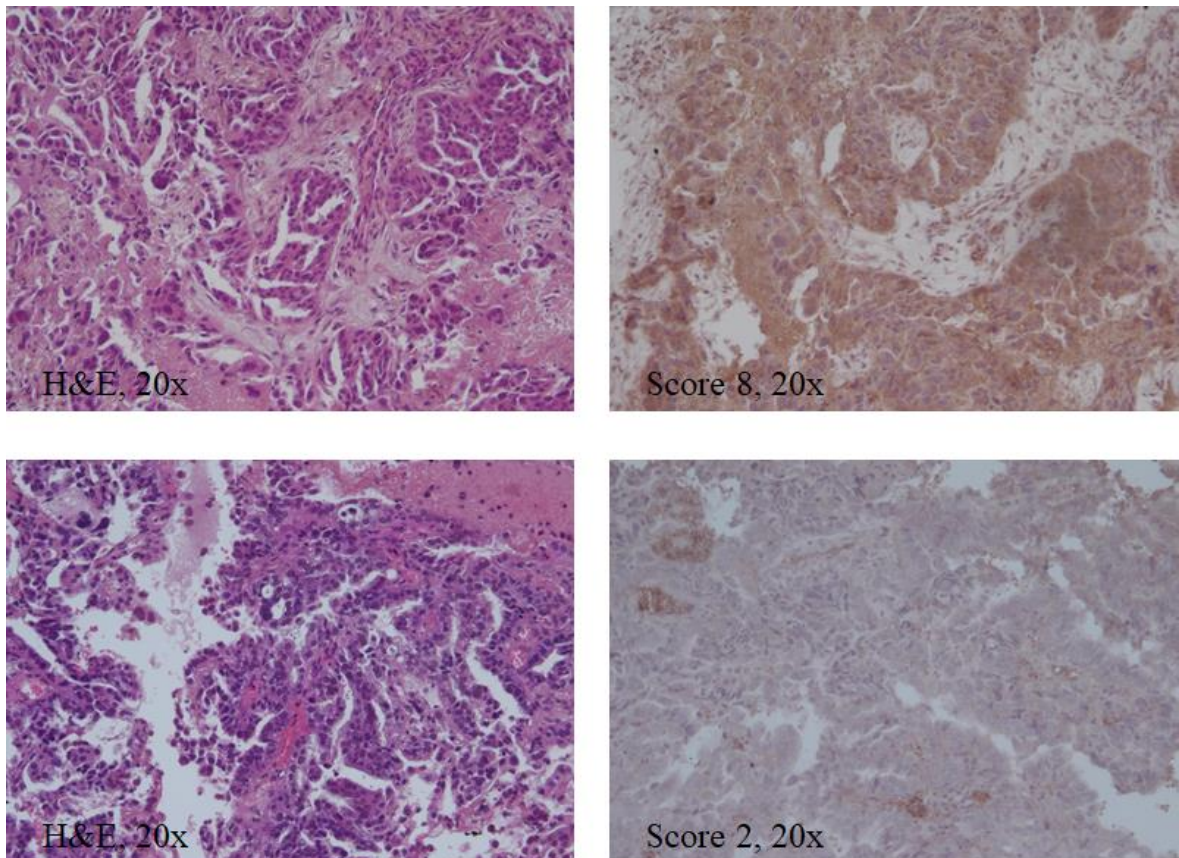
Figure 11. Representative images of IHC stainings for PD-L2 in human EC biopsies. *Stainings and scores of representative tumors. Pictures were taken at ×20 magnification (scale bar, 50 μm) and at ×40 magnification (scale bar, 20 μm).*

Representative images for the stainings and of the adopted scoring system are shown in Figure 11. Tissues were considered "high" at a score of six or higher, corresponding to weak staining in ≥ 67% of cells, moderate staining in ≥ 34% or strong staining in ≥ 10% of cells. "Moderate" staining at a score of 4-5.

PD-L2 is highly expressed in 64.44% of tumour specimens, 24.44% are moderate and 11.11% are low or negative. The highest staining was most frequently detected in serous type (69.23%) and mixed type (66.66%). Regarding peritumoral and normal tissues, PD-L2 was predominantly moderate or low. Number of normal samples are few respects to the initial cohort (10 samples) because the protocol used was incompatible with specimens rich in fat, according to H&E staining.

PD-L2 was expressed in epithelial component for 40% of specimens and in both stromal and epithelial components in 53.33% of samples (Figure 12).

Samples were classified according to FIGO staging system and the highest scores were detected for 76.47% stage I-II samples and for 75% stage IV samples. An increase of

	PD-L2		
	High	**Moderate**	**Low**
Tumour	29/45 (64.44%)	11/45 (24.44%)	5/45 (11.11%)
Serous	18/26 (69.23%)	4/26 (15.38%)	4/26 (15.38%)
Clear cell	3/7 (42.85%)	3/7 (42.85%)	1/7 (14.28%)
Mixed	8/12 (66.66%)	4/12 (33.33%)	0/12 (0%)
Peritumoural tissue	1/4 (25%)	2/4 (50%)	1/4 (25%)
Normal endometrium	0/2 (0%)	1/2 (50%)	1/2 (50%)
FIGO stage			
Stage I-II	13/17 (76.47%)	3/17 (17.64%)	1/17 (5.88%)
Serous	7/9 (77.77%)	1/9 (11.11%)	1/9 (11.11%)
Clear cell	1/2 (50%)	1/2 (50%)	0/2 (0%)
Mixed	5/6 (83.33%)	1/6 (16.66%)	0/6 (0%)
Stage III	7/16 (43.75%)	7/16 (43.75%)	2/16 (12.5%)
Serous	5/10 (50%)	3/10 (30%)	2/10 (20%)
Clear cell	0/2 (0%)	2/2 (100%)	0/2 (0%)
Mixed	2/4 (50%)	2/4 (50%)	0/4 (0%)
Stage IV	9/12 (75%)	1/12 (8.33%)	2/12 (16.66%)
Serous	6/7 (85.71%)	0/7 (0%)	1/7 (14.28%)
Clear cell	2/3 (66.66%)	0/3 (0%)	1/3 (33.33%)
Mixed	1/2 (50%)	1/2 (50%)	0/2 (0%)
Age			
= 68	11/19 (57.89%)	5/19 (26.31%)	3/19 (15.79%)
> 68	18/26 (69.23%)	6/26 (23.07%)	2/26 (7.69%)

Table 5. Expression of PD-L2 in EC, peritumoral tissue and normal endometrium. Percentages of samples according different clinicopathological characteristics.

percentage of samples with strong positivity was detected in patients over 68 years (Figure 13).
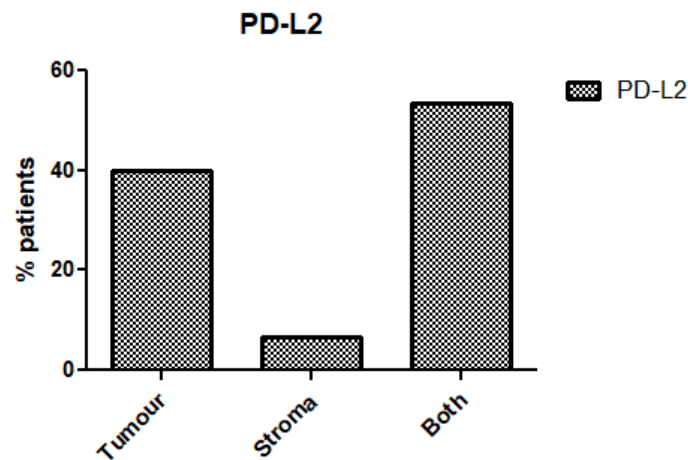
Figure 12. Percentages of patients classified according PD-L2 distribution inside tumoral mass.

Taken together, our data show that PD-L2 should be a potential target for non-endometrioid endometrial cancer, especially for serous and mixed subtypes, for low and high grade tumors.
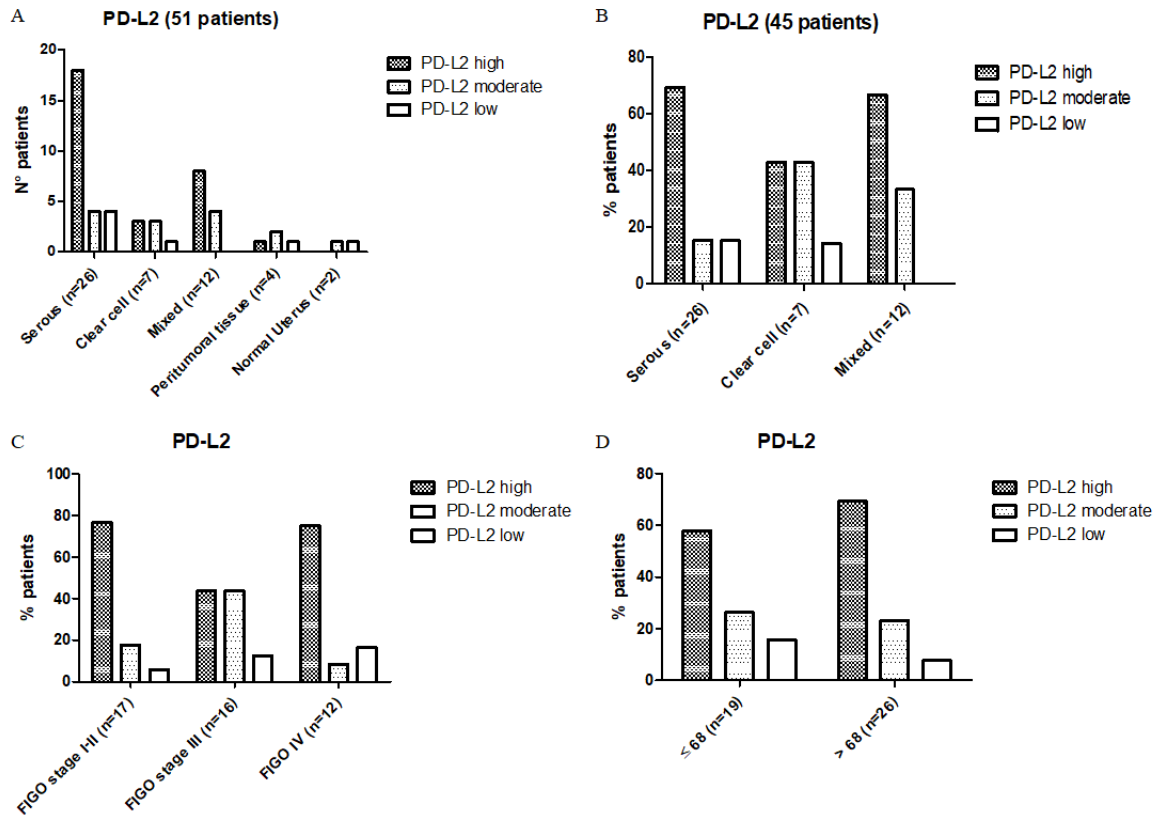
Figure 13. Classification of patients according PD-L2 expression and clinicopathological characteristics. A) Number of patients classified according PD-L2 expression in EC, peritumoral tissue and normal endometrium. B) Percentages of patients classified according PD-L2 expression in EC. C) Percentage of patients classified according PD-L2 expression and FIGO stage. D) Percentages of patients classified according PD-L2 expression and age.

4.3 High levels of PD-L2 correlates with poor prognosis

Figure 14. Survival of EC patients according to PD-L2 expression. *Kaplan–Meier survival curves showing OS and PFS of EC patients. The log-rank test with corresponding P values applies to the PD-L2–high and PD-L2–moderate curves.*

According to PD-L2 expression, Kaplan Meier analysis was performed, calculating overall survival (OS) and progression-free survival (PFS) for patients with high and moderate PD-L2 expression, while subgroup low was excluded because there were too few patients for a statistical analysis.

Kaplan Meier analysis revealed that OS was significant longer for patients who have a lower PD-L2 expression (PD-L2^{high} 34 months vs PD-L2^{moderate} 114 months, p= 0.0332, HR= 2.033, 95% CI= 0.9747 to 4.240) (fig X). For PFS, PD-L2 has a less impact on progression-free status (p >0.05, HR= 1.942, 95% CI= 0.7419 to 5.085) (Figure 14).

Additionally, OS and PFS were calculated according PD-L2 distribution, dividing patients for PD-L2 expression in tumour, stroma or both. Stroma subgroup was excluded because there were too few patients for a statistical analysis. PD-L2 distribution inside tumoral mass do not influence OS outcome (p> 0.05, HR= 0.5368, 95% CI= 0.2550 to 1.130) or PFS (p> 0.05, HR= 0.9280, 95% CI= 0.3610 to 2.386) (Figure 15).

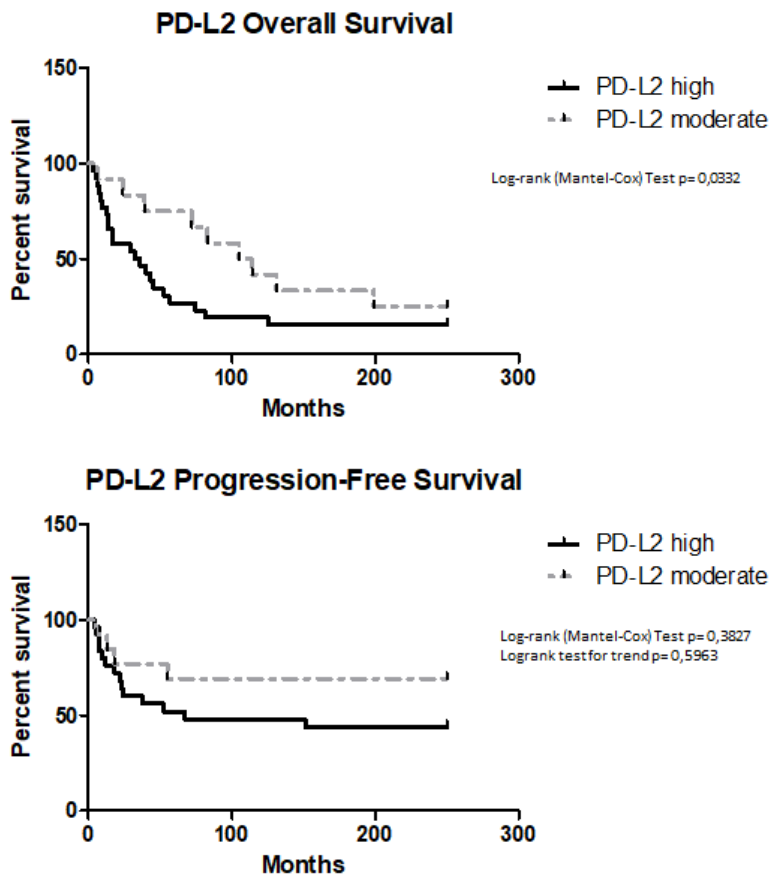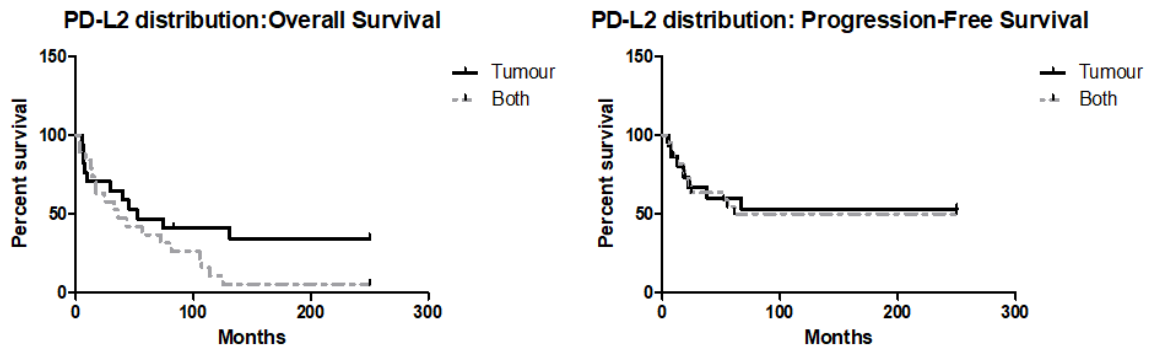*Figure 15. Survival of EC patients according to PD-L2 distribution.* *Kaplan–Meier survival curves showing OS and PFS of EC patients, according PD-L2 distribution inside tumoral mass (tumour, stroma or both). The log-rank test with corresponding P values applies to the PD-L2–tumour and PD-L2–both.*

4.4 PD-L2 expression stimulates migration and survival of endometrial cancer cells

To examine the role of PD-L2 in regulating proliferation and migration of endometrial cancer cells, the mixed type I/II PCEM004b cell line, that showed a low PD-L2 expression, was transfected with PD-L2 vector and Ishikawa cells, which are a Type I model PD-L2 positive, were silenced with a PD-L2 siRNA. PD-L2 expression was subsequently detected by western blot.

The results showed that the PD-L2$^+$ cells exhibited higher migratory capacities compared with control group (non-transfected cells) as determined by the wound-healing assay (p< 0.01) (Figure 16).
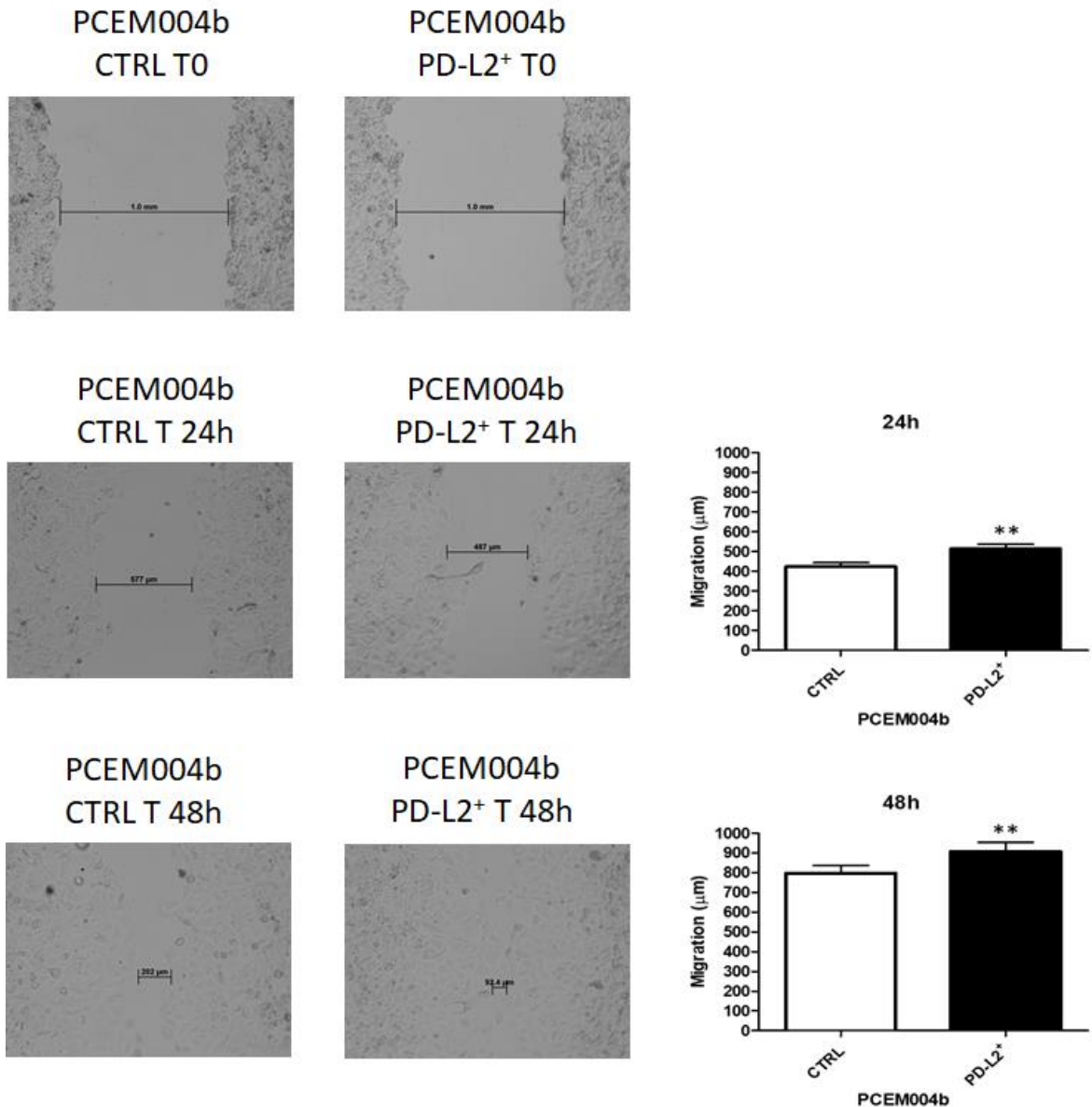
Figure 16. PD-L2 overexpression enhances migration of EC cells. *Wound-healing assays for PCEM004b cells after PD-L2 overexpression. All experiments were repeated three times. Data are presented as the mean ± SD. **P < 0.01 vs control.*

Similar result was obtained in a PD-L2-silenced Ishikawa cell line since PD-L2⁻ cells exhibited lower migratory capacities compared with control group as determined by the wound-healing assay (p< 0.001) (Figure 18).

These data indicate that PD-L2 is involved in migration of endometrial cancer cells and it could explain a worst OS for patients with high expression of PD-L2.
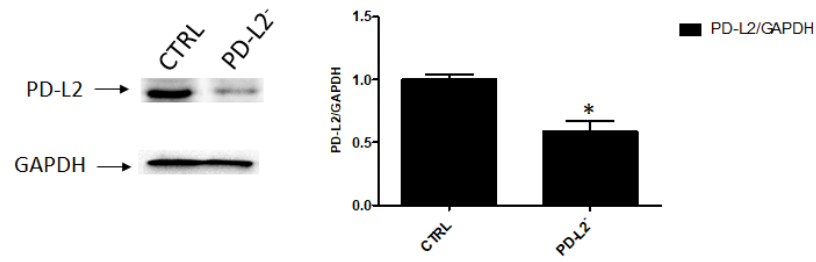
Figure 17. PD-L2 silencing in Ishikawa cells. Western blot analysis of PD-L2 and GAPDH protein levels in PD-L2⁻ Ishikawa cells. Blots are representative of one of three separate experiments. PD-L2 densitometry values were normalized to GAPDH used as loading control. Densitometric values shown are the mean ± SE of three separate experiments. *p < 0.05 vs control cells.
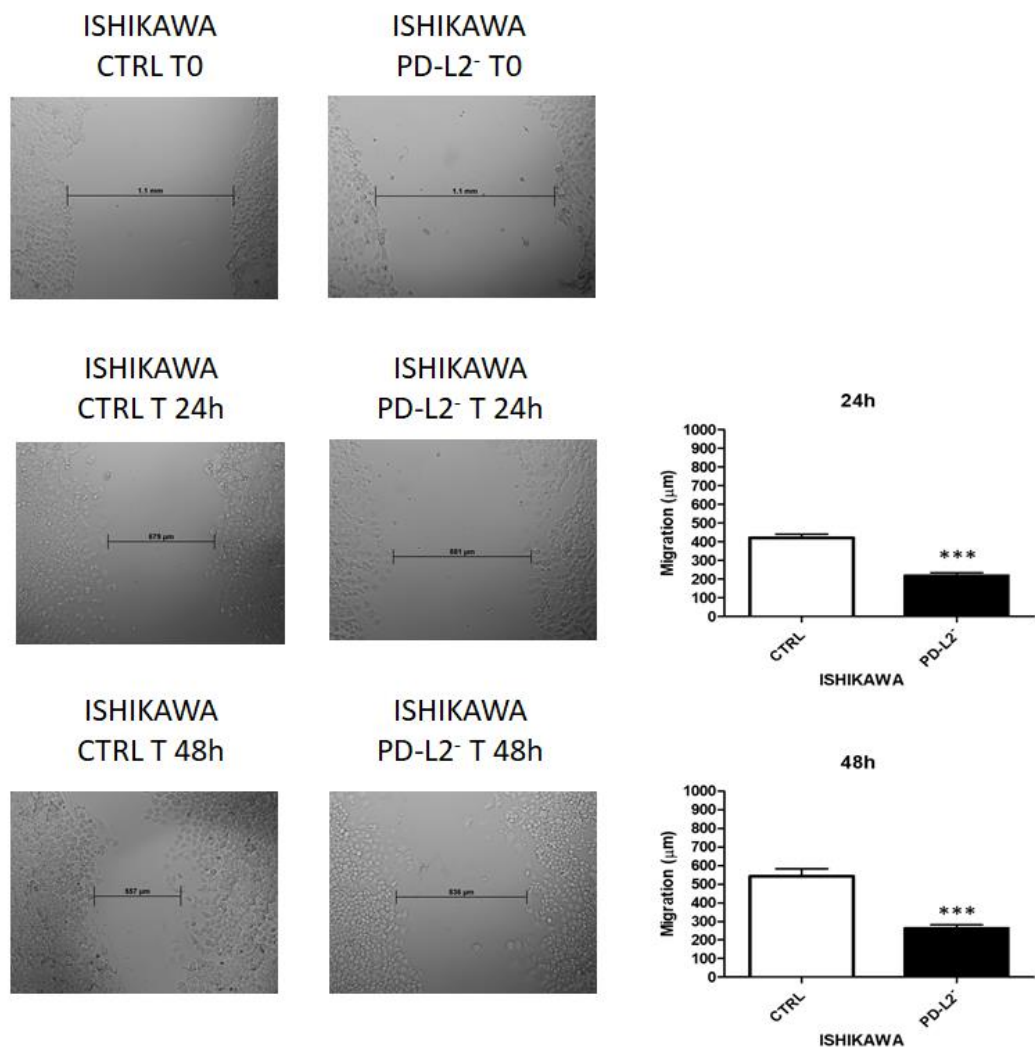
Figure 18. PD-L2 down-regulation reduced migration of EC cells. Wound-healing assays for PD-L2⁻ Ishikawa cells. All experiments were repeated three times. Data are presented as the mean ± SD. ***p < 0.001 vs control.

Additionally, to assess PD-L2 potential role in regulating cancer cell survival and migration, modulation of ERK and Akt/PKB pathways were evaluated through western blot analysis. Indeed, the phosphorylated form of AKT is significantly increased (p= 0.05) while phosphorylated ERK is significantly decreased in PD-L2$^+$ cells respect to the control (p<
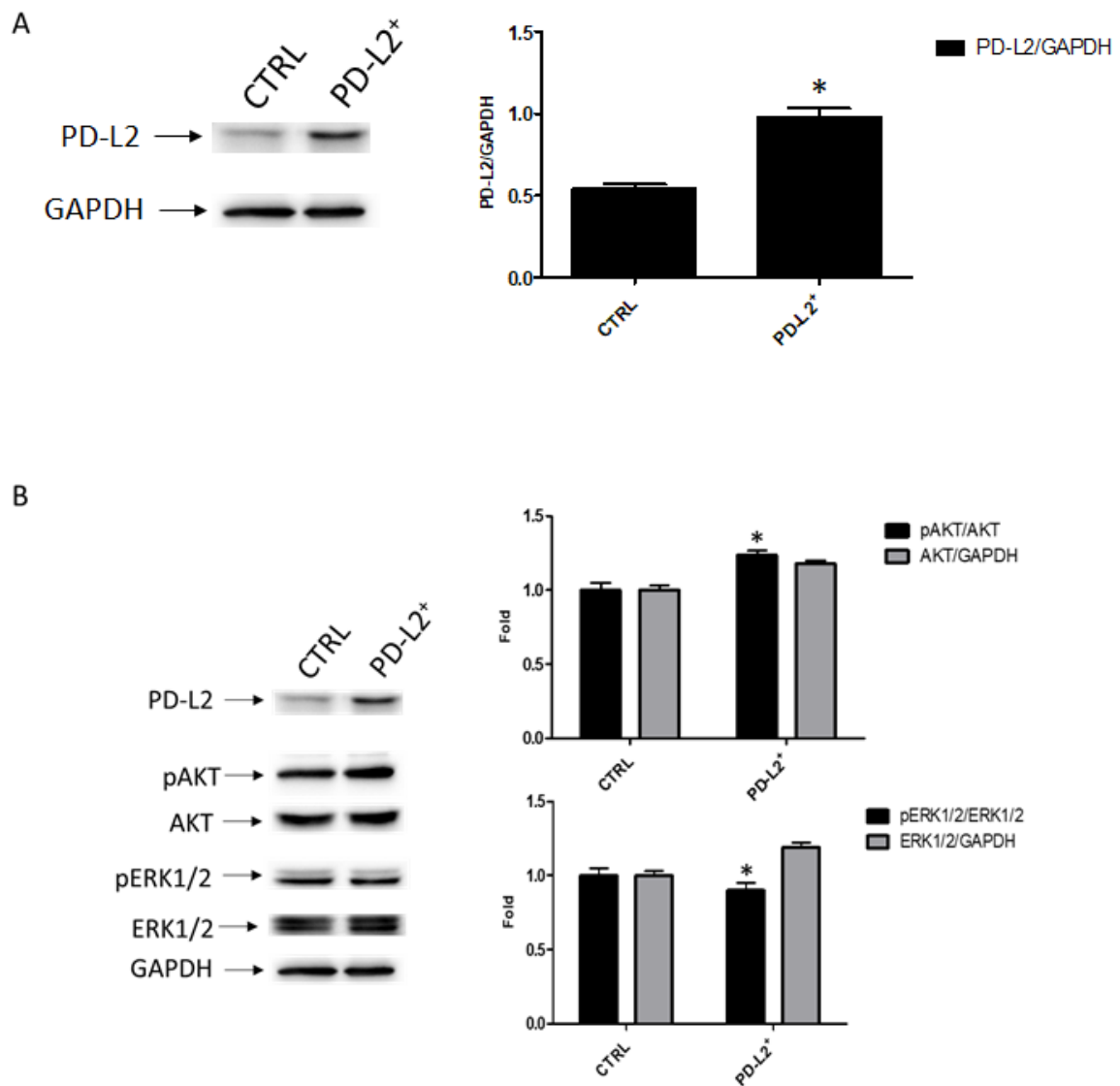
*Figure 19. PD-L2 overexpression modulates AKT and ERK pathways. A) Western blot analysis of PD-L2 and GAPDH protein levels in PD-L2$^+$ PCEM004b cells. Blots are representative of one of three separate experiments. PD-L2 densitometry values were normalized to GAPDH used as loading control. Densitometric values shown are the mean ± SE of three separate experiments. *p < 0.05 vs control cells. B) Western blot analysis of pAKT(Ser473), pERK1/2(Thr202/Tyr204), ERK1/2, AKT and GAPDH protein levels in PD-L2$^+$ EC cells. Blots are representative of one of three separate experiments. The pERK1/2(Thr202/Tyr204) and pAKT(Ser473) protein levels were determined with respect to ERK1/2 and AKT levels. ERK1/2 and AKT densitometry values were normalized to GAPDH used as loading control. Densitometric values shown are the mean ± SE of three separate experiments. *p < 0.05 vs control cells.*

0.05) (Figure 19B) and the opposite effect was observed by PD-L2 silencing in Ishikawa cells (p< 0.05) (Figure 20)
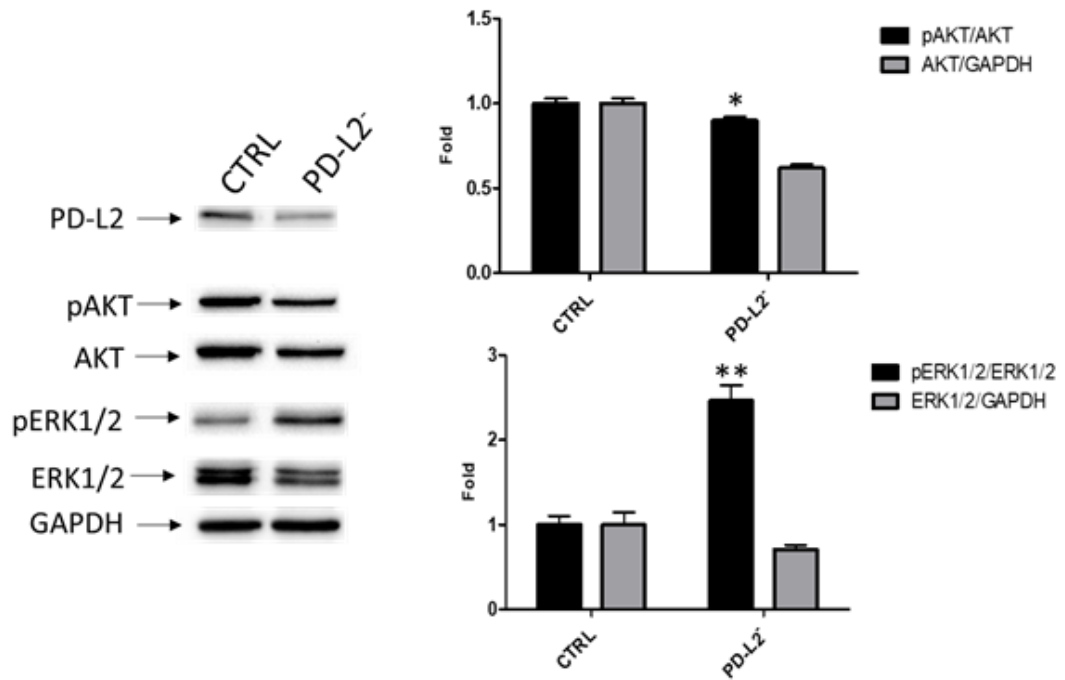
Figure 20. PD-L2 down-regulation modulates AKT and ERK pathways. *Western blot analysis of pAKT(Ser473), pERK1/2(Thr202/Tyr204), ERK1/2, AKT and GAPDH protein levels in PD-L2⁻ Ishikawa cells. Blots are representative of one of three separate experiments. The pERK1/2(Thr202/Tyr204) and pAKT(Ser473) protein levels were determined with respect to ERK1/2 and AKT levels. ERK1/2 and AKT densitometry values were normalized to GAPDH used as loading control. Densitometric values shown are the mean ± SE of three separate experiments. *p < 0.05 vs control cells, **p < 0.01 vs control cells.*

4.5 PD-L2 expression influences chemoresistance of endometrial cancer cells

Treating cells with the common chemotherapeutic drugs used in therapy, Cisplatin and Doxorubicin (from 0.0064 µg/mL to 100 µg/mL) and Paclitaxel (from 0.0064 µg/mL to 100 µg/mL for PCEM004b and from 0.00025 µg/mL to 4 µg/mL for Ishikawa) for 72 hs, tumour PD-L2 did not significantly alter sensitivity of both transfected/silenced cells to the chemotherapeutic agents Cisplatin and Doxorubicin ($p > 0.05$) but increased the effect of Paclitaxel ($p < 0.05$) in PD-L2$^+$ cells, especially at concentration of 0.16 µg/mL (Figure 21) and decreased the effect in PD-L2$^-$ cells, up to 0.8 µg/mL ($p < 0.05$) ($p < 0.05$) (Figure 22).
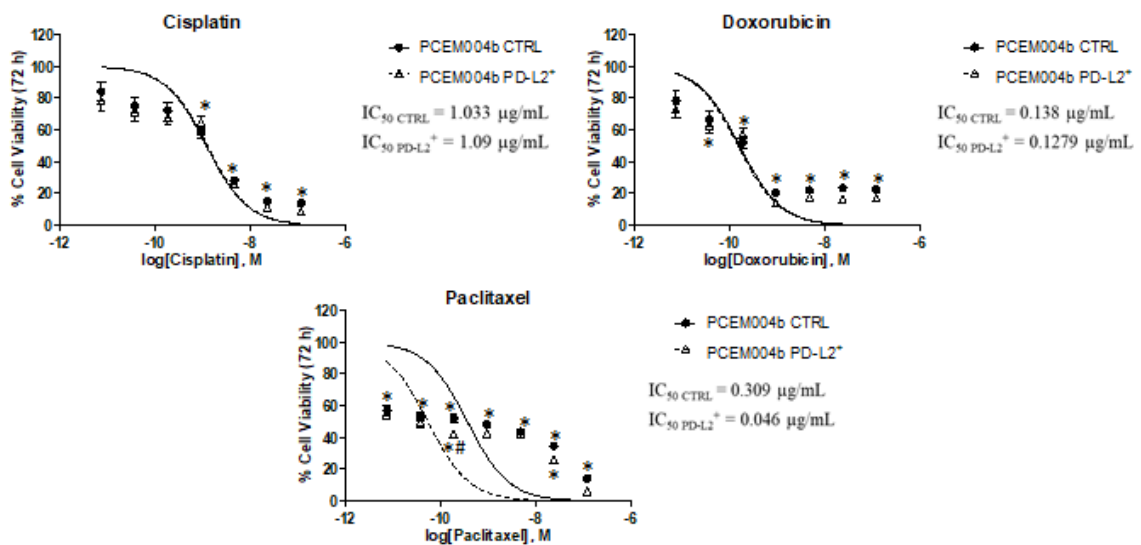
Figure 21. Cell viability was determined by MTT assay. *PD-L2$^+$ cells and control were treated for 72 hs with different concentrations of Cisplatin, Doxorubicin and Paclitaxel (up to 100 µg/mL). Data shown are expressed as mean ± SE of three separate experiments. *p < 0.05 treated vs vehicle, #p < 0.05 PD-L2$^+$ vs control.*
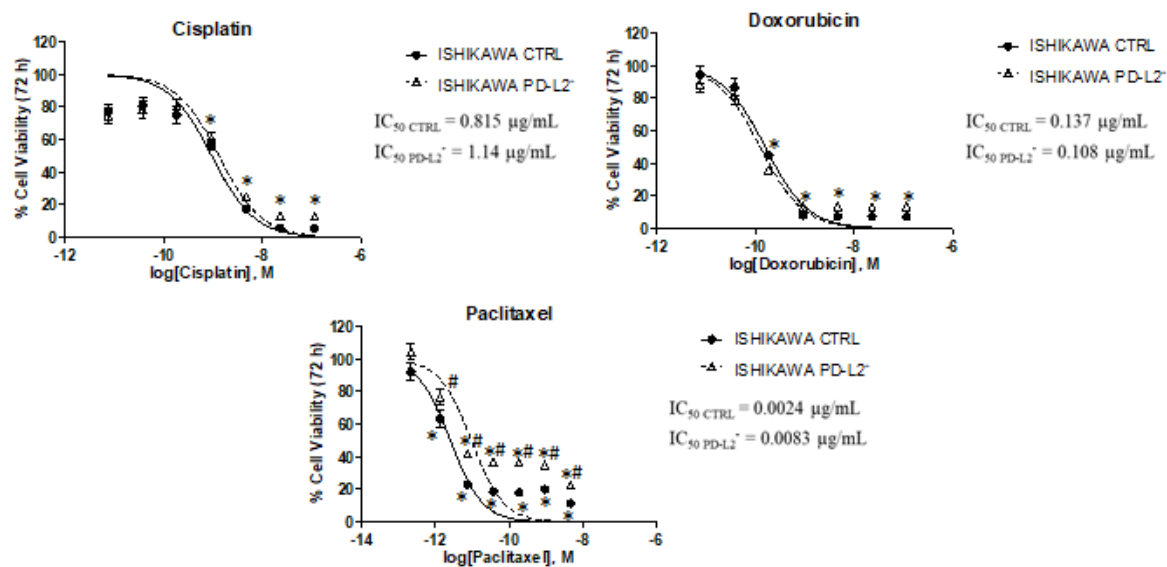
Figure 22. Cell viability was determined by MTT assay. PD-L2⁻ Ishikawa cells and control were treated for 72 hs with different concentrations of Cisplatin and Doxorubicin (up to 100 μg/mL), and Paclitaxel (up to 4 μg/mL). Data shown are expressed as mean ± SE of three separate experiments. *p < 0.05 treated vs vehicle, #p < 0.05 PD-L2⁺ vs control.

4.6 EC expresses several CBD targets

As previously described, CBD acts in a CB1 and CB2-dependent and -independent manner then, in order to evaluate CBD biological effect in EC cell lines, we characterized EC cell lines, analysing which of the CBD target receptors are expressed by RT-PCR and western blot for CB1, CB2, TRPV1 and TRPV2 genes. The results showed that EC cell lines did not significantly express CBs receptor, except for MFE-280 that expressed CB1 (Figure 23). Regarding TRPVs channels, only for TRPV2 there is an increase in expression with increasing of non-endometrioid component. Regarding TRPV1, mRNA is expressed in all EC cell lines while only the mixed type I/II PCEM004a cell line expressed significantly TRPV1 protein (Figure 24).
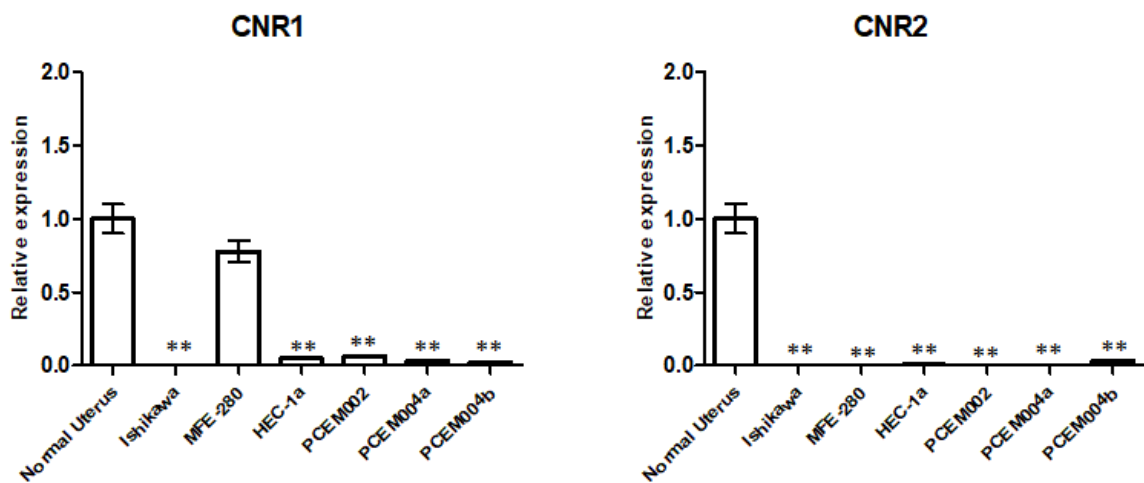
Figure 23. CB1 (CNR1) and CB2 (CNR2) expression on normal human uterus and EC cell lines. CB1 and CB2 mRNA expression was evaluated by qRT-PCR in normal human uterus and six EC cell lines. CB1 and CB2 mRNA levels were normalized for GAPDH expression. Data are expressed as fold mean ± SD. **p<0.01 vs normal control.
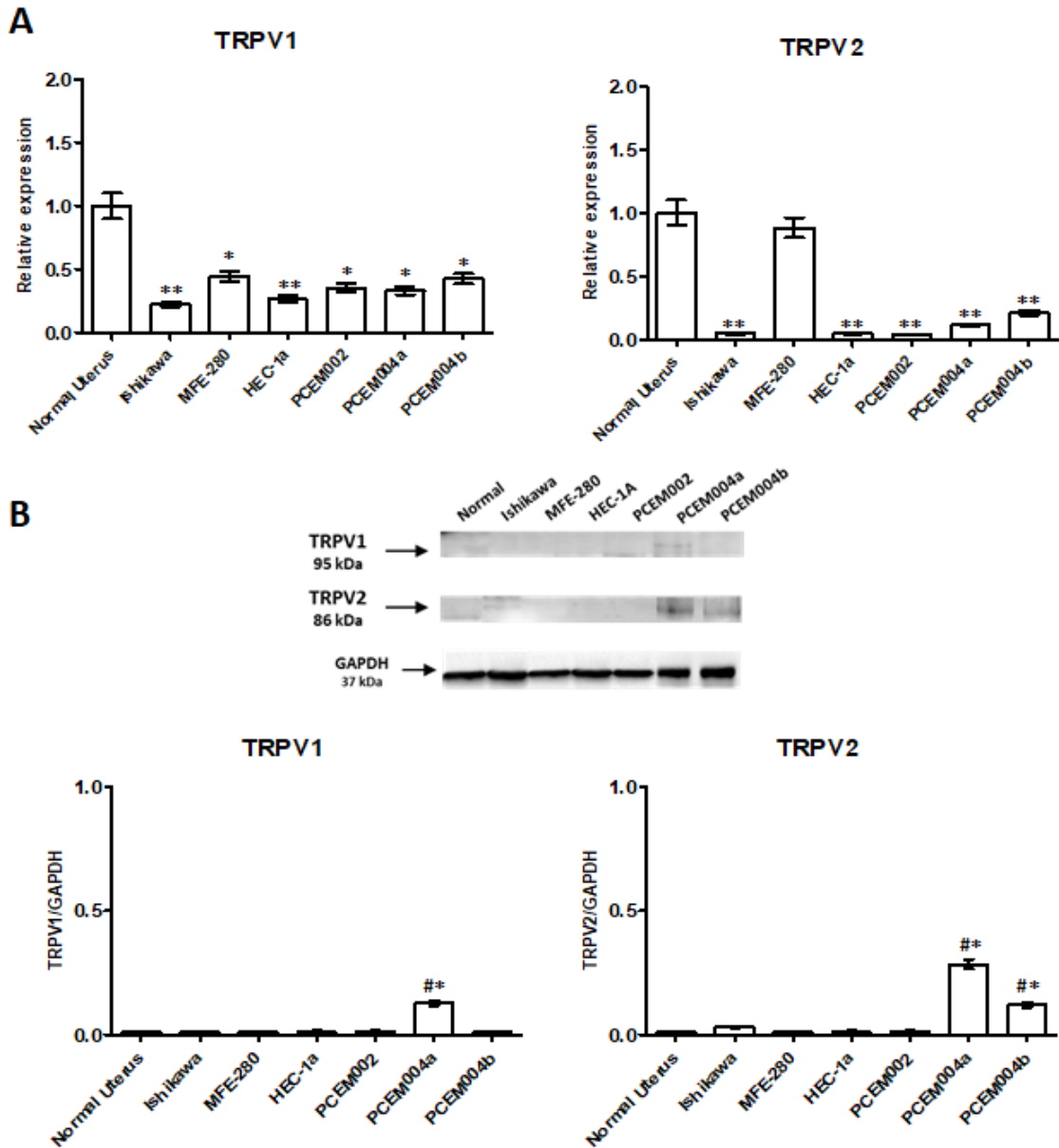
Figure 24. TRPV1 and TRPV2 expression on normal human uterus and EC cell lines. *(A) TRPV1 and TRPV2 mRNA expression was evaluated by qRT-PCR in normal human uterus and six EC cell lines. TRPV1 and TRPV2 mRNA levels were normalized for GAPDH expression. Data are expressed as fold mean ± SD. *p<0.05 vs normal control, **p<0.01 vs normal control, #p<0.05 vs type I primary EC cell line PCEM002. (B) TRPV1 and TRPV2 protein expression was evaluated by western blot in normal human uterus and six EC cell lines. TRPV1 and TRPV2 densitometry values were normalized to GAPDH used as loading control. Densitometric values shown are the mean ± SE of three separate experiments. *p < 0.05 vs normal control, #p < 0.05 vs type I primary EC cell line PCEM002.*

According to these gene expression profile, we decided to focus the attention on TRPV2 expression in a cohort of human EC type II.

4.7 Determination of CB receptors and TRPVs gene expression in EC samples from TCGA

We assessed CB receptors and TRPVs gene expression in 506 EC data samples from TCGA, queried with cBioportal (TCGA, PanCancer Atlas). Samples were divided in endometrioid (397 samples) and serous type (109 samples) and the mRNA levels were expressed in $\log_2$.
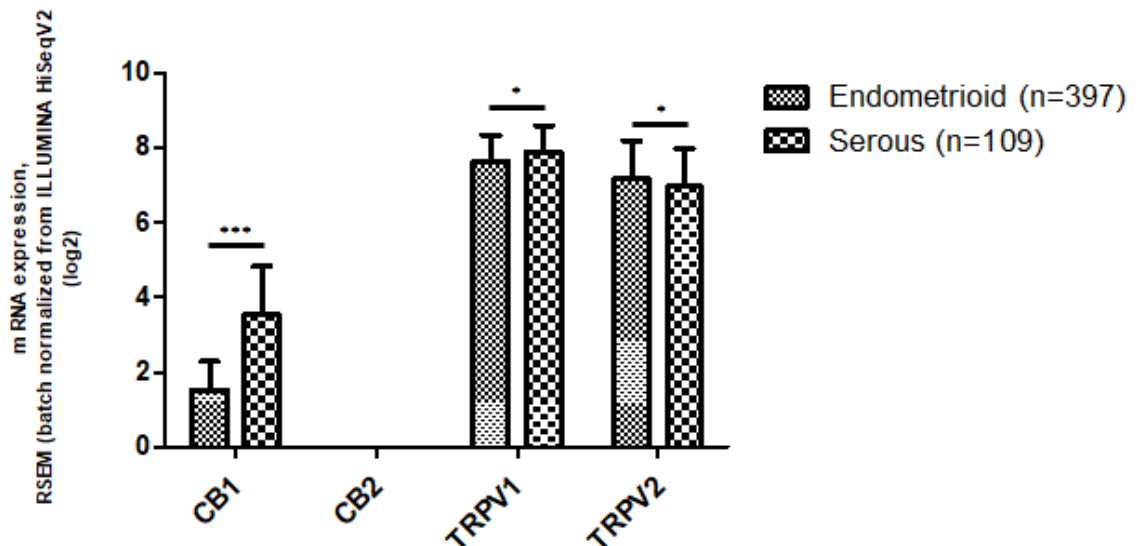
*Figure 25. The expression of CBD targets in EC patients. The mRNA expression ($\log_2$) of CB1, CB2, TRPV1 and in 506 EC samples, divided in 397 for Type I and 109 for Type II, from TCGA database. ***$p < 0.001$ Type II vs Type I, *$p < 0.05$ Type II vs Type I.*

CB1 receptor was expressed more in serous type samples ($p < 0.001$), while CB2 was not expressed, confirming RT-PCR analysis in EC cell lines. TRPV1 and TRPV2 were expressed in EC samples of both types. TRPV1 was expressed more in serous subtype ($p < 0.05$) while TRPV2 was expressed more in endometrioid subtype ($p < 0.05$) (Figure 25).

4.8 TRPV2 expression increases with the malignancy of type II EC and correlates with a shorter PFS

TRPV2 expression level was determined in a total of 68 patients, including serous, clear cell, mixed type, peritumoral tissues and normal endometrium. Expression data are summarized in Table 6, divided for histological subgroups, FIGO stage, age and localization. Representative images for the staining and of the adopted scoring system are shown in Figure 26. Tissues were considered "high" at a score of six or higher, corresponding to weak

staining in $\geq 67\%$ of cells, moderate staining in $\geq 34\%$ or strong staining in $\geq 10\%$ of cells. "Moderate" staining at a score of 4-5.
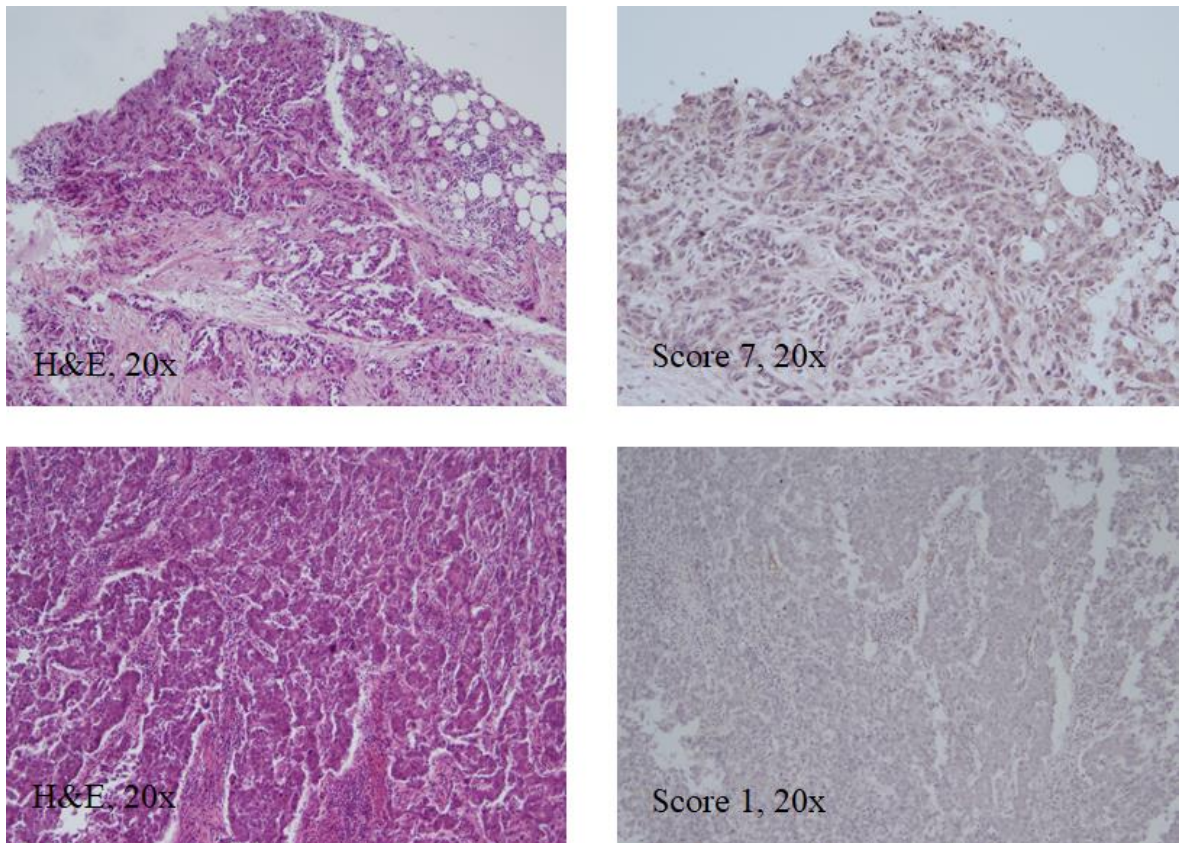
Figure 26. Representative images of IHC stainings for TRPV2 in human EC biopsies. *Stainings and scores of representative tumors. Pictures were taken at ×20 magnification (scale bar, 50 µm) and at ×40 magnification (scale bar, 20 µm).*

TRPV2 was highly expressed in 18.86% of tumour specimens, 30.19% were moderate and 50.94% are low or negative. The highest staining was most frequently detected in serous type (24.13%) while the lowest staining was found in clear cell type (71.43%). Regarding peritumoral and normal tissues, TRPV2 was predominantly moderate or low. No significant difference in TRPV2 expression was detected in patients ≤ 68 or > 68 years (Figure 27). Samples were classified according to FIGO staging system and we found that TRPV2 expression increases with increasing of tissue malignancy (Figure 27c). TRPV2 was expressed in epithelial component for 43.48% of specimens and in both stromal and

epithelial components in 50% of samples (Figure 28). Furthermore, Kaplan Meier analysis was performed, calculating overall survival (OS) and progression-free survival (PFS).

	TRPV2		
	High	Moderate	Low
Tumour	10/53 (18.86%)	16/53 (30.19%)	27/53 (50.94%)
Serous	7/29 (24.13%)	9/29 (31.03%)	13/29 (45.89%)
Clear cell	1/7 (14.28%)	1/7 (14.28%)	5/7 (71.43%)
Mixed	2/17 (11.76%)	6/17 (35.29%)	9/17 (52.94%)
Peritumoural tissue	0/5 (0%)	1/5 (20%)	4/5 (80%)
Normal endometrium	0/10 (0%)	4/10 (40%)	6/10 (60%)
FIGO stage			
Stage I-II	3/20 (15%)	5/20 (25%)	12/20 (60%)
Serous	1/10 (10%)	3/10 (30%)	6/10 (60%)
Clear cell	0/2 (0%)	1/2 (50%)	1/2 (50%)
Mixed	2/8 (25%)	1/8 (12.5%)	5/8 (62.5%)
Stage III	3/17 (17.65%)	6/17 (35.29%)	8/17 (47.06%)
Serous	3/10 (30%)	4/10 (40%)	3/10 (30%)
Clear cell	0/2 (0%)	0/2 (0%)	2/2 (100%)
Mixed	0/5 (0%)	2/5 (40%)	3/5 (60%)
Stage IV	4/16 (25%)	5/16 (31.25%)	7/16 (43.75%)
Serous	4/9 (44.44%)	2/9 (22.22%)	3/9 (33.33%)
Clear cell	1/3 (33.33%)	0/3 (0%)	2/3 (66.66%)
Mixed	0/4	3/4 (75%)	1/4 (25%)
Age			
= 68	4/26 (15.38%)	6/26 (23.07%)	16/26 (61.54%)
> 68	6/27 (22.22%)	10/27 (37.04%)	11/27 (40.74%)

Table 6. Expression of TRPV2 in EC, peritumoral tissue and normal endometrium. Percentages of samples according different clinicopathological characteristics.
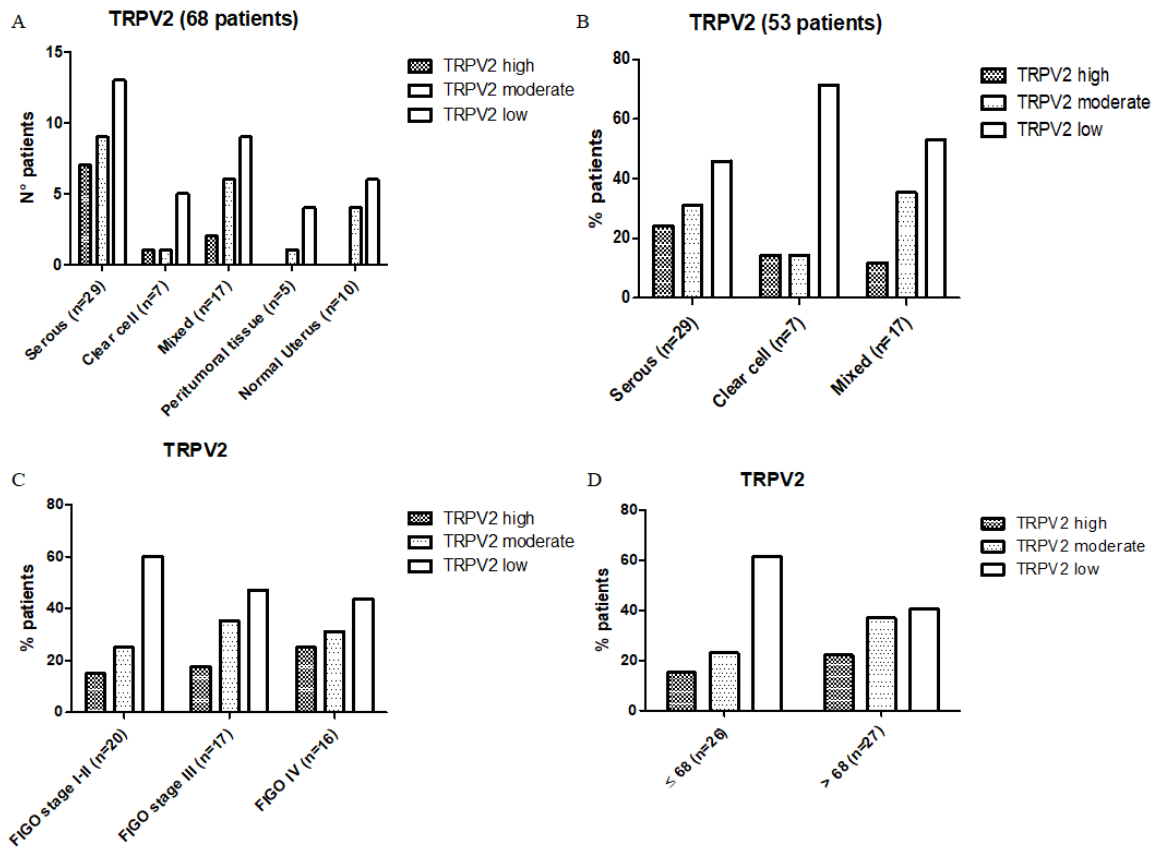
Figure 27. Classification of patients according TRPV2 expression and clinicopathological characteristics. *A) Number of patients classified according TRPV2 expression in EC, peritumoral tissue and normal endometrium. B) Percentages of patients classified according TRPV2 expression in EC. C) Percentage of patients classified according TRPV2 expression and FIGO stage. D) Percentages of patients classified according TRPV2 expression and age.*
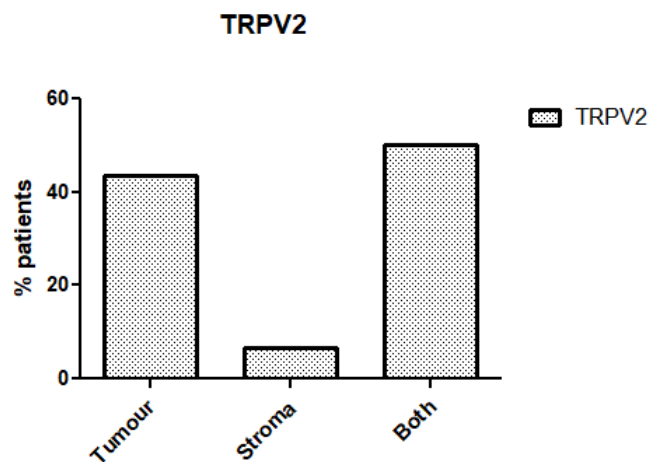
Figure 28. Percentages of patients classified according TRPV2 distribution inside tumoral mass.

TRPV2 Overall Survival

TRPV2 Progression-Free Survival
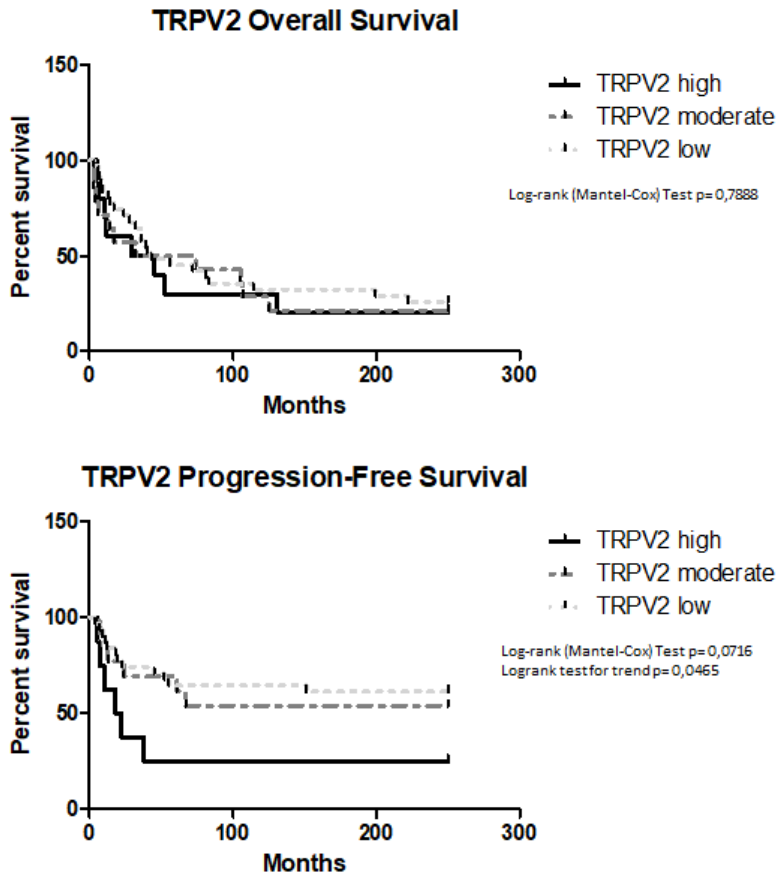
Figure 29. Survival of EC patients according to TRPV2 expression. Kaplan–Meier survival curves showing OS and PFS of EC patients. The log-rank test with corresponding P values applies to the TRPV2–high, TRPV2–moderate and TRPV2-low curves.

Kaplan Meier analysis revealed that TRPV2 does not influence OS (TRPV2^{high} 37 months vs TRPV2^{moderate} 53 months, p= 0.9346, HR= 1.039, 95% CI= 0.4131 to 2.615, TRPV2^{high} 37 months vs TRPV2^{low} 43 months, p= 1.326, HR= 1.039, 95% CI= 0.5579 to 3.149, TRPV2^{moderate} 53 months vs TRPV2^{low} 43 months, p= 1.326, HR= 1.199, 95% CI= 0.5665 to 2.537) (Figure 28). High TRPV2 expression is correlated with a shorter PFS (TRPV2^{high} vs TRPV2^{low} p= 0.0224, HR= 4.675, 95% CI= 1.244 to 17.57, TRPV2^{high} vs TRPV2^{moderate}, p= 0.1172, HR= 2.755, 95% CI= 0.7754 to 9.790, TRPV2^{moderate} vs TRPV2^{low} , p= 0.6896, HR= 1.232, 95% CI= 0.4433 to 3.422) (Figure 29).

Additionally, OS and PFS were calculated according TRPV2 distribution, dividing patients for TRPV2 expression in tumour, stroma or both. Stroma subgroup was excluded because there were too few patients for a statistical analysis. TRPV2 distribution inside tumoral mass do not influence OS outcome (p>0.05, HR= 0.6764, 95% CI= 0.3391 to 1.349) or PFS (p>0.05, HR= 0.8102, 95% CI= 0.3201 to 2.051) (Figure 30).

Taken together, our data show that TRPV2 is involved in malignancy of non-endometrioid endometrial cancer and support the investigation of CBD biological effect in EC treatment.

Figure 30. Survival of EC patients according to TRPV2 distribution. *Kaplan–Meier survival curves showing OS and PFS of EC patients, according TRPV2 distribution inside tumoral mass (tumour, stroma or both). The log-rank test with corresponding P values applies to the TRPV2–tumour and TRPV2–both.*

4.9 TRPV2 expression stimulates migration and survival of endometrial cancer cells

To examine the biological role of TRPV2 expression on proliferation and migration of endometrial cancer cells, Ishikawa cells, that showed a low TRPV2 expression, were transfected with TRPV2 vector and TRPV2 expression was subsequently detected by western blot.

The result showed that TRPV2$^+$ cells exhibited higher migratory capacities compared with non-transfected cells, after 48 hs, as determined by the wound-healing assay (p< 0.05) (Figure 31).
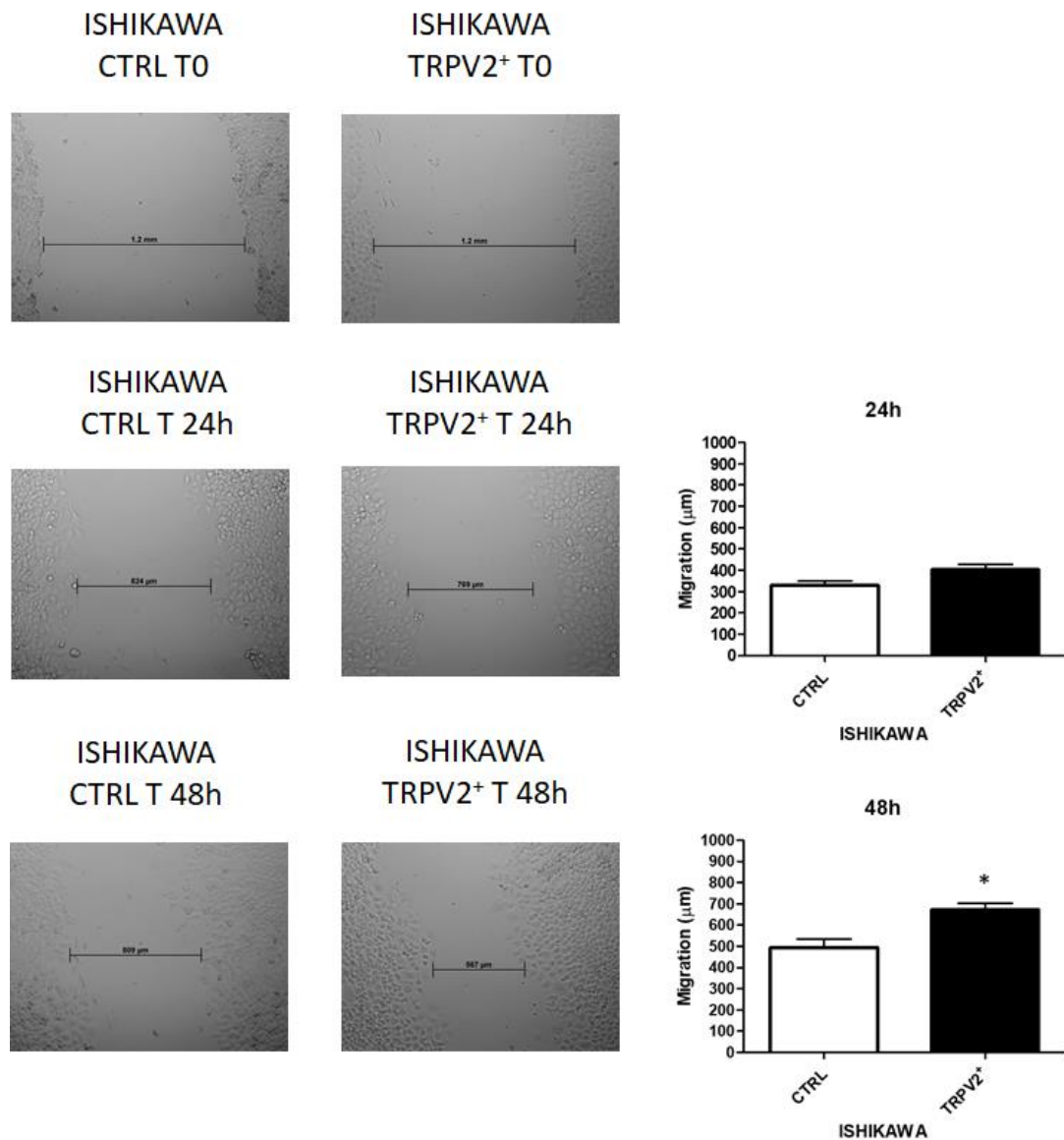
Figure 31. TRPV2 overexpression enhances migration of EC cells. *Wound-healing assays for Ishikawa cells after TRPV2 overexpression. All experiments were repeated three times. Data are presented as the mean ± SD. *P < 0.05 vs control.*

Additionally, to assess TRPV2 potential role in regulating cancer cell proliferation, modulation of Akt/PKB pathway was evaluated through western blot analysis.

Indeed, AKT phosphorylated form is significantly increased in TRPV2$^+$ cells (p< 0.001) supporting the hypothesis that TRPV2 expression increases cancer aggressiveness (Figure 32).
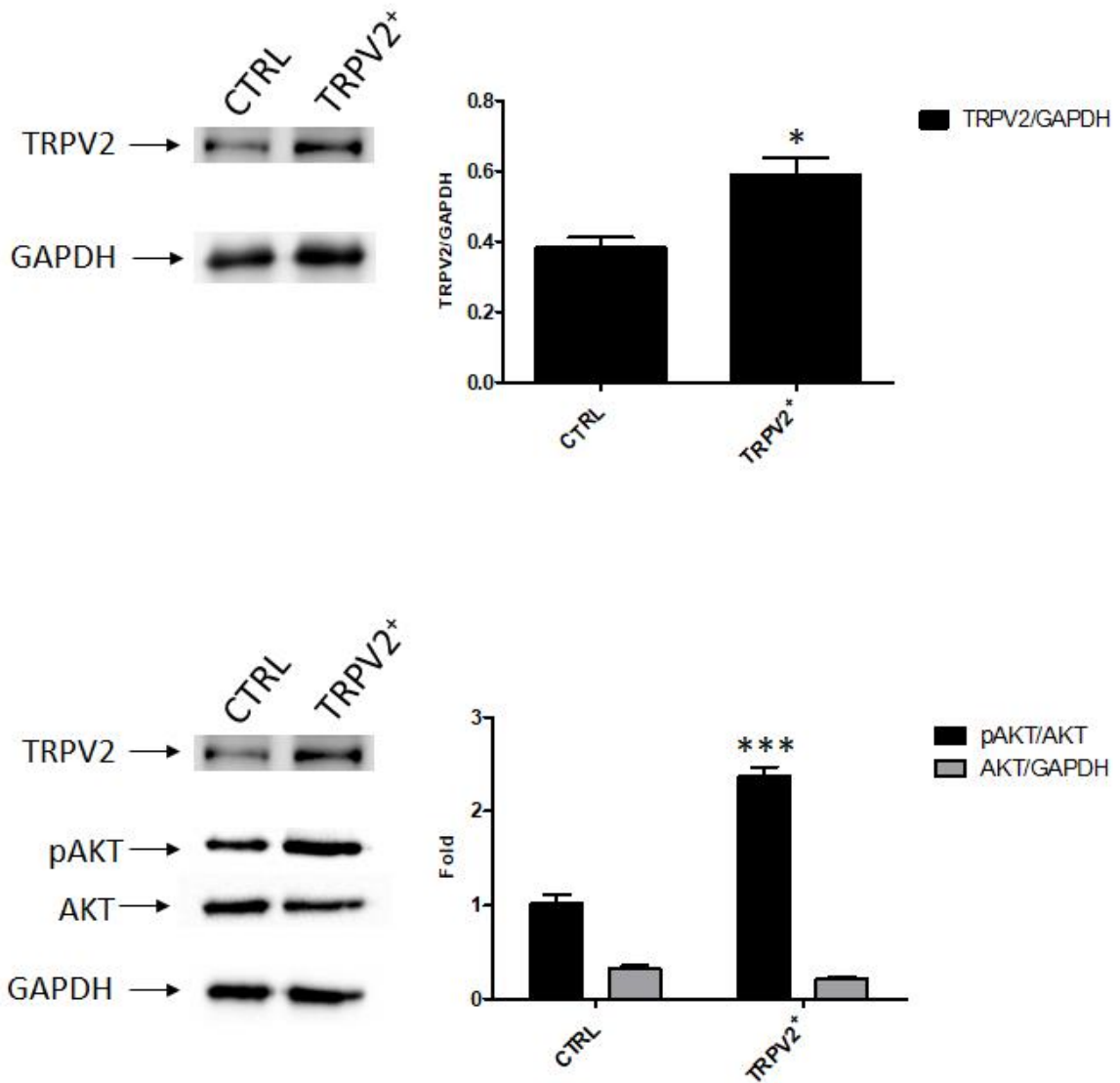
Figure 32. TRPV2 overexpression stimulates EC cells proliferation. *Western blot analysis of pAKT(Ser473), AKT and GAPDH protein levels in TRPV2⁺ EC cells. Blots are representative of one of three separate experiments. The pAKT(Ser473) protein levels were determined with respect to and AKT levels. AKT densitometry values was normalized to GAPDH used as loading control. Densitometric values shown are the mean ± SE of three separate experiments. ***p < 0.001 vs control cells.*

4.10 TRPV2 expression influences the effect of chemo-drugs in endometrial cancer cells

TRPV2⁺ cells were treated with Cisplatin and Doxorubicin (from 0.0064 µg/mL to 100 µg/mL) and Paclitaxel (from 0.00025 µg/mL to 4 µg/mL) for 72 hs. Results showed that

TRPV2 expression increased chemo-sensitivity in Ishikawa cells, especially for Cisplatin (p<0.05), while did not particularly modulate the effect of Doxorubicin and Paclitaxel (Figure 33).
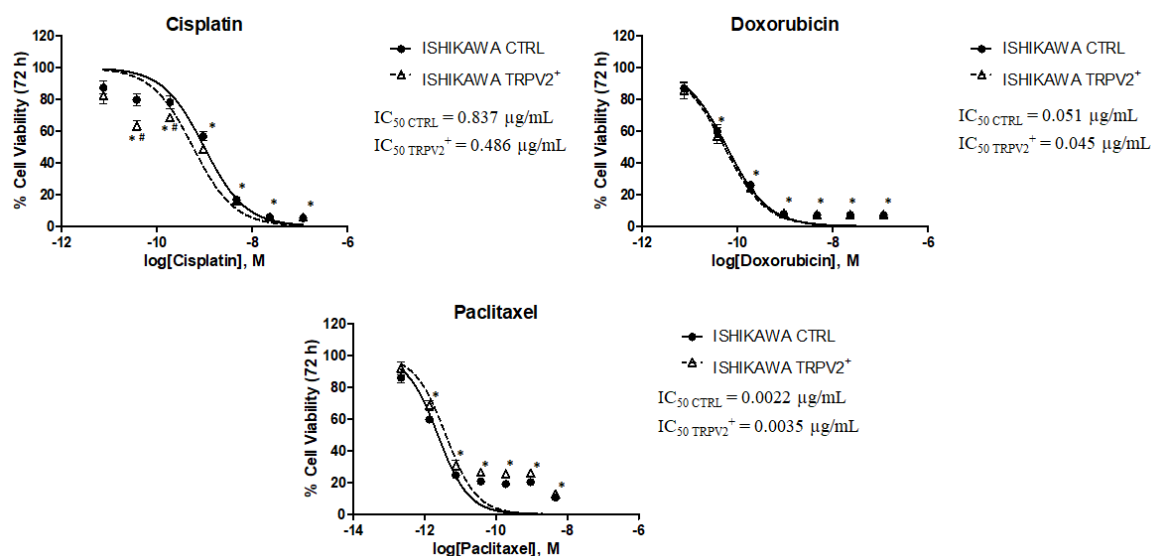
Figure 33. Cell viability was determined by MTT assay. TRPV2+ cells and control were treated for 72 hs with different concentrations of Cisplatin, Doxorubicin (up to 100 µg/mL) and Paclitaxel (up to 4 µg/mL). Data shown are expressed as mean ± SE of three separate experiments. *p < 0.05 treated vs vehicle, #p < 0.05 TRPV2+ vs control.

4.11 CBD induces cytotoxicity in EC cell lines in single and daily administration

The effect of CBD in reducing cell viability was evaluated in EC cell lines for 72 hs, in single and daily administration. Cells were treated with CBD (up to 15.72 µg/ml) and percentage of cell viability was evaluated by the MTT assay. The results showed a dose dependent CBD effect in all EC cell lines, IC_{50} values are reported in Table 7. Additionally, daily administration induces a higher cytotoxicity when compared with CBD single administration (Figure 34), but not for PCEM004b. According to the basal expression of the main CBD targets, CB1, CB2, TRPV1 and TRPV2, the higher sensibility of PCEM004b cell line already with single administration compared with other cell lines, could be explained by the fact that CBD acts also with other TRP channels and receptors (e.g. GPR55) or with receptor-independent mechanism. So, we decided to work with the doses of 3.92, 7.85 and 15.72 µg/ml, according with the IC_{50} of each EC cell line.

Endometrial cancer cell lines	IC$_{50}$ CBD µg/ml single administration	IC$_{50}$ CBD µg/ml daily administration
Ishikawa	5.89 ± 0.4	3.56 ± 0.2
MFE-280	6.33 ± 0.5	2.39 ± 0.1
HEC-1a	23.38 ± 0.8	13.16 ± 0.6
PCEM002	6.58 ± 0.2	3.59 ± 0.1
PCEM004a	20.02 ± 0.7	14.01 ± 0.6
PCEM004b	8.29 ± 0.5	7.05 ± 0.4

Table 7. IC50 values in endometrial cancer cell lines.
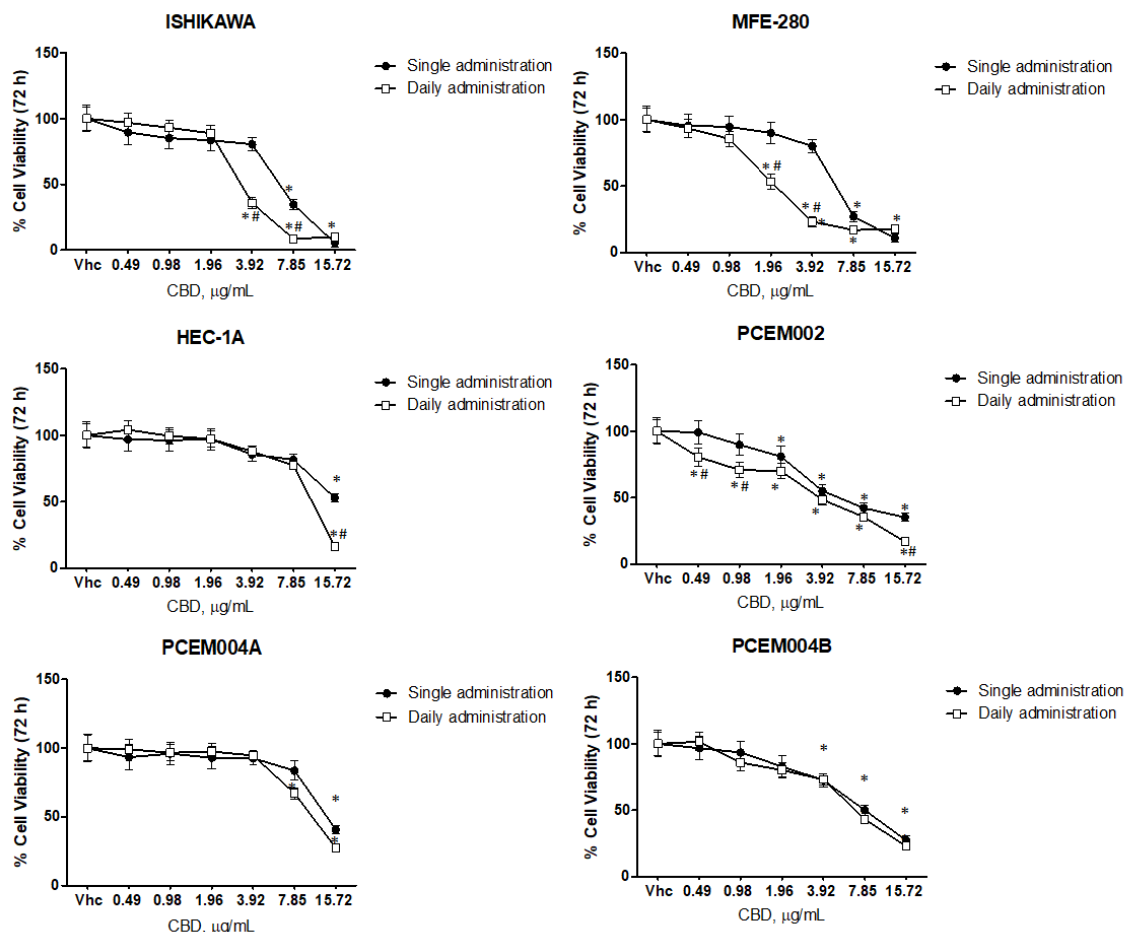
Figure 34. CBD induces cytotoxicity in endometrial cancer cell lines. Cell viability was determined by MTT assay. Ishikawa, MFE-280, HEC-1a, PCEM002, PCEM004a and PCEM004b cells were treated for 72 hs with different concentrations of CBD (up to 15.72 µg/mL). Data shown are expressed as mean ± SE of three separate experiments. *p < 0.05 treated vs vehicle, #p < 0.05 daily vs single administration.

4.12 CBD induces cell cycle arrest in EC cell lines

We evaluated the role of CBD in single and in daily administration in influencing the cell cycle of EC cell lines. The results showed that CBD was able to induce cell accumulation in the G1 phase, starting from 24 hs post-treatment, accompanied by accumulation in the sub-G1 phase (hypodiploid DNA) mostly after daily treatments, in all cell lines, especially for MFE-280 cell line (Figure 35). These data evidenced that CBD-reduced cell viability, especially in daily administration, was partially due to inhibition of cell cycle.

ISHIKAWA 24h

ISHIKAWA 48h

MFE-280 24h

MFE-280 48h

HEC-1A 24h

HEC-1A 48h

PCEM002 24h

PCEM002 48h

PCEM004A 24h

PCEM004A 48h

PCEM004B 24h

PCEM004B 48h

77
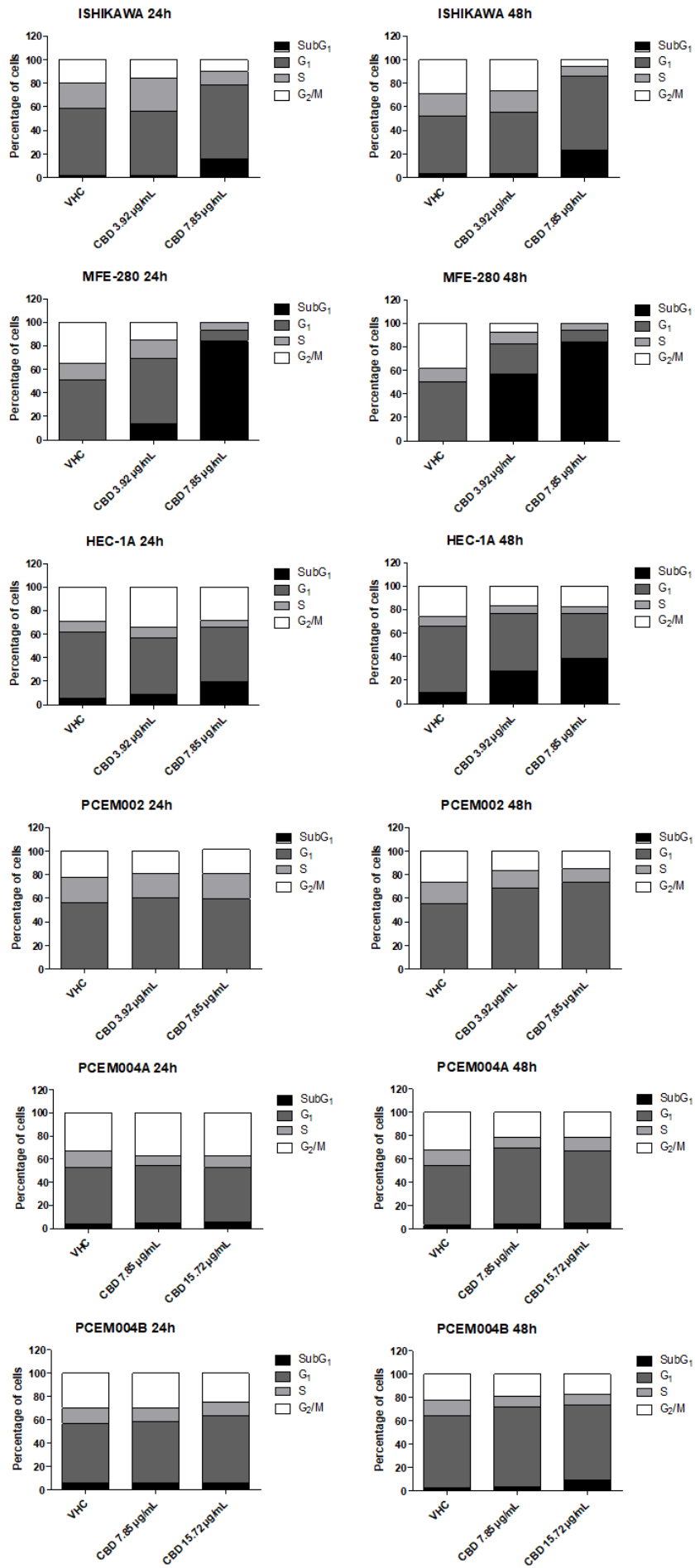
Figure 35. CBD induces cell cycle arrest in EC cell lines. *EC cell lines were treated with CBD up to 15.72 µg/mL for 48 hs. Percentage of cells are represented as histograms representation of the cell cycle phases in the EC cell lines.*

4.13 Daily administration induces autophagy in mixed type I/II primary cell lines

This study investigated the cytotoxic effect of CBD exposure in EC cells by Annexin V-FITC/PI staining. The cell lines were treated with vehicle or CBD in single and daily administration up to 48 hs. Then, fluorescence was analysed by flow cytometry. The results evidenced that CBD treatment induced Annexin V^+ or Annexin V^+PI^+ cells in HEC-1a and all primary cell lines, indicating apoptotic cell death, while only PI^+ cells in Ishikawa and MFE-280 cell lines, indicating a necrotic cell death (Figure 36).

Additionally, we investigated whether increasing of the sub-G1 cell accumulation by CBD treatment was due to an autophagic process in mixed type I/II primary cell lines. We analysed the conversion of the soluble form of LC3 (LC3-I) to the lipidated and autophagosome-associated form (LC3-II), marker of autophagy activation after 48 hs and 72 hs of treatment, using western blot analysis. We found that CBD induced a strong increase of the cleaved LC3-II form and the LC3-II/LC3-I ratio, especially in PCEM004a after 72 hs (Figure 37A). We also evaluated the variation of p62 levels. The results evidenced that CBD is able to induce a slight decrease of the p62 protein level in both cell lines after 48 hs, while an increase was evidenced after 72 hs in PCEM004A cell line (Figure 37A).

Further, to precisely investigate if autophagy was induced CBD treatments, we used acridine orange dye which accumulates in acidic spaces, such as acidic vesicular organelles, considered as indicative marker of autophagy. They emit bright red fluorescence, the intensity of which is proportional to the degree of the acidity and the volume of these structures and we assessed their presence under fluorescence microscope.

As depicted in Figure 37B, CBD treatment promoted acidic vesicular organelles formation after 24 hs, especially at 15.72 µg/ml.
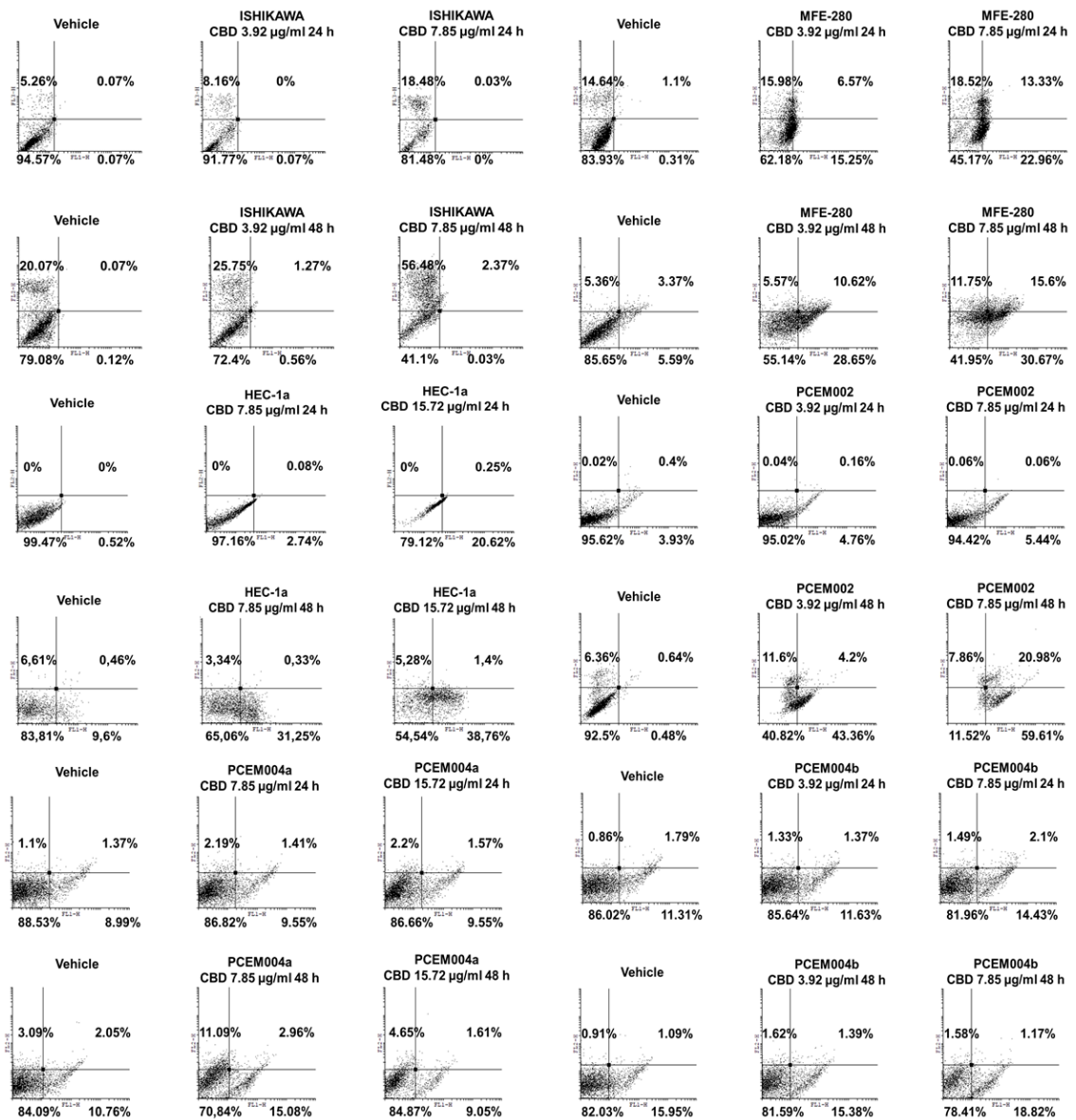
Figure 36. CBD induces apoptosis in endometrial cancer cell lines. *EC cell lines were treated with CBD up to 15.72 μg/mL for 48 hs. Flow cytometry was performed by Annexin V and PI double-staining. Data represent the percentage of PI and/or Annexin V positive cells and are representative of one of three separate experiments.*
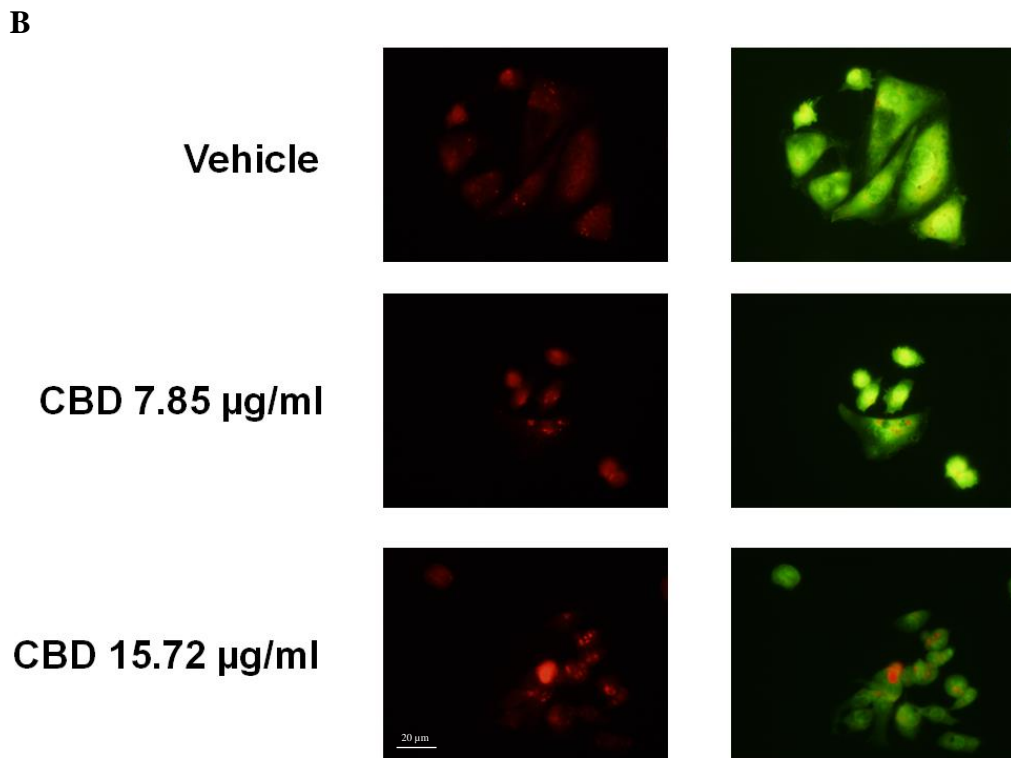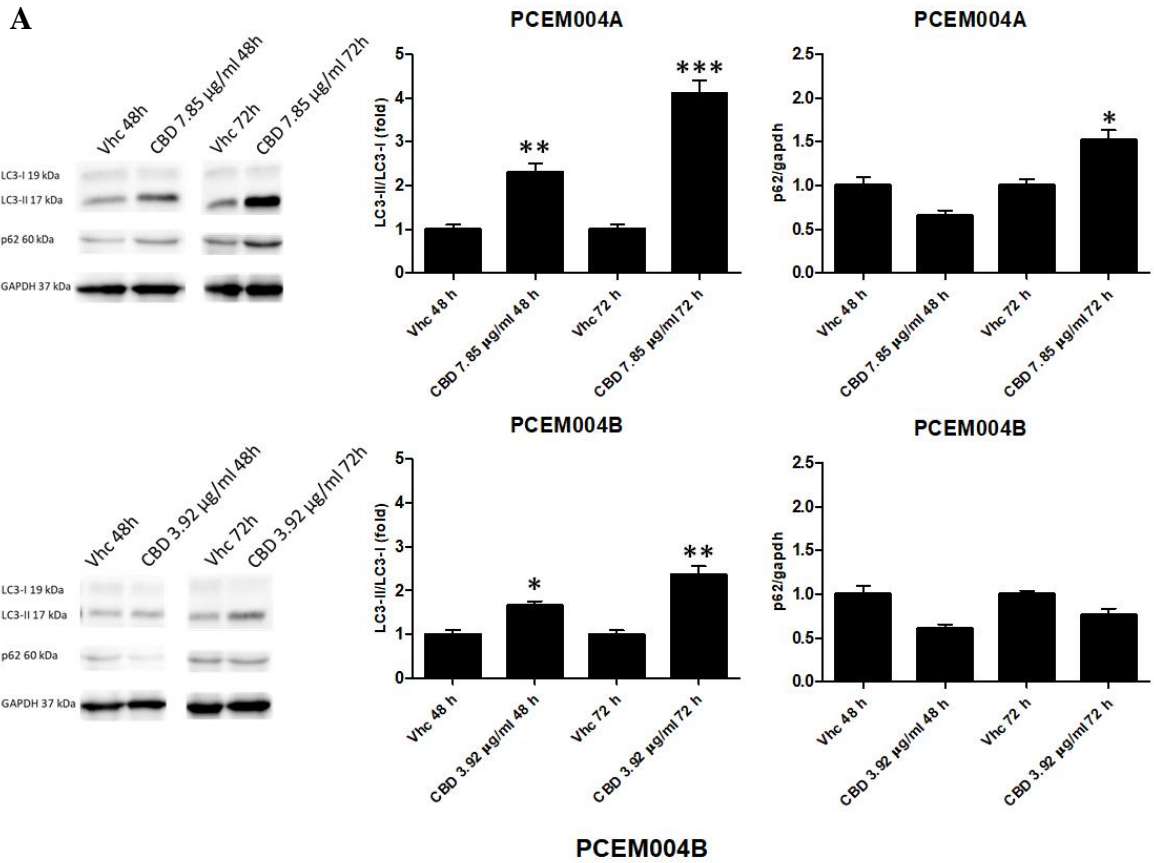
Figure 37. CBD induces autophagy in mixed type I/II endometrial cancer cell lines. *A. Western blot analysis and densitometric quantification of LC3 and p62 protein levels PCEM004a and PCEM004b mixed type EC cell lines treated for up to 72 hs with CBD 7.85 µg/mL and 3.92 µg/mL, respectively. Densitometric values were normalized to GAPDH used as loading control. Blots are representative of one of three separate experiments, *p < 0.05 treated vs untreated cells, #p < 0.05 72 hs vs 48 hs of treatment. B. PCEM004b were treated with CBD up to 15.72 µg/mL for 72 hs and stained with acridine orange. Calibration bar, 20 µm*

4.14 CBD inhibits migratory ability of EC cells

To further investigate anti-tumour effect of CBD, we treated for 24 hs Ishikawa and PCEM004b cells with the appropriate dose of CBD and then we measured cell migration. The results showed that CBD was able to reduce migratory capacity of Ishikawa cells compared with vehicle-treated cells in a dose-dependent manner, with a significant effect at 7.85 µg/mL (p< 0.05) (Figure 38).

In PCEM004b cells, CBD strongly reduced migratory ability of EC cells, already from the lowest doses of 3.92 µg/mL (p< 0.01), up to inhibit completely the migration at 7.85 µg/mL (p< 0.001) (Figure 39).
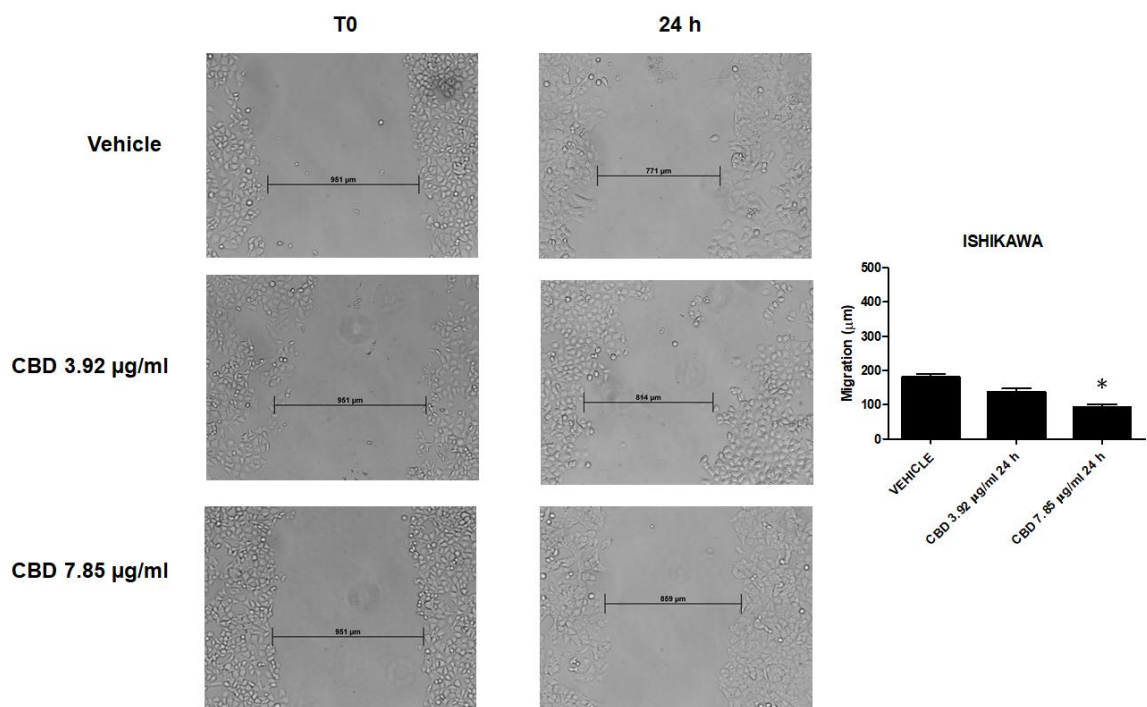
Figure 38. CBD treatment inhibits migration of EC cells. Wound-healing assays for Ishikawa cells after treatment with CBD 7.85 µg/mL and 3.92 µg/mL for 24 hs. All experiments were repeated three times and images were taken at 0 and 24 hs (20x). Data are presented as the mean ± SD. *p < 0.05 vs untreated.
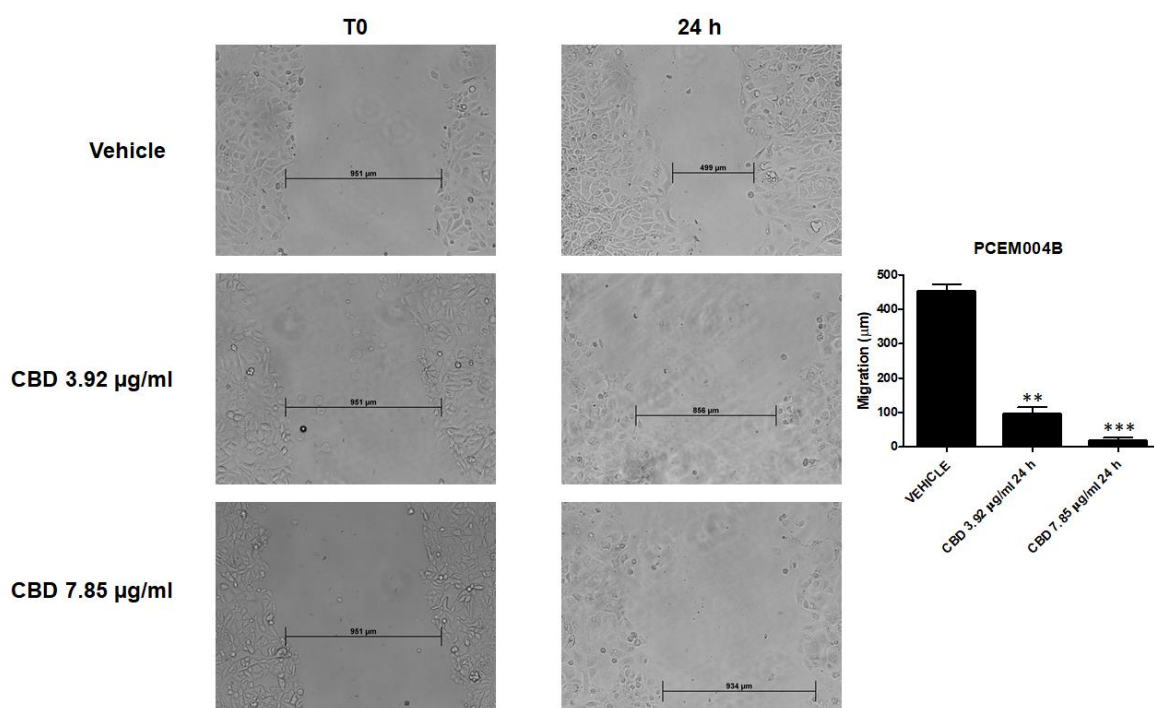
*Figure 39. **CBD treatment inhibits migration of EC cells.** Wound-healing assays for PCEM004b cells after treatment with CBD 7.85 µg/mL and 3.92 µg/mL for 24 hs. All experiments were repeated three times and images were taken at 0 and 24 hs (20x). Data are presented as the mean ± SD. **p < 0.01 vs untreated, ***p < 0.001 vs untreated.*

4.15 CBD synergizes with chemo-drugs used for endometrial cancer treatment

The possible synergism between CBD and chemo-drugs in the three EC cell lines has been evaluated with the aim to reduce the chemo-drugs dosage and toxicity. Ishikawa, PCEM004a and PCEM004b were treated with different doses of Cisplatin, Doxorubicin and Paclitaxel (up to 100 µg/mL) in single administration for 72 hs, in order to find non cytotoxic doses of each chemo-drug. Subsequently, Ishikawa cell line was exposed to CBD at 3.92 µg/mL while PCEM004a and PCEM004b were exposed to CBD at 7.85 µg/mL, in combination with two doses of each chemo-drug (cisplatin 0.5 and 1 µg/mL, Doxorubicin 0.15 and 0.3 µg/mL, Paclitaxel 0.0015 and 0.003 µg/mL for Ishikawa, Cisplatin 0.75 and 1.5 µg/mL, Doxorubicin 0.15 and 0.3 µg/mL for both types of PCEM004, Paclitaxel 0.025 and 0.05 µg/mL for PCEM004a, Paclitaxel 0.1 and 0.2 µg/mL for PCEM004b) for 72 hs. Chemo-drugs were administered once, while CBD was administered daily washing cells with medium after 24 hs. The combined treatment induced an increased level of cytotoxicity, as compared with either CBD or chemo-drugs alone (Figure 40). These results suggest a

synergistic interaction between CBD and chemo-drugs on EC cell lines, thus supporting the feasible use of CBD as an adjuvant in the treatment of human EC.
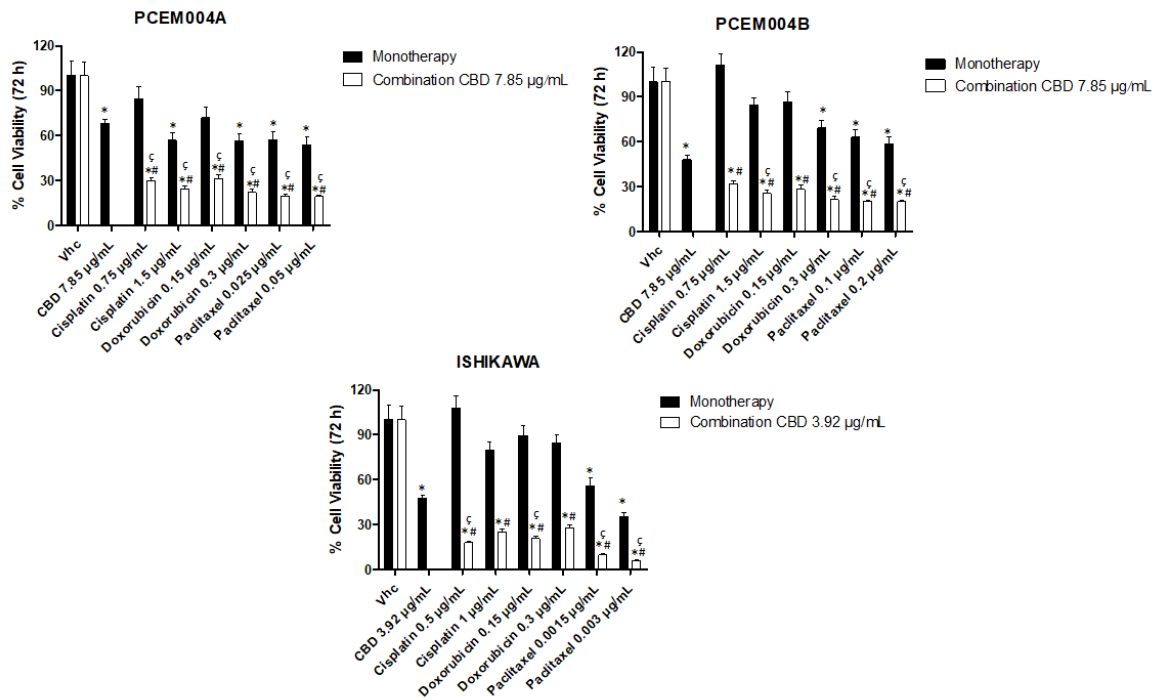
Figure 40. CBD synergizes with chemo-drugs in endometrial cancer cell lines. *Cell viability was determined in EC cell lines by MTT assay. Cells were treated for 72 hs with CBD up to 7.85 µg/mL, alone and in combination with different doses of Cisplatin, Doxorubicin and Paclitaxel. Data shown are expressed as mean ± SE of three separate experiments. *p < 0.05 treated vs vehicle, #p < 0.05 vs chemo-drug alone, çp < 0.05 vs CBD.*

5. DISCUSSION

Endometrial cancer is still the most frequently diagnosed malignancy of the female genital tract, particularly in developed countries (184). The non-endometrioid type II EC is responsible for most EC-related deaths because it is characterized by an aggressive behaviour, a late stage detection and high resistance to the common therapy. Furthermore, there are no targeted therapies for this subtype, and it is still treated in the same way as endometrioid type I EC, which is characterized by good prognosis and good response to therapy. Therefore, type II ECs need new treatment options and molecular target (185).

PD-L1 and PD-L2 are ligands of PD-1 that negatively regulate the activation of T cells allowing tumour immune escape and survival (1), but emerging evidence shows that they also have tumour-intrinsic functions (186-188). The role of immune checkpoints in suppression T cell anti-tumour response, have led to the development of immune checkpoint inhibitor for cancer treatment. Indeed, the blocking antibody (Ab) against PD-1 (Nivolumab and Pembrolizumab) and Ab against PD-L1 (Atezolizumab) have been approved by the US Food and Drug Administration (FDA) to treatment of melanoma and non-small-cell lung cancer (23).

About PD-L2, less is known about its role in cancer and, up to now, there are few information in EC, especially for non-endometrioid EC (189).

Recently, regarding non-endometrioid EC, it is shown that, in a cohort of 53 cases, the expression levels of PD-L1 was detected in tumour and microenvironment in 8 (15%) and in 15 cases (28%), respectively and its expression in tumour area was associated with shorter survival ($p = 0.001$) (190), while regarding PD-L2 in type II ECs, its expression was evaluated in 12 patients and 7 (58,3%) were positive to PD-L2 without a significant difference among patients with different ages, differentiation status, clinical stages, histological types or status of vascular invasion in the tumour (5).

It was reported an unfavourable prognostic effect of PD-L2 significant for OS in glioma (191) and both for OS and DFS/PFS in hepatocellular carcinoma, but, in esophageal cancer, high PD-L2 expression implied a favourable prognosis trend suggesting that PD-L2 has different effects on immune suppression among different cancer types (192).

The current study confirms that EC expresses both PD-1 ligands but PD-L2 is expressed more than its homolog PD-L1. Additionally, we show that PD-L2 expression is higher in serous subtype non-endometrioid EC (69,23% and 15,38% with high and moderate expression respectively) compared with other subtypes. PD-L2 expression correlates with a shorter overall survival (p= 0.0332) and, according to FIGO staging system, a high PD-L2 expression was detected predominantly in stage I-II samples and stage IV samples.

Therefore, we have analyzed the possible molecular mechanisms supporting the negative prognostic role of PD-L2 in EC. Emerging evidence show that PD-L1 and PD-L2 also activate tumor-intrinsic functions (186, 187, 193). Cell-intrinsic PD-L1 regulates cancer cell resistance against apoptosis (186), cell proliferation, AKT/mTOR signalling pathway and autophagy in ovarian cancer cells (187, 188).

Currently, literature describing an intrinsic role of PD-L2 in cancer is scarce.

A recent study demonstrates that cell-intrinsic PD-L2 signals promote invasion and metastasis through the Rhoa-ROCK-LIMK2 and autophagy pathways in osteosarcoma cells (193). In this study, we demonstrate that PD-L2 increases migration and proliferation of mixed type I/II PCEM004b cell line, while the effects are reverted silencing Ishikawa cell line, a type I model that expresses PD-L2.

The Ras/Raf/MEK/ERK and Ras/PI3K/PTEN/Akt pathways interact with each other, regulating a variety of oncogenic processes including cell proliferation, survival, epithelial mesenchymal transition, enhanced motility, angiogenesis and genetic alterations leading to increased PI3K/AKT/mTOR signaling are reported in both type I and type II ECs (194, 195). Previous results clearly suggest that PD-L1 is able to activate an intrinsic signal through the mTOR/AKT pathway, supporting cancer cell proliferation and regulating cell autophagy (187, 188), but there is no evidence for PD-L2 and this pathway. We first demonstrated that PD-L2 overexpression induces an increase in AKT/mTOR activation and a reduction in ERK phosphorylation. Indeed, the Ras-ERK and PI3K-AKT pathways can negatively regulate each other's activity. It has been reported that this cross-inhibition is often revealed when one pathway is chemically blocked, activating thereby the other pathway (195). Furthermore, the clinical significance of the PD-L2 expression and chemotherapy has not been fully investigated. Tanaka *et al*. demonstrated that oesophageal patients with PD-L2 positive tumor had significantly inferior responses to chemotherapy suggesting that PD-1/PD-Ls pathway might be an immunological mechanism associated with resistance to

chemotherapy in oesophageal cancer patients (196). Herein, we found that PD-L2$^+$ EC cells are more sensitive to Paclitaxel than control, and the opposite effect is observed in the PD-L2-silenced cells. However, PD-L2 expression levels did not alter the response to Cisplatin and Doxorubicin. It has been found that a specific inhibition of MEK1/2 kinase activity, associated with a decrease in phospho-ERK, enhanced the effects of nab-Paclitaxel-based chemotherapy in pancreatic ductal adenocarcinoma patients (197). Similarly, elevated levels of activated ERK have been found in paclitaxel-resistant hematopoietic cells and ectopic activation of Raf induces resistance to Doxorubicin and Paclitaxel in breast cancer cells (198). These evidences support our results in which PD-L2 silencing, associated with an increase in pERK1/2/ERK1/2 ratio, are more resistant to Paclitaxel than PD-L2$^+$ cells.

PD-1 ligands are transmembrane protein that binds PD-1 expressed on the cellular surface of activated T and B cells, monocytes, natural killer (NK), and dendritic cells (DCs) (2,5). Recent studies showed also an intracellular distribution, suggesting that these proteins might have an unexpected function, different from what has previously been described for its membranous counterpart (187, 193, 199-201). It has been demonstrated high cytoplasmic PD-L1 levels in SKOV3 and HO8910 ovarian cancer cell lines and, in SKOV3 cells, cytoplasmic PD-L1 increased cancer cell growth and migration (199). In addition to a membrane expression, cytoplasmic PD-L1 was detected also in lymphoma (200) and lung cancer (201). For PD-L2, previous studies reported an expression both membranous and cytoplasmic (193,201-202).

The relative lack of robust diagnostic/prognostic biomarkers for EC, compared with other tumours, and its often-late presentation, interferes with the amelioration of the morbidity and mortality rates associated with this type of cancer. Indeed, the prognosis of EC is based solely on hormone receptor status but is therefore inefficient. This suggests that novel markers should be considered for clinical value (203). Previous reports have documented the expression of all the endocannabinoid system elements in a healthy endometrium while few data are shown about CB receptors and TRPVs expression in EC. Recently, Ayakannu *et al.* have demonstrated that CB1 and CB2 receptors expression, at both the transcript and protein level, were reduced in human samples of both endometrioid and non-endometrioid EC (203). These findings are in contrast with previous studies of Guida *et al.* (204) and Fonseca *et al.* (182) in which is reported, respectively, that CB2 receptor and CB1 receptor are highly expressed in human samples and two EC cell lines, Ishikawa and Hec50co. Our data obtained from TCGA and in six EC cell lines are in accordance with Ayakannu *et al.*

findings. The reason for this could be related to methodological differences, as suggested by the authors (203).

Regarding TRPVs, only Fonseca *et al*. demonstrated that TRPV1 was expressed by Ishikawa and Hec50co cell lines, but no data are provided for another CBD target, TRPV2 (182). In contrast with this finding, we found that TRPV1, at transcript level, is detected in all EC cell lines used but not at protein level. The difference could be explained with the different antibody used and its specificity. We first proved that TRPV2 expression increased with increasing of non-endometrioid component and its expression in human EC samples of Type II and mixed type is associated with a reduced PFS. Additionally, its expression increases with increasing of malignancy, according to FIGO stage. Previously, it has been demonstrated that TRPV2 expression correlates with worse OS and PFS for triple negative breast cancer (140), esophageal squamous cell carcinoma (141), multiple myeloma (144) and gastric cancer (145). Furthermore, its expression increases with increasing of tumour stage in urothelial cancer (138), gastric cancer (145) and esophageal squamous cell carcinoma (141).

TRPV2-mediated signaling pathways modulate some pathological processes, including, cancer (129). Its stimulation by growth factors, cytokines, hormones, and endocannabinoids induces TRPV2 translocation from the endosome to the plasma membrane affecting, in normal cells, both cell proliferation and cell death (137). Indeed, previous evidences show that inactivation of TRPV2-mediated signals in cancer leads to an uncontrolled proliferation and cell death-resistance whereas TRPV2 activation increases migratory capability and invasiveness of cancer cells (135). TRPV2 enhanced migration process of prostate cancer cells through a TRPV2-mediated calcium influx, via Gq/Go, phosphatidylinositol-3,4 kinase (PI3,4K) signaling and translocation of TRPV2 from endosome to the plasma membrane (138). Here, we show that TRPV2$^+$ EC cells have a high migratory ability, and its expression induced an increase of pAKT/AKT ratio supporting the activation of PI3K pathway in TRPV2$^+$ cells that leads to high migratory ability and survival. These data could support the evidence that high expression of TRPV2 in patients correlates with a shorter PFS.

Additionally, increasing TRPV2 expression and activity, CBD, as TRPV2 agonist, is able to enhance drug-uptake. The pore region of TRPV2 has been demonstrated to be critical for ion channel permeation and the resulting increase of glioma chemosensitivity and cytotoxic effects (137) and similar results are shown also for triple negative breast cancer (140).

Treating TRPV2$^+$ EC cells with common chemotherapeutic drugs used in EC therapy, Cisplatin, Doxorubicin and Paclitaxel, the cytotoxic effect of Cisplatin is increased in transfected cells compared to control, suggesting that TRPV2 can increase the chemo-sensitivity and its expression in EC could be considered as a marker useful for optimize the therapy.

During the last twenty years it has been well demonstrated the antitumor effects of cannabinoids in different human cancer cell lines and *in vivo* preclinical models (163-182). The main effects of cannabinoids in inducing an impairment of tumor progression were related to their anti-proliferative, pro-cell death and anti-migratory activities, which were shown in solid and haematological cancers. In glioblastoma, CBD alone and in combination with THC, induced a cell viability reduction and apoptosis *in vitro* and *in vivo* (205, 206). CBD induced apoptotic cell death also in *in vitro* model of lung cancer and in primary cells from patients, and tumour regression in *in vivo* model (167). In breast cancer, CBD inhibited AKT and mTOR signalling inducing autophagic-cell death (172). In multiple myeloma, CBD was able to reduce cell proliferation and induce a necrotic cell death (178). In the present study, data show that CBD induces cell viability impairment in EC cell lines, inducing cell cycle arrest in sub-G0 and in G1-phase in primary cell lines. These data support previous findings regarding the efficacy of CBD as anticancer molecule in different human cancer models. Our data in EC cells confirm anti-cancer effects of CBD. EC cells were treated with different concentration of CBD in single and daily administration and, except for PCEM004b, daily administration was more effective than single administration. Furthermore, MFE-280 cells, a type I model expressing CB1 receptor, showed a higher sensitivity to CBD exposure, compared with the other EC cells.

Recently, Fonseca *et al*. published preliminary data regarding anticancer effect of eCBs, THC and CBD in Ishikawa and Hec50co cell lines, which expressed some characteristics of type II EC. They found that a significant reduction in cell viability was observed with eCBs and CBD in both EC cell types, while, with THC treatment (0.01–25 μM), no changes were observed. In Ishikawa cells, CBD at 5 μM (1.57 μg/mL) induced chromatin condensation, increased levels of ROS/RNS, induced a decrease in mitochondrial membrane potential and an increase of 23% in caspase-3/7 activities, resulting in an apoptotic cell death. Additionally, the proteolytic cleavage of poly(ADP-ribose) polymerase (PARP), an enzyme involved in DNA repair, is a biochemical event that support apoptosis in many cell types

and they found that CBD increased cleaved PARP in Ishikawa cells. Furthermore, although the eCBs were more effective in reducing cell viability in Hec50co cells, they did not cause any increase in the apoptotic markers (182). These data are quite in contrast with our findings. Indeed, CBD induces apoptotic cell death in MFE-280, HEC-1a, and PCEM002 but, in Ishikawa cell line, CBD treatment results in increased PI$^+$/annexin$^-$ cell population and for mixed type I/II cells treatments leads to an autophagic cell death. The main difference is probably related with CBD concentration used and treatment protocol. Indeed, in our study, cells were treated daily and a necrotic cell death in Ishikawa cell line was detected with a higher concentration of CBD compared with Fonseca *et al.* experiments. Additionally, it has been demonstrated that excessive consumption of intracellular ATP or the inhibition of ATP synthesis may convert apoptosis to necrosis. For example, substantial DNA damage leads to the activation of PARP, resulting in a high consumption of NAD$^+$ and ATP molecules and subsequent necrotic death. Furthermore, mitochondria dysfunction can trigger necrosis by ATP depletion and excessive mitochondrial ROS formation and the onset of the mitochondrial permeability transition are also causally linked to the conversion of apoptosis to necroptosis (207).

For cannabinoids, previous data suggest that the combination of cannabinoids and other anti-cancer drugs commonly used in therapy, could act synergistically to reduce tumour growth and chemoresistance. CBD combination with Temozolomide and Carmustine, increases GBM cells death both in vitro and in vivo, overpowering resistance mechanisms and lowering the chemotherapeutic doses, thereby leading to few adverse events (205,206). In triple negative breast cancer, CBD enhanced doxorubicin uptake increasing significantly its anti-tumorigenic effects (173). In multiple myeloma, the CBD and Bortezomib combination was found to be more effective in inducing cancer cell death, compared with bortezomib alone (178). Herein, we confirm that CBD combination with anti-cancer drugs could improve anti-cancer therapy effectiveness. Indeed, combination with Cisplatin, Doxorubicin and Paclitaxel, used at lower doses, induces an increased reduction of cell viability, compared with CBD and chemo-drugs alone.

Another potential anti-cancer activity of cannabinoids is demonstrated in glioma (166), breast cancer (208), lung cancer (168) and multiple myeloma (179), in which cannabinoids treatments were able to reduce cell migration.

CBD reduces migratory capacity of Ishikawa and PCEM004b cells as demonstrated by wound-healing assay, confirming its capability in modulating several pro-tumoral pathways.

6. CONCLUSION

PD-L2, a ligand of PD-1 receptor, is involved in regulating the immune response but, about endometrial cancer, there are few reports. Results show that PD-L2 is involved in aggressiveness and progression of EC. Its overexpression stimulates migration and survival of EC cells, through Akt/mTOR pathway activation. Its intracellular signal could explain the shorter survival of patients with high PD-L2 expression. Indeed, patients with type II and mixed type EC, with high PD-L2 expression, showed a worse overall survival but its expression did not influence progression free-survival. These evidences could support role of PD-L2 as prognostic factor.

It is known that TRPV2 is involved in several intracellular and pathological processes, among them, cancer. In EC, TRPV2 enhances cancer cell proliferation and migration, in an Akt/mTOR-dependent manner, supporting the hypothesis that TRPV2 expression can increase cancer aggressiveness. Additionally, TRPV2 expression influences the clinical outcome of patients. Indeed, Type II EC and mixed type patients with high TRPV2 expression, showed a worse progression-free survival.

Cannabidiol is a TRPV2 agonist that acts in a receptor-dependent and -independent manner. Data show that it is able to induce a cytotoxic effect in EC, inducing cell cycle arrest, cell death and reducing migratory ability of both Type I and Type II EC cells. Additionally, it increases chemo-drugs response allowing an anti-tumour effect with a lower dose. These data support the hypothesis that cannabidiol could be used as novel anti-cancer molecule in an integrative therapy for EC management.

7. BIBLIOGRAPHY

1. Rozali EN, Hato SV, Robinson BW, Lake RA, Lesterhuis WJ. Programmed death ligand 2 in cancer-induced immune suppression. Clin Dev Immunol. (2012) 2012:656340. doi: 10.1155/2012/656340

2. Yang S, Zhang Q, Liu S,Wang AR, You Z. PD-1, PD-L1 and PD-L2 expression in mouse prostate cancer. Am J Clin Exp Urol. (2016) 4:1–8.

3. Ohigashi Y, Sho M, Yamada Y, Tsurui Y, Hamada K, Ikeda N, et al. Clinical significance of programmed death-1 ligand-1 and programmed death-1 ligand-2 expression in human esophageal cancer. Clin Cancer Res. (2005) 11:2947–53. doi: 10.1158/1078-0432.CCR-04-1469

4. Bardhan K, Anagnostou T, Boussiotis VA. The PD1:PD-L1/2 pathway from discovery to clinical implementation. Front Immunol. (2016) 7:550. doi: 10.3389/fimmu.2016.00550

5. Mo Z, Liu J, Zhang Q, Chen Z, Mei J, Liu L, et al. Expression of PD-1, PDL1 and PD-L2 is associated with differentiation status and histological type of endometrial cancer. Oncol Lett. (2016) 12:944–50. doi: 10.3892/ol.2016.4744

6. Liu J, Liu Y, Wang W, Wang C, Che Y. Expression of immune checkpoint molecules in endometrial carcinoma. Exp Ther Med. (2015) 10:1947–52. doi: 10.3892/etm.2015.2714

7. Vanderstraeten A, Luyten C, Verbist G, Tuyaerts S, Amant F. Mapping the immunosuppressive environment in uterine tumors: implications for immunotherapy. Cancer Immunol Immunother. (2014) 63:545–57. doi: 10.1007/s00262-014-1537-8

8. Chen J, Jiang CC, Jin L, Zhang XD. Regulation of PD-L1: a novel role of pro-survival signalling in cancer. Ann Oncol. (2016) 27:409–16. doi: 10.1093/annonc/mdv615

9. He XH, Liu Y, Xu LH, Zeng YY. Cloning and identification of two novel splice variants of human PD-L2. Acta Biochim Biophys Sin. (2004) 36:284–9. doi: 10.1093/abbs/36.4.284

10. Dong Y, Sun Q, Zhang X. PD-1 and its ligands are important immune checkpoints in cancer. Oncotarget. (2017) 8:2171–86. doi: 10.18632/oncotarget.13895

11. Ghiotto M, Gauthier L, Serriari N, Pastor S, Truneh A, Nunès JA, et al. PD-L1 and PD-L2 differ in their molecular mechanisms of interaction with PD-1. Int Immunol. (2010) 22:651–60. doi: 10.1093/intimm/dxq049

12. Zou W, Chen L. Inhibitory B7-family molecules in the tumour microenvironment. Nat Rev Immunol. (2008) 8:467–77. doi: 10.1038/nri2326

13. Chen L, Han X. Anti-PD-1/PD-L1 therapy of human cancer: past, present, and future. J Clin Invest. (2015) 125:3384–91. doi: 10.1172/JCI80011

14. Xiao Y, Yu S, Zhu B, Bedoret D, Bu X, Francisco LM, et al. RGMb is a novel binding partner for PD-L2 and its engagement with PDL2 promotes respiratory tolerance. J Exp Med. (2014) 211:943–59. doi: 10.1084/jem.20130790

15. Liu CQ, Xu J, Zhou ZG, Jin LL, Yu XJ, Xiao G, et al. Expression patterns of programmed death ligand 1 correlate with different microenvironments and patient prognosis in hepatocellular carcinoma. Br J Cancer. (2018) 119:80–8. doi: 10.1038/s41416-018-0144-4

16. Birtalan E, Danos K, Gurbi B, Brauswetter D, Halasz J, Kalocsane Piurko V, et al. Expression of PD-L1 on immune cells shows better prognosis in laryngeal, oropharygeal, and hypopharyngeal cancer. Appl Immunohistochem Mo Morphol. (2018) 26:e79–85. doi: 10.1097/PAI.00000000000 00590

17. Drakes ML, Mehrotra S, Aldulescu M, Potkul RK, Liu Y, Grisoli A, et al. Stratification of ovarian tumor pathology by expression of programmed cell death-1 (PD-1) and PD-ligand- 1 (PD-L1) in ovarian cancer. J Ovarian Res. (2018) 11:43. doi: 10.1186/s13048-018-0414-z

18. Pulko V, Harris KJ, Liu X, Gibbons RM, Harrington SM, Krco CJ, et al. B7-h1 expressed by activated CD8 T cells is essential for their survival. J Immunol. (2011) 187:5606–14. doi: 10.4049/jimmunol.1003976

19. Tang H, Liang Y, Anders RA, Taube JM, Qiu X, Mulgaonkar A, et al. PD-L1 on host cells is essential for PD-L1 blockade-mediated tumor regression. J Clin Invest. (2018) 128:580–8. doi: 10.1172/JCI96061

20. Sepesi B, Cuentas EP, Canales JR, Behrens C, Correa AM, Vaporciyan A, et al. Programmed death cell ligand 1 (PD-L1) is associated with survival in stage I non-small cell lung cancer. Semin Thorac Cardiovasc Surg. (2017) 29:408–15. doi: 10.1053/j.semtcvs.2017.05.008

21. Ojalvo LS, Thompson ED, Wang TL, Meeker AK, Shih IM, Fader AN, et al. Tumor-associated macrophages and the tumor immune microenvironment of primary and recurrent epithelial ovarian cancer. Hum Pathol. (2018) 74:135–47. doi: 10.1016/j.humpath.2017.12.010

22. Zhu J, Wen H, Bi R, Wu Y, Wu X. Prognostic value of programmed deathligand 1 (PD-L1) expression in ovarian clear cell carcinoma. J Gynecol Oncol. (2017) 28:e77. doi: 10.3802/jgo.2017.28.e77

23. Ventriglia J, Paciolla I, Pisano C, Cecere SC, Di Napoli M, Tambaro R, et al. Immunotherapy in ovarian, endometrial and cervical cancer: state of the art and future perspectives. Cancer Treat Rev. (2017) 59:109–16. doi: 10.1016/j.ctrv.2017.07.008

24. Hamanishi J, Mandai M, Abiko K, Matsumura N, Baba T, Yoshioka Y, et al. The comprehensive assessment of local immune status of ovarian cancer by the clustering of multiple immune factors. Clin Immunol. (2011) 141:338–47. doi: 10.1016/j.clim.2011.08.013

25. Duraiswamy J, Freeman GJ, Coukos G. Therapeutic PD-1 pathway blockade augments with other modalities of immunotherapy T-cell function to prevent immune decline in ovarian cancer. Cancer Res. (2013) 73:6900–12. doi: 10.1158/0008-5472.CAN-13-1550

26. Gatalica Z, Snyder C, Maney T, Ghazalpour A, Holterman DA, Xiao N, et al. Programmed cell death 1 (PD-1) and its ligand (PD-L1) in common cancers and their correlation with molecular cancer type. Cancer Epidemiol Biomarkers Prev. (2014) 23:2965–70. doi: 10.1158/1055-9965.EPI-14-0654

27. Turner TB, Buchsbaum DJ, Straughn JM Jr, Randall TD, Arend RC. Ovarian cancer and the immune system - the role of targeted therapies. Gynecol Oncol. (2016) 142:349–56. doi: 10.1016/j.ygyno.2016.05.007

28. Wang Q, Lou W, Di W, Wu X. Prognostic value of tumor PD-L1 expression combined with CD8(+) tumor infiltrating lymphocytes in high grade serous ovarian cancer. Int Immunopharmacol. (2017) 52:7–14. doi: 10.1016/j.intimp.2017.08.017

29. Wieser V, Gaugg I, Fleischer M, Shivalingaiah G, Wenzel S, Sprung S, et al. BRCA1/2 and TP53 mutation status associates with PD-1 and PD-L1 expression in ovarian cancer. Oncotarget. (2018) 9:17501–11. doi: 10.18632/oncotarget.24770

30. Xiao X, Dong D, He W, Song L, Wang Q, Yue J, et al. Mismatch repair deficiency is associated with MSI phenotype, increased tumor-infiltrating lymphocytes and PD-L1 expression in immune cells in ovarian cancer. Gynecol Oncol. (2018) 149:146–54. doi: 10.1016/j.ygyno.2018.02.009

31. Imai Y, Hasegawa K, Matsushita H, Fujieda N, Sato S, Miyagi E, et al. Expression of multiple immune checkpoint molecules on T cells in malignant ascites from epithelial ovarian carcinoma. Oncol Lett. (2018) 15:6457–68. doi: 10.3892/ol.2018.8101

32. Howitt BE, Sun HH, Roemer MG, Kelley A, Chapuy B, Aviki E, et al. Genetic basis for PD-L1 expression in squamous cell carcinomas of the cervix and vulva. JAMA Oncol. (2016) 2:518–22. doi: 10.1001/jamaoncol.2015.6326

33. Sloan EA, Ring KL, Willis BC, Modesitt SC, Mills AM. PD-L1 expressionin mismatch repair-deficient endometrial carcinomas, including lynch syndrome-associated and MLH1 promoter hypermethylated tumors. Am J Surg Pathol. (2017) 41:326–33. doi: 10.1097/PAS.0000000000000783

34. Bregar A, Deshpande A, Grange C, Zi T, Stall J, Hirsch H, et al. Characterization of immune regulatory molecules B7-H4 and PD-L1 in low and high grade endometrial tumors. Gynecol Oncol. (2017) 145:446–52. doi: 10.1016/j.ygyno.2017.03.006

35. Kim J, Kim S, Lee HS, YangW, Cho H, Chay DB, et al. Prognostic implication of programmed cell death 1 protein and its ligand expressions in endometrial cancer. Gynecol Oncol. (2018) 149:381–7. doi: 10.1016/j.ygyno.2018.02.013

36. Kharma B, Baba T, Matsumura N, Kang HS, Hamanishi J, Murakami R, et al. STAT1 drives tumor progression in serous papillary endometrial cancer. Cancer Res. (2014) 74:6519–30. doi: 10.1158/0008-5472.CAN-14-0847

37. Eggink FA, Van Gool IC, Leary A, Pollock PM, Crosbie EJ, Mileshkin L, et al. Immunological profiling of molecularly classified high-risk endometrial cancers identifies POLE-mutant and microsatellite unstable carcinomas as candidates for checkpoint inhibition. Oncoimmunology. (2016) 6:e1264565. doi: 10.1080/2162402X.2016.1264565

38. Yamashita H, Nakayama K, Ishikawa M, Nakamura K, Ishibashi T, Sanuki K, et al. Microsatellite instability is a biomarker for immune checkpoint inhibitors in endometrial cancer. Oncotarget. (2017) 9:5652–64. doi: 10.18632/oncotarget.23790

39. Cancer Genome Atlas Research Network, Albert Einstein College of Medicine, Analytical Biological Services, Barretos Cancer Hospital, Baylor College of Medicine, Beckman Research Institute of City of Hope, et al. Integrated genomic and molecular characterization of cervical cancer. Nature. (2017) 543:378–84. doi: 10.1038/nature21386

40. zur Hausen, H. Papillomaviruses in the causation of human cancers - a brief historical account. Virology. (2009) 384:260–5. doi: 10.1016/j.virol.2008.11.046

41. Zhang H, Zhang T, You Z, Zhang Y. Positive surgical margin, HPV persistence, and expression of both TPX2 and PD-L1 are associated with persistence/recurrence of cervical intraepithelial neoplasia after cervical conization. PLoS ONE. (2015) 10:e0142868. doi: 10.1371/journal.pone.0142868

42. Alexandrov LB, Nik-Zainal S, Wedge DC, Aparicio SA, Behjati S, Biankin AV, et al. Signatures of mutational processes in human cancer. Nature. (2013) 500:415–21. doi: 10.1038/nature12477

43. Lyford-Pike S, Peng S, Young GD, Taube JM, Westra WH, Akpeng B, et al. Evidence for a role of the PD-1:PD-L1 pathway in immune resistance of HPV-associated head and neck squamous cell carcinoma. Cancer Res. (2013) 73:1733–41. doi: 10.1158/0008-5472.CAN-12-2384

44. Yang W, Lu YP, Yang YZ, Kang JR, Jin YD, Wang HW. Expressions of programmed death (PD)-1 and PD-1 ligand (PD-L1) in cervical intraepithelial neoplasia and cervical squamous cell carcinomas are of prognostic value and associated with human papillomavirus status. J Obstet Gynaecol Res. (2017) 43:1602–12. doi: 10.1111/jog.13411

45. Reddy OL, Shintaku PI,Moatamed NA. Programmed death-ligand 1 (PD-L1) is expressed in a significant number of the uterine cervical carcinomas. Diagn Pathol. (2017) 12:45. doi: 10.1186/s13000-017-0631-6

46. Mezache L, Paniccia B, Nyinawabera A, Nuovo GJ. Enhanced expression of PD L1 in cervical intraepithelial neoplasia and cervical cancers. Mod Pathol. (2015) 28:1594–602. doi: 10.1038/modpathol.2015.108

47. Heeren AM, Punt S, Bleeker MC, Gaarenstroom KN, van der Velden J, Kenter GG, et al. Prognostic effect of different PD-L1 expression patterns in squamous cell carcinoma and adenocarcinoma of the cervix. Mod Pathol. (2016) 29:753–63. doi: 10.1038/modpathol.2016.64

48. Piersma SJ. Immunosuppressive tumor microenvironment in cervical cancer patients. Cancer Microenviron. (2011) 4:361–75. doi: 10.1007/s12307-011-0066-7

49. Pfaendler KS, Tewari KS. Changing paradigms in the systemic treatment of advanced cervical cancer. Am J Obstet Gynecol. (2016) 214:22–30. doi: 10.1016/j.ajog.2015.07.022

50. Heeren AM, de Boer E, Bleeker MC, Musters RJ, Buist MR, Kenter GG, et al. Nodal metastasis in cervical cancer occurs in clearly delineated fields of immune suppression in the pelvic lymph catchment area. Oncotarget. (2015) 6:32484–93. doi: 10.18632/oncotarget.5398

51. Hecking T, Thiesler T, Schiller C, Lunkenheimer JM, Ayub TH, Rohr A, et al. Tumoral PD-L1 expression defines a subgroup of poor-prognosis vulvar carcinomas with non-viral etiology. Oncotarget. (2017) 8:92890–903. doi: 10.18632/oncotarget.21641

52. Chinn Z, Stoler MH, Mills AM. PD-L1 and IDO expression in cervical and vulvar invasive and intraepithelial squamous neoplasias: implications for combination immunotherapy. Histopathology. (2019) 74:256–68. doi: 10.1111/his.13723

53. Thangarajah F, Morgenstern B, Pahmeyer C, Schiffmann LM, Puppe J, Mallmann P, et al. Clinical impact of PD-L1 and PD-1 expression in squamous cell cancer of the vulva. J Cancer Res Clin Oncol. (2019) 145:1651–60. doi: 10.1007/s00432-019-02915-1

54. Sznurkowski JJ, Zawrocki A, Sznurkowska K, Peksa R, Biernat W. PDL1 expression on immune cells is a favorable prognostic factor for vulvar squamous cell carcinoma patients. Oncotarget. (2017) 8:89903–12. doi: 10.18632/oncotarget.20911

55. Fleming GF, Emens LA, Eder JP, Hamilton EP, Liu JF, Liu B, et al. Clinical activity, safety and biomarker results from a phase Ia study of atezolizumab (atezo) in advanced/recurrent endometrial cancer (rEC). J Clin Oncol. (2017) 35(Suppl.):5585–5585. doi: 10.1200/JCO.2017.35.15_suppl.5585

56. Ott PA, Bang YJ, Berton-Rigaud D, Elez E, Pishvaian MJ, Rugo HS, et al. Safety and antitumor activity of pembrolizumab in advanced programmed death ligand 1-positive endometrial cancer: results from the KEYNOTE- 028 study. J Clin Oncol. (2017) 35:2535–41. doi: 10.1200/JCO.2017. 72.5952

57. Dai Y, Sun C, Feng Y, JiaQ, Zhu B. Potent immunogenicity in BRCA1-mutated patients with high-grade serous ovarian carcinoma. J Cell Mol Med. (2018) 22:3979–86. doi: 10.1111/jcmm.13678

58. Iwai Y, Hamanishi J, Chamoto K, Honjo T. Cancer immunotherapies targeting the PD 1 signaling pathway. J Biomed Sci. (2017) 24:26. doi: 10.1186/s12929-017-0329-9

59. Hamanishi J,MandaiM, Ikeda T,MinamiM, Kawaguchi A,Murayama T, et al. Safety and antitumor activity of anti-PD-1 antibody, nivolumab, in patients with platinum resistant ovarian cancer. J Clin Oncol. (2015) 33:4015–22. doi: 10.1200/JCO.2015.62.3397

60. Frenel JS, Le Tourneau C, O'Neil B, Ott PA, Piha-Paul SA, Gomez-Roca C, et al. Safety and efficacy of pembrolizumab in advanced, programmed death ligand 1-positive cervical cancer: results from the phase Ib KEYNOTE-028 trial. J Clin Oncol. (2017) 35:4035–41. doi: 10.1200/JCO.2017.74.5471

61. Chung HC, Schellens JHM, Delord JP, Perets R, Italiano A, Shapira-Frommer R, et al. Pembrolizumab treatment of advanced cervical cancer: updated results from the phase 2 KEYNOTE-158 study. J Clin Oncol. (2018) 36(Suppl.15):5522. doi: 10.1200/JCO.2018.36.15_suppl.5522

62. Callahan MK, Wolchok JD. At the bedside: CTLA-4- and PD-1-blocking antibodies in cancer immunotherapy. J Leukoc Biol. (2013) 94:41–53. doi: 10.1189/jlb.1212631

63. Zitvogel L, Kroemer G. Targeting PD-1/PD-L1 interactions for cancer immunotherapy. Oncoimmunology. (2012) 1:1223–5. doi: 10.4161/onci.21335 64. O'Donnell JS, Long GV, Scolyer RA, Teng MW, Smyth MJ. Resistance to PD1/PDL1 checkpoint inhibition. Cancer Treat Rev. (2017) 52:71–81.doi: 10.1016/j.ctrv.2016.11.007

65. Martins F, Sofiya L, Sykiotis GP, Lamine F, Maillard M, Fraga M, et al. Adverse effects of immune-checkpoint inhibitors: epidemiology, management and surveillance. Nat Rev Clin Oncol. (2019) 16:563–80. doi: 10.1038/s41571-019-0218-0

66. Swart M, Verbrugge I, Beltman JB. Combination approaches with immunecheckpoint blockade in cancer therapy. Front Oncol. (2016) 6:233. doi: 10.3389/fonc.2016.00233

67. Jin L, Lee EM, Ramshaw HS, Busfield SJ, Peoppl AG, Wilkinson L, et al. Monoclonal antibody-mediated targeting of CD123, IL-3 receptor alpha chain, eliminates human acute myeloid leukemic stem cells. Cell Stem Cell. (2009) 5:31–42. doi: 10.1016/j.stem.2009.04.018

68. Muñoz L, Nomdedéu JF, López O, Carnicer MJ, Bellido M, Aventín A, et al. Interleukin-3 receptor alpha chain (CD123) is widely expressed in hematologic malignancies. Haematologica. (2001) 86:1261–9.

69. Kobold S, Pantelyushin S, Rataj F, Vom Berg J. Rationale for combining bispecific T cell activating antibodies with checkpoint blockade for cancer therapy. Front Oncol. (2018) 8:285. doi: 10.3389/fonc.2018.00285

70. Krupka C, Kufer P, Kischel R, Zugmaier G, Lichtenegger FS, Köhnke T, et al. Blockade of the PD-1/PD-L1 axis augments lysis of AML cells by the CD33/CD3 BiTE antibody construct AMG 330: reversing a T cell- induced immune escape mechanism. Leukemia. (2016) 30:484–91. doi: 10.1038/leu.2015.214

71. Waldmann TA. Cytokines in cancer immunotherapy. Cold Spring Harb Perspect Biol. (2018) 10:a028472. doi: 10.1101/cshperspect. a028472

72. Charych DH, Hoch U, Langowski JL, Lee SR, Addepalli MK, Kirk PB, et al. NKTR 214, an engineered cytokine with biased IL2 receptor binding, increased tumor exposure, and marked efficacy in mouse tumor models. Clin Cancer Res. (2016) 22:680–90. doi: 10.1158/1078-0432.CCR- 15-1631

73. Siefker-Radtke AO, Baron AD, Necchi A, Plimack ER, Pal SK, Bedke J, et al. Nivolumab monotherapy in patients with advanced platinum-resistant urothelial carcinoma: efficacy and safety update from CheckMate 275. J Clin Oncol. (2019) 37:(Suppl. 15):4524. doi: 10.1200/JCO.2019.37.15_suppl.4524

74. Garris CS, Arlauckas SP, Kohler RH, Trefny MP, Garren S, Piot C, et al. Successful anti-PD-1 cancer immunotherapy requires T cell-dendritic cell crosstalk involving the cytokines IFN-g and IL-12. Immunity. (2018) 49:1148–61. doi: 10.1016/j.immuni.2018.09.024

75. PDQ Adult Treatment Editorial Board. Uterine Sarcoma Treatment (PDQ®): Patient Version. 2019 Jun 12. PDQ Cancer Information Summaries [Internet]. Bethesda (MD): National Cancer Institute (US); 2002-.

76. Human Anatomy and Physiology. 27.2 Anatomy and Physiology of the Female Reproductive System by Rice University.

77. Di Blasio AM, Vignali M, Gentilini D. The endocannabinoid pathway and the female reproductive organs. J Mol Endocrinol. (2013) 50(1):R1-9.

78. Keefe DL, Wright KP. Chapter 2 - Reproductive Physiology, Editor(s): Andrew I. Sokol, Eric R. Sokol, General Gynecology, Mosby (2007) 21-41, ISBN 9780323032476, doi.org/10.1016/B978-032303247-6.10002-4.

79. Lessey BA, Young SL, Chapter 9 - Structure, Function, and Evaluation of the Female Reproductive Tract, Editor(s): Jerome F. Strauss, Robert L. Barbieri, Yen and Jaffe's Reproductive Endocrinology (Eighth Edition), (2019), 206-247.e13, ISBN 9780323479127. doi.org/10.1016/B978-0-323-47912-7.00009-3.

80. Siegel R, Naishadham D, Jemal A. Cancer statistics, 2013. CA Cancer J Clin. (2013) 63: 11–30.

81. Cancer Research UK. Uterine cancer statistics. http://info.cancerresearchuk.org/cancerstats/types/uterus/ (accessed Nov,2019).

82. Doll A, Abal M, Rigau M, et al. Novel molecular profiles of endometrial cancer-new light through old windows. J Steroid Biochem Mol Biol. (2008) 108(3-5): 221-229.

83. Ma X, Ma C and Wang J. Endometrial Carcinogenesis and Molecular Signaling Pathways. American Journal of Molecular Biology. (2014) 4: 134-149. doi: 10.4236/ajmb.2014.43015.

84. Talhouk A, McAlpine JN. New classification of endometrial cancers: the development and potential applications of genomic-based classification in research and clinical care. Gynecol Oncol Res Pract. (2016) 3:14. doi: 10.1186/s40661-016-0035-4.

85. Bansal N, Yendluri V, Wenham RM. The molecular biology of endometrial cancers and the implications for pathogenesis, classification, and targeted therapies. Cancer Control. (2009) 16(1): 8-13.

86. Mutter GL, Lin MC, Fitzgerald JT, et al. Altered PTEN expression as a diagnostic marker for the earliest endometrial precancers. J Natl Cancer Inst. (2000) 92(11): 924-930.

87. Sonoda K. Molecular biology of gynecological cancer. Oncol Lett. (2016) 1: 16-22.

88. Orbo A, Nilsen MN, Arnes MS, Pettersen I, Larsen K. Loss of expression of MLH1, MSH2, MSH6, and PTEN related to endometrial cancer in 68 patients with endometrial hyperplasia. Int J Gynecol Pathol. (2003) (2):141-8.

89. Żyła MM, Wilczyński JR, Kostrzewa M, Księżakowska-Łakoma K, Nowak M, Stachowiak G, et al. The significance of markers in the diagnosis of endometrial cancer. Prz Menopauzalny. (2016) 15(3): 176-185.

90. Merritt MA, Cramer DW. Molecular pathogenesis of endometrial and ovarian cancer. Cancer Biomark. (2010) 9(1-6): 287-305. doi: 10.3233/CBM-2011-0167.

91. Hoffman BL, Schorge JO, Schaffer JI, Halvorson LM, Bradshaw KD, Cunningham FG. "Endometrial Cancer". Williams Gynecology (2nd ed.). McGraw-Hill. (2012) p. 823. ISBN 978-0-07-171672-7.

92. American Joint Committee on Cancer. Corpus Uteri-Carcinoma and Carcinosarcoma. In: AJCC Cancer Staging Manual. 8th ed. New York, NY: Springer; (2017) :661-669.

93. Khatuja R., Rai S. Endometrial Carcinoma: Epidemiology and Risk Factors. In: Mehta S., Singla A. (eds) Preventive Oncology for the Gynecologist. (2019) Springer, Singapore

94. Calle EE, Rodriguez C, Walker-Thurmond K, Thun MJ. Overweight, obesity, and mortality from cancer in a prospectively studied cohort of U.S. Adults. N Engl J Med. (2003) 348:1625–38.

95. Renehan AG, Tyson M, Egger M, et al. Body-mass index and incidence of cancer: a systematic review and meta-analysis of prospective observational studies. Lancet. (2008) 371:569.

96. Setiawan VW, Yang HP, Pike MC, McCann SE, Yu H, Xiang YB, et al. Type I and II endometrial cancers: have they different risk factors? J Clin Oncol. (2013) 31(20):2607-18. doi: 10.1200/JCO.2012.48.2596.

97. Angeles MA, Martínez-Gómez C, Migliorelli F, Voglimacci M, Figurelli J, Motton S, et al. Novel Surgical Strategies in the Treatment of Gynecological Malignancies. Curr Treat Options Oncol. (2018) ;19(12):73.

98. Cowan M, Strauss JB, Barber EL, Matei D. Updates on adjuvant chemotherapy and radiation therapy for endometrial cancer. Curr Opin Obstet Gynecol. (2019) 31(1):31-37

99. McDonald ME, Bender DP. Endometrial Cancer: Obesity, Genetics, and Targeted Agents. Obstet Gynecol Clin North Am. (2019) 46(1):89-105.

100. de Haydu C, Black JD, Schwab CL, English DP, Santin AD. An update on the current pharmacotherapy for endometrial cancer. Expert Opin Pharmacother. (2016) 17(4):489-499.

101. Lee YC, Lheureux S, Oza AM. Treatment strategies for endometrial cancer: current practice and perspective. Curr Opin Obstet Gynecol. (2017) 29(1):47-58. doi: 10.1097/GCO.0000000000000338.

102. ElSohly MA, Radwan MM, Gul W, Chandra S, Galal A. Phytochemistry of Cannabis sativa L. Prog Chem Org Nat Prod. (2017) 103:1-36.

103. Zuardi AW. History of cannabis as a medicine: a review. Braz J Psychiatry. (2006) 28(2):153-7.

104. Spitzer-Rimon B, Duchin S, Bernstein N, Kamenetsky R. Architecture and Florogenesis in Female Cannabis sativa Plants. Front Plant Sci. (2019) 10:350.

105. Solymosi K, Köfalvi A. Cannabis: A Treasure Trove or Pandora's Box? Mini Rev Med Chem. (2017) 17(13): 1223-1291.

106. Lu HC, Mackie K. An Introduction to the Endogenous Cannabinoid System. Biol Psychiatry. (2016) 79(7): 516-25.

107. Walker OS, Holloway AC, Raha S. The role of the endocannabinoid system in female reproductive tissues. J Ovarian Res. 2019 Jan 15;12(1):3. doi: 10.1186/s13048-018-0478-9.

108. Di Marzo V, Melck D, Bisogno T, De Petrocellis L. Endocannabinoids: endogenous cannabinoid receptor ligands with neuromodulatory ac-tion. Trends Neurosci. (1998) 21(12):521-8.

109. Laprairie RB, Bagher AM, Denovan-Wright EM. Cannabinoid receptor ligand bias: implications in the central nervous system. Curr Opin Pharmacol. (2017) 32: 32-43.

110. Guzmán M. Cannabinoids: potential anticancer agents. Nat Rev Cancer. (2003) 3(10): 745-55.

111. Appendino G, Chianese G, Taglialatela-Scafati O. Cannabinoids: occurrence and medicinal chemistry. Curr Med Chem. 2011;18(7):1085-99.

112. Grotenhermen F. Pharmacokinetics and pharmacodynamics of cannabinoids. Clin Pharmacokinet. (2003) 42(4):327-60.

113. Grant KS, Petroff R, Isoherranen N, Stella N, Burbacher TM. Cannabis use during pregnancy: Pharmacokinetics and effects on child development. Pharmacol Ther. (2018) 82: 133-151. doi: 10.1016/j.pharmthera.2017.08.014.

114. Lucas CJ, Galettis P, Schneider J. The pharmacokinetics and the pharmacodynamics of cannabinoids. Br J Clin Pharmacol. (2018) 84(11): 2477-2482. doi: 10.1111/bcp.13710.

115. Laprairie RB, Bagher AM, Kelly ME, Denovan-Wright EM. Cannabidiol is a negative allosteric modulator of the cannabinoid CB1 receptor. Br J Pharmacol. (2015) 172(20):4790-805. doi: 10.1111/bph.13250.

116. Das SK, Paria BC, Chakraborty I and Dey SK. Cannabinoid ligand receptor signaling in the mouse uterus. PNAS (1995) 92. 4332–4336. doi:10.1073/pnas.92.10.4332

117. Schmid PC, Paria BC, Krebsbach RJ, Schmid HH and Dey SK. Changes in anandamide levels in mouse uterus are associated with uterine receptivity for embryo implantation. PNAS (1997) 94: 4188–4192. doi:10.1073/pnas.94.8.4188

118. Taylor AH, Abbas MS, Habiba MA and Konje JC. Histomorphometric evaluation of cannabinoid receptor and anandamide modulating enzyme expression in the human endometrium through the menstrual cycle. Histochemistry and Cell Biology (2010a) 133: 557–565. doi:10.1007/s00418-010-0695-9

119. Resuehr D, Glore DR, Taylor HS, Bruner-Tran KL and Osteen KG. Progesterone dependent regulation of endometrial cannabinoid receptor type 1 (CB1-R) expression is disrupted in women with endometriosis and in isolated stromal cells exposed to 2,3,7,8-tetrachlorodibenzo-p-dioxin (TCDD). Fertility and Sterility (2012) 98: 948.e1–956.e1. doi:10.1016/j.fertnstert.2012.06.009

120. Taylor AH, Amoako AA, Bambang K, Karasu T, Gebeh A, Lam PM, et al. Endocannabinoids and pregnancy. Clinica Chimica Acta (2010b) 411: 921–930. doi:10.1016/j.cca.2010.03.012

121. Maccarrone M, Bisogno T, Valensise H, Lazzarin N, Fezza F, Manna C, et al. Low fatty acid amide hydrolase and high anandamide levels are associated with failure to achieve ongoing pregnancy after IVF and embryo transfer. Molecular Human Reproduction (2002) 8: 188–195. doi:10.1093/molehr/8.2.188

122. Gentilini D, Besana A, Vigano P, Dalino P, Vignali M, Melandri M, et al. The Endocannabinoid system regulates migration of endometrial stromal cells via cannabinoid receptor 1 through the activation of PI3K and ERK1/2 pathways. Fertility and Sterility (2010) 93: 2588–2593. doi:10.1016/j.fertnstert.2010.02.006

123. McHugh DJ, Page Dunn E and Bradshaw HB. Delta(9)-THC and N-arachidonyl glycine are full agonists at GPR18 and cause migration in the human endometrial cell line, HEC-1B. British Journal of Pharmacology (2011) 8. 2411–2413.

124. Leconte M, Nicco C, Ngo C, Arkwright S, Chereau C, Guibourdenche J, et al. Antiproliferative effects of cannabinoid agonists on deep infiltrating endometriosis. American Journal of Pathology (2010) 177 2963–2970. doi:10.2353/ajpath. 2010.100375

125. Ellert-Miklaszewska A, Ciechomska I and Kaminska B. Cannabinoid signaling in glioma cells. Advances in Experimental Medicine and Biology (2013) 986: 209–220.

126. Santoni G, Morelli MB, Amantini C, Santoni M, Nabissi M, Marinelli O, et al. "Immuno-Transient Receptor Potential Ion Channels": The Role in Monocyte- and Macrophage-Mediated Inflammatory Responses. Front Immunol. (2018) 9:1273. doi: 10.3389/fimmu.2018.01273

127. Muller C, Morales P, Reggio PH. Cannabinoid Ligands Targeting TRP Channels. Front Mol Neurosci. (2019) 11:487. doi: 10.3389/fnmol.2018.00487.

128. De Petrocellis L, Nabissi M, Santoni G, Ligresti A. Actions and Regulation of Ionotropic Cannabinoid Receptors. Adv Pharmacol. (2017) 80: 249-289.

129. Santoni G, Amantini C, Maggi F, Marinelli O, Santoni M, Nabissi M, Morelli MB. The TRPV2 cation channels: from urothelial cancer invasiveness to glioblastoma multiforme interactome signature. Lab Invest. (2019). [Epub ahead of print] doi: 10.1038/s41374-019-0333-7

130. De Clercq K, Held K, Van Bree R, Meuleman C, Peeraer K, Tomassetti C, et al. Functional expression of transient receptor potential channels in human endometrial stromal cells during the luteal phase of the menstrual cycle. Hum Reprod. (2015) 30(6):1421-36. doi: 10.1093/humrep/dev068.

131. Persoons E, Hennes A, De Clercq K, Van Bree R, Vriens G, O DF, et al. Functional Expression of TRP Ion Channels in Endometrial Stromal Cells of Endometriosis Patients. Int J Mol Sci. (2018) 19(9). pii: E2467. doi: 10.3390/ijms19092467.

132. Gambade A, Zreika S, Guéguinou M, Chourpa I, Fromont G, Bouchet A.M, et al. Activation of TRPV2 and BKCa channels by the LL-37 enantiomers stimulates calcium entry and migration of cancer cells. Oncotarget (2016) 7: 23785–23800. doi:10.18632/oncotarget.8122.

133. Waning J, Vriens J, Owsianik G, Stüwe L, Mally S, Fabian A, et al. A novel function of capsaicin-sensitive TRPV1 channels: Involvement in cell migration. Cell Calcium (2007) 42: 17–25.

134. Graziani A, Poteser M, Heupel W.M, Schleifer H, Krenn M, Drenckhahn D, et al. Cell-cell contact formation governs Ca2+ signaling by TRPC4 in the vascular endothelium: Evidence for a regulatory TRPC4-β-catenin interaction. J. Biol. Chem. (2010) 285: 4213–4223. doi: 10.1074/jbc.M109.060301.

135. Liberati S, Morelli MB, Amantini C, Farfariello V, Santoni M, Conti A, et al. Loss of TRPV2 Homeostatic Control of Cell Proliferation Drives Tumor Progression. Cells (2014) 3: 112–128. doi: 10.3390/cells3020660

136. Sagredo AI, Sagredo EA, Cappelli C, Báez P, Andaur RE, Blanco C, et al. TRPM4 regulates Akt/GSK3 activity and enhances catenin signaling and cell proliferation in prostate cancer cells. Mol. Oncol. (2018) 12: 151–165. doi: 10.1002/1878-0261.12100.

137. Liberati S, Morelli MB, Amantini C, Santoni M, Nabissi M, Cardinali C, et al. Advances in transient receptor potential vanilloid-2 channel expression and function in tumor growth and progression. Curr Protein Pept Sci. (2014) 15:732–7.

138. Monet M, Gkika D, Lehen'kyi V, Pourtier A, Vanden Abeele F, Bidaux G, et al. Lysophospholipids stimulate prostate cancer cell migration via TRPV2 channel activation. Biochim Biophys Acta. (2009)1793: 528–39.

139. Monet M, Lehen'kyi V, Gackiere F, Firlej V, Vandenberghe M, Roudbaraki M, et al. Role of cationic channel TRPV2 in promoting prostate cancer migration and progression to androgen resistance. Cancer Res. (2010) 70:1225–35. doi: 10.1158/0008-5472.CAN-09-2205.

140. Elbaz M, Ahirwar D, Xiaoli Z, Zhou X, Lustberg M, Nasser MW, et al. TRPV2 is a novel biomarker and therapeutic target in triple negative breast cancer. Oncotarget. (2016) 9(71): 33459-33470. doi: 10.18632/oncotarget.9663.

141. Zhou K, Zhang SS, Yan Y, Zhao S. Overexpression of transient receptor potential vanilloid 2 is associated with poor prognosis in patients with esophageal squamous cell carcinoma. Med Oncol. (2014) 31(7):17. doi: 10.1007/s12032-014-0017-5.

142. Liu G, Xie C, Sun F, Xu X, Yang Y, Zhang T, et al. Clinical significance of transient receptor potential vanilloid 2 expression in human hepatocellular carcinoma. Cancer Genet Cytogenet. (2010) 197(1):54-9. doi: 10.1016/j.cancergencyto.2009.08.007.

143. Alptekin M, Eroglu S, Tutar E, Sencan S, Geyik MA, Ulasli M, et al. Gene expressions of TRP channels in glioblastoma multiforme and relation with survival. Tumour Biol. (2015) 36(12): 9209-13. doi: 10.1007/s13277-015-3577-x.

144. Bai H, Zhu H, Yan Q, Shen X, Lu X, Wang J, et al. TRPV2-induced Ca(2+)-calcineurin NFAT signaling regulates differentiation of osteoclast in multiple myeloma. Cell Commun Signal. (2018) 16(1):68. doi: 10.1186/s12964-018-0280-8.

145. Zoppoli P, Calice G, Laurino S, Ruggieri V, La Rocca F, La Torre G, et al. TRPV2 Calcium Channel Gene Expression and Outcomes in Gastric Cancer Patients: A Clinically Relevant Association. J Clin Med. (2019) 8(5). pii: E662. doi: 10.3390/jcm8050662.

146. Zheng J, Liu F, Du S, Li M, Wu T, Tan X, et al. Mechanism for Regulation of Melanoma Cell Death via Activation of Thermo-TRPV4 and TRPV2. J Oncol. (2019) 2019:7362875. doi: 10.1155/2019/7362875.

147. Pellati F, Borgonetti V, Brighenti V, Biagi M, Benvenuti S, Corsi L. Cannabis sativa L. and Nonpsychoactive Cannabinoids: Their Chemistry and Role against Oxidative Stress,

Inflammation, and Cancer. Biomed Res Int. (2018) 2018: 1691428. doi: 10.1155/2018/1691428.

148. Pisanti S, Malfitano AM, Ciaglia E, Lamberti A, Ranieri R, Cuomo Get al. Cannabidiol: State of the art and new challenges for therapeutic applications. Pharmacol Ther. (2017) 175: 133-150. doi: 10.1016/j.pharmthera.2017.02.041.

149. Kargl J, Andersen L, Hasenöhrl C, Feuersinger D, Stančić A, Fauland A, et al. GPR55 promotes migration and adhesion of colon cancer cells indicating a role in metastasis. Br J Pharmacol. (2016) 173(1) :142-54. doi: 10.1111/bph.13345.

150. Silvestro S, Mammana S, Cavalli E, Bramanti P, Mazzon E. Use of Cannabidiol in the Treatment of Epilepsy: Efficacy and Security in Clinical Trials. Molecules. (2019) 24(8). pii: E1459. doi: 10.3390/molecules24081459.

151. Grotenhermen F. Pharmacokinetics and pharmacodynamics of cannabinoids. Clin Pharmacokinet. (2003) 42(4):327-60.

152. Harvey DJ, Mechoulam R. Metabolites of cannabidiol identified in human urine. Xenobiotica. (1990) 20(3):303-20.

153. Samara E, Bialer M, Harvey DJ. Identification of glucose conjugates as major urinary metabolites of cannabidiol in the dog. Xenobiotica. (1990) 20(2):177-83.

154. Rosenkrantz H, Fleischman RW, Grant RJ. Toxicity of short-term administration of cannabinoids to rhesus monkeys. Toxicol Appl Pharmacol. (1981) 58(1):118-31.

155. Ribeiro A, Ferraz-de-Paula V, Pinheiro ML, Vitoretti LB, Mariano-Souza DP, Quinteiro-Filho WM, et al. Cannabidiol, a non-psychotropic plant-derived cannabinoid, decreases inflammation in a murine model of acute lung injury: role for the adenosine A(2A) receptor. Eur J Pharmacol. (2012) 678(1-3): 78-85. doi: 10.1016/j.ejphar.2011.12.043.

156. Ribeiro A, Almeida VI, Costola-de-Souza C, Ferraz-de-Paula V, Pinheiro ML, Vitoretti LB, et al. Cannabidiol improves lung function and inflammation in mice submitted to LPS-induced acute lung injury. Immunopharmacol Immunotoxicol. (2015) 37(1):35-41. doi: 10.3109/08923973.2014.976794.

157. Saijo K, Glass CK. Microglial cell origin and phenotypes in health and disease. Nat Rev Immunol. (2011) 11(11): 775-87. doi: 10.1038/nri3086.

158. Kozela E, Pietr M, Juknat A, Rimmerman N, Levy R, Vogel Z. Cannabinoids Delta(9)-tetrahydrocannabinol and cannabidiol differentially inhibit the lipopolysaccharide-activated NF-kappaB and interferon-beta/STAT proinflammatory pathways in BV-2 microglial cells. J Biol Chem. (2010) 285(3): 1616-26. doi: 10.1074/jbc.M109.069294.

159. De Filippis D, Esposito G, Cirillo C, Cipriano M, De Winter BY, Scuderi C, et al. Cannabidiol reduces intestinal inflammation through the control of neuroimmune axis. PLoS One. (2011) 6(12):e28159. doi: 10.1371/journal.pone.0028159.

160. Hegde VL, Singh UP, Nagarkatti PS, Nagarkatti M. Critical Role of Mast Cells and Peroxisome Proliferator-Activated Receptor γ in the Induction of Myeloid-Derived Suppressor Cells by Marijuana Cannabidiol In Vivo. J Immunol. (2015) 194(11): 5211-22. doi: 10.4049/jimmunol.1401844.

161. Ali TH, Pisanti S, Ciaglia E, Mortarini R, Anichini A, Santinami M, et al. Enrichment of KIR+CD57+ highly cytotoxic NK cells in sentinel lymph nodes of melanoma patients. J Transl Med. (2014) 12(Suppl 1):P10. doi: 10.1186/1479-5876-12-S1-P10.

162. Childs RW, Carlsten M. Therapeutic approaches to enhance natural killer cell cytotoxicity against cancer: the force awakens. Nat Rev Drug Discov. (2015) 14(7):487-98. doi: 10.1038/nrd4506.

163. Nabissi M, Morelli MB, Amantini C, Liberati S, Santoni M, Ricci-Vitiani L, et al. Cannabidiol stimulates Aml-1a-dependent glial differentiation and inhibits glioma stem-like cells proliferation by inducing autophagy in a TRPV2-dependent manner. Int J Cancer. (2015) 137(8):1855-69. doi: 10.1002/ijc.29573.

164. Ivanov VN, Wu J, Hei TK. Regulation of human glioblastoma cell death by combined treatment of cannabidiol, γ-radiation and small molecule inhibitors of cell signalling pathways. Oncotarget. (2017) 8(43):74068-74095. doi: 10.18632/oncotarget.18240.

165. Massi P, Vaccani A, Ceruti S, Colombo A, Abbracchio MP, Parolaro D. Antitumor effects of cannabidiol, a nonpsychoactive cannabinoid, on human glioma cell lines. J Pharmacol Exp Ther. (2004) 308(3):838-45.

166. Vaccani A, Massi P, Colombo A, Rubino T, Parolaro D. Cannabidiol inhibits human glioma cell migration through a cannabinoid receptor-independent mechanism. Br J Pharmacol. (2005) 144(8):1032-6.

167. Ramer R, Heinemann K, Merkord J, Rohde H, Salamon A, Linnebacher M, et al. COX-2 and PPAR-γ confer cannabidiol-induced apoptosis of human lung cancer cells. Mol Cancer Ther. (2013) 12(1):69-82. doi: 10.1158/1535-7163.MCT-12-0335.

168. Ramer R, Bublitz K, Freimuth N, Merkord J, Rohde H, Haustein M, et al. Cannabidiol inhibits lung cancer cell invasion and metastasis via intercellular adhesion molecule-1. FASEB J. (2012) 26(4):1535-48. doi: 10.1096/fj.11-198184.

169. Ramer R, Rohde A, Merkord J, Rohde H, Hinz B. Decrease of plasminogen activator inhibitor-1 may contribute to the anti-invasive action of cannabidiol on human lung cancer cells. Pharm Res. 2010 Oct;27(10):2162-74. doi: 10.1007/s11095-010-0219-2.

170. Zhang X, Qin Y, Pan Z, Li M, Liu X, Chen X, et al. Cannabidiol Induces Cell Cycle Arrest and Cell Apoptosis in Human Gastric Cancer SGC-7901 Cells. Biomolecules. (2019) 9(8). pii: E302. doi: 10.3390/biom9080302.

171. Sultan AS, Marie MA, Sheweita SA. Novel mechanism of cannabidiol-induced apoptosis in breast cancer cell lines. Breast. (2018) 41:34-41. doi: 10.1016/j.breast.2018.06.009.

172. Shrivastava A, Kuzontkoski PM, Groopman JE, Prasad A. Cannabidiol induces programmed cell death in breast cancer cells by coordinating the cross-talk between apoptosis and autophagy. Mol Cancer Ther. (2011) 10(7):1161-72. doi: 10.1158/1535-7163.MCT-10-1100.

173. Elbaz M, Nasser MW, Ravi J, Wani NA, Ahirwar DK, Zhao H, et al. Modulation of the tumor microenvironment and inhibition of EGF/EGFR pathway: novel anti-tumor mechanisms of Cannabidiol in breast cancer. Mol Oncol. (2015) 9(4):906-19. doi: 10.1016/j.molonc.2014.12.010.

174. Simmerman E, Qin X, Yu JC, Baban B. Cannabinoids as a Potential New and Novel Treatment for Melanoma: A Pilot Study in a Murine Model. J Surg Res. (2019) 235:210-215. doi: 10.1016/j.jss.2018.08.055.

175. Aviello G, Romano B, Borrelli F, Capasso R, Gallo L, Piscitelli F, et al. Chemopreventive effect of the non-psychotropic phytocannabinoid cannabidiol on experimental colon cancer. J Mol Med (Berl). (2012) 90(8):925-34. doi: 10.1007/s00109-011-0856-x.

176. Sreevalsan S, Joseph S, Jutooru I, Chadalapaka G, Safe SH. Induction of apoptosis by cannabinoids in prostate and colon cancer cells is phosphatase dependent. Anticancer Res. (2011) 31(11):3799-807.

177. Fisher T, Golan H, Schiby G, PriChen S, Smoum R, Moshe I, et al. In vitro and in vivo efficacy of non-psychoactive cannabidiol in neuroblastoma. Curr Oncol. (2016) 23(2):S15-22. doi: 10.3747/co.23.2893.

178. Morelli MB, Offidani M, Alesiani F, Discepoli G, Liberati S, Olivieri A, et al. The effects of cannabidiol and its synergism with bortezomib in multiple myeloma cell lines. A role for transient receptor potential vanilloid type-2. Int J Cancer. (2014) 134(11):2534-46. doi: 10.1002/ijc.28591.

179. Nabissi M, Morelli MB, Offidani M, Amantini C, Gentili S, Soriani A, et al. Cannabinoids synergize with carfilzomib, reducing multiple myeloma cells viability and migration. Oncotarget. (2016) 7(47):77543-77557. doi: 10.18632/oncotarget.12721.

180. Massi P, Solinas M, Cinquina V, Parolaro D. Cannabidiol as potential anticancer drug. Br J Clin Pharmacol. (2013) 75(2):303-12. doi: 10.1111/j.1365-2125.2012.04298.x.

181. Sharafi G, He H, Nikfarjam M. Potential Use of Cannabinoids for the Treatment of Pancreatic Cancer. J Pancreat Cancer. (2019) 5(1):1-7. doi: 10.1089/pancan.2018.0019.

182. Fonseca BM, Correia-da-Silva G, Teixeira NA. Cannabinoid-induced cell death in endometrial cancer cells: involvement of TRPV1 receptors in apoptosis. J Physiol Biochem. (2018) 74(2):261-272. doi: 10.1007/s13105-018-0611-7.

183. Solinas M, Massi P, Cantelmo AR, Cattaneo MG, Cammarota R, Bartolini D, et al. Cannabidiol inhibits angiogenesis by multiple mechanisms. Br J Pharmacol. (2012) 167(6):1218-31. doi: 10.1111/j.1476-5381.2012.02050.x.

184. Nabissi M, Amant F, Gehrig P. Endometrial Cancer: From Biological to Clinical Approaches. Lausanne: Frontiers Media. eds. (2019). doi: 10.3389/978-2-88963-049-3

185. Remmerie M, Janssens V. Targeted Therapies in Type II Endometrial Cancers: Too Little, but Not Too Late. Int J Mol Sci. (2018) 19(8). pii: E2380. doi: 10.3390/ijms19082380.

186. Azuma T, Yao S, Zhu G, Flies AS, Flies SJ, Chen L. B7-H1 is a ubiquitous antiapoptotic receptor on cancer cells. Blood. (2008) 111(7):3635-43. doi: 10.1182/blood-2007-11-123141.

187. Clark CA, Gupta HB, Sareddy G, Pandeswara S, Lao S, Yuan B, et al. Tumor-Intrinsic PD-L1 Signals Regulate Cell Growth, Pathogenesis, and Autophagy in Ovarian Cancer and Melanoma. Cancer Res. (2016) 76(23):6964-6974.

188. Escors D, Gato-Cañas M, Zuazo M, Arasanz H, García-Granda MJ, Vera R, et al. The intracellular signalosome of PD-L1 in cancer cells. Signal Transduct Target Ther. (2018) 3:26. doi: 10.1038/s41392-018-0022-9.

189. Marinelli O, Annibali D, Aguzzi C, Tuyaerts S, Amant F, Morelli MB, et al. The Controversial Role of PD-1 and Its Ligands in Gynecological Malignancies. Front Oncol. (2019) 9:1073. doi: 10.3389/fonc.2019.01073.

190. Kucukgoz Gulec U, Kilic Bagir E, Paydas S, Guzel AB, Gumurdulu D, Vardar MA. Programmed death-1 (PD-1) and programmed death-ligand 1 (PD-L1) expressions in type 2 endometrial cancer. Arch Gynecol Obstet. (2019) 300(2):377-382. doi: 10.1007/s00404-019-05180-2.

191. Wang ZL, Li GZ, Wang QW, Bao ZS, Wang Z, Zhang CB, et al. PD-L2 expression is correlated with the molecular and clinical features of glioma, and acts as an unfavorable prognostic factor. Oncoimmunology. (2018) 8(2):e1541535. doi: 10.1080/2162402X.2018.1541535.

192. Yang H, Zhou X, Sun L, Mao Y. Correlation Between PD-L2 Expression and Clinical Outcome in Solid Cancer Patients: A Meta-Analysis. Front Oncol. (2019) 9:47. doi: 10.3389/fonc.2019.00047.

193. Ren T, Zheng B, Huang Y, Wang S, Bao X, Liu K, et al. Osteosarcoma cell intrinsic PD-L2 signals promote invasion and metastasis via the RhoA-ROCK-LIMK2 and autophagy pathways. Cell Death Dis. (2019) 10(4):261. doi: 10.1038/s41419-019-1497-1.

194. Shi X, Wang J, Lei Y, Cong C, Tan D, Zhou X. Research progress on the PI3K/AKT signaling pathway in gynecological cancer (Review). Mol Med Rep. (2019) 19(6):4529-4535. doi: 10.3892/mmr.2019.10121.

195. Mendoza MC, Er EE, Blenis J. The Ras-ERK and PI3K-mTOR pathways: cross-talk and compensation. Trends Biochem Sci (2011) 36(6): 320–328. doi:10.1016/j.tibs.2011.03.006

196. Tanaka K, Miyata H, Sugimura K, Kanemura T, Hamada-Uematsu M, Mizote Y, et al. Negative influence of programmed death-1-ligands on the survival of esophageal cancer patients treated with chemotherapy. Cancer Sci. (2016) 107(6):726-33. doi:10.1111/cas.12938.

197. Awasthi N, Monahan S, Stefaniak A, Schwarz MA, Schwarz RE. Inhibition of the MEK/ERK pathway augments nab-paclitaxel-based chemotherapy effects in preclinical models of pancreatic cancer. Oncotarget (2017) 9(4): 5274–5286. doi:10.18632/oncotarget.23684

198. McCubrey JA, Steelman LS, Chappell WH, Abrams SL, Wong EW, Chang F, et al. Roles of the Raf/MEK/ERK pathway in cell growth, malignant transformation and drug resistance. Biochim Biophys Acta (2007) 1773(8):1263–1284. doi:10.1016/j.bbamcr.2006.10.001

199. Qu QX, Xie F, Huang Q, Zhang XG. Membranous and Cytoplasmic Expression of PD-L1 in Ovarian Cancer Cells. Cell Physiol Biochem. (2017) 43(5): 1893-1906. doi: 10.1159/000484109.

200. Panjwani PK, Charu V, DeLisser M, Molina-Kirsch H, Natkunam Y, Zhao S. Programmed death-1 ligands PD-L1 and PD-L2 show distinctive and restricted patterns of expression in lymphoma subtypes. Hum Pathol. (2018) 71: 91-99. doi: 10.1016/j.humpath.2017.10.029.

201. Inoue Y, Yoshimura K, Mori K, Kurabe N, Kahyo T, Mori H, et al. Clinical significance of PD-L1 and PD-L2 copy number gains in non-small-cell lung cancer. Oncotarget. (2016) 7(22): 32113-28. doi: 10.18632/oncotarget.8528.

202. Calles A, Liao X, Sholl LM, Rodig SJ, Freeman GJ, Butaney M, et al. Expression of PD-1 and Its Ligands, PD-L1 and PD-L2, in Smokers and Never Smokers with KRAS-Mutant Lung Cancer. J Thorac Oncol. (2015) 10(12):1726-35. doi: 10.1097/JTO.0000000000000687.

203. Ayakannu T, Taylor AH, Konje JC. Cannabinoid receptor expression in estrogen-dependent and estrogen-independent endometrial cancer. J Recept Signal Transduct Res. (2018) 38(5-6):385-392. doi: 10.1080/10799893.2018.1531890.

204. Guida M, Ligresti A, De Filippis D, D'Amico A, Petrosino S, Cipriano M, et al. The levels of the endocannabinoid receptor CB2 and its ligand 2-arachidonoylglycerol are elevated in endometrial carcinoma. Endocrinology. (2010) 151(3):921-8. doi: 10.1210/en.2009-0883.

205. Nabissi M, Morelli MB, Santoni M, Santoni G. Triggering of the TRPV2 channel by cannabidiol sensitizes glioblastoma cells to cytotoxic chemotherapeutic agents. Carcinogenesis. (2013) 34(1):48-57. doi: 10.1093/carcin/bgs328.

206. Torres S, Lorente M, Rodríguez-Fornés F, Hernández-Tiedra S, Salazar M, García-Taboada E, et al. A combined preclinical therapy of cannabinoids and temozolomide against glioma. Mol Cancer Ther. (2011) 10(1):90-103. doi: 10.1158/1535-7163.MCT-10-0688.

207. Chen Q, Kang J, Fu C. The independence of and associations among apoptosis, autophagy, and necrosis. Signal Transduct Target Ther. (2018) 3:18. doi: 10.1038/s41392-018-0018-5.

208. Qamri Z, Preet A, Nasser MW, Bass CE, Leone G, Barsky SH, et al. Synthetic cannabinoid receptor agonists inhibit tumor growth and metastasis of breast cancer. Mol Cancer Ther. (2009) 8(11):3117-29. doi: 10.1158/1535-7163.MCT-09-0448.

8. OTHER PROJECTS AND PUBLICATIONS

Santoni G, Maggi F, Morelli MB, Santoni M, **Marinelli O**. Transient Receptor Potential Cation Channels in Cancer Therapy. Med. Sci. 2019, 7, 108.

Marinelli O, Annibali D, Aguzzi C, Tuyaerts S, Amant F, Morelli MB, Santoni G, Amantini C, Maggi F, Nabissi M. The Controversial Role of PD-1 and Its Ligands in Gynecological Malignancies. Front Oncol. 2019 Oct 15;9:1073. doi: 10.3389/fonc.2019.01073.

Santoni G, Amantini C, Maggi F, **Marinelli O**, Santoni M, Nabissi M, Morelli MB. The TRPV2 cation channels: from urothelial cancer invasiveness to glioblastoma multiforme interactome signature. Lab Invest. 2019 Oct 25. doi: 10.1038/s41374-019-0333-7.

Santoni G, Morelli MB, Santoni M, Nabissi M, **Marinelli O**, Amantini C. Targeting Transient Receptor Potential Channels by MicroRNAs Drives Tumor Development and Progression. Adv Exp Med Biol. 2020;1131:605-623. doi: 10.1007/978-3-030-12457-1_24.

Santoni G, Morelli MB, **Marinelli O**, Nabissi M, Santoni M, Amantini C. Calcium Signaling and the Regulation of Chemosensitivity in Cancer Cells: Role of the Transient Receptor Potential Channels. Adv Exp Med Biol. 2020;1131:505-517. doi: 10.1007/978-3-030-12457-1_20.

Scheiner M, Dolles D, Gunesch S, Hoffmann M, Nabissi M, **Marinelli O**, Naldi M, Bartolini M, Petralla S, Poeta E, Monti B, Falkeis C, Vieth M, Hübner H, Gmeiner P, Maitra R, Maurice T, Decker M. Dual-Acting Cholinesterase-Human Cannabinoid Receptor 2 Ligands Show Pronounced Neuroprotection in Vitro and Overadditive and Disease-Modifying Neuroprotective Effects in Vivo. J Med Chem. 2019 Oct 24;62(20):9078-9102. doi: 10.1021/acs.jmedchem.9b00623.

Amantini C, Morelli MB, Nabissi M, Piva F, **Marinelli O**, Maggi F, Bianchi F, Bittoni A, Berardi R, Giampieri R, Santoni G. Expression Profiling of Circulating Tumor Cells in Pancreatic Ductal Adenocarcinoma Patients: Biomarkers Predicting Overall Survival. Front Oncol. 2019 Sep 10;9:874. doi: 10.3389/fonc.2019.00874.

Brunetti A, **Marinelli O**, Morelli MB, Iannarelli R, Amantini C, Russotti D, Santoni G, Maggi F, Nabissi M. Isofuranodiene synergizes with temozolomide in inducing glioma cells death. Phytomedicine. 2019 Jan;52:51-59. doi: 10.1016/j.phymed.2018.09.220.

Nabissi M, **Marinelli O**, Morelli MB, Nicotra G, Iannarelli R, Amantini C, Santoni G, Maggi F. Thyme extract increases mucociliary-beating frequency in primary cell lines from chronic obstructive pulmonary disease patients. Biomed Pharmacother. 2018 Sep;105:1248-1253. doi: 10.1016/j.biopha.2018.06.004.

Santoni G, Morelli MB, Amantini C, Santoni M, Nabissi M, **Marinelli O**, Santoni A. "Immuno-Transient Receptor Potential Ion Channels": The Role in Monocyte- and

Macrophage-Mediated Inflammatory Responses. Front Immunol. 2018 Jun 6;9:1273. doi: 10.3389/fimmu.2018.01273.

Marinelli O, Nabissi M, Morelli MB, Torquati L, Amantini C, Santoni G. ICOS-L as a Potential Therapeutic Target for Cancer Immunotherapy. Curr Protein Pept Sci. 2018;19(11):1107-1113. doi: 10.2174/1389203719666180608093913.

Santoni G, Amantini C, Morelli MB, Tomassoni D, Santoni M, **Marinelli O**, Nabissi M, Cardinali C, Paolucci V, Torniai M, Rinaldi S, Morgese F, Bernardini G, Berardi R. High CTLA-4 expression correlates with poor prognosis in thymoma patients. Oncotarget. 2018 Mar 30;9(24):16665-16677. doi: 10.18632/oncotarget.24645.

Dolles D, Hoffmann M, Gunesch S, **Marinelli O**, Möller J, Santoni G, Chatonnet A, Lohse MJ, Wittmann HJ, Strasser A, Nabissi M, Maurice T, Decker M. Structure-Activity Relationships and Computational Investigations into the Development of Potent and Balanced Dual-Acting Butyrylcholinesterase Inhibitors and Human Cannabinoid Receptor 2 Ligands with Pro-Cognitive in Vivo Profiles. J Med Chem. 2018 Feb 22;61(4):1646-1663. doi: 10.1021/acs.jmedchem.7b01760.

Amantini C, Farfariello V, Cardinali C, Morelli MB, **Marinelli O**, Nabissi M, Santoni M, Bonfili L, Cecarini V, Eleuteri AM, Santoni G. The TRPV1 ion channel regulates thymocyte differentiation by modulating autophagy and proteasome activity. Oncotarget. 2017 Oct 11;8(53):90766-90780. doi: 10.18632/oncotarget.21798.

Oral Presentation

THE INTERNATIONAL RETREAT OF PhD STUDENTS IN IMMUNOLOGY (Camogli, GE) organized by SIICA 5-6/12/2019

PD-L2 expression in endometrial cancer cell lines and biopsies. Biological functions and correlation with overall survival.

Marinelli Oliviero, Annibali Daniela, Amant Frédéric, Morelli Maria Beatrice, Santoni Giorgio, Amantini Consuelo, Maggi Federica, Nabissi Massimo

PURPOSE: The role of immune checkpoints (IC) in suppression T cell response is well established. So far, IC inhibitors were used in immuno-oncology, with promising outcomes. It is still needed identifying other markers, especially for endometrial cancer (EC). EC is a gynaecological tumour classified in type I and the most aggressive type II. Programmed death (PD) ligand-2 (PD-L2) leads to T-cell exhaustion but, very few data were provided about its cell-intrinsic signal and its role in EC. The aim of this work was to characterize PD ligands profile in EC focusing the attention on PD-L2 biological role and its prognostic impact in human type II EC.METHODS: PD ligands expression was analysed in a cohort of 506 patients by a silico analysis of TCGA data and in primary human EC cell lines by RT-PCR and Western Blot analysis. PD-L2 was evaluated in human type II EC samples by

immunohistochemistry, correlating with Overall Survival (OS). We also investigated the effects of PD-L2 over-expression on EC in vitro. RESULTS: Supported by TCGA, PD-L2 was more expressed than PD-L1 in EC. PD-L2 was highly expressed in 64.44% of tumour specimens, while in peritumoral and normal tissues, it was predominantly moderate or low. Its expression correlated with a shorter OS. Additionally, PD-L2 over-expression enhanced proliferation by increasing AKT phosphorylation and leaded to migration of EC cells in vitro. DISCUSSION: It was shown that PD-L2 has different effects on immune suppression among different tumours. Currently, data about its intrinsic role are scarce. Recently, it is shown that it promotes invasion through the ROCK pathway in osteosarcoma. PD-L1 activate intrinsic mTOR/AKT pathway, involved in cancer proliferation, survival and invasion, but there is no evidence for PD-L2.CONCLUSIONS: Our work clearly shows that PD-L2 activates an intrinsic signal supporting invasion and proliferation, through AKT signaling pathway, supporting its role as negative prognostic factor for EC.

Posters

Oliviero Marinelli, Daniela Annibali, Frédéric Amant, Massimo Nabissi (2019). Characterization of B7 members expression in endometrial cancer and clinical significance of PD-L2 in type II subtype. In: (a cura di): Bioevents, The Immuno-Oncology 2019 World Congress (Immuno-Oncology2019). vol. The Immuno-Oncology 2019 World Congress (Immuno-Oncology2019), p. 1-39, Tel Aviv-Yafo:BioEvents, Barcelona, 23-24 Maggio 2019

Background: In cancer, up-regulation of co-inhibitory B7 ligands is associated with immune evasion. So far, anti-PD-1 and anti-PD-L1 antibodies has been used in immune-oncology, with promising outcomes but only a small proportion of patients respond successfully. It is still needed identifying other markers, especially for endometrial cancer (EC). EC is a gynecological malignancy classified into two types, endometrioid type I and the most aggressive non-endometrioid type II. Up to now, very few information were provide about B7 members in EC. Furthermore, no molecular prognostic biomarkers are available for type II EC. Objective: Characterization of B7 members profile in EC and evaluation of PD-L2 prognostic impact in human type II EC biopsies. Methods: B7 members were evaluated in six human EC cell lines and one cancer-associated fibroblasts (CAFs), compared to normal endometrial samples. Additionally, using data from cBioportal, we performed a molecular profiling in a cohort of 506 patients. PD-L2 staining was evaluated in a cohort of 23 human type II EC samples, evaluating Overall Survival (OS) and Progression-Free Survival (PFS). Results: EC expresses several B7 members. PD-L2 was significantly over-expressed by one EC Type-I cell line and CAFs, ICOS-L and B7-H4 were expressed especially in mixed type I/II cell lines and type II patients. B7-H3 was expressed in EC cell lines and it was more expressed in type I patients. Additionally to these preliminary data, High PD-L2 expression correlated with shorter OS ($p < 0.033$) but not with PFS ($p > 0.05$). Conclusions: We firstly evidenced that some B7 members were expressed in EC with differences between Type I and Type II, compared with normal tissues. PD-L2 could be a potential predictive biomarker

for Type II EC. These preliminary results suggest investigating better the B7 molecular role in EC.

Oliviero Marinelli, Massimo Nabissi, Maria Beatrice Morelli, Consuelo Amantini, Giorgio Santoni (2018). Investigation of Biological Function of Costimulatory b7 Family Members in Endometrial Cancer. In: The Immuno-Oncology 2018 World Congress (Immuno-Oncology2018). p. 1-61, Tel Aviv-Yafo:BioEvents, Vienna, 25-26 Giugno 2018

Background Endometrial cancer (EC) is a gynecological malignancy classified into two clinicopathological types, endometroid type I and non-endometroid type II. Type I is characterized by slow growth and a good prognosis, while type II is very aggressive and with a poor survival. Recently, in immune-oncology there is a growing interest towards the costimulatory B7 family members as possible promising targets for immunotherapy. These proteins are cell-surface protein ligands, binding to receptors on lymphocytes to regulate immune responses, but previous evidence have demonstrated that inhibitory B7 molecules are frequently up-regulated in different tumors, which may contribute to immune evasion, invasiveness and chemoresistance. Up to now, very few information were provide about B7 members in EC. Objective Our objective was to characterize the expression profile of B7 members in EC. Methods B7 members were evaluated by RT-PCR and Western Blot analysis, in five different human EC cell lines and compared to normal endometrial samples. Results EC cell lines express several B7 members, such as, PD-L1, PD-L2, ICOS-L and B7-H3 with a significant difference compared with normal tissues. Specifically, PD-L2 is significantly over-expressed by an EC Type-II cell line, suggesting its correlation with tumour aggressiveness. Conclusions The role of inhibitory B7 molecules is not completely understood in cancer. Since no information are actually present in regard to B7 members and their roles in EC, we firstly evidenced that some B7 members were expressed in EC cell lines and their expression levels were different compared with normal tissues. These preliminary results are the basis for the development of a project focused in a better understanding of the B7 molecular role in EC.

Transient Receptor Potential Cation Channels in Cancer Therapy

Giorgio Santoni [1,*], **Federica Maggi** [1,2], **Maria Beatrice Morelli** [1], **Matteo Santoni** [3] **and Oliviero Marinelli** [1,4]

[1] School of Pharmacy, University of Camerino, via Madonna delle Carceri 9, 62032 Camerino (MC), Italy; federica.maggi@uniroma1.it (F.M.); mariabeatrice.morelli@unicam.it (M.B.M.); oliviero.marinelli@unicam.it (O.M.)

[2] Department of Molecular Medicine, Sapienza University, Viale Regina Elena 324, 00161 Rome (RM), Italy

[3] Medical Oncology Unit, Hospital of Macerata, Via Santa Lucia 2, 62100 Macerata (MC), Italy; mattymo@alice.it

[4] School of Biosciences and Veterinary Medicine, University of Camerino, via Madonna delle Carceri 9, 62032 Camerino (MC), Italy

[*] Correspondence: giorgio.santoni@unicam.it; Tel.: +39-0737403319; Fax: +39-0737403325

Abstract: In mammals, the transient receptor potential (TRP) channels family consists of six different families, namely TRPC (canonical), TRPV (vanilloid), TRPM (melastatin), TRPML (mucolipin), TRPP (polycystin), and TRPA (ankyrin), that are strictly connected with cancer cell proliferation, differentiation, cell death, angiogenesis, migration, and invasion. Changes in TRP channels' expression and function have been found to regulate cell proliferation and resistance or sensitivity of cancer cells to apoptotic-induced cell death, resulting in cancer-promoting effects or resistance to chemotherapy treatments. This review summarizes the data reported so far on the effect of targeting TRP channels in different types of cancer by using multiple TRP-specific agonists, antagonists alone, or in combination with classic chemotherapeutic agents, microRNA specifically targeting the TRP channels, and so forth, and the in vitro and in vivo feasibility evaluated in experimental models and in cancer patients. Considerable efforts have been made to fight cancer cells, and therapies targeting TRP channels seem to be the most promising strategy. However, more in-depth investigations are required to completely understand the role of TRP channels in cancer in order to design new, more specific, and valuable pharmacological tools.

Keywords: transient receptor potential channels; tumor progression; chemotherapy resistance

1. Introduction

Despite advances in findings and medical care for various cancers, there are still high rates of treatment failure and mortality worldwide. This high frequency is mainly due to the powerful capability of cancer cells to proliferate and migrate. Recent studies regarding transient receptor potential (TRP) channels have indicated that they mark a specific phase of cancer progression and that they could represent potential targets for cancer treatment. TRP channels are important as calcium- permeable and non-selective ion channels expressed in different tissues and cell types in mammals and are crucial regulators of calcium, sodium, and magnesium ions. They are grouped into six subfamilies: TRPC ("C" for canonical), TRPV ("V" for vanilloid), TRPM ("M" for melastatin), TRPA ("A" for ankyrin), TRPP ("P" for polycystic), and TRPML ("ML" for mucolipin) [1]. They show common features in structure, such as the presence of six transmembrane segments with intracellular N- and C-terms and various degrees of sequence homology. TRP subfamilies have been linked to

many physiological and pathological functions, including cell differentiation, proliferation, apoptosis, and ionic homeostasis.

Upregulation and downregulation in TRP channel subfamily expression are linked with the different phases of tumor progression and strongly correlate with clinical parameters (e.g., overall survival (OS), progression-free survival, and more) as shown by Kaplan–Meier, univariate, and multivariate Cox regression analysis. Indeed, high TRPM8 expression is related to a worse OS in pancreatic cancer (PC) patients ($p = 0.001$) [2]; and increased TRPM7 expression represents an unfavorable factor in human bladder cancer (BCa) ($p < 0.05$) [3]. In esophageal squamous cell carcinoma (OSCC), TRPM7 expression represents an independent prognostic factor of good post-operative survival ($p < 0.05$) [4], whereas TRPV6 downregulation is associated with an unfavorable 3-year disease-specific survival ($p = 0.027$) [5]. Overexpression of TRPV3 correlates with tumor progression and short OS in non-small cell lung carcinoma (NSCLC) ($p = 0.020$) [6]; and loss or reduction of TRPML1 mRNA expression correlates with short survival in glioblastoma (GBM) patients ($p < 0.0298$) [7]. In addition, in diffuse large B cell lymphoma, TRPM4 positivity confers worse OS ($p = 0.004$) and progression-free survival ($p = 0.005$) in rituximab-, cyclophosphamide-, doxorubicin-, vincristine-, and prednisone-treated lymphoma cells [8].

Therefore, TRP channels represent promising potential diagnostic, prognostic, and therapeutic tools for different types of cancer [9,10]. In this review, we report the results regarding the in vitro and in vivo therapeutic approach with different compounds that affect the expression and functions of TRP channels in cancer therapy.

2. TRPC Channels in Cancer Therapy

Several channels belonging to the TRPC subfamily have been found to be a target in cancer therapy. Treatment of colorectal cancer (CRC) cells with 10 μM of 20-*O*-β-D-glucopyranosil-20(*S*)-protopanaxadiol (20-GPPD), a metabolite of ginseng saponin, induces activation of Ca^{2+} influx through TRPC channels, leading to apoptosis [11]. Treatment of CT-26 murine colon cancer cells with 20-GPPD for 24 h triggers an accumulation of cells in the sub-G1 cell phase and apoptosis. In addition, this compound is able to stimulate the phosphorylation of AMP-activated protein kinase (AMPK), leading to AMPK activation and consequently inhibition of cell viability. The 20-GPPD induces an increase in AMPK activation, triggered by TRPC-dependent enhancement in intracellular Ca^{2+} concentration ($[Ca^{2+}]_i$), as demonstrated by the capability of the TRPC non-selective blockers, Gd^{3+} and SKF96365, to completely inhibit Ca^{2+} influx.

Several GBM cell lines express different members of the TRPC channels (e.g., TRPC1, 3, 4 and 5). Sustained treatment of glioma cells with the inhibitors SKF96365 (25 μM) and aminoethoxydiphenyl borate (2-APB) (100 μM) reduced cell proliferation, with an accumulation of glioma cells in the G2/M phase and impairment of cytokinesis [12,13]. However, 2-APB is not only a TRPC inhibitor, but it can also activate both TRPV2 and TRPV3 and, in addition, works as an inositol triphosphate (IP_3)-induced Ca^{2+}-release inhibitor. However, data on cell viability should be confirmed in TRPC1-silenced cells to verify the specific role of this channel. On the other hand, a role for TRPC1 in glioma cell chemotaxis induced by epidermal growth factor (EGF) has been demonstrated [14]. In this regard, in GBM cells, TRPC1 silencing or blockade using SKF96365 at 25 μM, 2-APB at 100 μM, or MRS1845 at 25 μM inhibits the chemotactic migration induced by EGF but not basal migration. The localization of TRPC1 in lipid rafts has been found to be essential for TRPC function as well as for EGF-induced chemotaxis [13].

The inhibition of TRPC1 using 2-APB or TRPC1 silencing reduces the adhesive and invasive capabilities of nasopharyngeal cancer cells, suggesting that TRPC1 can modulate metastasis spreading [15].

The sesquiterpene (-) Englerin A (EA, 250 nM) from the plant *Phyllanthus engleri* induces cytotoxicity in different cancer types, including renal cell carcinoma (RCC), but not in normal cells. A common feature in RCC lines is the expression of heteromeric TRPC1/C4/C5 channels. TRPC4 expression is required for EA-induced calcium influx, membrane depolarization, and growth inhibition. EA is a TRPC4 agonist; however it also activates TRPC1/C5 channels. TRPC4 stimulation

in cancer cells induced growth inhibition, which can be blocked by ML204, a TRPC4/C5 inhibitor. EA also weakly inhibits the TRPA1, TRPV3/V4, and TRPM8 channels, suggesting that it can bind a common domain present in the TRP ion channels [16].

Triple-negative breast cancers (TNBCs) are an aggressive heterogeneous group of tumors resistant to several target therapies, resulting in high relapse and poorer OS. A recent report has identified a group of TNBC cell lines responsive to EA treatment. The BT-549 and Hs578T TNBC BC cell lines, which express high TRPC4 and TRPC1/C4 heterodimer levels, are more sensitive to EA than other TNBC cell lines. In Hs578T TNBC cells, EA induces Na^+ and Ca^{2+} accumulation, whereas in BT-549 cells, it increases cytosolic Ca^{2+} levels and induces mitochondrial depolarization [17]. In human SW982 synovial sarcoma cells (SSCs), EA induces TRPC1/C4 heterodimer activation and cell cytotoxicity, which is inhibited by Pico145, an inhibitor of the TRPC1/C4 channels. EA cytotoxicity is due to TRPC1 or TRPC4 suppression. Ouabain (10 nM), an Na^+/K^+-ATPase inhibitor, increases EA-induced cytotoxicity; Na^+ entry by the Na^+ loading ionophore, gramicidin-A, causes cell death of SW982 cells, which are resistant to Pico145 (10 nM), suggesting that Na^+ loading is itself cytotoxic even without TRPC1/C4 activation. Overall, these results evidenced that EA-mediated cytotoxicity in human SSCs depends both on TRPC1/C4 channels and Na^+ loading [18].

EA exerts a rapid cytotoxic effect on TRPC4-positive A498 RCCs and Hs578T TNBC. Different members of the TRP channel family have been found to assembly to form homo- and heterodimers [16,17]. Regarding the effect of EA, it is mediated by TRPC1/TRPC4 heterodimers and both TRPC4 and TRPC1 are required; however, although TRPC4 was necessary for the EA-evoked Ca^{2+} elevation, TRPC1 negatively regulated Ca^{2+} entry. By contrast, both TRPC4 and TRPC1 were necessary for monovalent cation entry evoked by EA, and EA-evoked cell death was dependent upon entry of Na^+. Therefore, it can be hypothesized that Na^+/K^+-ATPase might protect cells by counteracting the sustained Na^+ entry. Indeed, inhibition of Na^+/K^+-ATPase by ouabain increases the EA-evoked cytotoxicity, suggesting that EA-mediated cancer cell cytotoxicity sustains Na^+ entry through the heteromeric TRPC1/TRPC4 channels and EA cytotoxicity can be increased by Na^+/K^+-ATPase inhibition [19].

The diterpene ester tonantzitlolone (TZL) is a natural product, which shows at a nanomolar dose cytotoxicity toward RCCs. Although chemically distinct to EA, its effects are similar to other drugs that target TRPC1/4/5 channels. TZL enhances the intracellular Ca^{2+} and induces TRPC4 and TRPC5 overexpression and the assembly of TRPC1-TRPC4 and TRPC1-TRPC5 heterodimers in A498 RCC line, which are inhibited by Pico145. No activated endogenous store-operated Ca^{2+} entry (SOCE) or TRPC3, TRPV4, or TRPM2 overexpression is induced by TZL in HEK293 cells [20].

An analogue of the xanthine-based Pico145 inhibitor, AM237 at 15 to 20 nM, activates TRPC5 in the A498 RCC line and potentiates TRPC5 activation by sphingosine-1-phosphate. AM237 also activates TRPC5 channels and potently inhibits EA-dependent activation [21]. By contrast, it did not activate TRPC4-C4, TRPC1-C4, and TRPC1-C5 channels.

MTI-101 is a peptidomimetic compound that binds the CD44/Integrin Subunit Alpha 4 complex and triggers necrosis in multiple myeloma (MM) cell lines. The MTI-10 stimulates an increase in intracellular Ca^{2+} levels in MM cells. Pharmacological inhibition of store-operated channels or reduction in TRPC1 expression blocks MTI-101-induced death. The effect of MTI-101 in MM is more evident in relapsed myeloma patients, suggesting an increased sensitivity to Ca^{2+} overload-mediated cell death in relapsed MM. Moreover, MTI-101 synergized with bortezomib in both MM cell lines and primary myeloma patients [22].

In NSCLC, the expression of TRPC1, C3, C4, and C6 channels correlates with tumor differentiation grade [23]. Treatment of A549 cells with GBM cells with SKF96365 (25 μM) and 2-APB (100 μM), all-trans retinoic acid (ATRA, 1 μM) for 96 h increased TRPC3, C4, and C6 expression and enhanced Ca^{2+} influx. The A549 cell proliferation is more sensitive to 2-APB, following chronic application of ATRA [23]. However, ATRA shows no direct effect on TRPC channel function, and the increased Ca^{2+} influx is probably due to *TRPC* gene upregulation.

The SOCE controls the proliferation and metastasis of several cancer types. Their role in nicotine-promoted proliferation of NSCLC A549 cells has been investigated. A549 cells express high levels of

TRPC1 and C6 and Orai1 store-operated calcium channels and low TRPC3 and TRPC4 levels. Nicotine at 1 μM upregulates TRPC1, TRPC6, Orai1, mRNA, and protein expression; increases basal $[Ca^{2+}]_i$; and enhances SOCE. The promotion of cell proliferation is observed in nicotine-treated cells, which is inhibited by the SOCE inhibitor, SKF-96365. Furthermore, nicotine upregulates hypoxia inducible factor 1α (HIF-1α) expression in A549 and NCI-H292 cells; silencing of HIF-1α stimulates an increase in TRPCs and Orai1 and decreases basal $[Ca^{2+}]_i$ and SOCE. In conclusion, nicotine promotes lung cancer cell proliferation by upregulating HIF-1α and Orai1 store-operated calcium channel components and therefore enhancing SOCE and increasing $[Ca^{2+}]_i$ [24].

Abnormal expression of TRPC5 has been associated with cancer progression and chemoresistance. A role for the overexpression of TRPC5 and P-glycoprotein (P-gp) in adriamycin-resistant (ADMR) MCF-7 BC cells has been demonstrated [25]. The TRPC5 expression is higher in ADMR-MCF-7 cells compared to controls. A marked downregulation of P-gp expression and an increase of adriamycin accumulation was evidenced in ADMR-MCF-7 cells using an anti-TRPC5 T5E3 antibody. In addition, miR-230a, which specifically targets TRPC5 and nuclear factor of activated T-cells 3 (NFATc3) mRNAs, is found to be downregulated in ADMR-MCF-7 cells, suggesting its involvement in chemoresistance, and a low expression of miR-230a is associated with poor patient outcomes. Finally, in regard to NFATc3, but not the other NFAT isoforms, it stimulates the transcriptional activity of the promoter of Multi Drug Reactivity 1 gene, suggesting that Ca^{2+} entry through TRPC5 stimulates NFATc3 to enhance P-gp production [25].

Cancer cells produce soluble factors and secrete extracellular vesicles (EVs), including exosomes, microvesicles, and apoptotic bodies [26]. TRPC5 is involved in EVs' formation and secretion in ADMR-MCF-7 [27]. TRPC5 is packaged in EVs and transported in recipient cells, where it promotes P-gp expression by increasing calcium (Ca^{2+}) influx. EVs levels containing TRPC5 are related to the acquired chemoresistance [26]. Zhang and colleagues also demonstrated that TRPC5 regulates chemotherapy-induced autophagy in BC cells via calcium/calmodulin-dependent protein kinase, AMPKα, and the mammalian target of rapamycin pathway. TRPC5-induced autophagy functions as a pro-survival mechanism promoting chemoresistance [28]. Overexpression of TRPC5 is also involved in 5-Fluorouracil (5-Fu) resistance in CRC [29]. Previously it has been reported that TRPC5 mediated Ca^{2+} entry, stimulating the ATP-binding cassette, subfamily B, member 1 (ABCB1) pump overproduction in drug-resistant BC cells, and suppressing TRPC5, reversing drug resistance through the TRPC5-NFATc3-Ca^{2+}-ABCB1 pathways [25]. TRPC5 and the ABCB1 pump are also found to be upregulated in human-resistant HCT-8 and LoVo CRC cell lines. TRPC5 activation promotes β-catenin translocation in the nucleus, increases glycolysis and ATP production, and stimulates the expression of ABCB1 and cyclin D1 proteins, contributing to 5-Fu resistance. Thus, suppressing TRPC5 expression weakens the ABCB1 pump and causes a reversal of 5-Fu resistance in HCT-8/5-Fu and LoVo/5-Fu cells. High expression of TRPC5 is associated with upregulation of glucose transporter 1 in CRCs, and an increase in glycolysis occurs in chemoresistance cells [30].

TRPC6 channels are essential for the G2/M phase transition in gastric cancer (GaC) and OSCC [31,32]. In these studies, SKF96365 (10 μM) blocks TRPC6 channel activity, leading to cell growth arrest and accumulation in the G2/M phase. The specific role of TRPC6 channels is confirmed by the heterologous expression of a dominant negative of TRPC6 in GaC cells. The regulation of cancer cell proliferation by TRPC6 involves an elevation of $[Ca^{2+}]_i$ that is essential for G2/M phase transition in GaCs and OSCCs.

In hepatocellular carcinoma (HCC), doxorubicin chemoresistance occurs through epithelial mesenchymal transition (EMT) induction, with vimentin upregulation and downregulation of E-cadherin and claudin1 EMT-associated proteins. Long treatment with doxorubicin, increasing Ca^{2+} influx, stimulates chemoresistance, which promotes EMT. The TRPC6 channel induces EMT by signal transducer and activator of transcription 3 activation, which is a downstream regulator in the TRPC6 calcium signaling pathway. In an HCC xenograft model, TRPC6 silencing resulted in slower growth and greater doxorubicin sensitivity with respect controls [33].

Data relative to TRPC channel-related effects are synthetized in Table 1.

Table 1. Pharmacological modulation of TRPC channel expression and functions by natural and/or chemical agents in cancer cells.

Pharmacological Agent	TRP Target	Cancer Type	Effects	Mechanisms	References
20-GPPD	TRPC (?)	CRC	Cell apoptosis (+)	Ca^{2+} entry ↑	[11]
SKF96365/2-APB/MRS1845	TRPC1	GBM	Cell growth (−)	SOCE ↓	[13]
SKF96365/2-APB/MRS1845	TRPC1	GBM	Cell migration (−)	SOCE ↓	[14]
MTI-101	TRPC1	MM	Necrosis (+)	Ca^{2+} entry ↑	[22]
SKF96365/2-APB	TRPC1, C3, C4, C5	GBM	Cell growth (−)	Cytokinesis ↑	[12]
ATRA	TRPC3, C4, C6	NSCLC	Proliferation (−)	Ca^{2+} entry ↑	[23]
EA	TRPC4/C5	RCC	Cell proliferation (−)	Ca^{2+} entry ↑	[16]
	TRPC1/4/5	SSC	Cytotoxicity (+)	Na^{+} entry ↑	[19]
TZL	TRPC1/4/5	RCC	Cytotoxicity (+)	PKC θ activity ↑	[20]
Nicotine	TRPC1/C6	NSCLC	Proliferation (+)	HIF-1α and SOCCs ↑	[24]
AM237	TRPC5	RCC	Viability (+)	Sphingosine-1-phosphate activity ↑	[21]
SKF96365	TRPC6	GCa, OSCC	Cell growth (−)	Ca^{2+} entry ↑	[31,32]

Abbreviations: 2-APB, 2-Aminoethoxydiphenyl borate; 20-GPPD, 20-*O*-β-D-glucopyranosyl-20(S)-protopanaxadiol; ATRA, all-trans retinoic acid; GBM, glioblastoma; BC, breast carcinoma; CRC, colorectal carcinoma; HIF-1α, hypoxia Inducible Factor 1α; EA, Englerin A; GCa, gastric carcinoma; MM, multiple myeloma; NSCLC non small lung cell carcinoma; OSCC, eosophageal carcinoma; RCC, renal cell carcinoma; SOCE, Store Operated Calcium Entry; SOCCs, Store Operated Calcium

Channels; SSC, synovial sarcoma cell. (?) no conclusive data. (↑) increment. (↓) reduction. (+) increase. (−) decrease.

3. TRPM Channels in Cancer Therapy

Among the TRPM family, an important antitumor effect has been mediated by TRPM2, TRPM5, TRPM7, and TRPM8 channels.

The histone deacetylase inhibitors Tricostatin A (100 nM) and sodium butyrate (5 mM) induce TRPM2 upregulation and apoptosis in a TRPM2-dependent manner in T24 BCa cells. The TRPM2 upregulation induced by histone deacetylases inhibition is due to an enhancement of acetylated H3K9 in the TRPM2 promoter. A previous report on TRPM2 modulators evaluated in *Xenopus* oocytes evidenced that H_2O_2, AMP, cyclic ADPR, dinucleotide phosphate, and nicotinic acid adenine dinucleotide do not affect TRPM2 channels in physiological conditions [34]. 5-Fu and Leucovorin (LCV) are widely used in BC and CRC for chemotherapy. It has been reported that the expression of TRPM2 channels increases in cancer cells. In BC (MCF-7) and CRC (Caco-2) cell lines, 5-Fu (5 μM) and LCV (2 μM), in combination or alone, result in TRPM2 activation with increased $[Ca^{2+}]i$ levels and oxidative stress-induced apoptosis. The effects of 5-Fu and LCV is directly related to TRPM2. These channels play an important role in the apoptosis of cancer cells by elevating Ca^{2+} and intracellular reactive oxygen species (ROS) levels and mitochondrial depolarization [35].

A recent report evidenced that Selenium (Se, 1 μM) enhances the apoptotic efficacy of docetaxel (DTX, 10 nM), through the activation of TRPM2 in the DBTRG GBM cell line [36]. DTX induces cancer cell death through excessive ROS production and increases Ca^{2+} entry. TRPM2 activated by ROS and Se stimulates the apoptosis of DTX-resistant GBM cells. DTX and Se in combination induce mitochondrial membrane depolarization and ROS production, and increase NAD-dependent DNA repair enzyme poly (ADP-ribose) polymerase-1 (PARP-1) activity and apoptosis in DBTRG cells.

A recent report of Maeda and collaborators discusses a role of TRPM5 in lung metastasis [37]. Acid extracellular pH has been found to increase intracellular Ca^{2+} and matrix metalloproteinase-9 (MMP-9) expression in the mouse B16 melanoma (ME) model. TRPM5 silencing reduces extracellular acid-induced MMP-9 expression, whereas enforced TRPM5 expression shows the opposite effect as well as increasing lung metastasis. Treatment of ME-bearing mice with the TRPM5 inhibitor triphenylphoshine oxide reduces spontaneous lung metastasis. Moreover, in ME and GaC patients, high TRPM5 mRNA expression correlates with poor OS rates.

TRPM7 has been found to regulate BC cell proliferation, migration, invasion, and metastasis; however, the effect of the TRPM7 kinase domain in the control of BC migration and invasion has only recently been evaluated by using a TRPM7 kinase assay and a new TRPM7 kinase inhibitor TG100-115. This inhibitor shows little effect on the proliferation of MDA-MB-231 on BCs, but significantly inhibits the migration and invasion of BC cells as a consequence of reduced myosin IIA heavy chain and focal adhesion kinase (FAK) phosphorylation. TG100-115 also suppressed the TRPM7 channel activity [38].

Waixenicin A (WA) is an extract from *Sarcotheliaedmondsoni* (syn. *Anthelia edmondsoni*), a soft coral from Hawaii, that inhibits TRPM7 in a dose-dependent manner [39]. Moreover, WA (10 μM) completely inhibits the TRPM7 current in TRPM7-transfected HEK293 cells. The inhibitory effects of WA on TRPM7 are strongly dependent on $[Mg^{2+}]i$, indicating that this compound enhances Mg^{2+} blockade of the channels or that Mg^{2+} enhances the binding affinity of WA. Importantly, WA does not exert an effect on TRPM6 channels, the closest homologues of TRPM7 channels. Zierler et al. showed that WA at 50 μM inhibits the proliferation of human Jurkat T cells and rat basophilic leukemia cells in a TRPM7-dependent manner [39]. Recently, Kim et al. demonstrated that WA is a potent inhibitor of GaC and BC proliferation in a TRPM7-dependent manner [40,41]. Indeed, WA is able to inhibit AGS GaC cell and MCF-7 BC cell proliferation as well as reduce the TRPM7 currents in these cell lines. Moreover, ginsenoside Rd, one of the more active ginseng saponin components, used at 500 μM, has been shown to block TRPM7 channels and to induce cell death in GaC and BC cells [41]. Indeed, ginsenoside Rd decreases cell viability in MCF-7 and AGS in a dose-dependent manner, while it increases cell viability in HEK293 cells. Ginsenoside Rd-induced cell death is due to

intrinsic apoptosis signaling via mitochondrial membrane depolarization. Moreover, ginsenoside Rd increases caspase-3 activity in both MCF-7 and AGS cancer cells. Importantly, ginsenoside Rd inhibits TRPM7 currents in MCF-7 and AGS cells.

Recent findings in glioma have shown that vacquinol-1 (Vac) promotes cell death as a consequence of inefficient vacuole–lysosome fusion, which is reversed by exogenous ATP in GBM [42]. Exogenous ATP activates TRPM7, Ca^{2+} and Mg^{2+} influx and phosphoinositide 3-kinases (PI3K) activation that promotes vesicle fusion with lysosomes. Thus, the inhibitory effect on ATP-mediated cell death induced by Vac depends to TRPM7 activation that stimulates the PI3K pathway, restoring vacuole–lysosome fusion. Overexpression of TRPM7 is responsible for Vac resistance in glioma cells. TRPM7 is required to prevent apoptosis in PC. Silencing TRPM7 in PC cells induces the replicative senescence program [43]. Downregulation of TRPM7 enhances gemcitabine cytotoxicity in PC [43].

TRPM8 is expressed or overexpressed in different cancer types (e.g., CRC, PCa, OSCC, and BC). Tsaveler et al. originally identified *TRPM8* by screening a prostate cDNA library; the gene was described as a novel prostate-specific gene with increased expression during the transformation of PCa [44]. Regarding agonists or antagonists of TRPM8 channels, several are now considered in cancer prevention and therapy, although some of those reported in the literature lack selectivity for TRPM8 because they also act on TRPV1 and TRPA1 [45,46].

In normal prostate cells, there is a slight level of TRPM8 expression, while in PCa, the expression of TRPM8 is increased [47]. Asuthkar et al. demonstrated that TRPM8 is an ionotropic testosterone receptor [48]. In early PCa tumors with high androgen levels, TRPM8 is expressed, while anti-androgen therapy reduced its expression [49]. Although TRPM8 mRNA is expressed at high levels, TRPM8 protein undergoes ubiquitination and degradation in PCa cells. Overexpression of TRPM8 induces anti-proliferation and pro-apoptotic effects. The cell cycle arrest and reduced cell motility is through downregulation of Cdk4/6 and focal adhesion kinase (FAK), respectively [50]. Treatment of PCa cells with TRPM8 agonist menthol accompanied by androgen receptor (AR) inhibition or TRPM8 overexpression, respectively, showed greater anti-proliferative effect [48]. Furthermore, the TRPM8 agonist WS12 encapsulated into lipid nanocapsules is able to impair cancer cell migration ability [51]. On the other hand, testosterone is able to inhibit TRPM8 activity [52]. Indeed, low (10 nM), but not high (100 nM), testosterone concentrations decrease TRPM8-mediated Ca^{2+} influx, resulting in a significant increase in cell migration. This process is induced by TRPM8/AR colocalization in lipid raft microdomains of the plasma membrane, where AR inhibits TRPM8 activity. As a result, increased FAK phosphorylation leads to PCa cell migration.

In the T24 BCa cell line, menthol (1 mM) induces cell death [53]. At 0.1 mM augments, the migration and invasion abilities of both TRPM8-overexpressing HSC3 and HSC4 oral squamous carcinoma (OSC) cell lines were shown by potentiating the MMP-9 activity, and this effect is completely suppressed by a novel TRPM8 antagonist RQ-00203078 used at a 10-μM dose [54].

Moreover, cannabigerol (CBG), a non-psychotropic cannabis-derived cannabinoid, used at 10 μM, potently blocks TRPM8 in CRC and protects against cancer development and progression [55]. CBG promotes ROS-dependent apoptosis, upregulates CCAAT-enhancer-binding protein homologous protein (CHOP) mRNA expression, and inhibits cell growth in CRC cells. TRPM8 silencing reduces the effect of CBG on cell growth and on CHOP mRNA expression. In vivo, CBG inhibits in a TRPM8-dependent manner the growth of xenograft tumors as well as chemically induced colon carcinogenesis. Although, in CRC, CBG is able to induce TRPA1, TRPV1, and TRPV2 channel activation, its proapoptotic effects are TRPA1, TRPV1, and TRPV2 independent [55].

TRPM8 blockers, such as BCTC, clotrimazole, and DD01050, as well as more specific blockers like AMTB and JNJ41876666, have been used in different human PCa cell lines [56,57]. BCTC (10 μM), clotrimazole (10 μM), AMTB (10 μM), and JNJ41876666 (10 μM) inhibit cell proliferation in all PCa cell lines but not in normal prostate cells. Moreover, RQ-00203078, another TRPM8 antagonist, is used in HSC3 and HSC4 OSC cell lines [54]. RQ-00203078 (10 μM) completely abolishes menthol-induced TRPM8 whole-cell currents and SOCE in both cell lines. Moreover, RQ-00203078 inhibits both menthol-induced basal cell proliferation as well as menthol-induced basal migration and invasion. Menthol-induced MMP-9 activity is also suppressed by RQ-00203078 [54]. In addition, recently,

tetrahydroisoquinoline-derived urea and 2,5-Diketopiperazine derivatives as selective antagonists of TRPM8 with high anti-PCa activity (at 10 nM) were synthetized by the De Petrocellis and colleagues [58].

TRPM8 is involved in cancer proliferation, invasion, and migration of LLC-2 lung cancer cells [59]. TRPM8, activating the uncoupling protein 2, induces resistance both against activated CD8$^+$T lymphocytes of the spleen and doxorubicin. In PCa cells, TRPM8 enhances HIF-1α, a subunit of the transcription factor HIF-1, which promotes hypoxic growth capacity, angiogenesis, and drug resistance in cancer cells. TRPM8 promotes in vitro hypoxic growth, drug resistance, in vivo tumorigenicity, and increased HIF-1α protein levels. TRPM8-induced suppression of HIF-1α ubiquitination and enhanced HIF-1α transactivation are attenuated by forced expression of receptor of activated protein C kinase 1 (RACK1); TRPM8 overexpression reduces phospho-RACK1 levels, thus affecting its dimerization status, and promotes RACK1 binding to HIF-1α and calcineurin [60].

TRPM8 is necessary for proliferation and invasion of PCa cells and is closely related to PCa gemcitabine sensitivity [61]. In PCa cell lines, PACN-1 and BxPC-3 sensitivity to gemcitabine is increased, while proliferation and invasion have been suppressed after TRPM8 RNA interference-mediated silencing. The mechanism of TRPM8 in gemcitabine-based chemotherapy is a consequence of the reduction in the expression and activity of multidrug resistance-associated proteins, such as P-gp in response to TRPM8 silencing. Moreover, TRPM8 knockdown significantly increased human equilibrative nucleoside transporter 1 protein levels and the Bax/Bcl-2 pro-apoptotic ratio, while reducing ribonucleotide reductase M1 protein levels.

Furthermore, in osteosarcoma cells, TRPM8 knockdown induces Ca^{2+}imbalance, inhibition of protein kinase B (Akt)-Glycogen synthase kinase (GSK)-3β, extracellular signal–regulated kinases (ERK)1/2 and FAK pathways, decreases proliferation, invasion, and migration, and improves apoptosis induced by epirubicin [62].

Immunotherapies might represent promising alternatives for the treatment of patients with hormone-refractory PCa. Results of phase I clinical trial reported the efficacy of vaccination with dendritic cells (DC) loaded with a cocktail consisting of HLAA*0201-restricted peptides derived from five different PCa-associated antigens prostate-specific antigen (PSA), prostate-specific membrane antigen, survivin, prostein, and also an HLA-A*0201-restricted T cell epitope derived from the PCa-associated protein TRPM8 (TRPM8 187–195, GLMKYIGEV) [63]. Eight hormone-refractory PCa patients received a total of four vaccinations every week. One patient displayed a partial response (PSA decrease >50%) and three other patients showed stable PSA values or decelerated PSA increases. Three of four PSA responders also showed antigen-specific CD8$^+$T-cell activation against prostein, survivin, and prostate-specific membrane antigen. A TRPM8-restricted peptide specifically upregulated in PCa has been identified [44,49] and its ability to induce in vitro a specific T cell response and in vivo a partial response when loaded on myeloid DC cells has been demonstrated [63]. However, no increase of TRPM8-reactive CD8$^+$T-lymphocytes was detected after vaccination. These results, although partially positive for TRPM8 protein, evidenced that the application of cocktail-loaded DCs induces a transient protective clinical response [64]. Further study of the molecular structure of the TRPM8 channels is required to further improve this therapeutic approach.

Microribonucleic acids (miRNAs), small non-coding RNAs of approximately 22 bp, induce RNA interference by base-pairing with the 3′ untranslated region of mRNA, which triggers either mRNA translational repression or RNA degradation [65]. Thus, miRNAs function as sequence-specific inhibitors of gene expression. miRNAs are initially transcribed as precursor transcripts called primary miRNAs. Over 1000 different miRNAs are encoded by the human genome; approximately 20% to 30% of all genes are targeted by miRNAs, and a single miRNA may target up to 200 genes [66]. In human cancers, specific miRNAs are expressed in different tissues, and changes in the control of gene expression have been associated with carcinogenesis [67]. Furthermore, miRNAs regulate the expression of different TRP genes involved in human diseases. The analysis of a possible correlation between the expression of selected miRNAs and the *TRPM8* gene have shown an inverse correlation between high TRPM8 expression and low miR-26a expression. It was found that miR-26a expression was decreased in PCa tissues and cell lines, with androgen-independent PCa showing lower miR-26a

expression compared to androgen-dependent PCa [68]. Overexpression of miR-26a enhances apoptosis, and this upregulation is triggered by cytochrome c oxidase subunit II inhibition. In addition, a low miR-26a density results in an evidently poor prognosis.

TRPM3 plays a major role in the development and progression of clear cell renal cell carcinoma (ccRCC) with von Hippel-Lindau (VHL) loss mutation. TRPM3 expression is enhanced in human ccRCC with inactivated or deleted VHL. Loss of VHL inhibits the expression of miR204, that in turn leads to an increase of the oncogenic autophagy in ccRCC, resulting in augmented TRPM3 expression, a direct target of miR204 [69].

About 50% of the malignant ME show a somatic missense mutation at the amino acid residue V600 of the proto-oncogene B-raf (BRAF[600]). The BRAF inhibitor vemurafenib induces a regression of metastatic ME harboring BRAF[600] and extracellular vesicles from vemurafenib-treated ME show increased miR211-5p expression. In BRAF[600] ME cells, the increase of microphthalmia-associated transcription factor (MITF) that upregulates the TRPM1 gene expression and also miR211-5p transcription, resulting in the activation of anti-apoptotic molecules and in the survival of ME cells [70].

Further research is required to confirm a direct regulatory effect of miRNA on their potential TRP target genes and to the development of miRNA-based therapy.

Data relative to the effects of TRPM channel-related effects are synthetized in Table 2.

Table 2. Pharmacological modulation of TRPM channel expression and functions by natural and/or chemical agents in cancer cells.

Pharmacological Agent	TRP Target	Cancer Type	Effects	Mechanisms	References
Tricostatin A/ Sodium butirrate	TRPM2	BCa	Apoptosis (+)	Ca^{2+} entry↑	[71]
5FU/Leucoverin	TRPM2	BC, CRC	Apoptosis (+)	Ca^{2+} entry ↑	[35]
Se/Docetaxel	TRPM2	GBM	Apoptosis (+)	ROS generation ↑ Ca^{2+} entry ↑	[36]
WA	TRPM7	LK	Cell proliferation (-)	Mg^{2+}-dependent TRPM7 block ↑	[39]
WA	TRPM7	BC, GCa	Cell proliferation (-)	Mg^{2+}-dependent TRPM7 block ↑	[40]
Ginseroside Rd	TRPM7	GCa, BC	Apoptosis (+)	TRPM7 currents ↑	[41]
TG100-115 activity ↓	TRPM7	BC	Cell migration (-) Invasion(-)	TRPM7 Kinase	[38]
WS-12	TRPM8	PCa	Migration (-)	ND	[51,52]
Menthol	TRPM8	BCa	Cell viability (-) and death (+)	Mitochondrial depolarization ↑	[53]
BCTC	TRPM8	PCa	Cell proliferation (-)	Ca^{2+} entry ↓	[56]
Clotrimazole	TRPM8	PCa	Cell proliferation (-)	Ca^{2+} entry ↓	[56]
DD01050	TRPM8	PCa	Cell proliferation (-)	Ca^{2+} entry ↓	[56]

AMTB TRPM8		PCa	Cell proliferation (-)	ND	[57]
JNJ41876666 TRPM8		PCa	Cell proliferation (-)	ND	[57]
RQ	TRPM8	OSC	Cell migration and Invasion (-)	SOCE and MMP-9 activity ↓	[54]
CBG	TRPM8	CRC	Cell growth (-) Apoptosis (-)	Endocannabinoids reuptake ↑	[55]
Thisoquinoline-derived Urea 2,5'DKpiperazine derivates	TRPM8	PCa	Viability, cell growth and apoptosis (-)	Ca^{2+} entry ↓	[58]
Triphanyphosphine oxide TRPM5		ME	Lung metastasis (-)	ETA-induced $[Ca^{2+}]i$ ↓ MMP9 ↑	[37]

Abbreviation: 5-FU, fluorouracil; BC, breast carcinoma; BCa, bladder cancer; CBG, cannabigerol; CRC, colorectal carcinoma; ETA, extracellular acid; GBM, glioblastoma; GCa, gastric carcinoma; ME, melanoma; MMP-9, Metallo-proteases 9; OSC, oral squamous carcinoma; PCa, prostate carcinoma; ROS, reactive oxygen species; RQ, RQ-0023078; Se, Selenium; SOCE, Store Operated Calcium Entry; TRPM7, transient receptor potential melastanin 7; WA, Waixenicin A. ND, not detected. (↑) increment. (↓) reduction. (+) increase. (−) decrease..

4. TRPV Channels in Cancer Therapy

TRPV1 is a Ca^{2+}-permeable channel gated by oxidative stress and capsaicin (CPS) and inhibited by the TRPV1 blocker capsazepine (CPZ).

Targeting BC cells with MRS1477, a dihydropyridine derivative acting as a positive allosteric modulator of TRPV1 channels, induces apoptotic cell death. MRS1477 (2 μM) evokes Ca^{2+} signals in MCF-7 BC cells, but not in primary breast epithelial cells. Incubation with CPS (10 μM) for 72 h increases ROS production, caspase activity, and apoptosis of BC cells. These effects are further increased when cells are incubated with MRS1477 alone or in combination with CPS. The effects are TRPV1 specific, since CPZ inhibits both the effect of CPS and MRS1477. However, the tumor growth in MCF-7 tumor-bearing immunodeficient mice is not inhibited by MRS1477, suggesting that in vivo further studies are required [72].

In the same view, treatment of MCF-7 BC cells with cisplatin and/or alpha-lipoic acid (ALA) by activating TRPV1 increases $[Ca^{2+}]_i$ levels, ROS production, lipid peroxidation, mitochondrial membrane depolarization, PARP-1, caspase activation, and apoptosis, and these effects are decreased by CPZ [73].

Recently, static magnetic field application together with CPS (50 μM) has been found to increase its anticancer effects in HepG2 cancer cells by enhancing the CPS-induced mitochondrial-dependent apoptosis. These synergistic effects could be the result of an increased binding efficiency of CPS to TRPV1, induced by a static magnetic field [74].

In the human PC-3 PCa cell line, CPS (20 μM) induces a $[Ca^{2+}]_i$ increase that is antagonized by CPZ [75]. Moreover, CPS inhibits the DNA synthesis and increases the apoptotic bodies number. Addition of CPZ does not reduce CPS-induced apoptosis but stimulates apoptosis in a similar manner. Both CPS and CPZ increase the production of ROS and mitochondrial potential ($\Delta\Psi$m) dissipation, suggesting that oxidant stress induced by vanilloids in PC-3 cells is a TRPV1-independent effect. CPS and CPZ further induce caspase-3 activation and reduce tumor growth in vivo. Thus, vanilloids could be used as pharmacological tools against hormone-refractory PCa; however, the contribution of TRPV1 as a potential target is still unclear [75].

The TRPV1 channel has been reported to be the main target of CPS-induced apoptosis in GBM. In the GBM cell line U373, CPS (50 μM) increases $[Ca^{2+}]_i$ and induces p38 activation, $\Delta\Psi$m dissipation, and caspase-3 activation, leading to apoptosis. All these effects are reverted by CPZ. Interestingly, the TRPV1 expression is inversely correlated with the grade in GBM, suggesting that TRPV1 may negatively control cancer progression. The loss of TRPV1 in high-grade GBM may represent a mechanism by which cancer cells can evade anti-proliferative and pro-apoptotic signals [76].

Stock et al. showed that in high-grade astrocytomas (AS), neural precursor cells, by releasing endovanilloids that activate TRPV1 channels in cancer cells, induce cell death [77]. Treatment of high-grade AS with arvanil (50 nM) induces a TRPV1-dependent cell death as a consequence of endoplasmic reticulum (ER) stress triggering and TRPV1 expression in the ER membrane. CPZ reversed cell death in high-grade AS in a TRPV1-dependent manner.

In BCa, the TRPV1 agonist CPS (80 μM) promotes Fas/CD95-mediated apoptosis [78]. CPS reduces in a dose-dependent manner the proliferation of the human well-differentiated low-grade papillary RT4 BCa cell line. Moreover, CPS induces the upregulation of pro-apoptotic genes as well as TRPV1-Fas/CD95 receptor clustering and activation, which trigger both extrinsic and intrinsic mitochondrial-dependent pathways. Importantly, all of these effects are reversed by CPZ. Similarly, to GBM, TRPV1 expression decreased in invasive BCas with a complete loss of TRPV1 in high-grade cancers [78]. Moreover, a more aggressive gene phenotype and invasiveness has been evidenced in BCa cells lacking TRPV1 [79].

The agonist CPS evokes Ca^{2+} influx in etoposide-resistant but not in etoposide-sensitive WERI-Rb1 retinoblastoma cells [80]. A recent report [81] shows the synergistic effect of CPS in combination with the tyrosine kinase inhibitor, sorafenib, in HCC patients. The drug combination exerts a potent anti-tumor effect by suppressing the EGFR and the PI3K/Akt/mTOR signaling pathways. At present, the contribution of TRPV1 to the CPS-mediated effect has not been addressed so far.

TRPV1 is also involved in increasing the chemosensitivity of cisplatin induced by ALA in BC cells. ALA administration, through TRPV1 activation, increases cisplatin-induced apoptosis, stimulating mitochondrial membrane depolarization, ROS production, lipid peroxidation, caspase-3 and -9 expression, and the first responder of DNA damage, PARP-1. ALA-dependent stimulation of TRPV1 enhances oxidative stress, making BC cells more sensitive to the action of chemotherapeutic drug [73]. TRPV1 channels are sensitive to endocannabinoid exposure, which suppresses cell invasion. Indeed, Ramer et al. showed that low concentrations of R(+)- methanandamide decreased cell invasion and this effect was reversed by CPZ in human cervical cancer cells (HeLa, C33A) as well as human lung carcinoma cells (A549) [82].

Finally, CPZ has been studied as a potential pharmacological tool in cancer. Indeed, at the 50 nM concentration, CPZ sensitizes CRC cells to apoptosis stimulated by tumor necrosis factor (TNF)-related apoptosis-induced ligand [83].

The role of TRPV2 in cancer is still unclear. While it has been described as a regulator of stem-like cell differentiation and chemotherapeutics uptake in GBM, it is also associated with the metastatic status of PCa and BCa, where it stimulates cell migration and invasion.

Cannabidiol (CBD) is a non-psychoactive cannabinoid with anti-tumor activities, acting as a TRPV2 agonist. Nabissi et al. showed that CBD (about 20 µM) increased drug uptake and potentiated cytotoxic activity in GBM when co-administered with cytotoxic agents [84]. Moreover, TRPV2 has been shown to promote, both in vitro and in vivo, differentiation of glioma stem-like cells, leading to a decreased proliferation rate [85].

Over-expression of TRPV2 in GBM increases the sensitivity to Fas/CD95 and Carmustine (BCNU)-induced cytotoxicity [84,85]. In addition, CBD-induced TRPV2 activation reduced BCNU resistance in GBM cells. In fact, CBD inhibits the Ras/Raf/MEK/ERK pathway and promotes drug retention in GBM cells, by restoring the chemoresistant phenotype, improving the apoptosis induced by temozolomide (TMZ), BCNU, and doxorubicin. Mutations of the TRPV2 pore completely inhibit CBD-induced chemoresistance. CBD, through TRPV2 activation, stimulates autophagy in glioma stem-like cells, promoting cell differentiation, and increasing the sensitivity to BCNU- and TMZ-mediated apoptosis [85]**.**

Furthermore, in MM cells, CBD induces TRPV2 upregulation and enhances the sensitivity to Bortezomib, improving cell growth inhibition, cell cycle arrest at the G1 phase, and mitochondrial and ROS-dependent necrosis, mainly in TRPV2-transfected RPMI8226 and U266 MM cells.

TRPV2 activation by CBD (20 µM) decreases proliferation and increases susceptibility to the proteasome inhibitor, bortezomib (3 ng/mL)-induced cell death in human MM cells. Previous studies have found the presence of heterogeneous $CD138^+TRPV2^+$ and $CD138^+TRPV2^-$ plasma cell subpopulations in MM patients. CBD, itself or in synergy with bortezomib, is able to inhibit growth, arrest cell cycle progression, and induce MM cell death by regulating the ERK, Akt, and NF-κB pathways with major effects in $CD138^+TRPV2^+$ MM cells [86,87]**.**

It has also been shown that endogenous lysophospholipids, including lysophosphatidylcholine and lysophosphatidylinositol, enhance the migration of human PCa (PC-3) cells via Ca^{2+} influx through TRPV2 channels by promoting its translocation to the membrane [88]. Similarly, adrenomedullin promote migration and invasion of PC-3 and T24/83 UC cells, through TRPV2 translocation to the plasma membrane, increase resting Ca^{2+} levels [89].

Recent reports suggest that TRPV2 is involved in the maintenance of cancer stem cells (CSCs). By microarray analysis, TRPV2 is found to be upregulated in CSCs. Tranilast, a TRPV2 inhibitor, at 50 µM, suppress OSCC stem cells, generated from ALDH1A1-positive OSCC TE8 cells, more than non-CSC and decreases tumor sphere numbers. Furthermore, tranilast reduces the cell population, which express ALDH1A1 among TE8 cells, suggesting a potential role as a targeted therapeutic agent against cisplatin-resistant OSCC, since CSCs, generated from TE8 cells, are resistant to cisplatin and have the ability to re-differentiate [90]. In addition to TRPV2, tranilast is also a weak TRPM2 inhibitor [91].

The antimicrobial peptide hCAP18/LL-37 stimulates cell migration and metastasis in several cancers. In BC, LL-37 (2 mM) induces migration by activating the TRPV2 and recruiting it to

pseudopodia in a PI3K/AKT-dependent manner. Ca^{2+}entry, through TRPV2, cooperates with a K^+ efflux through the large conductance Ca^{2+}-activated K^+ (BKCa) channels. However, LL-37 attaches to the membranes of caveolae and pseudopods and decreases the fluidity of the membrane, suggesting it as a mechanism of changes in the physical properties of the bilayer lipid membrane [92], instead of TRPV2-specific binding.

The TRPV6 channel is overexpressed in different cancers [93]. Soricidin and its derivatives (SOR-C13, 14 nM ;and SOR-C27, 65 nM) inhibit TRPV6-dependent Ca^{2+} uptake and bind TRPV6 with a high affinity in ovarian cancer (OC) [94]. Soricidin is a 54-amino acid peptide found in the paralytic venom of the short-tailed shrew *Blarinabrevicauda.* Recently, Bowen et al. described the use of the TRPV6-binding properties of SOR-C13 and SOR-C27 to target human OCs in a xenograft mouse model [94]. In addition, the side effects and best dose as well as safety/tolerability, pharmacokinetics, pharmacodynamics, and efficacy in treating patients with solid tumors, were evaluated in two different clinical trials (NCT03784677, NCT01578564, respectively). The first trial is in the recruiting stage (clinicaltrials.gov accessed 4 November 2019), whereas the data of the second one trial has been recently published. These data show that the administration of SO-C13, up to 6.2 mg/kg, induces in 54.5% of patients (n = 22 patients) a stable disease, ranging from 2.8 to 12.5 months, and the best response was a 27% reduction in PC, with a 55% reduction in CA19-9 marker levels [95]. TRPV6 has been shown to mediate the CPS-induced apoptosis (at 50 μM dose) in GaC cells [96] and, interestingly, GaC cells are more sensitive to CPS-induced apoptosis than normal gastric cells. The pretreatment with CPZ prevents CPS-induced TRPV6 expression and apoptosis of GaC cells. The mechanism involved in CPS-induced apoptosis of AGS cells depends on increased Ca^{2+} influx via TRPV6 channels; moreover, CPS induces apoptosis by stabilization of p53 through c-Jun N-terminal kinases activation.

Calcitriol, in combination with dietary soy, enhances anticancer activity and increases hypercalcemic toxicity in a mouse xenograft model of PCa. This combination upregulates the expression of anti-proliferative (p21, IGFBP-3) and pro-apoptotic (Bax) genes, increasing the inhibition of anti-apoptotic (Bcl-2) and cell cycle-promoting (cyclin D1) genes, thus suppressing prostaglandin (PG) synthesis and signaling (COX-2, 15-PGDH). These effects seem to be TRPV6-dependent; in fact, the calcium increase in serum is associated with elevated TRPV6 and calbindin-9k, an intestinal calcium absorption gene [97].

The TRPV6 channel is upregulated in BC cell lines and in BC samples compared to normal tissue. TRPV6 overexpression is associated with reduced OS in estrogen receptor-negative BCs as well as HER2-positive tumors. Downregulation of TRPV6 expression reduces basal Ca^{2+}influx, leading to a reduction in cell proliferation and DNA synthesis [98]. In *Xenopus* oocytes transfected with TRPV6, tamoxifen inhibits Ca^{2+}uptake and the expression of TRPV6 at mRNA levels in BC cell lines. The silencing of TRPV6 improves the pro-apoptotic activity of tamoxifen, suggesting that the increase of Ca^{2+}influx, mediated by TRPV6 overexpression in BCs, is responsible for the reduced sensitivity to tamoxifen treatment [99]. Tamoxifen is also able to inhibit TRPV6 activity through estrogen receptor-independent pathways in TRPV6-overexpressing MCF-7 BC cells. Tamoxifen reduces the basal intracellular Ca^{2+}concentration and this inhibitory effect is not blocked by the estrogen receptor antagonist, ICI 182,720. The effect of tamoxifen is completely blocked by activation of protein kinase C (PKC). After inhibiting the PKC with calphostin C, the activity of TRPV6 is decreased but does not alter the effect of tamoxifen, suggesting that the therapeutic effect of tamoxifen and PKC inhibitors might lead to the entry of TRPV6-mediated calcium [100].

The expression level of TRPV6, assessed using laser capture microdissection, is higher in invasive BC tissue than in the non-invasive one. In addition to MCF-7 cell migration inhibition, TRPV6 silencing can inhibit MDA-MB-231 migration and invasion [27]. Moreover, limited estrogen receptor signaling leads to lower levels of TRPV6 expression and the antitumor effect of tamoxifen seem to be related to inhibition of TRPV6 channel expression [101].

Data relative to the effects of TRPV channel-related effects are synthetized in Table 3.

Table 3. Pharmacological modulation of TRPV channel expression and functions by natural and/or chemical agents in cancer cells.

Pharmacological Agent	TRP Target	Cancer Type	Effects	Mechanisms	References
CPS	TRPV1	PCa	Cell growth (−)and apoptosis (+)	$[Ca^{2+}]$ ↑ Oxidative stress ↑	[75]
CPS	TRPV1	GBM	Apoptosis (+)	Ca^{2+} entry ↑	[76]
CPS	TRPV1	BCa	Cell growth (−)	$[Ca^{2+}]i$ ↑	[78]
Arvanil	TRPV1	AS	Apoptosis (+)	ER stress ↑	[77]
ALA/cisplatin	TRPV1	BC	ROS-induced apoptosis (+)	$[Ca^{2+}]$ ↑	[73]
CPS /MRS1477	TRPV1	BC	Cell viability (−) and apoptosis (+)	Oxidative Stress ↑	[72]
CPS /SM field	TRPV1	HCC	Apoptosis (+)	Binding affinity ↑	[74]
CPS /Sorafenib	TRPV1 (?)	HCC	Invasion (−) and autophagy (+)	AMPK activity ↓	[81]
CBD	TRPV2	GBM	Apoptosis (+) and drug sensitization (+)	Ca2+ entry ↑	[84]
CBD/Bortezomib	TRPV2	MM	Cell proliferation (−)and Drug sensitivity (+)	ERK activity ↓	[86]
LL-37 peptides	TRPV2 and BKCa	BC	Cell migration (+)	Ca^{2+} and K^+ entry ↑	[92]
Tranilast	TRPV2	OSCC	Cytotoxicity (+)	Stemness ↓	[90]

CPS	TRPV6	GCa	Apoptosis (+)	Ca^{2+} entry ↑	[96]
Tamoxifen	TRPV6	BC	Transport Ca2+ rate (−)	PKC inhibition ↑	[100]
Calcitriol	TRPV6	BC	Cell growth (+)	Ca^{2+} entry ↑	[93]
	TRPV6	LK	Cell differentiation (+)	Ca^{2+} entry (?)	[93]
SOR-C13/SOR-C27	TRPV6	OC, PCa	Cell proliferation (−)	[Ca^{2+}]i ↓	[94]

Abbreviation: ALA, Lipoich acid; AS, astrocytoma; GBM, glioblastoma; BC, breast carcinoma; BKCa, large-conductance voltage-and Ca2+ activated K+ channel; CBD, cannabidiol; CPS, Capsaicin; ER, endoplasmatic reticulum; ERK, extracellular signal–regulated kinases; GCa, gastric carcinoma; HCC, hepatocarcinoma; MM, multiple myeloma; OC, ovarian carcinoma; OSCC, eosophageal squamous carcinoma; PCa, Prostate carcinoma; Se, selenium; SM field, static magnetic field. (↑) increment. (↓) reduction. (+) increase. (−) decrease. (?) no conclusive data.

5. TRPA1 Channels in Cancer Therapy

Recent evidence shows that TRPA1 is involved in chemotherapy-induced pain syndrome. Thus, dacarbazine (DBZ), used mainly to treat metastatic melanoma, is reported to cause painful symptoms. Experiments using mouse dorsal root ganglion neurons and human TRPA1-transfected HEK293 (hTRPA1-HEK293) cells as well as naïve mice and TRPA1-knockout mice (1 mg/Kg/day) and B16-F10 melanoma cells treated with DBZ, demonstrated that DBZ directly activates TRPA1 and sensitizes it indirectly by generating oxidative stress products. Moreover, DBZ causes mechanical and cold allodynia in naïve but not in TRPA1-knockout mice. Pharmacological blockade of TRPA1 also reduces DBZ-induced nociception in a tumor-associated pain model [102].

On the other hand, in GBM cells, it has been shown that inhibition of TRPA1 is not a good strategy to kill cancer cells. Indeed, the ALA at 50 μM inhibits the TRPA1 channel in human GBM (DBTRG) cells, attenuating hypoxia-induced apoptosis, inflammation, and TRPA1-mediated mitochondrial oxidative stress [103].

Resveratrol induces activation of mutated TRPA1 in human PCa-associated fibroblasts. Previous studies have shown the effects of Resveratrol (6.5 μM) in inducing apoptosis in PCa cells without taking into consideration its impact on the tumor microenvironment. Recently, it has been reported that resveratrol activates N-terminal-mutated TRPA1, leading to intracellular calcium increase, and increases HGF and VEGF expression and secretion, without inducing apoptosis in these cells [104].

The steroidal and non-steroidal third-generation aromatase inhibitors, exemestane, letrozole and anastrozole, used in BCs, induce pain-like symptoms through TRPA1, suggesting that TRPA1 antagonists can be used for the treatment of pain associated with aromatase inhibitors [105]. Methyl syringate (100 μM), a TRPA1 agonist, has been reported to repress hypoxia-induced cyclooxygenase-2 (COX-2) in lung A549 cancer cells [106]. Methyl syringate suppresses in a TRPA1-dependent manner hypoxia-induced COX-2 and promoter activity and reduced hypoxia-induced migration and invasion and secretion of vascular endothelial growth factor.

Stimulation of TRPA1 by allyl isothiocyanate (AITC), at 10 mM, promotes cell survival of small cell lung cancer cells (SCLCs) [107]. TRPA1 mRNA is significantly expressed in SCLC patients as compared to non-SCLC samples or non-malignant lung tissue. Stimulation of SCLC cells with AITC leads to a rise of $[Ca^{2+}]_i$. Furthermore, AITC stimulates ERK in TRPA1-expressing HEK293 cells and in SCLC cells via an Src- and calcium-dependent mechanism. In addition, TRPA1 activation in SCLC cells prevents apoptosis and induces survival in a TRPA1- and ERK-dependent manner. On the contrary, downregulation of TRPA1 impairs the growth of SCLC cells. These data suggest that exogenous inhalable activators of TRPA1 exert tumor-promoting effects in SCLC cells. Finally, blockade of TRPA1 by its antagonist HC-030031 prevents chemotherapy-induced peripheral neuropathy [108].

Data relative to the effects of TRPA1 channel-related effects are synthetized in Table 4.

Table 4. Pharmacological modulation of TRPA channel expression and functions by natural and/or chemical agents in cancer cells.

	TRP Target	Cancer Type	Effects	Mechanisms	References
Dacarbazine	TRPA1	ME	Hypersensitivity (+)	Oxidative stress ↑	[102]
ALA	TRPA1	GBM	Apoptosis (−)	Mitochondrial oxidative stress ↓	[103]
Res	TRPA1	PCa	Apoptosis (−)	Growth Factor release ↑	[104]
Exemestane, Letrozole Anastrozole (Als)	TRPA1	BC	Nociception and allodynia (+)	Ca^{2+} entry ↑	[105]
Methyl syringate	TRPA1	NSCLC	Migration and invasion(−) VEGF (−)	Hypoxia induced COX-2/PGE2 activity ↓	[106]
AITC	TRPA1	NSCLC	Apoptosis (−)	Ca^{2+} entry ↑	[107]

Abbreviations: ALA, Alpha Lipoic acid; Als, aromatase inhibitors; AITC, Allyl isothiocyanate; BC, breast carcinoma; GBM, glioblastoma; ME, melanoma; NSCLC, non small cell lung carcinoma; OSC, oral squamous carcinoma; PCa, prostate carcinoma; Res, Resveratrol. (↑) increment. (↓) reduction. (+) increase. (−) decrease.

6. Conclusions

Despite advances in the detection of more specific therapies for various tumors, high rates of treatment failure and mortality still exist. These high rates depend on the ability of tumors to progress from local to systemic disease. TRP channels are Ca^{2+}-selective ion channels involved in cancer development and metastatic spreading by controlling different stages of tumor progression. Several pharmacological approaches targeting the TRP channels in cancer have been employed. However, the major obstacle in evaluating the effects of TRP agonists/antagonists and inhibitors/activators in cell lines or in other experimental models is due with their reduced specificity. Although most of these studies have provided interesting data on the cellular and molecular mechanisms driving tumor progression, the development of new specific drugs targeting TRP channels is only just beginning. In addition, although it is well known that the expression of TRP channels is altered during cancer progression, the TRP signaling pathways conditioning the behaviors of cancer cells as well as the pharmacological response are still poorly elucidated.

In this regard, previously, we demonstrated that ERK-induced TRPV2 activation by treatment with TRPV2 agonist, CBD, overcomes drug resistance in GBM [84,109]. Moreover, recently, it has been reported that the endolysosomal TRPML1 channel, belonging to the mucolipin TRP channel family, is required for cancer cell proliferation bearing HRAS mutations and that TRPML1 expression was significantly elevated in HRAS-positive tumors and inversely correlated with poor prognosis. Mutations of KRAS and HRAS in cancer affect the efficacy of chemotherapy; changes in TRP channel expression could overcome drug resistance and increase the sensitivity of cancer cells to chemotherapy [110]. The mucolipin TRPML1 receptor is also required in ME cells to negatively regulate MAPK and mTORC1 signaling [111] and in TNBC, where it regulates cancer development by promoting mTORC1 and purinergic signaling pathways [112].

Overall, we are only beginning to develop drugs specifically targeting TRP channels and TRP-mediated signaling pathways.

Furthermore, the role of changes in the epigenetics of TRP channels in cancers should also be considered. It has been demonstrated that inactivation of *TRP* genes by aberrant methylation (hyper- and hypo-methylation) of GC-rich DNA regions, CpG islands, is suggested to be involved in tumor development and progression. In this regard, hydrogen peroxide has been found to induce demethylation of the TRPM2 promoter region and increase the expression of TRPM2 in melanocytes [113]; the TRPM6 and TRPM7 ion channels have been found to bind to the chromatin-remodeling complexes, induce histone phosphorylation, and decrease arginine methylation, resulting in changes in the transcription of hundreds of genes [114,115]; transactivation of TRPA1 promoter by Notch1 receptor intracellular domain, which promotes TRPA1 expression in erytroleukemic cells, suppresses erythroid differentiation [116]. Moreover, regarding cancer chemoresistance, miR-320a is a mediator of the chemoresistance of BC cells by targeting TRPC5 and NFATc3 and the expression of miR320a is regulated by methylation of its promoter and the transcription factor, v-ets erythroblastosis virus E26 oncogene homolog 1 [117].

Aberrations in the expression of different splice variants, and their expression during tumor progression, may trigger a variety of Ca^{2+} signaling, which may contribute to the generation of more aggressive tumor clones. Thus, in PCa cells, two short splice variants of TRPM8, named TRPM8α and TRPM8β, with reducing activity, have been identified [118], and two different TRPM1 isoforms have been reported in human ME [119]. Finally, in BCa, an alternative splice variant of TRPV2 that acts as a dominant negative mutant of wild-type TRPV2 has been identified [120].

Epigenetic changes of TRP channels could be the rationale to approach a personalized therapy in cancer patients. Further studies are required to completely achieve this important issue. Deeper studies on TRP ion channels in cancer are required in order to have a major impact on the development of new drugs targeting the TRP signaling network and TRP isoforms in cancer cells.

Conflicts of Interest: The authors declare no conflict of interest

Abbreviations

2-APB	2-Aminoethoxydiphenyl borate
20-GPPD	20-O-β-D-glucopyranosyl-20(S)-protopanaxadiol
5-Fu	5-Fluorouracil
ADMR	adriamycin resistant
AITC	allyl isothiocyanate
AKT	protein kinase B
ALA	α-lipoic acid
AMPK	AMP-activated protein kinase
AR	androgen receptor
AS	astrocytoma
ATRA	all-trans retinoic acid
BC	breast cancer
BKCa	large-conductance voltage-and Ca^{2+}activated K^+channel
CBD	cannabidiol
CBG	cannabigerol
ccRCC	clear cell renal cell carcinoma
CHOP	CCAAT-enhancer-binding protein homologous protein
CPS	capsaicin
CPZ	capsazepine
CRC	colorectal cancer
CSC	cancer stem cell
DBZ	dacarbazine
DC	dendritic cell
DTX	docetaxel
EA	Englerin A
EGF	epidermal growth factor
EMT	epithelial mesenchymal transition
ERK	extracellular signal–regulated kinases
EV	extracellular vessicle
GaC	gastric cancer
GBM	glioblastoma
GSK-3β	glycogen synthase kinase-3β
HCC	hepatocellular carcinoma
HIF-1α	hypoxia Inducible Factor 1α
IP$_3$	inositol triphosphate
LCV	leucovorin
ME	melanoma
MEL	melatonin
miRNA	microribonucleic acid
MM	multiple myeloma
MMP-9	matrix metalloproteinase-9
MITF	microphthalmia-associated transcription factor

NFATc3	nuclear factor of activated T-cells 3
NSCLC	non-small cell lung cancer
OC	ovarian carcinoma
OS	overall survival
OSCC	eosophageal carcinoma
OSC	oral squamous carcinoma
PARP-1	poly (ADP-ribose) polymerase-1
PC	pancreatic cancer
PCa	prostate cancer
PG	prostaglandin
P-gp	P-glycoprotein
PI3K	phosphatidylinositole–3-kinase
PKC	protein kinase C
PSA	prostate-specific antigen
RACK1	receptor of activated protein C kinase 1
RCC	renal cell carcinoma
RES	resveratrol
ROS	reactive oxigen species
Se	selenium
SSC	synovial sarcoma cell
SOCC	store operated calcium channels
SOCE	store-operated calcium entry
TNBC	triple-negative breast cancer
TRP	transient potential receptor
TRPA	transient potential receptor ankyrin
TRPC	transient potential receptor canonical
TRPM	transient potential receptor melastatin
TRPML	transient potential receptor mucolipidin
TRPP	transient potential receptor polycystic
TRPV	transient potential receptor vanilloid
TZL	tonantzitlolone
Vac	vacquinol-1
VHL	von Hippel-Lindau
WA	waixenicin A

References

1. Zheng, J. Molecular mechanism of TRP channels. *Compr. Physiol.* **2013**, *3*, 221–242.
2. Du, J.-D.; Zheng, X.; Chen, Y.-L.; Huang, Z.-Q.; Cai, S.-W.; Jiao, H.-B.; Zhu, Z.-M.; Hu, B. Elevated Transient Receptor Potential Melastatin 8 (TRPM8) Expression Is Correlated with Poor Prognosis in Pancreatic Cancer. *Med. Sci. Monit.* **2018**, *24*, 3720–3725.
3. Gao, S.-L.; Kong, C.-Z.; Zhang, Z.; Li, Z.-L.; Bi, J.-B.; Liu, X.-K. TRPM7 is overexpressed in bladder cancer and promotes proliferation, migration, invasion and tumor growth. *Oncol. Rep.* **2017**, *38*, 1967–1976.
4. Nakashima, S.; Shiozaki, A.; Ichikawa, D.; Hikami, S.; Kosuga, T.; Konishi, H.; Komatsu, S.; Fujiwara, H.; Okamoto, K.; Kishimoto, M.; et al. Transient Receptor Potential Melastatin 7 as an Independent Prognostic Factor in   Human Esophageal Squamous Cell Carcinoma. *Anticancer Res.* **2017**, *37*, 1161–1167.
5. Zhang, S.-S.; Xie, X.; Wen, J.; Luo, K.-J.; Liu, Q.-W.; Yang, H.; Hu, Y.; Fu, J.-H. TRPV6 plays a new role in predicting survival of patients with esophageal squamous cell carcinoma. *Diagn. Pathol.* **2016**, *11*, 14.
6. Li, X.; Zhang, Q.; Fan, K.; Li, B.; Li, H.; Qi, H.; Guo, J.; Cao, Y.; Sun, H. Overexpression of TRPV3 Correlates with Tumor Progression in Non-Small Cell Lung Cancer. *Int. J. Mol. Sci.* **2016**, *17*, 437.
7. Morelli, M.B.; Amantini, C.; Tomassoni, D.; Nabissi, M.; Arcella, A.; Santoni, G. Transient Receptor Potential Mucolipin-1 Channels in Glioblastoma: Role in Patient's Survival. *Cancers* **2019**, *11*, 525.

8. Loo, S.K.; Ch'ng, E.S.; Md Salleh, M.S.; Banham, A.H.; Pedersen, L.M.; Moller, M.B.; Green, T.M.; Wong, K.K. TRPM4 expression is associated with activated B cell subtype and poor survival in diffuse large B cell lymphoma. *Histopathology* **2017**, *71*, 98–111.

9. Santoni, G.; Farfariello, V. TRP channels and cancer: New targets for diagnosis and chemotherapy. *Endocr. Metab. Immune Disord. Drug Targets* **2011**, *11*, 54–67.

10. Liberati, S.; Morelli, M.B.; Nabissi, M.; Santoni, M.; Santoni, G. Oncogenic and anti-oncogenic effects of transient receptor potential channels. *Curr. Top. Med. Chem.* **2013**, *13*, 344–366.

11. Hwang, J.A.; Hwang, M.K.; Jang, Y.; Lee, E.J.; Kim, J.-E.; Oh, M.H.; Shin, D.J.; Lim, S.; og Ji, G.; Oh, U.; et al. 20-O-beta-d-glucopyranosyl-20(S)-protopanaxadiol, a metabolite of ginseng, inhibits colon cancer growth by targeting TRPC channel-mediated calcium influx. *J. Nutr. Biochem.* **2013**, *24*, 1096–1104.

12. Bomben, V.C.; Sontheimer, H.W. Inhibition of transient receptor potential canonical channels impairs cytokinesis in human malignant gliomas. *Cell Prolif.* **2008**, *41*, 98–121.

13. Bomben, V.C.; Sontheimer, H. Disruption of transient receptor potential canonical channel 1 causes incomplete cytokinesis and slows the growth of human malignant gliomas. *Glia* **2010**, *58*, 1145–1156.

14. Bomben, V.C.; Turner, K.L.; Barclay, T.-T.C.; Sontheimer, H. Transient receptor potential canonical channels are essential for chemotactic migration of human malignant gliomas. *J. Cell. Physiol.* **2011**, *226*, 1879–1888.

15. He, B.; Liu, F.; Ruan, J.; Li, A.; Chen, J.; Li, R.; Shen, J.; Zheng, D.; Luo, R. Silencing TRPC1 expression inhibits invasion of CNE2 nasopharyngeal tumor cells. *Oncol. Rep.* **2012**, *27*, 1548–1554.

16. Carson, C.; Raman, P.; Tullai, J.; Xu, L.; Henault, M.; Thomas, E.; Yeola, S.; Lao, J.; McPate, M.; Verkuyl, J.M.; et al. Englerin A Agonizes the TRPC4/C5 Cation Channels to Inhibit Tumor Cell Line Proliferation. *PLoS ONE* **2015**, *10*, e0127498.

17. Grant, C.V.; Carver, C.M.; Hastings, S.D.; Ramachandran, K.; Muniswamy, M.; Risinger, A.L.; Beutler, J.A.; Mooberry, S.L. Triple-negative breast cancer cell line sensitivity to englerin A identifies a new, targetable subtype. *Breast Cancer Res. Treat.* **2019**, *177*, 345–355.

18. Muraki, K.; Ohnishi, K.; Takezawa, A.; Suzuki, H.; Hatano, N.; Muraki, Y.; Hamzah, N.; Foster, R.; Waldmann, H.; Nussbaumer, P.; et al. Na$^+$ entry through heteromeric TRPC4/C1 channels mediates (−)Englerin A-induced cytotoxicity in synovial sarcoma cells. *Sci. Rep.* **2017**, *7*, 16988.

19. Ludlow, M.J.; Gaunt, H.J.; Rubaiy, H.N.; Musialowski, K.E.; Blythe, N.M.; Vasudev, N.S.; Muraki, K.; Beech, D.J. (-)-Englerin A-evoked Cytotoxicity Is Mediated by Na$^+$ Influx and Counteracted by Na$^+$/K$^+$-ATPase. *J. Biol. Chem.* **2017**, *292*, 723–731.

20. Rubaiy, H.N.; Seitz, T.; Hahn, S.; Choidas, A.; Habenberger, P.; Klebl, B.; Dinkel, K.; Nussbaumer, P.; Waldmann, H.; Christmann, M.; et al. Identification of an (-)-englerin A analogue, which antagonizes (-)-englerin A at TRPC1/4/5 channels. *Br. J. Pharmacol.* **2018**, *175*, 830–839.

21. Minard, A.; Bauer, C.C.; Chuntharpursat-Bon, E.; Pickles, I.B.; Wright, D.J.; Ludlow, M.J.; Burnham, M.P.; Warriner, S.L.; Beech, D.J.; Muraki, K.; et al. Potent, selective, and subunit-dependent activation of TRPC5 channels by a xanthine derivative. *Br. J. Pharmacol.* **2019**, *176*, 3924–3938.

22. Emmons, M.F.; Anreddy, N.; Cuevas, J.; Steinberger, K.; Yang, S.; McLaughlin, M.; Silva, A.; Hazlehurst, L.A. MTI-101 treatment inducing activation of Stim1 and TRPC1 expression is a determinant of response in multiple myeloma. *Sci. Rep.* **2017**, *7*, 2685.

23. Jiang, H.-N.; Zeng, B.; Zhang, Y.; Daskoulidou, N.; Fan, H.; Qu, J.-M.; Xu, S.-Z. Involvement of TRPC channels in lung cancer cell differentiation and the correlation analysis in human non-small cell lung cancer. *PLoS ONE* **2013**, *8*, e67637.

24. Wang, Y.; He, J.; Jiang, H.; Zhang, Q.; Yang, H.; Xu, X.; Zhang, C.; Xu, C.; Wang, J.; Lu, W. Nicotine enhances storeoperated calcium entry by upregulating HIF1alpha and SOCC components in nonsmall cell lung cancer cells. *Oncol. Rep.* **2018**, *40*, 2097–2104.

25. Ma, X.; Cai, Y.; He, D.; Zou, C.; Zhang, P.; Lo, C.Y.; Xu, Z.; Chan, F.L.; Yu, S.; Chen, Y.; et al. Transient receptor potential channel TRPC5 is essential for P-glycoprotein induction in drug-resistant cancer cells. *Proc. Natl. Acad. Sci. USA* **2012**, *109*, 16282–16287.

26. Ma, X.; Chen, Z.; Hua, D.; He, D.; Wang, L.; Zhang, P.; Wang, J.; Cai, Y.; Gao, C.; Zhang, X.; et al. Essential role for TrpC5-containing extracellular vesicles in breast cancer with chemotherapeutic resistance. *Proc. Natl. Acad. Sci. USA* **2014**, *111*, 6389–6394.

27. Xu, Y.; Wu, X.; Li, F.; Huang, D.; Zhu, W. CDCA4, a downstream gene of the Nrf2 signaling pathway, regulates cell proliferation and apoptosis in the MCF7/ADM human breast cancer cell line. *Mol. Med. Rep.* **2018**, *17*, 1507–1512.

28. Zhang, P.; Liu, X.; Li, H.; Chen, Z.; Yao, X.; Jin, J.; Ma, X. TRPC5-induced autophagy promotes drug resistance in breast carcinoma via CaMKKbeta/AMPKalpha/mTOR pathway. *Sci. Rep.* **2017**, *7*, 3158.

29. Wang, T.; Chen, Z.; Zhu, Y.; Pan, Q.; Liu, Y.; Qi, X.; Jin, L.; Jin, J.; Ma, X.; Hua, D. Inhibition of transient receptor potential channel 5 reverses 5-Fluorouracil resistance in human colorectal cancer cells. *J. Biol. Chem.* **2015**, *290*, 448–456.

30. Wang, T.; Ning, K.; Lu, T.-X.; Hua, D. Elevated expression of TrpC5 and GLUT1 is associated with chemoresistance in colorectal cancer. *Oncol. Rep.* **2017**, *37*, 1059–1065.

31. Cai, R.; Ding, X.; Zhou, K.; Shi, Y.; Ge, R.; Ren, G.; Jin, Y.; Wang, Y. Blockade of TRPC6 channels induced G2/M phase arrest and suppressed growth in human gastric cancer cells. *Int. J. Cancer* **2009**, *125*, 2281–2287.

32. Shi, Y.; Ding, X.; He, Z.-H.; Zhou, K.-C.; Wang, Q.; Wang, Y.-Z. Critical role of TRPC6 channels in G2 phase transition and the development of human oesophageal cancer. *Gut* **2009**, *58*, 1443–1450.

33. Wen, L.; Liang, C.; Chen, E.; Chen, W.; Liang, F.; Zhi, X.; Wei, T.; Xue, F.; Li, G.; Yang, Q.; et al. Regulation of Multi-drug Resistance in hepatocellular carcinoma cells is TRPC6/Calcium Dependent. *Sci. Rep.* **2016**, *6*, 23269.

34. Toth, B.; Csanady, L. Identification of direct and indirect effectors of the transient receptor potential melastatin 2 (TRPM2) cation channel. *J. Biol. Chem.* **2010**, *285*, 30091–30102.

35. Guler, Y.; Ovey, I.S. Synergic and comparative effect of 5-fluorouracil and leucoverin on breast and colon cancer cells through TRPM2 channels. *Bratisl. Lekarske Listy* **2018**, *119*, 692–700.

36. Ertilav, K.; Naziroglu, M.; Ataizi, Z.S.; Braidy, N. Selenium Enhances the Apoptotic Efficacy of Docetaxel Through Activation of TRPM2 Channel in DBTRG Glioblastoma Cells. *Neurotox. Res.* **2019**, *35*, 797–808.

37. Maeda, T.; Suzuki, A.; Koga, K.; Miyamoto, C.; Maehata, Y.; Ozawa, S.; Hata, R.-I.; Nagashima, Y.; Nabeshima, K.; Miyazaki, K.; et al. TRPM5 mediates acidic extracellular pH signaling and TRPM5 inhibition reduces spontaneous metastasis in mouse B16-BL6 melanoma cells. *Oncotarget* **2017**, *8*, 78312–78326.

38. Song, C.; Bae, Y.; Jun, J.; Lee, H.; Kim, N.D.; Lee, K.-B.; Hur, W.; Park, J.-Y.; Sim, T. Identification of TG100-115 as a new and potent TRPM7 kinase inhibitor, which suppresses breast cancer cell migration and invasion. *Biochim. Biophys. Acta Gen. Subj.* **2017**, *1861*, 947–957.

39. Zierler, S.; Yao, G.; Zhang, Z.; Kuo, W.C.; Porzgen, P.; Penner, R.; Horgen, F.D.; Fleig, A. Waixenicin A inhibits cell proliferation through magnesium-dependent block of transient receptor potential melastatin 7 (TRPM7) channels. *J. Biol. Chem.* **2011**, *286*, 39328–39335.

40. Kim, B.J.; Nam, J.H.; Kwon, Y.K.; So, I.; Kim, S.J. The role of waixenicin A as transient receptor potential melastatin 7 blocker. *Basic Clin. Pharmacol. Toxicol.* **2013**, *112*, 83–89.

41. Kim, B.J. Involvement of melastatin type transient receptor potential 7 channels in ginsenoside Rd-induced apoptosis in gastric and breast cancer cells. *J. Ginseng Res.* **2013**, *37*, 201–209.

42. Sander, P.; Mostafa, H.; Soboh, A.; Schneider, J.M.; Pala, A.; Baron, A.-K.; Moepps, B.; Wirtz, C.R.; Georgieff, M.; Schneider, M. Vacquinol-1 inducible cell death in glioblastoma multiforme is counter regulated by TRPM7 activity induced by exogenous ATP. *Oncotarget* **2017**, *8*, 35124–35137.

43. Yee, N.S.; Zhou, W.; Lee, M.; Yee, R.K. Targeted silencing of TRPM7 ion channel induces replicative senescence and produces enhanced cytotoxicity with gemcitabine in pancreatic adenocarcinoma. *Cancer Lett.* **2012**, *318*, 99–105.

44. Tsavaler, L.; Shapero, M.H.; Morkowski, S.; Laus, R. Trp-p8, a novel prostate-specific gene, is up-regulated in prostate cancer and other malignancies and shares high homology with transient receptor potential calcium channel proteins. *Cancer Res.* **2001**, *61*, 3760–3769.

45. Gentry, C.; Stoakley, N.; Andersson, D.A.; Bevan, S. The roles of iPLA2, TRPM8 and TRPA1 in chemically induced cold hypersensitivity. *Mol. Pain* **2010**, *6*, 4.

46. Weil, A.; Moore, S.E.; Waite, N.J.; Randall, A.; Gunthorpe, M.J. Conservation of functional and pharmacological properties in the distantly related temperature sensors TRVP1 and TRPM8. *Mol. Pharmacol.* **2005**, *68*, 518–527.

47. Zhang, L.; Barritt, G.J. TRPM8 in prostate cancer cells: A potential diagnostic and prognostic marker with a secretory function? *Endocr. Relat. Cancer* **2006**, *13*, 27–38.

48. Asuthkar, S.; Velpula, K.K.; Elustondo, P.A.; Demirkhanyan, L.; Zakharian, E. TRPM8 channel as a novel molecular target in androgen-regulated prostate cancer cells. *Oncotarget* **2015**, *6*, 17221–17236.

49. Henshall, S.M.; Afar, D.E.H.; Hiller, J.; Horvath, L.G.; Quinn, D.I.; Rasiah, K.K.; Gish, K.; Willhite, D.; Kench, J.G.; Gardiner-Garden, M.; et al. Survival analysis of genome-wide gene expression profiles of prostate cancers identifies new prognostic targets of disease relapse. *Cancer Res.* **2003**, *63*, 4196–4203.

50. Yang, Z.-H.; Wang, X.-H.; Wang, H.-P.; Hu, L.-Q. Effects of TRPM8 on the proliferation and motility of prostate cancer PC-3 cells. *Asian J. Androl.* **2009**, *11*, 157–165.

51. Grolez, G.P.; Hammadi, M.; Barras, A.; Gordienko, D.; Slomianny, C.; Volkel, P.; Angrand, P.O.; Pinault, M.; Guimaraes, C.; Potier-Cartereau, M.; et al. Encapsulation of a TRPM8 Agonist, WS12, in Lipid Nanocapsules Potentiates PC3 Prostate Cancer Cell Migration Inhibition through Channel Activation. *Sci. Rep.* **2019**, *9*, 7926.

52. Grolez, G.P.; Gordiendko, D. V.; Clarisse, M.; Hammadi, M.; Desruelles, E.; Fromont, G.; Prevarskaya, N.; Slomianny, C.; Gkika, D. TRPM8-androgen receptor association within lipid rafts promotes prostate cancer cell migration. *Cell Death Dis.* **2019**, *10*, 652.

53. Li, Q.; Wang, X.; Yang, Z.; Wang, B.; Li, S. Menthol induces cell death via the TRPM8 channel in the human bladder cancer cell line T24. *Oncology* **2009**, *77*, 335–341.

54. Okamoto, Y.; Ohkubo, T.; Ikebe, T.; Yamazaki, J. Blockade of TRPM8 activity reduces the invasion potential of oral squamous carcinoma cell lines. *Int. J. Oncol.* **2012**, *40*, 1431–1440.

55. Borrelli, F.; Pagano, E.; Romano, B.; Panzera, S.; Maiello, F.; Coppola, D.; De Petrocellis, L.; Buono, L.; Orlando, P.; Izzo, A.A. Colon carcinogenesis is inhibited by the TRPM8 antagonist cannabigerol, a Cannabis-derived non-psychotropic cannabinoid. *Carcinogenesis* **2014**, *35*, 2787–2797.

56. Valero, M.; Morenilla-Palao, C.; Belmonte, C.; Viana, F. Pharmacological and functional properties of TRPM8 channels in prostate tumor cells. *Pflugers Arch.* **2011**, *461*, 99–114.

57. Valero, M.L.; de Queiroz, F.M.; Stuhmer, W.; Viana, F.; Pardo, L.A. TRPM8 ion channels differentially modulate proliferation and cell cycle distribution of normal and cancer prostate cells. *PLoS ONE* **2012**, *7*, e51825.

58. De Petrocellis, L.; Arroyo, F.J.; Orlando, P.; Schiano Moriello, A.; Vitale, R.M.; Amodeo, P.; Sanchez, A.; Roncero, C.; Bianchini, G.; Martin, M.A.; et al. Tetrahydroisoquinoline-Derived Urea and 2,5-Diketopiperazine Derivatives as Selective Antagonists of the Transient Receptor Potential Melastatin 8 (TRPM8) Channel Receptor and Antiprostate Cancer Agents. *J. Med. Chem.* **2016**, *59*, 5661–5683.

59. Du, G.-J.; Li, J.-H.; Liu, W.-J.; Liu, Y.-H.; Zhao, B.; Li, H.-R.; Hou, X.-D.; Li, H.; Qi, X.-X.; Duan, Y.-J. The combination of TRPM8 and TRPA1 expression causes an invasive phenotype in lung cancer. *Tumour Biol.* **2014**, *35*, 1251–1261.

60. Yu, S.; Xu, Z.; Zou, C.; Wu, D.; Wang, Y.; Yao, X.; Ng, C.-F.; Chan, F.L. Ion channel TRPM8 promotes hypoxic growth of prostate cancer cells via an O2 -independent and RACK1-mediated mechanism of HIF-1alpha stabilization. *J. Pathol.* **2014**, *234*, 514–525.

61. Liu, J.; Hu, G.; Gong, Y.; Yu, Q.; He, B.; Li, W.; He, Z.; Hao, W.; He, Z.; Liu, Y. Silencing of TRPM8 inhibits aggressive tumor phenotypes and enhances gemcitabine sensitivity in pancreatic cancer. *Pancreatology* **2018**, *18*, 935–944.

62. Wang, Y.; Yang, Z.; Meng, Z.; Cao, H.; Zhu, G.; Liu, T.; Wang, X. Knockdown of TRPM8 suppresses cancer malignancy and enhances epirubicin-induced apoptosis in human osteosarcoma cells. *Int. J. Biol. Sci.* **2013**, *10*, 90–102.

63. Kiessling, A.; Fussel, S.; Schmitz, M.; Stevanovic, S.; Meye, A.; Weigle, B.; Klenk, U.; Wirth, M.P.; Rieber, E.P. Identification of an HLA-A*0201-restricted T-cell epitope derived from the prostate cancer-associated protein trp-p8. *Prostate* **2003**, *56*, 270–279.

64. Fuessel, S.; Meye, A.; Schmitz, M.; Zastrow, S.; Linne, C.; Richter, K.; Lobel, B.; Hakenberg, O.W.; Hoelig, K.; Rieber, E.P.; et al. Vaccination of hormone-refractory prostate cancer patients with peptide cocktail-loaded dendritic cells: Results of a phase I clinical trial. *Prostate* **2006**, *66*, 811–821.

65. Bartel, D.P. MicroRNAs: Genomics, biogenesis, mechanism, and function. *Cell* **2004**, *116*, 281–297.

66. Krek, A.; Grun, D.; Poy, M.N.; Wolf, R.; Rosenberg, L.; Epstein, E.J.; MacMenamin, P.; da Piedade, I.; Gunsalus, K.C.; Stoffel, M.; et al. Combinatorial microRNA target predictions. *Nat. Genet.* **2005**, *37*, 495–500.

67. Lu, J.; Getz, G.; Miska, E.A.; Alvarez-Saavedra, E.; Lamb, J.; Peck, D.; Sweet-Cordero, A.; Ebert, B.L.; Mak, R.H.; Ferrando, A.A.; et al. MicroRNA expression profiles classify human cancers. *Nature* **2005**, *435*, 834–838.

68. Zhang, J.; Liang, J.; Huang, J. Downregulated microRNA-26a modulates prostate cancer cell proliferation and apoptosis by targeting COX-2. *Oncol. Lett.* **2016**, *12*, 3397–3402.

69. Cost, N.G.; Czyzyk-Krzeska, M.F. Regulation of autophagy by two products of one gene: TRPM3 and miR-204. *Mol. Cell. Oncol.* **2015**, *2*, e1002712.

70. Lunavat, T.R.; Cheng, L.; Einarsdottir, B.O.; Olofsson Bagge, R.; Veppil Muralidharan, S.; Sharples, R.A.; Lasser, C.; Gho, Y.S.; Hill, A.F.; Nilsson, J.A.; et al. BRAF(V600) inhibition alters the microRNA cargo in the vesicular secretome of malignant melanoma cells. *Proc. Natl. Acad. Sci. USA* **2017**, *114*, E5930–E5939.

71. Cao, Q.; Qian, S.; Wang, N.; Zhang, L.; Wang, W.; Shen, H. TRPM2 mediates histone deacetylase inhibition-induced apoptosis in bladder cancer cells. *Cancer Biother. Radiopharm.* **2015**, *30*, 87–93.

72. Naziroglu, M.; Cig, B.; Blum, W.; Vizler, C.; Buhala, A.; Marton, A.; Katona, R.; Josvay, K.; Schwaller, B.; Olah, Z.; et al. Targeting breast cancer cells by MRS1477, a positive allosteric modulator of TRPV1 channels. *PLoS ONE* **2017**, *12*, e0179950.

73. Nur, G.; Naziroglu, M.; Deveci, H.A. Synergic prooxidant, apoptotic and TRPV1 channel activator effects of alpha-lipoic acid and cisplatin in MCF-7 breast cancer cells. *J. Recept. Signal Transduct. Res.* **2017**, *37*, 569–577.

74. Chen, W.-T.; Lin, G.-B.; Lin, S.-H.; Lu, C.-H.; Hsieh, C.-H.; Ma, B.-L.; Chao, C.-Y. Static magnetic field enhances the anticancer efficacy of capsaicin on HepG2 cells via capsaicin receptor TRPV1. *PLoS ONE* **2018**, *13*, e0191078.

75. Sanchez, A.M.; Sanchez, M.G.; Malagarie-Cazenave, S.; Olea, N.; Diaz-Laviada, I. Induction of apoptosis in prostate tumor PC-3 cells and inhibition of xenograft prostate tumor growth by the vanilloid capsaicin. *Apoptosis* **2006**, *11*, 89–99.

76. Amantini, C.; Mosca, M.; Nabissi, M.; Lucciarini, R.; Caprodossi, S.; Arcella, A.; Giangaspero, F.; Santoni, G. Capsaicin-induced apoptosis of glioma cells is mediated by TRPV1 vanilloid receptor and requires p38 MAPK activation. *J. Neurochem.* **2007**, *102*, 977–990.

77. Stock, K.; Kumar, J.; Synowitz, M.; Petrosino, S.; Imperatore, R.; Smith, E.S.J.; Wend, P.; Purfürst, B.; Nuber, U.A.; Gurok, U.; et al. Neural precursor cells induce cell death of high-grade astrocytomas through stimulation of TRPV1. *Nat. Med.* **2012**, *18*, 1232–1238.

78. Amantini, C.; Ballarini, P.; Caprodossi, S.; Nabissi, M.; Morelli, M.B.; Lucciarini, R.; Cardarelli, M.A.; Mammana, G.; Santoni, G. Triggering of transient receptor potential vanilloid type 1 (TRPV1) by capsaicin induces Fas/CD95-mediated apoptosis of urothelial cancer cells in an ATM-dependent manner. *Carcinogenesis* **2009**, *30*, 1320–1329.

79. Caprodossi, S.; Amantini, C.; Nabissi, M.; Morelli, M.B.; Farfariello, V.; Santoni, M.; Gismondi, A.; Santoni, G. Capsaicin promotes a more aggressive gene expression phenotype and invasiveness in null-TRPV1 urothelial cancer cells. *Carcinogenesis* **2011**, *32*, 686–694.

80. Mergler, S.; Cheng, Y.; Skosyrski, S.; Garreis, F.; Pietrzak, P.; Kociok, N.; Dwarakanath, A.; Reinach, P.S.; Kakkassery, V. Altered calcium regulation by thermosensitive transient receptor potential channels in etoposide-resistant WERI-Rb1 retinoblastoma cells. *Exp. Eye Res.* **2012**, *94*, 157–173.

81. Dai, N.; Ye, R.; He, Q.; Guo, P.; Chen, H.; Zhang, Q. Capsaicin and sorafenib combination treatment exerts synergistic antihepatocellular carcinoma activity by suppressing EGFR and PI3K/Akt/mTOR signaling. *Oncol. Rep.* **2018**, *40*, 3235–3248.

82. Ramer, R.; Hinz, B. Inhibition of cancer cell invasion by cannabinoids via increased expression of tissue inhibitor of matrix metalloproteinases-1. *J. Natl. Cancer Inst.* **2008**, *100*, 59–69.

83. Sung, B.; Prasad, S.; Ravindran, J.; Yadav, V.R.; Aggarwal, B.B. Capsazepine, a TRPV1 antagonist, sensitizes colorectal cancer cells to apoptosis by TRAIL through ROS-JNK-CHOP-mediated upregulation of death receptors. *Free Radic. Biol. Med.* **2012**, *53*, 1977–1987.

84. Nabissi, M.; Morelli, M.B.; Santoni, M.; Santoni, G. Triggering of the TRPV2 channel by cannabidiol sensitizes glioblastoma cells to cytotoxic chemotherapeutic agents. *Carcinogenesis* **2013**, *34*, 48–57.

85. Nabissi, M.; Morelli, M.B.; Amantini, C.; Liberati, S.; Santoni, M.; Ricci-Vitiani, L.; Pallini, R.; Santoni, G. Cannabidiol stimulates Aml-1a-dependent glial differentiation and inhibits glioma stem-like cells proliferation by inducing autophagy in a TRPV2-dependent manner. *Int. J. Cancer* **2015**, *137*, 1855–1869.

86. Morelli, M.B.; Offidani, M.; Alesiani, F.; Discepoli, G.; Liberati, S.; Olivieri, A.; Santoni, M.; Santoni, G.; Leoni, P.; Nabissi, M. The effects of cannabidiol and its synergism with bortezomib in multiple myeloma cell lines. A role for transient receptor potential vanilloid type-2. *Int. J. Cancer* **2014**, *134*, 2534–2546.

87. Morelli, M.B.; Nabissi, M.; Amantini, C.; Farfariello, V.; Ricci-Vitiani, L.; di Martino, S.; Pallini, R.; Larocca, L.M.; Caprodossi, S.; Santoni, M.; et al. The transient receptor potential vanilloid-2 cation channel impairs glioblastoma stem-like cell proliferation and promotes differentiation. *Int. J. Cancer* **2012**, *131*, E1067–E1077.

88. Monet, M.; Gkika, D.; Lehen'kyi, V.; Pourtier, A.; Vanden Abeele, F.; Bidaux, G.; Juvin, V.; Rassendren, F.; Humez, S.; Prevarsakaya, N. Lysophospholipids stimulate prostate cancer cell migration via TRPV2 channel activation. *Biochim. Biophys. Acta Mol. Cell Res.* **2009**, *1793*, 528–539.

89. Oulidi, A.; Bokhobza, A.; Gkika, D.; Vanden Abeele, F.; Lehen'kyi, V.; Ouafik, L.; Mauroy, B.; Prevarskaya, N. TRPV2 Mediates Adrenomedullin Stimulation of Prostate and Urothelial Cancer Cell Adhesion, Migration and Invasion. *PLoS ONE* **2013**, *8*, e64885.

90. Shiozaki, A.; Kudou, M.; Ichikawa, D.; Fujiwara, H.; Shimizu, H.; Ishimoto, T.; Arita, T.; Kosuga, T.; Konishi, H.; Komatsu, S.; et al. Esophageal cancer stem cells are suppressed by tranilast, a TRPV2 channel inhibitor. *J. Gastroenterol.* **2018**, *53*, 197–207.

91. Darakhshan, S.; Pour, A.B. Tranilast: A review of its therapeutic applications. *Pharmacol. Res.* **2015**, *91*, 15–28.

92. Gambade, A.; Zreika, S.; Guéguinou, M.; Chourpa, I.; Fromont, G.; Bouchet, A.M.; Burlaud-Gaillard, J.; Potier-Cartereau, M.; Roger, S.; Aucagne, V.; et al. Activation of TRPV2 and BKCa channels by the LL-37 enantiomers stimulates calcium entry and migration of cancer cells. *Oncotarget* **2016**, *7*, 23785–23800.

93. Lehen'kyi, V.; Raphaël, M.; Prevarskaya, N. The role of the TRPV6 channel in cancer. *J. Physiol.* **2012**, *590*, 1369–1376.

94. Bowen, C.V.; DeBay, D.; Ewart, H.S.; Gallant, P.; Gormley, S.; Ilenchuk, T.T.; Iqbal, U.; Lutes, T.; Martina, M.; Mealing, G.; et al. In vivo detection of human TRPV6-rich tumors with anti-cancer peptides derived from soricidin. *PLoS ONE* **2013**, *8*, e58866.

95. Fu, S.; Hirte, H.; Welch, S.; Ilenchuk, T.T.; Lutes, T.; Rice, C.; Fields, N.; Nemet, A.; Dugourd, D.; Piha-Paul, S.; et al. First-in-human phase I study of SOR-C13, a TRPV6 calcium channel inhibitor, in patients with advanced solid tumors. *Investig. New Drugs* **2017**, *35*, 324–333.

96. Chow, J.; Norng, M.; Zhang, J.; Chai, J. TRPV6 mediates capsaicin-induced apoptosis in gastric cancer cells—Mechanisms behind a possible new "hot" cancer treatment. *Biochim. Biophys. Acta* **2007**, *1773*, 565–576.

97. Wang, J.Y.; Swami, S.; Krishnan, A.V.; Feldman, D. Combination of calcitriol and dietary soy exhibits enhanced anticancer activity and increased hypercalcemic toxicity in a mouse xenograft model of prostate cancer. *Prostate* **2012**, *72*, 1628–1637.

98. Peters, A.A.; Simpson, P.T.; Bassett, J.J.; Lee, J.M.; Da Silva, L.; Reid, L.E.; Song, S.; Parat, M.-O.; Lakhani, S.R.; Kenny, P.A.; et al. Calcium channel TRPV6 as a potential therapeutic target in estrogen receptor-negative breast cancer. *Mol. Cancer Ther.* **2012**, *11*, 2158–2168.

99. Bolanz, K.A.; Hediger, M.A.; Landowski, C.P. The role of TRPV6 in breast carcinogenesis. *Mol. Cancer Ther.* **2008**, *7*, 271–279.

100. Bolanz, K.A.; Kovacs, G.G.; Landowski, C.P.; Hediger, M.A. Tamoxifen inhibits TRPV6 activity via estrogen receptor-independent pathways in TRPV6-expressing MCF-7 breast cancer cells. *Mol. Cancer Res.* **2009**, *7*, 2000–2010.

101. Singh, S.S.; Vats, S.; Chia, A.Y.Q.; Tan, T.Z.; Deng, S.; Ong, M.S.; Arfuso, F.; Yap, C.T.; Goh, B.C.; Sethi, G.; et al. Dual role of autophagy in hallmarks of cancer. *Oncogene* **2018**, *37*, 1142–1158.

102. Brusco, I.; Li Puma, S.; Chiepe, K.B.; da Silva Brum, E.; de David Antoniazzi, C.T.; de Almeida, A.S.; Camponogara, C.; Silva, C.R.; De Logu, F.; de Andrade, V.M.; et al. Dacarbazine alone or associated with melanoma-bearing cancer pain model induces painful hypersensitivity by TRPA1 activation in mice. *Int. J. Cancer* **2019**, doi:10.1002/ijc.32648.

103. Deveci, H.A.; Akyuva, Y.; Nur, G.; Naziroglu, M. Alpha lipoic acid attenuates hypoxia-induced apoptosis, inflammation and mitochondrial oxidative stress via inhibition of TRPA1 channel in human glioblastoma cell line. *Biomed. Pharmacother.* **2019**, *111*, 292–304.

104. Vancauwenberghe, E.; Noyer, L.; Derouiche, S.; Lemonnier, L.; Gosset, P.; Sadofsky, L.R.; Mariot, P.; Warnier, M.; Bokhobza, A.; Slomianny, C.; et al. Activation of mutated TRPA1 ion channel by resveratrol in human prostate cancer associated fibroblasts (CAF). *Mol. Carcinog.* **2017**, *56*, 1851–1867.

105. Fusi, C.; Materazzi, S.; Benemei, S.; Coppi, E.; Trevisan, G.; Marone, I.M.; Minocci, D.; De Logu, F.; Tuccinardi, T.; Di Tommaso, M.R.; et al. Steroidal and non-steroidal third-generation aromatase inhibitors induce pain-like symptoms via TRPA1. *Nat. Commun.* **2014**, *5*, 5736.

106. Park, J.; Shim, M.K.; Jin, M.; Rhyu, M.-R.; Lee, Y. Methyl syringate, a TRPA1 agonist represses hypoxia-induced cyclooxygenase-2 in lung cancer cells. *Phytomedicine* **2016**, *23*, 324–329.

107. Schaefer, E.A.M.; Stohr, S.; Meister, M.; Aigner, A.; Gudermann, T.; Buech, T.R.H. Stimulation of the chemosensory TRPA1 cation channel by volatile toxic substances promotes cell survival of small cell lung cancer cells. *Biochem. Pharmacol.* **2013**, *85*, 426–438.

108. Trevisan, G.; Materazzi, S.; Fusi, C.; Altomare, A.; Aldini, G.; Lodovici, M.; Patacchini, R.; Geppetti, P.; Nassini, R. Novel therapeutic strategy to prevent chemotherapy-induced persistent sensory neuropathy by TRPA1 blockade. *Cancer Res.* **2013**, *73*, 3120–3131.

109. Nabissi, M.; Morelli, M.B.; Amantini, C.; Farfariello, V.; Ricci-Vitiani, L.; Caprodossi, S.; Arcella, A.; Santoni, M.; Giangaspero, F.; De Maria, R.; et al. TRPV2 channel negatively controls glioma cell proliferation and resistance to Fas-induced apoptosis in ERK-dependent manner. *Carcinogenesis* **2010**, *31*, 794–803.

110. Jung, J.; Cho, K.-J.; Naji, A.K.; Clemons, K.N.; Wong, C.O.; Villanueva, M.; Gregory, S.; Karagas, N.E.; Tan, L.; Liang, H.; et al. HRAS-driven cancer cells are vulnerable to TRPML1 inhibition. *EMBO Rep.* **2019**, *20*, e46685.

111. Kasitinon, S.Y.; Eskiocak, U.; Martin, M.; Mathews, T.; Aurora, A.B.; Morrison, S.J. TRPML1 Promotes Protein Homeostasis in Melanoma Cells by Negatively Regulating MAPK and Article TRPML1 Promotes Protein Homeostasis in Melanoma Cells by Negatively Regulating MAPK and mTORC1 Signaling. *Cell Rep.* **2019**, *28*, 2293–2305 e9.

112. Xu, M.; Almasi, S.; Yang, Y.; Yan, C.; Sterea, A.M.; Rizvi Syeda, A.K.; Shen, B.; Richard Derek, C.; Huang, P.; Gujar, S.; et al. The lysosomal TRPML1 channel regulates triple negative breast cancer development by promoting mTORC1 and purinergic signaling pathways. *Cell Calcium* **2019**, *79*, 80–88.

113. Kang, P.; Zhang, W.; Chen, X.; Yi, X.; Song, P.; Chang, Y.; Zhang, S.; Gao, T.; Li, C.; Li, S. TRPM2 mediates mitochondria-dependent apoptosis of melanocytes under oxidative stress. *Free Radic. Biol. Med.* **2018**, *126*, 259–268.

114. Wrighton, K.H. Epigenetics: The TRPM7 ion channel modifies histones. *Nat. Rev. Mol. Cell Biol.* **2014**, *15*, 427.

115. Krapivinsky, G.; Krapivinsky, L.; Renthal, N.E.; Santa-Cruz, A.; Manasian, Y.; Clapham, D.E. Histone phosphorylation by TRPM6's cleaved kinase attenuates adjacent arginine methylation to regulate gene expression. *Proc. Natl. Acad. Sci. USA* **2017**, *114*, E7092–E7100.

116. Chen, J.-L.; Ping, Y.-H.; Tseng, M.-J.; Chang, Y.-I.; Lee, H.-C.; Hsieh, R.-H.; Yeh, T.-S. Notch1-promoted TRPA1 expression in erythroleukemic cells suppresses erythroid but enhances megakaryocyte differentiation. *Sci. Rep.* **2017**, *7*, 42883.

117. He, D.-X.; Gu, X.-T.; Jiang, L.; Jin, J.; Ma, X. A methylation-based regulatory network for microRNA 320a in chemoresistant breast cancer. *Mol. Pharmacol.* **2014**, *86*, 536–547.

118. Bidaux, G.; Beck, B.; Zholos, A.; Gordienko, D.; Lemonnier, L.; Flourakis, M.; Roudbaraki, M.; Borowiec, A.-S.; Fernandez, J.; Delcourt, P.; et al. Regulation of activity of transient receptor potential melastatin 8 (TRPM8) channel by its short isoforms. *J. Biol. Chem.* **2012**, *287*, 2948–2962.

119. Oancea, E.; Vriens, J.; Brauchi, S.; Jun, J.; Splawski, I.; Clapham, D.E. TRPM1 forms ion channels associated with melanin content in melanocytes. *Sci. Signal.* **2009**, *2*, ra21.

120. Caprodossi, S.; Lucciarini, R.; Amantini, C.; Nabissi, M.; Canesin, G.; Ballarini, P.; Di Spilimbergo, A.; Cardarelli, M.A.; Servi, L.; Mammana, G.; et al. Transient Receptor Potential Vanilloid Type 2 (TRPV2) Expression in Normal Urothelium and in Urothelial Carcinoma of Human Bladder: Correlation with the Pathologic Stage. *Eur. Urol.* **2008**, *54*, 612–620.

The Controversial Role of PD-1 and Its Ligands in Gynecological Malignancies

Oliviero Marinelli[1,2†], Daniela Annibali[3†], Cristina Aguzzi[1], Sandra Tuyaerts[3], Frédéric Amant[3,4*], Maria Beatrice Morelli[1,2], Giorgio Santoni[1], Consuelo Amantini[2], Federica Maggi[5] and Massimo Nabissi[1*]

[1] School of Pharmacy, University of Camerino, Camerino, Italy, [2] School of Bioscience and Veterinary Medicine, University of Camerino, Camerino, Italy, [3] Gynecological Oncology, Oncology Department, LKI Leuven Cancer Institute KU Leuven-University of Leuven, Leuven, Belgium, [4] Centre for Gynecologic Oncology Amsterdam (CGOA), Antoni Van Leeuwenhoek-Netherlands Cancer Institute (AvL-NKI), University Medical Center (UMC), Amsterdam, Netherlands, [5] Department of Molecular Medicine, Sapienza University, Rome, Italy

The programmed death-1 (PD-1, CD279) receptor with its ligands, programmed death ligand 1 (PD-L1, CD274, B7-H1), and programmed death ligand 2 (PD-L2, CD273, B7-DC), are the key players of one of the immune checkpoint pathways inhibiting T-cell activation. PD-L1 and PD-L2 are expressed in different cancer cells and their microenvironment, including infiltrating immune cells. However, their prognostic value is still debated and their role in the tumor microenvironment has not been fully elucidated yet. Considering the importance that cancer immunotherapy with anti-PD-1 and anti-PD-L1 antibodies gained in several tumor types, in this review article we aim to discuss the role of the PD-1/PD-L1/PD-L2 axis in gynecological cancers. PD-1 ligands have been detected in ovarian, cervical, vulvar and uterine cancers, and correlation with prognosis seems dependent from their distribution. About PD-L2, very few reports are available so far in gynecological malignancies, and its role is still not completely understood. Clinical trials using anti-PD-1 or anti-PD-L1 antibodies, but not anti-PD-L2, are currently ongoing, in all types of gynecological cancers. They have shown good safety profiles in a certain cohort of patients, but response rates remain low and many aspects remain controversial. In this review, we propose possible solutions to enhance the clinical efficacy of PD-1 axis targeting therapies. Regarding PD-L2, it might be useful to better clarify its role in order to improve the efficiency of immunotherapy in female malignancies.

Keywords: PD-L2, PD-L1, PD-1, ovarian cancer, endometrial cancer, cervical cancer, immunotherapy

INTRODUCTION

PD-1 and Its Ligands, PD-L1 (B7-H1) and PD-L2 (B7-DC)

Programmed death-1 (PD-1, CD279) receptor and its ligands, programmed death ligand 1 (PD-L1, CD274, B7-H1) and programmed death ligand 2 (PD-L2, CD273, B7- DC), play crucial roles in one of the immune checkpoint pathways responsible for the inhibition of T-cell activation (1).

PD-1 receptor belongs to the CD28 family and is mainly expressed on the cellular surface of activated T and B cells, monocytes, natural killer (NK), and dendritic cells (DCs), with a role in the induction and maintenance of peripheral tolerance and for the maintenance of the stability and

the integrity of T cells (2–5). PD-1 ligands are glycoproteins, members of the B7 family, with 40% homology in amino acids sequence, but have quite distinct expression patterns, being expressed by a wide variety of immune and non-immune cells (1, 3, 4).

PD-L1 is a type I transmembrane glycoprotein with a single N-terminal immunoglobulin variable (IgV)-like domain sharing 21–33% sequence identity with CTLA-4, CD28, and ICOS, about 20 amino acids that separate the IgV domain from the plasma membrane, a transmembrane domain and a cytoplasmic tail (4). It is constitutively expressed on activated T and B cells, DCs, macrophages, mesenchymal stem cells, and bone marrow-derived mast cells (4, 6). Additionally, it is expressed on a wide variety of non-hematopoietic cells including the vascular endothelium, fibroblastic reticular cells, keratinocytes, lung, non-parenchymal cells of the liver, mesenchymal stem cells, pancreatic islet cells, astrocytes, and neurons (4, 5, 7). PD-L1 expression on human T cells is induced by common γ chain cytokines (IL-2, IL-7, and IL-15), whereas PD-L1 expression on B cells is stimulated by IL-21 (4). In cancer cells, PD-L1 expression is regulated by the MAPK and PI3K/AKT pathways, as well as by HIF-1α, STAT-3, NF-κB and epigenetic mechanisms via microRNAs (8). PD-L1 also exists in a soluble form (sPD-L1) that originates from the cleavage of membrane-bound PD-L1 by matrix metalloproteinases. Such PD-L1 soluble isoform, mainly produced by myeloid-derived cells, retains the IgV-like domain, necessary for the interaction with PD-1, and it is able to suppress T-cell activation. However, its physiological role is still unknown. Interestingly, sPD-L1 has been found in several human cancer cell lines, including H1299 non-small cell lung cancer cells, U-937 lymphoma cells, HO8910 ovarian carcinoma cells, SPCA-1 lung adenocarcinoma cells and U251 glioblastoma cells. In addition, high plasma levels of sPD-L1 have been associated with metastasis and poor prognosis in breast cancer and diffuse large B-cell lymphoma (8).

PD-L2 is a type I transmembrane protein containing an IgV-like domain and an immunoglobulin constant (IgC)-like domain in its extracellular region (9). PD-L2 expression is mainly restricted to antigen-presenting cells (APCs), including macrophages and myeloid DCs (6, 7), and non-hematopoietic tissues, such as the lung (10), human umbilical vein endothelial cells, and fibroblasts (1, 5). Three isoforms of PD-L2 have been described that might influence the outcome of the immune response (9). The most common splice variant contains all 6 exons. In humans, an alternative variant with a spliced-out exon 3, resulting in a protein lacks the IgC-like domain and with a shorter—extracellular region has been reported. A third isoform misses the transmembrane domain, because exon 3 is spliced out to an alternative acceptor site within exon 4, and the protein is secreted as a soluble form. This evidence underscores the importance of post-transcriptional regulation in the expression and function of PD-L2. He et al. suggested that isoforms II and III should be able to interact with PD-1, but further confirmation is needed (9).

Exposure to IL-4, IFN-γ, IL-2, IL-7, IL-15, IL-21, and toll-like receptor ligands induces PD-L2 upregulation in DCs and macrophages (1). Additionally, IL-4, in the presence of respiratory syncytial virus infection, stimulates PD-L2 expression in alveolar epithelial cells (1, 10).

Stimulation by tumor necrosis factor alpha (TNF-α) and interferon gamma (IFN-γ) enhances the constitutive expression of PD-L2 on endothelial cells from human umbilical vein *in vitro* (1). The NF-κB and the STAT-6 pathways are two major signaling reported to regulate PD-L2 expression (1).

Different molecular mechanisms dictate PD-Ls binding to PD-1, as demonstrated by the crystallographic structures of the complexes, showing that PD-Ls cross-compete and that the concurrent presence of both ligands might modify the functional outcome of the binding (11). Specifically, PD-L1 binding to PD-1 requires complex conformational changes of the ligand, while PD-L2 directly interacts with PD-1, explaining its reported 2 to 6-fold higher affinity for the receptor (1). Consequently, when both ligands are expressed at similar levels, PD-L2 would be expected to outcompete PD-L1 for binding to PD-1. However, PD-L2 is generally expressed at lower levels in physiological conditions, such as during maturation of DCs by LPS, when PD-L1 acts as the main ligand of PD-1. A known exception is Th2 responses, where PD-L2 is predominant (1, 11).
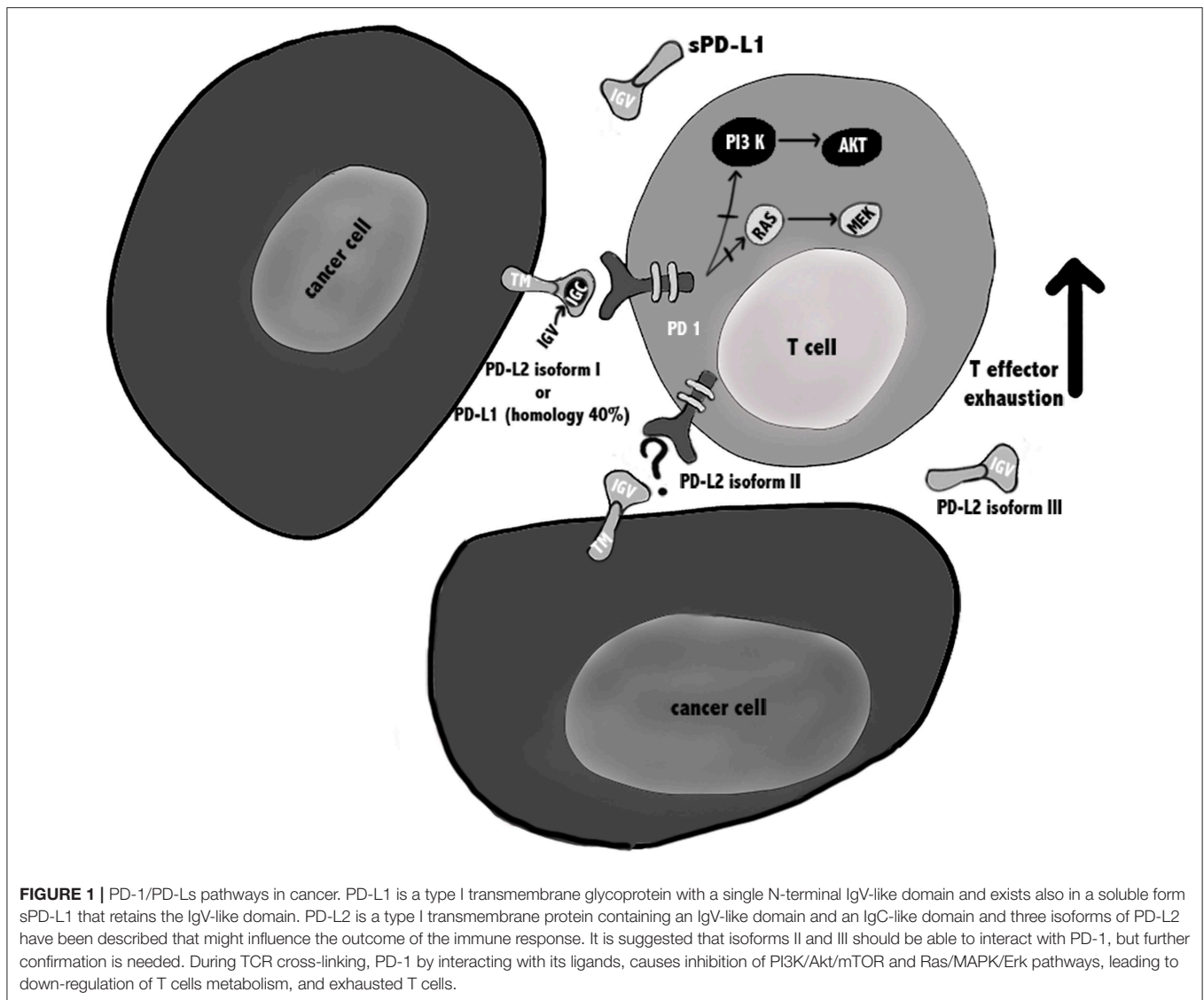
Regarding the PD-1/PD-L1 and PD-1/PD-L2 pathways involved in T cell immune evasion, different reports have been published, mainly regarding the biochemical signaling regulated by the PD-1/PD-L1. It was reported that the binding of PD-L1 to PD-1 may cause T cell apoptosis, anergy, exhaustion, and interleukin-10 (IL-10) expression, suggesting that PD-L1 can act as a defender for PD-L1+ cancer cells from CD8+ T cell–mediated lysis (12, 13) (**Figure 1**).

Regarding the PD-L2/PD-1 signaling pathways, it may not be biologically identical, since Repulsive Guidance Molecule B (RGMb) is also a binding partner for PD-L2 (14). Thus, the PD-L2 blockade may evocate different cellular responses, depending on the binding partner interaction, which can lead to potential varied biological outcomes. Up to now, in human anti-tumor immunity, the relationship between PD-1, PD-L1, and PD-L2 in their cellular expression profile and regulation, potential interactions and biological is considered not completely defined.

PD-1 Ligands in the Tumor Microenvironment Influence the Anti-tumor Response

PD-L1 and PD-L2 are expressed in different cancer cells and in their microenvironment (4, 8), including infiltrating immune cells (15, 16). However, their prognostic value is still debated and the role they might play when expressed in the tumor microenvironment has not be fully elucidated yet (17).

Previous evidence shows that PD-L1 expression by cancer cells correlates with poor prognosis (18), while PD-L1 expression by tumor-infiltrating immune cells is associated with improved overall survival (OS) (16). Furthermore, it seems that PD-L1 expressed by APC, rather than cancer cells, is essential for the response to immune checkpoint blockade therapy (19). Specifically, survival analysis showed that the presence of PD-L1 on macrophages had a protective role and enhanced the prognosis of patients with hepatocellular carcinoma.

FIGURE 1 | PD-1/PD-Ls pathways in cancer. PD-L1 is a type I transmembrane glycoprotein with a single N-terminal IgV-like domain and exists also in a soluble form sPD-L1 that retains the IgV-like domain. PD-L2 is a type I transmembrane protein containing an IgV-like domain and an IgC-like domain and three isoforms of PD-L2 have been described that might influence the outcome of the immune response. It is suggested that isoforms II and III should be able to interact with PD-1, but further confirmation is needed. During TCR cross-linking, PD-1 by interacting with its ligands, causes inhibition of PI3K/Akt/mTOR and Ras/MAPK/Erk pathways, leading to down-regulation of T cells metabolism, and exhausted T cells.

Macrophages are involved in maintaining an active immune microenvironment, with high numbers of infiltrating CD8$^+$ T cells and high immune-related gene expression levels (15).

Sepesi et al. investigated PD-L1 expression in surgically resected stage I non-small cell lung cancer and, in contrast, demonstrated that lower PD-L1 expression in the tumor, but also in tumor-infiltrating macrophages, was associated with significantly better OS (20).

The existence of conflicting reports about PD-L1 and−2 prognostic value can be generally attributed to technical disparities (e.g., variations in staining protocols across individual laboratories and use of different primary antibody clones to identify PD-Ls in tumor tissue), as well as different clinical features of the analyzed samples (site and size of cancer, treatments, follow-up time, etc.). Moreover, PD-L1 and−2 are dynamic markers that can be up- or downregulated over time, making their evaluation complicated (17, 21).

Direct activation of the PD-1 axis by cancer cells leads to a potent inhibitory signal in T lymphocytes resulting in anti-tumor immunity impairment and tumor cells ability to escape immunosurveillance (4, 19). Specifically, it has been shown that PD-1 activation inhibits glucose consumption, cytokine production, proliferation and survival in T lymphocytes, thus preventing the expression of transcription factors associated with effector T cell functions, such as GATA-3, T-bet, and Eomesodermin (Eomes) (4). PD-1/PD-Ls binding attenuates TCR-mediated signaling, thus impairing PI3K/Akt and Ras/MEK/Erk pathways, both required for T-cell activation (4).

PD-Ls are expressed in several solid tumors (8, 22), and immune checkpoint inhibitors, such as anti-PD-1 and anti-PD-L1 antibodies, showed efficacy in cancers with high mutational load, including lung cancer, melanoma, and microsatellite instable (MSI) tumors (23). It was shown that this efficacy is linked to the presence of tumor specific neoantigens that induce a Th1/CTL response that is counterbalanced by overexpression

of multiple immune checkpoints such as PD-1/PD-L1 (23). In addition, PD-1/PD-L1 axis blockade might activate tumor-specific T lymphocytes to kill tumor cells by inducing TNF-α and IFN-γ (22).

For gynaecologic malignancies, the expression of PD-1 ligands has been reported in ovarian (17, 21, 22, 24–31), uterine (5–7, 32–38), cervical (23, 32, 39–50), and vulvar (32, 51–54) cancers, which we describe in detail in the next section.

PD-1 AND PD-LS EXPRESSION IN ENDOMETRIAL CANCER

In normal endometrium the role of the immune system is extremely complex, since it must prevent sexually transmitted infections but should also be able to help the growth of an allogenic fetus during pregnancy (23). So far, few reports characterized PD-1 and its ligands' expression in gynecological cancer and data are quite controversial. The expression profile of these immune checkpoints has been analyzed predominantly by immunohistochemistry, in biopsies obtained from both healthy subjects and cancer patients.

PD-1 in Endometrial Cancer

The PD-1 receptor has been found almost exclusively in immune cells infiltrating the tumor (32, 37, 38), and not in normal endometrium (5). Additionally, a deep analysis performed on 183 patients showed that high expression of PD-1 within and at the margins of a tumor, with a high PD-1/CD8$^+$ ratio in the center, was associated with favorable OS (35).

Additional reports found a correlation between PD-1 expression in intraepithelial and peritumoural lymphocytes with DNA polymerase ε (POLE) mutation and MSI status of the patients (32, 37, 38). Specifically, it has been reported that PD-1 expression in tumor-infiltrating immune cells was more frequently found in moderately, poorly differentiated endometrial cancers, non-endometrioid type II (serous, clear cell, mucinous) endometrial cancers (5, 35, 36), and POLE and MSI subgroups (32, 37, 38).

PD-L1 in Endometrial Cancer

Regarding PD-1 ligands, all data concordantly showed that PD-L1 is expressed in most of the analyzed specimens (5–7, 32–35, 37), predominantly located in the cytoplasm (5–7). Several studies showed that PD-L1 was expressed in a similarly high percentage of samples in both normal endometrium and endometrial tumors (5–7).

PD-L1 expression in cancer cells correlates with post-menopausal status, high histological grade (grade 3), deep myometrial invasion (≥1/2), lymphovascular invasion, adjuvant therapy, and MSI status (35). High PD-L1 immuno-reactivity on immune cells, and not on tumor cells, is an independent predictor of adverse progression-free survival (PFS) in all patients, including the microsatellite stable (MSS) subgroup (35). In addition, some reports evidenced that PD-L1 expression in intraepithelial immune cells was significantly more frequent in POLE mutant and MSI tumors, compared to MSS tumors (32, 37, 38), while PD-L1 expression in tumor cells did not differ between POLE mutant, MSI and MSS patients (32).

However, data regarding PD-L1 expression in cancer cells are controversial: one study showed that only 1 out of 116 tumors expressed PD-L1 on tumor cells, but this under-estimation could be linked with the use of tissue microarrays, since PD-L1 expression is known to be heterogenous (37).

Another study regarding gynecological samples, in 47 uterine sarcoma samples, found that PD-L1 expression was upregulated in comparison with normal endometrium, suggesting that this protein is a potential target for immunotherapy (7), while Bregar et al., using a smaller number of samples (10 patients), found that PD-L1 is expressed in only 30% of specimens (34).

PD-L2 in Endometrial Cancer

For PD-L2 very few data are available so far, and its expression seems to differ from PD-L1, with no significant difference between normal endometrium and tumor (5–7).

High PD-L2 expression was shown in 30% of primary endometrial carcinoma patients and 16% of uterine sarcoma patients, demonstrating the potential of PD-L2 blockade in a limited proportion of uterine cancer patients (7). It has been shown that PD-L1 and PD-L2 expression was more frequent in moderately, poorly differentiated, non-endometrioid endometrial cancer and seems to be correlated with POLE and MSI status (5, 33, 36). Type II endometrial cancer and poorly differentiated histological features are generally associated with worse prognosis and, in addition, PD-1 axis expression suggests that it may cause immunosuppression to favor tumor growth, thus negatively affecting patients' survival (5).

EXPRESSION OF PD-1, PD-L1, AND PD-L2 IN OVARIAN CANCER

Ovarian cancer is the most lethal disease among gynecological cancers (17, 22, 29–31) and is known to be an immunogenic tumor.

PD-1 and PD-L1 in Ovarian Cancers

Some reports showed that PD-L1 expression is found in epithelial ovarian cancers (EOC) (17, 20, 21, 24–26, 30), especially in serous ovarian cancers (SOC) (28, 29), ovarian clear cell carcinomas (OCCC) and in malignant ascites (31), a sign of peritoneal carcinomatosis derived from ovarian cancer (22).

In a cohort of 122 patients with OCCC, Zhu et al. showed that 55 cases (44.7%), classified as having high PD-L1 expression (PD-L1^{high}), were significantly associated with advanced stages (III–IV) (22). Cases with high PD-L1 and PD-1 expression showed significantly poorer PFS and OS, compared to those with low PD-L1/PD-1 expression (22, 24, 28, 29). In subgroup analysis, PD-L1^{high} was associated with poorer prognosis compared to PD-L1^{low} in platinum-resistant and advanced stages (III–IV) patients (22). Drake et al. analyzed 55 ovarian cancer biopsies and showed that PD-1 was detected in 87% of the tumors in both stroma and epithelium, while PD-L1 was only present in 33% of patients, exclusively in high-grade tumors (17). Additionally, they found that low density of PD-1 and PD-L1 expressing cells in tumor tissue was significantly associated with advanced disease, failing to show any significant association between survival and PD-1 or PD-L1 expression in ovarian

cancer (17), while patients with recurrent tumors and increased infiltrating PD-1^{+} immune cells had longer OS (21). The correlation of PD-1 and PD-L1 expression with high-grade tumors and stage IV International Federation of Gynecology and Obstetrics (FIGO) disease has also been confirmed by other studies (28, 29).

Wieser et al. showed that, in a cohort of 158 patients with high-grade serous ovarian cancers, BRCA1/2 mutated tumors were characterized by high PD-1 expression, and that PD-L1 was observed mainly in BRCA1/2 and TP53 mutated cancers (29). Xiao et al. reported that PD-1 is expressed in tumor infiltrating lymphocytes and PD-L1 in tumor cells and in intratumoural immune cells, but there was no significant difference of PD-1^{+} intratumoural immune cells in tumors with different mismatch repair (MMR) status (30). MSI ovarian cancers exhibited a significantly higher number of PD-L1[+] intratumoural immune cells compared to MSS ovarian cancers, while PD-L1 expression was not different in tumors, irrespectively from their MMR status (30).

In addition, no significant difference regarding PD-L1 expression in tumor cells and tumor infiltrating lymphocytes, and PD-1 expression in infiltrating lymphocytes, has been found between primary and recurrent disease (21).

PD-L2 in Ovarian Cancers

So far, only few studies investigated the expression of PD-L2 in ovarian cancer. An analysis on 70 patients showed that PD-L2 expression was not related to patient prognosis or other clinical variables, but negatively correlated with the number of FOXP3^{+} T regulatory cells (Tregs) (24). Imai et al. analyzed the expression of PD-L1 and PD-L2 on tumor cells and APCs in malignant ascites from epithelial ovarian cancer patients (31), and found differential PD-L1 expression in tumor cells between patients with high or low PD-1-expressing CD4^{+} T cells (43.9 and 27.3%, respectively), while no difference in PD-L1 expression was observed between patients with high and low PD-1 expression on CD8^{+} T cells (34.1 and 27.3%, respectively). Between 2.3 and 3.2% of the patients with high or low PD-1 on CD4^{+} T cells and CD8^{+} T cells also expressed PD-L2. No correlation was found between PD-L1/2 expression and clinical variables or outcomes (31).

To support a potential role of PD-1 and PD-L1/ PD-L2 axis as targets in ovarian cancer, it has been reported in syngeneic orthotopic mouse model of epithelial ovarian cancer, that treatment with anti-PD-1 or anti-PD-L1 antibodies resulted in tumor rejection in 75% of the treated-mice, while mice treated with anti-PD-L2 antibody did not reject tumors (25). These data can be explained considering the selected models that expressed lower levels of PD-L2 than PD-1 and PD-L1. Additionally, PD-1 and PD-L1 blockade significantly increased the CD8^{+} to Tregs and CD4^{+} to Tregs ratios within the tumor, while, on the contrary, there was no significant change in the CD8^{+} or CD4^{+} to Tregs ratios (25).

EXPRESSION OF PD-1, PD-L1, AND PD-L2 IN OTHER GYNECOLOGICAL CANCERS

Cervical cancer is the third most common gynecological malignancy in Europe (23). Little information is available, up to now, regarding the expression of PD-1 ligands (23, 32, 39, 43–47).

A report from Howitt et al. showed that cervical cancer is a potential candidate for clinical trials testing PD-1 blockade (23, 32, 39). In fact, using FISH analysis on 48 Formalin-Fixed Paraffin-Embedded (FFPE) tissue specimens of cervical squamous cell carcinoma, they observed co-amplification or co-gain of PD-L1 and PD-L2 in 32 out of 48 cases (67%). Immunohistochemical staining for PD-L1 revealed high expression in 95% of the tumors with membranous staining pattern (32).

Persistent infection with human papilloma virus (HPV) is an essential step in the development of most cervical cancers (40). Some studies hypothesized that HPV may activate PD-1/PD-L1 to evade host immune responses, resulting in persistence of the cervical intraepithelial neoplasia (41). The identification of HPV as an etiological factor leads to antigen production and presentation, thereby making cervical cancer immunogenic (42). Recently, the role of the PD-1/PD-L1 axis in HPV associated head and neck squamous cell cancer (HPV-HNSCC) creating an "immune-privileged" site for initial viral infection and subsequent adaptive immune resistance suggests a rationale for therapeutic blockade of this pathway in patients with HPV-associated tumors (43). Significant PD-L1 expression in cervical carcinoma has been confirmed in several studies (44–47). As a consequence, this immunogenic disease requires a highly immunosuppressive microenvironment to progress and metastasize (48, 49) which has been demonstrated in tumor-positive lymph nodes where high Treg levels, low CD8^{+} T cell/Treg ratio and high levels of PD-L1^{+} and HLA-DR^{+} myeloid cells were found (50).

Regarding another gynecological malignancy, vulvar cancer, the clinical relevance of PD-L1 expression has not been completely studied so far (32).

Although rare, incidence rates of vulvar cancer are increasing and, in locally advanced, metastatic or recurrent disease, prognosis is poor and new treatment modalities are needed (51). Screening of 23 vulvar squamous cell carcinomas revealed 6 cases (26%) with co-amplification of PD-1 ligands, 4 cases (17%) showed co-gain, 6 cases (26%) showed polysomy, and 7 cases (30%) showed disomy. Immunohistochemical staining for PD-L1 across all cases revealed the highest median PD-L1 protein expression in cases with co-amplification of PD-L1 and PD-L2, and decreasing values with decreasing genetic complexity (32). Previous studies showed that PD-L1 is expressed in the majority of vulvar squamous cell carcinoma samples (51–54), in both cancer cells and peritumoural immune cells (52–54). Additionally, its expression was related with several components of immune system (CD3^{+}, CD20^{+}, and CD68^{+} intra-tumor immunocytes) (51, 54), while a significant correlation with immunosuppressive cell populations (FOxP3^{+} Treg cells) was reported only by Sznurkowski et al. (54). Data analyzing the

TABLE 1 | Ongoing immunotherapy clinical trials for patients with endometrial cancer.

ClinicalTrials.gov identifier	Status	Interventions/alone or in combination	Phase
NCT02630823	Active, not recruiting	Pembrolizumab (anti-PD-1) + Paclitaxel/Carboplatin/Radiation (standard of care)	I
NCT02725489	Active, not recruiting	Durvalumab (anti-PD-L1)	II
NCT02728830	Active, not recruiting	Pembrolizumab (anti-PD-1)	Early I
NCT02646748	Active, not recruiting	Pembrolizumab (anti-PD-1) + itacitinib/INCB050465	I
NCT02914470	Active, not recruiting	Atezolizumab (anti-PD-L1) + cyclophosphamide/Carboplatin	I
NCT02521844	Active, not recruiting	Pembrolizumab (anti-PD-1) + ETC-1922159	I

TABLE 2 | Ongoing immunotherapy clinical trials for patients with ovarian cancer.

ClinicalTrials.gov identifier	Status	Interventions (alone or in combination)	Phase
NCT02608684	Active, not recruiting	Pembrolizumab (anti-PD-1) + Gemcitabine/Cisplatin	II
NCT02728830	Active, not recruiting	Pembrolizumab (anti-PD-1)	Early I
NCT03287674	Active, not recruiting	Nivolumab (anti-PD-1) + Cyclophosphamide/Fludarabine/TIL infusion/Interleukin-2/Ipilimumab	I/II
NCT03277352	Active, not recruiting	Pembrolizumab (anti-PD-1) + INCAGN01876/Epacadostat	I/II
NCT03312114	Active, not recruiting	Avelumab (anti-PD-L1)	II
NCT02674061	Active, not recruiting	Pembrolizumab (anti-PD-1)	II
NCT03029598	Active, not recruiting	Pembrolizumab (anti-PD-1) + Carboplatin	I/II
NCT02335918	Completed	Nivolumab (anti-PD-1) + varlilumab	I/II
NCT02915523	Active, not recruiting	Avelumab (anti-PD-L1) + entinostat	I/II
NCT02452424	Completed	Pembrolizumab (anti-PD-1) + PLX3397	I/II
NCT02644369	Active, not recruiting	Pembrolizumab (anti-PD-1)	II
NCT03073525	Active, not recruiting	Atezolizumab (anti-PD-L1)	II
NCT02526017	Active, not recruiting	Nivolumab (anti-PD-1) + FPA008	I
NCT02580058	Active, not recruiting	Avelumab (anti-PD-L1) + PLD	III
NCT03365791	Active, not recruiting	PDR001 (anti-PD-1) + LAG525	I
NCT02764333	Active, not recruiting	Durvalumab (anti-PD-L1) + TPIV200	II
NCT02431559	Active, not recruiting	Durvalumab (anti-PD-L1) + Pegylated Liposomal Doxorubicin	I/II
NCT02914470	Active, not recruiting	Atezolizumab (anti-PD-L1) + carboplatin, cyclophosphamide	I
NCT02725489	Active, not recruiting	Durvalumab (anti-PD-L1)	II
NCT01975831	Active, not recruiting	MEDI4736 (anti-PD-L1) + Tremelimumab	I
NCT03038100	Active, not recruiting	Atezolizumab (anti-PD-L1) + Carboplatin/Atezolizumab/Bevacizumab	III
NCT01772004	Active, not recruiting	Avelumab (anti-PD-L1)	I/II
NCT03574779	Active, not recruiting	TSR-042 (anti-PD-1) + Niraparib/Bevacizumab	II
NCT02521844	Active, not recruiting	Pembrolizumab (anti-PD-1) + ETC-1922159	I

clinical impact of PD-L1 expression in vulvar cancer reveal that it is not clear whether its expression correlates with clinicopathological parameters.

In summary, no significant associations were observed between PD-L1 presence and typical clinicopathological factors (51), except for tumor stage as reported by Sznurkowski et al. (54), and PD-L1 expression occurs more often in high risk HPV-negative samples (51). Regarding survival analysis, it is reported that PD-L1 expression did not influence the OS (51, 53), but patients with primary tumors positive for immune cells-PD-L1 expression had improved OS compared to negative ones (54).

The presence of PD-L1 also seems to be an independent prognostic factor for recurrence free survival (51).

ONGOING IMMUNOTHERAPY CLINICAL TRIALS IN GYNECOLOGICAL MALIGNANCIES

Several clinical trials are ongoing at the moment, according to the ClinicalTrials.gov database [accessed July 06, 2019], testing anti-PD-1/PD-L1 blockade alone or in combination in patients with endometrial, cervical, vulvar and ovarian cancer, while there are no ongoing clinical trials using anti-PD-L2 (**Tables 1–3**).

Clinical trials data were collected from ClinicalTrials.gov database, selecting only completed trials or in "Active, not recruiting" status.

TABLE 3 | Ongoing immunotherapy clinical trials for patients with cervical cancer.

ClinicalTrials.gov Identifier	Status	Interventions	phase
NCT01975831	Active, not recruiting	MEDI4736 (anti-PD-L1) + Tremelimumab	I
NCT02914470	Active, not recruiting	Atezolizumab (anti-PD-L1) + Carboplatin/Cyclophosphamide	I
NCT02725489	Active, not recruiting	Durvalumab (anti-PD-L1)	II
NCT02921269	Active, not recruiting	Atezolizumab (anti-PD-L1) + Bevacizumab	II
NCT02257528	Active, not recruiting	Nivolumab (anti-PD-1)	II
NCT03073525	Active, not recruiting	Atezolizumab (anti-PD-L1)	II

Endometrial Cancer

Regarding endometrial cancer, 6 clinical trials are ongoing (**Table 1**). Most of them are Phase I clinical trials and preliminary results, reported by the American Society of Clinical Oncology (asco.org), showed that atezolizumab (anti-PD-L1), and pembrolizumab (anti-PD-1) might be promising agents for endometrial cancer treatment.

Most relevant results showed that in a phase I study, 15 patients eligible based on PD-L1 status (>5% of positivity in tumor-infiltrating immune cells) were treated with atezolizumab and evaluated for safety and efficacy. Results showed that atezolizumab had a favorable safety profile and 13% (2/15) of patients showed a reduction in tumor size. A trend for higher PFS and OS has been observed in patients with high levels of tumor-infiltrating immune cells. Clinical benefit appeared to increase with higher PD-L1 expression, suggesting a link between PD-L1 status and response to atezolizumab. In addition, hypermutation, and/or high immune infiltration may be linked to response to PD-L1 blockade (Clinical trial information: NCT01375842) (55).

In a different phase I clinical trial, pembrolizumab was administered in 24 patients with endometrial carcinoma (excluding sarcomas), failure of prior systemic therapy, and PD-L1 expression in ≥1% of tumor or stromal cells. A reduction in tumor size was confirmed in 13.0% of the patients, while 3 patients achieved stable disease. PFS and OS rates were 19.0 and 68.8%, respectively. In conclusion, Pembrolizumab demonstrated an acceptable safety profile and anti-tumor activity (Clinical trial information: NCT02054806) (56).

Ovarian Cancer

For ovarian cancer 22 clinical trials are ongoing, 2 of which are completed (**Table 2**). Some of the early-phase clinical trials of anti-PD-1 or anti-PD-L1 antibodies have shown good safety profiles and durable anti-tumor response in certain patient population(s). However, their response rates remain between 10 and 15% (31, 57). Available interim reports from some of the trials show promising objective response rates (ORR) for the treatment of ovarian cancer with nivolumab (anti-PD-1) (ORR of 15%, $n = 20$ patients), pembrolizumab (ORR 11.5%, $n = 49$), or avelumab (anti-PD-L1) (ORR 10%, $n = 124$) (17, 58, 59). Preliminary data presented at the annual ASCO meeting in 2016 of a phase I trial evaluating

durvalumab (anti-PD-L1) in combination with olaparib (PARP inhibitor), showed a disease control rate (DCR) of 67% for the doublet olaparib - durvalumab in a cohort including BRCA wild type triple negative breast cancer and EOC cases (23).

In the KEYNOTE-28 trial, which explored the activity of pembrolizumab in several solid tumors, outcome of ovarian cancer was ORR of 11.5%, and only 23.1% showed tumor shrinkage from baseline (57).
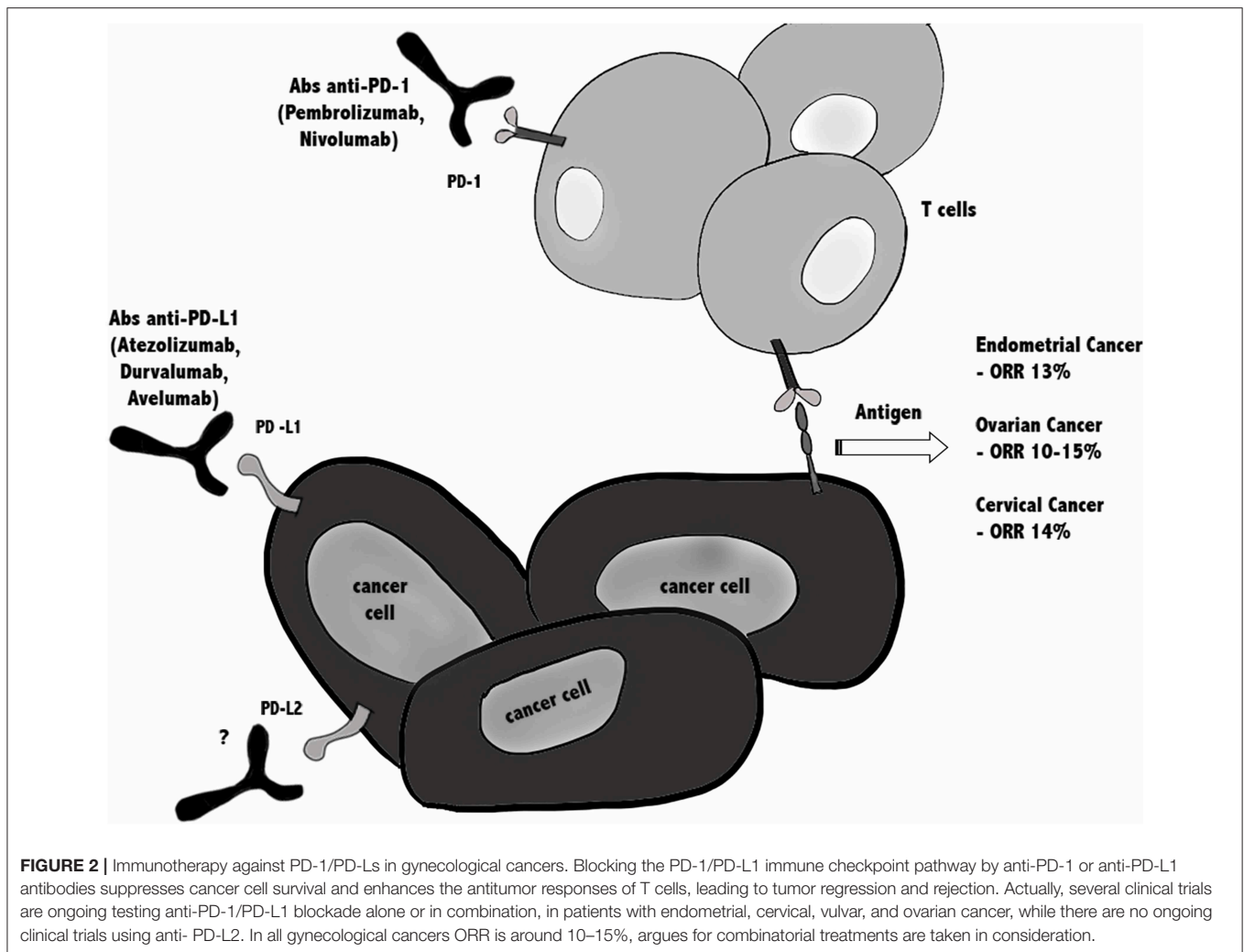
Cervical Cancer

For cervical cancer, 6 clinical trials are ongoing (**Table 3**). Most relevant findings showed that in a phase Ib study with 24 patients affected by advanced cervical squamous cell cancer and PD-L1 expression in ≥1% of tumor or stromal cells, pembrolizumab was well-tolerated and showed promising anti-tumor activity (Clinical trial information: NCT02054806) (60), while its clinical benefit was investigated in the phase 2 KEYNOTE-158 trial. Pembrolizumab administration has been also investigated in a single cohort trial enrolling 98 patients with recurrent or metastatic cervical cancer, expressing PD-L1 with a positive ratio of the number of all PD-L1–expressing cells (tumor cells, lymphocytes, macrophages) to the number of all tumor cells, or a Combined Positive Score (CPS) ≥1. The ORR in 77 patients was 14.3% (95% CI: 7.4, 24.1), including 2.6% complete responses and 11.7% partial responses. No responses were observed in patients with tumors negative for PD-L1 expression (CPS <1). Serious adverse reactions occurred in 39% of patients (Clinical trial information: NCT02628067) (61).

On June 12th 2018, pembrolizumab was approved by Food and Drug Administration (FDA), for treatment of patients with recurrent or metastatic cervical cancer, expressing PD-L1 (CPS ≥1) as determined by an FDA-approved test, with disease progression on or after chemotherapy[1].

In conclusion, since in all gynecological cancers ORR is around 10–15%, this emphasizes the need for combination treatments to improve efficacy of immune checkpoint (**Figure 2**).

---

[1]Merck & Co. Press Release Details. https://investors.merck.com/news/press-release-details/2018/FDA-Approves-Mercks-KEYTRUDA-pembrolizumab-for-Previously-Treated-Patients-with-Recurrent-or-Metastatic-Cervical-Cancer-Whose-Tumors-Express-PD-L1-CPS-Greater-Than-or-Equal-to-1/default.aspx

FIGURE 2 | Immunotherapy against PD-1/PD-Ls in gynecological cancers. Blocking the PD-1/PD-L1 immune checkpoint pathway by anti-PD-1 or anti-PD-L1 antibodies suppresses cancer cell survival and enhances the antitumor responses of T cells, leading to tumor regression and rejection. Actually, several clinical trials are ongoing testing anti-PD-1/PD-L1 blockade alone or in combination, in patients with endometrial, cervical, vulvar, and ovarian cancer, while there are no ongoing clinical trials using anti- PD-L2. In all gynecological cancers ORR is around 10–15%, argues for combinatorial treatments are taken in consideration.

FUTURE DIRECTIONS FOR IMMUNE CHECKPOINT INHIBITORS (ICIS) COMBINATION THERAPIES

Albeit ICIs therapies have been shown to induce durable responses and long-term remission in several cancer types, many patients fail to respond, develop resistance over the time or show immune-related adverse effects (62–65). The unresponsiveness or the toxicity of ICIs represents a strong rationale for the combination of ICIs with other treatments to increase the response rate of non-immunological tumors. For example, therapeutic approaches that induce the release and presentation of tumor antigens could be able to foster a *de novo* anti-tumor T cell response. In this regard, candidates for a combination therapy with ICIs could be cancer vaccines, oncolytic viruses, radiation, or low-dose chemotherapy (66).

Another potential combination approach with ICIs could be with bispecific antibodies, which recruit patient's T cells or NK cells against cancer cells expressing tumor-associated antigens. An example came from hematologic malignancies, wherein a bispecific antibody targeting both CD3 and CD123 (67, 68) was used but showed benefit in only a small fraction of patients. A major mechanism limiting the therapeutic efficacy was T cell anergy and exhaustion driven by ICIs pathways (mainly PD-L1/PD-1) (69). Inspired by this inhibitory role of ICIs pathway, combining ICIs with bispecific antibodies showed enhanced T cell proliferation and IFN-γ production (70).

One more possibility to improve ICI efficacy might be combination with cytokine therapy. The cytokine IL-2 has been approved for the treatment of metastatic renal cell carcinoma and advanced melanoma but is accompanied by severe side effects (71). However, modified IL-2 formulations such as bempegaldesleukin (NKTR-214) have an improved safety profile and have shown capabilities of enhancing the proliferation and activation of CD8$^+$ T cells and NK cells without increasing the number of Tregs (72). Recently, the PIVOT-02 trial (combination of NKTR-214 and nivolumab) has shown that this combination is safe and efficacious (ORR 48% in 23 patients) in metastatic urothelial carcinoma (73).

In addition, a recent study has demonstrated that DC-derived IL-12 is necessary for successful anti-PD-1 cancer therapy, suggesting that IL-12 and ICIs could be rationally combined (74).

Finally, there is strong rationale to combine anti-angiogenic therapies with ICI's, since anti-angiogenic therapies induce a normalization of the tumor vasculature, which leads to enhanced infiltration of T lymphocytes in the tumor.

CONCLUSION

Cancer immunotherapy is emerging as a promising component for cancer therapy. The most promising immunotherapy that showed good results involves antibodies targeting inhibitory immune checkpoint molecules (75).

Results obtained for patients with non-small cell lung cancer, renal cancer, and melanoma are evident and encouraging. However, in gynecological malignancies many aspects remain controversial in preclinical and clinical studies (23). Uncertain is the selection of patients because objective response rates remain low and retrospective analysis on biopsies showed opposing results for OS and PFS in patients with similar pattern of expression of PD-1 and its ligands (15, 17, 20–22, 24, 28, 29, 32, 34).

Regarding the second ligand PD-L2, it is needed to better clarify its role inside tumor microenvironment, together with the evaluation of other biological markers, in order to improve the efficiency of immunotherapy malignancies of the female genital tract.

AUTHOR CONTRIBUTIONS

OM, DA, CA, MN, FA, and ST wrote the paper. MM, GS, CA, and FM have revised the clinical trials and the paper.

FUNDING

ACKNOWLEDGMENTS

REFERENCES

1. Rozali EN, Hato SV, Robinson BW, Lake RA, Lesterhuis WJ. Programmed death ligand 2 in cancer-induced immune suppression. *Clin Dev Immunol.* (2012) 2012:656340. doi: 10.1155/2012/656340

2. Yang S, Zhang Q, Liu S, Wang AR, You Z. PD-1, PD-L1 and PD-L2 expression in mouse prostate cancer. *Am J Clin Exp Urol.* (2016) 4:1–8.

3. Ohigashi Y, Sho M, Yamada Y, Tsurui Y, Hamada K, Ikeda N, et al. Clinical significance of programmed death-1 ligand-1 and programmed death-1 ligand-2 expression in human esophageal cancer. *Clin Cancer Res.* (2005) 11:2947–53. doi: 10.1158/1078-0432.CCR-04-1469

4. Bardhan K, Anagnostou T, Boussiotis VA. The PD1:PD-L1/2 pathway from discovery to clinical implementation. *Front Immunol.* (2016) 7:550. doi: 10.3389/fimmu.2016.00550

5. Mo Z, Liu J, Zhang Q, Chen Z, Mei J, Liu L, et al. Expression of PD-1, PD-L1 and PD-L2 is associated with differentiation status and histological type of endometrial cancer. *Oncol Lett.* (2016) 12:944–50. doi: 10.3892/ol.2016.4744

6. Liu J, Liu Y, Wang W, Wang C, Che Y. Expression of immune checkpoint molecules in endometrial carcinoma. *Exp Ther Med.* (2015) 10:1947–52. doi: 10.3892/etm.2015.2714

7. Vanderstraeten A, Luyten C, Verbist G, Tuyaerts S, Amant F. Mapping the immunosuppressive environment in uterine tumors: implications for immunotherapy. *Cancer Immunol Immunother.* (2014) 63:545–57. doi: 10.1007/s00262-014-1537-8

8. Chen J, Jiang CC, Jin L, Zhang XD. Regulation of PD-L1: a novel role of pro-survival signalling in cancer. *Ann Oncol.* (2016) 27:409–16. doi: 10.1093/annonc/mdv615

9. He XH, Liu Y, Xu LH, Zeng YY. Cloning and identification of two novel splice variants of human PD-L2. *Acta Biochim Biophys Sin.* (2004) 36:284–9. doi: 10.1093/abbs/36.4.284

10. Dong Y, Sun Q, Zhang X. PD-1 and its ligands are important immune checkpoints in cancer. *Oncotarget.* (2017) 8:2171–86. doi: 10.18632/oncotarget.13895

11. Ghiotto M, Gauthier L, Serriari N, Pastor S, Truneh A, Nunès JA, et al. PD-L1 and PD-L2 differ in their molecular mechanisms of interaction with PD-1. *Int Immunol.* (2010) 22:651–60. doi: 10.1093/intimm/dxq049

12. Zou W, Chen L. Inhibitory B7-family molecules in the tumour microenvironment. *Nat Rev Immunol.* (2008) 8:467–77. doi: 10.1038/nri2326

13. Chen L, Han X. Anti-PD-1/PD-L1 therapy of human cancer: past, present, and future. *J Clin Invest.* (2015) 125:3384–91. doi: 10.1172/JCI80011

14. Xiao Y, Yu S, Zhu B, Bedoret D, Bu X, Francisco LM, et al. RGMb is a novel binding partner for PD-L2 and its engagement with PD-L2 promotes respiratory tolerance. *J Exp Med.* (2014) 211:943–59. doi: 10.1084/jem.20130790

15. Liu CQ, Xu J, Zhou ZG, Jin LL, Yu XJ, Xiao G, et al. Expression patterns of programmed death ligand 1 correlate with different microenvironments and patient prognosis in hepatocellular carcinoma. *Br J Cancer.* (2018) 119:80–8. doi: 10.1038/s41416-018-0144-4

16. Birtalan E, Danos K, Gurbi B, Brauswetter D, Halasz J, Kalocsane Piurko V, et al. Expression of PD-L1 on immune cells shows better prognosis in laryngeal, oropharyngeal, and hypopharyngeal cancer. *Appl Immunohistochem Mo Morphol.* (2018) 26:e79–85. doi: 10.1097/PAI.0000000000000590

17. Drakes ML, Mehrotra S, Aldulescu M, Potkul RK, Liu Y, Grisoli A, et al. Stratification of ovarian tumor pathology by expression of programmed cell death-1 (PD-1) and PD-ligand-1 (PD-L1) in ovarian cancer. *J Ovarian Res.* (2018) 11:43. doi: 10.1186/s13048-018-0414-z

18. Pulko V, Harris KJ, Liu X, Gibbons RM, Harrington SM, Krco CJ, et al. B7-h1 expressed by activated CD8 T cells is essential for their survival. *J Immunol.* (2011) 187:5606–14. doi: 10.4049/jimmunol.1003976

19. Tang H, Liang Y, Anders RA, Taube JM, Qiu X, Mulgaonkar A, et al. PD-L1 on host cells is essential for PD-L1 blockade-mediated tumor regression. *J Clin Invest.* (2018) 128:580–8. doi: 10.1172/JCI96061

20. Sepesi B, Cuentas EP, Canales JR, Behrens C, Correa AM, Vaporciyan A, et al. Programmed death cell ligand 1 (PD-L1) is associated with survival in stage I non-small cell lung cancer. *Semin Thorac Cardiovasc Surg.* (2017) 29:408–15. doi: 10.1053/j.semtcvs.2017.05.008

21. Ojalvo LS, Thompson ED, Wang TL, Meeker AK, Shih IM, Fader AN, et al. Tumor-associated macrophages and the tumor immune microenvironment of primary and recurrent epithelial ovarian cancer. *Hum Pathol.* (2018) 74:135–47. doi: 10.1016/j.humpath.2017.12.010

22. Zhu J, Wen H, Bi R, Wu Y, Wu X. Prognostic value of programmed death-ligand 1 (PD-L1) expression in ovarian clear cell carcinoma. *J Gynecol Oncol.* (2017) 28:e77. doi: 10.3802/jgo.2017.28.e77

23. Ventriglia J, Paciolla I, Pisano C, Cecere SC, Di Napoli M, Tambaro R, et al. Immunotherapy in ovarian, endometrial and cervical cancer: state of the art and future perspectives. *Cancer Treat Rev.* (2017) 59:109–16. doi: 10.1016/j.ctrv.2017.07.008

24. Hamanishi J, Mandai M, Abiko K, Matsumura N, Baba T, Yoshioka Y, et al. The comprehensive assessment of local immune status of ovarian cancer by the clustering of multiple immune factors. *Clin Immunol.* (2011) 141:338–47. doi: 10.1016/j.clim.2011.08.013

25. Duraiswamy J, Freeman GJ, Coukos G. Therapeutic PD-1 pathway blockade augments with other modalities of immunotherapy T-cell function to prevent immune decline in ovarian cancer. *Cancer Res.* (2013) 73:6900–12. doi: 10.1158/0008-5472.CAN-13-1550

26. Gatalica Z, Snyder C, Maney T, Ghazalpour A, Holterman DA, Xiao N, et al. Programmed cell death 1 (PD-1) and its ligand (PD-L1) in common cancers and their correlation with molecular cancer type. *Cancer Epidemiol Biomarkers Prev.* (2014) 23:2965–70. doi: 10.1158/1055-9965.EPI-14-0654

27. Turner TB, Buchsbaum DJ, Straughn JM Jr, Randall TD, Arend RC. Ovarian cancer and the immune system - the role of targeted therapies. *Gynecol Oncol.* (2016) 142:349–56. doi: 10.1016/j.ygyno.2016.05.007

28. Wang Q, Lou W, Di W, Wu X. Prognostic value of tumor PD-L1 expression combined with CD8(+) tumor infiltrating lymphocytes in high grade serous ovarian cancer. *Int Immunopharmacol.* (2017) 52:7–14. doi: 10.1016/j.intimp.2017.08.017

29. Wieser V, Gaugg I, Fleischer M, Shivalingaiah G, Wenzel S, Sprung S, et al. BRCA1/2 and TP53 mutation status associates with PD-1 and PD-L1 expression in ovarian cancer. *Oncotarget.* (2018) 9:17501–11. doi: 10.18632/oncotarget.24770

30. Xiao X, Dong D, He W, Song L, Wang Q, Yue J, et al. Mismatch repair deficiency is associated with MSI phenotype, increased tumor-infiltrating lymphocytes and PD-L1 expression in immune cells in ovarian cancer. *Gynecol Oncol.* (2018) 149:146–54. doi: 10.1016/j.ygyno.2018.02.009

31. Imai Y, Hasegawa K, Matsushita H, Fujieda N, Sato S, Miyagi E, et al. Expression of multiple immune checkpoint molecules on T cells in malignant ascites from epithelial ovarian carcinoma. *Oncol Lett.* (2018) 15:6457–68. doi: 10.3892/ol.2018.8101

32. Howitt BE, Sun HH, Roemer MG, Kelley A, Chapuy B, Aviki E, et al. Genetic basis for PD-L1 expression in squamous cell carcinomas of the cervix and vulva. *JAMA Oncol.* (2016) 2:518–22. doi: 10.1001/jamaoncol.2015.6326

33. Sloan EA, Ring KL, Willis BC, Modesitt SC, Mills AM. PD-L1 expression in mismatch repair-deficient endometrial carcinomas, including lynch syndrome-associated and MLH1 promoter hypermethylated tumors. *Am J Surg Pathol.* (2017) 41:326–33. doi: 10.1097/PAS.0000000000000783

34. Bregar A, Deshpande A, Grange C, Zi T, Stall J, Hirsch H, et al. Characterization of immune regulatory molecules B7-H4 and PD-L1 in low and high grade endometrial tumors. *Gynecol Oncol.* (2017) 145:446–52. doi: 10.1016/j.ygyno.2017.03.006

35. Kim J, Kim S, Lee HS, Yang W, Cho H, Chay DB, et al. Prognostic implication of programmed cell death 1 protein and its ligand expressions in endometrial cancer. *Gynecol Oncol.* (2018) 149:381–7. doi: 10.1016/j.ygyno.2018.02.013

36. Kharma B, Baba T, Matsumura N, Kang HS, Hamanishi J, Murakami R, et al. STAT1 drives tumor progression in serous papillary endometrial cancer. *Cancer Res.* (2014) 74:6519–30. doi: 10.1158/0008-5472.CAN-14-0847

37. Eggink FA, Van Gool IC, Leary A, Pollock PM, Crosbie EJ, Mileshkin L, et al. Immunological profiling of molecularly classified high-risk endometrial cancers identifies POLE-mutant and microsatellite unstable carcinomas as candidates for checkpoint inhibition. *Oncoimmunology.* (2016) 6:e1264565. doi: 10.1080/2162402X.2016.1264565

38. Yamashita H, Nakayama K, Ishikawa M, Nakamura K, Ishibashi T, Sanuki K, et al. Microsatellite instability is a biomarker for immune checkpoint inhibitors in endometrial cancer. *Oncotarget.* (2017) 9:5652–64. doi: 10.18632/oncotarget.23790

39. Cancer Genome Atlas Research Network, Albert Einstein College of Medicine, Analytical Biological Services, Barretos Cancer Hospital, Baylor College of Medicine, Beckman Research Institute of City of Hope, et al. Integrated genomic and molecular characterization of cervical cancer. *Nature.* (2017) 543:378–84. doi: 10.1038/nature21386

40. zur Hausen, H. Papillomaviruses in the causation of human cancers - a brief historical account. *Virology.* (2009) 384:260–5. doi: 10.1016/j.virol.2008.11.046

41. Zhang H, Zhang T, You Z, Zhang Y. Positive surgical margin, HPV persistence, and expression of both TPX2 and PD-L1 are associated with persistence/recurrence of cervical intraepithelial neoplasia after cervical conization. *PLoS ONE.* (2015) 10:e0142868. doi: 10.1371/journal.pone.0142868

42. Alexandrov LB, Nik-Zainal S, Wedge DC, Aparicio SA, Behjati S, Biankin AV, et al. Signatures of mutational processes in human cancer. *Nature.* (2013) 500:415–21. doi: 10.1038/nature12477

43. Lyford-Pike S, Peng S, Young GD, Taube JM, Westra WH, Akpeng B, et al. Evidence for a role of the PD-1:PD-L1 pathway in immune resistance of HPV-associated head and neck squamous cell carcinoma. *Cancer Res.* (2013) 73:1733–41. doi: 10.1158/0008-5472.CAN-12-2384

44. Yang W, Lu YP, Yang YZ, Kang JR, Jin YD, Wang HW. Expressions of programmed death (PD)-1 and PD-1 ligand (PD-L1) in cervical intraepithelial neoplasia and cervical squamous cell carcinomas are of prognostic value and associated with human papillomavirus status. *J Obstet Gynaecol Res.* (2017) 43:1602–12. doi: 10.1111/jog.13411

45. Reddy OL, Shintaku PI, Moatamed NA. Programmed death-ligand 1 (PD-L1) is expressed in a significant number of the uterine cervical carcinomas. *Diagn Pathol.* (2017) 12:45. doi: 10.1186/s13000-017-0631-6

46. Mezache L, Paniccia B, Nyinawabera A, Nuovo GJ. Enhanced expression of PD L1 in cervical intraepithelial neoplasia and cervical cancers. *Mod Pathol.* (2015) 28:1594–602. doi: 10.1038/modpathol.2015.108

47. Heeren AM, Punt S, Bleeker MC, Gaarenstroom KN, van der Velden J, Kenter GG, et al. Prognostic effect of different PD-L1 expression patterns in squamous cell carcinoma and adenocarcinoma of the cervix. *Mod Pathol.* (2016) 29:753–63. doi: 10.1038/modpathol.2016.64

48. Piersma SJ. Immunosuppressive tumor microenvironment in cervical cancer patients. *Cancer Microenviron.* (2011) 4:361–75. doi: 10.1007/s12307-011-0066-7

49. Pfaendler KS, Tewari KS. Changing paradigms in the systemic treatment of advanced cervical cancer. *Am J Obstet Gynecol.* (2016) 214:22–30. doi: 10.1016/j.ajog.2015.07.022

50. Heeren AM, de Boer E, Bleeker MC, Musters RJ, Buist MR, Kenter GG, et al. Nodal metastasis in cervical cancer occurs in clearly delineated fields of immune suppression in the pelvic lymph catchment area. *Oncotarget.* (2015) 6:32484–93. doi: 10.18632/oncotarget.5398

51. Hecking T, Thiesler T, Schiller C, Lunkenheimer JM, Ayub TH, Rohr A, et al. Tumoral PD-L1 expression defines a subgroup of poor-prognosis vulvar carcinomas with non-viral etiology. *Oncotarget.* (2017) 8:92890–903. doi: 10.18632/oncotarget.21641

52. Chinn Z, Stoler MH, Mills AM. PD-L1 and IDO expression in cervical and vulvar invasive and intraepithelial squamous neoplasias: implications for combination immunotherapy. *Histopathology.* (2019) 74:256–68. doi: 10.1111/his.13723

53. Thangarajah F, Morgenstern B, Pahmeyer C, Schiffmann LM, Puppe J, Mallmann P, et al. Clinical impact of PD-L1 and PD-1 expression in squamous cell cancer of the vulva. *J Cancer Res Clin Oncol.* (2019) 145:1651–60. doi: 10.1007/s00432-019-02915-1

54. Sznurkowski JJ, Zawrocki A, Sznurkowska K, Peksa R, Biernat W. PD-L1 expression on immune cells is a favorable prognostic factor for vulvar squamous cell carcinoma patients. *Oncotarget.* (2017) 8:89903–12. doi: 10.18632/oncotarget.20911

55. Fleming GF, Emens LA, Eder JP, Hamilton EP, Liu JF, Liu B, et al. Clinical activity, safety and biomarker results from a phase Ia study of atezolizumab (atezo) in advanced/recurrent endometrial cancer (rEC). *J Clin Oncol.* (2017) 35(Suppl.):5585–5585. doi: 10.1200/JCO.2017.35.15_suppl.5585

56. Ott PA, Bang YJ, Berton-Rigaud D, Elez E, Pishvaian MJ, Rugo HS, et al. Safety and antitumor activity of pembrolizumab in advanced programmed death ligand 1-positive endometrial cancer: results from the KEYNOTE-028 study. *J Clin Oncol.* (2017) 35:2535–41. doi: 10.1200/JCO.2017.72.5952

57. Dai Y, Sun C, Feng Y, Jia Q, Zhu B. Potent immunogenicity in BRCA1-mutated patients with high-grade serous ovarian carcinoma. *J Cell Mol Med.* (2018) 22:3979–86. doi: 10.1111/jcmm.13678

58. Iwai Y, Hamanishi J, Chamoto K, Honjo T. Cancer immunotherapies targeting the PD-1 signaling pathway. *J Biomed Sci.* (2017) 24:26. doi: 10.1186/s12929-017-0329-9

59. Hamanishi J, Mandai M, Ikeda T, Minami M, Kawaguchi A, Murayama T, et al. Safety and antitumor activity of anti-PD-1 antibody, nivolumab, in patients with platinum-resistant ovarian cancer. *J Clin Oncol.* (2015) 33:4015–22. doi: 10.1200/JCO.2015.62.3397

60. Frenel JS, Le Tourneau C, O'Neil B, Ott PA, Piha-Paul SA, Gomez-Roca C, et al. Safety and efficacy of pembrolizumab in advanced, programmed death ligand 1-positive cervical cancer: results from the phase Ib KEYNOTE-028 trial. *J Clin Oncol.* (2017) 35:4035–41. doi: 10.1200/JCO.2017.74.5471

61. Chung HC, Schellens JHM, Delord JP, Perets R, Italiano A, Shapira-Frommer R, et al. Pembrolizumab treatment of advanced cervical cancer: updated results from the phase 2 KEYNOTE-158 study. *J Clin Oncol.* (2018) 36(Suppl. 15):5522. doi: 10.1200/JCO.2018.36.15_suppl.5522

62. Callahan MK, Wolchok JD. At the bedside: CTLA-4- and PD-1-blocking antibodies in cancer immunotherapy. *J Leukoc Biol.* (2013) 94:41–53. doi: 10.1189/jlb.1212631

63. Zitvogel L, Kroemer G. Targeting PD-1/PD-L1 interactions for cancer immunotherapy. *Oncoimmunology.* (2012) 1:1223–5. doi: 10.4161/onci.21335

64. O'Donnell JS, Long GV, Scolyer RA, Teng MW, Smyth MJ. Resistance to PD1/PDL1 checkpoint inhibition. *Cancer Treat Rev.* (2017) 52:71–81. doi: 10.1016/j.ctrv.2016.11.007

65. Martins F, Sofiya L, Sykiotis GP, Lamine F, Maillard M, Fraga M, et al. Adverse effects of immune-checkpoint inhibitors: epidemiology, management and surveillance. *Nat Rev Clin Oncol.* (2019) 16:563–80. doi: 10.1038/s41571-019-0218-0

66. Swart M, Verbrugge I, Beltman JB. Combination approaches with immune-checkpoint blockade in cancer therapy. *Front Oncol.* (2016) 6:233. doi: 10.3389/fonc.2016.00233

67. Jin L, Lee EM, Ramshaw HS, Busfield SJ, Peoppl AG, Wilkinson L, et al. Monoclonal antibody-mediated targeting of CD123, IL-3 receptor alpha chain, eliminates human acute myeloid leukemic stem cells. *Cell Stem Cell.* (2009) 5:31–42. doi: 10.1016/j.stem.2009.04.018

68. Muñoz L, Nomdedéu JF, López O, Carnicer MJ, Bellido M, Aventín A, et al. Interleukin-3 receptor alpha chain (CD123) is widely expressed in hematologic malignancies. *Haematologica.* (2001) 86:1261–9.

69. Kobold S, Pantelyushin S, Rataj F, Vom Berg J. Rationale for combining bispecific T cell activating antibodies with checkpoint blockade for cancer therapy. *Front Oncol.* (2018) 8:285. doi: 10.3389/fonc.2018.00285

70. Krupka C, Kufer P, Kischel R, Zugmaier G, Lichtenegger FS, Köhnke T, et al. Blockade of the PD-1/PD-L1 axis augments lysis of AML cells by the CD33/CD3 BiTE antibody construct AMG 330: reversing a T-cell-induced immune escape mechanism. *Leukemia.* (2016) 30:484–91. doi: 10.1038/leu.2015.214

71. Waldmann TA. Cytokines in cancer immunotherapy. *Cold Spring Harb Perspect Biol.* (2018) 10:a028472. doi: 10.1101/cshperspect. a028472

72. Charych DH, Hoch U, Langowski JL, Lee SR, Addepalli MK, Kirk PB, et al. NKTR-214, an engineered cytokine with biased IL2 receptor binding, increased tumor exposure, and marked efficacy in mouse tumor models. *Clin Cancer Res.* (2016) 22:680–90. doi: 10.1158/1078-0432.CCR-15-1631

73. Siefker-Radtke AO, Baron AD, Necchi A, Plimack ER, Pal SK, Bedke J, et al. Nivolumab monotherapy in patients with advanced platinum-resistant urothelial carcinoma: efficacy and safety update from CheckMate 275. *J Clin Oncol.* (2019) 37:(Suppl. 15):4524. doi: 10.1200/JCO.2019.37.15_suppl.4524

74. Garris CS, Arlauckas SP, Kohler RH, Trefny MP, Garren S, Piot C, et al. Successful anti-PD-1 cancer immunotherapy requires T cell-dendritic cell crosstalk involving the cytokines IFN-γ and IL-12. *Immunity.* (2018) 49:1148–61. doi: 10.1016/j.immuni.2018.09.024

75. Arora E, Masab M, Mittar P, Jindal V, Gupta S, Dourado C. Role of immune checkpoint inhibitors in advanced or recurrent endometrial cancer. *Cureus.* (2018) 10:e2521. doi: 10.7759/ cureus.2521

USCAP

REVIEW ARTICLE

The TRPV2 cation channels: from urothelial cancer invasiveness to glioblastoma multiforme interactome signature

Giorgio Santoni[1] · Consuelo Amantini[2] · Federica Maggi[1,3] · Oliviero Marinelli[1,2] · Matteo Santoni[4] ·
Massimo Nabissi [1] · Maria Beatrice Morelli[1]

Abstract

Changes in transient receptor potential (TRP) Ca^{2+} permeable channels are associated with development and progression of different types of cancer. Herein, we report data relative to the expression and function of TRP vanilloid 2 (TRPV2) channels in cancer. Overexpression of TRPV2 is observed in high-grade urothelial cancers and treatment with the TRPV2 agonist cannabidiol induces apoptosis. In prostate cancer, TRPV2 promotes migration and invasion, and TRPV2 overexpression characterizes the castration-resistant phenotype. In breast cancer cells, inhibition of TRPV2 by tranilast reduces the insulin-like growth factor-1 stimulated proliferation. TRPV2 overexpression in triple-negative breast cancer cells is associated with high recurrence-free survival. Increased TRPV2 overexpression is present in patients with esophageal squamous cell carcinoma associated with advanced disease, lymph node metastasis, and poor prognosis. Increased TRPV2 transcripts have been found both in benign hepatoma and in hepatocarcinomas, where TRPV2 expression is associated with portal vein invasion and reduction of cancer stem cell expression. TRPV2 expression and function has been also evaluated in gliomagenesis. This receptor negatively controls survival, proliferation, and resistance to CD95- or BCNU-induced apoptosis. In glioblastoma stem cells, TRPV2 activation promotes differentiation and inhibits the proliferation in vitro and in vivo. In glioblastoma, the TRPV2 is part of an interactome-based signature complex, which is negatively associated with survival, and it is expressed in high risk of recurrence and temozolomide-resistant patients. Finally, also in hematological malignancies, such as myeloma or acute myeloid leukemia, TRPV2 might represent a target for novel therapeutic approaches. Overall, these findings demonstrate that TRPV2 exhibits an oncogenic activity in different types of cancers, controlling survival, proliferation, migration, angiogenesis, and invasion signaling pathways. Thus, it prompts the pharmacological use of TRPV2 targeting in the control of cancer progression.

These authors contributed equally: Giorgio Santoni, Consuelo Amantini

✉ Giorgio Santoni
giorgio.santoni@unicam.it

1 School of Pharmacy, University of Camerino, via Madonna delle Carceri 9, 62032 Camerino, MC, Italy

2 School of Biosciences and Veterinary Medicine, University of Camerino, via Madonna delle Carceri 9, 62032 Camerino, MC, Italy

3 Department of Molecular Medicine, Sapienza University, Viale Regina Elena 324, 00161 Rome, RM, Italy

4 Medical Oncology Unit, Hospital of Macerata, Via Santa Lucia 2, 62100 Macerata, MC, Italy

Introduction

Numerous recent studies demonstrate the role of ion channels in the pathogenesis of several chronic inflammatory disease, hence the term "channelopathies". At present, in mammalian cells, 28 transient receptor potential (TRP) Ca^{2+}-permeable channels, belonging to six subfamilies (TRPV, TRPM, TRPC, TRPA, TRPP, and TRPML) and activated by chemical and sensory agonists, have been reported [1]. The vanilloid subfamily (TRPV) is represented by six members (TRPV1–6). TRPV1 is the prototype of TRPV channels, it is activated by heat and synthetic or endogenous vanilloids [2]. TRPV2 shares about 50% sequence identity with TRPV1 [3, 4]. Nevertheless, TRPV2 shows distinct cellular functions from those mediated by TRPV1 [5]. TRPV1 expression is mainly localized in the plasma membrane [3, 4]; in contrast, TRPV2 is localized in the intracellular membranes [6].

SPRINGER NATURE

Moreover, TRPV2 is not stimulated by heat or in vivo by vanilloid exposure [3, 5–7]. In dorsal root ganglion neurons, TRPV2 showed a punctate distribution and Rab7 endosomal co-localization, where it promotes neuronal outgrowth and signaling [5]. TRPV2 activity is induced by 2-aminoethoxydiphenyl borate (2-APB), probenecid and cannabidiol (CBD), and inhibited by Ruthenium red (RR), Gadolinium (Gd), and tranilast [2, 4, 8–10]. Physiologically, post transcriptional modifications, lipid- and protein–protein interactions are involved in TRP regulation [1]. Phosphatidylinositol 4,5-bisphosphate (PIP2) and phosphorylation, due to extracellular signal-regulated kinase (ERKs), regulates the TRPV2 functions [5, 11].

For information regarding the structure of TRPV2, we refer the readers to the very informative and innovative works in which the TRPV2 full-length structure is described by cryo-electron microscopy [12], the conformational plasticity [13] and the distinct TRPV2 conformational states [14].

It is now clear that TRPV2, expressed not only in sensory neurons but also in motor neurons and in many nonneuronal tissues, displays tissue-specific physiological functions [15]. It is involved in perception of noxious stimuli, due to its stretch-dependent properties, and in the regulation of calcium homeostasis functioning as a mechanosensor, thermosensor, and lipid sensor.

TRPV2-mediated signaling pathways have profound effects on a variety of pathological processes such as cardiomyopathies [16, 17] and muscular dystrophy [18, 19], diabetes and obesity [20, 21], fibromyalgia [22, 23], infection diseases and so forth [24, 25], and cancer.

The aim of this review is to report the involvement of TRPV2 channels in the development, progression, and metastatic organ invasion in different tumor types. The stimulation of TRPV2 by growth factors, cytokines, hormones, and endocannabinoids induces the translocation of TRPV2 from the endosome to the plasma membrane, affecting both cell proliferation, and cell death [26]. Loss or changes of TRPV2-mediated signals result in uncontrolled proliferation and apoptotic-resistance, whereas TRPV2 activation enhances the migration and increases the invasiveness of cancer cells [27]. Finally, alternative splice variants of TRPV2 mRNA, evidenced in cancer cells, inhibit the TRPV2 trafficking/translocation [28].

In conclusion, the regulation of TRPV2 channel expression could control tumor progression and therefore these channels represent novel targets for diagnosis and therapy.

TRPV2 expression in urogenital cancer types

The history of the expression and functions of the TRPV2 channel in cancer cells begin in 2008 in the Santoni laboratory whereby a study from Caprodossi et al. demonstrated that TRPV2 expression in normal human urothelial tissues and its increased levels in high-grade and -stage urothelial cancer (UC) tissues and cell lines [29]. Both the full-length TRPV2 (f-TRPV2) and the short splice variant (s-TRPV2) are expressed in normal human urothelial cells and in normal bladder tissues; however, a progressive reduction of TRPV2 splice variant is detected from low stages (e.g., pTa, pT1, and pT2) to the high-stage (pT3 and pT4). In addition, a significant increase of full-length TRPV2 in high-grade and high-stage UC has been reported [29]. Subsequently, a functional role of the TRPV2 was demonstrated by Shimada and collaborators in the bladder cancer (BC) cell line T24 treated with CBD [30]. TRPV2 activation increases the intracellular calcium levels, decreases cell viability and induces apoptotic cell death [30]. Furthermore, the contribution of TRPV2 in matrix metalloproteinase-2 (MMP2)-mediated migration and invasion was demonstrated by Liu and Wang in the human 5637BC cell line transfected with rat TRPV2 [31]. Mizuno et al. reported higher TRPV2 expression levels in the murine MBT-2 BC cell line compared with normal mouse urothelial cells; the silencing of TRPV2 by RNA interference in MBT-2 cells increased cell proliferation, whereas the opposite effect was obtained by using TRPV2 activators. In addition, dominant-negative TRPV2 channel reduced Ca^{2+} permeability in MBT-2 cells, compared with controls [32].

A role for TRPV2 in cancer migration was further demonstrated in PC3 cell line by Prevarskaya's group [33]. It was reported that lysophospholipids (e.g., lysophosphatidylcholine and lysophosphatidylinositol) induce a TRPV2-mediated calcium influx, via Gq/Go and phosphatidylinositol-3,4 kinase (PI3,4K) signaling and translocation of TRPV2 from endosome to the plasma membrane, leading to increased PC3 prostate cancer (PCa) cell migration [33]. Moreover, the TRPV2 mRNA levels were higher in metastatic cancer patients compared with non metastatic primary tumors, with the higher TRPV2 expression characterizing the castration-resistant PCa phenotype. TRPV2 transfection in LNCaP prostate cell line increased cell migration and the expression of MMP-9 and cathepsin B [33]. Similarly, in a nude mice xenograft, TRPV2 silencing reduced PC3 cell growth and invasion, prompting TRPV2 as prognostic and therapeutic target in advanced PCa [34]. A recent publication reported that during cancer invasion TRPV2 activation and clustering by focal mechanical stimulation increases motility and causes actin reorganization that fuel the metastasis spreading [35].

Recent data show a role for adrenomedullin (AM), calcitonin (CT), and calcitonin gene-related peptide in PCa and bone metastasis. AM has been reported to induce a TRPV2-dependent prostate and BC cell migration and invasion; it affected the receptor activator of nuclear factor kappa-B ligand (RANKL) levels in the bone, favoring the metastasis formation [36, 37]. Moreover, CT acts on protein kinase-A

to promote PCa metastasis. Deletion of the PDZ-binding domain of CT receptor abrogates the bone metastasis in an orthotopic PCa model [37]. TRPV2 is also a positive modulator of tumor endothelial cell proliferation and, together with TRPC3 and TRPA1, represents an over-expressed prostate-associated gene in PCa [38].

Overall, TRPV2 activation promotes PI3,4K- and protein kinase A-dependent migration and metastasis in PCa cells, respectively, and through continuous Ca^{2+} influx, inhibits cell proliferation and induces apoptosis of BC cells. Altered transcription of TRPV2 generates a s-TRPV2 splice variant whose levels decrease during UC progression. Although the pathophysiological relevance of the splicing process is still not well understood in BCs, overexpression of s-TRPV2 demonstrated in leukemic blast cells (LBCs) was found to impair the f-TRPV2 translocation to plasma membrane and to inhibit its Ca^{2+} activity [39]. Thus, the ability of tranilast to restore the s-TRPV2 expression levels in LBCs [39], strongly suggest the possible usage of TRPV2 antagonist also in advanced UC.

Expression and function of TRPV2 in breast cancer cells

Breast cancer is the most frequent cancer type in women, with a high mortality rate in metastatic patients. It has been demonstrated that the TRPV2 antagonist, tranilast, reduces the IGF 1-induced calcium rise and cell proliferation in MCF-7 cell line by inducing hypo-phophosphorylation of

the retinoblastoma protein and G1 arrest [40, 41]. Moreover, reduced proliferation, promoted by the TRPV2 agonist CBD through a sustained upregulation of ERK activity, has been reported in aggressive breast cancer cells [42]. In addition, it has been shown that TRPV2 activation promotes cell differentiation in glioblastoma (GBM) stem cells [43] and reduces colony formation in liver cancer stem cells (CSC) [44] suggesting other TRPV2-mediated signals in stem cells-derived cancers. Thus, differences in TRPV2-signaling pathway activation may be responsible for para-doxical effects of the TRPV2-mediated functions.

TRPV2 has been also found to bind and inhibit Rac1 and RhoA in fibroblast-like synoviocytes from rheumatoid arthritis patients [45]. Concordantly in breast cancer cells, a reduction of TRPV2 levels by treatment with two Rho-kinase inhibitors, fasudil, and Y-27632, has been demon-strated in ZR-75-1, MCF-7, and MDA-MB-231 BC cell lines [46]. In addition, treatment of human breast cancer cell lines with the antimicrobial peptide hCAP18/LL-37 stimulated migration by recruiting the TRPV2 channel to pseudopodia through PI3K/Akt activation (Fig. 1). Ca^{2+} entry synergizes with a K^+ efflux through the bradykinin channel, BKCa. No major differences were observed by using the D- or L-enantiomer of LL-37 suggesting a TRPV2-independent decrease membrane fluidity [47].

Triple-negative breast cancer (TNBC) is highly aggres-sive and difficult to treat. Recent studies have demonstrated upregulation of the TRPV2 protein in TNBC tissues com-pared with normal tissues. Moreover, a direct correlation between TRPV2 overexpression and higher recurrence-free

Fig. 1 Mechanism proposed for the stimulatory activity of the LL-37 antimicrobial peptides on cell migration. LL-37 binds to the membranes of caveolae and pseudopodia [1], and activates PI3K/AKT signaling [2]. AKT induces the recruitment of the TRPV2 channel [3] from intracellular vesicles to plasma membranes of pseudopodia. The increase of intracellular Ca^{2+} induced by TRPV2 is accompanied by K^+ efflux through BKCa [4], which preserves the ion balance and maintain the Ca^{2+} entry, which promotes cancer cell migration. Courtesy by Gambade et al. [47]
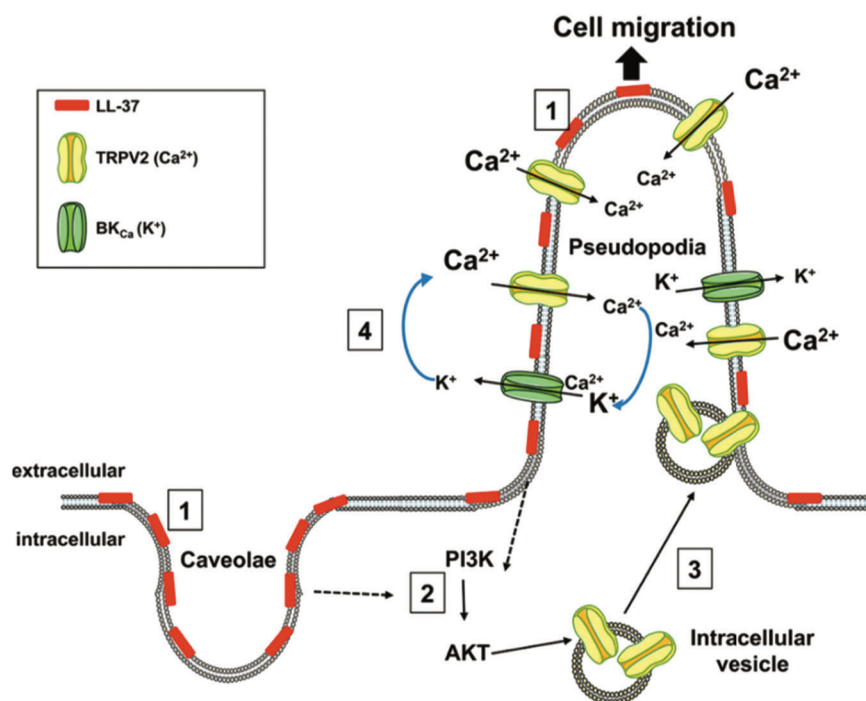
survival, was seen in TNBC and estrogen receptor β (ERβ)-negative breast cancer patients who underwent a chemotherapy regimen [48] (Fig. 2). TRPV2 overexpression or CBD treatment enhanced doxorubicin (DOXO) uptake and apoptotic cell death in TNBC cells. These effects were reverted by TRPV2 blocking or downregulation [48]. In an in vivo mouse model, increased apoptosis was observed in TNBC tumors from CBD plus DOX-treated mice, compared with mice treated with CBD or DOXO alone. Thus, these studies identify a good prognostic role for TRPV2 in TNBC and ERβ-negative BC patients, and suggest that TRPV2 activation may represent a new therapeutic strategy
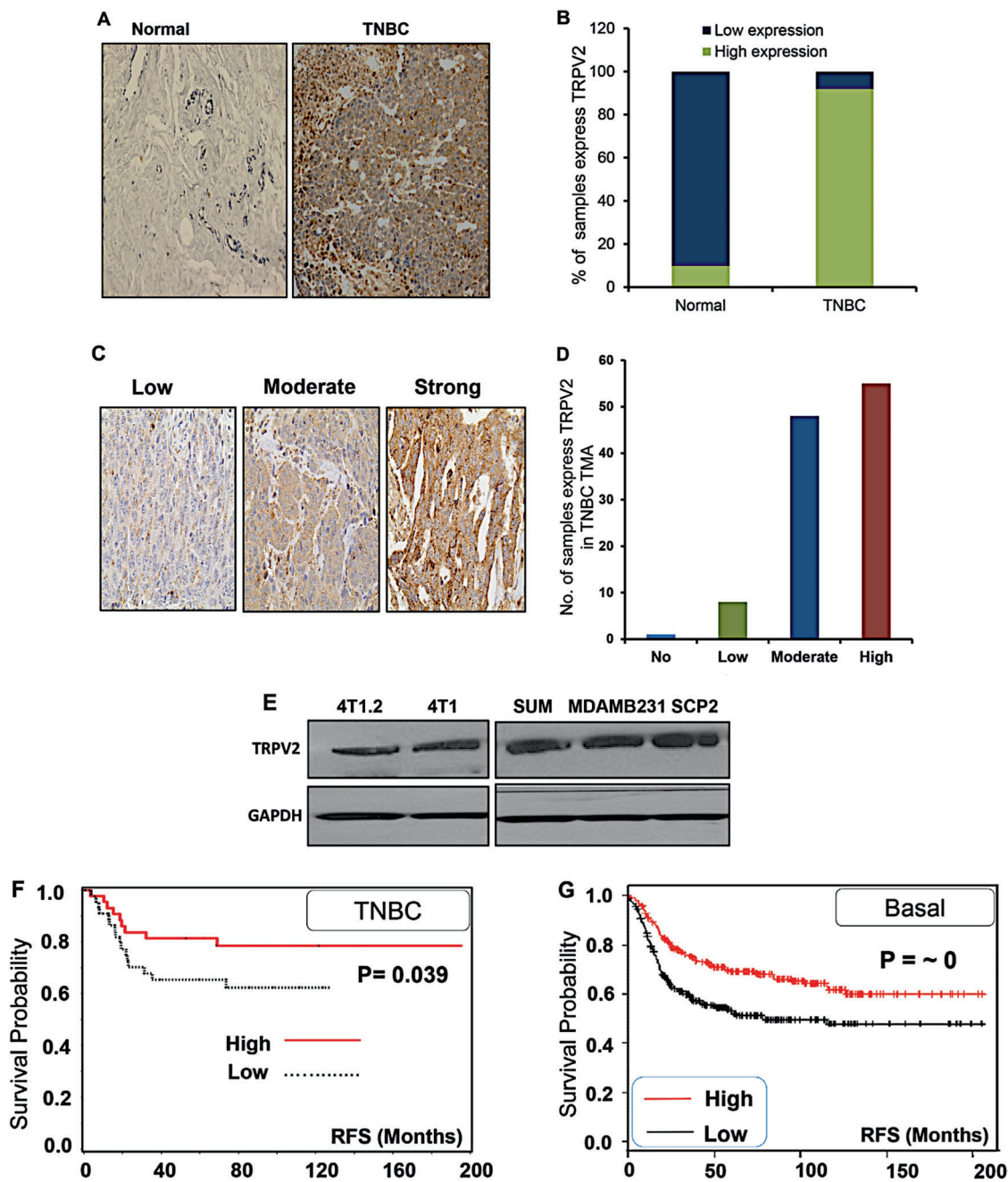
Fig. 2 TRPV2 is highly expressed in TNBC tissues and associated with better prognosis. **a** Representative image of immune-histochemical staining showing TRPV2 expression in normal and TNBC breast tissues. **b** Quantitation of TRPV2 expression of normal and TNBC breast tissues. **c** Representative image of IHC TRPV2 staining in the tissue microarray of TNBC patient samples. **d** Quantitation of TRPV2 expression in the tissue microarray of TNBC patients. **e** Western blot image showing TRPV2 protein expression of 4T1.2, 4T1, SUM159, MDA-MB231, and SCP2 cells. GAPDH used as a loading control. **f** Tissue microarray analysis showing the recurrence-free survival (RFS) of TNBC patients ($n = 116$) of high/low TRPV2 protein expression. **g** Kaplan–Meier blot showing RFS of high/low expressing TRPV2 breast cancer patients of basal subtypes ($n = 580$ patients). Courtesy of Elbaz et al. [48]

to increase the chemotherapic effects in these BC patients [48] (Fig. 3).

Overall, overexpression of TRPV2 in TNBC and ERβ-negative breast cancer plays a protective role by increasing the sensitivity of breast cancer cells to chemotherapy-induced apoptosis representing a positive prognostic factor. The increase of TRPV2 expression by CBD treatment, that sustains the ERK-dependent inhibition of breast cancer proliferation, or genetic/pharmacological downregulation of TRPV2 which reduces apoptosis, chemoresistance, and migration, may together represent a new therapeutic strategy for care this aggressive cancer.

Role of TRPV2 in in esophageal squamous cell carcinoma (ESCC)

TRPV2 mRNA overexpression was detected in ESCC tissues and ESCC cell lines respect to normal cells [49]. Moreover, recently, Huang et al. confirmed that TRPV2, but also TRPV1 and TRPV4, are functional and upregulated in ESCC. The TRPV2 channel was activated by exposure of ESCCs to high temperatures (53 °C) or to a newly developed cannabinoid, O1821 [50].

High TRPV2 expression was observed in patients with advanced disease, high-stage and lymph node metastasis. The 5-year disease-specific survival and disease-free survival were found to be worse in patients harboring high TRPV2 level compared with those showing low TRPV2 expression [49]. By multivariate analysis the TRPV2 mRNA expression and lymph node invasion were independent prognostic factors. TRPV2 mRNA overexpression represents a negative prognostic factor in ESCC patients surgical resected [49]. Moreover, CSC isolated from TE8 ESCC cell line also showed TRPV2 upregulation. CSCs were more sensitive than non-CSCs to tranilast effects that decreased the tumor sphere numbers. Furthermore, in TE8 cell line, tranilast reduced the stemness potential, by inhibiting the aldehyde dehydrogenase 1-positive CSCs, suggesting that TRPV2 might be involved in CSC
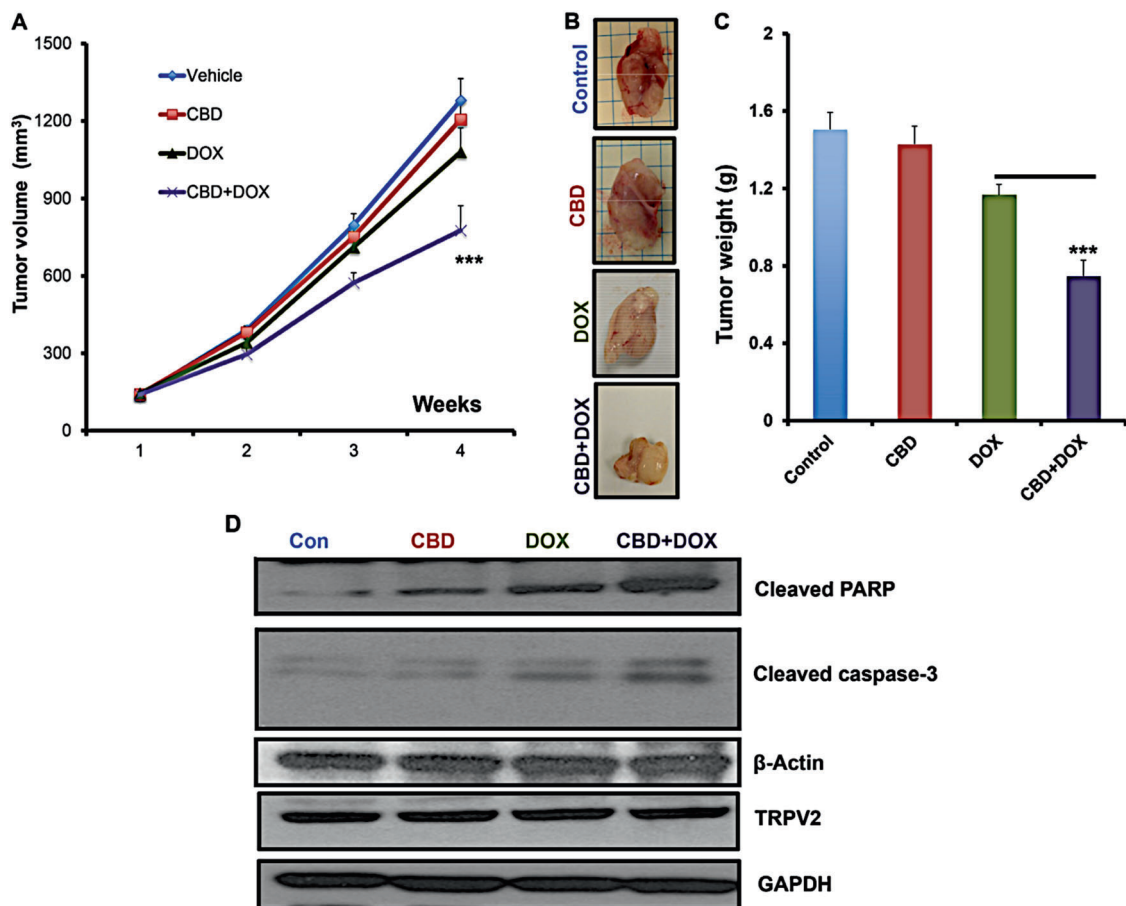
Fig. 3 CBD improves the antitumor chemotherapeutic efficacy in vivo. Nude mice were orthotopically injected into 4th mammary gland with SUM159 cells and subjected to the indicated treatments for 4 weeks and the tumor volume **a** has been measured every week and the weight **c** of the dissected tumors has been determined for each group. **b** Representative images of dissected tumors from the indicated experimental groups. **d** Tumor lysates from the experimental groups were used for western blot analysis and immunoblotted against the indicated proteins. Courtesy of Elbaz et al. [48]

maintenance; its specific inhibitor, tranilast, could represent a potential targeted therapeutic agent against ESCCs [51].

Role for TRPV2 in benign hepatoma and in hepatocarcinomas

Oxidative stress is involved in cancer initiation and progression. TRPV2-mediated oxidative stress in human hepatoma (HepG2 and Huh-7) cell lines has been reported [52]. TRPV2 mRNA overexpression has been found in H_2O_2-exposed HepG2 and Huh-7 cells [52]. Increased TRPV2 levels in H_2O_2-treated hepatoma cells, potentiating the Akt and Nrf2 oxidative-stress inhibition, enhanced the p38/JNK1 MAPK activation and cell death, suggesting that TRPV2 may act by increasing the oxidative stress-induced cytotoxicity and drug resistance in cancers [52].

The relationship between TRPV2 expression in human hepatocellular carcinoma (HCC), its role in hepatocarcinogenesis and the TRPV2 clinical significance has been also studied. qRT-PCR and immunoblotting revealed an increased TRPV2 mRNA and protein in ~30% of HCC cases and a statistical significant relation between TRPV2 expression, portal vein invasion and differentiation level [53]. The hepatocarcinoma phenotype is driven by liver cancer stem-like cells (LCSLCs) subpopulations CD133^{+},

CD90^{+}, CD44^{+}, CD13^{+}, and CD24^{+}, endowed of self-renewal [54]. Knockdown of TRPV2 in HepG2 cells increased the CD133, CD44, and ALDH1 expression and spheroid and colony formation, whereas the contrary effects were found in TRPV2-SMMC-7721 enforced cells. Furthermore, TRPV2 overexpression reverted the inhibition of spheroid and colony formation, whereas TRPV2 down-regulation reduced the stem cell expression in HepG2 cells. Probenecid and tranilast suppressed and increased respectively spheroid and colony formation in LCSLCs and liver cancer cell lines [50] as well as inhibited or promoted tumor growth of HepG2 xenografts in the severe combined immunodeficient (SCID) mouse model, respectively. Similarly, downregulation of CD133, CD44, and ALDH1 in TRPV2 knockdown liver cancer cells was reported (Fig. 4) [44].

TRPV2 channels in brain tumors: role of TRPV2 in gliomagenesis and glioma stem cells

TRPV2 mRNA and protein expression was found in normal human astrocytes, in U87MG cells, in primary glioma cells (MZC, FCL, and FSL lines) and glioma tissues; in particular, TRPV2 levels declined as histological grade
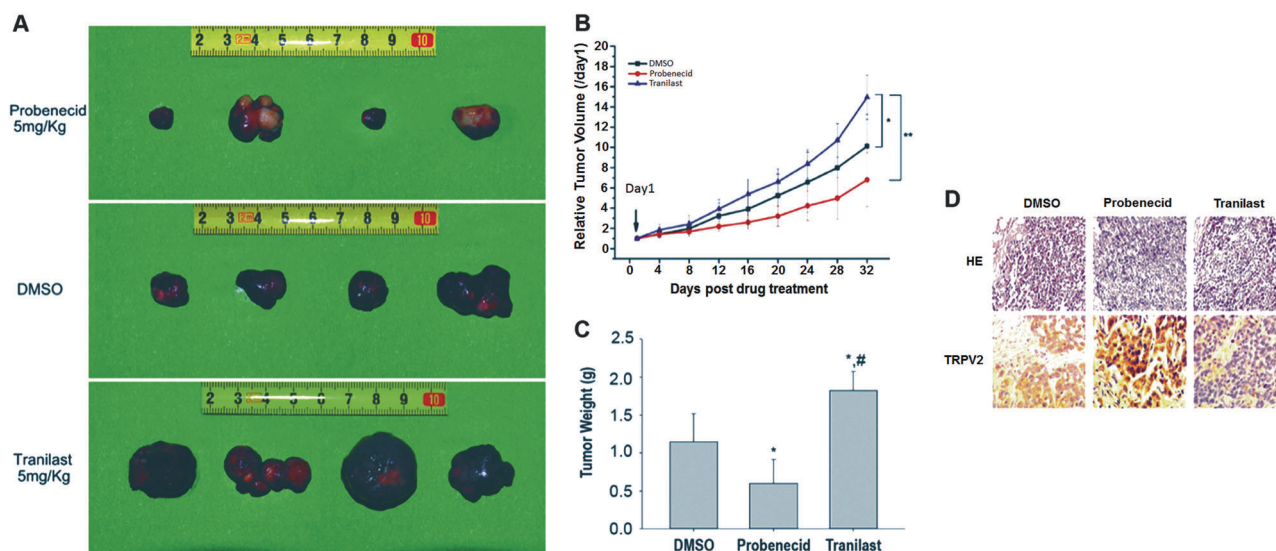
Fig. 4 In in vivo effects of probenecid and tranilast on the tumor growth of HepG2 SCID mouse xenografts. **a** Images of HepG2 xenografts following treatment of the mice with 5.0 mg/kg probenecid and tranilast. **b** Relative tumor volume of HepG2 xenografts in the SCID mouse model following treatment with 5.0 mg/kg probenecid and tranilast. Statistical analysis was conducted for the comparison of the SCID mice that were treated with 5.0 mg/kg tranilast, the animals treated with DMSO and those treated with 5.0 mg/kg of probenecid *$p < 0.05$, **$p < 0.01$. **c** Tumor weight of HepG2 xenografts in the SCID mouse model following treatment with 5.0 mg/kg probenecid and tranilast. Statistical analysis was conducted for the comparison of HepG2 cells treated with 0.1% DMSO, *$p < 0.05$. HepG2 cells treated with probenecid (5.0 mg/Kg) were compared with HepG2 cells treated with tranilast (5.0 mg/Kg), #$p < 0.05$. **d** The histological morphology and TRPV2 protein expression levels of HepG2 xenografts in the SCID mouse model following treatment of the animals with 5.0 mg/kg probenecid and tranilast. The histological evaluation was determined by H&E staining and immunohistochemistry. Courtesy of Hu et al. [44]

increased ($n = 49$ cases) [55]. A marked downregulation of Fas and procaspase-8 mRNA expression in association with upregulation of cyclin E1, cyclin-dependent kinase 2, E2F1 transcription factor-1, V-raf-1 murine leukemia viral oncogene homolog 1, and Bcl-2-associated X protein mRNA expression, was evidenced in TRPV2 silenced (siTRPV2) U87MG cells. Furthermore, increased proliferation and rescued glioma cells to Fas-induced apoptosis, in an ERK-dependent manner was evidenced in siTRPV2-U87MG cells. Indeed, treatment of siTRPV2-U87MG cells with PD98059, a specific MEK inhibitor, reduced Bcl-X(L), promoted CD95 expression and restoring Akt/PKB activation resulted in low U87MG cell proliferation, and increased CD95-mediated apoptosis. Enforced TRPV2 expression in primary glioma cells, by triggering CD95 overexpression, reduced cell viability and enhanced spontaneous and CD95-dependent apoptosis. Overall, in glioma cells, TRPV2 negatively controls the survival and proliferation, as well as resistance to CD95-induced apoptosis in ERK-dependent manner [55]. GBM are characterized by high invasiveness, proliferation, and drug resistance. Chemotherapy with temozolomide (TMZ), carmustine (BCNU) or DOXO was used in GBM treatment; however, their efficacy is limited. In this regard, TRPV2 activation leads to inhibition of GBM proliferation and overcoming of the BCNU resistance [56]. TRPV2 can be activated by CBD; this agonist increases drug uptake and cooperates with cytotoxic agents to induce Ca^{2+} flux and apoptosis of glioma cells, but not of normal astrocytes. In addition, deletion of TRPV2 pore domain, by affecting on channel permeation, inhibits CBD-induced Ca^{2+} rise, drug uptake and cytotoxic effects [56]. Furthermore, a significant relationship between TRPV2 overexpression and survival of GBM patients was reported by Alptekin et al. that demonstrated for the first time that TRP channels, including TRPV2, contribute to the progression/survival of GBM patients [57]. CSCs are considered as the origin of cancer. They represent a small population within the tumor mass, dynamically interchanging between a quiescent and proliferative state in response to stress or DNA damage. Elevated intra-tumor heterogeneity, diffuse parenchymal metastasis and resistance to chemotherapies, result in cancer relapse often leading to patient death. In brain tumors, CSCs seem to derive from neural/progenitor stem cells, and a relevant role for TRPV2 in neurogenesis and gliomagenesis has been suggested [58, 59].

In GBM, recent evidence indicates that cannabinoids inhibit gliomagenesis and promote glioblastoma stem-like cells (GSCs) differentiation. Data reported by Morelli et al. revealed TRPV2 expression in human GSCs suggesting a role in aberrant GSC differentiation. Treatment of GSC lines with RR, EDTA, or knockdown of TRPV2 gene during differentiation, decreases GFAP and β(III)-tubulin expression, conversely, phorbol ester, such as phorbol-12-myristate-13-acetate, reduces TRPV2 expression, enhances GSCs proliferation, and reverts the differentiation. Forced TRPV2 expression in GSC lines enhanced GFAP and β(III)-tubulin levels and inhibited the proliferation. In a xenograft mouse model, TRPV2 over-expression inhibits GSCs proliferation and promotes a glial phenotype differentiation. Therefore, deeper knowledge of TRPV2 molecular pathways in GSCs could improve the specificity and efficacy of the pharmacological approaches [43]. GSCs shown high radio- and chemoresistance are responsible of the recurrence and relapse of GBM. At present, drug-induced differentiation is an interesting approach to re-differentiated CSC subpopulations. CBD by stimulating TRPV2 triggers the GSCs differentiation by inducing autophagy and inhibiting GSCs proliferation and clonogenicity. Moreover, the CBD and BCNU combination overcame the GSC resistance to BCNU treatment, by inducing apoptosis [10]. Recently a role for Acute myeloid leukemia (Aml-1/Runx-1) transcription factor in GBM proliferation/differentiation has been demonstrated. In GSCs, three Aml-1 spliced variants (Aml-1a, b, and c) have been discovered to be modulated in their expression during GSC differentiation. In this regard, upregulation of Aml-1a form was observed during GSCs differentiation; and Aml-1a downregulation restores a stem cell immature phenotype in differentiated GSCs. The Aml-1a binds the TRPV2 promoters and CBD upregulated its expression in a TRPV2- and PI3K/AKT-dependent manner [10]. These data are particularly relevant in the view of the effects showed by CBD on the endothelial cells from blood–brain barrier (BBB). In these cells, CBD induces proliferation, migration, and tubulogenesis suggesting that it might be a potent target for modulating the BBB functions. Moreover, CBD-induced intracellular Ca^{2+} rise, increased cerebral endothelial human CMEC/D3 cell numbers, and increased the transendothelial electrical resistance of brain microvessel endothelial cells [60].

Accordingly, Perálvarez-Marín's group, using a systematic proteomics and computational analysis approach, confirmed the clinical relevance of TRPV2 overexpression in GBM, with the discovery of the TRPV2 interactome (Fig. 5) [61], thus opening new perspectives to identify new biomarkers for diagnosis, prognosis, and therapeutics in GBM. The TRPV2 interactome consists of TRPV2 plus 22 proteins that includes: transport proteins (TRPV2, KCNJ10, CACNG3, and SLC44A2), catalytic proteins (ALDH1A3, INPP5F, and PIP4K2B), trafficking proteins (ARF1, ARL15, ABR, SYT-9, and SNAPIN), signaling molecules (FGF1, ST18, SHISA6, CDH6, and SDC3), myelin components (PLP1, Opalin, and NTM), lipid metabolism proteins (SACM1L, PEBP1, INPP5F, and PIP4K2B), etc. In the TRPV2 interactome, the strongest protein interaction with

A

B

C
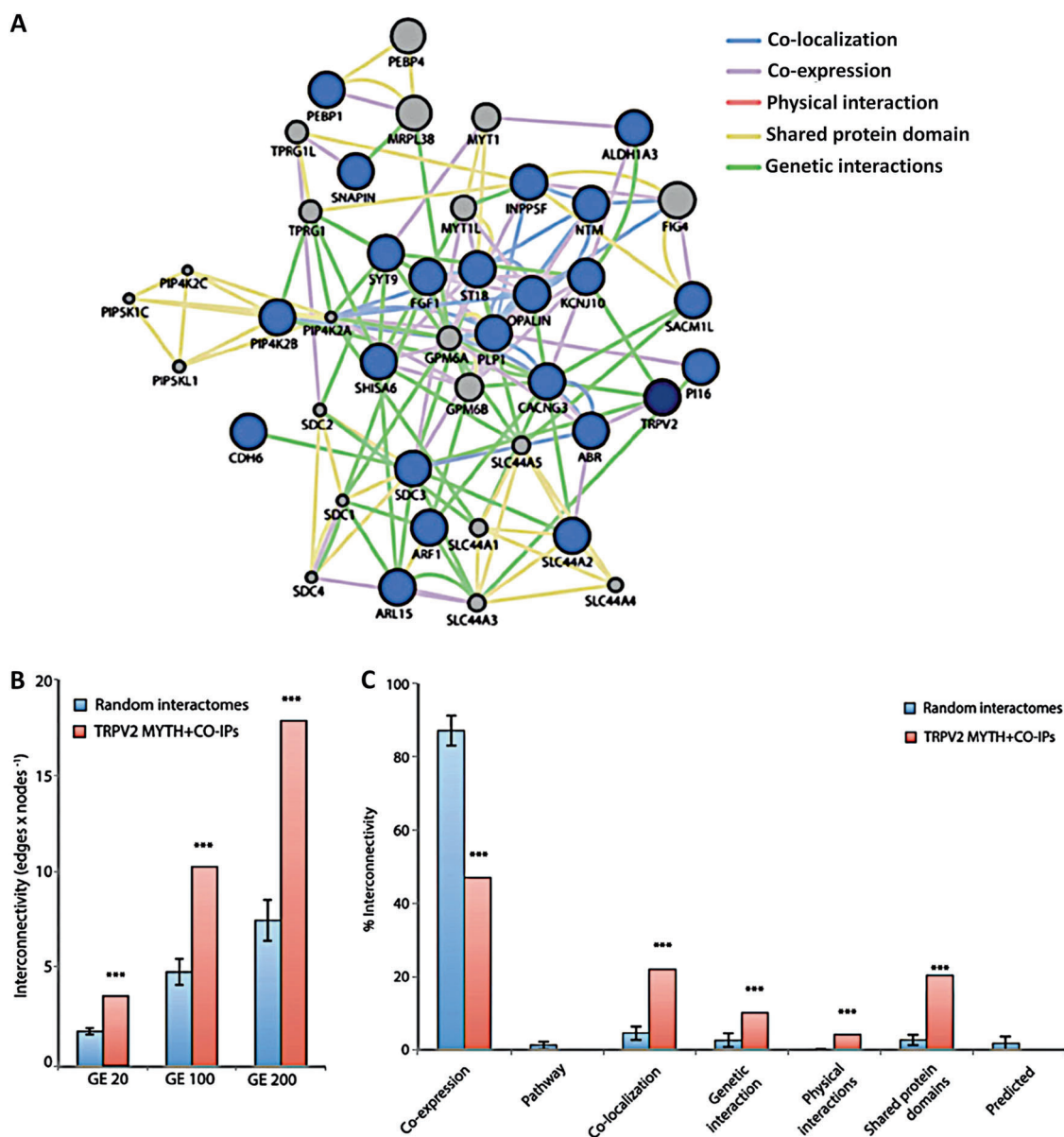
Fig. 5 TRPV2 interactome in GBM. **a** Gene enrichment using the 20 closest related genes. The network generated connects TRPV2 plus CoIP interactors (blue dots) and 20 closest related genes (grey dots) according with the following GO-terms: gene co-expression (purple lines); co-localization (blue lines); genetic interactions (green lines); physical interactions (red lines) and shared domains (brown lines). **b** Network interconnectivity measured as the ratio of edges: nodes within the network. TRPV2 interactome from MYTH plus CoIP was compared with randomly generated networks ($n = 16$). The analysis was performed using a gene enrichment of 20, 100, or 200 closest related genes (GE 20, GE100, and GE200, respectively). **c.** The nature of the network interconnectivity was assessed for TRPV2 interactome and randomly generated networks. The percentage of each type of connection over total connections within the network was represented. ***p values < 0.001 between compared groups. Courtesy of Donate-Macian et al. [61]

TRPV2 was reported for ABR, ARL15, NTM, Opalin, SACM1L, and ST18 proteins [61]. Neoplasms and diseases of the nervous system are strictly associated in the TRPV2 interactome, with the expression of ABR, FGF1, KNJ10, PEBP1, PLP1, and SOC3 proteins [43]. The TRPV2 interactome-based signature allows to discriminate among high- and low-risk GBM, in terms of overall survival (OS), with less survival in GBM patients expressing the TRPV2 protein interactome. Indeed, GBM patients with high TRPV2 interactome protein expression, show a negative prognosis, tumor progression, recurrence, and TMZ-resistance [61].

Expression and function of TRPV2 in the hematologic malignancies

The TRP channels mediate Ca^{2+} influx also in nonexcitable cells, such as in normal and neoplastic cells from

hematopoietic tissues. Several data evidenced that TRP expression was altered in hematologic malignancies: multiple myeloma (MM), acute, and chronic myeloid and lymphoid leukemia (AML, ALL, CML and CLL) and Hodgkin and non-Hodgkin, B- and T-lymphomas [62]. These effects are the result of the widespread roles played by the different subfamily of the TRP channels on hematopoietic cell proliferation, differentiation and apoptosis. The analysis of TRPV2 expression in different hematological malignancies, showed the expression of TRPV2 both in the myeloid and lymphoid leukemia [62]; moreover a very peculiar high TRPV2 expression in B cell lymphomas and MM [63, 64], that parallel the restricted TRPV2 expression in normal immune cells compared with its expression in other human body tissues was reported [65].

MM is a plasma cell (PC) malignancy characterized by the accumulation in the bone marrow of a monoclonal PC type. TRPV2 activation, induced by treatment of MM cells with CBD, decreases the proliferation and stimulates drug-induced cell death in human MM cells.

MM heterogeneity was evidenced by Morelli et al., with the CD138$^+$TRPV2$^+$ and CD138$^+$TRPV2-PC subpopulations expressed in MM patients, and the CD138$^+$ TRPV2-population only present in RPMI8226 and U266 MM cell lines analyzed [66]. In these cells, CBD alone or in synergy with bortezomib, normally used in MM treatment, strongly arrested cell cycle progression and induced cell death in CD138$^+$TRPV2- MM cells and MM cells transfected with TRPV2 (CD138$^+$TRPV2$^+$), by regulating the ERK, AKT, and NF-κB pathways, with more relevant effects in TRPV2-positive cells. Collectively, these findings suggest the use of CBD as adjuvant to increase the proteasome inhibitor activity in MM [66].

Myeloma causes bone destruction and increase Ca^{2+} levels in marrow microenvironment by triggering osteoclastic differentiation (Myeloma bone disease; MBD). Osteolysis during MBD, requires high TRPV2 expression and calcium flux. TRPV2 modulates the nuclear factor-κB ligand (RANKL)-dependent osteoclastic differentiation by activating the Ca^{2+}-calcineurin-nuclear factor of activated T cells signaling pathway, and systemic administration of SKF96365, a TRPV2 inhibitor, reduced the MM-induced osteoclast formation and osteolysis [67].

Pottosin et al. have recently reported the TRPV2 expression in human leukemic cells. TRPV2 is expressed in Jurkat T lymphoblasts, and its effects were blocked by amiloride, Gd^{3+}, RR, and SKF96365. TRPV2 silencing abolished the stretch-activated current in Jurkat T lymphoblasts, suggesting a role for TRPV2 in lymphocyte Ca^{2+} signaling in AML disease [68].

Leukemia patients, treated with chemotherapeutic drugs, showed an increased risk of pulmonary complications as the result of LBCs infiltration into the lung parenchyma. In this regard, LBCs showed increased TRPV2 expression compared with normal human peripheral blood mononuclear cells (PBMCs), which is correlated with increase oncogenic activity. In addition, upregulation of full-length isoform and downregulation of the nonfunctional short form pore-less variant of TRPV2 protein were found in LBCs, whereas the opposite effects were evidenced in PBMCs. It was also demonstrated that silencing or pharmacological targeting of TRPV2 by tranilast or SKF96365, enhances cell cycle arrest and caspase-dependent apoptosis [39]. Tranilast and SKF96365 inhibit the expression of chemotactic peptide that induces TRPV2-dependent migration and invasion and downregulates the CD38 surface expression, responsible for leukemia and lung airway inflammation. Overall, TRPV2 could represent a potential biomarker for patients with leukemia (with lung inflammation) and tranilast could be used as an adjuvant therapeutic strategy in these patients [39].

Expression of TRPV2 in other cancer types

The expression of TRPV2 in gastric cancer (GC) patients has been recently analyzed [58]. Among GC patients investigated, high levels of TRPV2 expression was associated with short OS. The expression of TRPV2 increases as tumor stage increase. In addition, GC showed a higher TRPV2 transcripts and protein levels compared with normal stomach specimens. Moreover, in Lauren's intestinal GCs and patients treated with adjuvant therapy, the TRPV2 levels positively associate with poor prognosis [69].

TRPV2 expression was also evaluated in epidermal melanocytes, two human malignant melanoma (A375, G361) and two metastatic melanoma (A2058, SK-MEL-3) cell lines [70]. Results evidenced that TRPV2, together with TRPV4, TRPA1, and TRPM8 was ectopically expressed in melanocytes and melanoma cells. TRPV2 channel activation reduced cell viability in melanoma A2058 and A375 cells. The 2-APB TRPV2 agonist induced cell necrosis in A2058 cells, suggesting that TRPV2 expression may serve as biomarker for targeting therapeutic drugs and for prognosis in melanomas [70]. Abnormal expression of TRPV channels has been also reported in meningiomas, tumors likely originating from arachnoid cap cells. A significant correlation between the TRPV1, TRPV2, TRPV3, and TRPV4 expression in different meningioma subtypes was evidenced [71].

Cancer adverse effects: role for the TRPV2 channel

Muscle wasting during cancer cachexia causes loss of body and skeletal muscle weight and diminished muscle force and

locomotor activity, so contributing to patient morbidity [72]. Cachexia of muscles results in myolysis, reduced sialic acid content of sarcolemma, enhanced lysosomal exocytosis, and sarcolemma localization of phosphorylated Ca^{2+}/calmodulin-dependent protein kinase II, abnormal autophagy with increased levels of autophagic markers and degradation of dystrophin [61]. Because of the role of TRPV2 in muscle dystrophy, a potential involvement of TRPV2 in cachexia-induced muscle damage has been considered. Studies in a murine model of cancer cachexia in mice bearing Lewis lung carcinoma/colon adenocarcinoma evidenced a slight accumulation of TRPV2 and TRPV2-dependent Ca^{2+} influx was low in cachexia-associated myotubes and cachexia was not ameliorated by dominant-negative inhibition of TRPV2 [73], suggesting a TRPV2-independent mechanisms mediating muscle damage in cancer cachexia.

Dysfunction of TRP channels contributes to the thermal hypersensitivity that accompanies painful conditions in several inflammatory and cancer diseases. Classical thermosensitive TRP channels are TRPV1, TRPV2, TRPV3, TRPV4, TRPM3, TRPM8, and TRPA1 [74]. In addition, althoughTRPV2 is also required for mechanical nociception and the stretch-evoked response of primary sensory neurons [75], no data on the analgesic effects of this compound or its derivates have been provided in cancer [76]. A role for TRPV2 in outgrowth of sensory neurons under neurothrophin-regulated signaling has been suggested [5]. However, although neurothrophin-3 (NT-3) has been found to alleviate perineural invasion and abdominal pain in pancreatic ductal adenocarcinoma patients (PDACs) and high levels of TRPV2 as well as the TRPV1 pain-related proteins were identified, no correlation between TRPV2 and

Table 1 Expression and functions of TRPV2 channels in different human cancer types

Cancer type	TRPV2	Effect	References
UC	Increase	(+) malignancy	[29]
	Activation	(−) viability, apotosis	[30]
	Overexpression	(+) migration, invasion	[31]
PCa	Activation	(+) migration, invasion	[33, 34, 36, 37]
BC	Inhibition	(−) proliferation	[40]
	Activation	(−) proliferation	[42]
	Inhibition	(−) migration	[47]
	Increase	(+) chemiosensitivity apoptosis	[48]
ESC	Increase	(+) progression	[49, 50]
	Increase	(+) stemness	[51]
HCC	Increase	(+) portal vein invasion	[53]
	Inhibition	(+) stemness, tumor growth	[44]
GBM	Inhibition	(−) Fas apoptosis	[55]
	Activation	(+) drug uptake, apoptosis	[56]
	Increase	progression	[57]
	Activation	(+) GSC differentiation Runx-1 activation	[10, 43]
		(+) drug sensitivity	
	Increase	(−) proliferation	[43]
		(+) angiogenesis	[47]
MM	Activation	(−) proliferation (+) cell death	[66]
ALL	Inhibition	(−) stretch-activated current	[68]
	Inhibition	(+) cycle arrest, apoptosis	[39]
		(−) migration, invasion	
GC	Increase	(+) progression	[69]
ME	Activation	(−) viability	[70]
		(+) necrosis	

(+) promote; (−) inhibit

UC Urothelial cancer, *PCa* prostate cancer, *BC* breast cancer, *ESCC* esophageal squamous cancer, *HCC* hepatocarcinoma, *GBM* glioblastoma maligno, *MM* multiple myeloma, *ALL* acute lymphoblastic leukemia, *GC* gastric cancer, *ME* melanoma, *CSC* cancer stem cell

TRPV2 channels control multiple processes involved in cancer progression by modulating survival, cell proliferation, angiogenesis, migration, and invasion in different cancer types. Clinical evidence demonstrates in glioblastoma, epatocarcinoma, and urogenital cancer a strictly relation between altered TRPV2 expression and negative prognosis. Thus, TRPV2 represents a novel prognostic biomarker for cancers

NT-3 pathway was identified in PDAC patients [77]. Moreover, Yamamoto et al., in a mouse model of bone cancer, have demonstrated that TRPV2 is involved in movement-related pain but not in ongoing pain [78].

Conclusions

TRPV2 exhibits an oncogenic activity in different types of cancer associated with changes in its expression levels (i.e., mainly TRPV2 overexpression) (Table 1). Since, it has been demonstrated by several reports that TRPV2 affects signaling pathways responsible for cancer growth/proliferation, migration/invasion, and apoptosis, TRPV2 represents a novel promising pharmacologic target especially in the management of the most aggressive cancers.

A TRPV2 interactome signature has been identified whose overexpression is associated with reduced OS, drug resistance and poor prognosis in GBM patients. Clinical studies are now required to confirm TRPV2 as a useful and sure molecular biomarker to be employed in the patient selection in order to promote a targeted therapy. Interestingly, tranilast, a TRPV2 inhibitor, was found to be effective in leukemia cells and primary blast so much so that it is now considered a potential candidate for further preclinical studies alone or in combination regimens. On the contrary, in UCs no experimental, preclinical, or clinical studies using tranilast have been provided so far. The clinical usage of them in murine cancer model as well as in preclinical studies could be essential to highlight the importance for targeting TRPV2 in high-risk cancer patients to propose a new therapeutic approach.

Compliance with ethical standards

Conflict of interest The authors declare that they have no conflict of interest.

Publisher's note Springer Nature remains neutral with regard to jurisdictional claims in published maps and institutional affiliations.

References

1. Venkatachalam K, Montell C. TRP Channels. Annu Rev Biochem. 2007;76:387–417.
2. Caterina MJ, Schumacher MA, Tominaga M, Rosen TA, Levine JD, Julius D. The capsaicin receptor: a heat-activated ion channel in the pain pathway. Nature. 1997;389:816–24.
3. Caterina MJ, Rosen TA, Tominaga M, Brake AJ, Julius D. A capsaicin-receptor homologue with a high threshold for noxious heat. Nature. 1999;398:436–41.
4. Perálvarez-Marín A, Doñate-Macian P, Gaudet R. What do we know about the transient receptor potential vanilloid 2 (TRPV2) ion channel? FEBS J. 2013;280:5471–87.
5. Cohen MR, Johnson WM, Pilat JM, Kiselar J, DeFrancesco-Lisowitz A, Zigmond RE, et al. Nerve growth factor regulates transient receptor potential vanilloid 2 via extracellular signal-regulated kinase signaling to enhance neurite outgrowth in developing neurons. Mol Cell Biol. 2015;35:4238–52.
6. Cohen MR, Huynh KW, Cawley D, Moiseenkova-Bell VY. Understanding the cellular function of TRPV2 channel through generation of specific monoclonal antibodies. PLoS ONE. 2013;8: e85392.
7. Park U, Vastani N, Guan Y, Raja SN, Koltzenburg M, Caterina MJ. TRP vanilloid 2 knock-out mice are susceptible to perinatal lethality but display normal thermal and mechanical nociception. J Neurosci. 2011;31:11425–36.
8. Bang S, Kim KY, Yoo S, Lee S-H, Hwang SW. Transient receptor potential V2 expressed in sensory neurons is activated by probenecid. Neurosci Lett. 2007;425:120–5.
9. Huynh KW, Cohen MR, Chakrapani S, Holdaway HA, Stewart PL, Moiseenkova-Bell VY. Structural insight into the assembly of TRPV channels. Structure. 2014;22:260–8.
10. Nabissi M, Morelli MB, Amantini C, Liberati S, Santoni M, Ricci-Vitiani L, et al. Cannabidiol stimulates Aml-1a-dependent glial differentiation and inhibits glioma stem-like cells proliferation by inducing autophagy in a TRPV2-dependent manner. Int J Cancer. 2015;137:1855–69.
11. Mercado J, Gordon-Shaag A, Zagotta WN, Gordon SE. Ca2+-dependent desensitization of TRPV2 channels is mediated by hydrolysis of phosphatidylinositol 4,5-bisphosphate. J Neurosci. 2010;30:13338–47.
12. Huynh KW, Cohen MR, Jiang J, Samanta A, Lodowski DT, Zhou ZH, et al. Structure of the full-length TRPV2 channel by cryo-EM. Nat Commun. 2016;7:11130.
13. Zubcevic L, Le S, Yang H, Lee S-Y. Conformational plasticity in the selectivity filter of the TRPV2 ion channel. Nat Struct Mol Biol. 2018;25:405–15.
14. Dosey TL, Wang Z, Fan G, Zhang Z, Serysheva II, Chiu W, et al. Structures of TRPV2 in distinct conformations provide insight into role of the pore turret. Nat Struct Mol Biol.2019;26:40–9.
15. Shibasaki K. Physiological significance of TRPV2 as a mechanosensor, thermosensor and lipid sensor. J Physiol Sci. 2016;66: 359–65.
16. Li Y, Li Q, Zhang O, Guan X, Xue Y, Li S, et al. miR-202-5p protects rat against myocardial ischemia reperfusion injury by downregulating the expression of Trpv2 to attenuate the Ca 2+ overload in cardiomyocytes. J Cell Biochem. 2019;120:13680–93.
17. Iwata Y, Matsumura T. Blockade of TRPV2 is a novel therapy for cardiomyopathy in muscular dystrophy. Int J Mol Sci. 2019; 20:3844.
18. Iwata Y, Katayama Y, Okuno Y, Wakabayashi S. Novel inhibitor candidates of TRPV2 prevent damage of dystrophic myocytes and ameliorate against dilated cardiomyopathy in a hamster model. Oncotarget. 2018;9:14042–57.
19. Matsumura T, Matsui M, Iwata Y, Asakura M, Saito T, Fujimura H, et al. A pilot study of tranilast for cardiomyopathy of muscular dystrophy. Intern Med. 2018;57:311–8.
20. Sawatani T, Kaneko YK, Doutsu I, Ogawa A, Ishikawa T. TRPV2 channels mediate insulin secretion induced by cell swelling in mouse pancreatic beta-cells. Am J Physiol Cell Physiol. 2019;316:C434–43.
21. Sun W, Li C, Zhang Y, Jiang C, Zhai M, Zhou Q, et al. Gene expression changes of thermo-sensitive transient receptor potential channels in obese mice. Cell Biol Int. 2017;41:908–13.
22. D'Agnelli S, Arendt-Nielsen L, Gerra MC, Zatorri K, Boggiani L, Baciarello M, et al. Fibromyalgia: genetics and epigenetics

insights may provide the basis for the development of diagnostic biomarkers. Mol Pain. 2019;15:174480691881994.

23. Park D-J, Kim S-H, Nah S-S, Lee JH, Kim S-K, Lee Y-A, et al. Polymorphisms of the TRPV2 and TRPV3 genes associated with fibromyalgia in a Korean population. Rheumatology. 2016;55:1518–27.

24. Leveque M, Penna A, Le Trionnaire S, Belleguic C, Desrues B, Brinchault G, et al. Phagocytosis depends on TRPV2-mediated calcium influx and requires TRPV2 in lipids rafts: alteration in macrophages from patients with cystic fibrosis. Sci Rep. 2018;8:4310.

25. Link TM, Park U, Vonakis BM, Raben DM, Soloski MJ, Caterina MJ. TRPV2 has a pivotal role in macrophage particle binding and phagocytosis. Nat Immunol. 2010;11:232–9.

26. Liberati S, Morelli MB, Amantini C, Santoni M, Nabissi M, Cardinali C, et al. Advances in transient receptor potential vanilloid-2 channel expression and function in tumor growth and progression. Curr Protein Pept Sci. 2014;15:732–7.

27. Liberati S, Morelli M, Amantini C, Farfariello V, Santoni M, Conti A, et al. Loss of TRPV2 Homeostatic Control of Cell Proliferation Drives Tumor Progression. Cells. 2014;3:112–28.

28. Gkika D, Prevarskaya N. Molecular mechanisms of TRP regulation in tumor growth and metastasis. Biochim Biophys Acta. 2009;1793:953–8.

29. Caprodossi S, Lucciarini R, Amantini C, Nabissi M, Canesin G, Ballarini P, et al. Transient receptor potential vanilloid type 2 (TRPV2) expression in normal urothelium and in urothelial carcinoma of human bladder: correlation with the pathologic stage. Eur Urol. 2008;54:612–20.

30. Yamada T, Ueda T, Shibata Y, Ikegami Y, Saito M, Ishida Y, et al. TRPV2 activation induces apoptotic cell death in human T24 bladder cancer cells: a potential therapeutic target for bladder cancer. Urology. 2010;76:509.e1–509.e7.

31. Liu Q, Wang X. Effect of TRPV2 cation channels on the proliferation, migration and invasion of 5637 bladder cancer cells. Exp Ther Med. 2013;6:1277–82.

32. Mizuno H, Suzuki Y, Watanabe M, Sokabe T, Yamamoto T, Hattori R, et al. Potential role of transient receptor potential (TRP) channels in bladder cancer cells. J Physiol Sci. 2014;64:305–14.

33. Monet M, Gkika D, Lehen'kyi V, Pourtier A, Vanden Abeele F, Bidaux G, et al. Lysophospholipids stimulate prostate cancer cell migration via TRPV2 channel activation. Biochim Biophys Acta. 2009;1793:528–39.

34. Monet M, Lehen'kyi V, Gackiere F, Firlej V, Vandenberghe M, Roudbaraki M, et al. Role of cationic channel TRPV2 in promoting prostate cancer migration and progression to androgen resistance. Cancer Res. 2010;70:1225–35.

35. Sugio S, Nagasawa M, Kojima I, Ishizaki Y, Shibasaki K. Transient receptor potential vanilloid 2 activation by focal mechanical stimulation requires interaction with the actin cytoskeleton and enhances growth cone motility. FASEB J. 2017;31:1368–81.

36. Oulidi A, Bokhobza A, Gkika D, Vanden Abeele F, Lehen'kyi V, Ouafik L, et al. TRPV2 mediates adrenomedullin stimulation of prostate and urothelial cancer cell adhesion, migration and invasion. PLoS ONE. 2013;8:e64885.

37. Warrington JI, Richards GO, Wang N. The role of the calcitonin peptide family in prostate cancer and bone metastasis. Curr Mol Biol Reports. 2017;3:197–203.

38. Bernardini M, Brossa A, Chinigo G, Grolez GP, Trimaglio G, Allart L, et al. Transient receptor potential channel expression signatures in tumor-derived endothelial cells: functional roles in prostate cancer angiogenesis. Cancers. 2019;11:956.

39. Siveen KS, Prabhu KS, Parray AS, Merhi M, Arredouani A, Chikri M, et al. Evaluation of cationic channel TRPV2 as a novel biomarker and therapeutic target in Leukemia-Implications concerning the resolution of pulmonary inflammation. Sci Rep. 2019;9:1554.

40. Nie L, Oishi Y, Doi I, Shibata H, Kojima I. Inhibition of proliferation of MCF-7 breast cancer cells by a blocker of Ca(2+)-permeable channel. Cell Calcium. 1997;22:75–82.

41. Kojima I, Nagasawa M. TRPV2: a calcium-permeable cation channel regulated by insulin-like growth factors. In: Liedtke WB, Heller S, editors.TRP ion channel function in sensory transduction and cellular signaling cascades. Chapter 7. Boca Raton, FL: CRC Press/Taylor & Francis; 2007.

42. McAllister SD, Murase R, Christian RT, Lau D, Zielinski AJ, Allison J, et al. Pathways mediating the effects of cannabidiol on the reduction of breast cancer cell proliferation, invasion, and metastasis. Breast Cancer Res Treat. 2011;129:37–47.

43. Morelli MB, Nabissi M, Amantini C, Farfariello V, Ricci-Vitiani L, di Martino S, et al. The transient receptor potential vanilloid-2 cation channel impairs glioblastoma stem-like cell proliferation and promotes differentiation. Int J Cancer. 2012;131:E1067–77.

44. Hu Z, Cao X, Fang Y, Liu G, Xie C, Qian K, et al. Transient receptor potential vanilloid-type 2 targeting on stemness in liver cancer. Biomed Pharmacother. 2018;105:697–706.

45. Laragione T, Harris C, Gulko PS. TRPV2 suppresses Rac1 and RhoA activation and invasion in rheumatoid arthritis fibroblast-like synoviocytes. Int Immunopharmacol. 2019;70:268–73.

46. Gogebakan B, Bayraktar R, Suner A, Balakan O, Ulasli M, Izmirli M, et al. Do Fasudil and Y-27632 affect the level of transient receptor potential (TRP) gene expressions in breast cancer cell lines? Tumor Biol. 2014;35:8033–41.

47. Gambade A, Zreika S, Guéguinou M, Chourpa I, Fromont G, Bouchet AM, et al. Activation of TRPV2 and BKCa channels by the LL-37 enantiomers stimulates calcium entry and migration of cancer cells. Oncotarget. 2016;7:23785–800.

48. Elbaz M, Ahirwar D, Xiaoli Z, Zhou X, Lustberg M, Nasser MW, et al. TRPV2 is a novel biomarker and therapeutic target in triple negative breast cancer. Oncotarget. 2018;9:33459–70.

49. Zhou K, Zhang S-S, Yan Y, Zhao S. Overexpression of transient receptor potential vanilloid 2 is associated with poor prognosis in patients with esophageal squamous cell carcinoma. Med Oncol. 2014;31:17.

50. Huang R, Wang F, Yang Y, Ma W, Lin Z, Cheng N, et al. Recurrent activations of transient receptor potential vanilloid-1 and vanilloid-4 promote cellular proliferation and migration in esophageal squamous cell carcinoma cells. FEBS Open Bio. 2019;9:206–25.

51. Shiozaki A, Kudou M, Ichikawa D, Fujiwara H, Shimizu H, Ishimoto T, et al. Esophageal cancer stem cells are suppressed by tranilast, a TRPV2 channel inhibitor. J Gastroenterol. 2018;53:197–207.

52. Ma W, Li C, Yin S, Liu J, Gao C, Lin Z, et al. Novel role of TRPV2 in promoting the cytotoxicity of H2O2-mediated oxidative stress in human hepatoma cells. Free Radic Biol Med. 2015;89:1003–13.

53. Liu G, Xie C, Sun F, Xu X, Yang Y, Zhang T, et al. Clinical significance of transient receptor potential vanilloid 2 expression in human hepatocellular carcinoma. Cancer Genet Cytogenet. 2010;197:54–9.

54. Liu L-L, Fu D, Ma Y, Shen X-Z. The power and the promise of liver cancer stem cell markers. Stem Cells Dev. 2011;20:2023–30.

55. Nabissi M, Morelli MB, Amantini C, Farfariello V, Ricci-Vitiani L, Caprodossi S, et al. TRPV2 channel negatively controls glioma cell proliferation and resistance to Fas-induced apoptosis in ERK-dependent manner. Carcinogenesis. 2010;31:794–803.

56. Nabissi M, Morelli MB, Santoni M, Santoni G. Triggering of the TRPV2 channel by cannabidiol sensitizes glioblastoma cells to cytotoxic chemotherapeutic agents. Carcinogenesis. 2013;34:48–57.

57. Alptekin M, Eroglu S, Tutar E, Sencan S, Geyik MA, Ulasli M, et al. Gene expressions of TRP channels in glioblastoma multiforme and relation with survival. Tumour Biol. 2015;36:9209–13.

58. Gimple RC, Bhargava S, Dixit D, Rich JN. Glioblastoma stem cells: lessons from the tumor hierarchy in a lethal cancer. Genes Dev. 2019;33:591–609.

59. Santoni G, Amantini C. The transient receptor potential vanilloid type-2(TRPV2) ion channels in neurogenesis and gliomagenesis: cross-talk between transcriptionfactors and signaling molecules. Cancers. 2019;11: p11 E322.

60. Luo H, Rossi E, Saubamea B, Chasseigneaux S, Cochois V, Choublier N, et al. Cannabidiol increases proliferation, migration, tubulogenesis, and integrity of human brain endothelial cells through TRPV2 activation. Mol Pharm. 2019;16:1312–26.

61. Donate-Macian P, Gomez A, Degano IR, Peralvarez-Marin A. A TRPV2 interactome-based signature for prognosis in glioblastoma patients. Oncotarget. 2018;9:18400–9.

62. Morelli MB, Liberati S, Amantini C, Nabiss M, Santoni M, Farfariello V, et al. Expression and function of the transient receptor potential ion channel family in the hematologic malignancies. Curr Mol Pharmacol. 2013;6:137–48.

63. Boyd RS, Jukes-Jones R, Walewska R, Brown D, Dyer MJS, Cain K. Protein profiling of plasma membranes defines aberrant signaling pathways in mantle cell lymphoma. Mol Cell Proteomics. 2009;8:1501–15.

64. Fabris S, Todoerti K, Mosca L, Agnelli L, Intini D, Lionetti M, et al. Molecular and transcriptional characterization of the novel 17p11.2-p12 amplicon in multiple myeloma. Genes Chromosomes Cancer. 2007;46:1109–18.

65. Santoni G, Farfariello V, Liberati S, Morelli MB, Nabissi M, Santoni M, et al. The role of transient receptor potential vanilloid type-2 ion channels in innate and adaptive immune responses. Front Immunol. 2013;4:34.

66. Morelli MB, Offidani M, Alesiani F, Discepoli G, Liberati S, Olivieri A, et al. The effects of cannabidiol and its synergism with bortezomib in multiple myeloma cell lines. A role for transient receptor potential vanilloid type-2. Int J Cancer. 2014;134:2534–46.

67. Bai H, Zhu H, Yan Q, Shen X, Lu X, Wang J, et al. TRPV2-induced Ca(2+)-calcineurin-NFAT signaling regulates differentiation of osteoclast in multiple myeloma. Cell Commun Signal. 2018;16:68.

68. Pottosin I, Delgado-Enciso I, Bonales-Alatorre E, Nieto-Pescador MG, Moreno-Galindo EG, Dobrovinskaya O. Mechanosensitive Ca(2)(+)-permeable channels in human leukemic cells: pharmacological and molecular evidence for TRPV2. Biochim Biophys Acta. 2015;1848(1 Pt A):51–9.

69. Zoppoli P, Calice G, Laurino S, Ruggieri V, La Rocca F, La Torre G, et al. TRPV2 calcium channel gene expression and outcomes in gastric cancer patients: a clinically relevant association. J Clin Med. 2019;8:pii E622.

70. Zheng J, Liu F, Du S, Li M, Wu T, Tan X, et al. Mechanism for regulation of melanoma cell death via activation of thermo-TRPV4 and TRPV2. J Oncol. 2019;2019:7362875.

71. Goutsou S, Tsakona C, Polia A, Moutafidi A, Zolota V, Gatzounis G, et al. Transient receptor potential vanilloid (TRPV) channel expression in meningiomas: prognostic and predictive significance. Virchows Arch. 2019;475:105–14.

72. Fearon K, Strasser F, Anker SD, Bosaeus I, Bruera E, Fainsinger RL, et al. Definition and classification of cancer cachexia: an international consensus. Lancet Oncol. 2011;12:489–95.

73. Iwata Y, Suzuki N, Ohtake H, Kamauchi S, Hashimoto N, Kiyono T, et al. Cancer cachexia causes skeletal muscle damage via transient receptor potential vanilloid 2-independent mechanisms, unlike muscular dystrophy. J Cachexia Sarcopenia Muscle. 2016;7:366–76.

74. Ferrer-Montiel A, Fernandez-Carvajal A, Planells-Cases R, Fernandez-Ballester G, Gonzalez-Ros JM, Messeguer A, et al. Advances in modulating thermosensory TRP channels. Expert Opin Ther Pat. 2012;22:999–1017.

75. Katanosaka K, Takatsu S, Mizumura K, Naruse K, Katanosaka Y. TRPV2 is required for mechanical nociception and the stretch-evoked response of primary sensory neurons. Sci Rep. 2018;8:16782.

76. Muller C, Morales P, Reggio PH. Cannabinoid ligands targeting TRP channels. Front Mol Neurosci. 2019;11:487.

77. Liu D, Song L, Dai Z, Guan H, Kang H, Zhang Y, et al. MiR-429 suppresses neurotrophin-3 to alleviate perineural invasion of pancreatic cancer. Biochem Biophys Res Commun. 2018;505:1077–83.

78. Yamamoto K, Tanaka S, Fuseya S, Ishida T, Zhang H, Kawamata T, et al. Knockdown of TRPV2 channels in sensory neurons increases limb use and weight bearing but does not affect spontaneous flinching behavior in a mouse model of bone cancer. Mol Pain. 2018;14:174480691881994.

Chapter 24
Targeting Transient Receptor Potential Channels by MicroRNAs Drives Tumor Development and Progression

Giorgio Santoni, Maria Beatrice Morelli, Matteo Santoni, Massimo Nabissi, Oliviero Marinelli, and Consuelo Amantini

Abstract Transient receptor potential (TRP) cation channel superfamily plays important roles in a variety of cellular processes such polymodal cellular sensing, adhesion, polarity, proliferation, differentiation and apoptosis. The expression of TRP channels is strictly regulated and their de-regulation can stimulate cancer development and progression.

In human cancers, specific miRNAs are expressed in different tissues, and changes in the regulation of gene expression mediated by specific miRNAs have been associated with carcinogenesis. Several miRNAs/TRP channel pairs have been reported to play an important role in tumor biology. Thus, the TRPM1 gene regulates melanocyte/melanoma behaviour via TRPM1 and microRNA-211 transcripts. Both miR-211 and TRPM1 proteins are regulated through microphthalmia-associated transcription factor (MIFT) and the expression of miR-211 is decreased during melanoma progression. Melanocyte phenotype and melanoma behaviour strictly depend on dual TRPM1 activity, with loss of TRPM1 protein promoting melanoma aggressiveness and miR-211 expression supporting tumour suppressor. TRPM3 plays a major role in the development and progression of human clear cell renal cell carcinoma (ccRCC) with von Hippel-Lindau (VHL) loss. TRPM3, a direct target of miR-204, is enhanced in ccRCC with inactivated or deleted VHL. Loss of VHL inhibits miR-204 expression that lead to increased oncogenic autophagy. Therefore,

G. Santoni (✉) · M. B. Morelli · M. Nabissi
School of Pharmacy, Experimental Medicine Section, University of Camerino, Camerino, Italy
e-mail: giorgio.santoni@unicam.it

M. Santoni
Clinic and Oncology Unit, Macerata Hospital, Macerata, Italy

O. Marinelli
School of Pharmacy, Experimental Medicine Section, University of Camerino, Camerino, Italy

School of Biosciences and Veterinary Medicine, University of Camerino, Camerino, Italy

C. Amantini
School of Biosciences and Veterinary Medicine, University of Camerino, Camerino, Italy

the understanding of specific TRP channels/miRNAs molecular pathways in distinct tumors could provide a clinical rationale for target therapy in cancer.

Keywords TRP channels · miRNAs · Channelopathies · Tumor progression · Target therapy · Calcium/calcineurin signaling · TRPV · TRPA1 · TRPP · TRPM

Abbreviations

BRAF	proto-oncogene protein B-raf
BRAF^{V600}	BRAF harbouring somatic missense mutations at the amino acid residue V600
BRN2	POU-domain transcription factor (POU3F2)
ccRCC	human clear cell renal cell carcinoma
CRC	colorectal cancer
EC	endometrial cancer
EOC	epithelial ovarian cancer
ETS-1	erythroblastosis virus E26 oncogene homolog 1
FGR2	fibroblast growth factor receptor type 2
HCC	hepatocellular carcinoma cells
LUAD	lung adenocarcinoma
MIFT	microphthalmia-associated transcription factor
miR	MicroRNAs
mRNA	messenger RNA
MTSS1	metastasis suppressor gene 1
NCX1	Na$^+$/Ca^{2+} exchanger-1
NFAT5	nuclear factor of activated T-cells 5
NFATC3	nuclear factor of activated T-cells isoform c3
NSCLC	non-small cell lung carcinoma
OC	ovarian cancer
PCa	prostate cancer
PKD	Polycystic kidney disease
pri-miRs	primary miRNAs
TrkB	Tropomyosin receptor kinase B
TRPA	Transient receptor potential ankyrin
TRPC	Transient receptor potential canonical
TRPM	Transient receptor potential melastatin
TRPP	Transient receptor potential polycystic
TRPV	Transient receptor potential vanilloid
UTR	untranslated region
VHL	von Hippel-Lindau

24.1 Introduction

Ion channels belonging to the Transient Receptor Potential (TRP) family are expressed in every living cell, where they participate in controlling a lot of biological processes and physiological functions, such as cell excitation, electrical activity, cellular osmolarity, as well as growth and death. They show common features in the structure such us the presence of six transmembrane segments with intracellular N- and C-termini and varying degrees of sequence homology. They are grouped into seven subfamilies: TRPC ("C" for canonical), TRPV ("V" for vanilloid), TRPM ("M" for melastatin), TRPN ("N" for no mechanoreceptor potential C), TRPA ("A" for ankyrin), TRPP ("P" for polycystic) and TRPML ("ML" for mucolipin). The majority of TRPs is permeable to Ca^{2+} and these channels are considered as multiple signal integrators. In fact they play critical roles in chemosensation, mechanosensation, thermosensation and nociception sensing stimuli from both external and local environments [1]. Expression of TRP channels is tightly regulated and their expression deregulation can trigger abnormal processes, leading to pathologies, called channelopathies. Several transcription factors play a critical role in controlling the transcriptome of TRP channels by acting on the 5′-flanking gene region. Microribonucleic acids (miRNAs), a small non-coding ribonucleic acids (RNAs) of approximately 22 bp, induce RNA interference by base-pairing with the 3′ untranslated region (UTR) of mRNA, which triggers either mRNA translational repression or RNA degradation [2, 3]. In this manner, miRNAs function as sequence-specific inhibitors of gene expression. miRNAs are initially transcribed as precursor transcripts called primary miRNAs (pri-miRNAs). pri-miRNAs are at first processed in the nucleus to precursor miRNAs (pre-miRNAs) by the class 2 RNase III enzyme Drosha, then, after the transport into the cytoplasm, they become mature miRNAs by the action of Dicer, an RNase III type protein. Finally they are integrated into the Argonaute protein to produce the effector RNA-induced silencing complex (RISC). RISCs target mRNAs recognized through partial sequence complementarity promoting either translational repression or mRNA degradation [4]. Over 1000 different miRNAs are encoded by the human genome; approximately 20–30% of all genes are targeted by miRNAs, and a single miRNA may target up to 200 genes [5]. In human cancers, specific miRNAs are expressed in different tissues, and changes in the control of gene expression have been associated with carcinogenesis [6], including in endometrial, colorectal, prostate cancers and melanomas [7–11]. Furthermore, miRNAs cooperatively exert their function with certain transcription factors in the regulation of mutual sets of target genes, allowing coordinated modulation of gene expression both transcriptionally and post-transcriptionally [12]. In addition, these small noncoding RNAs regulate the expression of different genes involved also in cardiac excitability, pain, brain edema etc. [3]. Future studies might decode other miRNAs/TRP deregulation in human diseases (Table 24.1).

Table 24.1 Expression of miRs and TRP channels in cancers

Tumors	TRP gene	miR	Refs.
Breast cancer	TRPC5	miR-320a (−)	[28]
Renal cell cancer	TRPM3	miR-204 (−)	[54, 56]
Melanoma	TRPM1	miR-211 (−)	[7, 8, 17–20]
Endometrial cancer	TRPM3	miR-204 (−)	[9]
Prostate cancer	TRPM8	miR-26a (+)	[11]
Colon-rectal cancer	TRPV6	miR-122 (+)	[30]
	TRPC1 (?)	miR-135a (+)	[73]
Epithelial ovarian cancer	TRPM1	miR-211 (−)	[26]
	TRPM3	mir-204 (−)	[62]
	TRPC1	miR-135b (+)	[76]
Hepatocarcinoma	TRPC6 (?)	miR-30 (?)	[64]
Lung adenocarcinoma	TRPA1	miR-142 (?)	[31]
Non small cell lung carcinoma	TRPP2	miR-106b (−)[a]	[29]

TRP: Transient receptor potential channels; (?): correlation has been suggested; (−): down-regulated; (+): up-regulated
[a]Cisplatin cell resistant vs sensitive

24.1.1 miR-211 and Its Target Genes in Melanoma Progression

Malignant melanoma has increased the frequency of its occurrence in the last years [13]. Surgical removal of superficial primary tumors is satisfactory in term of survival. However, metastatic melanoma shows a poor survival rate [14]. Transient receptor potential melastatin channel 1 (TRPM1) transcripts are over-expressed in benign nevi, dysplastic nevi and melanomas *in situ*; it is variably expressed in invasive melanomas and is absent in most melanoma metastasis [15]. TRPM1 is regulated by a microphthalmia-associated transcription factor (MITF) [16]. The expression of miR-211, which decreases during melanoma progression [7], is driven by the TRPM1 promoter sequences in a MITF-dependent manner [17]. The gene encoding miR-211 is located within the sixth intron of the TRPM1 gene, and both miR-211 and TRPM1 channel protein are regulated by MITF. The miR-211 directly targets potassium calcium-activated channel subfamily M alpha 1 (KCNMA1) which is often associated with both cell proliferation and migration/invasion in various cancers [7]. Moreover, it has been demonstrated that miR-211 expression is greatly decreased in melanoma cells compared to normal melanocytes [18]. Levy and co-workers have demonstrated by over-expression and knockdown of either TRPM1 channel protein or miR-211, respectively, that miR-211, rather than TRPM1 channel protein, modified the melanoma invasiveness [17]. They also identified that miR-211 regulates insulin-like growth factor 2 (IGF2R), transforming growth factor beta receptor II (TGFBR2), and nuclear factor of activated T-cells 5 (NFAT5) signal transduction pathways to have a suppressive effect on a tumour. These data support the hypothesis that TRPM1 gene regulates melanocyte/melanoma behaviour via generation of two transcripts including TRPM1 protein, and miR-211: the loss of TRPM1 protein is an excellent marker of melanoma aggressiveness while

the miR-211 expression is linked to the tumour suppressor functions. Therefore, different RNA transcription program (i.e. TRPM1 mRNA and/or miR-211) decides on the melanocyte phenotype and melanoma behaviour. Clarifying this phenomenon requires future in vitro studies with targeted modulation of TRPM1 expression and clinic-pathologic correlation using large clinical cohorts of melanoma patients [8]. Furthermore, another miR-211 target, BRN2, also known as POU-domain transcription factor (POU3F2) has been identified. In melanocyte, miR-211 modulates BRN2 expression by repressing its translation [18]. In melanoma miR-211 is expressed at low levels and is related to an over-expression of BRN2, that mediates the de-differentiated and invasive phenotype [18]. The identification of miR-211 and its TRPM1 and BRN2 target genes, could suggest a new therapeutic strategy for the treatment of metastatic melanomas.

24.1.2 miR-211/TRPM1 in BRAF^{V600} Malignant Melanoma

About 50% of malignant melanomas showed proto-oncogene protein B-raf (BRAF) somatic missense mutations at the amino acid residue V600 (BRAF^{V600}) [19]. Inhibition of BRAF^{V600} with vemurafenib induces a rapid regression of metastatic BRAF^{V600} melanomas. Recently, by studying the secretome of melanoma-derived extracellular CD81$^+$ and TSG-101$^+$ vesicles in vemurafenib-treated cells, an increased expression of several miRNAs including miR-211-5p was evidenced (Table 24.2). In melanomas harboring Braf^{V600} mutation, the expression of miR-211-5p because of BRAF inhibition was induced by increased MIFT expression. The later transcriptional factor that up-regulates the TRPM1 gene expression induces miR-211-5p expression, resulting in activation of survival pathway through the Bcl-2 and Melan-A anti-apoptotic molecules [20]. Bcl-2 is a direct target of

Table 24.2 Vemurofenib treatment increases the microRNA levels in exosomes-derived and BRAF^{V600} melanoma cells, compared to not treated cells

Type	Melanoma cells		Exosomes	
	Fold changes	p-value	Fold changes	p-value
microRNA-211-5p	4.07	0.03		
microRNA-34a-5p	1.91	0.04		
microRNA-15b-5p	−2.11	0.01		
microRNA-1307-3p	−1.72	0.01		
microRNA-1301-3p	−2.22	0.02		
microRNA-1307-5p	−2,25	0.03		
microRNA-339-5p	−2.23	0.01		
microRNA-574-3p			−1.40	0.00
microRNA-9-5p			−1.40	0.04
microRNA-7-5p			−1.50	0.04

Table shows the microRNA changes (fold expression) from sequencing analysis in exosome-secreted from and melanoma cells. Fold change is utilized as microRNA up- or down-regulation. Data are presented as the ±SEM. $p < 0.05$

MIFT and modulation of Bcl-2 regulates Melan-A [21]. Inhibition of BRAF^{V600} leads to down-regulation of pERK1/2 that increases MIFT expression [22].

MIFT transcriptionally activates TRPM1 and simultaneously up-regulates the intronic miR-211-5p. Recently has been reported that MIFT induces miR-211 target genes such as AP1S2, SOX11, IGFBP5 and SERINC3 that increase melanoma cell invasion. In addition, also a role for miR-211 as metabolic regulator in melanoma cells, by targeting the hypoxia inducible factor 1a (HIF-1α) has been reported [23].

24.1.3   miR-211 in Ovarian Cancer

The miR-211 is located on intron 6 of the TRPM1 gene at 15q13-q21, a locus frequently lost in neoplasms [24, 25]. It has been demonstrated that miR-211 expression is significantly down-regulated in ovarian cancer. The miR-211 negatively regulates the activity of CDK6 and Cyclin D1 by directly binding to 3'UTR sequences of the related mRNAs repressing their translation into proteins [26]. The cyclin D controls the CDK6 activity and has been reported to regulate angiogenesis, growth factor-stimulated proliferation and the promotion of G1 phase progression. Moreover, miR-211 suppresses the expression of PHF19, promoting apoptosis and inhibiting cell migration [27]. Overall, the cyclin D1/CDK6 and PHF19 are key players in epithelial ovarian cancer (EOC) tumorigenesis and TRPM1/miR-211 might provides new data in the diagnosis, prognosis and therapy for EOC [26, 27].

24.2   TRPC5/miR-320a and TRPP2/miR-106-5p in Breast and Lung Cancer Drug Sensitivity

Over-expression of the transient receptor potential canonical 5 (TRPC5) channel and the nuclear factor of activated T-cells isoform c3 (NFATC3) are essential for breast cancer chemoresistance. However, the mechanism by which TRPC5 and NFATC3 are regulated are unknown. The miR-320a was found to be downregulated in chemoresistant breast cancer cells. It directly targeted TRPC5 and NFATC3 and downregulation of miR-320a triggered TRPC5 and NFATC3 over-expression. In chemoresistant breast cancer cells, downregulation of miR-320a was associated with promoter methylation of the miR-320a coding sequence [28]. Furthermore, the transcription factor v-ets erythroblastosis virus E26 oncogene homolog 1 (ETS-1), which inhibits the miR-320a expression, was found to be activated in chemoresistant breast cancer cells and such activation was associated with hypomethylation of the ETS-1 promoter [28]. Finally, downregulation of miR-320a and enhanced expression of TRPC5, NFATC3, and ETS-1 were verified in clinically chemoresistant breast cancer samples. Low expression of miR-320a was also found to be a significant unfavourable predictor for clinic outcome.

In addition, a role for the miR-106b-5p and the transient receptor potential polycystic channel 2 (TRPP2) channel in the sensitivity of non-small cell lung

carcinoma (NSCLC) to cisplatin treatment has been reported [29]. Treatment of NSCL patients with cisplatin is hindered by cisplatin resistance. Yu e coworkers, have demonstrated in human lung adenocarcinoma MDRA549/cisplatin (A549/DDP) and its progenitor A549 cell line, that miR-106b-5p was decreased in A549/DDP cells. The miR-106b-5p affected the tolerance of cancer lung cells to cisplatin treatment, by negatively regulating the TRPP2 channel [29]. Up-regulation of the miR-106b-5p or down-regulation of the TRPP2 channel expression increased the sensitivity of A549/DDP cells to cisplatin treatment, suggesting that mR-106b-5p may represent a clinical strategy in the treatment of NSCLC [29].

24.3   TRPV6/miR-122 in Colorectal Liver Metastasis

Control of liver metastasis is an important goal in the treatment of colorectal cancer (CRC). In liver metastasis of primary CRCs, the most abundant miRNA, compared with primary tumors, is miR-122 [30].

The expression levels of transient receptor potential vanilloid channel 6 (TRPV6) channels, the cationic amino acid transporter 1 (CAT1), a negative target gene of miR-122, were found to be lower in liver metastases than in primary tumors. The expression levels of TRPV6 evaluated in 132 formalin-fixed paraffin-embedded primary tumors and their corresponding metastatic liver tumors isolated by using laser capture microdissection, were negatively correlated with synchronous liver metastasis and tumor stage. Results from the analysis on 121 CRC patients without synchronous liver metastasis, demonstrated that patients with low TRPV6 expression showed significantly shorter liver metastasis-free survival, but not disease-free survival. Over-expression of miR-122 and concomitant suppression of TRPV6 in the primary CRC appears to play important roles in the development of colorectal liver metastasis.

Thus, expression of TRPV6 in the primary CRC represents a novel biomarker to predict the risk of postoperative liver metastasis of CRC patients [30].

24.4   TRPA1 Channel-Targeting Exosomal miR-142-3p

The transient receptor potential ankyrin channel A1 (TRPA1) channel has been suggested to play an important role in lung cancers [31, 32]. Recent studies have demonstrated the capability of the TRPA1 to form a complex with the fibroblast growth factor receptor type 2 (FGR2) in lung adenocarcinoma (LUAD), a diffuse lung cancer that metastasizes in different organs and brain [33]. As in other lung tumors, in LUAD, FGFR2 is a major factor responsible of tumor progression [34, 35]. In this regard, the TRPA1 channel through the ankyrin repeats, has been demonstrated to bind the terminal prolin-rich region of FGR2. This binding that it is induced, independently by external stimulation, inhibits TRPA1 channel activity, resulting in FGFR2 signaling activation that leads to increased cell proliferation and metastatic spread invasion [33, 34]. In addition, Berrout and coworkers also

demonstrated that the dormant state of LUAD cells observed in the brain upon astrocytes encounter, may be related to a crosstalk between cancer cells and astrocytes. Previously, has been reported that the miR-142-3p targeting the TRPA1 channel can suppress NSC lung cancer progression [35, 36]. In regard to LUAD, astrocytes have been found to be able to transfer micro-vesicles called exosomes containing miRNA (e.g. miR-142-3p) specifically targeting the TRP channel. The binding of miRNA-142-3p to the 3'-UTR of TRPA1 triggers the depletion of TRPA1 expression in metastatic LUAD cells and subsequently abrogation of the FGFR2-driven cell proliferation and invasion of lung cancer cells in the brain.

24.5   TRPM8 and miRNAs in Prostate Cancer

Prostate cancer (PCa) is the second most frequent tumor and the 60 leading cause of cancer related death among males worldwide [37]. TRPM8 is an androgen-responsive gene and essential for the survival of PCa cells [38]. It is involved in the regulation of the intracellular Ca^{2+} concentration and exhibited an elevated expression in PCa cells. TRPM8 shows a significant association with age, serum prostate specific antigen concentration, tumor state, Gleason score or metastasis at prostatectomy. The analysis of a possible correlation between the expression of selected miRNAs and the TRPM8 gene, have evidenced a moderate inverse correlation between high TRPM8 expression and low miR-26a expression. It was found that miR-26a expression was decreased in PCa tissues and cell lines, with androgen-independent prostate cancer showing lower miR-26a expression compared to androgen-dependent prostate cancer [39]. Over-expression of miR-26a enhances apoptosis, and this upregulation is triggered by cytochrome *c* oxidase subunit II inhibition. In addition, a low miR-26a density resulted in an evidently poor prognosis. Further research is warranted to confirm a direct regulatory effect of miRNA on their potential target genes and to the development of miRNA-based therapy [11].

24.6   miR-17/TRPP Channels in Polycystic Kidney Disease and Cancers

The miR-17 and related miRNAs are derived from three miRNA clusters: miR-17 $\sim$ 92, miR-106a-363 and miR-106b $\sim$ 25 clusters. The genomic organization and coding sequences of these miRNA clusters are evolutionarily conserved in vertebrates. Based on their seed sequence, miRNAs derived from these three clusters can be classified into four families: the miR-17, miR-18, miR-19 and miR-25 families. Since members of each family have an identical seed sequence, they are predicted to target the same mRNAs. Interestingly, miR-17 $\sim$ 92 and related clusters

are enriched in developing tissues and are essential for heart and lung development [40]. The miR-17 and related miRNAs are also implicated in the pathogenesis of Polycystic kidney disease (PKD) [41], a most common genetic cause of chronic kidney failure characterized by the presence of numerous, progressively enlarging fluid-filled cysts in the renal parenchyma [41]. By bioinformatics analysis has been reported that miR-17 directly targets the 3′UTR of TRPP2 (PKD2) and post-transcriptionally represses its expression [42]. Dysregulated miRNA expression is observed in PKD, with miR-17 ∼ 92, that is upregulated in a mouse model of PKD. Kidney-specific transgenic over-expression of miR-17 ∼ 92 produces kidney cysts in mice. Conversely, kidney-specific inactivation of miR-17 ∼ 92 in a mouse model of PKD retards kidney cyst growth, improves renal function, and prolongs survival. miR-17 ∼ 92 may mediate these effects by promoting proliferation and through post-transcriptional repression of the TRPP1 and TRPP2 genes (Pkd1 and Pkd2, respectively) and of the hepatocyte nuclear factor-1β [41]. The cysts arise from renal tubules and are lined by abnormally functioning and hyperproliferative epithelial cells.

In addition, two major lines of evidence also implicate miR-17 and related miRs in the pathogenesis of various cancers [43, 44]. First, these miRs are amplified in numerous human cancers, promote proliferation [45] and cause tumor growth in vivo [44]. Second, the oncogenic transcription factor c-Myc has been demonstrated to bind to the miR-17 ∼ 92 promoter and to induce its transcription [46]. Further studies should be required to completely address the oncogenic role of miR-17 and TRPP channels.

24.6.1   *miR-204/TRPM3 and Cancer Survival and Apoptosis*

At present, several data on the role of miR-204 in cancers have been provided. Roldo and coworkers showed the upregulation of miR-204 in insulinoma [47]. Similar results were also reported by Zanette in the acute lymphoblastic leukemia [48]. By contrast, decreased miR-204 expression was reported in glioblastoma [49], gastric, bladder and lung cancers, suggesting that miR-204 may also be a tumor suppressor gene. In hepatocarcinoma, miR-204 has been found to inhibit the expression of long non-coding RNA (lncRNA) for homeobox A distal transcript antisense RNA (HOTTIP), through interference with the argonaute-2 pathway [50]. BCL-2 represents a target for miR-204, and apoptosis represents the suppressive mechanism regulated by miR-204 by binding to the 3′-UTR of BCL-2 [51]. The miR-204 suppression has been reported to inhibit the transition from epithelial to mesenchymal, IL-11, SOX4 and SIX1 target gene expression [52] and bone metastasis in breast cancer cells by reduction of the 68-kDa Src-associated protein in mitosis (SAM68) activity [53].

The miR-204-encoding gene is located in the sixth intron of TRPM3, and expression of mature miR-204 and pri-miR-204 strictly correlates in vitro and in vivo with that of TRPM3 gene [54].

24.6.2   Loss of miR-204 Triggers TRPM3-Mediated Oncogenic Autophagy in Clear Cell Renal Cell Carcinoma

Autophagy is an important homeostatic process for lysosome degradation of damaged organelles and proteins. Interestingly, alterations of the crosstalk between miRs and ion channels belonging to the TRP family, alter the homeostatic control and trigger oncogenic autophagy to survive to stressful stimuli [55]. Among TRP ion channels, TRPM3 plays a major role in the development and progression of clear cell renal cell carcinoma (ccRCC) with von Hippel-Lindau (VHL) loss mutation. TRPM3 expression is enhanced in human ccRCC with inactivated or deleted VHL. Loss of VHL inhibits the expression of miR-204 that in turn leads to increased oncogenic autophagy in ccRCC, resulting in an augmented expression of TRPM3, a direct target of miR-204 [54, 56, 57]. Binding of miR-204 to the 3′UTR of TRPM3 inhibits the TRPM3 translation. Similarly, binding of miR-204 to the 3′-UTR of caveolin 1 (CAV1) inhibits the CAV1 expression required for TRPM3 expression (Fig. 24.1). TRPM3 activation by stimulating of Ca^{2+} influx rise, triggers oncogenic autophagy through increased autophagosomes and CAMKK2
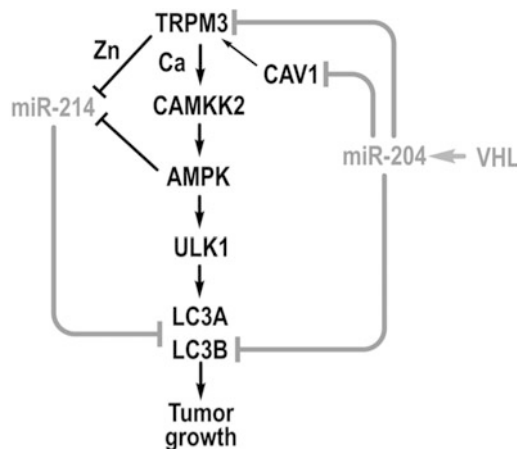
Fig. 24.1 Robust control of the autophagic network by microRNAs and calcium- and zinc-activated pathways. Calcium and zinc entering the cell through the TRPM3 channel stimulate oncogenic autophagy mediated by LC3A and LC3B through a dual mechanism. Calcium stimulates phagophore initiation through Ca^{2+}-dependent activation of CAMKK2 and AMPK, and the resulting phosphorylation of ULK1. Calcium and zinc also inhibit miR-214, which directly targets LC3A and LC3B. The VHL tumor suppressor inhibits expression of TRPM3 directly and indirectly through the effect of miR-204 on CAV1. In addition, miR-204 directly targets LC3B. AMPK, AMP-activated protein kinase; CAMKK2, calcium/calmodulin-dependent protein kinase kinase 2, β; CAV1, caveolin 1; LC3A, microtubule-associated protein 1 light chain 3 α; LC3B, microtubule-associated protein 1 light chain 3 β; TRPM3, transient receptor potential melastatin 3; ULK1, unc-51 like autophagy activating kinase 1; VHL, Von Hippel-Lindau [52]. (Courtesy Hall et al., Cancer Cell. 2014; 26(5): 738–753)
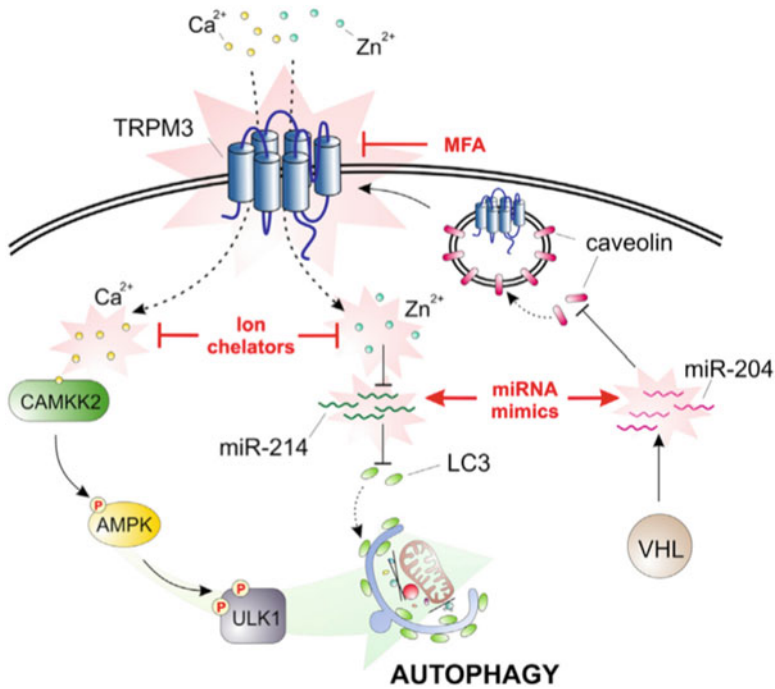
Fig. 24.2 Novel autophagy pathway important in ccRCC, centered on the ion channel TRPM3. The possible strategies to manipulate this pathway at several steps are indicated in red [53]. (Courtesy of Cecconi and Jaattela, Cancer Cell. 2014;26(5):599–600)

and AMPK activation, resulting in ULK1 phosphorylation; by contrast miR-204 inhibits oncogenic autophagy [56]. In addition, TRPM3-induced Ca^{2+} and Zn^{2+} influx and CAMKK2-AMPK pathway activation, inhibit the expression of miR-214 directly targeting the LC3A and LC3B proteins (Fig. 24.2) [58, 59]. Overall, the inhibition of TRPM3-induced oncogenic autophagy in VHL-mutated ccRCC may provide a clinical rationale therapy leading to ccRCC regression. On the other hand, the signal transducer and activator of transcription (STAT)-3 has been demonstrated to down-regulate the miR-204 expression in nasopharyngeal carcinoma [60] and endometrial carcinoma [9].

24.6.3 TRPM3/TrkB/miR-204 Interplay in the Endometrial Cancer

Endometrial carcinoma (EC) is the most common gynecological malignancy worldwide [61]. A recent study identifies a novel TrkB–STAT3–miR-204-5p signaling axis playing an important role in EC growth through the accumulation of the key
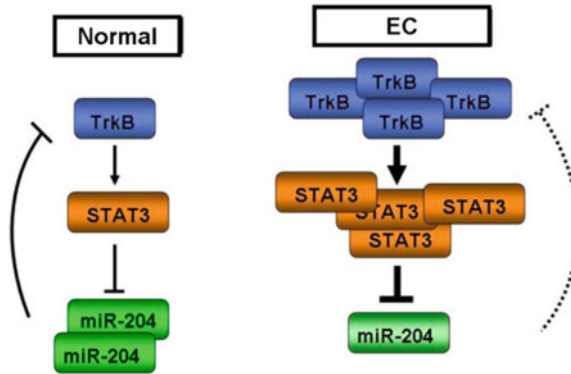
Fig. 24.3 Left: In normal cells, a recurrent auto-regulatory circuit involving the expression of TrkB induces phosphorylation of STAT3 to negatively regulate the expression of miR-204-5p. MiR-204-5p, in turn, represses TrkB expression. The expression of miR-204 within this circuit maintains endometrial cells in a normal differentiated state. Right: In endometrial cancer cells, this circuit becomes dysregulated due to increased activity of the TrkB–STAT3 component of the circuit, which constitutively represses miR-204-5p. In the absence of sufficient miR-204 tumor suppressor activity, TrkB is left uncontrolled, thereby leading to carcinogenesis [7]. (Courtesy of Bao et al. Mol Cancer. 2013; 12: 155)

tumor oncogene, TrkB [9]. The TrkB oncogene is a novel target of miR-204-5p. In normal cells, a recurrent auto-regulatory circuit involving the expression of TrkB induces phosphorylation of STAT3 that negatively regulates the miR-204-5p expression. The miR-204-5p in turn, represses the TrkB expression. The expression of miR-204 in this circuit maintains the endometrial cells in a normal differentiated state. On the other hand, in EC cells, this circuit becomes dysregulated due to increased activity of the TrkB–STAT3 component, which constitutively represses the miR-204-5p. In the absence of sufficient miR-204 tumor suppressor activity, the TrkB oncogene is left uncontrolled, thereby leading to carcinogenesis (Fig. 24.3).

Ectopic over-expression or knockdown of TrkB expression caused changes in miR expression in EC cells. qRT-PCR showed that elevated TrkB repressed miR-204-5p expression in EC cells. Furthermore, TrkB over-expression in Ishikawa[TrkB] cells increased JAK2 and STAT3 phosphorylation, which was aborted by TrkB knockdown in HEC-1B[shTrkB] cells. Moreover, by ChIP assays, phospho-STAT3 direct binding to STAT3-binding sites near the TRPM3 promoter region, upstream of miR-204-5p, has been reported [9]. The miR-204-5p suppresses the clonogenic growth, migration and invasion of EC cells and also inhibits the growth of tumor xenografts bearing human EC cells. Interestingly, lower miR-204-5p expression was associated with lymph node metastasis and lowered the survival in EC patients. Finally, it has been also recently reported in EOC [62] that IL-6 treated EOC via IL-6R, triggers STAT3 activation that in turn represses miR-204 near to the TRPM3 promoter. This effect is required for IL-6-induced cisplatin resistance [62]. Collectively, the reestablishment of miR-204-5p expression could be explored as a potential new therapeutic target for this disease.

24.6.4 TRPC6 and miR-30 in Hepatocellular Carcinoma Invasion

TRPC6 channel is a critical component of calcium/calcineurin signaling together with protein phosphatase 3 family member 3CA/B, R1 (PPP3CA/B, PPP3R1) and NFATC3. This channel is highly expressed in several types of cancer [63]. Recently, a role for TRPC6 in driven TGFβ-mediated migration and invasion of human hepatocellular carcinoma cells (HCC) by forming a complex with the Na^+/Ca^{2+} exchanger-1 (NCX1) has been reported [64]. This complex-mediating Ca^{2+} signaling regulates the effects of TGFβ on the migration, invasion in HepG2 and Huh7 cells, and intrahepatic metastasis of human HCC cells in nude mice. TGFβ upregulates TRPC6 and NCX1 expression and induces the formation and activation of the TRPC6/NCX1 molecular complex, generating a positive feedback between TRPC6/NCX1 and Smad signaling. The expression of both TRPC6 and NCX1 was markedly increased in native human HCC tissues, and their expression levels positively correlated with advancement of HCC in patients. These data reveal the relevance of TRPC6/NCX1 molecular complex in HCC suggesting it as potential targets for therapy [64]. TRPC6 is a target gene of miR-30 [65] found to inhibit cell proliferation and invasion in different tumors [66]. However, at present the mechanisms regulating the miR-30/TRPC6 molecular interaction in HCC are still unknown. In parallel to TRPC6 upregulation that increases cell proliferation, TRPC1 silencing suppressed proliferation. Thus, it may be suggested that miR-30 by targeting TRPC1 and TRPC6 channels may take a part in the mechanism regulating HCC cell proliferation [67].

24.6.5 MiR-135 by Targeting TRPC1 Promotes Cancer Invasion and Chemotherapy Resistance

The miR-135 family comprises two members, miR-135a and miR-135b. miR-135a functions as a tumor suppressor gene in gastric [68], prostate [69] and renal cancers [70], malignant glioma [71] and colon cancer [72]. An in vitro study has demonstrated that in SW480 and SW620 CRC cell lines miR-135a promotes mobility and invasion via the metastasis suppressor gene 1 (MTSS1) [73]. In contrast, inhibition of miR-135a reduced their invasive capability. The miR-135a-mediated cell mobility and invasion were reduced after MTSS1 knocked-down by small interfering RNA, indicating that miR-135a promotes the invasion of CRC cells, partially through targeting MTSS1 [73].

By luciferase reporter assay, TRPC1 was identified as other target gene of miR-135a [63]. In cultured podocytes, TGFβ stimulation and adriamycin treatment promote miR-135a expression and TRPC1 down-regulation. Ectopic expression of miR-135a led to severe podocyte injury and disarray of podocyte cytoskeleton, which was reversed by TRPC1 [63]. Thus, in the view of the important role of miR-

135a in cytoskeleton stability, a contribute of this miRNA in cancer migration and metastatic invasion could be suggested. A role of TRPC1 in cancer development and progression, such as a role in apoptosis of hepatocellular carcinoma [67], metastasis of nasopharyngeal carcinoma [74], proliferation of NSCL carcinoma [75] as well as proliferation and tumorigenesis in ovarian cancer (OC) has been reported. A marked decrease in TRPC1 mRNA levels in human OC and cisplatin-resistant OC cells was observed [76]. TRPC1 directly interacts with several proteins/genes (MORC4, EGFR, STAT3, PDCD4, MET, OGDHL, BCL2, PTEN, SPARCL1, PIK3C3) implicated in drug resistance of OC. In the same way 5 miRs (miR-135b, miR-186, miR-26a, miR-497 and miR-548b-3p) targeting TRPC1, controlling drug resistance in OC [76] have been identified, with increased miR-135b and miR-186 expression that significantly correlates with the reduction of TRPC1 expression. The miR-135a regulates HOXA10 expression in epithelial OC, which correlates with platinum resistance [77]; moreover, a role for the TRPC1/SPARCL1 in the regulation of the autophagy and drug resistance in OC has been suggested.

24.7   Conclusion

MicroRNA are single stranded 19–25 nucleotides short RNAs that modulate gene expression at posttranslational level by targeting mRNAs and through binding of the 3′-untranslated region (UTR) of mRNAs. In the last years, miRNAs have attracted great interest from the oncologists for their versatility to regulate every phase of the carcinogenesis processes. A growing body of evidence suggests that miRNAs are aberrantly expressed in many human cancers (Table 24.1). Some high expressed miRNAs may function as oncogenes by repressing tumor suppressors, whereas other miRNAs are down-regulated and negatively regulate oncogenes, thus functioning as tumor suppressor. miRNAs have a pivotal role in tumorigenesis and the understanding of their functions may help to provide new cancer therapies.

In the last years it was demonstrated that several members of TRP family are target of miRNAs. Considering that these not selective cation channels fulfill several roles in cell physiology and in pathology such as regulating tumorigenesis and tumor progression, they became promising therapeutic targets in cancer treatment. Indeed, the interruption of one or more of the above described signaling network could be more effective than a single target gene to overcome cancer.

Interestingly, RNA molecules are not only retained in the cytoplasm of the cells, but they can also be released into the extracellular milieu, often in extracellular vesicles. These extracellular vesicles can transfer functional RNA between cells. In addition, different types of vesicles such as apoptotic bodies, microvesicles and exosomes contain distinct RNA molecules, especially miRNAs.

MiRNAs dysregulation was also involved in cancer chemoresistance, by regulating specific TRP-mediated pathway developed as consequence of high selection pressure in response to a disadvantageous microenvironment.

Future studies should be required to identify the TRP channels and miRNAs expression and their role played in distinct phase of tumor development and progression. Much work still remains to do; we are only at the beginning to develop strategies to treat cancer manipulating the TRP/miRNA interactive network.

References

1. Zheng J (2013) Molecular mechanism of TRP channels. Compr Physiol 3:221–242
2. Bartel DP (2004) MicroRNAs: genomics, biogenesis, mechanism, and function. Cell 12:281–297
3. Wang Z (2013) miRNA in the regulation of ion channel/transporter expression. Compr Physiol 3:599–653
4. Hyun YJ, Changchun X (2015) MicroRNA mechanisms of action: what have we learned from mice? Front Genet 6:328
5. Krek A, Grun D, Poy MN, Wolf R, Rosenberg L, Epstein EJ, MacMenamin P, da Piedade I, Gunsalus KC, Stoffel M, Rajewsky N (2005) Combinatorial microRNA target predictions. Nat Genet 12:495–500
6. Lu J, Getz G, Miska EA, Alvarez-Saavedra E, Lamb J, Peck D, Sweet-Cordero A, Ebert BL, Mak RH, Ferrando AA (2005) MicroRNA expression profiles classify human cancers. Nature 12:834–838
7. Mazar J, DeYoung K, Khaitan D, Meister E, Almodovar A, Goydos J, Ray A, Perera RJ (2010) The regulation of miRNA-211 expression and its role in melanoma cell invasiveness. PLoS One 5:e13779
8. Guo H, Carlson JA, Slominski A (2012) Role of TRPM in melanocytes and melanoma. Exp Dermatol 21(9):650–654
9. Bao W, Wang HH, Tian FJ, He XY, Qiu MT, Wang JY (2013) A TrkB-STAT3-miR-204-5p regulatory circuitry controls proliferation and invasion of endometrial carcinoma cells. Mol Cancer 12:155
10. Banno K, Yanokura M, Kisu I, Yamagami W, Susumu N, Aoki D (2013) MicroRNAs in endometrial cancer. Int J Clin Oncol 12:186–192
11. Erdmann K, Kaulke K, Thomae C, Huebner D, Sergon M, Froehner M, Wirth MP, Fuessel S (2014) Elevated expression of prostate cancer-associated genes is linked to down-regulation of microRNAs. BMC Cancer 14:82
12. Shalgi R, Lieber D, Oren M, Pilpel Y (2007) Global and local architecture of the mammalian microRNA-transcription factor regulatory network. PLoS Comput Biol 3(7):e131
13. Australian Institute of Health and Welfare (AIHW) (2008) Australia Cancer Incidence and Mortality (ACIM) books: incidence numbers and rates from 1982 to 2005, and mortality numbers and rates from 1968 to 2006
14. Thompson JF, Scolyer RA, Kefford RF (2005) Cutaneous melanoma. Lancet 365(9460):687–701
15. Deeds J, Cronin F, Duncan LM (2000) Patterns of melastatin mRNA expression in melanocytic tumors. Hum Pathol 31(11):1346–1356
16. Miller AJ, Du J, Rowan S, Hershey CL, Widlund HR, Fisher DE (2004) Transcriptional regulation of the melanoma prognostic marker melastatin (TRPM1) by MITF in melanocytes and melanoma. Cancer Res 64(2):509–516
17. Levy C, Khaled M, Iliopoulos D, Janas MM, Schubert S, Pinner S, Chen PH, Li S, Fletcher AL, Yokoyama S, Scott KL, Garraway LA, Song JS, Granter SR, Turley SJ, Fisher DE, Novina CD (2010) Intronic miR-211 assumes the tumor suppressive function of its host gene in melanoma. Mol Cell 40:841–849

18. Boyle GM, Woods SL, Bonazzi VF, Stark MS, Hacker E, Aoude LG, Dutton-Regester K, Cook AL, Sturm RA, Hayward NK (2011) Melanoma cell invasiveness is regulated by miR-211 suppression of the BRN2 transcription factor. Pigment Cell Melanoma Res 24:525–537

19. Davies H, Bignell GR, Cox C, Stephens P, Edkins S, Clegg S, Teague J, Woffendin H, Garnett MJ, Bottomley W, Davis N, Dicks E, Ewing R, Floyd Y, Gray K, Hall S, Hawes R, Hughes J, Kosmidou V, Menzies A, Mould C, Parker A, Stevens C, Watt S, Hooper S, Wilson R, Jayatilake H, Gusterson BA, Cooper C, Shipley J, Hargrave D, Pritchard-Jones K, Maitland N, Chenevix-Trench G, Riggins GJ, Bigner DD, Palmieri G, Cossu A, Flanagan A, Nicholson A, Ho JW, Leung SY, Yuen ST, Weber BL, Seigler HF, Darrow TL, Paterson H, Marais R, Marshall CJ, Wooster R, Stratton MR, Futreal PA (2002) Mutation of the BRAF gene in human cancer. Nature 417:949–954

20. Lunavat TR, Cheng L, Einarsdottir BO, Olofsson Bagge R, Veppil Muralidharan S, Sharples RA, Lässer C, Gho YS, Hill AF, Nilsson JA, Lötvall J (2017) BRAF(V600) inhibition alters the microRNA cargo in the vesicular secretome of malignant melanoma cells. Proc Natl Acad Sci U S A 114(29):E5930–E5939

21. De Luca T, Pelosi A, Trisciuoglio D, D'Aguanno S, Desideri M, Farini V, Di Martile M, Bellei B, Tupone MG, Condiloro A, Regazzo G, Rizzo MG, Del Bufalo D (2016) miR-211 and MIFT modulation by Bcl-2 protein in melanoma cells. Mol Carcinog 55:2304–2312

22. Wellbrock C, Arozarena I (2015) Microphthalmia-associated transcription factor in melanoma development and MAP-kinase pathway targed therapy. Pigment Cell Melanoma Res 28:390–406

23. Margue C, Philippidou D, Reinsbach SE, Schmitt M, Behrmann I, Kreis S (2013) New target genes of MITF-induced microRNA-211 contribute to melanoma cell invasion. PLoS One 8(9):e73473

24. Natrajan R, Louhelainen J, Williams S, Laye J, Knowles MA (2003) High-resolution deletion mapping of 15q13.2-q21.1 in transitional cell carcinoma of the bladder. Cancer Res 63:7657–7662

25. Poetsch M, Kleist B (2006) Loss of heterozygosity at 15q21.3 correlates with occurrence of metastases in head and neck cancer. Mod Pathol 19:1462–1469

26. Xia B, Yang S, Liu T, Lou G (2015) miR-211 suppresses epithelial ovarian cancer proliferation and cell-cycle progression by targeting Cyclin D1 and CDK6. Mol Cancer 14:57

27. Tao F, Tian X, Ruan S, Shen M, Zhang Z (2018) miR-211 sponges lncRNA MALAT1 to suppress tumor growth and progression through inhibiting PHF19 in ovarian carcinoma. FASEB J 6:fj201800495RR

28. He DX, Gu XT, Jiang L, Jin J, Ma X (2014) A methylation-based regulatory network for microRNA 320a in chemoresistant breast cancer. Mol Pharmacol 86(5):536–547

29. Yu S, Qin X, Chen T, Zhou L, Xu X, Feng J (2017) MicroRNA-106b-5p regulates cisplatin chemosensitivity by targeting polycystic kidney disease-2 in non-small-cell lung cancer. Anti-Cancer Drugs 28(8):852–860

30. Iino I, Kikuchi H, Myyazaki S, Hiramatsu Y, Ohta M, Kamiya K, Kusama Y, Baba S, Setou M, Konno H (2013) Effect of mir-122 and its target gene cationic aminoacid transporter 1 on colorectal liver metastasis. Cancer Sci 104:624–630

31. Shapiro D, Deering-Rice CE, Romero EG, Hughen RW, Light AR, Veranth JM, Reilly CA (2013) Activation of transient receptor potential ankyrin-1 (TRPA1) in lung cells by wood smoke particulate material. Chem Res Toxicol 26(5):750–758

32. Zygmunt PM, Hogestatt ED (2014) Trpa1. Handb Exp Pharmacol 222:583–630

33. Berrout J, Kyriakopoulou E, Moparthi L, Hogea AS, Berrout L, Ivan C, Lorger M, Boyle J, Peers C, Muench S, Gomez JE, Hu X, Hurst C, Hall T, Umamaheswaran S, Wesley L, Gagea M, Shires M, Manfield I, Knowles MA, Davies S, Suhling K, Gonzalez YT, Carragher N, Macleod K, Abbott NJ, Calin GA, Gamper N, Zygmunt PM, Timsah Z (2017) TRPA1-FGFR2 binding event is a regulatory oncogenic driver modulated by miRNA-142-3p. Nat Commun 8(1):947

34. Turner N, Grose R (2010) Fibroblast growth factor signalling: from development to cancer. Nat Rev Cancer 10:116–129

35. Timsah Z, Berrout J, Suraokar M, Behrens C, Song J, Lee JJ, Ivan C, Gagea M, Shires M, Hu X, Vallien C, Kingsley CV, Wistuba I, Ladbury JE (2015) Expression pattern of FGFR2, Grb2 and Plcγ1 acts as a novel prognostic marker of recurrence recurrence-free survival in lung adenocarcinoma. Am J Cancer Res 5(10):3135–3148

36. Peng X, Liu WL (2015) MiR-142-3p functions as a potential tumour suppressor directly targeting HMGB1 in non-small-cell lung carcinoma. Int J Clin Exp Pathol 8(9):10800

37. Jemal A, Bray F, Center MM, Ferlay J, Ward E, Forman D (2011) Global cancer statistics. CA Cancer J Clin 61(2):69–90

38. Zhang L, Barritt GJ (2004) Evidence that TRPM8 is an androgen-dependent Ca^{2+} channel required for the survival of prostate cancer cells. Cancer Res 64(22):8365–8373

39. Zhang J, Liang J, Huang J (2016) Downregulated microRNA-26a modulates prostate cancer cell proliferation and apoptosis by targeting COX-2. Oncol Lett 12(5):3397–3402

40. Tong MH, Mitchell DA, McGowan SD, Evanoff R, Griswold MD (2012) Two miRNA clusters, Mir-17-92 (Mirc1) and Mir-106b-25 (Mirc3), are involved in the regulation of spermatogonial differentiation in mice. Biol Reprod 86(3):72

41. Patel V, Williams D, Hajarnis S, Hunter R, Pontoglio M, Somlo S, Igarashi P (2013) miR-17∼92 miRNA cluster promotes kidney cyst growth in polycystic kidney disease. Proc Natl Acad Sci U S A 110(26):10765–10770

42. Sun H, Li QW, Lv XY, Ai JZ, Yang QT, Duan JJ, Bian GH, Xiao Y, Wang YD, Zhang Z, Liu YH, Tan RZ, Yang Y, Wei YQ, Zhou Q (2010) MicroRNA-17 post-transcriptionally regulates polycystic kidney disease-2 gene and promotes cell proliferation. Mol Biol Rep 37:2951–2958

43. Mendell JT (2008) miRiad roles for the miR-17-92 cluster in development and disease. Cell 133(2):217–222

44. Conkrite K, Sundby M, Mukai S, Thomson JM, Mu D, Hammond SM, MacPherson D (2011) miR-17∼92 cooperates with RB pathway mutations to promote retinoblastoma. Genes Dev 25(16):1734–1745

45. Cloonan N, Brown MK, Steptoe AL, Wani S, Chan WL, Forrest AR, Kolle G, Gabrielli B, Grimmond SM (2008) The miR-17-5p microRNA is a key regulator of the G1/S phase cell cycle transition. Genome Biol 9(8):R127

46. O'Donnell KA, Wentzel EA, Zeller KI, Dang CV, Mendell JT (2005) c-Myc-regulated microRNAs modulate E2F1 expression. Nature 435(7043):839–843

47. Roldo C, Missiaglia E, Hagan JP, Falconi M, Capelli P, Bersani S, Calin GA, Volinia S, Liu CG, Scarpa A, Croce CM (2006) MicroRNA expression abnormalities in pancreatic endocrine and acinar tumors are associated with distinctive pathologic features and clinical behavior. J Clin Oncol 24(29):4677–4684

48. Zanette DL, Rivadavia F, Molfetta GA, Barbuzano FG, Proto-Siqueira R, Silva WA Jr, Falcão RP, Zago MA (2007) miRNA expression profiles in chronic lymphocytic and acute lymphocytic leukemia. Braz J Med Biol Res 40(11):1435–1440

49. Xin J, Zheng L-M, Sun D-K, Li X-F, Xu P, Tian L-Q (2018) miR-204 functions as a tumor suppressor gene, at least partly by suppressing CYP27A1 in glioblastoma. Oncol Lett 16:1439–1448

50. Ge Y, Yan X, Jin Y, Yang X, Yu X, Zhou L, Han S, Yuan Q, Yang M (2015) fMiRNA-192 and miRNA-204 directly suppress lncRNA HOTTIP and interrupt GLS1-mediated glutaminolysis in hepatocellular carcinoma. Terracciano L ed. PLoS Genet 11(12):e1005726

51. Kuwano Y, Nishida K, Kajita K, Satake Y, Akaike Y, Fujita K, Kano S, Masuda K, Rokutan K (2015) Transformer 2beta and miR-204 regulate apoptosis through competitive binding to 3′ UTR of BCL2 mRNA. Cell Death Differ 22(5):815–825

52. Imam JS, Plyler JR, Bansal H, Prajapati S, Bansal S, Rebeles J, Chen HI, Chang YF, Panneerdoss S, Zoghi B, Buddavarapu KC, Broaddus R, Hornsby P, Tomlinson G, Dome J, Vadlamudi RK, Pertsemlidis A, Chen Y, Rao MK (2012) Genomic loss of tumor suppressor miRNA-204 promotes cancer cell migration and invasion by activating AKT/mTOR/Rac1 signaling and actin reorganization. PLoS One 7(12):e52397

53. Wang L, Tian H, Yuan J, Wu H, Wu J, Zhu X (2015) CONSORT. Sam68 is directly regulated by MiR-204 and promotes the self-renewal potential of breast cancer cells by activating the Wnt/Beta-catenin signaling pathway. Medicine 94(49):e2228

54. Hall DP, Cost NG, Hegde S, Kellner E, Mikhaylova O, Stratton Y, Ehmer B, Abplanalp WA, Pandey R, Biesiada J, Harteneck C, Plas DR, Meller J, Czyzyk-Krzeska MF (2014) TRPM3 and miR-204 establish a regulatory circuit that controls oncogenic autophagy in clear cell renal cell carcinoma. Cancer Cell 26(5):738–753

55. Cecconi F, Jäättelä M (2014) Targeting ions-induced autophagy in cancer. Cancer Cell 26(5):599–600

56. Cost NG, Czyzyk-Krzeska MF (2015) Regulation of autophagy by two products of one gene: TRPM3 and miR-204. Mol Cell Oncol 2(4):e1002712

57. Harteneck C (2005) Function and pharmacology of TRPM cation channels. Naunyn Schmiedeberg's Arch Pharmacol 371:307–314

58. Chow TF, Youssef YM, Lianidou E, Romaschin AD, Honey RJ, Stewart R, Pace KT, Youssef GM (2010) Differential expression profiling of microRNAs and their potential involvement in renal cell carcinoma pathogenesis. Clin Biochem 43:150–158

59. Osanto S, Qin Y, Buermans HP, Berkers J, Lerut E, Goeman JJ, van Poppel H (2012) Genome-wide microRNA expression analysis of clear cell renal cell carcinoma by next generation deep sequencing. PLoS One 7:e38298

60. Ma L, Deng X, Wu M, Zhang G, Huang J (2014) Down-regulation of miRNA-204 by LMP-1 enhances CDC42 activity and facilitates invasion of EBV-associated nasopharyngeal carcinoma cells. FEBS Lett 588(9):1562–1570

61. Siegel R, Naishadham D, Jemal A (2013) Cancer statistics, 2013. CA Cancer J Clin 12:11–30

62. Zhu X, Shen H, Yin X, Long L, Chen X, Feng F, Liu Y, Zhao P, Xu Y, Li M, Xu W, Li Y (2017) IL-6R/STAT3/miR-204 feedback loop contributes to cisplatin resistance of epithelial ovarian cancer cells. Oncotarget 8(24):39154–39166

63. Shapovalov G, Ritaine A, Skryma R, Prevarskaya N (2016) Role of TRP ion channels in cancer and tumorigenesis. Semin Immunopathol 38(3):357–369

64. Xu J, Yang Y, Xie R, Liu J, Nie X, An J, Wen G, Liu X, Jin H, Tuo B (2018) The NCX1/TRPC6 complex mediates TGFβ-driven migration and invasion of human hepatocellular carcinoma cells. Cancer Res 78(10):2564–2576

65. Wu J, Zheng C, Wang X, Yun S, Zhao Y, Liu L, Lu Y, Ye Y, Zhu X, Zhang C, Shi S, Liu Z (2015) MicroRNA-30 family members regulate calcium/calcineurin signaling in podocytes. J Clin Invest 125(11):4091–4106

66. Liu Y, Zhou Y, Gong X, Zhang C (2017) MicroRNA-30a-5p inhibits the proliferation and invasion of gastric cells by targeting insulin-like growth factor 1 receptor. Exp Ther Med 14:173–180

67. Selli C, Erac Y, Tosun M (2015) Simultaneous measurement of cytosolic and mitochondrial calcium levels: observations in TRPC1-silenced hepatocellular carcinoma cells. J Pharmacol Toxicol Methods 72:29–34

68. Zhang C, Chen X, Chen X, Wang X, Ji A, Jiang L, Sang F, Li F (2016) miR-135a acts as a tumor suppressor in gastric cancer in part by targeting KIFC1. Onco Targets Ther 9:3555–3563

69. Wan X, Pu H, Huang W, Yang S, Zhang Y, Kong Z, Yang Z, Zhao P, Li A, Li T, Li Y (2016) Androgen-induced miR-135a acts as a tumor suppressor through downregulating RBAK and MMP11, and mediates resistance to androgen deprivation therapy. Oncotarget 7:51284–51300

70. Yamada Y, Hidaka H, Seki N, Yoshino H, Yamasaki T, Itesako T, Nakagawa M, Enokida H (2013) Tumor-suppressive microRNA-135a inhibits cancer cell proliferation by targeting the c-MYC oncogene in renal cell carcinoma. Cancer Sci 104:304–312

71. Wu S, Lin Y, Xu D, Chen J, Shu M, Zhou Y, Zhu W, Su X, Zhou Y, Qiu P, Yan G (2012) MiR-135a functions as a selective killer of malignant glioma. Oncogene 31:3866–3874

72. Nagel R, le Sage C, Diosdad B, van der Waal M, Oude Vrielink JA, Bolijn A, Meijer GA, Agami R (2008) Regulation of the adenomatous polyposis coli gene by the miR-135 family in colorectal cancer. Cancer Res 68:5795–5802

73. Zhou W, Li X, Liu F, Xiao Z, He M, Shen S, Liu S (2012) MiR-135a promotes growth and invasion of colorectal cancer via metastasis suppressor 1 in vitro. Acta Biochim Biophys Sin Shanghai 44:838–846

74. He B, Liu F, Ruan J, Li A, Chen J, Li R, Shen J, Zheng D, Luo R (2012) Silencing TRPC1 expression inhibits invasion of CNE2 nasopharyngeal tumor cells. Oncol Rep 27:1548–1554
75. Tajeddine N, Gailly P (2012) TRPC1 protein channel is major regulator of epidermal growth factor receptor signaling. J Biol Chem 287:16146–16157
76. Liu X, Zou J, Su J, Lu Y, Zhang J, Li L, Yin F (2016) Downregulation of transient receptor potential cation channel, subfamily C, member 1 contributes to drug resistance and high histological grade in ovarian cancer. Int J Oncol 48(1):243–252
77. Tang W, Jiang Y, Mu X, Xu L, Cheng W, Wang X (2014) MiR-135a functions as a tumor suppressor in epithelial ovarian cancer and regulates HOXA10 expression. Cell Signal 26:1420–1426

Chapter 20
Calcium Signaling and the Regulation of Chemosensitivity in Cancer Cells: Role of the Transient Receptor Potential Channels

Giorgio Santoni, Maria Beatrice Morelli, Oliviero Marinelli, Massimo Nabissi, Matteo Santoni, and Consuelo Amantini

Abstract Cancer cells acquire the ability to modify the calcium signaling network by altering the expression and functions of cation channels, pumps or transporters. Calcium signaling pathways are involved in proliferation, angiogenesis, invasion, immune evasion, disruption of cell death pathways, ECM remodelling, epithelial-mesenchymal transition (EMT) and drug resistance. Among cation channels, a pivotal role is played by the Transient Receptor Potential non-selective cation-permeable receptors localized in plasma membrane, endoplasmic reticulum, mitochondria and lysosomes. Several findings indicate that the dysregulation in calcium signaling induced by TRP channels is responsible for cancer growth, metastasis and chemoresistance. Drug resistance represents a major limitation in the application of current therapeutic regimens and several efforts are spent to overcome it. Here we describe the ability of Transient Receptor Potential Channels to modify, by altering the intracellular calcium influx, the cancer cell sensitivity to chemotherapeutic drugs.

G. Santoni · M. Nabissi
School of Pharmacy, Immunopathology and Molecular Medicine Laboratory, University of Camerino, Camerino, Italy

M. B. Morelli · O. Marinelli
School of Pharmacy, Immunopathology and Molecular Medicine Laboratory, University of Camerino, Camerino, Italy

School of Biosciences and Veterinary Medicine, University of Camerino, Camerino, Italy

M. Santoni
Clinic and Oncology Unit, Macerata Hospital, Macerata, Italy

C. Amantini (✉)
School of Biosciences and Veterinary Medicine, University of Camerino, Camerino, Italy
e-mail: consuelo.amantini@unicam.it

20.1 Calcium Signaling in Cancer

Intracellular calcium ions (Ca^{2+}), the most abundant and important second messenger, play a pivotal role in controlling cell proliferation, differentiation, migration and death [1–4]. Thus, it is essential to keep under tight control the Ca^{2+} signals in the form of oscillations, wave or spikes [2]. The disruption of normal Ca^{2+} signaling contributes to the development of the malignant phenotypes; in fact, cancer cells are able to modify the Ca^{2+} signaling network in order to increase proliferation, immortalization, angiogenesis, invasion, immune evasion, disruption of cell death pathways, ECM remodelling, epithelial-mesenchymal transition (EMT) and drug resistance [5, 6]. Several Ca^{2+} channels, transporters and Ca^{2+}-ATPases, as voltage-gated Ca^{2+} channel (VGCC), Transient Receptor Potential (TRP), Ca^{2+} release activated Ca^{2+} channel (CRAC), inositol 1,4,5-triphosphate receptor (IP3R) and mitochondrial Ca^{2+} uniporter (MCU) are altered in cancer. Moreover, their impairment has been found to be involved in the tumorigenesis [2] (Fig. 20.1). The aim of this chapter is to address the role of TRP channels in modulating sensitivity to chemotherapeutic drugs in different cancer types.
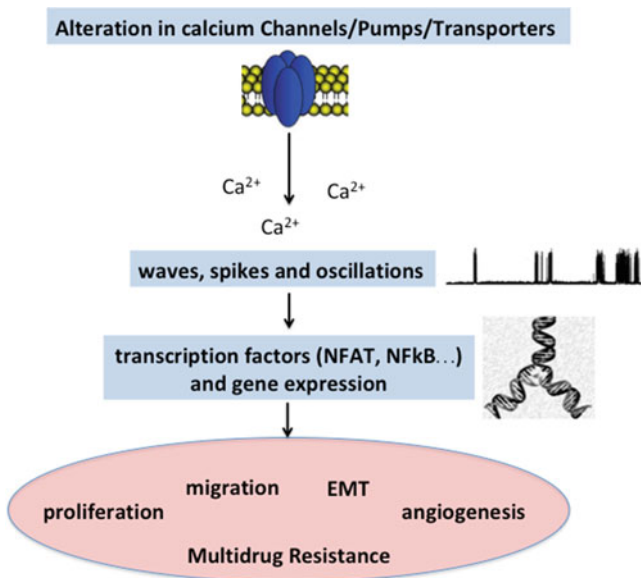
Fig. 20.1 Alterations in expression and functions of Ca^{2+} channels/pumps/transporters lead to dysregulation in calcium signaling promoting malignant phenotype and chemoresistance

20.1.1 Cation Disruption in Cancer: The Transient Receptor Potential Family

The TRP channels are non-selective cation permeable receptors localized in plasma membrane, endoplasmic reticulum, mitochondria and lysosomes [7]. They play a key role in regulating cellular Ca^{2+} concentration and membrane voltage. To date, about 30 TRPs have been identified and, on the basis of their structural homology, they are classified in: TRPC1-7, TRPV1-6, TRPM1-8, TRPP2,3,5, TRPML1-3 and TRPA1 [8]. Several findings indicate that alterations in expression and functions of TRP channels are responsible for cancer growth, metastasis and chemoresistance [9]. In particular, dysregulation of TRPC, TRPM or TRPV members has been mainly correlated with malignant growth and progression [10], so that cancer can now be considered like a "channellopathy" [11]. The central role of TRPs in cancer is to impair the Ca^{2+} homeostasis by stimulating Ca^{2+} entry or altering membrane potential. For this reason, in the recent years an increased interest in discovering agents targeting TRP channels in cancer, has been emerged and several pharmacological modulators are now used to characterize the implications of TRP channels in whole-cell membrane currents, resting membrane potential regulation or intracellular Ca^{2+} signaling [12, 13].

20.2 Drug Resistance in Cancer

Initially, cancers are susceptible to chemotherapy but over time they develop resistance by activating different strategies to limit drug efficacy eluding cell death. Thus, cancer cells become tolerant to pharmacological treatments [14]. Drug resistance can be achieved through several mechanisms involving Ca^{2+} signaling as drug inactivation, drug efflux, drug target alterations, acquisition of EMT, evasion from cell death pathways, increased DNA damage tolerance and dysregulation of critical genes (Fig. 20.2). Many chemotherapeutic agents require metabolic
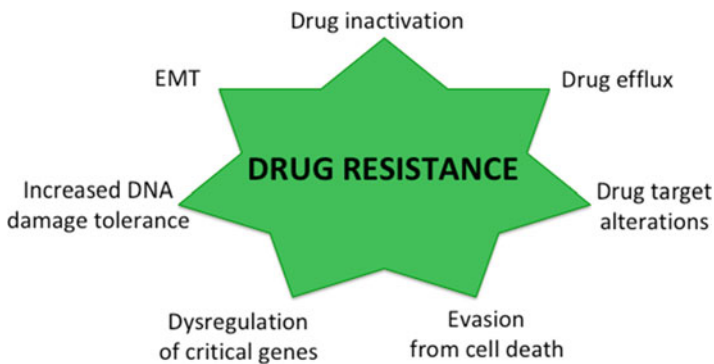
Fig. 20.2 Mechanisms promoting the acquisition of chemoresistance in cancer

conversion to be active; mutations or down-regulation of the enzymes responsible for the drug activation, as cytochrome P 450 system, glutathione-S-transferase (GST) and uridine diphospho-glucuronosyltransferase (UGT) super-families, are often present in cancer cells [15]. In addition, changes in the expression or functions of drug targets such as topoisomerase II, epidermal growth factor receptor family, Ras, Src, Raf, MEK, AKT and PTEN, lead to resistance. One of the most studied mechanisms of cancer drug resistance involves the increasing drug efflux with subsequent reduction in cellular drug concentration. ATP-binding cassette (ABC) members, multidrug resistance protein 1 (MDR1), known as P glycoprotein (P-gp), multidrug resistance-associated protein 1 (MRP1), and breast cancer resistance protein (BCRP), represent the main transporters involved in the efflux mechanism causing the non-accumulation of anti-tumoral agents in cancer cells [16].

20.2.1 TRPC5 and TRPC6 in Multidrug Resistance

TRPC5 forms homo and hetero-oligomeric complex with other TRPs and it stimulates Ca^{2+} flux in response to different stimuli as stress, growth factors, lysophospholipids, nitric oxide or thioredoxin [17]. Abnormal expression of this channel has been found to be associated with several diseases. In addition, it is well known that TRPC5 alterations, interfering with the normal Ca^{2+} homeostasis, are involved in the development of cancer progression and acquisition of chemoresistance. During therapy, the majority of cancer cell types starts to over-express P-gp, a well-known membrane efflux pump [18]. Recently [19], TRPC5 channel has been found to be overexpressed together with P-gp in adriamycin-resistant breast cancer cell line (MCF-7/ADM). As demonstrated by patch clamp, the TRPC5-dependent calcium current was higher in MCF-7/ADM cells compared to wild type indicating that the over-expressed TRPC5 is functional.

By using the TRPC5-specific blocking antibody T5E3, authors showed that the TRPC5 inhibition is associated with both marked down-regulation of P-gp expression and increase of adriamycin accumulation, demonstrating that TRPC5 is crucial for P-gp expression and chemoresistance in MCF-7/ADM cells. Moreover, the high Ca^{2+} current generated by TRPC5 activation was able to activate the nuclear factor of activated T cells cytoplasmic 3 (NFAT$_C$3) that, stimulating the transcription, promotes P-gp over-expression. In vivo studies using athymic nude mouse model of ADM-human breast tumor, showed an evident decrease of cancer growth induced by the suppression of TRPC5 channel. Thus, the TRPC5-NFATc3-P-gp signaling cascade plays an important role in promoting drug-resistance in breast cancer cells [19].

Micro RNAs (miRNAs) are single-stranded 19–25 nucleotide short RNAs that modulate gene expression at post-transcriptional stage by targeting mRNAs. It is now well accepted that they can regulate several processes closely associated with tumor progression as chemoresistance, apoptosis, cell cycle or stemness transition. In the recent years, the attention was mainly focused on miR-230a

since its expression has been found to be strongly down-regulated in MCF-7/ADM cells compared to MCF-7 cells, suggesting that it is involved in the development of chemoresistance [20]. Moreover, low miR-320a expression is associated with clinical chemoresistance and poor patient outcome. As showed by Targescan and miRDB software analysis, this miRNA specifically targets TRPC5 and NFATC3 mRNAs. Therefore, its down-regulation has been found to be responsible for TRPC5 over-expression and related drug resistance in breast cancer [20].

For cancer progression, cell-cell communication in the tumor microenvironment is fundamental [21]. To this aim, cancer cells produce soluble factors and secrete membrane-encapsulated vesicles containing regulatory signals. These membrane-limited vesicles are known as Extracellular Vesicles (EVs) and they include exosomes, microvesicles and apoptotic bodies [21]. It has been recently demonstrated [22] that TRPC5, involved in growth factor-regulated local vesicular trafficking, by mediating Ca^{2+} flux, plays a role in the EVs formation and secretion in MCF-7/ADM. Since EVs membrane phospholipid bilayer is composed by the plasma membrane of the donor cells, TRPC5 channel is packaged in the developing vesicles and, in this way, transported into recipient cells where it promotes P-gp expression by increasing Ca^{2+} flux. Thus, the TRPC5-containing EVs represent a mechanism used by cancer cells to disseminate the acquisition of chemoresistance. Furthermore, immunohistochemistry analysis performed on breast cancer tissues, collected before and after the chemotherapy, showed a marked increase in the TRPC5 expression mainly in samples from not responsive patients indicating the close association between TRPC5 and chemoresistance [22]. Since TRPC5-containing EV levels correlate with acquired chemoresistance and EVs can be easily monitored in the blood of breast cancer patients [23], TRPC5-containing EVs represent a new potential diagnostic biomarker for real time measurement of chemoresistance in breast cancer.

In addition, it has been demonstrated that endothelial cells of the tumor microenvironment acquire resistance thanks to TRPC5-containing EVs released by ADM/MCF-7 [24]. As already described, the transmitted TRPC5, by activating NFATC3 in a Ca^{2+} dependent manner, stimulates the expression of P-gp.

Autophagy, an evolutionarily conserved lysosomal pathway, has been reported to show paradoxical roles in cancer: it can inhibit or promote tumorigenesis by inducing cell death or survival, respectively [25]. Since intracellular Ca^{2+} plays an important role in both basal and induced autophagy, TRP channels are now recognized as autophagy regulators [26].

Zhang and co-workers demonstrated that TRPC5 regulates the chemotherapy-induced autophagy in breast cancer cells. In fact, TRPC5, by inducing Ca^{2+} flux, initiates the autophagy via CaMKKβ/AMPKα/mTOR pathway in response to chemotherapy. Authors also showed that the TRPC5-induced autophagy functions as pro-survival mechanism promoting chemoresistance, as demonstrated by the reduction in autophagy and enhancement in ADM sensitivity in TRPC5 silenced MCF-7 cells [27].

Over-expression of TRPC5 was also found to be involved in the development of 5-Fluorouracil (5-Fu) resistance in colon rectal cancer [28]. TRPC5 is up-regulated

together with the efflux pump ABC subfamily B, both at mRNA and protein levels, in resistant human HCT-8 and LoVo colon rectal cancer cells. TRPC5, by inducing intracellular Ca^{2+} flux, promotes β-catenin translocation in the nucleus, increases glycolysis and provides ATP production to avoid Ca^{2+} influx overload. Moreover it stimulates ACB and cyclin D1 expression contributing to the development of 5-Fu resistance. In fact, its suppression markedly inhibits the canonical Wnt/β-catenin signal pathway and reduces efflux pump activity reverting the chemoresistance. By contrast, the forced expression of TRPC5 results in an activated Wnt/β-catenin signal pathway and up-regulation of ABC. High expression of TRPC5 has also been found to be associated with glucose transporter 1 (GLUT1) up-regulation in colon rectal cancer cells and increased glycolysis often occurs in chemoresistance cells [29]. Taken together, these findings demonstrate in human colon rectal cancer cells an important role of TRPC5 in drug resistance via stimulating nuclear β-catenin, ABC and GLUT1 over-expression [28–30].

Cancer cells become more resistant to drugs also thanks to the EMT, a process involved in the acquisition of invasive and migratory phenotype [31]. In hepatocellular carcinoma (HCC), it has been recently demonstrated that chemoresistance to doxorubicin occurs through up-regulation of Vimentin and down-regulation of E-cadherin and Claudin1, typical EMT markers. In fact, prolonged treatment with doxorubicin, by enhancing Ca^{2+} influx, induces EMT promoting chemoresistance. The channel involved in this process is TRPC6 that, via calcium signaling, stimulates STAT3 activation inducing the EMT [32]. The role of TRPC6 in chemoresistance was also explored in xenograft models of HCC using TRPC6-silenced and wild type Huh-7 HCC cells. Results showed that tumors, derived from the injection of TRPC6-silenced cells, grow slower than normal cells and they are more sensitive to doxorubicin [32].

20.2.2 TRPM Channels in Chemoresistance

TRPM7 is a highly Ca^{2+} and Mg^{2+} permeable member of the TRPM family activated by ATP and characterized in the C-terminal region by the presence of a kinase domain. Recent findings showed that Vacquinol-1 (Vac) promotes in glioma cells the methuosis cell death based on cell blebbing followed by rupture of the plasma membrane. This new type of cell death, caused by inefficient vacuole-lysosome fusion, is caspase-dependent and it is reverted by exogenous ATP [33]. The ATP-mediated inhibitory effect on Vac-induced cell death is due to TRPM7 activation that, by a marked Ca^{2+} influx, stimulates the phosphoinositide 3-kinase (PI3K) restoring the vacuole-lysosome fusion. Thus, the Ca^{2+} current induced by TRPM7, often found to be overexpressed in cancer cells, is responsible for the development of Vac-resistance in glioma cell lines (Fig. 20.3). It has also been demonstrated that the expression of TRPM7 is required to prevent apoptotic cell death in pancreatic adenocarcinoma [34]. The targeted silencing of TRPM7
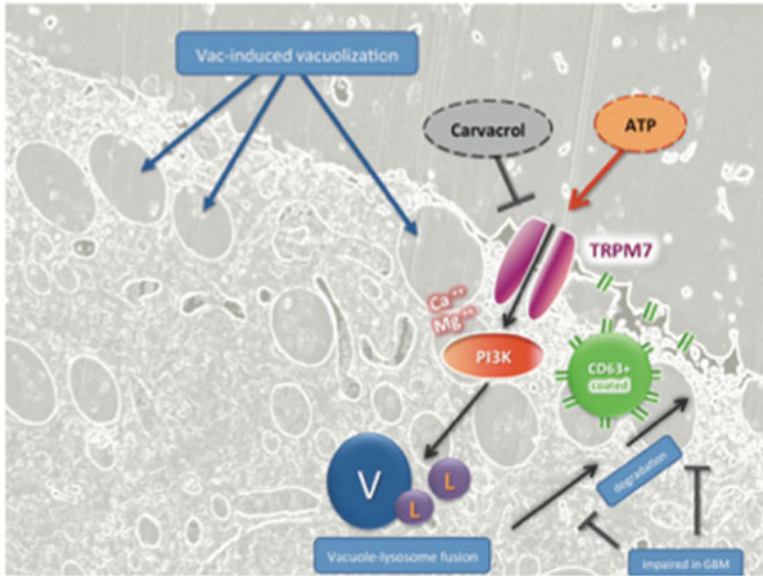
Fig. 20.3 TRPM7 activation induced by exogenous ATP stimulates Ca^{2+} influx that promotes PI3K activation increasing vesicle fusion (V) with lysosomes (L). [From reference 33]

increases the expression of senescence-associated genes inducing the replicative senescence in pancreatic cancer cells. The down-regulation of TRPM7 expression also enhances the cytotoxicity mediated by gemcitabine treatment in pancreatic cancer suggesting that its expression is strongly associated with resistance to apoptosis induction [34].

Moreover, in Lewis lung cancer cells (LLC-2), TRPM8, showing a plasma membrane and a membrane rafts localisation, is involved in the induction of proliferation, invasion and migration [35]. In addition, TRPM8, by activating Uncoupling Protein 2, contributes to the acquisition of resistance against both activated spleen CD8 T lymphocytes and doxorubicin contributing to the development of the malignant phenotype. The ability of TRPM8 to promote the acquisition of chemoresistance is also supported by data obtained in in vitro studies on prostate cancer cells [36]. By enhancing the HIF-1α protein levels, the cold-sensitive Ca^{2+} channel protein TRPM8 promotes hypoxic growth capacities and drug resistance. In particular, the TRPM8 activation induces the suppression of HIF-1α ubiquitination and enhances HIF-1 transactivation both in hypoxia- and normoxia-exposed prostate cancer cells. The potential involvement of TRPM8 channel in chemosensitivity has been also shown in osteosarcoma cells [37]. Knockdown of TRPM8 by siRNA in osteosarcoma cells leads to alterations in intracellular Ca^{2+} concentration. This Ca^{2+} imbalance induces the inhibition of several pathways as Akt-GSK-3β, ERK1/2 and FAK, promoting strong decrease in proliferation, invasion and migration.

Moreover, although TRPM8 silencing alone does not increase apoptotic cell death, it enhances the epirubicin-induced apoptosis indicating that the over expression of TRPM8 in osteosarcoma cells is associated with impaired Ca^{2+} signaling and induction of drug resistance [37].

20.2.3 Chemosensitivity and TRPV-Mediated Calcium Signaling

Calcium signaling is also required for the development of the neoplastic features in Retinoblastoma, a common intraocular pediatric cancer arising from immature cells of the retina [38]. TRPs and cannabinoid receptors are expressed in retinoblastoma cells. Their expression levels are considered useful as prognostic factors, since they correlate with tumor progression and are associated with the acquisition of etoposide-resistance. Interestingly, capsaicin, the specific agonist of TRPV1 receptor, is able to evoke Ca^{2+} influx in etoposide-resistant but not in etoposide-sensitive WERI-Rb1 retinoblastoma cells, suggesting the key role played by TRPV1-mediated calcium signaling in the acquisition of drug chemoresistance [38].

TRPV1 is also involved in the enhancement of chemosentitivity to cisplatin induced by Alpha-lipoic acid (ALA) in breast cancer cells. ALA administration, through TRPV1 activation, increases the apoptosis induced by cisplatin stimulating mitochondrial membrane depolarization, reactive oxygen species (ROS) production, lipid peroxidation, PARP1, caspase 3 and 9 expression. The ALA-dependent stimulation of TRPV1, via calcium signaling, enhances the oxidative stress making breast cancer cells more sensitive to the action of the chemotherapeutic drug [39].

Among TRPV family members, the role of TRPV2, with Ca^{2+} permeation properties, in the regulation of glioblastoma cell growth and progression, has been addressed. The aggressive behaviour of glioblastoma is mainly due to high resistance to the standard chemotherapy as Temozolomide (TMZ), Carmustine (BCNU) or Doxorubicin characterized by limited efficacy. The over-expression of TRPV2 by gene transfection in glioma cells increases the sensitivity to FAS- and BCNU-induced cytotoxicity [40, 41]. Moreover, the activation of the TRPV2 channel, induced by treatment with cannabidiol (CBD), strongly reduced the BCNU resistance in glioma cells. In fact, CBD, by generating a TRPV2-dependent Ca^{2+} influx, inhibits the Ras/Raf/MEK/ERK pathway and promotes the drug retention in glioma cells, reverting the chemoresistant phenotype and improving the apoptosis induced by TMZ, BCNU and doxorubicin [40, 41]. Mutations of the TRPV2 pore completely cancel the CBD-induced Ca^{2+} signaling demonstrating the essential role of the TRPV2 permeant cation region in chemoresistance. In addition, glioma stem-like cells represent a major problem in the treatment of glioblastoma because they maintain stem cell properties and show marked resistance to radiation and conven-

tional drugs. Reduce their drug resistance is fundamental to increase the patient survival. At this regard, CBD, through TRPV2 activation, stimulates autophagy in glioma stem-like cells promoting cell differentiation and increasing the sensitivity to the apoptosis induced by BCNU and TMZ [42].

Furthermore, TRPV2 is expressed in multiple myeloma cells, a malignancy characterised by clonal proliferation of plasma cells and subsequent accumulation in the bone marrow [43]. Recent data demonstrated that CBD treatment induces in myeloma cells up-regulation of TRPV2 expression enhancing the sensitivity to Bortezomib, a specific proteosome inhibitor. The specific TRPV2 activation, induced by CBD, strongly reduces proliferation and improves cytotoxic effects of bortezomib by enhancing cell growth inhibition, cell cycle arrest at the G1 phase, mitochondrial and ROS-dependent necrosis mainly in TRPV2-transfected RPMI8226 and U266 multiple myeloma cells. The cell death induced by the co-administration of CBD and Bortezomib is also characterized by down-regulation of the ERK, AKT and NF-κB pathways. These findings provide a rationale for the use of TRPV2 activators (e.g., CBD) to increase the activity of proteasome inhibitors in myeloma multiple patients [43].

The TRPV6 channel, which is highly selective for Ca^{2+}, is upregulated, by a gene amplification mechanism, in breast cancer cell lines and in breast carcinoma samples compared with normal mammary gland tissue. By microarray analysis, it has been shown that the TRPV6 over-expression, associated with reduced patient overall survival, is a feature of estrogen receptor-negative breast tumors as well as HER2-positive tumors. Down-regulation of TRPV6 expression reduces the basal Ca^{2+} influx leading to decrease in cellular proliferation and DNA synthesis [44]. It has been showed, using TRPV6-transfected *Xenopus* oocytes, that tamoxifen, the most common therapy used in breast cancer treatment, inhibits the Ca^{2+} uptake regulated by this channel. In addition, tamoxifen treatment markedly reduces the expression of TRPC6 at mRNA levels in breast cancer cell lines [45]. Silencing of TRPV6 enhances the pro-apoptotic activity of tamoxifen suggesting that the increase of Ca^{2+} influx, mediated by TRPV6 over-expression in breast cancer cells, is responsible for the reduced sensitivity to tamoxifen treatment. These findings support the hypothesis that a combination therapy using tamoxifen and TRPV6 inhibitor could represent a promising strategy to improve the treatment of breast cancer [44, 46].

20.3   Conclusion

It is becoming evident that dysregulation in Ca^{2+} homeostasis plays a pivotal role in tumor progression, functioning as a driving signal in the acquisition of the aggressive phenotype. In fact, cancer cells, by changing the expression of ion channels/transporters/pumps acquire the ability to modulate Ca^{2+} intracellular concentration creating pro-survival conditions. Several evidences support the idea that Ca^{2+} signaling pathways are also involved in regulating sensitiv-

Table 20.1 Chemosensitivity and TRP roles in cancer cells

TRPs activation	Pathway mediated by Ca^{2+} dysregulation	Drug	Cancer cell line	References
TRPCS	NFATc3 activation promoting P-gp over-expression	↑Adryamycin	MCF-7	[19]
	Prosurvival autophagy via CaMKKβ/AMPKα/mTOR	↑Adryamycin	MCF-7	[27]
	ACB and cyclin D1 over-expression via β-catenin	↑5-Fluorouracil	HCT8 and LoVo	[28–30]
TRPC6	STAT3 activation inducing EMT	↑Doxorubicin	Huh-7	[32]
TRPM7	PI3K activation restoring vacuole/lysosome fusion	↑Vaquinol-1	U-87 and #12537-GB	[33]
	Prevention of non apoptotic cell death	↑Gemcitabine	BxPC3 and PANIC-1	[34]
TRPM8	Uncoupling Protein 2 activation	↑Doxorubicin	LLC-2	[35]
	Akt-GSK-3β, ERK1/2 and FAK activation	↑Epirubicin	MG-63, U2OS, SaOS2 and HOS	[37]
TRPV1	Oxidative stress	↓Cisplatin	MCF-7	[39]
TRPV2		↓Temozolomide		
	Ras/Raf/MEK/ERK activation	↓Carmustine	U-37, MZC, GSC,	[40–42]
		↓Doxorubicine		
	Inhibition of NF-kB	↓Bortezomib	RPMI3226 and U266	[43]
TRPV6	Promotes cell proliferation	↑Tamoxifen	T47D	[46]

ity to chemotherapeutic drugs. Drug resistance represents a major limitation in the application of current therapeutic regimens and several efforts are spent to overcome it. The targeting of the Ca^{2+} channels, by altering their expression and functions, has been demonstrated be effective in improving of cytotoxicity induced by the most common chemotherapeutic agents. Among Ca^{2+} channels, TRPs influence the expression and function of many drug resistance-related proteins and pathways contributing to the development of pharmacological tolerance in cancer (Table 20.1). Therefore, targeting the TRP expression and activity, can be now considered a promising and fascinating strategy to inhibit cancer growth and progression and restore/improve the sensitivity of cancer cells to chemotherapeutic drugs [10].

References

1. Giorgi C, Danese A, Missiroli S, Patergnani S, Pinton P (2018) Calcium dynamics as a machine for decoding signals. Trends Cell Biol 28(4):258–273
2. Cui C, Merritt R, Fu L, Pan Z (2017) Targeting calcium signaling in cancer therapy. Acta Pharm Sin B 7(1):3–17
3. Zhang X, Yuan D, Sun Q, Xu L, Lee E, Lewis AJ, Zuckerbraun BS, Rosengart MR (2017) Calcium/calmodulin-dependent protein kinase regulates the PINK1/Parkin and DJ-1 pathways of mitophagy during sepsis. FASEB J 31(10):4382–4395
4. Bootman MD, Chehab T, Bultynck G, Parys JB, Rietdorf K (2018) The regulation of autophagy by calcium signals: do we have a consensus? Cell Calcium 70:32–46
5. Busselberg D, Florea AM (2017) Targeting intracellular calcium signaling ($[Ca^{2+}]_i$) to overcome multiddrug resistance of cancer cells: a mini-overview. Cancers 9:48
6. Xu MM, Seas A, Kijan M, Ji KSY, Bell HN (2018) A temporal examination of calcium signaling in cancer-from tumorigenesis, to immune evasion, and metastasis. Cell Biosci 8:25
7. La Rovere RM, Roest G, Bultynck G, Parys JB (2016) Intracellular Ca^{2+} signaling and Ca^{2+} microdomains in the control of cell survival, apoptosis and autophagy. Cell Calcium 60(2):74–87
8. Nilius B, Owsianik G (2011) The transient receptor potential family of ion channels. Genome Biol 12(3):218
9. Shapovalov G, Ritaine A, Skryma R, Prevarskaya N (2016) Role of TRP ion channels in cancer and tumorigenesis. Semin Immunopathol 38(3):357–369
10. Gautier M, Dhennin-Duthille I, Ay AS, Rybarczyk P, Korichneva I, Ouadid-Ahidouch H (2014) New insights into pharmacological tools to TR(i)P cancer up. Br J Pharmacol 171:2582–2592
11. Litan A, Langhans SA (2015) Cancer as a channelopathy: ion channels and pumps in tumor development and progression. Front Cell Neurosci 9:86
12. Santoni G, Farfariello V, Amantini C (2011) TRPV channels in tumor growth and progression. Adv Exp Med Biol 704:947–967
13. Santoni G, Farfariello V (2011) TRP channels and cancer: new targets for diagnosis and chemotherapy. Endocr Metab Immune Disord Drug Targets 11:54–67
14. Housman G, Byler S, Heerboth S, Lapinska K, Longacre M, Snyder N, Sarkar S (2014) Drug resistance in cancer: an overview. Cancers (Basel) 6:1769–1792
15. Michael M, Doherty MM (2005) Tumoral drug metabolism: overview and its implications for cancer therapy. J Clin Oncol 23:205–229
16. Stavrovskaya AA (2000) Cellular mechanisms of multidrug resistance of tumor cells. Biochemistry (Mosc) 65:95–106
17. He DX, Ma X (2016) Transient receptor potential channel C5 in cancer chemoresistance. Acta Pharmacol Sin 37:19–24
18. Binkhathlan Z, Lavasanifar A (2013) P-glycoprotein inhibition as a therapeutic approach for overcoming multidrug resistance in cancer: current status and future perspectives. Curr Cancer Drug Targets 13:326–346
19. Ma X, Cai Y, He D, Zou C, Zhang P, Lo CY, Xu Z, Chan FL, Yu S, Chen Y, Zhu R, Lei J, Jin J, Yao X (2012) Transient receptor potential channel TRPC5 is essential for P-glycoprotein induction in drug-resistant cancer cells. Proc Natl Acad Sci U S A 109:16282–16287
20. He DX, Gu XT, Jiang L, Jin J, Ma X (2014) A methylation-based regulatory network for microRNA 320a in chemoresistant breast cancer. Mol Pharmacol 86:536–547
21. Xu R, Rai A, Chen M, Suwakulsiri W, Greening DW, Simpson RJ (2018) Extracellular vesicles in cancer – implications for future improvements in cancer care. Nat Rev Clin Oncol 15(10):617–638. https://doi.org/10.1038/s41571-018-0036-9
22. Ma X, Chen Z, Hua D, He D, Wang L, Zhang P, Wang J, Cai Y, Gao C, Zhang X, Zhang F, Wang T, Hong T, Jin L, Qi X, Chen S, Gu X, Yang D, Pan Q, Zhu Y, Chen Y, Chen D, Jiang L, Han X, Zhang Y, Jin J, Yao X (2014) Essential role for TrpC5-containing extracellular vesicles in breast cancer with chemotherapeutic resistance. Proc Natl Acad Sci U S A 111:6389–6394

23. Wang T, Ning K, Lu TX, Sun X, Jin L, Qi X, Jin J, Hua D (2017) Increasing circulating exosomes-carrying TRPC5 predicts chemoresistance in metastatic breast cancer patients. Cancer Sci 108:448–454

24. Dong Y, Pan Q, Jiang L, Chen Z, Zhang F, Liu Y, Xing H, Shi M, Li J, Li X, Zhu Y, Chen Y, Bruce IC, Jin J, Ma X (2014) Tumor endothelial expression of P-glycoprotein upon microvesicular transfer of TrpC5 derived from adriamycin-resistant breast cancer cells. Biochem Biophys Res Commun 446:85–90

25. Singh SS, Vats S, Chia AY, Tan TZ, Deng S, Ong MS, Arfuso F, Yap CT, Goh BC, Sethi G, Huang RY, Shen HM, Manjithaya R, Kumar AP (2018) Dual role of autophagy in hallmarks of cancer. Oncogene 37:1142–1158

26. Sukumaran P, Schaar A, Sun Y, Singh BB (2016) Functional role of TRP channels in modulating ER stress and autophagy. Cell Calcium 60:123–132

27. Zhang P, Liu X, Li H, Chen Z, Yao X, Jin J, Ma X (2017) TRPC5-induced autophagy promotes drug resistance in breast carcinoma via CaMKKβ/AMPKα/mTOR pathway. Sci Rep 7(1):3158

28. Wang T, Chen Z, Zhu Y, Pan Q, Liu Y, Qi X, Jin L, Jin J, Ma X, Hua D (2015) Inhibition of transient receptor potential channel 5 reverses 5-fluorouracil resistance in human colorectal Cancer cells. J Biol Chem 290:448–456

29. Wang T, Ning K, Lu TX, Hua D (2017) Elevated expression of TrpC5 and GLUT1 is associated with chemoresistance in colorectal cancer. Oncol Rep 37:1059–1065

30. Wang T, Ning K, Sun X, Zhang C, Jin L-f, Hua D (2018) Glycolysis is essential for chemoresistance induced by transient receptor potential channel C5 in colorectal cancer. BMC Cancer 18:207

31. Bhatia S, Monkman J, Toh AKL, Nagaraj SH, Thompson EW (2017) Targeting epithelial-mesenchymal plasticity in cancer: clinical and preclinical advances in therapy and monitoring. Biochem J 474:3269–3306

32. Wen L, Liang C, Chen E, Chen W, Liang F, Zhi X, Wei T, Xue F, Li G, Yang Q, Gong W, Feng X, Bai X, Liang T (2016) Regulation of multi-drug resistance in hepatocellular carcinoma cells is TRPC6/calcium dependent. Sci Rep 6:23269

33. Sander P, Mostafa H, Soboh A, Schneider JM, Pala A, Baron AK, Moepps B, Wirtz CR, Georgieff M, Schneider M (2017) Vacquinol-1 inducible cell death in glioblastoma multiforme is counter regulated by TRPM7 activity induced by exogenous ATP. Oncotarget 8:35124–35137

34. Yee NS, Zhou W, Lee M, Yee RK (2012) Targeted silencing of TRPM7 ion channel induces replicative senescence and produces enhanced cytotoxicity with gemcitabine in pancreatic adenocarcinoma. Cancer Lett 318:99–105

35. Du GJ, Li JH, Liu WJ, Liu YH, Zhao B, Li HR, Hou XD, Li H, Qi XX, Duan YJ (2014) The combination of TRPM8 and TRPA1 expression causes an invasive phenotype in lung cancer. Tumour Biol 35:1251–1261

36. Yu S, Xu Z, Zou C, Wu D, Wang Y, Yao X, Ng CF, Chan FL (2014) Ion channel TRPM8 promotes hypoxic growth of prostate cancer cells via an O2 -independent and RACK1-mediated mechanism of HIF-1α stabilization. J Pathol 234:514–525

37. Wang Y, Yang Z, Meng Z, Cao H, Zhu G, Liu T, Wang X (2013) Knockdown of TRPM8 suppresses cancer malignancy and enhances epirubicin-induced apoptosis in human osteosarcoma cells. Int J Biol Sci 10:90–102

38. Mergler S, Cheng Y, Skosyrski S, Garreis F, Pietrzak P, Kociok N, Dwarakanath A, Reinach PS, Kakkassery V (2012) Altered calcium regulation by thermosensitive transient receptor potential channels in etoposide-resistant WERI-Rb1 retinoblastoma cells. Exp Eye Res 94:157–173

39. Nur G, Nazıroğlu M, Deveci HA (2017) Synergic prooxidant, apoptotic and TRPV1 channel activator effects of alpha-lipoic acid and cisplatin in MCF-7 breast cancer cells. J Recept Signal Transduct Res 37:569–577

40. Nabissi M, Morelli MB, Amantini C, Farfariello V, Ricci-Vitiani L, Caprodossi S, Arcella A, Santoni M, Giangaspero F, De Maria R, Santoni G (2010) TRPV2 channel negatively controls glioma cell proliferation and resistance to Fas-induced apoptosis in ERK-dependent manner. Carcinogenesis 31(5):794–803

41. Nabissi M, Morelli MB, Santoni M, Santoni G (2013) Triggering of the TRPV2 channel by cannabidiol sensitizes glioblastoma cells to cytotoxic chemotherapeutic agents. Carcinogenesis 34:48–57
42. Nabissi M, Morelli MB, Amantini C, Liberati S, Santoni M, Ricci-Vitiani L, Pallini R, Santoni G (2015) Cannabidiol stimulates Aml-1a-dependent glial differentiation and inhibits glioma stem-like cells proliferation by inducing autophagy in a TRPV2-dependent manner. Int J Cancer 137:1855–1869
43. Morelli MB, Nabissi M, Amantini C, Farfariello V, Ricci-Vitiani L, di Martino S, Pallini R, Larocca LM, Caprodossi S, Santoni M, De Maria R, Santoni G (2012) The transient receptor potential vanilloid-2 cation channel impairs glioblastoma stem-like cell proliferation and promotes differentiation. Int J Cancer 131:E1067–E1077
44. Peters AA, Simpson PT, Bassett JJ, Lee JM, Da Silva L, Reid LE, Song S, Parat MO, Lakhani SR, Kenny PA, Roberts-Thomson SJ, Monteith GR (2012) Calcium channel TRPV6 as a potential therapeutic target in estrogen receptor-negative breast cancer. Mol Cancer Ther 11:2158–2168
45. Bolanz KA, Kovacs GG, Landowski CP, Hediger MA (2009) Tamoxifen inhibits TRPV6 activity via estrogen receptor-independent pathways in TRPV6-expressing MCF-7 breast cancer cells. Mol Cancer Res 7:2000–2010
46. Bolanz KA, Hediger MA, Landowski CP (2008) The role of TRPV6 in breast carcinogenesis. Mol Cancer Ther 7:271–279

Dual-Acting Cholinesterase−Human Cannabinoid Receptor 2 Ligands Show Pronounced Neuroprotection in Vitro and Overadditive and Disease-Modifying Neuroprotective Effects in Vivo

Matthias Scheiner,[†] Dominik Dolles,[†] Sandra Gunesch,[†] Matthias Hoffmann,[†] Massimo Nabissi,[‡] Oliviero Marinelli,[‡] Marina Naldi,[§] Manuela Bartolini,[§] Sabrina Petralla,[∥] Eleonora Poeta,[∥] Barbara Monti,[∥] Christina Falkeis,[⊥] Michael Vieth,[⊥] Harald Hübner,[#] Peter Gmeiner,[#] Rangan Maitra,[∇] Tangui Maurice,[○] and Michael Decker*,[†]

[†]Pharmaceutical and Medicinal Chemistry, Institute of Pharmacy and Food Chemistry, Julius Maximilian University of Würzburg, Am Hubland, 97074 Würzburg, Germany

[‡]School of Pharmacy, University of Camerino, Via Madonna delle Carceri 9, 62032 Camerino, Italy

[§]Department of Pharmacy and Biotechnology, University of Bologna, Via Belmeloro 6, 40126 Bologna, Italy

[∥]Department of Pharmacy and Biotechnology, University of Bologna, Via Selmi 3, 40126 Bologna, Italy

[⊥]Pathology, Clinical Center Bayreuth, Preuschwitzer Straße 101, 95445 Bayreuth, Germany

[#]Medicinal Chemistry, Department of Chemistry and Pharmacy, Friedrich-Alexander University Erlangen-Nürnberg, Schuhstraße 19, 91052 Erlangen, Germany

[∇]Center for Drug Discovery, Research Triangle Institute, Research Triangle Park, North Carolina 27709, United States

[○]MMDN, University of Montpellier, INSERM, EPHE, UMR-S1198, 34095 Montpellier, France

S *Supporting Information*

ABSTRACT: We have designed and synthesized a series of 14 hybrid molecules out of the cholinesterase (ChE) inhibitor tacrine and a benzimidazole-based human cannabinoid receptor subtype 2 (hCB$_2$R) agonist and investigated them in vitro and in vivo. The compounds are potent ChE inhibitors, and for the most promising hybrids, the mechanism of human acetylcholinesterase (hAChE) inhibition as well as their ability to interfere with AChE-induced aggregation of β-amyloid (Aβ), and Aβ self-aggregation was assessed. All hybrids were evaluated for affinity and selectivity for hCB$_1$R and hCB$_2$R. To ensure that the hybrids retained their agonist character, the expression of cAMP-regulated genes was quantified, and potency and efficacy were determined. Additionally, the effects of the hybrids on microglia activation and neuroprotection on HT-22 cells were investigated. The most promising in vitro hybrids showed pronounced neuroprotection in an Alzheimer's mouse model at low dosage (0.1 mg/kg, i.p.), lacking hepatotoxicity even at high dose (3 mg/kg, i.p.).
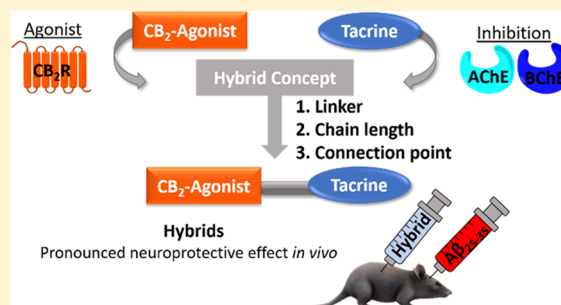
INTRODUCTION

About 50 million people worldwide had to live with dementia in 2018.[1] In about 30 years, an increase of cases up to 152 million is expected. The most common form of dementia is Alzheimer's disease (AD). People aged 65 and over are considered at risk and are most likely to be affected.[1] Unfortunately, pharmacotherapy is very limited. Currently, only four drugs are approved for the treatment of AD. Three of them (donepezil, rivastigmine, and galantamine) are cholinesterase (ChE) inhibitors, while the fourth (memantine) is an *N*-methyl-D-aspartate (NMDA) receptor noncompetitive antagonist. All approved drugs are only symptomatically effective in the moderate stages of the disease and reduce but do not stop the progression and do not affect the cause of the disease.[2] The exact molecular mechanisms, as well as the causes for an AD outbreak still remain unknown. However, a variety of biochemical changes during the pathological process take place. AD hallmarks are the formation of amyloid-beta (Aβ) plaques in the extracellular brain parenchyma,[3] the abnormal hyperphosphorylation of the microtubule-associated tau protein, and the formation of neurofibrillary tangles (NFTs) within neurons.[4] Both the Aβ aggregates and the NTFs lead to a progressive loss of cholinergic neurons in the brain, memory deficits, and cognitive dysfunction.[5−7] Aβ itself has been shown to exert cytotoxic effects on cultured neurons,[8] induce oxidative stress, and modify ionic homeostasis.[9,10] Furthermore, in the post-mortem analysis of AD brain, an increased expression of inflammatory mediators

has been observed.[11,12] The increase seems to be partly triggered by microglia activation. Microglia cells are activated by various stimuli, including misfolded $A\beta$, its precursor protein (APP), and misfolded tau.[13,14] In the early stage of AD, stimulation leads to a neuroprotective M2 microglia phenotype and can, therefore, promote $A\beta$ clearance via microglia's scavenger receptors (SRs), which hinder AD progression.[15,16] However, it has been shown that there is a switch from the neuroprotective M2 to a more classically activated M1 phenotype at the later stage of AD. The M1 phenotype generally mediates defense from pathogens and tumor cells, and it is characterized by the production of proinflammatory cytokines, such as TNF-α, IL1β, or reactive oxygen species (ROS), which are associated with the loss of neurons. Therefore, this switch can lead to an increased $A\beta$ production, a decreased $A\beta$ clearance, and, ultimately, to neuronal damage and progression of AD.[16]

The human endocannabinoid system has been intensively investigated, and two cannabinoid receptor (hCBR) subtypes have been discovered. The hCBR subtype 1 (hCB$_1$R) is the most abundant metabotropic receptor in the brain, and it is involved in a variety of physiological processes.[17−19] The psychoactive effect of tetrahydrocannabinol (THC), the main psychoactive constituent of cannabis, is due to hCB$_1$R agonism.[20] The hCB$_2$R is mainly expressed in peripheral immune cells and has been originally described as the peripheral CBR,[21] but later, it was found also in the central nervous system (CNS) where it is expressed on microglia and astrocytes.[22,23] While the expression of the hCB$_1$R remains unchanged, the hCB$_2$R is abundantly and selectively expressed in neuritic plaque-associated astrocytes and microglia.[24,25] In several in vitro and in vivo models of acute and chronic neurodegenerative disorders, the activation of the hCB$_2$R was shown to exert beneficial effects.[26] hCB$_2$R agonists can suppress microglia activation and the production of neurotoxic factors such as ROS, nitric oxide (NO), and proinflammatory mediators (TNF-α and cytokines).[27−29] Administration of an hCB$_2$R agonist to rats, previously and intracerebrally treated with $A\beta_{40}$, the forty-amino acid long isoform of $A\beta$, promoted $A\beta$ clearance, decreased secretion of proinflammatory mediators, and, ultimately, led to an increased synaptic plasticity, cognition, and memory.[30] Furthermore, in vivo studies with transgenic Tg2576 mice overexpressing hAPP$_{Swe}$ showed a lower $A\beta$ production, reduced reactive microglia cells, and improved cognition performance upon treatment with an hCB$_2$R agonist.[31] Additionally, an hCB$_2$R knockout experiment with APP transgenic mice supports the potential of cannabinoid therapies targeting hCB$_2$R to reduce $A\beta$, as the knockout results in an increased $A\beta$ pathology and an alternation in tau processing.[32]

Acetylcholinesterase (AChE)-inhibiting drugs for symptomatic cognition improvement in AD patients are related to the oldest theory of AD pathophysiology, the cholinergic hypothesis.[2] The theory describes the loss of cholinergic neurons and reduction of the neurotransmitter acetylcholine (ACh).[33] Inhibition of the metabolizing enzyme AChE raises ACh levels, leading to an improved cognitive performance. However, since AChE level decreases with the progression of AD,[34−36] AChE inhibition seems to be only effective at early stages of disease. On the other hand, the levels of the less specific butyrylcholinesterase (BChE) remain unaltered or increase with AD progression.[35−38] BChE can hydrolyze ACh and, thereby, compensate the reduction of AChE activity. An experiment with AChE knockout mice supported this hypothesis. Indeed, no cholinergic hyperactivation in the absence of AChE was observed since BChE can take over the hydrolysis of ACh.[39] Results from further studies were in accordance with the role of the BChE in AD brains and showed a positive correlation between selective BChE inhibition and improved cognitive performance and memory.[40−44]

There is even more diversity in the pathological processes and reasons for AD beyond the ones herein described. Because of this multifactorial and sporadic nature of AD, the classical approach "one target−one disease" reaches its limits or even makes it ineffective to develop an effective drug.[45] Conversely, a more promising approach seems to be the development of a multitarget drug capable of simultaneously acting at different targets.[46] To obtain such multitarget drugs, there are two common strategies: the hybrid and the "merged ligand".[47] In the merged ligand strategy, two pharmacophores are fused into a single small molecule. The hybrid strategy foresees the combination of two molecules with two different pharmacologically active moieties by using a linker to form a larger molecule.[45,47] Through the merged ligand strategy, we have recently achieved low-molecular-weight hCB$_2$R ligands endowed with hBChE inhibitory activity, which proved to exert neuroprotection even in vivo.[48] The design and improvement of such multi-target directed ligands (MTDLs) are challenging since minor chemical alternations can improve affinity at one target and diminish activity at the second one. Here, we describe hybrids out of similar benzimidazole units with the established tacrine unit to yield higher affinity at both targets.

Design. Since AChE is a well-established target for the treatment of AD at the early and moderate stages, while BChE is a promising target for the moderate-to-advanced forms of AD, an inhibitor that is able to tackle both ChEs should be effective for a longer time span along AD progression. Such dual inhibitors have been described in the literature, among which tacrine **1**.[49] Tacrine was the first approved drug for the treatment of AD but was withdrawn from the market because of its dose-dependent hepatotoxicity.[50,51] Due to its low molecular weight and excellent ChE inhibitory activity, tacrine **1** is an ideal starting point for the development of multitarget drugs (for recent review articles, see refs 52 and 53).

In developing tacrine hybrids, it is important to keep the potential hepatotoxic effect in mind. Linking or coupling with hepatoprotective compounds can reduce or even eliminate such a side effect.[54−56]

In addition to the inhibition of the ChEs, the activation of the hCB$_2$R, as previously mentioned, represents a promising strategy in the treatment of AD. An example of a selective hCB$_2$R agonist is the benzimidazole-based derivative **2** described by AstraZeneca (see Figure 1)[57] and further investigated by us.[48,58−60]

■ RESULTS AND DISCUSSION

Following the hybrid concept, coupling of structures **1** and **2** into a single molecule through a linker should yield a molecule with inhibitory properties toward ChEs and affinity for the hCB$_2$R. Defining a suitable connecting position for the linker chain is a crucial task because an unsuitable connection between the two pharmacophore units can easily lead to a complete loss of activity or can reverse the behavior of the drug at the target, especially with regard to the hCB$_2$R (e.g., turn an agonist into an antagonist).[60] Linkage at the primary amine moiety at the position 9 of **1** is chemically easy to access, and substituted derivatives still show pronounced inhibitory properties toward ChEs.[61]
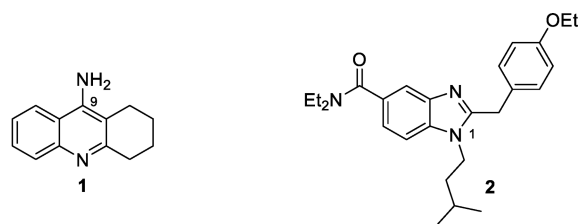
pIC$_{50}$ (hAChE): 6.8 K_i (hCB$_2$R): 36.7 nM[58]
pIC$_{50}$ (hBChE): 7.9   displ. (hCB$_1$R) at 10 μM: 24%[58]

**Figure 1.** Tacrine **1** and selective hCB$_2$R agonist **2**.[58]

Taking advantage of the previous work on the structure–activity relationships (SARs) of the hCB$_2$R ligand **2**, two possible attachment positions for a linker were identified, that is, the amide moiety and the N^1 of the imidazole.[58] Connection of structures **1** and **2** through these two connection points lead to two sets of hybrid compounds: **3a–e** and **4a–e** (see Figure 2).

Modification of the tertiary amide group of the parent molecule **2** into a secondary amide group in derivatives **4a–e** might affect affinity and activity at the target. Hence, to investigate a possible effect of the number of substituents at this position, we designed a tertiary amide hybrid (hybrid **5**). After optimizing the spacer length, we designed hybrids with a functionalized linker. Therefore, we introduced a 2-poly-(ethylene glycol) (PEG) linker for higher rigidity and polarity (hybrids **6** and **7**). In addition, cystamine was introduced as a linker at the amide position to archive neuroprotective and putative hepatoprotective properties (**8**, see Figure 3).[62]

Synthesis. Based on these design strategies, tacrine-amine derivatives **12a–g** and **14** were synthesized and coupled to the benzimidazole core. Anthranilic acid **9** and cyclohexanone **10** were heated up with an excess of phosphoroxylchloride to yield the tetrahydroacridine derivative **11**.[63] By substitution with the corresponding diamine in excess, the tacrine-amine derivatives **12a–g** were obtained (Scheme 1).

For the synthesis of derivative **14**, the primary amine of tacrine-amine derivative **12c** was acetylated to form amide **13** in quantitative yield. In the next step, the amide was reduced to the secondary amine **14** in the presence of lithium aluminum hydride (Scheme 1).

Synthesis of derivatives **3a–e** and **6** started with 4-fluoro-3-nitrobenzoic acid **15**. To form the diethylamide **16**, oxalyl chloride and a catalytic amount of DMF were used, and then diethylamine was added. In the next step, the fluorine atom was substituted with the respective amine derivatives **12a–f** to form compounds **17a–f**, the reaction gave good to quantitative yield.
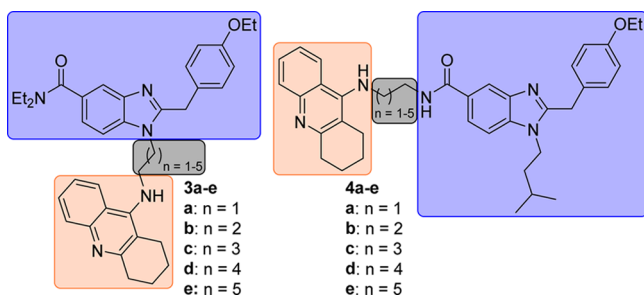
Figure 2. Designed hybrids **3a–e** and **4a–e** used to investigate the optimal spacer length and the attachment point.

The nitro moiety was then reduced with tin(II) chloride dihydrate to obtain the anilinic amines **18a–f**, which were directly used for the next step. 2-(4-Ethoxyphenyl)acetic acid was activated with HBTU and added to amines **18a–f**. In the last step, the amides **19a–f** were cyclized in acetic acid to yield compounds **3a–e** and **6** (Scheme 2).

4-Fluoro-3-nitrobenzoic acid **15** served as the starting material for derivatives **4a–e**, **5**, **7**, and **8**. In the first step, the ethyl ester was formed as a protection group, and the fluorine atom was substituted with 3-methylbutan-1-amine to yield substituted ester **20** in a good yield. In the next step, the nitro moiety was reduced with hydrogen over Pd/C to yield amine **21**, which was then directly reacted with HBTU-activated 2-(4-ethoxyphenyl)acetic acid to form amide **22**. Benzimidazole **23** was formed by stirring **22** in acetic acid under reflux. The ester was hydrolyzed under basic conditions. In the last step, acid **24** was activated with HBTU and reacted with the respective amines **12a–g** and **14** to yield hybrids **4a–e**, **5**, **7**, and **8** (Scheme 3).

■ PHARMACOLOGICAL PROFILE

Inhibition of Cholinesterases. All synthesized compounds were assayed for their ability to inhibit human butyrylcholinesterase (hBChE) and human acetylcholinesterase (hAChE) using the colorimetric Ellman's assay (Table 1).[64] Tacrine **1** was selected as the reference compound and showed an pIC$_{50}$(hBChE) = 7.9 and pIC$_{50}$(hAChE) = 6.8. Previous studies showed no significant ChE inhibitory activity of the hCB$_2$R agonist **2** at 10 μM.[58] According to our expectations, all synthesized hybrids acted as ChE inhibitors. Compared to **1**, hybrids **3a**, **3b**, **3e**, and **4b** showed an increased inhibitory potency toward hBChE, while **3a** and **4b**, in addition, also showed a higher inhibitory activity toward hAChE. The higher inhibitory potency might be due to interaction with the PAS of the AChE (see Inhibition and Mode of Action toward hAChE), which was consequently followed up (cf. Figure 5). For a better overview of the selectivity, we correlated pIC$_{50}$ values of hAChE and hBChE in Figure 4.

Inhibition Constants and Mode of Action toward hAChE. To get further insights into the inhibition of hAChE, the mechanism of inhibition was investigated for one hybrid of each set with a pronounced inhibition of AChE. Specifically, hybrid **3e** of set 1 and **4b** of set 2 were selected. Additionally, cystamine hybrid **8** was investigated.

For the three selected compounds, the mechanism of inhibition was investigated by monitoring the catalytic rate at several substrate and inhibitor concentrations (see Experimental Section for details). Lineweaver–Burk reciprocal plots showed increasing slope (decreasing V_{max}) and increasing x intercept (increasing K_m values) at increasing inhibitor concentration (see Figure 5). This trend indicates a mixed-type inhibition, and thus, the inhibitor could bind simultaneously with the CAS and the PAS of hAChE. The inhibitor inhibition constant K_i and the inhibition constant for the enzyme–substrate–inhibitor complex (K_i') were estimated for each hybrid and are reported in Figure 5.

Inhibition of Aβ Aggregation. Compounds able to bind the AChE's PAS may interfere with the AChE-induced Aβ oligomerization and fibrillization.[65,66] Hence, given the ability of **3e**, **4b**, and **8** to contact AChE's PAS, the inhibitory activity on AChE-induced Aβ$_{40}$ aggregation was investigated by a thioflavin T (ThT)-based fluorometric assay[65] and compared with that of the anti-AD drug **1** (see Figure 6). Results showed that
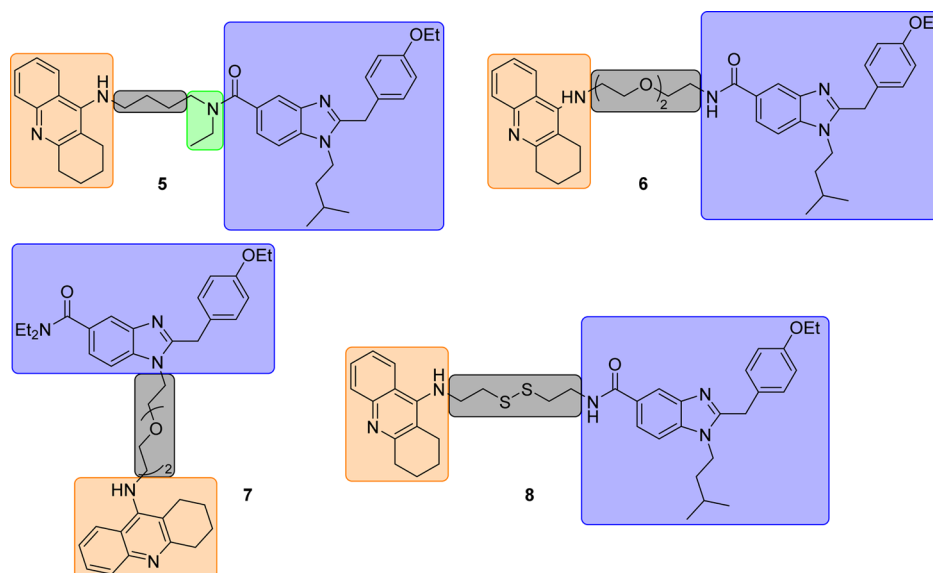
Figure 3. Designed hybrids **5**−**8**.

Scheme 1. Synthesis of Tacrine-Amine Intermediates 12a−g and 14[a]
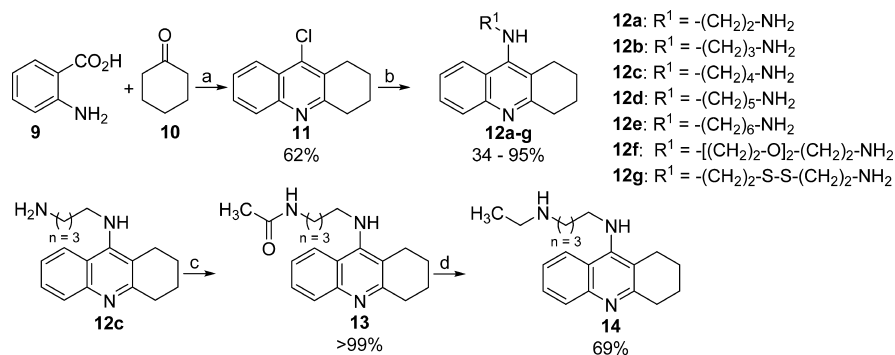
[a]Reagents and conditions: (a) POCl$_3$, reflux; (b) respective diamine, hexanol, reflux; (c) Ac$_2$O, r.t.; (d) LiAlH$_4$, THF, reflux.

## Scheme 2. Synthesis of Hybrids 3a−e and 6[a]
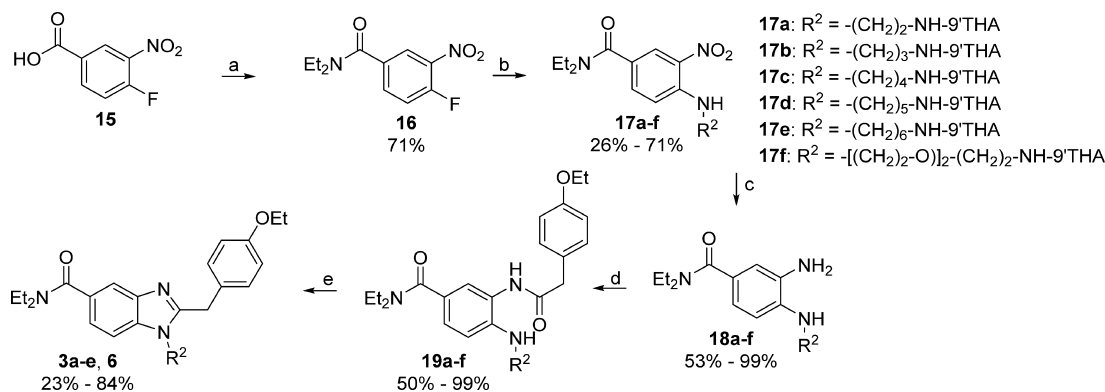
[a]Reagents and conditions: (a) HNEt$_2$, cat. DMF, (COCl)$_2$, CH$_2$Cl$_2$ at 0 °C → r.t.; (b) respective amines **12a−f**, THF, NEt$_3$, r.t.; (c) SnCl$_2$·2H$_2$O, EtOH, reflux; (d) 2-(4-ethoxyphenyl)acetic acid, HBTU, NEt$_3$, DMF, r.t.; (e) AcOH, reflux.

compounds **3e** and **4b** were able to significantly reduce the proaggregating action of hAChE, while **1** was inactive, in agreement with a previous study.[65] Interestingly, percent inhibition values archived for **3e** and **4b** are close to activity values previously obtained for the well-known multifunctional compound bis(7)tacrine (68.0% inhibition in the same assay conditions).[67] In the same experimental conditions, the

cystamine derivate **8** was not able to significantly inhibit the AChE-induced Aβ_{40} aggregation.

Although **1** is not able to inhibit amyloid self-aggregation at a significant extent, several studies have shown that tacrine homo- and heterodimers may be endowed with such a beneficial property.[52] Hence, the three selected hybrids were also assayed for their ability to inhibit Aβ_{42} self-aggregation by a similar ThT

Scheme 3. Synthesis of Hybrids 4a−e, 5, 7, and 8[a]
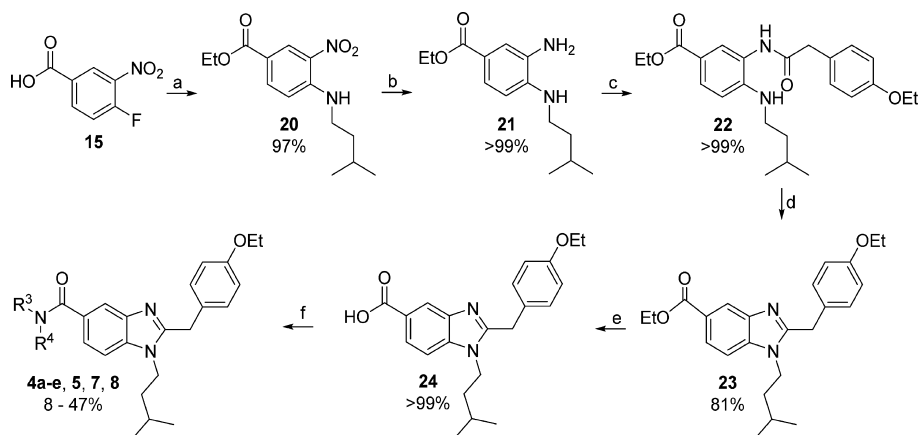
[a]Reagents and conditions: (a) (I) cat. H_2SO_4 (97%), EtOH, reflux; (II) NEt_3 3-methylbutan-1-amine, r.t.; (b) cat. Pd/C (10%), MeOH, H_2 atm, 8 bar, r.t.; (c) 2-(4-ethoxyphenyl)acetic acid, HBTU, NEt_3, DMF, r.t.; (d) AcOH, reflux; (e) LiOH, H_2O, reflux; (f) respective amines **12a−g**, **14**, HBTU, NEt_3, DMF, r.t.

fluorescence assay.[68] Quite interestingly, compounds **3e** and **8** strongly inhibited $A\beta_{42}$ aggregation when assayed at a 1:1 ratio with $A\beta_{42}$, while, in the same conditions, inhibition by **4b** was quite weak (see Figure 6) since each compound is representative of a different subset of hybrids, SARs cannot be derived. However, it is clear that the spatial arrangement of pharmacophore fragments and the nature of the spacer chain strongly affect the inhibitory ability toward the spontaneous aggregation of the 42-amino acid isoform of $A\beta$.
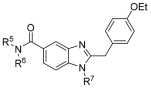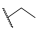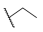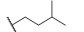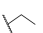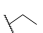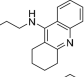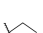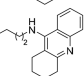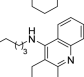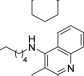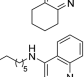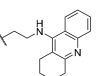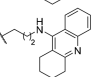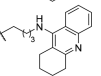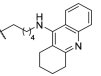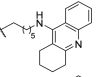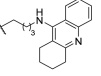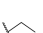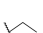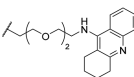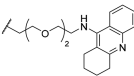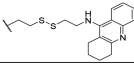
The three hybrids showed different inhibition profiles toward the two aggregation phenomena. While hybrid **8** was able to significantly interfere with $A\beta$ self-aggregation but not with the chaperonic action of hAChE toward $A\beta$, hybrid **4b** was able to significantly interfere with the chaperonic action of hAChE toward $A\beta$ but only weakly with $A\beta$ self-aggregation, and, finally, hybrid **3e** able to significantly inhibit both aggregation phenomena. Because of the strong inhibitory potency toward $A\beta$ self-aggregation exerted by **3e**, it cannot be excluded that this activity can also synergistically contribute to the good inhibitory potency recorded in the AChE-induced amyloid aggregation assay. This might also explain the high inhibition value recorded in this assay, notwithstanding a K_i' value in the submicromolar range.

Radioligand Binding Assays at hCB_1R and hCB_2R. All synthesized compounds were tested for affinity to hCB_1R and hCB_2R using radioligand binding assays. Briefly, hCBRs were isolated from cell lines stably expressing receptors (CHO cells for hCB_1R or HEK cells in the case of hCB_2R). [3H]CP 55,940 was used as radioligand. As a positive control, the hCB_2R selective ligand **2** was used. In our tests, we measured a $K_i(hCB_2R) = 37$ nM and selectivity over hCB_1R [24% replacement (hCB_1R) of radioligand at 10 μM)]. All compounds showed affinity to hCB_2R within single- to two-digit micromolar range. In the case of compounds **3a−e**, the affinity toward hCB_2R increased with the length of the spacer, from $K_i = 38.5$ μM (**3a**) to $K_i = 4.5$ μM (**3e**). Part of this effect might be due to an increasing lipophilicity, which is a favorable feature for high-affinity hCB_2R ligands.[71] Compounds **4a−e** all show a single-digit micromolar affinity toward hCB_2R. Experimental data did not support the correlation between affinity and chain length. The tertiary amide derivative **5**, which is the equivalent of derivative **4c**, showed the same affinity

toward hCB_2R but a higher affinity toward hCB_1R, resulting in low selectivity. Hence, the number of substituents at the amide group influences selectivity. Hybrids **6** and **7** with a 2-PEG-linker, which confers a higher hydrophilicity and rigidity, showed a weaker affinity toward hCB_2R compared to the compounds with the longest alkylene linkers (**3e** and **4e**). The disulfide bond in hybrid **8** has no significant effect on affinity toward hCB_2R as the equivalent derivative **4e** showed almost the same affinity (Table 1). Overall, the linkage of the two molecules has been associated with a loss of affinity at the hCB_2R compared to the parent molecule **2**, but the ligands still retain moderate affinity and good selectivity at hCB_2R. Since parent molecule **2** shares a high structural similarity with the known μ-opioid receptor (MOR) ligand etonitazene,[48] we investigated potential affinity and found a significant affinity of hybrids **3a**, **4a**, and **4e** (see Supplementary Table 1). In our previous work, we were able to show that an MOR "design out" approach is possible, if this is required with regard to the side effect profile.[48]

Efficacy at hCB_2R. The hCB_2R is coupled through $G_{i/0}$ protein, so adenylate cyclase is inhibited in the case of activation. This results in a lower level of intracellular cAMP in the case of agonist binding or to an increased cAMP level in the case of an inverse agonist binding.[72] The cAMP increase by forskolin (FSK) is further enhanced by an antagonist/reverse agonist binding, while the binding of an agonist reverts the effect.[73] This makes the intracellular detection of cAMP levels by immuno-assays a common method for the characterization of the efficacy of hCB_2R ligands. Going down the signaling pathway mediated by a conformational change of the receptor, the resulting difference in the cellular cAMP level changes the expression of cAMP-regulated genes (the reporter). The transcription of these genes is regulated by the transcription factor cAMP response element-binding protein (CREB). Binding of CREB to the cAMP responding element (CRE) is upstreaming gene expression.[74] A high cAMP level, induced by an antagonist binding, leads to a high expression of cAMP-regulated genes, while an agonist leads to the opposite effect. By quantifying the expression of these genes, it is possible to investigate the behavior of the ligand at the receptor. An example of a cAMP-regulated gene is the macrophage migration inhibitory factor (MIF) with a CRE in the proximal promoter region.[75] A further example is the signal transducer and activator of transcription

Table 1. Results of the in Vitro Evaluation of the Inhibitory Effect of AChE/BChE and Radioligand Binding Studies at hCB$_1$R/hCB$_2$R^a

Cpd.	R^5	R^6	R^7	pIC$_{50}$ ± SD or Inhibition [%] hBChE^a	hAChE^b	SI^c	K_i ± SD or [^{3}H]CP 55,940 displ. @10 μM hCB$_2$R^d	hCB$_1$R^e
Tacrine **1**				7.9 ± 0.1	6.8 ± 0.1	1.0	29%	24%
Rimonabant				n.d.	n.d.	n.d.	4%	143 nM ± 15 25.0 nM[69]
SR-144,528				n.d.	n.d.	n.d.	19.7 ± 4.1 nM 5.7 nM[70]	687 nM ± 107 264 nM[70]
2				n.a.	n.a.	n.d.	36.7 ± 4.0 nM 4.5 nM[57]	24% >5 μM[57]
3a				8.9 ± 0.1	8.6 ± 0.1	2.3	38.5 ± 16.0 μM	36%
3b				8.5 ± 0.1	6.3 ± 0.1	193	30.7 ± 3.5 μM	15%
3c				7.5 ± 0.1	6.4 ± 0.1	12.0	26.9 ± 3.5 μM	32%
3d				8.2 ± 0.1	6.2 ± 0.1	109	7.3 ± 0.9 μM	21%
3e				8.7 ± 0.1	7.1 ± 0.1	45.3	4.5 ± 0.9 μM	17%
4a				7.1 ± 0.1	7.4 ± 0.1	0.4	2.5 ± 0.8 μM	5%
4b				8.5 ± 0.1	8.2 ± 0.1	1.8	5.0 ± 0.8 μM	20%
4c				8.0 ± 0.1	6.8 ± 0.1	15.7	2.4 ± 0.3 μM	9%
4d				8.1 ± 0.1	6.6 ± 0.1	3.1	4.0 ± 0.7 μM	15%
4e				7.7 ± 0.1	7.1 ± 0.1	4.6	9.6 ± 1.3 μM	54%
5				7.2 ± 0.1	6.6 ± 0.1	4.3	3.0 ± 0.5 μM	36%
6				7.0 ± 0.1	6.4 ± 0.1	4.3	28.7 ± 8.8 μM	11%
7				6.4 ± 0.1	5.9 ± 0.1	3.7	17.4 ± 2.7 μM	32%
8				7.1 ± 0.1	7.9 ± 0.1	0.2	6.8 ± 1.3 μM	45%

^{a}n.a. activity lower than 10% at the highest tested concentration (10 μM); n.d., not determined. ^{b}Values are the means of at least three independent determinations; hBChE from human serum. ^{c}Values are the means of at least three independent determinations; recombinant hAChE. ^{d}Selectivity index (SI) toward hBChE = IC$_{50}$(hAChE)/IC$_{50}$(hBChE). ^{e}Screened on membranes of HEK cells stably expressing hCB$_2$R using 10 μM of the compound; values are mean values from at least two independent experiments, each performed in triplicate. ^{f}Screened on membranes of CHO cells stably expressing hCB$_1$R using 10 μM of the compound; values are mean values from at least two independent experiments, each performed in triplicate.

(STAT-3) gene, which expression is also under CRE promoter control.[76] Both genes are highly expressed in multiple myeloma cells.[77,78] Compounds **3e** and **4c** were evaluated, as previously described, at a concentration of 50 μM.[48] In general, before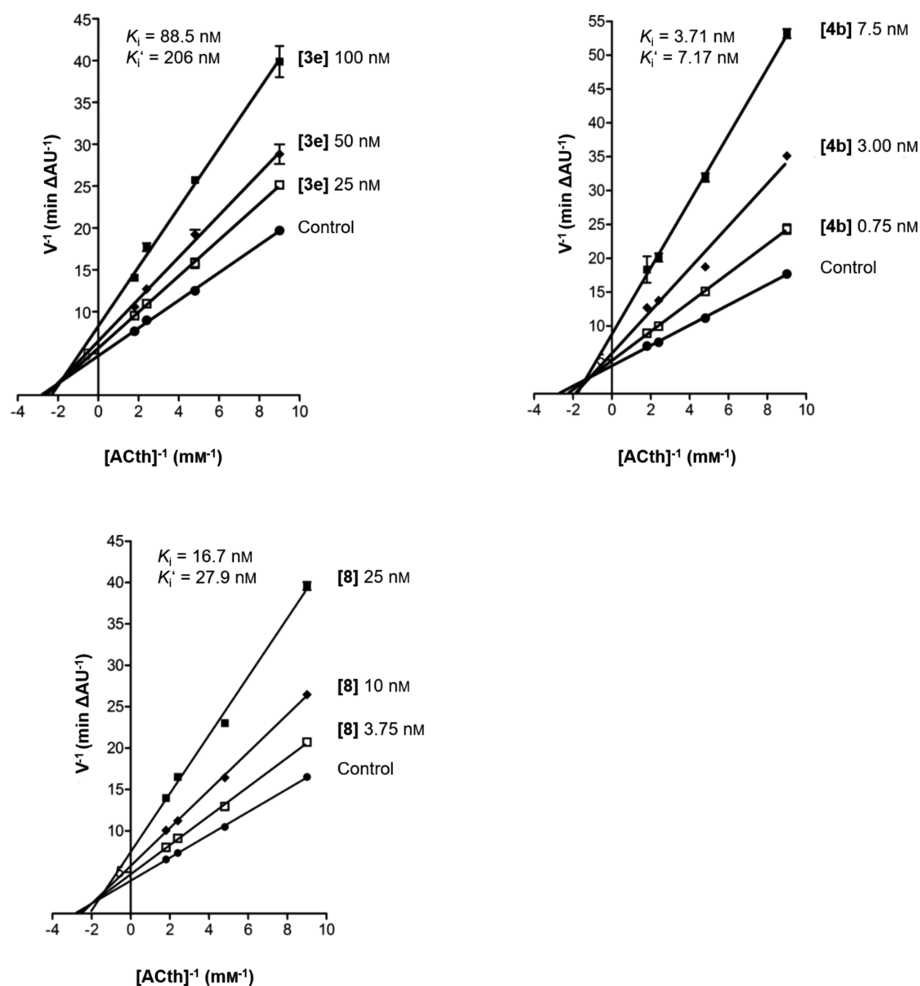 examining the efficacy of the compounds, an MTT assay was carried out on U266 myeloma cells to evaluate a nontoxic concentration of the compounds (see Supplementary Figure 1). The efficacy of the compounds was investigated by the quantification of the cAMP-regulated MIF and STAT-3 genes by a qRT-PCR methodology. AM630 was measured as a
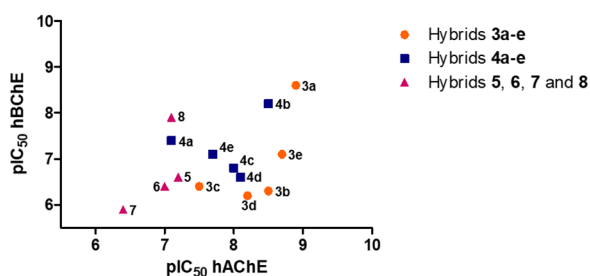
Figure 4. Plot of pIC_{50} values toward hBChE against pIC_{50} values toward hAChE of all hybrids.

	% inhibition Aβ aggregation	
	self-induced[a]	AChE-induced[b]
3e	81.5 ± 0.2	62.9 ± 5.4
4b	16.4 ± 4.2	47.8 ± 9.6
8	83.4 ± 6.4	5.0 ± 2.6
1	< 5	< 5

Figure 6. AChE-mediated and self-induced Aβ aggregation. Footnote a denotes inhibition of $A\beta_{42}$ self-aggregation investigated by the thioflavin T fluorescence assay. Assays were carried out in the presence of 50 μM inhibitor and 50 μM $A\beta_{42}$ ([I] = [$A\beta_{42}$]). Values are expressed as means ± SEM of two independent experiments, and each was performed in duplicate. Footnote b denotes % inhibition of hAChE-induced $A\beta_{40}$ aggregation at [I] = 100 μM. The $A\beta_{40}$/hAChE ratio was equal to 100:1. Values are expressed as means ± SEM of two independent experiments, and each was performed in duplicate.

reference antagonist/reverse agonist. Cells were treated with compound **2** as a reference agonist, **3e** and **4c** alone, and in combination with AM630. Compared to the vehicle, compounds **2**, **3e**, and **4c** show a decreased expression of both genes. Also, in combination experiments, all three compounds show a decreased level of both genes compared to the levels of only the AM630-treated cells (see Figure 7 and Supplementary Figure 2).

Furthermore, compounds **3e** and **4c** were characterized using a functional fluorescent hCB2-activated $G_{\alpha q16}$-coupled intracellular calcium mobilization assay in CHO-K1 cells overexpressing the receptor.[79,80] Briefly, CHO-K1 cells were

engineered to stably co-express hCB1 or hCB2 and $G_{\alpha q16}$. Activation of hCB_1/CB_2 by an agonist then leads to generation of inositol phosphatase 3 (IP3) and activation of IP3 receptors, which, in turn, mobilizes intracellular calcium. Compounds **3e** and **4c** were identified as agonists of hCB2R with an EC_{50} of 911 ± 42 nM for compound **4c** and an E_{max} = 39%. Compound **3e** shows an EC_{50} of 3.05 ± 0.2 μM and an E_{max} = 51%. Therefore,
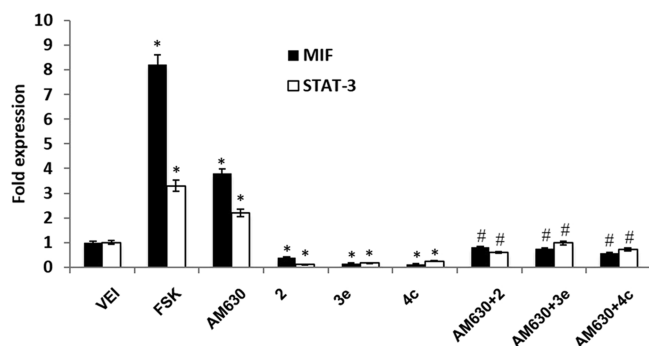

Figure 5. Kinetic study on the mechanism of hAChE inhibition by **3e**, **4b**, and **8**. Lineweaver–Burk reciprocal plots of hAChE initial velocity at increasing substrate (acetylthiocholine, ACth) concentration in the absence of the inhibitor (control) and the presence of increasing concentrations of the inhibitor are shown. Values are the means of at least three independent determinations.

Figure 7. Test compounds (**2**, **3e**, and **4c**) reduce MIF and STAT-3 gene expression. U266 cells were treated with hybrid compounds (50 μM), FSK (10 μM), or AM630 (25 μM) for 2 h. In a combined experiment (AM630 plus test compounds), U266 cells were preincubated with AM630 for 30 min. Before adding the test compounds, MIF and STAT-3 mRNA levels were determined by qRT-PCR. GAPDH was used for normalization. Data are expressed as relative fold with respect to vehicle-treated cells used as the control. Values are means of at least two independent experiments, and each was performed in duplicate. Data are expressed as means $\pm$ SD *$p < 0.01$ vs untreated; # vs AM630.

both compounds are partial agonists at hCB$_2$R. Both compounds were devoid of activity at hCB$_1$R. (see Figure 8).

Compounds **3e** and **4c** are therefore partial agonists at the hCB$_2$R as confirmed in two different assays. Since in our previous work, we also found agonist behavior for structurally related derivatives and because of the high structural similarity of all the hybrids described, we assume that all hybrids are agonists.[48]

Effects on Microglia Activation. To test a possible immunomodulatory effect, that is, the shift from the M1 neurotoxic to the M2 neuroprotective phenotype, of compounds **2**, **3e**, and **4a**, the murine microglial cell line N9 was exposed to 100 ng/mL lipopolysaccharide (LPS), which induces an M1 activation state, in the presence or absence of increasing concentrations (1, 2.5, and 5 μM) of the test compounds. After 24 h of treatment, microglial conditioned media were collected, partly used for nitrite measurement, and partly concentrated for Western blot analysis. In parallel, microglial cells were collected, and the protein content was determined. Accumulation of nitrite in microglial conditioned media was measured by a colorimetric assay based on the Griess reaction, while the release of IL1β and

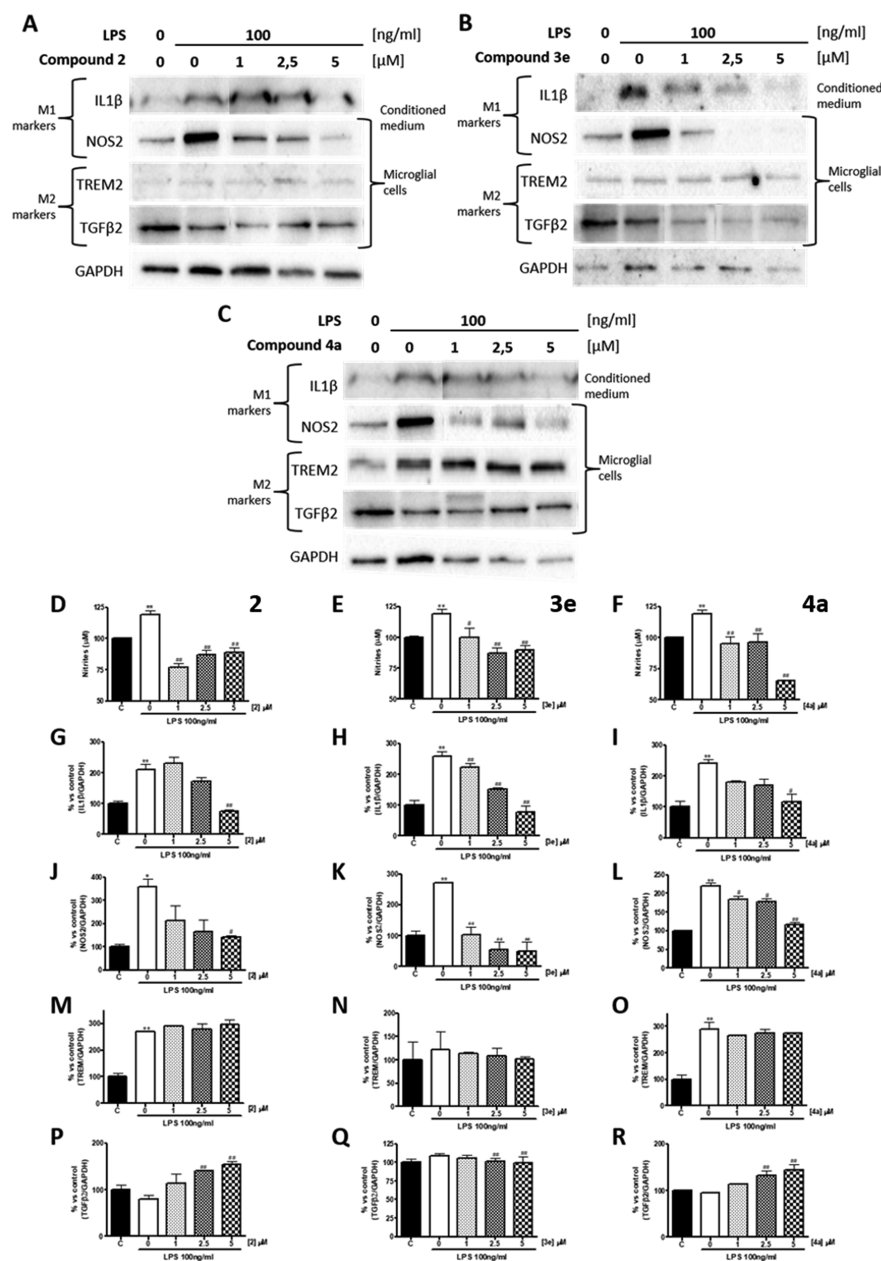the expression of iNOS, TREM2, and TGFβ2 were tested through Western blot analysis.

Nitrite production due to iNOS induction and IL1β release is the marker of M1, neurotoxic activated microglia, and induced by the LPS treatment, while the phagocytic proteins TREM2 and TGFβ2 are both makers of M2, neuroprotective microglia. As shown in Figure 9, compound **3e** strongly reduces in a dose-dependent way IL1β release and nitrite accumulation, as well as iNOS expression induced by LPS-mediated activation of microglial cells, with no parallel change in TREM2 and TGFβ2 expression, thus indicating an immunomodulatory effect of the compound, which is similar to compounds **2** and **4a**.

Neuroprotective Properties on HT-22 Cells. For the biological evaluation of compound **8** regarding its effects on murine hippocampal neurons (HT-22), we performed a glutamate assay as previously described.[81,82] This neuronal cell line is derived from murine hippocampal tissue and is glutamate sensitive.[83] HT-22 cells lack ionotropic glutamate receptors. The addition of extracellular glutamate at high concentrations can be used to introduce intracellular ROS accumulation by blocking the cystine/glutamate antiporter, resulting in glutathione depletion. This neuronal oxidative stress results in cell injuries and eventually cell death.[84−86] Before performing the neuroprotectivity assays, potential neurotoxicity of both compounds **4e** and **8** were evaluated in an MTT assay (see Figure 10A). Compound **8** showed concentration-dependent neuroprotectivity starting at 1 μM (see Figure 10C). Treatment with 5 μM compound **8** leads to neuroprotection comparable to the positive control quercetin at 25 μM. Compound **4e** shows a similar neuroprotective behavior but decreases viability at 10 μM due to the neurotoxic effect at this dose (see Figure 10B). The use of cystamine as a linker yielded a hybrid with lower neurotoxicity compared to the sulfur-free analogue **4e** with a neuroprotective behavior at a comparable low concentration. Furthermore, compounds **3a**, **3d**, **3e**, **4a**, and **4b** were also investigated toward their neurotoxicity and neuroprotective behavior. In summary, compounds **3a**, **3d**, and **3e** show no neurotoxicity at the doses tested (max. 10 μM), while **4a** is toxic above 5 μM, and **4b** shows first toxicity effects at 5 μM. Compounds **4b** and **4a** show neuroprotective behavior only at 5 μM, while other compounds tested showed low neuroprotective behavior (**3e**) or none (**3a** and **3d**) (see Supplementary Figure 3).

In Vivo Studies. The most promising compounds were tested regarding their procognitive effects in an in vivo AD mouse model. To induce AD such as neuroinflammation and
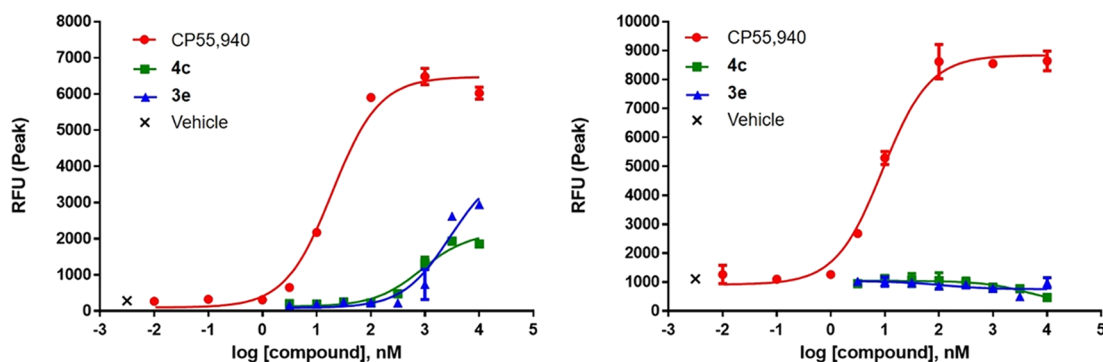
Figure 8. Calcium mobilization assay in CHO-K1 cells overexpressing hCB$_1$ or hCB$_2$ and G$_{\alpha q16}$. Compounds were tested in each cell type as described under Experimental Section. Agonism was noted in cells expressing hCB$_2$ (left) but not in cells expressing hCB$_1$ (right). The synthetic full agonist CP 55,040 served as a comparator and positive control. No significant signal was noted in vehicle control cells.

Figure 9. Effect of compounds **2**, **3e**, and **4a** on microglial activation in N9 cells previously activated by LPS (100 ng/mL). IL1β release and expression of iNOS, TREM2, and TGFβ2 were tested through Western blot analysis after 24 h of treatment with LPS in the presence of increasing concentrations (1, 2.5, and 5 μM) of compounds (A) **2**, (B) **3e**, and (C) **4a**, respectively, and (G−R) quantified through densitometry. NO release was evaluated through the Griess reaction in media conditioned for 24 h by microglial cells treated by LPS in the presence of compounds (D) **2**, (E) **3e**, and (F) **4a**, showing an increase in NO release in media conditioned by LPS-treated cells that are reduced by the co-treatment with the compounds, with the strongest effect of compound **2**. Both (G−I) IL1β release and (J−L) iNOS expression, which are markers of M1 neurotoxic microglia, strongly increase in LPS-treated cells but significantly decrease in cells co-treated with compounds (G, J) **2**, (H, K) **3e**, and (I, L) **4a** in a dose-dependent way, while the expression of the M2 microglial markers (M−O) TREM2 and (P−R) TGFβ2 is not reduced by co-treatment with the compounds. All quantitative data are presented as means $\pm$ SEM from at least three independent experiments. Statistical significance between different treatments was calculated by using one-way analysis of variance (ANOVA) followed by post hoc comparison through Bonferroni's test. *$p < 0.05$; **$p < 0.01$ compare to control; [#]$p < 0.05$; [##]$p < 0.01$ compare to LPS.

cognitive deficits, oligomerized A$\beta_{25−35}$ peptide was intracerebroventricularly injected into the mouse brain.[44,87,88] Since the addressed targets are located in the brain, hybrids must be able to penetrate the BBB. We first tested compounds, with the shortest spacer lengths, **3a** and **4a** with a low molecular weight. After the first positive results, we also tested compounds with a more pronounced in vitro profile.

Compounds were injected once daily (o.d.) and intraperitoneally (i.p.) from day 1, 20 min after the peptide injection, until day 7. Compounds were solubilized in pure DMSO at a concentration of 2 mg/mL and then diluted in water. Final DMSO concentration in the vehicle solution remained, however, high (60%), and innocuity was controlled by a daily observation on the mice behavior and weight gain control. None of the treatment affected significantly the weight gain during the
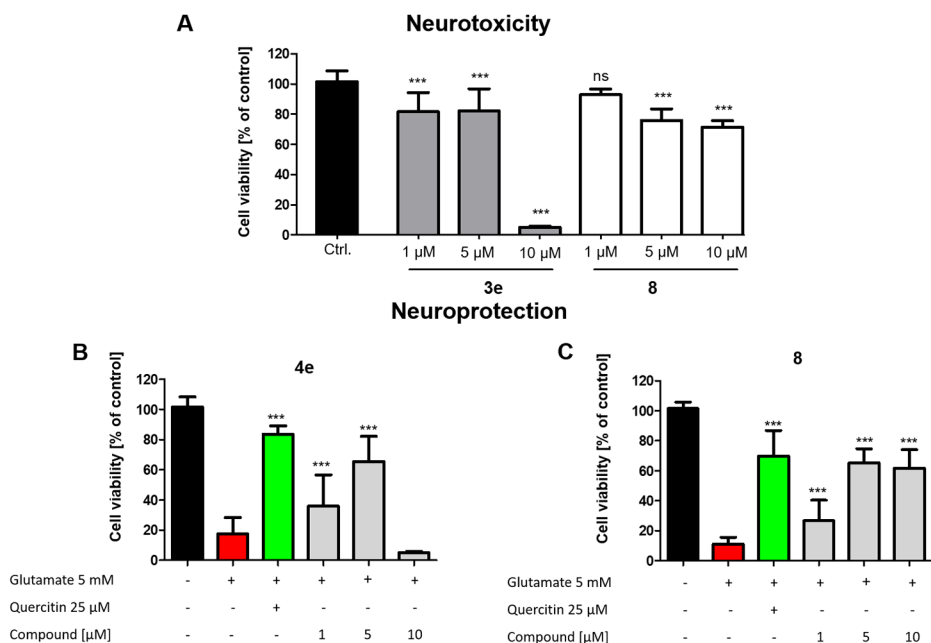
Figure 10. Compounds **4e** and **8** were studied on neuronal HT-22 cells for (A) neurotoxicity effects and (B, C) neuroprotection against glutamate-induced oxidative stress at $1-25$ μM. Results of the modified MTT test are presented as means $\pm$ SD of three independent experiments, each performed in sextuplicate, and refer to untreated control cells, which were set as 100% values. Statistical analysis was achieved by applying one-way ANOVA followed by Dunnett's multiple comparison post-test. Levels of significance: *$p < 0.005$; **$p < 0.01$; ***$p < 0.001$. Treated cells were compared to (A) untreated cells and (B) cells treated with glutamate only.
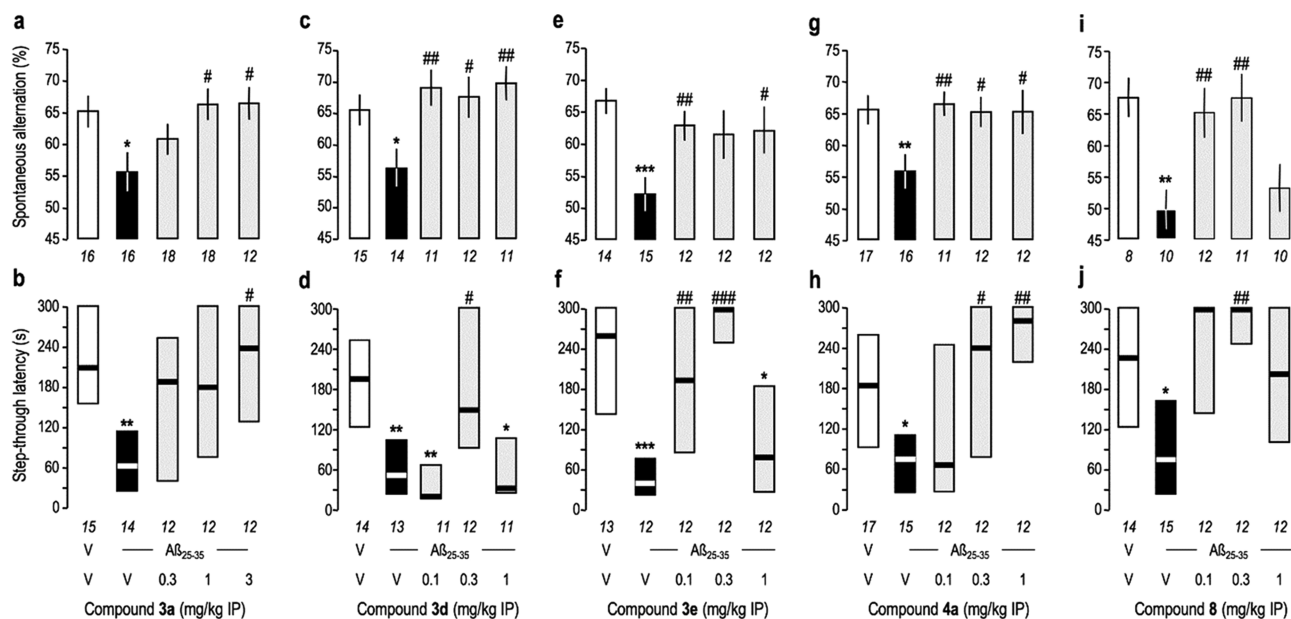
Figure 11. Effect of the compounds on $A\beta_{25-35}$-induced learning impairments in mice: spontaneous alternation performance (upper panels) and passive avoidance response (lower panels). Mice received $A\beta_{25-35}$ (9 nmol, i.c.v.) or vehicle solution (3 μL, i.c.v.) on day 1 and then compound (a, b) **3a**, (c, d) **3d**, (e, f) **3e**, (g, h) **4a**, or (i, j) **8** in the $0.1-3$ mg/kg, i.p. dose range, o.d. between day 1 to 7. Mice were then tested for (a, c, e, g, and i) spontaneous alternation on day 8 and (b, d, f, h, and j) passive avoidance on days 9 and 10. Data show means $\pm$ SEM (upper panels) or median and interquartile range (lower panels). ANOVA: $F_{(4,79)} = 3.05$, $p < 0.05$, $n = 12-18$ in (a); $F_{(4,62)} = 3.77$, $p > 0.01$, $n = 11-15$ in (c); $F_{(4,64)} = 3.85$, $p < 0.01$, $n = 10-15$ in (e); $F_{(4,67)} = 3.14$, $p < 0.05$, $n = 11-17$ in (g); $F_{(4,50)} = 5.40$, $p < 0.01$, $n = 8-12$ in (i). Kruskal−Wallis ANOVA: $H = 9.87$, $p < 0.05$, $n = 12-15$ in (b); $H = 17.4$, $p < 0.01$, $n = 11-14$ in (d); $H = 21.9$, $p < 0.001$, $n = 12-13$ in (f); $H = 13.9$, $p < 0.01$, $n = 12-17$ in (h); $H = 11.8$, $p < 0.05$, $n = 12-15$ in (j). Post hoc: *$p < 0.05$, **$p < 0.01$, and ***$p < 0.001$ vs (V + V)-treated group; #$p < 0.05$, ##$p < 0.01$, and ###$p < 0.001$ vs (V + Aβ_{25-35})-treated group; Dunnett's (upper panels) or Dunn's test (lower panels).

week of treatment. Animals lost up to 1 g after the peptide injection but then regained regularly between 0.2 and 0.4 g daily (see Supplementary Figure 4).

Behavioral examination was performed between day 8 and 10 according to the procedure schematized in Supplementary

Table 2. Results of the Liver Histology Performed with High Dose (3 mg/kg)-Treated Mice

	microvesicular steatosis			necrosis		
treatment	positive/specimen	% of specimen	reported area %	positive/specimen	% of specimen	reported area %
V/V	6/10	60	30−40	5/10	50	2−30
Aß/V	7/10	58	10−30	11/12	91	1−30
Aß/**3a** (3 mg/kg)	8/12	66	5−30	8/12	66	2−50
Aß/**3d** (3 mg/kg)	6/6	100	3−45	5/6	83	5−15
Aß/**4a** (3 mg/kg)	2/9	22	10−30	6/9	66	5−10
Aß/**8** (3 mg/kg)	8/11	72	20−40	8/11	72	5−50

Figure 5. All animals were sacrificed on day 11 (see Supplementary Figure 5).

Spontaneous alternation performance, which is an index of spatial working memory, was tested on day 8 in the Y-maze test. Long-term memory response was measured on day 10, in a step-through type passive avoidance task, with retention assessed for 24 h after training. Results confirmed that $A\beta_{25-35}$ induced significant learning impairments in the behavioral tests. Moreover, all compounds tested showed significant attenuations of $A\beta_{25-35}$-induced learning impairments in both the short-term and the long-term memory responses (see Figure 11). Effective doses were slightly lower in the spontaneous alternation test (see Figure 11, upper panels) than in the passive avoidance test (see Figure 11, lower panels) and appeared often bell-shaped (see Figure 11d,f,i,j). Compound **3a** significantly prevented $A\beta_{25-35}$-induced learning impairments at doses of 1 mg/kg and higher (see Figure 11b, 1). All other compounds, namely, **3d**, **3e**, **4a**, and **8**, significantly prevented the learning deficits at the lower dose of 0.3 mg/kg (see Figure 11c−j). Notably, compounds **3e**, **4a**, and **8** completely prevented $A\beta_{25-35}$ impairments in both tests at the most effective doses (resp., 0.3, 1, and 0.3 mg/kg), outlining the high efficiency of the compounds. It should be noted, at this point, that the hybrids show a significantly higher efficacy compared to the parent molecules **1** and **2**, which were also investigated in vivo in our previous work.[48,87] It is possible that MOR activity of the compounds may marginally contribute to the neuroprotective effect observed here. However, the only indirect measure we get from our experiments was that no significant change in pain sensitivity to footshock was measured, even at the highest drug dose during the passive avoidance training session. Shock sensitivity was 1.1 ± 0.3 for the group treated with compound **3a**, 3 mg/kg, and 0.9 ± 0.3 for compound **4a**, 1 mg/kg, versus 1.4 ± 0.3 for Veh-treated animals, suggesting that pain response was not affected by the compound treatments. Nevertheless, MORs have been shown to be involved in memory formation, particularly, in the context of memory formation associated with opiate drug abuse, by regulating GABAergic inputs and facilitating neuronal excitatory activity through the hippocampal CA1 area.[89] Therefore, the agonist (or antagonist) activity of the compounds at MORs and synergy of MOR and CB₂R activities on memory and neuroprotection is—at least in principle—possible. Indeed, the compounds tested exhibit a remarkably high in vivo efficacy, with sub-mg/kg active doses as compared with their low micromolar affinities in vitro on CB₂Rs or MORs. Their precise PK/PD profiles and any possible synergy between pharmacological targets should be examined to confirm that the compounds exhibit a very unique and interesting pharmacological activity.

Liver Histology. Livers of mice treated with the high dose (3 mg/kg) were dissected out on day 12, after the behavioral experiments, post-fixed in buffered formalin 4%, and cut into 2 mm slices. At least two-thirds of the parenchyma was embedded, including all macroscopically visible abnormalities. The material underwent standardized dehydration and paraffin embedding as well as hematoxylin−eosin staining after well-established routine protocols. All slides were assessed by the same pathologist, completely blinded to the treatment protocols. The assessment included all typical liver changes seen with drug toxicity: Necrosis was reported focal, segmental, diffuse, or zonal in percentages and divided between fresh and long-standing necrosis. Steatosis was reported as macro- or microvesicular, given in percentages, as diffuse or zonal (lobular zones I−III). Fibrosis was assessed according to stages I to IV after Batts and Ludwig.[90] Inflammation is reported semiquantitatively in a four-tiered system 0−3 and divided into portal and/or lobular. Cholestasis was also reported in a four-tiered system 0−3 specified to intrahepatocytic or canalicular. Cell ballooning was also stated in percentage. After the assessment, the findings were realigned with the treating groups. Microvesicular steatosis was present in all groups, including controls (6/10) showing the highest ratio in group **3d** (6/6) and the lowest in group **4a** (2/9). Necrosis was differentiated into fresh necrosis and older necrosis. The fresh necrosis in these specimen was completed without reaction, only hours old. It was seen in all groups, including controls. The highest ratio was observed in the Aß/V group (11/12) and group **3d** (5/6) with nearly all specimen affected. Older necrosis was reported in two specimen only, both in group Aß/V. Other findings, such as discrete lobular inflammation, were seen only in a single specimen, not related to treatment groups. The results suggest drug-independent reasons for steatosis and fresh necrosis because they were also found in the control groups in a high percentage. One possible cause of the observed liver damage could be the high level of DMSO used for compound injection.[91] No hepatotoxic relation to compound treatment could be established. Further experiments for long-time toxicity must be performed.

CONCLUSIONS

In the current study, sets of hybrid compounds combining tacrine **1** as ChE inhibitor and the hCB₂R agonist **2** were designed and synthesized using different molecular attachment points in the benzimidazole core, different spacer lengths, and structures. The newly synthesized compounds were first evaluated in a series of experiments to confirm activity on AD-relevant targets, namely, AChE, BChE, and hCB₂R. The hybrid compounds showed higher inhibition of ChEs compared to **1**. To follow this up, a kinetic study was performed. The study showed a mixed-type inhibition by compounds tested and suggests binding to a second site in ChE leading to higher inhibition. While **1** has no effect on $A\beta$ aggregation when assayed at 1/1 ratio, all hybrids tested had an effect. Above all, **3e** showed a pronounced inhibition of self- and AChE-induced $A\beta$ aggregation. Radioligand binding studies on hCB₂R showed a

lower affinity from the nanomolar range of **2** to the single-digit micromolar range for the hybrids. Hybrids **3e** and **4c**, representative for the two different sets, were investigated by a cAMP-regulated gene expression experiment, which showed they maintained their agonist behavior at the hCB$_2$R. To investigate the effectiveness, microglial activity was investigated. Therefore, different M1 and M2 markers were quantified. Despite the significantly lower affinity for the hCB$_2$R compared to **2**, the compounds showed an immunomodulatory effect similar to the parent molecule **2**. The concept of incorporating a disulfide into the linker to introduce neuroprotection was investigated in a HT22 cell assay. Both tested compounds, **8** and the sulfur-free analogue **3e**, showed neuroprotection against glutamate-induced oxidative stress. Due to the promising in vitro profile, several compounds were tested in vivo and showed pronounced effects on short- and long-term memory, proving their ability to cross the BBB. Keeping the hepatotoxicity of **1** in mind, liver histology of high dose-treated animals (3 mg/kg) was carried out (Table 2). In first-line experiments, the tested hybrids showed no hepatotoxicity effect, but this must be further investigated. The high in vivo efficacy of the compounds should be emphasized, which is significantly higher in particular for the compounds **3e** and **8** (0.1 mg/kg), than for the parent molecules **1** and **2**, which were investigated in our previous work.[48,87] Due to the significantly lower dosage compared to **1**, a lower liver-damaging side effect of the novel hybrids in a potential clinical application might be assumed. We consider these data also of interest for other drug discovery efforts with regard to tacrine-containing experimental therapeutics as well as hybrid molecules with higher molar mass aiming at CNS activity.

■ EXPERIMENTAL SECTION

Chemistry. *General Information. Reagents and Solvents.* All reagents were used without further purification and bought from common commercial suppliers. For anhydrous reaction conditions, THF was dried prior to use by refluxing over sodium slices with benzophenone as an indicator under an argon atmosphere.

Thin-Layer Chromatography (TLC). To monitor reaction progress, thin-layer chromatography (precoated plates with silica gel, from Machery-Nagel: ALUGRAM Xtra SIL G/UV$_{254}$) was carried out. The spots were visualized by UV light (254 and 366 nm), by staining in the iodine chamber, orby using spray reagents (Ehrlich's reagent: primary amines turn red). The eluent systems are indicated in volume (v) ratios of the respective solvents (v/v).

Preparative Thin-Layer Chromatography. Silica gel (Merck KGaA: Silica gel 60 GF$_{254}$) was mixed with water. Glass plates were coated evenly with the mixture and dried at room temperature. The compound was dissolved in CH$_2$Cl$_2$ and applied to the starting line in small drops. The plate was then transferred to a preparative TLC chamber with the mobile phase. After successful separation, the plate was dried, and the product was detected under UV light (254 and 366 nm), scraped off, and then extracted with MeOH.

Column Chromatography. Silica gel (particle size, 0.063–0.2 mm; Merck) was used for column chromatography. The eluent systems are indicated in volume (v) ratios of the respective solvents (v/v). Column chromatography was also performed using an Interchim Puri Flash 430 (Ultra Performance Flash Purification) instrument (Montluçon, France) connected to an Interchim Flash ELSD. Used columns were Silica 25 g (30 μm) (Interchim, Montluçon, France).

Nuclear Magnetic Resonance Spectroscopy (NMR). Measurements of NMR spectra were performed on a Bruker Advance 400 (^{1}H NMR: 400 MHz; ^{13}C NMR: 101 MHz). ^{1}H and ^{13}C NMR spectra were calibrated with the hydrogen signal of the respective solvent as the internal standard. In this work, CDCl$_3$, CD$_3$OD, and D$_2$O were used as solvents (^{1}H: CDCl$_3$, 7.26 ppm; ^{1}H: CD$_3$OD, 3.31 ppm; ^{1}H: D$_2$O, 4.79 ppm; ^{13}C: CDCl$_3$, 77.16 ppm; ^{13}C: CD$_3$OD, 49.0 ppm). *J* is the

coupling constant in hertz (s^{-1}). The abbreviations of the indicated signal diversities were s = singlet, d = doublet, t = triplet, q = quartet, and m = multiplet.

Liquid Chromatography/Mass Spectrometry (LC/MS). Measurements for verification and purity of the compounds were performed by LC/MS (from Shimadzu), comprising a DGU-20A3R controller, pump LC-20AB, degasser DGU-20A, and SPD-20A UV/Vis detector. ESI ionization was accomplished by an LCMS-2020 single quadrupol mass spectrometer. As a stationary phase, for analytical purpose, a Synergi 4U fusion-RP 80 Å (150 × 4.6 mm) column and for preparative purpose, a Synergi 4U fusion-RP 80 Å (250 × 10.0 mm) were used. As a mobile phase, a gradient of MeOH/water (both containing 0.1% formic acid) (phase A/phase B) was used. The compounds were dissolved in MeOH and filtered through syringe filters.

The parameters for the methods are given as follows: flow rate, 1.0 mL/min; UV detection, 254 nm; scan range, 100–800 *m/z*; gradient: A, H$_2$O (0.1% CF$_3$COOH) and B, MeOH (0.1% CF$_3$COOH); 0–8 min 5% → 90% B, 8–13 min 90% B, 13–14 min 90% → 10% B, and 14–18 min 10% → 5% B.

Compounds were only used for biological evaluation if the purity was ≥95%.

General Procedures. General Procedure I for Nucleophilic Substitution of Aryl Chloride by a Diamine (for Compounds 12a–g). The chloride compound **11** was dissolved in hexanol, and the corresponding diamine was added. The mixture was stirred for 24 h under reflux conditions under an argon atmosphere. The solvent was evaporated under high vacuum using an evaporator. The residue was dissolved in CH$_2$Cl$_2$ and extracted with water. The organic layer was dried over anhydrous MgSO$_4$, and the solvent was removed in vacuo.

General Procedure II for Aromatic Substitution of Fluoride by Amines (for Compounds 17a–f and 20). The respective fluoride compound and the respective amine were dissolved in THF, and then NEt$_3$ was added. The mixture was stirred at room temperature overnight. The solvent was then removed in vacuo, and the residue was dissolved in CH$_2$Cl$_2$ and washed with water. The organic layers were combined and dried over anhydrous MgSO$_4$, and the solvent was removed in vacuo.

General Procedure III for Reduction of an Aromatic Nitro Moiety with Stannous Chloride Dihydrate (for Compounds 18a–f). The respective nitro compound was dissolved in ethanol, and SnCl$_2$·2H$_2$O was added. The mixture was stirred under reflux conditions under an argon atmosphere for 5 h. Then, the mixture was basified with NH$_{3(aq)}$ (25%), and the precipitate was filtered off by suction. The filtrate was concentrated in vacuo. The residue was dissolved in CH$_2$Cl$_2$ and washed with 1M NaOH. The organic layers were combined and dried over anhydrous MgSO$_4$, and the solvent was removed in vacuo. The product was directly used in the next reaction, without further purification, and just characterized by mass spectrometry.

General Procedure IV for Amide Formation with HBTU-Activated Ester (for Compounds 19a–f and 22). The respective acid was dissolved in DMF then NEt$_3$, and HBTU was added. This mixture was added to a solution of the respective amine in DMF. The mixture was stirred overnight at room temperature, and the solvent was then removed in vacuo. The residue was dissolved in CH$_2$Cl$_2$ and washed with a saturated NaHCO$_3$ solution. The organic layers were combined and dried over anhydrous MgSO$_4$, and the solvent was removed in vacuo.

General Procedure V for Ring Closure to Benzimidazole (for Compounds 3a–e, 6, and 23). The respective amide was dissolved in glacial acetic acid. The mixture was stirred depending on the reaction progress for 2–6 h under reflux conditions and was then concentrated in vacuo. The residue was basified with NH$_{3(aq)}$ (25%) and extracted with CH$_2$Cl$_2$. The organic layers were combined, dried over anhydrous MgSO$_4$, and concentrated in vacuo.

Synthesis. 2-(4-Ethoxybenzyl)-N,N-diethyl-1-(2-((1,2,3,4-tetrahydroacridin-9-yl)amino)ethyl)-1H-benzo[d]imidazole-5-carboxamide (3a). The reaction was carried out according to general procedure V using 3-(2-(4-ethoxyphenyl)acetamido)-N,N-diethyl-4-((2-((1,2,3,4-tetrahydroacridin-9-yl)amino)ethyl)amino)benzamide **19a** (258 mg, 0.43 mmol). The crude product was purified by column chromatography (20:1:0.1 CH$_2$Cl$_2$/MeOH/NH$_{3(aq)}$ (25%)), and

product **3a** (210 mg, 0.36 mmol, 84%) was obtained as a yellow oil. ^{1}H NMR (400 MHz, CDCl$_3$): δ 7.86 (d, J = 8.2 Hz, 1H), 7.70 (s, 1H), 7.57 (d, J = 8.3 Hz, 1H), 7.51−7.45 (m, 1H), 7.24−7.15 (m, 2H), 7.11 (d, J = 8.3 Hz, 1H), 6.90 (d, J = 8.6 Hz, 2H), 6.66−6.61 (m, 2H), 4.13 (t, J = 6.6 Hz, 2H), 4.04 (s, 2H), 3.88 (s, 1H), 3.82 (q, J = 7.0 Hz, 2H), 3.56−3.23 (m, 6H), 2.96 (t, J = 6.4 Hz, 2H), 2.31 (t, J = 6.3 Hz, 2H), 1.83−1.75 (m, 2H), 1.74−1.66 (m, 2H), 1.27 (t, J = 7.0 Hz, 3H), 1.15 (s, 6H) ppm. ^{13}C NMR (101 MHz, CDCl$_3$): δ 171.7, 158.8, 158.2, 154.9, 149.2, 147.2, 142.2, 135.9, 131.6, 129.4, 128.9, 128.7, 127.7, 124.6, 122.0, 121.7, 120.6, 118.0, 117.9, 114.9, 109.5, 63.5, 47.3, 44.5, 34.0, 33.8, 24.8, 22.9, 22.7, 14.9, 14.2 ppm. ESI: m/z calcd for C$_{36}$H$_{42}$N$_5$O$_2$ [M + H]$^+$, 576.33; found, 576.25; retention time, 7.90 min; HPLC purity, 97%.

2-(4-Ethoxybenzyl)-N,N-diethyl-1-(3-((1,2,3,4-tetrahydroacridin-9-yl)amino)propyl)-1H-benzo[d]imidazole-5-carboxamide (3b). The reaction was carried out according to general procedure V using 3-(2-(4-ethoxyphenyl)acetamido)-N,N-diethyl-4-((3-((1,2,3,4-tetra-hydroacridin-9-yl)amino)propyl)amino)benzamide **19b** (104 mg, 0.17 mmol). The crude product was purified by preparative thin-layer chromatography (10:1:0.1 CH$_2$Cl$_2$/MeOH/NH$_{3(aq)}$ (25%)), and product **3b** (23 mg, 39.0 μmol, 23%) was obtained as a yellow oil. ^{1}H NMR (400 MHz, CDCl$_3$): δ 8.16 (d, J = 7.8 Hz, 1H), 8.06 (d, J = 8.0 Hz, 1H), 7.74 (s, 1H), 7.56−7.49 (m, 2H), 7.27−7.22 (m, 2H), 7.15 (d, J = 7.9 Hz, 2H), 6.62 (d, J = 8.3 Hz, 2H), 4.43 (s, 2H), 4.00−3.92 (m, 2H), 3.77 (q, J = 6.9 Hz, 2H), 3.57−3.48 (m, 2H), 3.40−3.13 (m, 4H), 3.08−3.03 (m, 2H), 2.59−2.51 (m, 2H), 2.20−2.12 (m, 2H), 1.75−1.71 (m, 4H), 1.29−1.17 (m, 8H) ppm. ^{13}C NMR (101 MHz, CDCl$_3$): δ 171.0, 158.4, 156.7, 154.2, 151.0, 145.9, 142.3, 134.2, 132.2, 129.8, 128.4, 128.1, 127.5, 124.5, 122.4, 121.8, 119.7, 117.7, 115.9, 115.0, 111.7, 63.5, 46.0, 42.8, 33.9, 32.0, 29.8, 24.8, 22.4, 22.1, 14.9, 14.2 ppm. ESI: m/z calcd for C$_{37}$H$_{45}$N$_5$O$_2$ [M + 2H]$^{2+}$, 295.68; found, 295.60; retention time, 7.82 min; HPLC purity, 98%.

2-(4-Ethoxybenzyl)-N,N-diethyl-1-(4-((1,2,3,4-tetrahydroacridin-9-yl)amino)butyl)-1H-benzo[d]imidazole-5-carboxamide (3c). The reaction was carried out according to general procedure V using 3-(2-(4-ethoxyphenyl)acetamido)-N,N-diethyl-4-((4-((1,2,3,4-tetrahydroacridin-9-yl)amino)butyl)amino)benzamide **19c** (166 mg, 0.27 mmol). The crude product was purified by column chromatography (10:1:0.1 CH$_2$Cl$_2$/MeOH/NH$_{3(aq)}$ (25%)), and product **3c** (46 mg, 76.2 μmol, 28%) was obtained as a yellow oil. ^{1}H NMR (400 MHz, CDCl$_3$): δ 7.90 (d, J = 8.3 Hz, 1H), 7.82 (d, J = 8.3 Hz, 1H), 7.75 (s, 1H), 7.55 (t, J = 11.1, 4.0 Hz, 1H), 7.34 (t, J = 7.3 Hz, 1H), 7.29−7.26 (m, 1H), 7.18 (d, J = 8.3 Hz, 1H), 7.09 (d, J = 8.6 Hz, 2H), 6.76 (d, J = 8.6 Hz, 2H), 4.20 (s, 2H), 3.97 (t, J = 7.1 Hz, 2H), 3.87 (q, J = 7.0 Hz, 2H), 3.64−3.36 (m, 4H), 3.30 (t, J = 6.7 Hz, 2H), 3.05 (t, J = 5.8 Hz, 2H), 2.62 (t, J = 5.7 Hz, 2H), 1.92−1.83 (m, 4H), 1.61−1.49 (m, 4H), 1.30 (t, J = 7.0 Hz, 3H), 1.26−1.19 (m, 6H) ppm. ^{13}C NMR (101 MHz, CDCl$_3$): δ 171.8, 158.7, 157.2, 154.5, 150.3, 147.5, 142.2, 135.9, 131.3, 129.5, 128.9, 128.5, 127.9, 124.1, 122.5, 121.5, 120.6, 117.8, 116.9, 115.9, 109.5, 63.5, 48.7, 43.9, 33.9, 29.8, 28.9, 27.0, 25.0, 23.1, 22.9, 14.8, 14.2 ppm. ESI: m/z calcd for C$_{38}$H$_{47}$N$_5$O$_2$ [M + 2H]$^{2+}$, 302.69; found, 302.65; retention time, 7.92 min; HPLC purity, 98%.

2-(4-Ethoxybenzyl)-N,N-diethyl-1-(5-((1,2,3,4-tetrahydroacridin-9-yl)amino)pentyl)-1H-benzo[d]imidazole-5-carboxamide (3d). The reaction was carried out according to general procedure V using 3-(2-(4-ethoxyphenyl)acetamido)-N,N-diethyl-4-((5-((1,2,3,4-tetra-hydroacridin-9-yl)amino)pentyl)amino)benzamide **19d** (346 mg, 0.47 mmol). The crude product was purified by column chromatography (10:1:0.1 CH$_2$Cl$_2$/MeOH/NH$_{3(aq)}$ (25%)), and product **3d** (22 mg, 35.6 μmol, 51%) was obtained as a yellow oil. ^{1}H NMR (400 MHz, CDCl$_3$): δ 8.05−7.98 (m, 2H), 7.72 (s, 1H), 7.56 (t, J = 7.6 Hz, 1H), 7.33 (t, J = 7.7 Hz, 1H), 7.25−7.19 (m, 2H), 7.11 (d, J = 8.5 Hz, 2H), 6.78 (d, J = 8.5 Hz, 2H), 4.22 (s, 2H), 3.98 (t, J = 7.2 Hz, 2H), 3.92 (q, J = 7.0 Hz, 2H), 3.61 (t, J = 7.1 Hz, 2H), 3.56−3.32 (m, 4H), 3.06−3.01 (m, 2H), 2.55−2.49 (m, 2H), 1.83−1.75 (m, 4H), 1.67−1.52 (m, 4H), 1.32 (t, J = 7.0 Hz, 3H), 1.28−1.13 (m, 8H) ppm. ^{13}C NMR (101 MHz, CDCl$_3$): δ 172.0, 158.2, 154.7, 154.7, 153.4, 142.1, 141.1, 135.9, 131.1, 131.1, 129.6, 128.0, 124.7, 123.9, 122.7, 121.4, 117.6, 117.3, 115.0, 112.4, 109.7, 63.6, 48.1, 44.0, 33.8, 31.1, 26.7, 29.2, 24.5, 24.2, 22.3,

21.3, 14.8, 14.1 ppm. ESI: m/z calcd for C$_{39}$H$_{49}$N$_5$O$_2$ [M + 2H]$^{2+}$, 309.70; found, 309.65; retention time, 8.07 min; HPLC purity, 99%.

2-(4-Ethoxybenzyl)-N,N-diethyl-1-(6-((1,2,3,4-tetrahydroacridin-9-yl)amino)hexyl)-1H-benzo[d]imidazole-5-carboxamide (3e). The reaction was carried out according to general procedure V using 3-(2-(4-ethoxyphenyl)acetamido)-N,N-diethyl-4-((6-((1,2,3,4-tetrahydroa-cridin-9-yl)amino)hexyl)amino)benzamide **19e** (142 mg, 0.22 mmol). The crude product was purified by preparative thin-layer chromatography (10:1:0.1 CH$_2$Cl$_2$/MeOH/NH$_{3(aq)}$ (25%)), and product **3e** (70 mg, 0.11 mmol, 50%) was obtained as a yellow oil. ^{1}H NMR (400 MHz, CDCl$_3$): δ 7.96−7.90 (m, 2H), 7.75 (s, 1H), 7.55 (t, J = 8.1, Hz, 1H), 7.33 (t, J = 9.2 Hz 1H), 7.30−7.27 (m, 1H), 7.25−7.22 (m, 1H), 7.11 (d, J = 8.6 Hz, 2H), 6.79 (d, J = 8.6 Hz, 2H), 4.23 (s, 2H), 3.98−3.90 (m, 4H), 3.61−3.33 (m, 6H), 3.09−3.03 (m, 2H), 2.70−2.64 (m, 2H), 1.92−1.86 (m, 4H), 1.59−1.47 (m, 4H), 1.33 (t, J = 7.0 Hz, 3H), 1.30−1.13 (m, 10H) ppm. ^{13}C NMR (101 MHz, CDCl$_3$): δ 171.9, 158.2, 154.5, 151.1, 146.9, 142.19, 136.0, 131.2, 129.6, 128.7, 128.3, 128.1, 125.4, 123.9, 122.9, 121.5, 120.1, 117.7, 155.8, 115.0, 109.6, 63.6, 49.3, 44.1, 33.9, 33.7, 31.6, 29.5, 26.8, 26.7, 24.9, 23.1, 22.7, 14.9, 14.3 ppm. ESI: m/z calcd for C$_{40}$H$_{51}$N$_5$O$_2$ [M + 2H]$^{2+}$, 316.70; found, 316.90; retention time, 8.27 min; HPLC purity, 95%.

2-(4-Ethoxybenzyl)-1-isopentyl-N-(2-((1,2,3,4-tetrahydroacridin-9-yl)amino)ethyl)-1H-benzo[d]imidazole-5-carboxamide (4a). The reaction was carried out according to general procedure V using 2-(4-ethoxybenzyl)-1-isopentyl-1H-benzo[d]imidazole-5-carboxylic acid **24** (271 mg, 0.74 mmol), N^1-(1,2,3,4-tetrahydroacridin-9-yl)ethane-1,2-diamine **12a** (179 mg, 0.74 mmol), HBTU (281 mg, 0.74 mmol), and NEt$_3$ (145 μL, 1.05 mmol). The crude product was purified by preparative thin-layer chromatography (10:1:0.1 CH$_2$Cl$_2$/MeOH/NH$_{3(aq)}$ (25%)), and product **4a** (35.0 mg, 59.3 μmol, 8%) was obtained as a yellow oil. ^{1}H NMR (400 MHz, CDCl$_3$): δ 8.24 (s, 1H), 8.13 (d, J = 8.7 Hz, 1H), 7.84 (d, J = 8.5 Hz, 1H), 7.62 (d, J = 8.6 Hz, 1H), 7.44 (t, J = 7.7 Hz, 1H), 7.34 (d, J = 8.5 Hz, 1H), 7.30−7.24 (m, 2H), 7.06 (d, J = 8.4 Hz, 2H), 6.70 (d, J = 8.4 Hz, 2H), 4.21 (s, 2H), 4.04−3.99 (m, 4H), 3.92−3.83 (m, 4H), 2.83−2.79 (m, 2H), 2.69−2.62 (m, 2H), 1.85−1.71 (m, J = 25.6, 5.6 Hz, 4H), 1.63−1.52 (m, 1H), 1.44−1.39 (m, 2H), 1.34 (t, J = 7.0 Hz, 3H), 0.90 (d, J = 6.6 Hz, 6H) ppm. ^{13}C NMR (101 MHz, CDCl$_3$): δ 168.8, 158.2, 155.3, 155.0, 152.3, 147.8, 142.1, 138.0, 130.6, 129.7, 128.5, 127.5, 125.5, 124.7, 122.1, 120.0, 118.7, 117.1, 115.1, 114.9, 109.8, 63.6, 44.7, 42.5, 40.6, 38.3, 33.7, 31.5, 29.8, 26.3, 24.2, 22.5, 21.3, 14.9 ppm. ESI: m/z calcd for C$_{37}$H$_{45}$N$_5$O$_2$ [M + 2H]$^{2+}$: 295.68; found: 295.75; retention time: 8.96 min; HPLC purity, 96%.

2-(4-Ethoxybenzyl)-1-isopentyl-N-(3-((1,2,3,4-tetrahydroacridin-9-yl)amino)propyl)-1H-benzo[d]imidazole-5-carboxamide (4b). The reaction was carried out according to general procedure V using 2-(4-ethoxybenzyl)-1-isopentyl-1H-benzo[d]imidazole-5-carboxylic acid **24** (370 mg, 1.01 mmol), N^1-(1,2,3,4-tetrahydroacridin-9-yl)propane-1,3-diamine **12b** (200 mg, 0.78 mmol), HBTU (326 mg, 1.33 mmol), and NEt$_3$ (184 μL, 1.33 mmol). The crude product was purified by column chromatography (20:1:0.1 CH$_2$Cl$_2$/MeOH/NH$_{3(aq)}$ (25%)), and product **4b** (67.0 mg, 0.11 mmol, 14%) was obtained as a yellow oil. ^{1}H NMR (400 MHz, CDCl$_3$): δ 8.37 (s, 1H), 8.24 (d, J = 8.7 Hz, 1H), 8.20 (d, J = 8.4 Hz, 1H), 7.97 (d, J = 8.5 Hz, 1H), 7.54 (t, J = 7.7 Hz, 1H), 7.35 (t, J = 7.8 Hz, 1H), 7.25 (d, J = 10.0 Hz, 1H), 7.08 (d, J = 8.4 Hz, 2H), 6.76 (d, J = 8.4 Hz, 2H), 4.19 (s, 2H), 3.97−3.88 (m, 6H), 3.71−3.65 (m, 2H), 3.14−3.09 (m, 2H), 2.75 (t, J = 5.8 Hz, 2H), 2.07−2.00 (m, 2H), 1.85−1.74 (m, 4H), 1.57−1.48 (m, 1H), 1.35 (t, J = 7.0 Hz, 3H), 1.33−1.24 (m, 2H), 0.87 (d, J = 6.6 Hz, 6H) ppm. ^{13}C NMR (101 MHz, CDCl$_3$): δ 169.4, 158.2, 155.5, 155.0, 152.0, 148.3, 142.3, 137.7, 131.6 129.6, 128.1, 127.8, 125.0, 124.2, 122.2, 119.1, 117.8, 116.6, 115.6, 114.9, 109.4, 63.6, 44.3, 42.8, 38.2, 36.2, 36.7, 33.8, 31.2, 29.3, 26.2, 24.6, 22.5, 21.1, 14.9 ppm. ESI: m/z calcd for C$_{38}$H$_{47}$N$_5$O$_2$ [M + 2H]$^{2+}$, 302.69; found, 302.75; retention time, 8.82 min; HPLC purity, 98%.

2-(4-Ethoxybenzyl)-1-isopentyl-N-(4-((1,2,3,4-tetrahydroacridin-9-yl)amino)butyl)-1H-benzo[d]imidazole-5-carboxamide (4c). The reaction was carried out according to general procedure V using 2-(4-ethoxybenzyl)-1-isopentyl-1H-benzo[d]imidazole-5-carboxylic acid **24** (286 mg, 0.78 mmol), N^1-(1,2,3,4-tetrahydroacridin-9-yl)butane-1,4-

diamine **12c** (161 mg, 0.60 mmol), HBTU (250 mg, 0.66 mmol), and NEt₃ (141 μL, 1.02 mmol). The crude product was purified by preparative thin-layer chromatography (10:1:0.1 CH₂Cl₂/MeOH/NH₃₍aq₎ (25%)), and product **4c** (38.0 mg, 0.62 mmol, 10%) was obtained as a yellow oil. ^{1}H NMR (400 MHz, CDCl₃): δ 8.26 (s, 1H), 8.18 (d, J = 8.7 Hz, 1H), 8.07 (d, J = 8.4 Hz, 1H), 7.86 (d, J = 8.5, 1H), 7.51 (t, J = 7.6, 1H), 7.32 (t, J = 7.6 Hz, 1H), 7.23 (d, J = 8.5 Hz, 1H), 7.06 (d, J = 8.6 Hz, 2H), 6.72 (d, J = 8.4 Hz, 2H), 4.18 (s, 2H), 3.96–3.88 (m, 6H), 3.56–3.49 (m, 2H), 3.03 (t, J = 5.9 Hz, 2H), 2.60 (t, J = 5.7 Hz, 2H), 1.96–1.88 (m, 2H), 1.81–1.70 (m, 6H), 1.56–1.48 (m, 1H), 1.34 (t, J = 7.0 Hz, 3H), 1.31–1.23 (m, 2H), 0.86 (d, J = 6.6 Hz, 6H) ppm. ^{13}C NMR (101 MHz, CDCl₃): δ 168.4, 158.2, 155.8, 154.9, 153.2, 142.9, 142.1, 137.5, 132.2, 129.6, 128.6, 127.7, 125.1, 124.7, 122.1, 120.5, 118.6, 116.5, 116.0, 114.9, 109.4, 63.6, 47.9, 42.8, 39.3, 38.3, 33.7, 29.8, 28.6, 28.1, 26.8, 26.2, 23.9, 22.4, 20.8, 14.9 ppm. ESI: m/z calcd for C₃₉H₄₉N₅O₂ [M + 2H]²⁺, 309.70; found, 309.70; retention time, 8.77 min; HPLC purity, 98%.

2-(4-Ethoxybenzyl)-1-isopentyl-N-(5-((1,2,3,4-tetrahydroacridin-9-yl)amino)pentyl)-1H-benzo[d]imidazole-5-carboxamide (4d). The reaction was carried out according to general procedure V using 2-(4-ethoxybenzyl)-1-isopentyl-1H-benzo[d]imidazole-5-carboxylic acid **24** (286 mg, 0.78 mmol), N^1-(1,2,3,4-tetrahydroacridin-9-yl)pentane-1,5-diamine **12d** (170 mg, 0.60 mmol), HBTU (250 mg, 0.66 mmol), and NEt₃ (141 μL, 1.02 mmol). The crude product was purified by column chromatography (20:1:0.1 CH₂Cl₂/MeOH/NH₃₍aq₎ (25%)), and product **4d** (57.0 mg, 0.32 mmol, 15%) was obtained as a yellow oil. ^{1}H NMR (400 MHz, CDCl₃): δ 8.15 (d, J = 8.7 Hz, 1H), 8.04 (s, 1H), 7.85 (d, J = 8.5, 1H), 7.82–7.77 (m, 1H), 7.60 (t, J = 7.3 Hz, 1H), 7.40–7.34 (m, 2H), 7.08 (d, J = 8.1 Hz, 2H), 6.67 (d, J = 7.0 Hz, 2H), 4.28 (s, 2H), 4.10–4.04 (m, 2H), 3.91–3.84 (m, 4H), 3.49–3.45 (m, 2H), 2.89–2.85 (m, 2H), 2.43–2.38 (m, 2H), 1.90–1.85 (m, 2H), 1.65–1.58 (m, 2H), 1.60–1.56 (m, 4H), 1.46–1.43 (m, 1H), 1.32 (t, J = 7.0 Hz, 4H), 1.26–1.25 (m, 5H), 0.94 (d, J = 6.8 Hz, 6H) ppm. ^{13}C NMR (101 MHz, CDCl₃): δ 169.5, 158.2, 155.5, 154.2, 153.6, 143.3, 142.3, 137.4, 130.7, 129.8, 128.5, 127.4, 125.2, 124.2, 122.5, 119.7, 118.0, 117.3, 115.8, 114.9, 109.9, 63.6, 47.5, 43.0, 39.2, 38.3, 33.1, 29.8, 29.0, 28.2, 27.9, 26.8, 26.3, 23.6, 22.5, 20.4, 14.9 ppm. ESI: m/z calcd for C₄₀H₅₁N₅O₂ [M + 2H]²⁺, 316.70; found, 316.75; retention time, 8.82 min; HPLC purity, 98%.

2-(4-Ethoxybenzyl)-1-isopentyl-N-(6-((1,2,3,4-tetrahydroacridin-9-yl)amino)hexyl)-1H-benzo[d]imidazole-5-carboxamide (4e). The reaction was carried out according to general procedure V using 2-(4-ethoxybenzyl)-1-isopentyl-1H-benzo[d]imidazole-5-carboxylic acid **24** (114 mg, 0.31 mmol), N^1-(1,2,3,4-tetrahydroacridin-9-yl)hexane-1,6-diamine **12e** (92.2 mg, 0.31 mmol), HBTU (118 mg, 0.31 mmol), and NEt₃ (65.1 μL, 0.47 mmol). The crude product was purified by column chromatography (20:1:0.1 CH₂Cl₂/MeOH/NH₃₍aq₎ (25%)), and product **4e** (40.0 mg, 61.9 μmol, 20%) was obtained as a yellow oil. ^{1}H NMR (400 MHz, CDCl₃): δ 8.11 (s, 1H), 8.05 (d, J = 8.2 Hz, 1H), 7.78–7.75 (m, 2H), 7.55–7.50 (m, 1H), 7.37–7.32 (m, 1H), 7.29–7.26 (m, 1H), 7.08 (d, J = 8.8 Hz, 2H), 6.74 (d, J = 8.8 Hz, 2H), 4.21 (s, 2H), 4.02–3.86 (m, 6H), 3.64 (t, J = 6.6 Hz, 2H), 3.47–3.40 (m, 2H), 2.62 (t, J = 5.7 Hz, 2H), 1.87–1.80 (m, 4H), 1.75–1.68 (m, 2H), 1.65–1.59 (m, 2H), 1.56–1.51 (m, 1H), 1.42–1.32 (m, 9H), 0.88 (d, J = 6.6 Hz, 6H) ppm. ^{13}C NMR (101 MHz, CDCl₃): δ 168.3, 158.2, 155.2, 154.7, 153.4, 143.3, 142.2, 137.5, 130.5, 129.6, 128.9, 127.7, 124.4, 124.0, 122.0, 118,1, 118.0, 117,0, 115,1, 114,9, 109.6, 63.6, 48.9, 42.8, 42.5, 39.9, 38.2, 36.6, 33.8, 31.3, 31.1, 29.5, 26.4, 26.2, 24.1, 22.4, 21.8, 14.9 ppm. ESI: m/z calcd for C₄₁H₅₃N₅O₂ [M + 2H]²⁺, 323.71; found, 323.80; retention time, 8.94 min; HPLC purity, 95%.

2-(4-Ethoxybenzyl)-N-ethyl-1-isopentyl-N-(4-((1,2,3,4-tetrahydroacridin-9-yl)amino)butyl)-1H-benzo[d]imidazole-5-carboxamide (5). The reaction was carried out according to general procedure V using 2-(4-ethoxybenzyl)-1-isopentyl-1H-benzo[d]imidazole-5-carboxylic acid **24** (23.7 mg, 64.6 μmol), N^1-ethyl-N^4-(1,2,3,4-tetrahydroacridin-9-yl)butane-1,4-diamine **14** (16.0 mg, 53.8 μmol), HBTU (24.5 mg, 64.6 μmol), and NEt₃ (14.9 μL, 0.11 mmol). The solvent was removed in vacuo, and the residue was dissolved in CH₂Cl₂ and washed with NaHCO₃₍aq₎. The crude product was purified by preparative TLC (20:1:0.1 CH₂Cl₂/MeOH/NH₃₍aq₎ (25%)). The

product **5** (21 mg, 32.5 μmol, 60%) was obtained as a brown oil. ^{1}H NMR (400 MHz, CDCl₃): δ 7.89 (d, J = 8.1 Hz, 1H), 7.75–7.73 (s, 1H), 7.56–7.51 (m, 1H), 7.36–7.30 (m, 1H), 7.27–7.23 (m, 3H), 7.14 (d, J = 8.6 Hz, 2H), 6.82 (d, J = 8.6 Hz, 2H), 4.24 (s, 2H), 4.02–3.95 (m, 4H), 3.58–3.42 (m, 4H), 3.08–3.03 (m, 2H), 2.77–2.69 (m, 2H), 1.94–1.88 (m, 4H), 1.83–1.65 (m, 6H), 1.59–1.51 (m, 1H), 1.41–1.35 (m, 6H), 1.29–1.23 (m, 2H), 0.90 (d, J = 6.6 Hz, 6H) ppm. ^{13}C NMR (101 MHz, CDCl₃): δ 168.4, 158.2, 155.4, 154.8, 153.7, 142.2, 142.2, 137.5, 130.5, 129.6, 128.9, 127.9, 125.0, 124.0, 121.3, 119.9, 117.8, 116.9, 115.2, 115.0, 109.7, 63.6, 52.4, 48.0, 44.1, 42.8, 41.1, 38.3, 33.9, 30.5, 28.3, 26.3, 24.2, 22.5, 22.3, 21.2, 14.9, 14.2. ppm. ESI: m/z calcd for C₄₁H₅₂N₅O₂ [M + 1H]¹⁺, 646.41; found, 646.25; retention time 8.94 min; HPLC purity, 99%.

2-(4-Ethoxybenzyl)-N,N-diethyl-1-(2-(2-(2-((1,2,3,4-tetrahydroacridin-9-yl)amino)ethoxy)ethoxy)ethyl)-1H-benzo[d]imidazole-5-carboxamide (6). The reaction was carried out according to general procedure V using 3-(2-(4-ethoxyphenyl)acetamido)-N,N-diethyl-4-((2-(2-(2-((1,2,3,4-tetrahydroacridin-9-yl)amino)ethoxy)ethoxy)ethyl)amino)benzamide **19f** (398 mg, 0.58 mmol). The crude product was purified by column chromatography (CH₂Cl₂/MeOH/NH₃₍aq₎ (25%) 16:1:0.1), and product **6** (220 mg, 33.1 mmol, 57%) was obtained as a brown oil. ^{1}H NMR (400 MHz, CDCl₃): δ 7.95–7.89 (m, 2H), 7.68 (s, 1H), 7.50 (t, J = 6.9 Hz, 1H), 7.31–7.27 (m, 1H), 7.22 (d, J = 8.3, 1H), 7.07 (d, J = 8.4 Hz, 2H), 6.73 (d, J = 8.4 Hz, 2H), 4.25 (s, 2H), 4.13 (t, J = 5.4 Hz, 2H), 3.90 (q, J = 7.0 Hz, 2H), 3.58 (t, J = 5.1 Hz, 2H), 3.51 (t, J = 5.4 Hz, 2H), 3.46–3.41 (m, 4H), 3.54–3.32 (m, 4H), 3.39–3.35 (m, 2H), 3.02 (t, J = 6.0 Hz, 2H), 2.62 (t, J = 5.9 Hz, 2H), 1.86–1.75 (m, 4H), 1.31 (t, J = 7.0 Hz, 3H), 1.21–1.06 (m, 6H) ppm. ^{13}C NMR (101 MHz, CDCl₃): δ 171.7, 158.0, 157.1, 155.3, 151.6, 145.5, 142.0, 135.1, 131.1, 129.5, 129.1, 127.9, 126.9, 124.1, 123.0, 122.2, 119.7, 117.4, 116.4, 114.8, 109.8, 70.8, 70.3, 69.4, 63.4, 48.2, 47.9, 44.1, 33.5, 32.6, 24.4, 22.7, 22.3, 14.8, 14.1 ppm. ESI: m/z calcd for C₄₀H₅₁N₅O₄ [M + 2H]²⁺, 332.70; found, 332.70; retention time, 7.89 min; HPLC purity, 99%.

2-(4-Ethoxybenzyl)-1-isopentyl-N-(2-(2-(2-((1,2,3,4-tetrahydroacridin-9-yl)amino)ethoxy)ethoxy)ethyl)-1H-benzo[d]imidazole-5-carboxamide (7). The reaction was carried out according to general procedure V using 2-(4-ethoxybenzyl)-1-isopentyl-1H-benzo[d]imidazole-5-carboxylic acid **24** (40 mg, 0.11 mmol), N-(2-(2-(2-aminoethoxy)ethoxy)ethyl)-1,2,3,4-tetrahydroacridin-9-amine **12f** (36.2 mg, 0.11 mmol), HBTU (41.7 mg, 0.11 mmol), and NEt₃ (23.6 μL, 0.17 mmol). The crude product was purified by column chromatography (16:1:0.1 CH₂Cl₂/MeOH/NH₃₍aq₎ (25%)), and product **7** (33.0 mg 48.7 μmol, 44%) was obtained as a brown oil. ^{1}H NMR (400 MHz, CDCl₃): δ 8.08 (s, 1H), 8.00 (d, J = 8.1 Hz, 1H), 7.94 (d, J = 8.4 Hz, 1H), 7.72 (d, J = 8.5, 1H), 7.56–7.52 (m, 1H), 7.32 (t, J = 8.0, 1H), 7.15 (d, J = 8.5 Hz, 1H), 7.08 (d, J = 8.6 Hz, 2H), 6.76 (d, J = 8.7 Hz, 2H), 4.17 (s, 2H), 3.95–3.90 (m, 4H), 3.85–3.81 (m, 2H), 3.72–3.67 (m, 10H), 3.02–2.98 (m, 2H), 2.58 (t, J = 7.8 Hz, 2H), 1.85–1.78 (m, 4H), 1.56–1.49 (m, 1H), 1.35 (t, J = 7.0 Hz, 3H), 1.30–1.27 (m, 2H), 0.86 (d, J = 6.6 Hz, 6H) ppm. ^{13}C NMR (101 MHz, CDCl₃): δ 168.0, 158.2, 155.2, 154.95, 153.3, 143.0, 142.1, 137.5, 130.5, 129.7, 128.5, 127.7, 124.6, 123.7, 122.1, 118.4, 117.9, 117.0, 114.7, 114.9, 109.5, 70.4, 70.3, 70.0, 69.9, 63.6, 48.1, 42.8, 39.8, 38.2, 33.8, 31.2, 29.8, 26.2, 23.9, 22.4, 21.8, 14.9 ppm. ESI: m/z calcd for C₄₁H₅₃N₅O₄ [M + 2H]²⁺, 339.80; found, 339.70; retention time, 8.75 min; HPLC purity, 98%.

2-(4-Ethoxybenzyl)-1-isopentyl-N-(2-((2-((1,2,3,4-tetrahydroacridin-9-yl)amino)ethyl)disulfaneyl)ethyl)-1H-benzo[d]imidazole-5-carboxamide (8). The reaction was carried out according to general procedure V using 2-(4-ethoxybenzyl)-1-isopentyl-1H-benzo[d]imidazole-5-carboxylic acid **24** (48 mg, 0.13 mmol), N-(2-((2-aminoethyl)disulfaneyl)ethyl)-1,2,3,4-tetrahydroacridin-9-amine (35 mg, 0.11 mmol), HBTU (49 mg, 0.13 mmol), and NEt₃ (26 μL, 0.19 mmol). The crude product was purified by preparative thin-layer chromatography (18:1:0.1 CH₂Cl₂/MeOH/NH₃₍aq₎ (25%)), and product **8** (35 mg, 51.4 μmol, 47%) was obtained as a yellow oil. ^{1}H NMR (400 MHz, CDCl₃): δ = 8.15 (d, J = 1.3 Hz, 1H), 8.00–7.96 (m, 1H), 7.84 (dd, J = 8.5, 0.8 Hz, 1H), 7.77 (dd, J = 8.5, 1.6 Hz, 1H), 7.53–7.50 (m, 1H), 7.35–7.32 (m, 1H), 7.29–7.25 (m, 1H), 7.13–7.08 (m,

2H), 6.86 (t, J = 5.8 Hz, 1H), 6.80−6.76 (m, 2H), 4.23 (s, 2H), 4.01−3.92 (m, 4H), 3.89−3.82 (m, 2H), 3.75 (q, J = 6.3 Hz, 2H), 3.04−2.96 (m, 2H), 2.95−2.86 (m, 4H), 2.71 (s, 2H), 1.86 (t, J = 2.8 Hz, 4H), 1.62−1.50 (m, 1H), 1.42−1.33 (m, 5H), 0.88 (d, J = 5.3 Hz, 6H) ppm. ^{13}C NMR (101 MHz, CDCl$_3$): δ 168.3, 158.2, 157.4, 155.3, 151.2, 145.8, 142.3, 137.7, 129.6, 129.4, 128.4, 127.7, 127.1, 124.4, 123.1, 122.1, 119.9, 118.2, 116.6, 115.0, 109.6, 63.6, 46.9, 42.9, 39.0, 38.9, 38.2, 37.9, 33.8, 33.0, 26.3, 24.8, 22.8, 22.5, 14.9 ppm. ESI: m/z calcd for C$_{39}$H$_{49}$N$_5$O$_2$S$_2$ [M + 2H]$^{2+}$, 341.66; found, 341.70; retention time, 9.38 min; HPLC purity, 96%.

9-Chloro-1,2,3,4-tetrahydroacridine (11). 2-Aminobenzoic acid **9** (1.00 g, 7.29 mmol) and cyclohexanone **10** (883 μL, 8.53 mmol) were combined in a flask and cooled down to 0 °C. Then, POCl$_3$ (8.00 mL) was slowly added. Afterward, the mixture was stirred for 3 h under reflux conditions and then concentrated to a slurry in vacuo. The slurry was dissolved in ethyl acetate and neutralized with aqueous sodium hydroxide. The mixture was extracted with ethyl acetate. The organic layers were combined and dried over anhydrous MgSO$_4$, and the solvent was removed in vacuo. The crude product was purified by recrystallization from acetone. The product **11** (988 mg, 4.54 mmol, 62%) was obtained as a brown solid. mp = 66 °C. ^{1}H NMR (400 MHz, CDCl$_3$): δ 8.17 (d, J = 8.4, 1H), 7.98 (d, J = 8.5 Hz, 1H), 7.69−7.63 (m, 1H), 7.56−7.50 (m, 1H), 3.13 (t, J = 5.6 Hz, 2H), 3.03 (t, J = 6.4 Hz, 2H), 1.97−1.93 (m, 4H) ppm. ^{13}C NMR (101 MHz, CDCl$_3$): δ 159.4, 146.2, 141.8, 129.4, 128.9, 128.3, 126.6, 125.4, 123.7, 33.9, 27.5, 22.6, 21.5 ppm. ESI: m/z calcd for C$_{13}$H$_{13}$ClN [M + H]$^+$, 218.07; found, 218.00; retention time, 9.97 min.

N^1-(1,2,3,4-Tetrahydroacridin-9-yl)ethane-1,2-diamine (12a). The reaction was carried out according to general procedure I using 9-chloro-1,2,3,4-tetrahydroacridine **11** (800 mg, 3.67 mmol) and ethane-1,2-diamine (1.23 mL, 18.35 mmol). The product **12a** (557 mg, 2.31 mmol, 63%) was obtained as a brown oil. ^{1}H NMR (400 MHz, CDCl$_3$): δ 7.94 (d, J = 8.4 Hz, 1H), 7.85 (d, J = 8.5 Hz, 1H), 7.48 (t, J = 10.0, 5.1 Hz, 1H), 7.26 (t, 1H), 4.75 (s, 1H), 3.43−3.36 (m, 2H), 3.03−2.97 (m, 2H), 2.89−2.81 (m, 2H), 2.72−2.65 (m, 2H), 1.86−1.80 (m, 4H) ppm. ^{13}C NMR (101 MHz, CDCl$_3$): δ 157.5, 149.9, 146.4, 127.7, 127.2, 122.6, 121.8, 119.5, 115.5, 50.0, 41.4, 33.0, 23.8, 22.0, 21.8 ppm. ESI: m/z calcd for C$_{15}$H$_{20}$N$_3$ [M + H]$^+$, 242.17; found, 242.10; retention time, 4.09 min.

N^1-(1,2,3,4-Tetrahydroacridin-9-yl)propane-1,3-diamine (12b). The reaction was carried out according to general procedure I using 9-chloro-1,2,3,4-tetrahydroacridine **11** (600 mg, 2.76 mmol) and propane-1,3-diamine (1.15 mL, 13.8 mmol). The product **12b** (530 mg, 1.97 mmol, 80%) was obtained as a brown oil (417 mg, 1.63 mmol, 59%). ^{1}H NMR (400 MHz, CDCl$_3$): δ 7.87 (m, 1H), 7.83−7.79 (m, 1H), 7.46−7.39 (m, 1H), 7.24−7.19 (1 H), 3.48 (t, J = 6.7 Hz, 2H), 3.01 (t, J = 6.1 Hz, 2H), 2.89 (t, J = 6.2 Hz, 2H), 2.60 (t, J = 5.9 Hz, 2H), 1.85−1.76 (m, 4H), 1.85−1.76 (m, 2H) ppm. ^{13}C NMR (101 MHz, CDCl$_3$): δ 157.3, 149.9, 146.3, 127.6, 127.2, 122.6, 121.9, 119.1, 114.8, 47.0, 39.4, 33.1, 26.4, 24.1, 22.1, 21.8 ppm. ESI: m/z calcd for C$_{16}$H$_{22}$N$_3$ [M + H]$^+$, 256.18; found, 256.10; retention time, 4.26 min.

N^1-(1,2,3,4-Tetrahydroacridin-9-yl)butane-1,4-diamine (12c). The reaction was carried out according to general procedure I using 9-chloro-1,2,3,4-tetrahydroacridine **11** (535 mg, 2.45 mmol) and butane-1,4-diamine (1.08 g, 12.3 mmol). The product **12c** (530 mg, 1.97 mmol, 80%) was obtained as a brown oil. ^{1}H NMR (400 MHz, CDCl$_3$): δ 7.99−7.92 (m, 2H), 7.57−7.52 (m, 1H), 7.36−7.31 (m, 1H), 3.53 (t, J = 7.1 Hz, 2H), 3.07 (t, J = 6.3 Hz, 2H), 2.76 (t, J = 6.9 Hz, 2H), 2.71 (t, J = 6.2 Hz, 2H), 1.93−1.88 (m, 4H), 1.76−1.68 (m, 2H), 1.61−1.52 (m, 2H) ppm. ^{13}C NMR (101 MHz, CDCl$_3$): δ 157.9, 151.1, 146.7, 128.6, 128.1, 123.7, 122.9, 119.9, 115.6, 49.29, 41.72, 33.56, 30.76, 29.06, 24.82, 22.98, 22.61 ppm. ESI: m/z calcd for C$_{17}$H$_{24}$N$_3$ [M + H]$^+$, 270.20; found, 270.10; retention time, 4.26 min.

N^1-(1,2,3,4-Tetrahydroacridin-9-yl)pentane-1,5-diamine (12d). The reaction was carried out according to general procedure I using 9-chloro-1,2,3,4-tetrahydroacridine **11** (600 mg, 2.76 mmol) and pentane-1,5-diamine (1.62 mL, 13.8 mmol). The product **12d** (427 mg, 1.51 mmol, 55%) was obtained as a brown oil. ^{1}H NMR (400 MHz, CDCl$_3$): δ 8.09 (d, J = 8.4 Hz, 1H), 7.91−7.86 (m, 1H), 7.62−7.56 (m, 1H), 7.30−7.24 (m, 1H), 3.41 (t, J = 7.0 Hz, 2H), 3.07−3.03 (m, 2H),

3.02−2.98 (m, 2H), 2.96−2.89 (m, 2H), 2.66−2.60 (m, 4H), 1.62−1.39 (m, 6H) ppm. ^{13}C NMR (101 MHz, CDCl$_3$): δ 158.5, 150.6, 146.6, 128.6, 128.2, 123.5, 122.7, 120.3, 115.9, 49.3, 41.9, 33.2, 32.8, 31.7, 27.4, 24.8, 23.0, 22.6 ppm. ESI: m/z calcd for C$_{18}$H$_{26}$N$_3$ [M + H]$^+$, 284.21; found, 284.15; retention time, 4.66 min.

N^1-(1,2,3,4-Tetrahydroacridin-9-yl)hexane-1,6-diamine (12e). The reaction was carried out according to general procedure I using 9-chloro-1,2,3,4-tetrahydroacridine **11** (500 mg, 2.30 mmol) and hexane-1,6-diamine (1.50 mL, 11.5 mmol). The product **12e** was obtained as a brown oil (343 mg, 1.15 mmol, 50%). ^{1}H NMR (400 MHz, CDCl$_3$): δ 7.94 (d, J = 8.4 Hz, 1H), 7.89 (d, J = 8.4 Hz, 1H), 7.53 (t, J = 6.8 Hz, 1H), 7.32 (t, J = 6.8 Hz, 1H), 3.47 (t, J = 7.2 Hz, 2H), 3.04 (t, J = 6.5 Hz, 2H), 2.72−2.65 (m, 4H), 1.92−1.88 (m, 4H), 1.69−1.60 (m, 2H), 1.46−1.35 (m, 6H) ppm. ^{13}C NMR (101 MHz, CDCl$_3$): δ 158.8, 151.0, 147.74, 129.0, 128.8, 124.1, 123.3, 120.6, 116.2, 49.9, 42.5, 34.4, 34.0, 32.2, 27.3, 27.1, 25.2, 23.4, 23.2 ppm. ESI: m/z calcd for C$_{19}$H$_{28}$N$_3$ [M + 2H]$^{2+}$, 149.62; found, 149.65; retention time, 5.38 min.

N-(2-(2-(2-Aminoethoxy)ethoxy)ethyl)-1,2,3,4-tetrahydroacridin-9-amine (12f). The reaction was carried out according to general procedure I using 9-chloro-1,2,3,4-tetrahydroacridine **11** (600 mg, 2.76 mg) and 2,2′-(ethane-1,2-diylbis(oxy))bis(ethan-1-amine) (2.00 mL, 13.8 mmol). The product **12f** (864 mg, 2.62 mmol, 95%) was obtained as a brown oil. ^{1}H NMR (400 MHz, CDCl$_3$): δ = 7.95 (d, J = 8.5 Hz, 1H), 7.89 (d, J = 8.5 Hz, 1H), 7.58−7.59 (m, 1H), 7.37−75.30 (m, 1H), 3.67−3.56 (m, 8H), 3.50 (t, J = 5.2 Hz, 2H), 3.05 (t, J = 6.0 Hz, 2H), 2.88−2.84 (m, 2H), 2.76 (t, J = 5.7 Hz, 2H), 1.94−1.86 (m, 4H) ppm. ^{13}C NMR (101 MHz, CDCl$_3$): δ 158.7, 150.4, 147.5, 128.8, 128.2, 123.8, 122.7, 120.8, 117.5, 73.6, 70.5, 70.3, 70.3, 48.6, 41.8, 24.7, 23.1, 22.9, 22.6 ppm. ESI: m/z calcd for C$_{19}$H$_{28}$N$_3$O$_2$ [M + H]$^+$, 330.22; found, 330.05; retention time, 4.60 min.

N-(2-((2-Aminoethyl)disulfaneyl)ethyl)-1,2,3,4-tetrahydroacridin-9-amine (12g). 2,2′-Dithiobis(ethylamine)dihydrochloride (608 mg, 2.70 mmol) was suspended in hexanol, and NEt$_3$ (1.49 mL, 10.8 mmol) was added. The reaction vessel was closed and stirred for 30 min at 160 °C. Then, 9-chloro-1,2,3,4-tetrahydroacridine **11** (117 mg, 0.54 mg) was added, and the mixture was stirred for further 12 h at 160 °C. The solvent was removed under high vacuum at 60 °C. The crude product was purified using RP flash chromatography to yield **12g** (80 mg, 0.33 mmol, 44%) as a pale yellow oil. ^{1}H NMR (400 MHz, MeOD): δ 8.44 (d, J = 8.7 Hz, 1H), 7.88−7.86 (m, 2H), 7.65−7.61 (m, 1H), 4.33 (t, J = 6.6 Hz, 2H), 3.34−3.29 (m, 2H), 3.24 (t, J = 6.6 Hz, 2H), 3.08 (t, J = 5.3 Hz, 2H), 3.03 (t, J = 6.9 Hz, 2H), 2.79 (t, J = 5.7 Hz, 2H), 2.02−1.94 (m, 4H) ppm. ^{13}C NMR (101 MHz, MeOD): δ = 156.8, 151.0, 138.2, 132.8, 125.3, 124.9, 118.9, 115.9, 112.3, 46.29, 38.0, 36.7, 33.7, 28.1, 23.9, 21.6, 20.4 ppm. ESI: m/z calcd for C$_{17}$H$_{24}$N$_3$S$_2$ [M + H]$^+$, 334.14; found, 334.00; retention time, 5.31 min.

N-(4-((1,2,3,4-Tetrahydroacridin-9-yl)amino)butyl)acetamide (13). N^1-(1,2,3,4-Tetrahydroacridin-9-yl)butane-1,4-diamine **12c** (51.0 mg, 0.19 mmol) was dissolved in CH$_2$Cl$_2$, and acetic acid anhydride (359 μL, 3.80 mmol) was added at room temperature. After stirring for 5 min, the mixture was basified by washing with a saturated NaHCO$_3$ solution. The organic layer was dried over anhydrous MgSO$_4$ and concentrated in vacuo. The product **13** (59.2 mg, 0.19 mmol, quant.) was obtained as a pale yellow oil. ^{1}H NMR (400 MHz, CDCl$_3$): δ 8.13−8.10 (m, 1H), 7.95−7.91 (m, 1H), 7.53−7.48 (m, 1H), 7.34−7.30 (m, 1H), 3.79 (t, J = 7.1 Hz, 2H), 3.26 (q, J = 6.5 Hz, 2H), 2.99 (t, J = 6.0 Hz, 2H), 2.55 (t, J = 5.7 Hz, 2H), 1.84−1.75 (m, 6H), 1.66−1.59 (m, 2H), 1.23 (s, 3H) ppm. ^{13}C NMR (101 MHz, CDCl$_3$): δ 171.2, 155.11 151.7, 139.3, 131.6, 124.7, 124.3, 120.8, 116.2, 111.3, 47.8, 38.7, 28.5, 28.1, 26.5, 24.1, 23.1, 22.0, 20.8 ppm. ESI: m/z calcd for C$_{19}$H$_{26}$N$_3$O [M + H]$^+$, 312.21; found, 312.05; retention time, 6.58 min.

N^1-Ethyl-N^4-(1,2,3,4-tetrahydroacridin-9-yl)butane-1,4-diamine (14). N-(4-((1,2,3,4-Tetrahydroacridin-9-yl)amino)butyl)acetamide **13** (218 mg, 0.70 mmol) was dissolved in dry THF. LiAlH$_4$ (133 mg, 3.50 mmol) was added, the mixture was stirred for 48 h under reflux conditions, and then NH$_{3(aq)}$ (25%) was carefully added to the mixture on ice. The mixture was concentrated in vacuo, dissolved in ethyl acetate, and washed with a mixture of water/NH$_{3(aq)}$ (25%) (1:1). The combined organic layers were dried over anhydrous MgSO$_4$ and concentrated in vacuo. The crude product was purified by column

chromatography (4:1:0.1 CH_2Cl_2/MeOH/$NH_{3(aq)}$ (25%)). The product **14** (144 mg, 0.48 mmol, 69%) was obtained as a yellow oil. ^1H NMR (400 MHz, $CDCl_3$): δ 7.98–7.90 (m, 2H), 7.56–7.51 (m, 1H), 7.35–7.29 (m, 1H), 3.52 (t, J = 6.8 Hz, 2H), 3.07–3.03 (m, 2H), 2.72–2.65 (m, 6H), 1.92–1.86 (m, 4H), 1.76–1.61(m, 4H), 1.14 (t, J = 7.2 Hz, 3H) ppm. ^{13}C NMR (101 MHz, $CDCl_3$): δ = 157.8, 151.2, 146.6, 128.7, 127.9, 123.8, 123.0, 119.9, 115.6, 49.2, 49.0, 44.0, 33.5, 29.3, 27.1, 24.8, 23.0, 22.6, 14.7 ppm. ESI: m/z calcd for $C_{19}H_{28}N_3$ [M + 2H]$^{2+}$, 149.62; found, 149.65; retention time, 4.77 min.

N,N-Diethyl-4-fluoro-3-nitrobenzamide (16). 4-Fluoro-3-nitrobenzoic acid **15** (1.00 g, 5.4 mmol) was dissolved in CH_2Cl_2 and cooled down to 0 °C. A catalytic amount of *N,N*-dimethylformamide was added, and oxalylchloride (2.31 mL, 27.01 mmol) was added dropwise. The mixture was stirred for 10 min at 0 °C, allowed to come to room temperature, and then stirred again for 1 h. The mixture was then evaporated, and the residue was dissolved in CH_2Cl_2 and cooled down to 0 °C. Then, a mixture of HNEt$_2$ (621 μL, 1.1 mmol) and NEt$_3$ (2.24 mL, 16.2 mmol) in CH_2Cl_2 was slowly added to the cold mixture. After stirring for 3 h at room temperature, the mixture was washed with water. The combined organic layers were dried over anhydrous MgSO$_4$ and concentrated in vacuo. The product **16** (918 mg, 3.82 mmol, 71%) was obtained as a yellow oil. ^1H NMR (400 MHz, $CDCl_3$): δ 8.11 (d, J = 7.0 Hz, 1H), 7.66–7.70 (m, 1 H), 7.35 (d, J = 10.4 Hz, 1H), 3.65–3.18 (m, 4H), 1.30–1.11 (m, 6H) ppm. ^{13}C NMR (101 MHz, $CDCl_3$): δ 167.5, 156.8, 154.1, 136.9, 133.8, 124.4, 118.8, 43.4, 14.0 ppm. ESI: m/z calcd for $C_{11}H_{14}FN_2O_3$ [M + H]$^+$, 241.10; found, 241.10.

N,N-Diethyl-3-nitro-4-((2-((1,2,3,4-tetrahydroacridin-9-yl)-amino)ethyl)amino)benzamide (17a). The reaction was carried out according to general procedure II using *N,N*-diethyl-4-fluoro-3-nitrobenzamide **16** (351 mg, 1.46 mmol), **12a** (388 mg, 1.61 mmol), and NEt$_3$ (304 μL, 2.19 mmol). The crude product was purified by column chromatography (20:1:0.1 CH_2Cl_2/MeOH/$NH_{3(aq)}$ (25%)). The product **17a** (475 mg, 1.03 mmol, 71%) was obtained as a yellow oil. ^1H NMR (400 MHz, $CDCl_3$): δ 8.27 (t, J = 5.2 Hz, 1H), 8.24 (d, J = 1.8 Hz, 1H), 7.91 (t, J = 8.5 Hz, 2H), 7.53 (t, J = 7.6 Hz, 1H), 7.46 (d, J = 8.8 Hz, 1H), 7.33 (t, J = 7.6 Hz, 1H), 6.76 (d, J = 8.8 Hz, 1H), 4.27 (s, 1H), 3.77–3.70 (m, 2H), 3.55–3.48 (m, 2H), 3.46–3.32 (m, 4H), 3.04 (t, J = 6.0 Hz, 2H), 2.71 (t, J = 5.8 Hz, 2H), 1.91–1.81 (m, 4H), 1.18 (t, J = 7.0 Hz, 6H) ppm. ^{13}C NMR (101 MHz, $CDCl_3$): δ 169.2, 158.9, 149.5, 147.3, 145.5, 135.1, 131.3, 128.9, 128.6, 125.7, 124.5, 124.4, 122.2, 120.8, 118.2, 113.8, 47.4, 43.6, 34.0, 25.0, 22.9, 22.7 ppm. ESI: m/z calcd for $C_{26}H_{33}N_5O_3$ [M + H]$^+$, 462.57; found, 462.15; retention time, 7.718 min.

N,N-Diethyl-3-nitro-4-((3-((1,2,3,4-tetrahydroacridin-9-yl)-amino)propyl)amino)benzamide (17b). The reaction was carried out according to general procedure II using *N,N*-diethyl-4-fluoro-3-nitrobenzamide **16** (173 mg, 0.72 mmol), **12b** (165 mg, 0.65 mmol), and NEt$_3$ (136 μL, 0.98 mmol). The crude product was purified by flash chromatography (gradient CH_2Cl_2, MeOH), and the product **17b** (110 mg, 0.23 mmol, 36%) was obtained as a brown oil. ^1H NMR (400 MHz, $CDCl_3$): δ 8.23 (d, J = 2.0 Hz, 1H), 8.16 (t, J = 5.1 Hz, 1H), 7.89 (d, J = 8.4, 2H), 7.54–7.50 (m, 1H), 7.49–7.45 (m, 1H), 7.33–7.27 (m, 1H), 6.74 (d, J = 8.9 Hz, 1H), 3.60 (t, J = 6.9 Hz, 2H), 3.49–3.30 (m, 6H), 3.03 (t, J = 5.3 Hz, 2H), 2.68 (t, J = 5.5 Hz, 2H), 2.09–1.98 (m, 2H), 1.90–1.81 (m, 4H), 1.18 (t, J = 7.1 Hz, 6H) ppm. ^{13}C NMR (101 MHz, $CDCl_3$): δ = 169.9, 154.6, 151.6, 145.9, 143.1, 135.8, 130.3, 129.1, 128.6, 124.2, 124.8, 123.5, 122.6, 119.0, 115.5, 113.8, 52.9, 42.6, 41.6, 34.7, 26.9, 24.5, 22.4, 22.0, 13.3 ppm. ESI: m/z calcd for $C_{27}H_{34}N_5O_3$ [M + H]$^+$, 476.26; found, 476.15; retention time, 7.83 min.

N,N-Diethyl-3-nitro-4-((4-((1,2,3,4-tetrahydroacridin-9-yl)-amino)butyl)amino)benzamide (17c). The reaction was carried out according to general procedure II using *N,N*-diethyl-4-fluoro-3-nitrobenzamide **16** (430 mg, 1.79 mmol), **12c** (439 mg, 1.63 mmol), and NEt$_3$ (340 μL, 2.45 mmol). The crude product was purified by flash chromatography (gradient CH_2Cl_2, MeOH), and the product **17c** (212 mg, 0.43 mmol, 26%) was obtained as a brown oil. ^1H NMR (400 MHz, $CDCl_3$): δ 8.26 (d, J = 2.0 Hz, 1H), 8.16 (t, J = 4.9 Hz, 1H), 7.96–7.92 (m, 2H), 7.58–7.51 (m, 2H), 7.37–7.32 (m, 1H), 6.81 (d, J = 8.9 Hz, 1H), 3.57 (t, J = 6.2 Hz, 2H), 3.45–3.33 (m, 6H), 3.09–3.05 (m, 2H), 2.72–2.67 (m, 2H), 1.92–1.86 (m, 4H), 1.85–1.79 (m, 4H), 1.20 (t, J

= 7.1 Hz, 6H) ppm. ^{13}C NMR (101 MHz, $CDCl_3$): δ 169.4, 154.4, 151.0, 146.6, 145.8, 135.4, 131.0, 128.9, 128.1, 125.8, 124.2, 124.1, 122.8, 120.0, 116.1, 113.9, 53.6, 48.9, 42.9, 33.5, 29.3, 26.5, 25.0, 23.0, 22.7, 13.8 ppm. ESI: m/z calcd for $C_{28}H_{36}N_5O_3$ [M + H]$^+$, 490.28; found, 490.15; retention time, 8.04 min.

N,N-Diethyl-3-nitro-4-((5-((1,2,3,4-tetrahydroacridin-9-yl)-amino)pentyl)amino)benzamide (17d). The reaction was carried out according to general procedure II using *N,N*-diethyl-4-fluoro-3-nitrobenzamide **16** (221 mg, 0.92 mmol), **12d** (237 mg, 0.84 mmol), and NEt$_3$ (173 μL, 1.26 mmol). The crude product was purified by flash chromatography (gradient CH_2Cl_2, MeOH), and the product **17d** (160 mg, 0.32 mmol, 38%) was obtained as a brown oil. ^1H NMR (400 MHz, $CDCl_3$): δ 8.21 (d, J = 2.0 Hz, 1H), 8.13–8.05 (m, 3H), 7.56–7.51 (m, 1H), 7.50–7.46 (m, 1H), 7.35–7.30 (m, 1H), 6.81 (d, J = 8.9 Hz, 1H), 3.72 (t, J = 7.2 Hz, 2H), 3.45–3.35 (m, 3H), 3.33–3.27 (m, 2H), 3.12–3.07 (m, 2H), 2.67–2.63 (m, 2H), 1.87–1.79 (m, 6H), 1.77–1.70 (m, 2H), 1.58–1.50 (m, 2H), 1.17 (t, J = 7.1 Hz, 6H) ppm. ^{13}C NMR (101 MHz, $CDCl_3$): δ 169.4, 154.6, 153.3, 145.8, 142.7, 135.2, 130.7, 130.4, 125.7, 124.5, 124.3, 123.8, 123.7, 118.0, 114.0, 113.5, 53.1, 48.5, 42.9, 31.1, 30.0, 28.6, 24.6, 24.3, 22.5, 21.7, 13.7 ppm. ESI: m/z calcd for $C_{29}H_{38}N_5O_3$ [M + H]$^+$, 504.30; found, 504.15; retention time, 8.36 min.

N,N-Diethyl-3-nitro-4-((6-((1,2,3,4-tetrahydroacridin-9-yl)-amino)hexyl)amino)benzamide (17e). The reaction was carried out according to general procedure II using *N,N*-diethyl-4-fluoro-3-nitrobenzamide **16** (341 mg, 1.42 mmol), **12e** (458 mg, 1.56 mmol), and NEt$_3$ (297 μL, 2.13 mmol). The product **17e** (230 mg, 0.44 mmol, 31%) was obtained as a brown oil and used in the next reaction step without further purification. ^1H NMR (400 MHz, $CDCl_3$): δ 8.55 (d, J = 8.4 Hz, 1H), 8.26 (d, J = 2.0 Hz, 1H), 8.18–8.13 (m, 2H), 7.73–7.67 (m, 1H), 7.57–7.52 (m, 1H), 7.48–7.42 (m, 1H), 6.86 (d, J = 8.9 Hz, 1H), 3.94 (t, J = 7.0 Hz, 2H), 3.51–3.37 (m, 4H), 3.36–3.29 (m, 4H), 2.60 (t, J = 6.2 Hz, 2H), 1.91–1.83 (m, 4H), 1.69–1.58 (m, 4H), 1.57–1.53 (m, 4H), 1.21 (t, J = 7.1 Hz, 6H) ppm. ^{13}C NMR (101 MHz, $CDCl_3$): δ 168.5, 155.45, 152.0, 146.0, 142.04 135.4, 129.52, 129.2, 125.4, 124.9, 123.7, 123.2, 121.6, 118.7, 114.0, 113.6, 53.1, 48.2, 43.0, 31.3, 31.2, 28.8, 26.8, 26.6, 26.3, 23.8, 20.8, 13.8 ppm. ESI: m/z calcd for $C_{30}H_{40}N_5O_3$ [M + H]$^+$, 518.31; found, 518.40; retention time, 8.55 min.

N,N-Diethyl-3-nitro-4-((2-(2-(2-((1,2,3,4-tetrahydroacridin-9-yl)-amino)ethoxy)ethoxy)ethyl)amino)benzamide (17f). The reaction was carried out according to general procedure II using *N,N*-diethyl-4-fluoro-3-nitrobenzamide **16** (475 mg, 1.98 mmol), **12f** (718 mg, 2.18 mmol), and NEt$_3$ (410 μL, 2.97 mmol). The crude product was purified by flash chromatography (gradient CH_2Cl_2/MeOH), and product **17f** (575 mg, 1.05 mmol, 53%) was obtained as a brown oil and used in the next reaction step without further purification. ^1H NMR (400 MHz, $CDCl_3$): δ 8.41–8.35 (m, 2H), 8.22 (d, J = 2.0 Hz, 1H), 8.11–8.07 (m, 1H), 7.66–7.60 (m, 1H), 7.56–7.52 (m, 1H), 7.42–7.37 (m, 1H), 6.86 (d, J = 8.9 Hz, 1H), 4.01–3.95 (m, 2H), 3.83–3.73 (m, 4H), 3.75–3.70 (m, 4H), 3.52–3.48 (m, 2H), 3.47–3.35 (m, 4H), 3.27–3.22 (m, 2H), 2.68–2.63 (m, 2H), 1.90–1.83 (m, 4H), 1.20 (t, J = 7.1 Hz, 6H) ppm. ^{13}C NMR (101 MHz, $CDCl_3$): δ 169.3, 154.30, 151.4, 145.8, 143.1, 135.4, 131.1, 125.7, 125.0, 124.3, 124.2, 123.6, 121.3, 117.6, 116.0, 114.1, 70.9, 70.5, 70.0, 69.0, 52.7, 48.1, 42.8, 30.1, 23.9, 22.4, 21.4, 13.7 ppm. ESI: m/z calcd for $C_{30}H_{40}N_5O_5$ [M + H]$^+$, 550.30; found, 550.25; retention time, 8.05 min.

3-Amino-N,N-diethyl-4-((2-((1,2,3,4-tetrahydroacridin-9-yl)-amino)ethyl)amino)benzamide (18a). The reaction was carried out according to general procedure III using *N,N*-diethyl-3-nitro-4-((2-((1,2,3,4-tetrahydroacridin-9-yl)amino)ethyl)amino)benzamide **17a** (475 mg, 1.03 mmol) and SnCl$_2$·2H$_2$O (1.44 g, 6.39 mmol). The product **18a** (325 mg, 0.75 mmol, 73%) was obtained as a colorless oil and directly used for the next reaction without purification. ESI: m/z calcd for $C_{26}H_{35}N_5O$ [M + H]$^+$, 432.28; found, 432.30; retention time, 7.534 min.

3-Amino-N,N-diethyl-4-((3-((1,2,3,4-tetrahydroacridin-9-yl)-amino)propyl)amino)benzamide (18b). The reaction was carried out according to general procedure III using *N,N*-diethyl-3-nitro-4-((3-((1,2,3,4-tetrahydroacridin-9-yl)amino)propyl)amino)benzamide **17b**

(110 mg, 0.23 mmol) and SnCl$_2$·2H$_2$O (323 mg, 1.43 mmol). The product **18b** (89.1 mg, 0.20 mmol, 87%) was obtained as a colorless oil and directly used for the next reaction without purification. ESI: *m/z* calcd for C$_{27}$H$_{36}$N$_5$O [M + H]$^+$, 223.65; found, 223.65; retention time, 7.84 min.

3-Amino-N,N-diethyl-4-((4-((1,2,3,4-tetrahydroacridin-9-yl)-amino)butyl)amino)benzamide (18c). The reaction was carried out according to general procedure III using *N,N*-diethyl-3-nitro-4-((4-((1,2,3,4-tetrahydroacridin-9-yl)amino)butyl)amino)benzamide **17c** (212 mg, 0.43 mmol) and SnCl$_2$·2H$_2$O (602 mg, 2.67 mmol). The product **18c** (154 mg, 0.34 mmol, 79%) was obtained as a colorless oil and directly used for the next reaction without purification. ESI: *m/z* calcd for C$_{28}$H$_{38}$N$_5$O [M + 2H]$^{2+}$, 230.66; found, 230.60; retention time, 7.17 min.

3-Amino-N,N-diethyl-4-((5-((1,2,3,4-tetrahydroacridin-9-yl)-amino)pentyl)amino)benzamide (18d). The reaction was carried out according to general procedure III using *N,N*-diethyl-3-nitro-4-((5-((1,2,3,4-tetrahydroacridin-9-yl)amino)pentyl)amino)benzamide **17d** (236 mg, 0.47 mmol) and SnCl$_2$·2H$_2$O (657 mg, 2.91 mmol). The product **18d** (222 mg, 0.47 mmol, quant.) was obtained as a colorless oil and directly used for the next reaction without purification. ESI: *m/z* calcd for C$_{29}$H$_{40}$N$_5$O [M + 2H]$^{2+}$, 237.67; found, 237.65; retention time, 7.73 min.

3-Amino-N,N-diethyl-4-((6-((1,2,3,4-tetrahydroacridin-9-yl)-amino)hexyl)amino)benzamide (18e). The reaction was carried out according to general procedure III using *N,N*-diethyl-3-nitro-4-((6-((1,2,3,4-tetrahydroacridin-9-yl)amino)hexyl)amino)benzamide **17e** (230 mg, 0.44 mmol) and SnCl$_2$·2H$_2$O (616 mg, 2.73 mmol). The product **18e** (140 mg, 0.29 mmol, 66%) was obtained as a colorless oil and directly used for the next reaction without purification. ESI: *m/z* calcd for C$_{30}$H$_{42}$N$_5$O [M + 2H]$^{2+}$, 244.68; found, 244.65; retention time, 7.93 min.

3-Amino-N,N-diethyl-4-((2-(2-(2-((1,2,3,4-tetrahydroacridin-9-yl)amino)ethoxy)ethoxy)ethyl)amino)benzamide (18f). The reaction was carried out according to general procedure III using *N,N*-diethyl-3-nitro-4-((2-(2-(2-((1,2,3,4-tetrahydroacridin-9-yl)amino)-ethoxy)ethoxy)ethyl)amino)benzamide **17f** (575 mg, 1.05 mmol) and SnCl$_2$·2H$_2$O (1.47 g, 8.51 mmol). The product **18f** (290 mg, 0.56 mmol, 53%) was obtained as a colorless oil and directly used for the next reaction without purification. ESI: *m/z* calcd for C$_{30}$H$_{42}$N$_5$O$_3$ [M + 2H]$^{2+}$, 260.67; found, 260.60; retention time, 7.50 min.

3-(2-(4-Ethoxyphenyl)acetamido)-N,N-diethyl-4-((2-((1,2,3,4-tetrahydroacridin-9-yl)amino)ethyl)amino)benzamide (19a). The reaction was carried out according to general procedure IV using 3-amino-*N,N*-diethyl-4-((2-((1,2,3,4-tetrahydroacridin-9-yl)amino)-ethyl)amino)benzamide **18a** (325 mg, 0.75 mmol), 2-(4-ethoxyphenyl)acetic acid (30 mg, 0.83 mmol), HBTU (313 mg, 0.83 mmol), and triethylamine (156 μL, 1.13 mmol). The product **19a** (258 mg, 0.43 mmol, 57%) was obtained as an orange/brown oil. ^{1}H NMR (400 MHz, CDCl$_3$): δ 8.72 (s, 1H), 7.97 (d, *J* = 8.5 Hz, 1H), 7.89 (d, *J* = 8.4 Hz, 1H), 7.52 (t, *J* = 7.6 Hz, 1H), 7.32 (t, *J* = 7.6 Hz, 1H), 7.23 (d, *J* = 8.5 Hz, 2H), 7.15 (d, *J* = 1.4 Hz, 1H), 7.00 (dd, *J* = 8.3, 1.4 Hz, 1H), 6.74 (d, *J* = 8.5 Hz, 2H), 6.46 (d, *J* = 8.4 Hz, 1H), 4.73 (s, 1H), 4.64 (t, *J* = 5.3 Hz, 1H), 3.85 (q, *J* = 7.0 Hz, 2H), 3.66−3.59 (m, 4H), 3.39 (s, 4H), 3.26−3.18 (m, 2H), 3.01 (t, *J* = 6.1 Hz, 2H), 2.63 (t, *J* = 6.0 Hz, 2H), 1.89−1.75 (m, 4H), 1.32 (t, *J* = 7.0 Hz, 3H), 1.15 (s, 6H) ppm. ^{13}C NMR (101 MHz, CDCl$_3$): δ 171.7, 171.1, 158.1, 157.9, 150.9, 146.5, 143.2, 130.2, 128.7, 127.8, 127.2, 125.3, 125.2, 124.7, 124.0, 123.8, 122.9, 120.2, 116.9, 114.7, 111.1, 63.4, 47.6, 44.3, 42.9, 33.5, 24.8, 22.9, 22.6, 14.8 ppm. ESI: *m/z* calcd for C$_{36}$H$_{45}$N$_5$O$_3$ [M + H]$^+$, 594.78; found, 594.25; retention time, 8.101 min.

3-(2-(4-Ethoxyphenyl)acetamido)-N,N-diethyl-4-((3-((1,2,3,4-tetrahydroacridin-9-yl)amino)propyl)amino)benzamide (19b). The reaction was carried out according to general procedure IV using 3-amino-*N,N*-diethyl-4-((3-((1,2,3,4-tetrahydroacridin-9-yl)amino)-propyl)amino)benzamide **18b** (154 mg, 0.34 mmol), 2-(4-ethoxyphenyl)acetic acid (136 mg, 0.37 mmol), HBTU (140 mg, 0.37 mmol), and triethylamine (70.6 μL, 0.51 mmol). The product **19b** (104 mg, 0.17 mmol, 50%) was obtained as an orange/brown oil. ^{1}H NMR (400 MHz, CDCl$_3$): δ 8.07 (s, 1H), 8.02 (d, *J* = 9.5 Hz, 1H),

7.59−7.55 (m, 1H), 7.47−7.44 (m, 1H), 7.29−7.28 (m, 1H), 7.24 (d, *J* = 8.4 Hz, 2H), 7.05−7.02 (m, 1H), 6.76−6.74 (m, 2H), 6.56−6.52 (m, 1H), 3.92−3.83 (m, 4H), 3.73 (s, 2H), 3.42−3.36 (m, 4H), 3.22−3.15 (m, 2H), 2.73−2.68 (m, 2H), 2.43−2.36 (m, 2H), 2.03−1.97 (m, 2H), 1.71−1.65 (m, 4H), 1.32 (t, *J* = 7.0 Hz, 3H), 1.20−1.09 (m, 6H) ppm. ^{13}C NMR (101 MHz, CDCl$_3$): δ 172.1, 171.9, 162.7, 157.2, 151.9, 146.6, 143.5, 130.6, 129.4, 127.3, 126.7, 125.8, 124.7, 124.6, 123.0, 121.1, 119.5, 118.5, 115.5, 114.8, 111.0, 63.5, 46.1, 42.8, 42.5, 39.4, 29.8, 29.5, 24.8, 22.4, 22.1, 14.9, 13.7 ppm. ESI: *m/z* calcd for C$_{37}$H$_{47}$N$_5$O$_3$ [M + 2H]$^{2+}$, 304.69; found, 304.70; retention time, 8.23 min.

3-(2-(4-Ethoxyphenyl)acetamido)-N,N-diethyl-4-((4-((1,2,3,4-tetrahydroacridin-9-yl)amino)butyl)amino)benzamide (19c). The reaction was carried out according to general procedure IV using 3-amino-*N,N*-diethyl-4-((4-((1,2,3,4-tetrahydroacridin-9-yl)amino)-butyl)amino)benzamide **18c** (139 mg, 0.30 mmol), 2-(4-ethoxyphenyl)acetic acid (121 mg, 0.33 mmol), HBTU (125 mg, 0.33 mmol), and triethylamine (62.3 μL, 0.45 mmol). The product **19c** (166 mg, 0.27 mmol, 90%) was obtained as a brown oil. ^{1}H NMR (400 MHz, CDCl$_3$): δ 7.97 (s, 1H), 7.79−7.77 (m, 1H), 7.53−7.50 (m, 1H), 7.34−7.31 (m, 1H), 7.24 (d, *J* = 8.6 Hz, 2H), 7.17−7.14 (m, 1H), 7.06−7.02 (m, 1H), 6.81 (d, *J* = 8.6 Hz, 2H), 6.50−6.46 (m, 1H), 4.03−3.91 (m, 4H), 3.64 (s, 2H), 3.42−3.31 (m, 4H), 3.05−3.00 (m, 2H), 2.94−2.90 (m, 2H), 2.63−2.57 (m, 2H), 1.87−1.80 (m, 4H), 1.73−1.56 (m, 4H), 1.33 (t, *J* = 7.0 Hz, 3H), 1.19−1.11 (m, 6H) ppm. ^{13}C NMR (101 MHz, CDCl$_3$): δ 171.7, 171.4, 162.1, 158.4, 152.4, 144.7, 143.8, 130.5, 129.8, 127.2, 126.9, 125.9, 124.9, 124.3, 123.6, 121.9, 119.5, 118.9, 115.7, 115.1, 111.1, 63.6, 48.9, 47.2, 44.4, 43.1, 32.2, 28.7, 26.3, 24.7, 22.7, 22.2, 14.9, 13.6 ppm. ESI: *m/z* calcd for C$_{38}$H$_{49}$N$_5$O$_3$ [M + 2H]$^{2+}$, 311.69; found, 311.70; retention time, 8.39 min.

3-(2-(4-Ethoxyphenyl)acetamido)-N,N-diethyl-4-((5-((1,2,3,4-tetrahydroacridin-9-yl)amino)pentyl)amino)benzamide (19d). The reaction was carried out according to general procedure IV using 3-amino-*N,N*-diethyl-4-((5-((1,2,3,4-tetrahydroacridin-9-yl)amino)-pentyl)amino)benzamide **19d** (222 mg, 0.47 mmol), 2-(4-ethoxyphenyl)acetic acid (191 mg, 0.52 mmol), HBTU (197 mg, 0.52 mmol), and triethylamine (98.4 μL, 0.71 mmol). The product **19d** (299 mg, 0.47 mmol, quant.) was obtained as a brown oil. ^{1}H NMR (400 MHz, CDCl$_3$): δ 8.11 (d, *J* = 8.7 Hz, 1H), 7.59−7.56 (m, 2H), 7.43−7.36 (m, 2H), 7.27−7.25 (m, 2H), 6.92−6.87 (m, 1H), 6.79 (d, *J* = 8.6 Hz, 2H), 6.33 (d, *J* = 8.5 Hz, 1H), 3.95 (q, *J* = 14.0, 7.0 Hz, 2H), 3.86−3.82 (m, 2H), 3.69 (s, 2H), 3.46−3.37 (m, 4H), 3.00−2.95 (m, 2H), 2.69−2.64 (m, 2H), 2.50−2.45 (m, 2H), 1.80−1.72 (m, 6H), 1.69−1.63 (m, 2H), 1.37−1.33 (m, 5H), 1.30−1.21 (m, 6H) ppm. ^{13}C NMR (101 MHz, CDCl$_3$): δ 171.8, 171.2, 161.4, 157.6, 153.1, 146.7, 143.7, 130.5, 129.5, 127.3, 126.7, 125.8. 124.8, 124.5, 123.5, 122.2, 119.6, 118.8, 115.7, 114.9, 111.3, 63.6, 48.6, 47.4, 45.1, 43.2, 30.2, 29.9, 28.4, 28.2, 23.56, 22.2, 22.1, 14.9, 13.7 ppm. ESI: *m/z* calcd for C$_{39}$H$_{51}$N$_5$O$_3$ [M + 2H]$^{2+}$, 318.70; found, 318.65; retention time, 8.75 min.

3-(2-(4-Ethoxyphenyl)acetamido)-N,N-diethyl-4-((6-((1,2,3,4-tetrahydroacridin-9-yl)amino)hexyl)amino)benzamide (19e). The reaction was carried out according to general procedure IV using 3-amino-*N,N*-diethyl-4-((6-((1,2,3,4-tetrahydroacridin-9-yl)amino)-hexyl)amino)benzamide **18e** (140 mg, 0.29 mmol), 2-(4-ethoxyphenyl)acetic acid (52.3 mg, 0.29 mmol), HBTU (133 mg, 0.35 mmol), and triethylamine (61.0 μL, 0.44 mmol). The product **19e** (142 mg, 0.22 mmol, 76%) was obtained as a brown oil. ^{1}H NMR (400 MHz, CDCl$_3$): δ 8.56 (s, 1H), 8.15 (d, *J* = 8.7 Hz, 1H), 7.88 (d, *J* = 8.4 Hz, 1H), 7.53 (t, *J* = 7.2 Hz, 1H), 7.35 (t, *J* = 8.0 Hz, 1H), 7.25 (d, *J* = 8.6 Hz 2H), 7.04−7.00 (m, 1H), 6.75 (d, *J* = 8.6 Hz, 2H), 6.48−6.44 (m, 1H), 3.92 (q, *J* = 7.0 Hz, 2H), 3.81 (m, 2H), 3.71 (s, 2H), 3.49−3.32 (m, 4H), 2.96−2.91 (m, 2H), 2.88−2.83 (m, 2H), 2.54−2.49 (m, 2H), 1.80−1.68 (m, 6H), 1.54−1.47 (m, 2H), 1.37−1.31 (m, 4H), 1.25 (t, *J* = 7.3 Hz, 3H), 1.14−1.09 (m, 6H) ppm. ^{13}C NMR (101 MHz, CDCl$_3$): δ 172.0, 170.8, 162.7, 158.1, 156.0, 150.5, 144.07, 130.4, 129.4, 127.6, 127.0, 125.8, 125.1, 124.9, 123.8, 122.6, 119.9, 119.0, 115.7, 114.7, 111.3, 63.5, 48.1, 46.3, 45.2, 43.2, 31.5, 30.3, 28.6, 28.3,

26.2, 25.9, 21.8, 20.7, 14.9, 13.7 ppm. ESI: *m/z* calcd for C$_{40}$H$_{53}$N$_5$O$_3$ [M + 2H]$^{2+}$, 325.70; found: 325.75; retention time: 8.76 min.

3-(2-(4-Ethoxyphenyl)acetamido)-N,N-diethyl-4-((2-(2-(2-((1,2,3,4-tetrahydroacridin-9-yl)amino)ethoxy)ethoxy)ethyl)-amino)benzamide (19f). The reaction was carried out according to general procedure IV using 3-amino-*N,N*-diethyl-4-((2-(2-(2-((1,2,3,4-tetrahydroacridin-9-yl)amino)ethoxy)ethoxy)ethyl)amino)-benzamide **18f** (290 mg, 0.56 mmol), 2-(4-ethoxyphenyl)acetic acid (122 mg, 0.62 mmol), HBTU (235 mg, 0.62 mmol), and triethylamine (116 μL, 0.84 mmol). The product **19f** (398 mg, 0.58 mmol, quant.) was obtained as a brown oil.¹H NMR (400 MHz, CDCl₃): δ 8.03–7.96 (m, 2H), 7.87 (d, *J* = 8.3 Hz, 1H), 7.51 (t, *J* = 8.0 Hz, 1H), 7.31 (t, *J* = 7.2 Hz 1H), 7.20 (d, *J* = 8.6 Hz, 2H), 7.07–7.03 (m, *J* = 8.4, 1.9 Hz, 1H), 6.81 (d, *J* = 8.6 Hz, 2H), 6.56–6.52 (m, 1H), 3.99–3.92 (m, 2H), 3.71–3.67 (m, 2H), 3.63–3.56 (m, 10H), 3.42–3.31 (m, 4H), 3.17 (t, *J* = 5.3 Hz, 2H), 2.99–2.94 (m, 2H), 2.67–2.62 (m, 2H), 1.84–1.76 (m, 4H), 1.36 (t, *J* = 7.2 Hz, 3H), 1.14–1.09 (m, 6H) ppm. ¹³C NMR (101 MHz, CDCl₃): δ 171.5, 170.9, 158.3, 156.6, 152.1, 144.9, 143.4, 130.5, 129.5, 127.0, 126.4, 125.7, 124.6, 124.3, 123.5, 123.3, 119.5, 118.7, 115.9, 115.0, 111.6, 70.4, 70.3, 70.2, 69.6, 63.5, 53.5, 48.3, 45.8, 43.5, 29.8, 24.4, 22.8, 22.3, 14.9, 13.7 ppm. ESI: *m/z* calcd for C$_{40}$H$_{51}$N$_5$O$_5$ [M + 2H]$^{2+}$, 341.70; found, 341.70; retention time, 8.34 min.

Ethyl 4-(Isopentylamino)-3-nitrobenzoate (20). 4-Fluoro-3-nitrobenzoic acid **15** (1.00 g, 5.40 mmol) was dissolved in ethanol, and a cat. amount (few drops) of H₂SO₄ (95–97%) was added. After stirring overnight under reflux conditions, the mixture was basified with triethylamine, and 3-methylbutan-1-amine (691 μL, 5.94 mmol) was added. After stirring under reflux conditions overnight, the mixture was concentrated in vacuo. The residue was dissolved in CH₂Cl₂ and washed with 1 M HCl$_{(aq)}$ and NaHCO₃ solution. The organic layers were combined, dried over anhydrous MgSO₄, and concentrated in vacuo. The product **20** (1.46 g, 5.22 mmol, 97%) was obtained as a yellow oil. ¹H NMR (400 MHz, CDCl₃): δ 8.88–8.85 (m, 1H), 8.31 (s, 1H), 8.07–8.03 (m, 1H), 6.88–6.83 (m, 1H), 4.35 (q, *J* = 7.1 Hz, 2H), 3.39–3.33 (m, 2H), 1.83–1.72 (m, 1H), 1.65 (q, *J* = 7.1 Hz, 2H), 1.38 (t, *J* = 7.1 Hz, 3H), 0.99 (d, *J* = 6.7 Hz, 6H) ppm. ¹³C NMR (101 MHz, CDCl₃): δ 165.3, 147.9, 136.5, 131.3, 129.6, 117.5, 113.6, 61.1, 41.6, 37.8, 26.1, 22.6, 14.5 ppm. ESI: *m/z* calcd for C$_{14}$H$_{21}$N$_2$O$_4$ [M + H]$^+$, 281.15; found, 281.00; retention time, 11.85 min.

Ethyl 3-Amino-4-(isopentylamino)benzoate (21). Ethyl 4-(isopentylamino)-3-nitrobenzoate **20** (1.46 g, 5.22 mmol) was dissolved in MeOH and a cat. amount of Pd/C (10%) was added. The mixture was stirred under a hydrogen atmosphere (8 bar) at room temperature for 3 h. The clear mixture was filtered off by suction over Celite. The combined organic layers were dried over anhydrous MgSO₄ and concentrated in vacuo, and product **36** (1.31 g, 5.22 mmol, quant.) was obtained as a colorless oil. The product was directly used for the next reaction step without further purification. ESI: *m/z* calcd for C$_{14}$H$_{23}$N$_2$O$_2$ [M + H]$^+$, 251.18; found, 251.05; retention time, 10.34 min.

Ethyl 3-(2-(4-Ethoxyphenyl)acetamido)-4-(isopentylamino)-benzoate (22). The reaction was carried out according to general procedure V using 3 ethyl 3-amino-4-(isopentylamino)benzoate **21** (1.31 g, 5.22 mmol), 2-(4-ethoxyphenyl)acetic acid (1.03 g, 5.74 mmol), HBTU (2.18 g, 5.74 mmol), and NEt₃ (1.08 mL, 7.83 mmol). The product **22** (2.15 g, 5.22 mmol, quant.) was obtained as an orange/brown oil. ¹H NMR (400 MHz, CDCl₃): δ 7.86–7.82 (m, 1H), 7.73–7.71 (m, 1H), 7.32–7.29 (m, 2H), 6.97–6.94 (m, 2H), 6.65 (d, *J* = 8.7 Hz, 1H), 4.32 (q, *J* = 7.1 Hz, 2H), 4.17 (q, *J* = 7.1 Hz, 2H), 3.74 (s, 2H), 3.14–3.08 (m, 2H), 1.70–1.65 (m, 1H), 1.50–1.40 (m, 5H), 1.37 (t, *J* = 7.1 Hz, 3H), 0.96 (d, *J* = 6.6 Hz, 6H) ppm. ¹³C NMR (101 MHz, CDCl₃): δ 170.8, 158.6, 147.2, 130.5, 130.2, 130.1, 127.8, 126.5, 121.5, 118.4, 115.4, 114.6, 63.7, 60.5, 41.8, 38.8, 38.3, 26.1, 22.7, 14.9, 14.6 ppm. ESI: *m/z* calcd for C$_{24}$H$_{33}$N$_2$O$_4$ [M + H]$^+$, 413.24; found, 413.10; retention time, 11.04 min.

Ethyl 2-(4-Ethoxybenzyl)-1-isopentyl-1H-benzo[d]imidazole-5-carboxylate (23). The reaction was carried out according to general procedure V using ethyl 3-(2-(4-ethoxyphenyl)acetamido)-4-(isopentylamino)benzoate **22** (2.15 g, 5.22 mmol). The crude product was purified by column chromatography (20:1:0.1 CH₂Cl₂/MeOH/

NH$_{3(aq)}$ (25%)), and product **23** (1.67 g, 4.23 mmol, 81%) was obtained as a purple oil. ¹H NMR (400 MHz, CDCl₃): δ 8.44 (s, 1H), 7.95–7.91 (m, 1H), 7.21 (d, *J* = 8.4 Hz, 1H), 7.10 (d, *J* = 8.8 Hz, 2H), 6.78 (d, *J* = 8.8 Hz, 2H), 4.35 (q, *J* = 7.1 Hz, 2H), 4.20 (s, 2H), 3.96–3.89 (m, 4H), 1.56–1.46 (m, 1H), 1.39–1.28 (m, 8H), 0.85 (d, *J* = 6.8 Hz, 6H) ppm. ¹³C NMR (101 MHz, CDCl₃): δ 167.2, 158.1, 155.1, 142.2, 138.5, 129.5, 127.7, 124.4, 123.8, 121.7, 114.9, 108.9, 63.4, 60.7, 42.7, 38.0, 33.8, 26.1, 22.3, 14.7, 14.4 ppm. ESI: *m/z* calcd for C$_{24}$H$_{31}$N$_2$O$_3$ [M + H]$^+$, 395.23; found, 395.15; retention time, 11.11 min.

2-(4-Ethoxybenzyl)-1-isopentyl-1H-benzo[d]imidazole-5-carboxylic Acid (24). Ethyl 2-(4-ethoxybenzyl)-1-isopentyl-1*H*-benzo[*d*]-imidazole-5-carboxylate **23** (250 mg, 0.63 mmol) was dissolved in THF, and lithium hydroxide (150 mg, 0.63 mmol) in water was added. After 48 h of harsh stirring under reflux conditions, the mixture was concentrated in vacuo, and the residue was acidified with 2 M HCl$_{(aq)}$. Then, CH₂Cl₂ was added, and the organic layer was washed with water. The organic layers were combined, dried over anhydrous MgSO₄, and concentrated in vacuo. Product **24** (231 mg, 0.63 mmol, quant.) was obtained as a purple oil. ¹H NMR (400 MHz, D₂O): δ 8.10–8.07 (m, 1H), 7.80–7.75 (m, *J* = 9.9 Hz, 1H), 7.29 (d, *J* = 8.5 Hz, 1H), 7.06 (d, *J* = 8.5 Hz, 2H), 6.78 (d, *J* = 8.3 Hz, 2H), 4.10 (s, 2H), 3.94–3.88 (m, 2H), 3.86–3.80 (m, 2H), 1.36–1.27 (m, 1H), 1.21 (t, *J* = 6.9 Hz, 3H), 1.08–1.01 (m, 2H), 0.66 (d, *J* = 6.6 Hz, 6H) ppm. ¹³C NMR (101 MHz, DMSO): δ 167.6, 166.2, 158.4, 135.7, 132.8, 130.6, 128.0, 126.5, 125.3, 125.2, 117.2, 115.5, 63.7, 43.8, 37.1, 31.1, 25.8, 22.2, 14.8 ppm. ESI: *m/z* calcd for C$_{22}$H$_{27}$N$_2$O$_3$ [M + H]$^+$, 367.20; found, 367.15; retention time, 10.13 min.

Pharmacology. *Inhibition of hBChE.* BChE (E.C. 3.1.1.8, from humans) was kindly provided by Oksana Lockridge from the University of Nebraska Medical Center. 5,5′-Dithiobis(2-nitrobenzoic acid) and ATC iodide were obtained from Fluka Analytical, and tacrine hydrochloride was purchased from Sigma-Aldrich. Inhibitory activities were evaluated using Ellman's method.[64] The stock solutions of the test compounds were prepared in ethanol (33.3 mM) and diluted to the desired concentrations. For the testing, 50 μL of 5,5′-dithiobis(2-nitrobenzoic acid) and 50 μL of enzyme were added to 1.5 mL of the buffer. After 50 μL of the test compound was added, the mixture was incubated for 4.5 min. Afterward, 10 μL of acetylthiocholine iodide was added, and the mixture was allowed to incubate for further 2.5 min. Enzyme activity was then observed via UV (λ = 412 nm). IC$_{50}$ values were determined graphically from inhibition curves using Pad Prism 5.0 software. Experiments were carried out three times independently.

Inhibition of hAChE and hBChE. The hAChE inhibitory activity was evaluated spectrophotometrically at 37 °C by Ellman's method.[64] AChE stock solution was prepared by dissolving recombinant hAChE lyophilized powder (Sigma, Italy) in 0.1 M phosphate buffer (pH = 8.0) containing Triton X-100 0.1%. The stock solution of BChE from human serum (Sigma, Italy) was prepared by dissolving the lyophilized powder in an aqueous solution of gelatin 0.1%. Stock solutions of inhibitors (1 or 2 mM) were prepared in methanol. The assay solution consisted of a 0.1 M phosphate buffer at pH 8.0, with the addition of 340 μM 5,5′-dithiobis(2-nitrobenzoic acid), 0.02 unit/mL hAChE or hBChE, and 550 μM substrate (acetylthiocholine iodide or butyrylthiocholine iodide for AchE or BchE, respectively). Fifty microliter aliquots of increasing concentration of the tested compound were added to the assay solution and preincubated for 20 min at 37 °C with the enzyme. Upon addition of the substrate, the increase in absorbance at 412 nm was monitored for 3 min. Assays were carried out with a blank containing all components except the enzyme to account for the nonenzymatic reaction. The reaction rates were compared, and the percent inhibition was calculated. IC$_{50}$ values were determined graphically from inhibition curves using GraphPad Prism 4.03 software. Experiments were carried out three times independently.

Investigation of Inhibitory Constants and Mode of Inhibition toward hAChE. To assess the mechanism of action and inhibitory constant reciprocal plots of 1/*V* versus 1/[S] were constructed using relatively low concentrations of substrate (ACTh, 0.111–0.554 mM). The evaluation of the enzyme activity was carried out by Ellman's method.[64] The plots were assessed by a weighted least square analysis

that assumed the variance of V to be a constant percentage of V for the entire data set. The mechanism of inhibition was assessed by comparing the overlaid Lineweaver–Burk plots with the theoretical trends for competitive, mixed-type, and noncompetitive inhibition. To determine the inhibition constant K_i, slopes of reciprocal plots were replotted against the concentration of the tested inhibitor (3e, range 0–100 nM; 4b, range 0–7.5 nM; 8, range 0–25.0 nM), and K_i was determined as the intersect on the negative x axis. The K_i' (dissociation constant for the enzyme–substrate–inhibitor complex) value was determined by plotting the apparent $1/V_{max}$ versus inhibitor concentration.[92] Data analysis was performed using GraphPad Prism 4.03 software. Experiments were carried out three times independently.

Inhibition of AChE-Induced Aβ$_{40}$ Aggregation.[65] Aβ$_{40}$, supplied as trifluoroacetate salt, was purchased from Bachem AG (Switzerland). Aβ$_{40}$ (2 mg mL^{-1}) was dissolved in 1,1,1,3,3,3-hexafluoro-2-propanol (HFIP), lyophilized, and redissolved in DMSO to achieve a 2.3 mM stock solution. Stock solutions of tested inhibitors were prepared in methanol (2.0 mM) and diluted in the assay buffer. Aliquots of Aβ$_{40}$ peptide (2 μL) were incubated for 24 h at room temperature in 0.215 M sodium phosphate buffer (pH 8.0) at a final concentration of 230 μM. For co-incubation experiment aliquots (16 μL) of hAChE solution (final concentration, 2.30 μM; Aβ/AChE molar ratio, 100:1) and hAChE in the presence of 2 μL of the tested inhibitor (final inhibitor concentration, 100 μM) in 0.215 M sodium phosphate buffer solution (pH 8.0) were added. Blanks containing Aβ$_{40}$ alone, hAChE alone, and Aβ$_{40}$ plus tested inhibitors in 0.215 M sodium phosphate buffer (pH 8.0) were also prepared. The final volume of each sample was 20 μL. To quantify amyloid fibril formation, the thioflavin T fluorescence method was then applied.[93] The fluorescence intensities related to fibril formation were monitored for 300 s at λ_{em} = 490 nm (λ_{exc} = 446 nm). Fluorescence intensities of samples without and with an inhibitor were compared, and percent inhibition was calculated.[65] The experiment was carried out two times independently, and each was performed in duplicate.

Inhibition of Aβ$_{42}$ Self-Aggregation. As reported in a previously published protocol,[68] HFIP-pretreated Aβ$_{42}$ samples (Bachem AG, Switzerland) were solubilized with a CH$_3$CN/0.3 mM Na$_2$CO$_3$/250 mM NaOH (48.4:48.4:3.2) mixture to obtain a 500 μM stock solution. Experiments were performed by diluting (final Aβ concentration, 50 μM) and incubating the peptide in 10 mM phosphate buffer (pH = 8.0) containing 10 mM NaCl, at 30 °C for 24 h with and without an inhibitor (50 μM, Aβ/inhibitor = 1:1). Blanks containing the tested inhibitors were also prepared. Each assay was run in duplicate. To quantify amyloid fibril formation, the thioflavin T fluorescence method was used.[93] After incubation, samples were diluted to a final volume of 2.0 mL with 50 mM glycine–NaOH buffer (pH 8.5) containing 1.5 μM thioflavin T. A 300 s time scan of the fluorescence intensity was carried out (λ_{exc} = 446 nm; λ_{em} = 490 nm, FP-6200 fluorometer, Jasco Europe), and values at the plateau were averaged after subtracting the background fluorescence of 1.5 μM thioflavin T solution. The fluorescence intensities obtained in the absence and in the presence of tested inhibitors were compared, and the percent inhibition due to the presence of the inhibitor was calculated by the following formula: $100 - (\mathrm{IF}_i/\mathrm{IF}_o \times 100)$, where IF_i and IF_o are the fluorescence intensities obtained for Aβ$_{42}$ in the presence and in the absence of inhibitor, respectively. The experiment was carried out two times independently, and each was performed in duplicate.

Radioligand Binding Studies on hCB$_2$R and hCB$_1$R and Efficacy. HEK hCB$_2$R Cell Line. Human embryonic kidney cells (HEK) stably expressing the hCB$_2$R were grown in Dulbecco's modified Eagle's medium containing high glucose supplemented with 8% fetal calf serum and 25 μg/mL zeocin in a 37 °C incubator in the presence of 5% CO$_2$. Cells were passaged twice a week.

CHO hCB$_1$R Cell Line. Chinese hamster ovary cells (CHO) stably expressing the hCB$_1$R were grown in Ham's F-12 Nutrient Mix supplemented with 8% fetal calf serum and 400 μg/mL geneticin in a 37 °C incubator in the presence of 5% CO$_2$. Cells were passaged twice a week.

U266 Cell Line. The U266 cell line was purchased from ATCC (LGC Standards, Milan, IT). Cell authentication was performed by IST (Genova, Italy). Cells were cultured in an RPMI 1640 medium (Lonza, Milan, IT) supplemented with 10% fetal bovine serum (FBS), 2 mM L-glutamine, 100 IU/mL penicillin, 100 μg/mL ampicillin/streptomycin, 1 mM sodium pyruvate and grown at 37 °C with 5% CO$_2$ and 95% humidity.

Cell Thawing. Cells were removed from liquid nitrogen stocks and warmed up in a 37 °C water bath. Then, the cells were resuspended in 10 mL of DMEM (high glucose) and 8–10% FCS. The suspension was centrifuged for 5 min at 1000 rpm, and the supernatant was discarded. The pellet was resuspended in 10 mL of DMEM (high glucose) with 2.5 μL (25 μg/mL) of zeocin and 8–10% FCS. The suspension was transferred into a tissue culture flask and then placed in an incubator (37 °C, 5% CO$_2$, humid). The medium was changed on the following day.

Cell Passaging. The passaging rate was determined by examining the cells under the light microscope. The medium was discarded, and cells were washed gently by adding 5 mL of PBS. The PBS was discarded, and 3 mL of Trypsin/EDTA was added. The flask was placed in the incubator for 5 min. After incubation, 7 mL of DMEM (high glucose) with 8–10% FCS was added. The cells were washed down and transferred into a falcon tube. The tube was centrifuged for 5 min at 1000 rpm. The supernatant was discarded, and 5–10 mL of DMEM (high glucose) with zeocin (25 μg/mL) and 8–10% FCS was added. The cell suspension was divided into aliquots according to the passaging rate of the cells. Cells were passaged twice a week.

Binding Studies. Membrane Preparation. The cells were passaged according to their passaging rate (1:8) and plated on petri dishes 3 days before preparation. The preparation itself was carried out on ice. The medium was dispensed, and the cells were washed with 5 mL of PBS. Then, 3.5 mL of preparation buffer (50 mM Tris, 1 mM MgCl$_2$·6H$_2$O, 1 mM EDTA, pH 7.4) were added. The cells were scrubbed from the surface, and the cell suspensions were combined. The combined suspension was treated two times for 10 s with an ultraturrax. The cell lysate was then centrifuged for 10 min at 3200 rpm at 4 °C. The supernatant was transferred to ultracentrifugation tubes and centrifugated for 50 min at 37,000 rpm at 4 °C. The supernatant was discarded, and the pellet was resuspended in binding buffer (50 mM Tris, 5 mM MgCl$_2$·6 H$_2$O, 2.5 mM EDTA, pH 7.4). The protein concentration of the pellet was determined using the Bradford assay (according to vendor's description). The suspension was passaged, and the aliquots were shock-frosted in liquid nitrogen and stored at −80 °C until further use.

Radioligand Binding Assay. SR-144,528 (inverse agonist for hCB$_2$R) was purchased from Santa Cruz Biotechnology Inc. Unlabeled CP 55,940 (agonist for hCB$_2$R and hCB$_1$R) was obtained from Sigma-Aldrich Life Science. Radioactive labeled [^{3}H]CP 55,940 was acquired by Hartmann Analytic GmbH. Rimonabant (inverse agonist for hCB$_1$R) was obtained by an in-house synthesis. Saturation assays were carried out similar to Murkherjee et al.[94] to determine the K_D value of the membrane samples. Saturation assays were carried out using eight concentrations of [^{3}H]CP 55,940, ranging from 0.088 to 4.4 nM. Reactions were started by adding 8 μg membrane per well of a 96 well Multiscreen filter plate (Millipore) containing the radioligand in assay buffer (50 mM Tris-HCl, pH 7.4; 5 mM MgCl$_2$·6 H$_2$O; 2.5 mM EDTA; 2 mg/mL BSA). After incubating for 3 h at RT, the reaction was stopped by vacuum filtration, and each well was washed four times with 100 μL of cold binding buffer (50 mM Tris-HCl, pH 7.4; 5 mM MgCl$_2$·6 H$_2$O; 2.5 mM EDTA). The filter plate was dried at 40 °C. The activity was measured in a Microbeta Trilux counter (Wallac) using an IRGA Safe plus-scintillation cocktail (PerkinElmer). Competition assays were performed with 5–11 concentrations of replacing ligands (0.1 nM–0.4 mM) and 0.44 nM [^{3}H]CP 55,940. Nonspecific binding was determined using 10 μM 2 for hCB$_2$R and 10 μM rimonabant for hCB$_1$R.

Statistical Analysis. To determine the IC$_{50}$ values, statistical evaluations and sigmoidal dose–response curve fittings were performed using GraphPad Prism 5 software applying nonlinear regression and one site fit logIC$_{50}$ as curve fitting functions. K_i values were determined according to the Cheng–Prusoff equation when the displacement of

[^{3}H]CP 55,940 was higher than 60% at 100 μM test compound concentration

$$K_i = \frac{IC_{50}}{1 + \frac{[L^*]}{K_D}}$$

with [L*] as radioligand concentration (0.44 nM), and the K_i value was calculated for at least two individual experiments. K_D values and standard errors were determined for hCB$_2$R K_D(hCB$_2$R) = 4.16 ± 3.04 and for CB$_1$R K_D(hCB$_1$R) = 2.24 ± 1.15.

hCB$_2$R Efficacy. MTT Assay. The U266 cell line (4 × 104 cells/mL) was plated on 96-well plates to a final volume of 100 μL/ well. After incubating for 1 day, compounds or vehicles were added at different concentrations. Six replicates were used for each treatment. At the indicated time point, cell viability was assessed by adding 0.8 mg/mL 3-[4,5-dimethylthiazol-2-yl]-2,5-diphenyl tetrazolium bromide (MTT) (Sigma-Aldrich) to the medium. After 3 h, the plates were centrifuged, the supernatant was discarded, and the pellet was solubilized with 100 μL/well DMSO. The absorbance of the samples against a background control (medium alone) was measured at 570 nm using an ELISA reader microliter plate (BioTek Instruments, Winooski, VT, USA). For some experiments, 1 h of preincubation with Forskolin or AM630 was performed. Each sample was evaluated in six wells and in two independent experiments.

cAMP Assay. U266 cells (1 × 10^6/mL) were plated in 24-well plates and treated with the appropriate compounds for 2 h. After treatment, the cells were processed for the detection of cAMP levels, using the cAMP assay kit (Enzo Life Sciences, Farmingdale, NY, USA) in accordance to the manufacturer's protocol. U266 cells were treated with Forskolin (10 μM), AM630 (25 μM), or compound (50 μM) for 2 h. For combination treatments, U266 cells were preincubated with AM630 (25 μM) for 30 min before adding the compounds. The concentration of cAMP was calculated by measuring the absorbance at 450 nm with an ELISA reader. Each compound was evaluated in duplicate and in two independent assays. cAMP levels were stated as pmol/mg protein.

RNA Extraction and qRT-PCR. Total RNA from treated and vehicle U266 cells was extracted using the RNeasy Mini Kit (Qiagen) at the appropriate time points, and cDNA was synthesized using the High-Capacity cDNA Archive Kit (Applied Biosystems, Foster City, PA) according to the manufacturer's instructions. Quantitative real-time polymerase chain reactions (qRT-PCR) for MIF, STAT-3, and GAPDH were performed using the iQ5 multicolor real-time PCR detection system (Bio-Rad, Hercules, CA). The PCR reaction was performed with SYBR Green qPCR mastermix (Qiagen) using 500 ng of cDNA for the reaction, following the amplification protocol indicated by the manufacturer's instruction. All samples were tested in triplicates in the same plate, GAPDH levels were used to normalize mRNA contents, and target gene levels were calculated by the $2^{-\Delta\Delta CT}$ method. cDNA from Forskolin-treated cells was used as CREB-induced MIF and STAT-3 as a positive control. cDNA from MD-48-treated cells was used for CB$_2$ agonist MIF and STAT-3 gene expression control. cDNA from AM630-treated cells was used for antagonist/inverse agonist CB$_2$ MIF and STAT-3 expression control. Each sample was evaluated in triplicate and in three different experiments.

Statistical Analysis. The statistical significance for MTT and qRT-PCR assays was determined using the analysis of variance (ANOVA) test. The calculation of IC$_{50}$ was performed by a nonlinear fit of log-dose versus response, using GraphPad Prism 5.01 software. cAMP concentration was calculated utilizing a four-parameter logistic (4PL) curve fitting program.

Calcium Mobilization Assay. Compounds were tested using a fluorescence-based assay. Briefly, CHO-K1 cells were engineered to either co-express hCB$_1$R and G$_{\alpha q16}$ or hCB$_2$R and G$_{\alpha q16}$. Activation of the receptor therefore leads to mobilization of intracellular calcium. Cells were seeded out in 96-well plates and incubated overnight. The next day, cells were loaded with the fluorescent dye calcein-4 AM. Calcium flux was monitored using an automated plate reader (FlexStation, Molecular Devices). Statistical analysis was performed using GraphPad Prism 5 software.

Effects on Microglia. *Cell Cultures.* Mouse N9 microglial cells were cultured in Dulbecco's modified Eagle's medium (DMEM) supplemented with 10% heat-inactivated fetal bovine serum (FBS), 1% penicillin/streptomycin, and 2 mM glutamine (all cell cultures' reagents were from Aurogene Srl, Rome, Italy). At confluence, after a short wash with sterile PBS, microglia were trypsinized for 5 min at 37 ° C, and trypsin was inactivated with a complete DMEM medium. Detached cells were then collected, centrifuged for 5 min at 300g, and resuspended to be counted. For experiments, microglial cells were plated at the density of 2.5 × 10^5 in a 35 mm Ø dish and exposed to 100 ng/mL lipopolysaccharide (LPS), in the presence or absence of increasing concentrations of the compound to be tested. After 24 h of treatment, microglial conditioned media were collected and partly used for nitrite measurement, partly filtered through 0.22 μm filters, concentrated using Microcon YM-3 (Millipore, Billerica, MA), and resuspended in 12 μL of 4× loading buffer (0.2 M Tris-HCl, pH 6.8; 8% sodium dodecyl sulfate; 40% glycerol; 0.4% bromophenol blue, and 0.4 M dithiothreitol; Sigma-Aldrich) for Western blot analysis. In parallel, microglial cells were collected in 2× loading buffer (LB; 50 μL per dish) for Western blot analysis.

Western Blotting. Concentrated microglial conditioned media and cell samples were briefly sonicated and loaded into 12% sodium dodecyl sulfate-polyacrylamide gel electrophoresis (SDS-PAGE; Bio-Rad). After electrophoresis and transfer onto nitrocellulose membranes (GE Healthcare, Milano, Italy), membranes were blocked for 1 h in blocking solution PBS−0.1% Tween-20 (Sigma-Aldrich), 4% nonfat dry milk (Bio-Rad) and incubated overnight at 4 °C with primary antibodies in PBS−0.1% Tween-20. Primary antibodies used were rabbit anti-iNOS, rabbit anti-IL1β, rabbit anti-TREM2, and rabbit anti-TGFβ2, and mouse anti-GAPDH (all 1:1000 dilution except for anti-GAPDH used 1:20,000 dilution, all from Santa Cruz Biotechnology). Membranes were then incubated with specific secondary antibodies conjugated to horseradish peroxidase (goat anti-rabbit and goat anti-mouse, both at 1:2000 dilution and from Santa Cruz) for 90 min at room temperature in PBS−0.1% Tween-20. Labeled proteins were visualized by using the Clarity Western ECL substrate (Bio-Rad) and detected using Bio-Rad Image Lab software with a ChemiDoc MP imaging system (Bio-Rad).

Nitrite Assay. Accumulation of nitrite in microglial conditioned media was measured by a colorimetric assay based on the Griess reaction. A nitrate standard curve was performed with NaNO$_2$ at known concentrations. Sulfanilamide (5 mM; Sigma-Aldrich) was added to the culture medium and the standard curve. Sulfanilamide reacts with nitrite under acidic conditions to form a diazonium cation, which subsequently couples to N-1-naphthyl-ethylenediamine dihydrochloride (NEDA, 40 mM; Sigma-Aldrich) to produce a colored azo dye. After 15 min of incubation at room temperature in the dark, absorbance was read at 540 nm with a multiplate spectrophotometric reader (Bio-Rad Laboratories Srl, Segrate, Milano, Italy).

Statistical Analysis. All quantitative data are presented as means ± SE from at least three independent experiments. Statistical significance between different treatments was calculated using GraphPad Prism 6 software applying one-way analysis of variance (ANOVA) followed by post hoc comparison through Bonferroni's test. A value of $p < 0.05$ was considered statistically significant.

Neuroprotection on HT-22 Cells. *Cell Culture.* HT-22 cells were grown in Dulbecco's modified Eagle's medium (DMEM, Sigma-Aldrich, Munich, Germany) supplemented with 10% (v/v) heat-inactivated fetal calf serum (FCS) and 1% (v/v) penicillin/streptomycin. Cells were passaged every 2 days and incubated at 37 °C with 5% CO$_2$ in a humidified incubator. Compounds were dissolved in DMSO, (Sigma-Aldrich, Munich, Germany) and diluted with medium. Generally, 80% confluent cells were seeded with 5000 cells per well into sterile 96-well plates and were incubated for 24 h.

Neurotoxicity. For the neurotoxicity assay, the previous medium was discarded, and different concentrations of the compound were added to the wells. DMSO (0.5%) in DMEM served as control. Cells were incubated for 24 h. After incubation, an MTT assay was performed.

Neuroprotection. For neuroprotection, 5 mM glutamate (mono-sodium-L-glutamate, Sigma-Aldrich, Munich, Germany) was co-

incubated with different concentrations of respective compounds for 24 h. Quercetin (25 μM, Sigma-Aldrich, Munich, Germany) served as a positive control. After 24 h of incubation, an MTT assay was performed.

MTT Assay. Cell viability was determined using the 3-(4,5-dimethylthiazol-2-yl)-2,5-diphenyl tetrazolium bromide (MTT, Sigma-Aldrich, Munich, Germany) assay. MTT solution (4 mg/mL in PBS) was diluted 1:10 with medium and added to the wells after removal of the previous medium. Cells were incubated for 3 h when the supernatant was removed and lysis buffer (10% SDS) was applied. The next day, absorbance at 560 nm was determined with a multiwell plate photometer (Tecan, SpectraMax 250).

Statistical Analysis. Results are presented as percentage to untreated control cells. Data are expressed as means $\pm$ SD of three different independent experiments, and each was performed in sextuplicate. Analysis was accomplished using GraphPad Prism 5 software applying one-way ANOVA followed by Dunnett's multiple comparison post-test. Levels of significance: *$p < 0.05$; **$p < 0.01$; ***$p < 0.001$.

In Vivo Studies. *Aim of the Study.* To test five compounds **3a**, **3d**, **3e**, **4a**, and **6** as protectant drugs in the in vivo mouse model of Alzheimer's disease induced by intracerebroventricular (i.c.v.) injection of oligomerized Aβ_{25-35} peptide. Each compound was injected intraperitoneally (i.p.) o.d. between day 1 and 7, as summarized in Supplementary Figure 4. The peptide was injected on day 1, and behavioral examination was performed between days 8 and 10. All animals were then sacrificed on day 11 and their brain stored at $-80\ ^\circ$C awaiting further biochemical analyses. In addition, the livers of high dose-treated animals (3 mg/kg) were removed and fixed in formaldehyde solution.

Animals. Male Swiss mice, 6 weeks old and weighing 30−35 g, from Janvier (Saint-Berthevin, France), were kept for housing, and experiments took place within the animal facility building of the University of Montpellier (CECEMA, Office of Veterinary Services agreement #B-34-172-23). Animals were housed in groups with access to food and water ad libitum, except during behavioral experiments. They were kept in a temperature and humidity-controlled animal facility on a 12 h/12 h light/dark cycle (lights off at 07:00 p.m.). All animal procedures were conducted in strict adherence to the European Union directive of September 22, 2010 (2010/63/UE) and authorized (file #1485-15034) by the National Ethic Committee (Paris, France).

Drug Preparation. Compounds were weighed and solubilized in pure DMSO, and a stock solution at 2 mg/mL was prepared in DMSO/ddH$_2$O. The percentage of DMSO in ddH$_2$O for 3 mg/kg dose was 30%. Stock solution in DMSO was stored for 1 week at +4 $^\circ$C, and the injection solutions were made fresh daily. Vehicle solutions used for control groups were DMSO 30% in H$_2$O.

Amyloid Peptide Preparation and Injection. Mice were anesthetized with isoflurane 2.5% and were injected i.c.v. with Aβ_{25-35} peptide (9 nmol/mouse) or vehicle solution (distilled water), in a final volume of 3 μL/mouse, according to the previously described method.[87,95−99] Homogeneous oligomeric preparation of Aβ_{25-35} peptide was performed by incubation for 4 days at 37 $^\circ$C according to Maurice et al.[87] Since it is well established that vehicle solution similar as a control scrambled Aβ_{25-35} peptide failed to induce toxicity and therefore affect learning abilities, vehicle-treated animals served as controls.[87,95−100]

Spontaneous Alternation Performances. On day 8, all animals were tested for spontaneous alternation performance in the Y maze, an index of spatial working memory. The Y maze is made of gray polyvinyl chloride. Each arm is 40 cm long, 13 cm high, 3 cm wide at the bottom, 10 cm wide at the top, and converging at an equal angle. Each mouse will be placed at the end of one arm and allowed to move freely through the maze during an 8 min session. The series of arm entries, including possible returns into the same arm, was checked visually. An alternation was defined as entries into all three arms on consecutive occasions. The number of maximum alternations is, therefore, the total number of arm entries minus two, and the percentage of alternation was calculated as (actual alternations/maximum alternations) × 100. Parameters included the percentage of alternation (memory index) and the total number of arm entries (exploration index).[87,95,96,98,99] Animals that shown an extreme behavior (alternation percentage of <20% or >90%

or number of arm entries <10) were discarded from the calculation. In this study, 11 animals were discarded accordingly (3.2% attrition).

Passive Avoidance Test. On days 9 and 10, a passive avoidance test was performed. The apparatus is a two-compartment (15 × 20 × 15 cm high) box with one compartment illuminated with white polyvinyl chloride walls and the other darkened with black polyvinyl chloride walls and a grid floor. A guillotine door separates each compartment. A 60 W lamp positioned 40 cm above the apparatus lights up the white compartment during the experiment. Scrambled foot shocks (0.3 mA for 3 s) were delivered to the grid floor using a shock generator scrambler (Lafayette Instruments, Lafayette, USA). The guillotine door was initially closed during the training session. During the training session, on day 9, each mouse was placed into the white compartment. After 5 s, the door was raised. When the mouse entered the darkened compartment and placed all its paws on the grid floor, the door was closed, and the foot shock was delivered for 3 s. The step-through latency, that is, the latency spent to enter the darkened compartment, and the number of vocalizations was recorded. The retention test was carried out 24 h after training, on day 10. Each mouse was placed again into the white compartment. After 5 s, the door was raised. The step-through and escape latencies (corresponding to the re-exit from the darkened compartment) were recorded up to 300 s. Animals that show all latencies during the training and retention session lower than 10 s are considered as failing to respond to the procedure and were discarded from the calculations. In this study, nine animals were discarded accordingly (2.6% attrition).

Sacrifice and Brain and Liver Sampling. On day 11, all animals were sacrificed, their brains dissected out to isolate the hippocampus and cortex. Samples were frozen in liquid nitrogen and stored at $-80\ ^\circ$C awaiting further analysis. For treated with the high dose (3 mg/kg) of compounds, the livers were also dissected out, post-fixed in formalin, and kept at 4 $^\circ$C.

Statistical Analyses. All values, except passive avoidance latencies, were expressed as means $\pm$ SEM. Statistical analyses were performed on the different conditions using one-way ANOVA (F value), followed by Dunnett's post hoc multiple comparison test. Passive avoidance latencies do not follow a Gaussian distribution since upper cutoff times are set. They were therefore analyzed using a Kruskal−Wallis nonparametric ANOVA (H value), followed by Dunn's multiple comparison test. $p < 0.05$ was considered as statistically significant.

■ ASSOCIATED CONTENT

ⓢ Supporting Information

The Supporting Information is available free of charge on the ACS Publications website at DOI: 10.1021/acs.jmedchem.9b00623.

> RP-HPLC chromatograms of the lead compounds (PDF)
> Molecular formula stings (CSV)

■ AUTHOR INFORMATION

Corresponding Author
*E-mail: michael.decker@uni-wuerzburg.de. Tel.: +49-931-31-89676.

ORCID ⓘ
Peter Gmeiner: 0000-0002-4127-197X
Rangan Maitra: 0000-0001-6663-6800
Michael Decker: 0000-0002-6773-6245

Author Contributions

Synthesis of the target compounds was performed by M.S. and D.D. Inhibitory, kinetic studies on hAChE and Aß aggregation were performed by M.O., M.N., and M.B. Inhibitory potency on hBChE and hAChE was performed by S.G. and M.H., radioligand binding studies on CBRs by M.S., and CB$_2$R efficacy by cAMP-regulated gene expression by M.N. The calcium mobilization assay on CBRs was performed by R.M. and

neuroprotection and neurotoxicity experiments by S.G. and M.S. Microglia effects were investigated by S.P., E.P., and B.M., and in vivo experiments were performed by M.S. and T.M. and liver histology by C.F. and M.V. Finally, MOR binding studies were performed by H.H. and P.G. All authors contributed to writing the manuscript and read and approved the final version.

■ ACKNOWLEDGMENTS

■ ABBREVIATIONS

Aβ, amyloid-beta; ACh, acetylcholine; AChE, acetylcholinesterase; ACth, acetylthiocholine; AD, Alzheimer's disease; ANOVA, analysis of variance; APP, amyloid precursor protein; BBB, blood−brain-barrier; BChE, butyrylcholinesterase; cAMP, cyclic adenosine monophosphate; CAS, catalytic active site; ChE, cholinesterase; CHO, Chinese hamster ovary; CNS, central nervous system; Cpd, compound; CRE, cAMP response element; CREB, cAMP response element-binding protein; DMSO, dimethyl sulfoxide; FSK, forskolin; GAPDH, glyceraldehyde-3-phosphat-dehydrogenase; GTP$_\gamma$S, guanosine 5′[γ-thio]triphosphate; HBTU, 2-(1H-benzotriazol-1-yl)-1,1,3,3-tetramethyluronium hexafluorophosphate; hCB$_{1/2}$R, human cannabinoid receptor 1/2; HEK, human embryotic kidney; i.c.v., intracerebroventricular; Il1β, interleukin 1 beta; iNOS, inducible nitric oxide synthase; i.p.., intraperitoneal; LPS, lipopolysaccharide; MIF, macrophage migration inhibitory factor; MTT, 3-(4,5-dimethylthiazol-2-yl)-2,5-diphenyltetrazolium bromide; NMDA, N-methyl-D-aspartate;; MOR, μ-opioid receptor; PAS, peripheral anionic site; PEG, polyethylene glycol; ROS, reactive oxygen species; (q)RT/PCR, (quantitative) reverse transcription polymerase chain reaction; SAR, structure−activity relationship; SD, standard deviation; SR, scavenger receptor; STAT-3, signal transducer and activator of transcription; ST-PA, step-through passive avoidance; TGFβ2, transforming growth factor beta-2; THC, tetrahydrocannabinol; THF, tetrahydrofuran; TNF, tumor necrosis factor; TREM2, triggering receptor expressed on myeloid cells 2; V or VEI, vehicle; YMT, Y-maze test

■ REFERENCES

(1) Patterson, C. *World Alzheimer report 2018*; ADI: London, 2018; pp 1−48.

(2) Zemek, F.; Drtinova, L.; Nepovimova, E.; Sepsova, V.; Korabecny, J.; Klimes, J.; Kuca, K. Outcomes of Alzheimer's disease therapy with acetylcholinesterase inhibitors and memantine. *Expert Opin. Drug Saf.* **2014**, *13*, 759−774.

(3) Glenner, G. G.; Wong, C. W. Alzheimer's disease: initial report of the purification and characterization of a novel cerebrovascular amyloid protein. *Biochem. Biophys. Res. Commun.* **1984**, *120*, 885−890.

(4) Grundke-Iqbal, I.; Iqbal, K.; Tung, Y. C.; Quinlan, M.; Wisniewski, H. M.; Binder, L. I. Abnormal phosphorylation of the microtubule-associated protein τ (tau) in Alzheimer cytoskeletal pathology. *Proc. Natl. Acad. Sci. U. S. A.* **1986**, *83*, 4913−4917.

(5) Ferrer, I. Defining Alzheimer as a common age-related neurodegenerative process not inevitably leading to dementia. *Prog. Neurobiol.* **2012**, *97*, 38−51.

(6) Tsai, J.; Grutzendler, J.; Duff, K.; Gan, W.-B. Fibrillar amyloid deposition leads to local synaptic abnormalities and breakage of neuronal branches. *Nat. Neurosci.* **2004**, *7*, 1181.

(7) Gómez-Isla, T.; Hollister, R.; West, H.; Mui, S.; Growdon, J. H.; Petersen, R. C.; Parisi, J. E.; Hyman, B. T. Neuronal loss correlates with but exceeds neurofibrillary tangles in Alzheimer's disease. *Ann. Neurol.* **1997**, *41*, 17−24.

(8) Loo, D. T.; Copani, A.; Pike, C. J.; Whittemore, E. R.; Walencewicz, A. J.; Cotman, C. W. Apoptosis is induced by beta-amyloid in cultured central nervous system neurons. *Proc. Natl. Acad. Sci. U.S.A.* **1993**, *90*, 7951−7955.

(9) Zhu, X.; Raina, A. K.; Lee, H. G.; Casadesus, G.; Smith, M. A.; Perry, G. Oxidative stress signalling in Alzheimer's disease. *Brain Res.* **2004**, *1000*, 32−39.

(10) LaFerla, F. M. Calcium dyshomeostasis and intracellular signalling in Alzheimer's disease. *Nat. Rev. Neurosci.* **2002**, *3*, 862−872.

(11) Akiyama, H.; Barger, S.; Barnum, S.; Bradt, B.; Bauer, J.; Cole, G. M.; Cooper, N. R.; Eikelenboom, P.; Emmerling, M.; Fiebich, B. L.; Finch, C. E.; Frautschy, S.; Griffin, W. S. T.; Hampel, H.; Hull, M.; Landreth, G.; Lue, L.-F.; Mrak, R.; Mackenzie, I. R.; McGeer, P. L.; O'Banion, M. B.; Pachter, J.; Pasinetti, G.; Plata-Salaman, C.; Rogers, J.; Rydel, R.; Shen, Y.; Streit, W.; Strohmeyer, R.; Tooyoma, I.; Van Muiswinkel, F. L.; Veerhuis, R.; Walker, D.; Webster, S.; Wegrzyniak, B.; Wenk, G.; Wyss-Coray, T. Inflammation and Alzheimer's disease. *Neurobiol. Aging* **2000**, *21*, 383−421.

(12) Wyss-Coray, T.; Mucke, L. Inflammation in neurodegenerative disease—a double-edged sword. *Neuron* **2002**, *35*, 419−432.

(13) Barger, S. W.; Harmon, A. D. Microglial activation by Alzheimer amyloid precursor protein and modulation by apolipoprotein E. *Nature* **1997**, *388*, 878−881.

(14) Meda, L.; Cassatella, M. A.; Szendrei, G. I.; Otvos, L., Jr.; Baron, P.; Villalba, M.; Ferrari, D.; Rossi, F. Activation of microglial cells by β-amyloid protein and interferon-γ. *Nature* **1995**, *374*, 647−650.

(15) Yang, C.-N.; Shiao, Y.-J.; Shie, F.-S.; Guo, B.-S.; Chen, P.-H.; Cho, C.-Y.; Chen, Y.-J.; Huang, F.-L.; Tsay, H.-J. Mechanism mediating oligomeric Aβ clearance by naïve primary microglia. *Neurobiol. Dis.* **2011**, *42*, 221−230.

(16) Wang, W.-Y.; Tan, M.-S.; Yu, J.-T.; Tan, L. Role of pro-inflammatory cytokines released from microglia in Alzheimer's disease. *Ann. Transl. Med.* **2015**, *3*, 136.

(17) Katona, I.; Freund, T. F. Multiple functions of endocannabinoid signaling in the brain. *Annu. Rev. Neurosci.* **2012**, *35*, 529−558.

(18) Mechoulam, R.; Parker, L. A. The endocannabinoid system and the brain. *Annu. Rev. Psychol.* **2013**, *64*, 21−47.

(19) Lutz, B.; Marsicano, G.; Maldonado, R.; Hillard, C. J. The endocannabinoid system in guarding against fear, anxiety and stress. *Nat. Rev. Neurosci.* **2015**, *16*, 705−718.

(20) Ameri, A. The effects of cannabinoids on the brain. *Prog. Neurobiol.* **1999**, *58*, 315−348.

(21) Munro, S.; Thomas, K. L.; Abu-Shaar, M. Molecular characterization of a peripheral receptor for cannabinoids. *Nature* **1993**, *365*, 61−65.

(22) Van Sickle, M. D.; Duncan, M.; Kingsley, P. J.; Mouihate, A.; Urbani, P.; Mackie, K.; Stella, N.; Makriyannis, A.; Piomelli, D.; Davison, J. S.; Marnett, L. J.; Di Marzo, V.; Pittman, Q. J.; Patel, K. D.; Sharkey, K. A. Identification and functional characterization of brainstem cannabinoid CB2 receptors. *Science* **2005**, *310*, 329−332.

(23) Núñez, E.; Benito, C.; Pazos, M. R.; Barbachano, A.; Fajardo, O.; González, S.; Tolón, R. M.; Romero, J. Cannabinoid CB2 receptors are expressed by perivascular microglial cells in the human brain: an immunohistochemical study. *Synapse* **2004**, *53*, 208−213.

(24) Grünblatt, E.; Zander, N.; Bartl, J.; Jie, L.; Monoranu, C. M.; Arzberger, T.; Ravid, R.; Roggendorf, W.; Gerlach, M.; Riederer, P. Comparison analysis of gene expression patterns between sporadic Alzheimer's and Parkinson's disease. *J. Alzheimer's Dis.* **2007**, *12*, 291−311.

(25) Benito, C.; Núñez, E.; Tolón, R. M.; Carrier, E. J.; Rábano, A.; Hillard, C. J.; Romero, J. Cannabinoid CB2 receptors and fatty acid amide hydrolase are selectively overexpressed in neuritic plaque-associated glia in Alzheimer's disease brains. *J. Neurosci.* **2003**, *23*, 11136−11141.

(26) Bisogno, T.; Oddi, S.; Piccoli, A.; Fazio, D.; Maccarrone, M. Type-2 cannabinoid receptors in neurodegeneration. *Pharmacol. Res.* **2016**, *111*, 721−730.

(27) Ehrhart, J.; Obregon, D.; Mori, T.; Hou, H.; Sun, N.; Bai, Y.; Klein, T.; Fernandez, F.; Tan, J.; Shytle, R. D. Stimulation of cannabinoid receptor 2 (CB 2) suppresses microglial activation. *J. Neuroinflammation* **2005**, *2*, 29.

(28) Molina-Holgado, F.; Molina-Holgado, E.; Guaza, C.; Rothwell, N. J. Role of CB1 and CB2 receptors in the inhibitory effects of cannabinoids on lipopolysaccharide-induced nitric oxide release in astrocyte cultures. *J. Neurosci. Res.* **2002**, *67*, 829−836.

(29) Sheng, W. S.; Hu, S.; Min, X.; Cabral, G. A.; Lokensgard, J. R.; Peterson, P. K. Synthetic cannabinoid WIN55, 212-2 inhibits generation of inflammatory mediators by IL-1β-stimulated human astrocytes. *Glia* **2005**, *49*, 211−219.

(30) Wu, J.; Bie, B.; Yang, H.; Xu, J. J.; Brown, D. L.; Naguib, M. Activation of the CB2 receptor system reverses amyloid-induced memory deficiency. *Neurobiol. Aging* **2013**, *34*, 791−804.

(31) Martín-Moreno, A. M.; Brera, B.; Spuch, C.; Carro, E.; García-García, L.; Delgado, M.; Pozo, M. A.; Innamorato, N. G.; Cuadrado, A.; de Ceballos, M. L. Prolonged oral cannabinoid administration prevents neuroinflammation, lowers β-amyloid levels and improves cognitive performance in Tg APP 2576 mice. *J. Neuroinflammation* **2012**, *9*, 1−15.

(32) Koppel, J.; Vingtdeux, V.; Marambaud, P.; d'Abramo, C.; Jimenez, H.; Stauber, M.; Friedman, R.; Davies, P. CB2 receptor deficiency increases amyloid pathology and alters tau processing in a transgenic mouse model of Alzheimer's disease. *Mol. Med.* **2013**, *19*, 29−36.

(33) Davies, P.; Maloney, A. J. F. Selective loss of central cholinergic neurons in Alzheimer's disease. *Lancet* **1976**, *308*, 1403.

(34) Arendt, T.; Brückner, M. K.; Lange, M.; Bigl, V. Changes in acetylcholinesterase and butyrylcholinesterase in Alzheimer's disease resemble embryonic development—a study of molecular forms. *Neurochem. Int.* **1992**, *21*, 381−396.

(35) Greig, N. H.; Utsuki, T.; Yu, Q. S.; Zhu, X.; Holloway, H. W.; Perry, T.; Lee, B.; Ingram, D. K.; Lahiri, D. K. A new therapeutic target in Alzheimer's disease treatment: attention to butyrylcholinesterase. *Curr. Med. Res. Opin.* **2001**, *17*, 159−165.

(36) Giacobini, E. Cholinergic function and Alzheimer's disease. *Int. J. Psychiatry* **2003**, *18*, S1−S5.

(37) Grossberg, G. T. Cholinesterase inhibitors for the treatment of Alzheimer's disease: getting on and staying on. *Curr. Ther. Res.* **2003**, *64*, 216−235.

(38) Darvesh, S.; Hopkins, D. A.; Geula, C. Neurobiology of butyrylcholinesterase. *Nat. Rev. Neurosci.* **2003**, *4*, 131−138.

(39) Mesulam, M. M.; Guillozet, A.; Shaw, P.; Levey, A.; Duysen, E.; Lockridge, O. Acetylcholinesterase knockouts establish central cholinergic pathways and can use butyrylcholinesterase to hydrolyze acetylcholine. *Neuroscience* **2002**, *110*, 627−639.

(40) Nordberg, A.; Ballard, C.; Bullock, R.; Darreh-Shori, T.; Somogyi, M. A review of butyrylcholinesterase as a therapeutic target in the treatment of Alzheimer's disease. *Prim. Care Companion CNS Disord.* **2013**, *15*, 1−30.

(41) Hartmann, J.; Kiewert, C.; Duysen, E. G.; Lockridge, O.; Greig, N. H.; Klein, J. Excessive hippocampal acetylcholine levels in acetylcholinesterase-deficient mice are moderated by butyrylcholinesterase activity. *J. Neurochem.* **2007**, *100*, 1421−1429.

(42) Furukawa-Hibi, Y.; Alkam, T.; Nitta, A.; Matsuyama, A.; Mizoguchi, H.; Suzuki, K.; Moussaoui, S.; Yu, Q. S.; Greig, N. H.; Nagai, T.; Yamada, K. Butyrylcholinesterase inhibitors ameliorate cognitive dysfunction induced by amyloid-β peptide in mice. *Behav. Brain Res.* **2011**, *225*, 222−229.

(43) Greig, N. H.; Utsuki, T.; Ingram, D. K.; Wang, Y.; Pepeu, G.; Scali, C.; Yu, Q. S.; Mamczarz, J.; Holloway, H. W.; Giordano, T.; Chen, D.; Furukawa, K.; Sambamurti, K.; Brossi, A.; Lahiri, D. K. Selective butyrylcholinesterase inhibition elevates brain acetylcholine, augments learning and lowers Alzheimer β-amyloid peptide in rodent. *Proc. Natl. Acad. Sci.* **2005**, *102*, 17213−17218.

(44) Maurice, T.; Strehaiano, M.; Siméon, N.; Bertrand, C.; Chatonnet, A. Learning performances and vulnerability to amyloid toxicity in the butyrylcholinesterase knockout mouse. *Behav. Brain Res.* **2016**, *296*, 351−360.

(45) Morphy, R.; Rankovic, Z. Designed multiple ligands. An emerging drug discovery paradigm. *J. Med. Chem.* **2005**, *48*, 6523−6543.

(46) Proschak, E.; Stark, H.; Merk, D. Polypharmacology by design: a medicinal chemist's perspective on multitargeting compounds. *J. Med. Chem.* **2019**, *62*, 420−444.

(47) Dolles, D.; Decker, M. Dual-acting compounds acting as receptor ligands and enzyme inhibitors. In *Design of hybrid molecules for drug development*, Elsevier: Amsterdam, 2017; pp 137−165.

(48) Dolles, D.; Hoffmann, M.; Gunesch, S.; Marinelli, O.; Möller, J.; Santoni, G.; Chatonnet, A.; Lohse, M. J.; Wittmann, H.-J.; Strasser, A.; Nabissi, M.; Maurice, T.; Decker, M. Structure−activity relationships and computational investigations into the development of potent and balanced dual-acting butyrylcholinesterase inhibitors and human cannabinoid receptor 2 ligands with pro-cognitive in vivo profiles. *J. Med. Chem.* **2018**, *61*, 1646−1663.

(49) Freeman, S. E.; Dawson, R. M. Tacrine: a pharmacological review. *Prog. Neurobiol.* **1991**, *36*, 257−277.

(50) Summers, W. K.; Majovski, L. V.; Marsh, G. M.; Tachiki, K.; Kling, A. Oral tetrahydroaminoacridine in long-term treatment of senile dementia, Alzheimer type. *N. Engl. J. Med.* **1986**, *315*, 1241−1245.

(51) Watkins, P. B.; Zimmerman, H. J.; Knapp, M. J.; Gracon, S. I.; Lewis, K. W. Hepatotoxic effects of tacrine administration in patients with Alzheimer's disease. *JAMA* **1994**, *271*, 992−998.

(52) Milelli, A.; De Simone, A.; Ticchi, N.; H. Chen, H.; Betari, N.; Andrisano, V.; Tumiatti, V. Tacrine-based multifunctional agents in Alzheimer's disease: an old story in continuous development. *Curr. Med. Chem* **2017**, *24*, 3522−3546.

(53) Lin, H.; Li, Q.; Gu, K.; Zhu, J.; Jiang, X.; Chen, Y.; Sun, H. Therapeutic agents in Alzheimer's disease through a multi-target directed ligands strategy: Recent progress based on tacrine core. *Curr. Top. Med. Chem.* **2017**, *17*, 3000−3016.

(54) Chen, X.; Zenger, K.; Lupp, A.; Kling, B.; Heilmann, J.; Fleck, C.; Kraus, B.; Decker, M. Tacrine-silibinin codrug shows neuro-and hepatoprotective effects in vitro and pro-cognitive and hepatoprotective effects in vivo. *J. Med. Chem.* **2012**, *55*, 5231−5242.

(55) McEneny-King, A.; Osman, W.; Edginton, A. N.; Rao, P. P. N. Cytochrome P450 binding studies of novel tacrine derivatives: predicting the risk of hepatotoxicity. *Bioorg. Med. Chem. Lett.* **2017**, *27*, 2443−2449.

(56) Zenger, K.; Chen, X.; Decker, M.; Kraus, B. In-vitro stability and metabolism of a tacrine−silibinin codrug. *J. Pharm. Pharmacol.* **2013**, *65*, 1765−1772.

(57) Pagé, D.; Balaux, E.; Boisvert, L.; Liu, Z.; Milburn, C.; Tremblay, M.; Wei, Z.; Woo, S.; Luo, X.; Cheng, Y.-X.; Yang, H.; Srivastava, S.; Zhou, F.; Brown, W.; Tomaszewski, M.; Walpole, C.; Hodzic, L.; St-

Onge, S.; Godbout, C.; Salois, D.; Payza, K. Novel benzimidazole derivatives as selective CB₂ agonists. *Bioorg. Med. Chem. Lett.* **2008**, *18*, 3695−3700.

(58) Dolles, D.; Nimczick, M.; Scheiner, M.; Ramler, J.; Stadtmüller, P.; Sawatzky, E.; Drakopoulos, A.; Sotriffer, C.; Wittmann, H.-J.; Strasser, A.; Decker, M. Aminobenzimidazoles and structural isomers as templates for dual-acting butyrylcholinesterase inhibitors and hCB2R ligands to combat neurodegenerative disorders. *ChemMedChem* **2016**, *11*, 1270−1283.

(59) Dolles, D.; Strasser, A.; Wittmann, H. J.; Marinelli, O.; Nabissi, M.; Pertwee, R. G.; Decker, M. The first photochromic affinity switch for the human cannabinoid receptor 2. *Adv. Ther.* **2018**, *1*, 1700032.

(60) Nimczick, M.; Pemp, D.; Darras, F. H.; Chen, X.; Heilmann, J.; Decker, M. Synthesis and biological evaluation of bivalent cannabinoid receptor ligands based on hCB2R selective benzimidazoles reveal unexpected intrinsic properties. *Bioorg. Med. Chem.* **2014**, *22*, 3938−3946.

(61) Mishra, P.; Kumar, A.; Panda, G. Anti-cholinesterase hybrids as multi-target-directed ligands against Alzheimer's disease (1998-2018). *Bioorg. Med. Chem.* **2019**, *27*, 895−930.

(62) Minarini, A.; Milelli, A.; Tumiatti, V.; Rosini, M.; Simoni, E.; Bolognesi, M. L.; Andrisano, V.; Bartolini, M.; Motori, E.; Angeloni, C.; Hrelia, S. Cystamine-tacrine dimer: a new multi-target-directed ligand as potential therapeutic agent for Alzheimer's disease treatment. *Neuropharmacology* **2012**, *62*, 997−1003.

(63) Hu, M.-K.; Wu, L.-J.; Hsiao, G.; Yen, M.-H. Homodimeric tacrine congeners as acetylcholinesterase inhibitors. *J. Med. Chem.* **2002**, *45*, 2277−2282.

(64) Ellman, G. L.; Courtney, K. D.; Andres, V., Jr.; Featherstone, R. M. A new and rapid colorimetric determination of acetylcholinesterase activity. *Biochem. Pharmacol.* **1961**, *7*, 88−95.

(65) Bartolini, M.; Bertucci, C.; Cavrini, V.; Andrisano, V. β-Amyloid aggregation induced by human acetylcholinesterase: inhibition studies. *Biochem. Pharmacol.* **2003**, *65*, 407−416.

(66) Castro, A.; Martinez, A. Targeting beta-amyloid pathogenesis through acetylcholinesterase inhibitors. *Curr. Pharm. Des.* **2006**, *12*, 4377−4387.

(67) Zha, X.; Lamba, D.; Zhang, L.; Lou, Y.; Xu, C.; Kang, D.; Chen, L.; Xu, Y.; Zhang, L.; De Simone, A.; Samez, S.; Persaresi, A.; Stojan, J.; Lopez, M. G.; Egea, J.; Andrisano, V.; Bartolini, M. Novel tacrine−benzofuran hybrids as potent multitarget-directed ligands for the treatment of Alzheimer's disease: design, synthesis, biological evaluation, and X-ray crystallography. *J. Med. Chem.* **2016**, *59*, 114−131.

(68) Bartolini, M.; Bertucci, C.; Bolognesi, M. L.; Cavalli, A.; Melchiorre, C.; Andrisano, V. Insight into the kinetic of amyloid β (1−42) peptide self-aggregation: elucidation of inhibitors' mechanism of action. *ChemBioChem* **2007**, *8*, 2152−2161.

(69) Lange, J. H. M.; van Stuivenberg, H. H.; Coolen, H. K. A. C.; Adolfs, T. J. P.; McCreary, A. C.; Keizer, H. G.; Wals, H. C.; Veerman, W.; Borst, A. J. M.; de Looff, W.; Verveer, P. C.; Kruse, C. G. Bioisosteric replacements of the pyrazole moiety of rimonabant: synthesis, biological properties, and molecular modeling investigations of thiazoles, triazoles, and imidazoles as potent and selective CB1 cannabinoid receptor antagonists. *J. Med. Chem.* **2005**, *48*, 1823−1838.

(70) Yao, B. B.; Hsieh, G. C.; Frost, J. M.; Fan, Y.; Garrison, T. R.; Daza, A. V.; Grayson, G. K.; Zhu, C. Z.; Pai, M.; Chandran, P.; Salyers, A. K.; Wensink, E. J.; Honore, P.; Sullivan, J. P.; Dart, M. J.; Meyer, M. D. In vitro and in vivo characterization of A-796260: a selective cannabinoid CB2 receptor agonist exhibiting analgesic activity in rodent pain models. *Br. J. Pharmacol.* **2008**, *153*, 390−401.

(71) Nimczick, M.; Decker, M. New approaches in the design and development of cannabinoid receptor ligands: multifunctional and bivalent compounds. *ChemMedChem* **2015**, *10*, 773−786.

(72) Howlett, A. C.; Barth, F.; Bonner, T. I.; Cabral, G.; Casellas, P.; Devane, W. A.; Felder, C. C.; Herkenham, M.; Mackie, K.; Martin, B. R.; Mechoulam, R.; Pertwee, R. G. International Union of Pharmacology. XXVII. Classification of cannabinoid receptors. *Pharmacol. Rev.* **2002**, *54*, 161−202.

(73) Ross, R. A.; Brockie, H. C.; Stevenson, L. A.; Murphy, V. L.; Templeton, F.; Makriyannis, A.; Pertwee, R. G. Agonist-inverse agonist characterization at CB1 and CB2 cannabinoid receptors of L759633, L759656 and AM630. *Br. J. Pharmacol.* **1999**, *126*, 665−672.

(74) Williams, C. cAMP detection methods in HTS: selecting the best from the rest. *Nat. Rev. Drug Discov.* **2004**, *3*, 125−135.

(75) Waeber, G.; Thompson, N.; Chautard, T.; Steinmann, M.; Nicod, P.; Pralong, F. P.; Calandra, T.; Gaillard, R. C. Transcriptional activation of the macrophage migration-inhibitory factor gene by the corticotropin-releasing factor is mediated by the cyclic adenosine 3′, 5′-monophosphate responsive element-binding protein CREB in pituitary cells. *Mol. Endocrinol.* **1998**, *12*, 698−705.

(76) Kato, K.; Nomoto, M.; Izumi, H.; Ise, T.; Nakano, S.; Niho, Y.; Kohno, K. Structure and functional analysis of the human STAT3 gene promoter: alteration of chromatin structure as a possible mechanism for the upregulation in cisplatin-resistant cells. *Biochim. Biophys. Acta Gene Struct. Expr.* **2000**, *1493*, 91−100.

(77) Alas, S.; Bonavida, B. Inhibition of constitutive STAT3 activity sensitizes resistant non-Hodgkin's lymphoma and multiple myeloma to chemotherapeutic drug-mediated apoptosis. *Clin. Cancer. Res.* **2003**, *9*, 316−326.

(78) Zheng, Y.; Wang, Q.; Li, T.; Qian, J.; Lu, Y.; Li, Y.; Bi, E.; Reu, F.; Qin, Y.; Drazba, J.; Hsi, E.; Yang, J.; Cai, Z.; Yi, Q. Role of myeloma-derived MIF in myeloma cell adhesion to bone marrow and chemotherapy response. *J. Natl. Cancer Inst.* **2016**, *108*, djw131.

(79) Fulp, A.; Zhang, Y.; Bortoff, K.; Seltzman, H.; Snyder, R.; Wiethe, R.; Amato, G.; Maitra, R. Pyrazole antagonists of the CB1 receptor with reduced brain penetration. *Bioorg. Med. Chem.* **2016**, *24*, 1063−1070.

(80) Seltzman, H. H.; Shiner, C.; Hirt, E. E.; Gilliam, A. F.; Thomas, B. F.; Maitra, R.; Snyder, R.; Black, S. L.; Patel, P. R.; Mulpuri, Y.; Spigelman, I. Peripherally selective cannabinoid 1 receptor (CB1R) agonists for the treatment of neuropathic pain. *J. Med. Chem.* **2016**, *59*, 7525−7543.

(81) Schramm, S.; Huang, G.; Gunesch, S.; Lang, F.; Roa, J.; Högger, P.; Sabaté, R.; Maher, P.; Decker, M. Regioselective synthesis of 7-O-esters of the flavonolignan silibinin and SARs lead to compounds with overadditive neuroprotective effects. *Eur. J. Med. Chem.* **2018**, *146*, 93−107.

(82) Schramm, S.; Gunesch, S.; Lang, F.; Saedtler, M.; Meinel, L.; Högger, P.; Decker, M. Investigations into neuroprotectivity, stability, and water solubility of 7-O-cinnamoylsilibinin, its hemisuccinate and dehydro derivatives. *Arch. Pharm.* **2018**, *351*, 1800206.

(83) Davis, J. B.; Maher, P. Protein kinase C activation inhibits glutamate-induced cytotoxicity in a neuronal cell line. *Brain Res.* **1994**, *652*, 169−173.

(84) Murphy, T. H.; Miyamoto, M.; Sastre, A.; Schnaar, R. L.; Coyle, J. T. Glutamate toxicity in a neuronal cell line involves inhibition of cystine transport leading to oxidative stress. *Neuron* **1989**, *2*, 1547−1558.

(85) Tan, S.; Wood, M.; Maher, P. Oxidative stress induces a form of programmed cell death with characteristics of both apoptosis and necrosis in neuronal cells. *J. Neurochem.* **1998**, *71*, 95−105.

(86) Tan, S.; Schubert, D.; Maher, P. Oxytosis: a novel form of programmed cell death. *Curr. Top. Med. Chem.* **2001**, *1*, 497−506.

(87) Maurice, T.; Lockhart, B. P.; Privat, A. Amnesia induced in mice by centrally administered β-amyloid peptides involves cholinergic dysfunction. *Brain Res.* **1996**, *706*, 181−193.

(88) Lahmy, V.; Meunier, J.; Malmström, S.; Naert, G.; Givalois, L.; Kim, S. H.; Villard, V.; Vamvakides, A.; Maurice, T. Blockade of Tau hyperphosphorylation and Aβ 1−42 generation by the amino-tetrahydrofuran derivative ANAVEX2-73, a mixed muscarinic and σ 1 receptor agonist, in a nontransgenic mouse model of Alzheimer's disease. *Neuropsychopharmacology* **2013**, *38*, 1706−1723.

(89) McQuiston, A. R.; Saggau, P. Mu-opioid receptors facilitate the propagation of excitatory activity in rat hippocampal area CA1 by disinhibition of all anatomical layers. *J. Neurophysiol.* **2003**, *90*, 1936−1948.

(90) Batts, K. P.; Ludwig, J. An update on terminology and reporting. *Am. J. Surg. Pathol.* **1995**, *19*, 1409−1417.

(91) Mathew, T.; Karunanithy, R.; Yee, M.; Natarajan, P. Hepatotoxicity of dimethylformamide and dimethylsulfoxide at and above the levels used in some aflatoxin studies. *Lab. Invest.* **1980**, *42*, 257−262.

(92) Silverman, R. B. *The organic chemistry of enzyme-catalyzed reactions*. Academic Press: London, 2002.

(93) Naiki, H.; Higuchi, K.; Nakakuki, K.; Takeda, T. Kinetic analysis of amyloid fibril polymerization in vitro. *Lab. Invest.* **1991**, *65*, 104−110.

(94) Mukherjee, S.; Adams, M.; Whiteaker, K.; Daza, A.; Kage, K.; Cassar, S.; Meyer, M.; Yao, B. B. Species comparison and pharmacological characterization of rat and human CB_2 cannabinoid receptors. *Eur. J. Pharmacol.* **2004**, *505*, 1−9.

(95) Maurice, T.; Su, T.-P.; Privat, A. Sigma1 (σ1) receptor agonists and neurosteroids attenuate β25−35-amyloid peptide-induced amnesia in mice through a common mechanism. *Neuroscience* **1998**, *83*, 413−428.

(96) Meunier, J.; Ieni, J.; Maurice, T. The anti-amnesic and neuroprotective effects of donepezil against amyloid beta25-35 peptide-induced toxicity in mice involve an interaction with the sigma1 receptor. *Br. J. Pharmacol.* **2006**, *149*, 998−1012.

(97) Meunier, J.; Villard, V.; Givalois, L.; Maurice, T. The γ-secretase inhibitor 2-[(1R)-1-[(4-chlorophenyl) sulfonyl](2, 5-difluorophenyl) amino] ethyl-5-fluorobenzenebutanoic acid (BMS-299897) alleviates Aβ1−42 seeding and short-term memory deficits in the Aβ25−35 mouse model of Alzheimer's disease. *Eur. J. Pharmacol.* **2013**, *698*, 193−199.

(98) Villard, V.; Espallergues, J.; Keller, E.; Alkam, T.; Nitta, A.; Yamada, K.; Nabeshima, T.; Vamvakides, A.; Maurice, T. Antiamnesic and neuroprotective effects of the aminotetrahydrofuran derivative ANAVEX1-41 against amyloid β 25−35-induced toxicity in mice. *Neuropsychopharmacology* **2009**, *34*, 1552−1566.

(99) Villard, V.; Espallergues, J.; Keller, E.; Vamvakides, A.; Maurice, T. Anti-amnesic and neuroprotective potentials of the mixed muscarinic receptor/sigma$_1$ (σ_1) ligand ANAVEX2-73, a novel aminotetrahydrofuran derivative. *J. Psychopharmacol.* **2011**, *25*, 1101−1117.

(100) Zussy, C.; Brureau, A.; Delair, B.; Marchal, S.; Keller, E.; Ixart, G.; Naert, G.; Meunier, J.; Chevallier, N.; Maurice, T.; Givalois, L. Time-course and regional analyses of the physiopathological changes induced after cerebral injection of an amyloid β fragment in rats. *Am. J. Pathol.* **2011**, *179*, 315−334.

Expression Profiling of Circulating Tumor Cells in Pancreatic Ductal Adenocarcinoma Patients: Biomarkers Predicting Overall Survival

Consuelo Amantini[1]*, Maria Beatrice Morelli[1,2], Massimo Nabissi[2], Francesco Piva[3], Oliviero Marinelli[1,2], Federica Maggi[4], Francesca Bianchi[5], Alessandro Bittoni[5], Rossana Berardi[5], Riccardo Giampieri[5] and Giorgio Santoni[2]*

[1] School of Biosciences and Veterinary Medicine, University of Camerino, Camerino, Italy, [2] School of Pharmacy, Experimental Medicine Section, University of Camerino, Camerino, Italy, [3] Department of Specialistic Clinical and Odontostomatological Sciences, Polytechnic University of Marche, Ancona, Italy, [4] Department of Molecular Medicine, Sapienza University of Rome, Rome, Italy, [5] Oncology Clinic, AOU Ospedali Riuniti, Polytechnic University of Marche, Ancona, Italy

The interest in liquid biopsy is growing because it could represent a non-invasive prognostic or predictive tool for clinical outcome in patients with pancreatic ductal adenocarcinoma (PDAC), an aggressive and lethal disease. In this pilot study, circulating tumor cells (CTCs), CD16 positive atypical CTCs, and CTC clusters were captured and characterized in the blood of patients with PDAC before and after palliative first line chemotherapy by ScreenCell device, immunohistochemistry, and confocal microscopy analysis. Gene profiles were performed by digital droplet PCR in isolated CTCs, five primary PDAC tissues, and three different batches of RNA from normal human pancreatic tissue. Welsh's t-test, Kaplan-Meier survival, and Univariate Cox regression analyses have been performed. Statistical analysis revealed that the presence of high CTC number in blood is a prognostic factor for poor overall survival and progression free survival in advanced PDAC patients, before and after first line chemotherapy. Furthermore, untreated PDAC patients with CTCs, characterized by high ALCAM, POU5F1B, and SMO mRNAs expression, have shorter progression free survival and overall survival compared with patients expressing the same biomarkers at low levels. Finally, high SHH mRNA levels are negatively associated to progression free survival, whereas high vimentin mRNA levels are correlated with the most favorable prognosis. By hierarchical clustering and correlation index analysis, two cluster gene signatures were identified in CTCs: the first, with high expression of VEGFA, NOTCH1, EPCAM, IHH, is the signature of PDAC patients before chemotherapy, whereas the second, with an enrichment in the expression of CD44, ALCAM, and POU5F1B stemness and pluripotency genes, is reported after palliative chemotherapy. Overall our data support the clinic value of the identification of CTC's specific biomarkers to improve the prognosis and the therapy in advanced PDAC patients.

Keywords: circulating tumor cells, pancreatic cancer, overall survival, gene signature, digital droplet PCR, atypical CTC

INTRODUCTION

Pancreatic ductal adenocarcinoma (PDAC) is an aggressive and lethal disease whose incidence rate is growing. The overall survival (OS) rate at 5 years is only 9%, the lowest percentage respect to other cancers (1). After diagnosis only 24% of patients survive 1 year and the 85% of them die within 5 years from diagnosis (2). This high death rate depends not only on the development of drug resistance, but also on late diagnosis. The majority of PDAC patients are treated with a first line palliative chemotherapy to reduce symptoms and prolong their survival (3). However, data obtained using combined therapy with gemcitabine plus paclitaxel or folfirinox, have demonstrated an increase in the chemotherapeutic efficacy (4, 5).

In PDAC, the development of metastases occurs very early and their presence is discovered already during the first diagnosis. Metastases represent the main cause of cancer-related deaths and the mechanisms of the metastatic spread are not yet well-known. Recently, the detection/isolation of circulating tumor cells (CTCs) in blood samples from cancer patients prompted high interest. CTCs, believed to be responsible for seeding and dissemination of cancer, originate from the primary tumor mass and spread in the peripheral circulation among immune cells and erythrocytes (6). In addition, CTCs are also able to aggregate forming clusters, termed circulating tumor microemboli, whose size and concentration have been found to influence the development of metastases. It is now accepted that CTC clusters have survival advantage in the circulation, since the aggregation protect tumor cells from apoptosis, shear stress, and immune response facilitating the colonization (7). Thus, CTCs have been utilized as prognostic or predictive tool for clinical outcome in patients with localized, metastatic and recurrent disease and the CTC number is now considered a prognostic factor in breast, colorectal, prostate, and lung cancers (8).

Among the different technologies employed to isolate and purify CTCs, the ScreenCell® microfiltration is an epitope-independent size-based device, able to capture CTCs, both EPCAM positive and negative. It has been used in CTC identification in rare tumors like hemangiopericytoma (9) as well as in more common tumors such as non-small cell lung, bladder, prostate, head, and neck cancers (10–13) including PDAC (14).

Several studies demonstrated that a large number of CTCs and circulating tumor microemboli is detected in blood samples from PDAC patients with high accuracy and this appears to be clinically relevant avoiding the need of invasive tumor biopsies (8, 15, 16). In this regard, Nagrath et al. by using the CTC-chip on blood samples from PDAC patients, identified the presence of CTCs in the 100% of cases and the number of CTCs detected ranged from 9 to 831/ml (17). CTCs are found in the blood of patients with all PDAC stages and their presence is associated with poor progression-free survival (PFS), shorter OS, liver metastases, and poor tumor differentiation (18–20). Remarkably, high number of CTCs and unfavorable number of CTC clusters are associated with a trend for short OS (21).

Moreover, the recurrence occurs earlier in patients with CTCs than those without them, suggesting that CTCs are involved in pancreatic cancer malignancy and can be used to predict outcome and prognosis (18, 20). In addition, preclinical studies, performed using a xenograft mouse model of pancreatic adenocarcinoma, demonstrated that CTC concentration is markedly reduced in the pharmacologically treated group compared to the untreated one, indicating CTCs as a promising biomarker to monitor treatment efficacy (22). Interestingly, a recent report showed that in the blood of PDAC patients, the CTC population is represented not only by cancer cells but also by atypical CTCs that are hybrid cells, also called tumacrophages, deriving from the fusion between macrophages and cancer cells (23, 24). It has also been shown that the presence of tumacrophages significantly correlates with advanced PDAC disease (23).

At present, little is known about the neoplastic features, clinical significance, and molecular profiles of CTCs in PDAC patients. Several altered signaling pathways have been found in pancreatic cancers as KRAS, EGFR, NOTCH, WNT, and Hedgehog signaling pathways (25, 26). However, specific biomarkers useful for the early detection or for predicting treatment response are still missing. The complexity to manage clinical situations absolutely needs of new therapeutic strategies and further efforts must be made to identify novel targets for the development of personalized treatment options (27). In addition, given the anatomical difficulty of reaching the primary site of the tumor, it is problematic to monitor disease progression by invasive repeated biopsies. Thus, a multimarkers' analysis represents a good strategy to better understand the features of CTCs in terms of aggressiveness and phenotype. This could make it possible to select the most effective treatment and to facilitate a personalized therapy.

The aim of this study was to evaluate the expression of different genes involved in several signaling pathways in CTCs, isolated from patients with metastatic PDAC, in order to correlate the gene expression profiles with clinical parameters, before and after the palliative chemotherapeutic treatments.

MATERIALS AND METHODS

Patient Recruitment and Sample Processing

The study population consisted of patients with a histologically/cytologically confirmed diagnosis of metastatic/locally advanced PDAC, who were candidates to receive 1st line palliative chemotherapy ($n = 20$) and with ages between 44 and 76, hospitalized from 2016 to 2018 at Università Politecnica delle Marche–Azienda Ospedaliero-Universitaria Ospedali Riuniti Umberto I—Lancisi—Salesi, Ancona, Italy. Scheduled evaluations of disease status were performed via computed tomography scan of the chest and abdomen. Database with demographic, pathologic, and relevant clinical outcome/survival variables was maintained in a prospective manner. RECIST 1.1 criteria were used to evaluate the radiological responses to treatment, at approximately 3 months after the beginning of 1st line chemotherapy and every 3 months thereafter. Data regarding OS (time between the diagnosis and the death or lost-at-follow-up visit), OS1 (the time between the 1st cycle of chemotherapy and death or lost-at-follow-up visit) and PFS (the time between the 1st

cycle of chemotherapy and the 1st radiological progression or lost-at-follow-up-visit) were collected. All patients gave their consent prior to blood draws and the local Ethical Committee approved the study.

Peripheral blood samples from patients (6 ml) were collected in a K2-EDTA tube, before and after 3 months the beginning of the chemotherapy. The blood samples were processed within 3 h by using ScreenCell devices (Sarcelles, France) according to the protocol with some modifications to better eliminate peripheral blood cells. Briefly, after filtration, ScreenCell filters were washed with RPMI 1640 medium and then with Red Blood Lysis Buffer (Milteny Biotec, Bologna, Italy). The isolated cells were then detached from the filter by pipetting, collected in RPMI medium and the resulting cell suspension was filtered again. Blood samples from 5 healthy donors were processed as negative control.

Cell Counting

CTCs, collected in the second filter, were observed by stereo-microscope with bright-field illumination. Two independent operators performed a blind evaluation for each sample of the selected isolated cells, dividing patients in two categories: those with more than 10 CTCs and those with less. The presence of CTC clusters was also assessed and patients were divided in positive (Yes) or negative (No) for this parameter.

RNA Extraction, Reverse Transcription, and Digital Droplet PCR (ddPCR)

Total RNA from isolated CTCs was extracted by using the Single Shot Cell Lysis Kit (Bio-Rad, Hercules, CA, USA) according to the protocol. As control, three different total RNAs from normal pancreas tissues were purchased (OriGene Technologies, Rockville, MA, USA) and total RNA was extracted from 5 different primary PDAC tissue specimens, not autologous to the patients from whom CTCs were isolated (from Università Politecnica delle Marche–Azienda Ospedaliero-Universitaria Ospedali Riuniti Umberto I—Lancisi—Salesi, Ancona), by "RNeasy® FFPE" kit (QIAGEN, Milan, Italy).

Total RNA was retro-transcribed by Iscript Advanced cDNA Synthesis kit (Bio-Rad) and the resulting cDNA was used to pre-amplify each sample for all primers used in the gene expression analysis by SSOADvancedPreAmp Kit and PrimePCRPreAMP Assays (Bio-Rad). The ddPCR Supermix for Probes (No dUTP) (Bio-Rad) and the specific PrimePCR™ ddPCR™ Expression Probe Assays conjugated with FAM or HEX fluorescent dyes (the same pool used in the pre-amplification step) (Bio-Rad) were then used to perform the ddPCR. The analyzed target genes were: CD44, DHH, ALCAM, IHH, VEGFA, NOTCH1, VEGFB, PTCH1, ZEB1, PTCH2, ZEB2, SHH, EPCAM, SMO, POU5F1B, SPARC, STAT3, vimentin (VIM), and NOTCH2. Data, normalized to β-actin concentration, were analyzed using the QuantaSoft Software (Bio-Rad). Since some of the analyzed transcripts could also be expressed, although at low levels, in normal blood cells, ddPCR analysis was carried out identifying the gene expression values obtained from white blood cells and taking them as negative threshold.

After ddPCR, according to the ROC analysis performed before and after palliative 1st line chemotherapy, patients were sub-grouped for each gene in high (H) and low (L) expression.

Heat-maps were generated with hierarchical clustering analysis by the software Multi Experiment Viewer (MeV) Version 4.9.0. To compare CTCs with PDAC biopsies, gene expression levels were expressed as fold changes respect to normal pancreas RNAs used as calibrator.

Immunohistochemistry

Purified CTCs were fixed by using paraformaldehyde (4%) for 5 min at room temperature. After washing with PBS, cells were permeabilized by using 0.3% Triton X-100 in PBS for 15 min at room temperature. To block endogenous peroxidase, samples were incubated with 0.3% H_2O_2 for 15 min and then the blocking solution (3% BSA, 0.3% Triton X-100 in PBS) was used for 60 min at room temperature. Thereafter, cells were firstly incubated with anti-human pancytokeratin antibody (pan-CK, 1:50, DAKO, Agilent, Santa Clara, CA, USA) overnight at 4°C and then with anti-mouse biotin-conjugated secondary antibody for 30 min (1:200, ThermoFisher Scientific, Waltham, MA, USA). The immunodetection was performed using the VECTASTAIN® Elite® ABC System (Vectastain Laboratories, Burlingame, CA, USA), according to the provided protocol and counterstaining

TABLE 1 | Patient demographics and clinical features.

Number of patients	20
Average age	64.04 ± 8.07
Median age	64.13
Sex	F (4)
	M (16)
T	T1 (1)
	T2 (6)
	T3 (8)
	T4 (5)
N	Yes (16)
	No (4)
M	Yes (13)
	Liver (8)
	Lung (1)
	Peritoneum (1)
	Liver + lung (1)
	Liver + peritoneum (1)
	Lung + peritoneum (1)
	No (7)
Chirurgical resection	Yes (4)
	No (16)
First-line chemotherapy	Yes (19)
	Gemcitabine (4)
	Folfirinox (4)
	Gemcitabine + abraxane (11)
	No (1)

with hematoxylin for 30 s. Four random fields of each filter were analyzed under 40X magnification using the Olympus BX51 Microscope and the ImageJ software (National Institutes of Health, Bethesda, MD, USA).

Confocal Microscope Analysis

Isolated CTCs were fixed with 4% paraformaldehyde for 5 min at room temperature and permeabilized as above described. For epithelial markers analysis, cells were stained with mouse anti-human pan-CK (1:50, Agilent), anti-human EPCAM (1:50, Cell Signaling Technology, Danvers, MA, USA), anti-human CD45, and anti-human CD16 (Cell Signaling Technology) antibodies followed by goat anti-mouse secondary antibody Alexa 594 (1:100, ThermoFisher Scientific), labeled with DAPI (ThermoFisher Scientific) and examined under 40X magnification using the Confocal Microscopy Nikon C2plus and the NIS software (Nikon, Otawara, Japan).

Statistical Analysis

This study was an exploratory research. Statistical analysis was performed by using the Welch's t-test (GraphPad). Patients were divided in two groups according to: high and low CTC/cluster number, high and low gene expression levels. In addition, the Welch's t-test was used to compare gene expression levels between PDAC biopsy and CTCs. $p < 0.05$ was considered as statistically significant. The Kaplan-Meier (KM) method was also used for survival analysis. For Univariate analysis of significance (MedCalc package, MedCalc® v16.4.3), the long-rank test or Cox analysis was used. $p < 0.05$ was considered as statistically significant.

We determined, by Relative Operating Characteristic (ROC) curve analysis, the expression value for each analyzed gene (cDNA copies/μl) that best discriminates between good and poor prognosis.

For hierarchical clustering, we applied the most common settings that is "average linkage" as agglomeration rule and Pearson correlation to measure the similarity among gene profiles.

The analysis of frequency distribution was performed using Chi-squared test selecting as expected frequencies <60 for age, male category for sex, yes for lymph node invasion, yes for distant metastasis and high for CTC number; $p < 0.05$ was considered as statistically significant. To study the survival time we considered: OS, OS1, and PFS.

RESULTS

Capture and Detection of CTCs From Blood of PDAC Patients

All the 20 patients, enrolled in this study, had histologically confirmed diagnosis of PDAC; the list of patients' characteristics, including average age, sex, TNM classification, chirurgical resection, and 1st line chemotherapy options, is shown in **Table 1**. The median OS, OS1, or PFS of the patient population were 11.87, 8.75, and 6.16 months, respectively. The KM analysis was carried out to evaluate OS and PFS in relation to the clinic-pathological characteristics of PDAC patients. No statistical significance was found among age, TNM stage, different 1st line palliative chemotherapy protocol and OS, OS1, and PFS. Sex showed positive correlation with PFS ($p = 0.0470$) (**Supplementary Table 1**).

CTCs were isolated from blood samples in patients before chemotherapy (20 patients) and after standard palliative 1st line chemotherapy (19 samples, since one patient died during treatment).

Both single CTCs and/or CTC clusters were captured by microfiltration. In particular, before chemotherapy, low CTCs number (<10 CTCs/ml blood) was evidenced in 6/20 (30%) and high number (more than 10 CTCs/ml blood) in 14/20 (70%) of the PDAC patients; 3 months later, after palliative chemotherapy, low CTCs number was found in 4/19 (21%) and high in 15/19 (79%) PDAC patients. Moreover, since

Patients	T0 CTC	T0 Cluster	T1 CTC	T1 Cluster
#1T	H	+	H	+
#2T	H	−	H	+
#3T	H	+	H	+
#4T	H	+	L	+
#5T	H	−	H	+
#6T	L	+	L	−
#7T	L	−	L	−
#8T	L	−	H	+
#9T	H	+	H	−
#10T	H	+	ND	ND
#11T	H	+	H	+
#12T	H	+	H	+
#13T	H	+	H	+
#14T	L	−	H	+
#15T	H	+	H	+
#16T	L	−	L	−
#17T	H	+	H	+
#18T	L	−	H	+
#19T	H	+	H	+
#20T	H	+	H	+

FIGURE 1 | CTC isolation from blood samples of PDAC patients. **(A)** After isolation of CTCs on the ScreenCell filter, PDAC patients were classified, according to the evaluation performed by stereo-microscope, in H (High, more than 10 CTCs); L (Low, <10 CTCs); —(no presence of clusters); + (presence of clusters); ND (not determined). T0 = before chemotherapy; T1 = after chemotherapy. **(B)** Representative image of isolated CTC stained with H&E. **(C)** Representative image of single CTC in ScreenCell filter stained with anti-human pan-CK and processed by immunohistochemistry. The omission of the primary antibody was used as negative control. **(D)** Representative image of CTC cluster in ScreenCell filter processed as described in **(C)**.

CTC clusters, composed by more than 3 cells, have a greater predisposition of forming distal metastasis than single CTCs (7), our attention was focused on the presence of CTC aggregates. CTC clusters were present in 13/20 (65%) patients before the chemotherapy and in 15/19 (79%) patients after palliative chemotherapy (**Figure 1A**). Neither single CTCs nor CTC clusters were found in the blood of healthy donors. After chemotherapy (T1), in three patients the number of CTCs was increased and in one was reduced. Regarding to CTC clusters, in five patients the number is increased and in other two they were reduced.

We confirmed the CTC phenotype by Hematoxylin and Eosin (H&E) staining, immunohistochemistry and confocal microscopy using anti-human pan-CK, anti-EPCAM, and anti-CD45 antibodies. The H&E staining evidenced, as previously described (15), that the single CTC displays a big size with a hyperchromatic nucleus larger than $14\,\mu m$ and scant well-defined small rim of cytoplasm (**Figure 1B**). By immunohistochemistry, we showed that both single CTCs and CTC clusters, forming irregular microemboli, were markedly pan-CK$^+$ (**Figures 1C,D**). Finally, the confocal microscopy analysis demonstrated the presence in the CTC population of both EPCAM$^+$ or pan-CK$^+$ CD45$^-$ cancer cells and EPCAM$^+$ or pan-CK$^+$ CD45$^+$ atypical CTCs (**Figure 2A**). Since it has been suggested that atypical CTCs derived from the fusion between cancer

FIGURE 2 | Confocal microscopy analyses of isolated CTCs. **(A)** Representative images of single CTC and atypical CTC stained with anti-human EPCAM or anti-human pan-CK and anti-human CD45 Abs. DAPI was used to counteract nuclei. The omission of the primary antibody was used as negative control. **(B)** Representative image of atypical CTC stained with anti-human pan-CK and anti-human CD16 Abs. DAPI was used to counteract nuclei. **(C)** Representative image of a CTC cluster stained with anti-human pan-CK and anti-human CD45 Abs. DAPI was used to counteract nuclei.

cells and macrophages (23), we also evaluated, in CTCs, the expression of CD16 found to be expressed by pro-tumorigenic macrophages (28). The isolated atypical CTCs expressed CD16 (**Figure 2B**) supporting the previous data about the origin of these hybrid cells. Finally, we demonstrated that CTC cluster is formed by both pan-CK$^+$ CD45$^-$ cancer cells and pan-CK$^+$ CD45$^+$ atypical CTCs (**Figure 2C**).

Increased CTC Number Correlates With Poor Prognosis in PDAC Patients

We found that, PDAC patients with high number of CTCs/ml (H), evaluated before the chemotherapy (T0), display a significant shorter survival respect to patients with low number (L) when considering OS and OS1 (**Figures 3A,B**). Concerning PFS, a tendency toward significance was found between high and low CTCs number (**Figure 3C**). Our results suggest that high number

FIGURE 3 | OS, OS1, and PFS according to CTC or CTC cluster number. **(A–C)** OS, OS1, and PFS were evaluated stratifying patients according to H (High, more than 10 CTCs/ml) or L (Low, <10 CTCs/ml) CTCs amount. **(D–F)** OS, OS1, and PFS, were evaluated stratifying patients according to presence (Yes) or not (No) of CTC clusters. $p < 0.05$ was considered as statistically significant.

FIGURE 4 | Gene expression profiles of CTCs from PDAC patients. **(A,B)** Hierarchical clustering was used to analyze the expression levels of 19 genes, assessed by ddPCR, in CTCs from PDAC patients before chemotherapy **(A)** and after palliative chemotherapy **(B)**. Two different main gene clusters were found, as shown with vertical bars and identified as 1 and 2, before chemotherapy ($p < 0.0001$) and after chemotherapy ($p < 0.038$). **(C,D)** Correlation matrix showing only the gene pairs whose expression levels were found to be positively correlated with a correlation coefficient more than 0.8500.

of CTCs represents a negative factor for survival in PDAC patients. No significant correlation between the presence of CTC cluster (T0) and OS, OS1, or PFS was observed (**Figures 3D–F**).
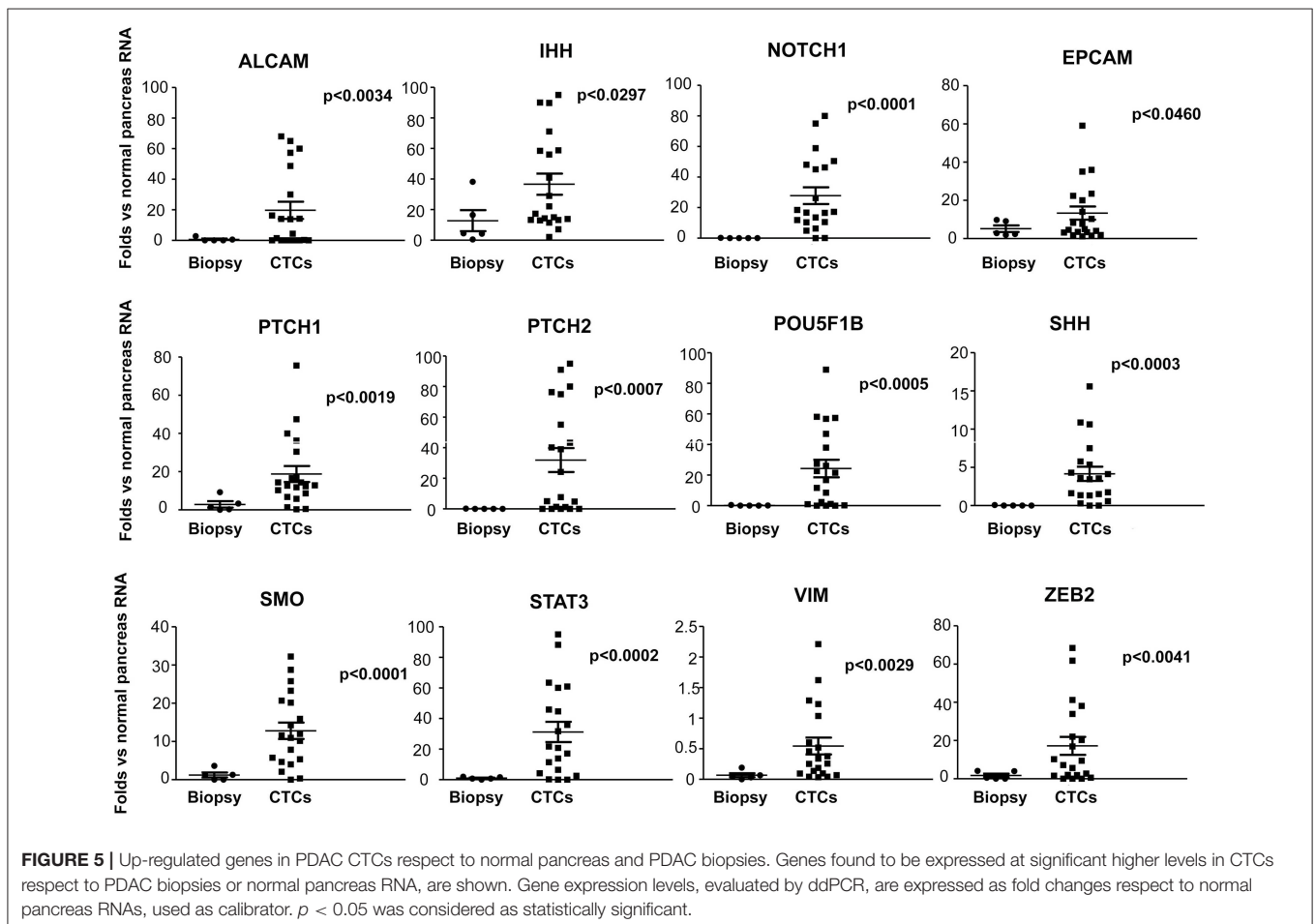
Gene Expression Profile of CTCs in PDAC Patients

The gene expression profile of CTCs from PDAC patients, before and after palliative chemotherapy, in PDAC biopsies and in normal pancreas RNAs, was evaluated.

At first, we found that the 19 genes analyzed by ddPCR analysis were differently expressed and clustered in the same patients, before and after therapy, as shown by the heat-map (**Figures 4A,B**). In fact, according to the expression levels, two different main gene clusters were identified in the hierarchical clustering before therapy: ZEB2, DHH, VEGFB, PTCH1, ZEB1, STAT3, SMO, SHH, PTCH2 (cluster 1) vs. CD44, IHH, VEGFA, NOTCH1, EPCAM, VIM, SPARC, NOTCH2, ALCAM, POU5F1B (cluster 2) (**Figure 4A**). Whereas, after 3 months of chemotherapy, the gene map showed a different grouping: ZEB2, SHH, VEGFA, NOTCH1, EPCAM (cluster 1) vs. DHH, VEGFB, PTCH1, ZEB1, STAT3, SMO, CD44, IHH, VIM, SPARC, NOTCH2, ALCAM, POU5F1B, PATCH2 (cluster 2) (**Figure 4B**). Since the gene grouping, based on the expression

profiles, changes after chemotherapy, our data suggest that the treatment is able to modify the gene expression levels in CTCs. The analysis of the correlation index for all studied genes (data not shown) also confirmed the presence of a strong association in the expression levels of specific genes and two different gene signature models for CTCs from PDAC patients were built before and after palliative chemotherapy, respectively. The VEGFA/EPCAM/NOTCH1/IHH network of functional genes marks the PDAC patients before chemotherapy (**Figure 4C**), whereas the VEGFB/ALCAM/PTCH1/2/POU5F1B/CD44 cluster characterizes CTCs from patients after the conditioned chemotherapy (**Figure 4D**).

Moreover, since CTCs are implicated in the metastatic spread, to better understand the differences between circulating and primary tumor mass cells, we compared the gene expression levels, evaluated as fold changes respect to normal pancreatic RNAs, of CTCs (T0) with PDAC biopsies. A significantly increased expression of ALCAM, SHH, IHH, PTCH1, PTCH2, ZEB2, SMO, VIM, EPCAM, POU5F1B, STAT3, and NOTCH1 was found in CTCs respect to normal pancreatic RNA and, even more interestingly, compared with PDAC biopsies (**Figure 5**). Overall, these results suggest that the ability of CTCs to circulate is associated with the enhancement in the expression levels of

FIGURE 5 | Up-regulated genes in PDAC CTCs respect to normal pancreas and PDAC biopsies. Genes found to be expressed at significant higher levels in CTCs respect to PDAC biopsies or normal pancreas RNA, are shown. Gene expression levels, evaluated by ddPCR, are expressed as fold changes respect to normal pancreas RNAs, used as calibrator. $p < 0.05$ was considered as statistically significant.

several genes mainly involved in the Hedgehog, angiogenesis, epithelial mesenchymal transition (EMT) and transcription regulation pathways.

Detection of Different EMT Phenotypes in CTCs From PDAC Patients

Among all the analyzed genes, our attention was focused on those strongly associated with the stemness and aggressiveness as well as EMT phenotype. On the basis of EMT markers (e.g., EPCAM/VIM) we demonstrated that about 40% of patients display epithelial CTCs (E-CTCs), whereas 60% show hybrid CTCs (H-CTCs) expressing both EPCAM and VIM (**Table 2**). No change in the percentage of patients showing E-CTCs was found 3 months after chemotherapy (42%), whereas a reduction of those with H-CTCs (37%) as well as the occurrence of patients (21%) with mesenchymal CTCs (M-CTCs) was observed (**Table 3**). We then analyzed the distribution of patients, according to the clinic-pathological features and the different EMT-phenotypes of CTCs, before and after palliative chemotherapy (**Tables 2**, **3**). We found that before chemotherapy, the distribution of patients for age, gender, lymph node metastasis, distant metastasis, and CTC number was significantly different between E-CTC and H-CTC groups (**Table 2**); similarly, after palliative chemotherapy, as respect to lymph node metastasis and distant metastasis, E-, H-, and M-CTC groups were significantly different (**Table 3**). Moreover, 1/20 (5%) and 3/19 (16%) PDAC patients, before and after palliative chemotherapy, respectively, evidenced a more aggressive CTC phenotype, characterized by high levels of CD44/ALCAM (29).

Correlation Between CTC Gene Expression and OS or PFS in PDAC Patients

The correlation between the expression level of the 19 analyzed genes in CTCs and OS, OS1, and PFS was evaluated (**Supplementary Tables 2**, **3**).

A statistically significant correlation was found for the expression of ALCAM, POU5F1B, and SMO and OS in CTCs from PDAC patients (**Figure 6A**); similar results were obtained by Univariate analysis (**Figure 6B**). No positive correlation was found for the other analyzed genes (**Supplementary Tables 2**, **3**). Similarly, after palliative chemotherapy, low ALCAM and high VIM levels were correlated with a longer OS1 (**Figure 7A**). These data were confirmed by Univariate analysis (**Figure 7B**). Regarding the PFS, high VIM, and low SHH levels were associated with a shorter PFS (**Figure 7C**). Similar results were obtained for SHH ($p = 0.022$) by Univariate Cox regression analysis (**Figure 7D**).

DISCUSSION

The majority of cancer patients dies from metastasis, regardless of chemotherapy approaches. Current cancer treatments are usually determined on primary tumor instead that on metastasis or cancer cells in blood circulation. Since distant metastases are considered to be the end-result of CTCs, the molecular characterization of these cells, including both cancer cells and tumacrophages (23), represents a promising approach to better evaluate the prognosis and select the therapy (30).

The identification of specific gene profiles and phenotypic changes occurring in CTCs could result in a better understanding of the metastatic process and lead to more effective and targeted therapeutic strategies. To our knowledge, very few reports have evaluated gene expression in blood CTCs. Moreover, this is the first study in which size-based CTC isolation method was coupled with ddPCR not only to confirm the CTCs phenotypes, but also to evaluate gene profiles.

Herein, we demonstrated the presence of single CTCs, atypical CTCs, and CTC clusters in the blood of PDAC patients before chemotherapy and 3 months later palliative first line chemotherapy. Our data are in agreement with recent data showing the presence of atypical CTCs, characterized by the expression of EPCAM, pan-CK, and CD45, in several cancer types. According to recent findings, they are hybrid cells deriving from the fusion of macrophages and tumor cells and for this reason, they are called tumacrophages. These cells, characterized by the expression of epithelial and hematopoietic markers as cytokeratins, CD45, and CD16, display progressive malignant behavior and tumorigenic abilities, contributing to the metastatic spread (23, 24).

High number of single CTCs and CTC clusters was captured in the blood of PDAC patients before and after chemotherapy. However, with regard to variations in the CTC number and cluster between before and after chemotherapy, in the majority of

TABLE 2 | PDAC patient distributions according to EMT phenotypes of CTCs and clinic-pathological features before chemotherapy.

|		Epithelial CTC (%)	Hybrid CTC (%)	
Age (year)	<60	5/20 (25%)	2/20 (10%)	
	>60	5/20 (25%)	8/20 (40%)	*
Gender	Male	10/20 (50 %)	8/20 (40%)	
	Female		2/20 (10%)	*
TNM stage	I	–	1/20 (5%)	
	II	2/20 (10%)	4/20 (20%)	
	III	5/20 (25%)	3/20 (15%)	
	IV	3/20 (15%)	2/20 (10%)	
Lymph node metastasis	Negative	1/20 (5%)	3/20 (15%)	
	Positive	9/20 (45%)	7/20 (35%)	*
Distant metastasis	Negative	5/20 (20%)	2/20 (10%)	
	Positive	5/20 (25%)	8/20 (40%)	*
Metastatis sites	Liver	4/13 (30.8%)	3/13 (23.1%)	
	Others	1/13 (7.6%)	5/13 (38.5%)	
CTC number	High	8/20 (40%)	7/20 (35%)	
	Low	1/20 (5%)	4/20 (20%)	*
CTC cluster	Yes	7/20 (35%)	6/20 (30%)	
	No	3/20 (15%)	4/20 (20%)	

*$p < 0.01$.

TABLE 3 | PDAC patient distributions according to the different EMT phenotypes of CTCs and clinic-pathological features after palliative chemotherapy.

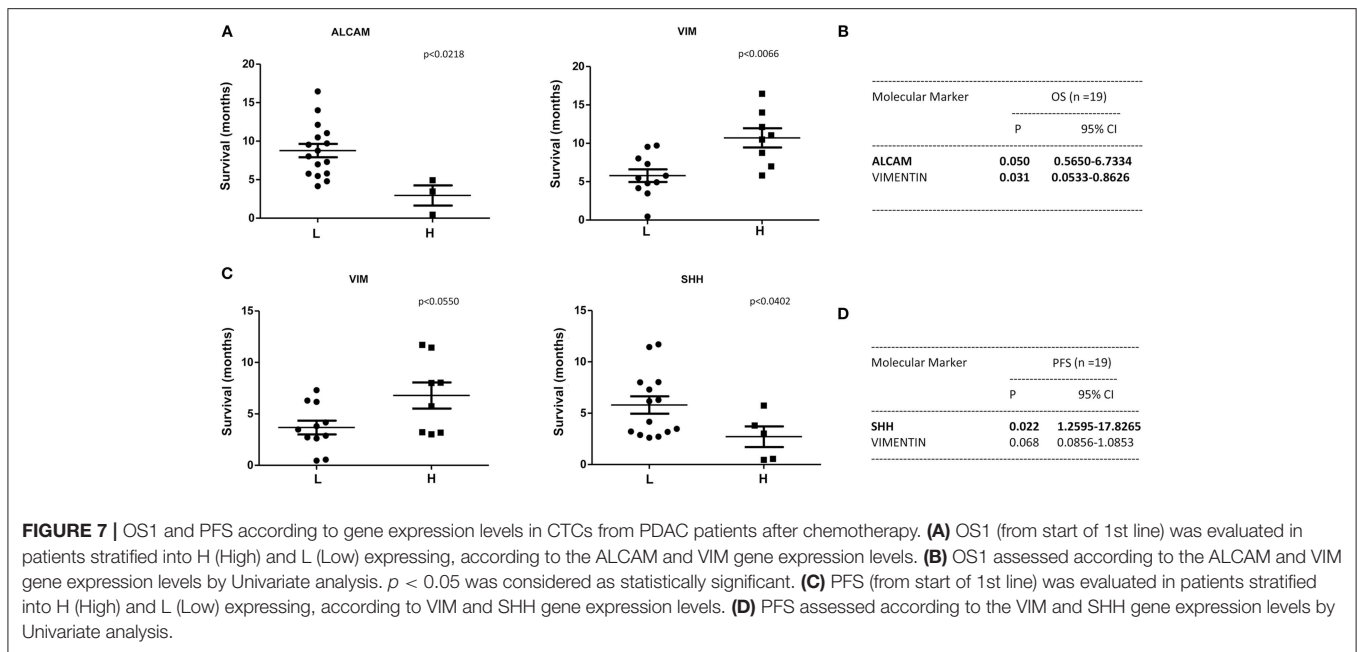|		Epithelial CTC 8/19 (42.1%)	Hybrid CTC 7/19 (36.8%)	Mesenchymal CTC 4/19 (21.1%)	
TNM stage	I		1/19 (5.3%)		
	II	3/19 (15.8%)	2/19 (10.1%)	1/19 (5.3%)	
	III	4/19 (21.1%)	3/19 (15.8%)		
	IV	1/19 (5.3%)	1/19 (5.3%)	3/19 (15.8%)	
Lymph node metastasis	Negative	3/19 (15.8%)	1/19 (5.3%)		
	Positive	6/19 (31.6%)	7/19 (36.9%)	2/19 (10.1%)	*
Distant metastasis	Negative	4/19 (21.1%)	1/19 (5.3%)	2/19 (10.1%)	
	Positive	4/19 (21.1%)	6/19 (31.6%)	2/19 (10.1%)	*
Metastasis sites	Liver	3/12 (25%)	4/12 (33.3%)		
	Other	1/12 (8.3%)	2/12 (16.7%)	2/12 (16.7%)	
CTC number	High	6/19 (31.6%)	5/19 (26.3%)	4/19 (21.1%)	
	Low	2/19 (10.1%)	2/19 (10.1%)		
CTC cluster	Yes	6/19 (31.6%)	5/19 (26.3%)	4/19 (21.1%)	
	No	2/19 (10.1%)	2/19 (10.1%)		

*$p < 0.01$.
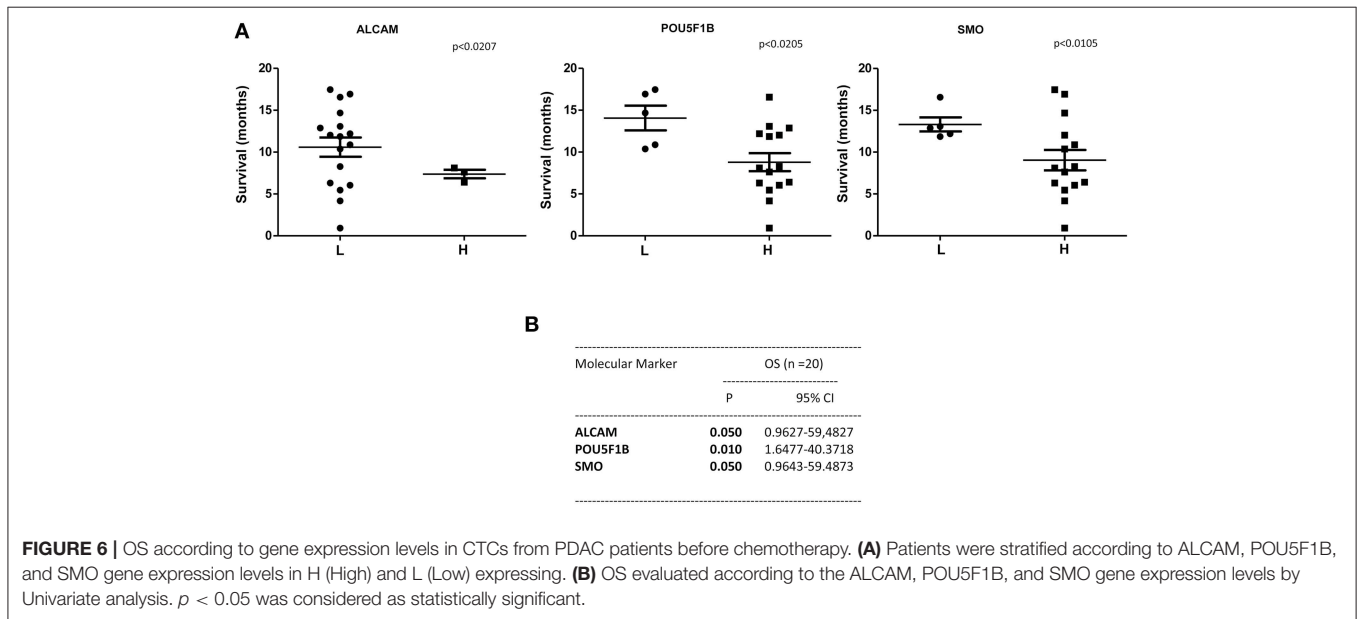
FIGURE 6 | OS according to gene expression levels in CTCs from PDAC patients before chemotherapy. **(A)** Patients were stratified according to ALCAM, POU5F1B, and SMO gene expression levels in H (High) and L (Low) expressing. **(B)** OS evaluated according to the ALCAM, POU5F1B, and SMO gene expression levels by Univariate analysis. $p < 0.05$ was considered as statistically significant.

the patients, chemotherapy is not able to induce changes. Overall, we evidenced that increased CTC number represents a negative prognostic factor for poor OS and PFS in PDAC patients.

EMT process arises during pancreatic cancer progression generating highly tumorigenic stem cells, characterized by motility and invasiveness. Multiple studies reported that EMT/MET (mesenchymal epithelial transition) processes are common in CTCs (31). Due to the high heterogeneity and plasticity of metastatic PDAC cells, pancreatic cells often cross between an EMT to MET phenotype during the metastatic adaption (32). In this regard, Zhao et al. using the Can Patrol system, identified the presence of three distinct CTC phenotypes in PDAC patients: E-CTC, M-CTC, and E/M or H-CTCs. The

CTC status correlated with lymph node invasion, TNM, and distant metastasis. In this study, KM survival analysis showed that patients with higher CTC count had significantly reduced OS and PFS compared with those showing lower CTC number (33). Moreover, by exploring the EMT phenomenon, it has been demonstrated that M-CTCs are associated with tumor progression and chemo-resistant cancer types (34). In this regard, we showed that E-CTCs and H-CSCs are found in PDAC patients before chemotherapy, whereas the M-CTCs subtype appears in chemotherapy-conditioned patients.

The identification of biomarkers in patients at high risk of poor prognosis might deserve additional/alternative therapeutic interventions also in advanced metastatic PDAC patients.

FIGURE 7 | OS1 and PFS according to gene expression levels in CTCs from PDAC patients after chemotherapy. **(A)** OS1 (from start of 1st line) was evaluated in patients stratified into H (High) and L (Low) expressing, according to the ALCAM and VIM gene expression levels. **(B)** OS1 assessed according to the ALCAM and VIM gene expression levels by Univariate analysis. $p < 0.05$ was considered as statistically significant. **(C)** PFS (from start of 1st line) was evaluated in patients stratified into H (High) and L (Low) expressing, according to VIM and SHH gene expression levels. **(D)** PFS assessed according to the VIM and SHH gene expression levels by Univariate analysis.

In this regard, isolation of CTCs from blood sample holds the promise of diagnosing and molecular profiling cancers. CTCs are thought to represent the intravasation tumor stage between the primary cancer and its distant metastases. Thus, by ddPCR assay, the molecular profile of genes, involved in EMT, angiogenesis, stemness and pluripotency, Hedgehog, Notch, and Stat pathways, have been evaluated in CTCs from PDAC patients before and after palliative chemotherapy, and compared with normal pancreatic RNAs and PDAC biopsies. We found a strong up-regulation of ALCAM, IHH, and SHH, NOTCH1, EPCAM, PTCH1, PTCH2, POU5F1B, SMO and ZEB2, STAT3, and VIM genes in the CTCs compared to normal pancreatic samples and, in particular, respect to the biopsies. Moreover, using hierarchical clustering to analyze gene expression levels, two different gene clusters were identified in CTCs from PDAC patients, before and after palliative chemotherapy. In particular, the first group consisted of VEGFA, NOTCH1 and 2, EPCAM, IHH, CD44, ALCAM, VIM, SPARC, and POU5F1B genes whereas the other consisted of VEGFB, DHH and SHH, PTCH1 and 2, ZEB1 and 2, SMO, and STAT3 genes. After chemotherapy, the VEGFA, NOTCH1 and EPCAM phenotype was maintained, whereas a phenotype enriched of stemness and pluripotency genes such as VEGFB, CD44, ALCAM, NOTCH2, POU5F1B, PTCH1 and 2, STAT3, DHH, IHH and SMO, SPARC, and VIM, emerged. To better characterize the gene clustering based on positive correlation, multiple correlation index analysis was performed. A significant high correlation coefficient for several gene pairs was found allowing the identification of specific gene signatures in CTCs from PDAC patients: VEGFA/NOTCH1/EPCAM/IHH gene cluster before chemotherapy and VEGFB/POU5F1B/PTCH1/PTCH2/ALCAM/CD44 after palliative chemotherapy.

There is growing evidence that CTC population is extremely heterogeneous, with a small percentage of tumor cells, called cancer stem cells (CSCs) expressing CD44, ALCAM, POU5F1B (35), able to proliferate and form new tumors. The presence of CSCs in tumors is associated with aggressive disease and poor prognosis (35). We showed high ALCAM, POU5F1B, and SMO mRNA expression levels in CTCs that are predictive of poor OS in both untreated and treated PDAC patients. In addition, high SHH mRNA expression level in CTCs has been demonstrated to represent a negative factor for PFS.

CSCs express several markers such as CD44, CD166, POU5F1B, EPCAM, NOTCH1 (36), and STAT3 (37). In this regard, we observed during PDAC progression, after palliative chemotherapy, an enrichment in the CTCs of the expression levels of stemness and pluripotency genes, as CD44, ALCAM, EPCAM, NOTCH1, POU5F1B, PTCH1, or CSC drivers as VEGFB and STAT3.

The role of VEGFB in tumor progression remains controversial. In fact, although VEGFB overexpression predicts for increased distant metastasis and shorter OS in advanced cancers (38), it was also shown to delay tumor growth in a mouse model of pancreatic neuroendocrine tumorigenesis (39). VEGFB is a part of VEGFB/GSK-β3/PI3K-Akt/CD44 signaling pathway controlling stem cell renewal, differentiation and development (40). The CD44 induces the EMT and triggers the expression of POU5F1B/OCT-4 stem cell marker, through the AKT/GSK-3β/β-catenin pathway (41). POU5F1B/OCT-4 maintains pluripotency and self-renewal by interacting with STAT3 and the Hedgehog pathway. Its overexpression in PDAC induces cell proliferation, migration, invasion and gemcitabine resistance (GR) (42) and its expression correlates with the N1/M1 status and worse prognosis. In several KRAS mutated cancers, the CD44 molecule associates with ALCAM/CD166 promoting an aggressive phenotype that predicts worse outcome and increased risk of liver and lung metastasis (e.g., colon cancer) (29). In addition, high ALCAM levels are associated with poor survival,

early tumor relapse (43) and chemoresistance (44). Regarding the Notch pathway, down-regulation of NOTCH1 reduces PDAC invasiveness (45), whereas NOTCH2 silencing reduces the expression of ZEB1, reverts the EMT phenotype, down-regulates the CSC marker expression (e.g., CD44) and decreases the invasiveness of GR-cells (46). In line with these findings, we showed the presence of CTCs expressing CD44/CD166 in PDAC patients with liver and lung metastasis. Thus, the analysis of gene expression levels in CTCs could permit to identify in KRAS mutated PDAC, patients expressing the CD44/CD166 phenotype associated with higher risk to develop lymph node invasion and distant metastasis. In addition, CTCs' characterization represents a non-invasive tool to identify, before palliative chemotherapy, patients predisposed to show GR-resistance, thus facilitating the design of individualized therapies.

Further support to our data, comes from *in vivo* experiments with metformin (met) treatment targeting several genes studied in our molecular analysis. In fact, met has been demonstrated to inhibit pancreatic intraepithelial neoplasia growth and the progression to PDAC, by reducing the CD44 or EPCAM stem cell marker expression in a transgenic mouse model (47).

On the contrary, we also showed that VIM expression positively correlates with a higher OS and PFS in PDAC patients after palliative first line chemotherapy. VIM, traditionally considered a marker of EMT, is also involved in angiogenesis, migration, invasion, metastasis, and drug-resistance (48, 49). For long time, high expression of VIM was only associated with poor prognosis in patients with different cancers (50). However, recently, high VIM expression was also correlated with a prolonged survival in endometrioid cancer patients (51) and better prognosis in ovarian cancer patients (46). This protective effect was explained by the role of VIM in the regulation of cancer cell-platinum resistance (52). Similarly to this study, it has been demonstrated that in Capan-1-GR cells the drug resistance is associated with VIM down-regulation (53). Thus, the increase of OS in patients showing CTCs with high VIM expression may be related to gemcitabine susceptibility in PDAC patients mainly treated with gemcitabine, alone or in combination with paclitaxel.

Overall, our data support the potential clinical value of CTCs from PDAC patients. CTC number, EMT/MET phenotype and molecular gene profile may contribute to the PDAC prognosis and therapy. Therefore, this study confirms that in PDAC high CTC number represents a negative prognostic factor, but also demonstrates that the identification of specific biomarkers could be useful to improve the prognosis and therapy in advanced PDAC patients. However, our pilot study includes a small sample size and large well-designed clinical trial is required to elucidate the real potential value of CTC gene profile in PDACs.

DATA AVAILABILITY

Data generated or analyzed during this study, with the only exception of correlation matrix analysis for all studied genes, are included in this published article and its additional information files. The whole correlation matrix is available from the corresponding author.

ETHICS STATEMENT

All patients gave their consent prior to blood draws and the local Ethical Committee of the Università Politecnica delle Marche–Azienda Ospedaliero-Universitaria Ospedali Riuniti Umberto I, Lancisi, Salesi, Ancona, Italy, approved the study. The patients/participants provided their written informed consent to participate in this study.

AUTHOR CONTRIBUTIONS

CA contributed to the acquisition, analysis, interpretation of the data, and drafted the manuscript. MM and MN performed acquisition and interpretation of the data. FM and FB revised the manuscript. FP and OM were responsible for analysis. AB and RG participated to the acquisition of the data. RB contributed to the conception of the work and revised the manuscript. GS designed the work and drafted the manuscript.

FUNDING

ACKNOWLEDGMENTS

A special thanks to Prof. Tomassoni for his support in immunohistochemical analysis.

SUPPLEMENTARY MATERIAL

The Supplementary Material for this article can be found online at: https://www.frontiersin.org/articles/10.3389/fonc.2019.00874/full#supplementary-material

REFERENCES

1. Siegel RL, Miller KD, Jemal A. Cancer statistics, 2019. *CA Cancer J Clin*. (2019) 69:7–34. doi: 10.3322/caac.21551

2. Rawla P, Sunkara T, Gaduputi V. Epidemiology of pancreatic cancer: global trends, etiology and risk factors. *World J Oncol*. (2019) 10:10–27. doi: 10.14740/wjon1166

3. Hidalgo M. Pancreatic cancer. *N Engl J Med*. (2010) 362:1605–17. doi: 10.1056/NEJMra0901557

4. Von Hoff DD, Ramanathan RK, Borad MJ, Laheru DA, Smith LS, Wood TE, et al. Gemcitabine plus nab-paclitaxel is an active regimen in patients with advanced pancreatic cancer: a phase I/II trial. *J Clin Oncol*. (2011) 29:4548–54. doi: 10.1200/JCO.2011.36.5742

5. Conroy T, Desseigne F, Ychou M, Bouché O, Guimbaud R, Bécouarn Y, et al. FOLFIRINOX versus gemcitabine for metastatic pancreatic cancer. *N Engl J Med*. (2011) 364:1817–25. doi: 10.1056/NEJMoa1011923

6. Jeong KY, Kim EK, Park MH, Kim HM. Perspective on cancer therapeutics utilizing analysis of circulating tumor cells. *Diagnostics*. (2018) 8:23. doi: 10.3390/diagnostics8020023

7. Fabisiewicz A, Grzybowska E. CTC clusters in cancer progression and metastasis. *Med Oncol*. (2017) 34:12. doi: 10.1007/s12032-016-0875-0

8. Khoja L, Backen A, Sloane R, Menasce L, Ryder D, Krebs M, et al. A pilot study to explore circulating tumour cells in pancreatic cancer as a novel biomarker. *Br J Cancer*. (2012) 106:508–16. doi: 10.1038/bjc.2011.545

9. Nicolazzo C, Colangelo L, Corsi A, Carpino G, Gradilone A, Sonato C, et al. Liquid biopsy in rare cancers: lessons from hemangiopericytoma. *Anal Cell Pathol*. (2018) 2018:9718585. doi: 10.1155/2018/9718585

10. Chudasama D, Barr J, Beeson J, Beddow E, McGonigle N, Rice A, et al. Detection of circulating tumour cells and survival of patients with non-small cell lung cancer. *Anticancer Res*. (2017) 37:169–73. doi: 10.21873/anticanres.11302

11. Awe JA, Saranchuk J, Drachenberg D, Mai S. Filtration-based enrichment of circulating tumor cells from all prostate cancer risk groups. *Urol Oncol*. (2017) 35:300–9. doi: 10.1016/j.urolonc.2016.12.008

12. Fina E, Necchi A, Bottelli S, Reduzzi C, Pizzamiglio S, Iacona C, et al. Detection of circulating tumour cells in urothelial cancers and clinical correlations: comparison of two methods. *Dis Markers*. (2017) 2017:3414910. doi: 10.1155/2017/3414910

13. Kulasinghe A, Perry C, Jovanovic L, Nelson C, Punyadeera C. Circulating tumour cells in metastatic head and neck cancers. *Int J Cancer*. (2015) 136:2515–23. doi: 10.1002/ijc.29108

14. Kulemann B, Pitman MB, Liss AS, Valsangkar N, Fernández-Del Castillo C, Lillemoe KD, et al. Circulating tumor cells found in patients with localized and advanced pancreatic cancer. *Pancreas*. (2015) 44:547–50. doi: 10.1097/MPA.0000000000000324

15. Iwanicki-Caron I, Basile P, Toure E, Antonietti M, Lecleire S, Di Fiore A, et al. Usefulness of circulating tumor cell detection in pancreatic adenocarcinoma diagnosis. *Am J Gastroenterol*. (2013) 108:152–5. doi: 10.1038/ajg.2012.367

16. Ankeny JS, Court CM, Hou S, Li Q, Song M, Wu D, et al. Circulating tumour cells as a biomarker for diagnosis and staging in pancreatic cancer. *Br J Cancer*. (2016) 114:1367–75. doi: 10.1038/bjc.2016.121

17. Nagrath S, Sequist LV, Maheswaran S, Bell DW, Irimia D, Ulkus L, et al. Isolation of rare circulating tumour cells in cancer patients by microchip technology. *Nature*. (2007) 450:1235–9. doi: 10.1038/nature06385

18. Poruk KE, Valero V III, Saunders T, Blackford AL, Griffin JF, Poling J, et al. Circulating tumor cell phenotype predicts recurrence and survival in pancreatic adenocarcinoma. *Ann Surg*. (2016) 264:1073–81. doi: 10.1097/SLA.0000000000001600

19. Han L, Chen W, Zhao Q. Prognostic value of circulating tumor cells in patients with pancreatic cancer: a meta-analysis. *Tumour Biol*. (2014) 35:2473–80. doi: 10.1007/s13277-013-1327-5

20. Okubo K, Uenosono Y, Arigami T, Mataki Y, Matsushita D, Yanagita S, et al. Corrigendum to "Clinical impact of circulating tumor cells and therapy response in pancreatic cancer" [43 (6) (2017) 1050-1055]. *Eur J Surg Oncol*. (2018) 44:860. doi: 10.1016/j.ejso.2018.03.015

21. Chang MC, Chang YT, Chen JY, Jeng YM, Yang CY, Tien YW, et al. Clinical significance of circulating tumor microemboli as a prognostic marker in patients with pancreatic ductal adenocarcinoma. *Clin Chem*. (2016) 62:505–13. doi: 10.1373/clinchem.2015.248260

22. Torphy RJ, Tignanelli CJ, Kamande JW, Moffitt RA, Herrera Loeza SG, Soper SA, et al. Circulating tumor cells as a biomarker of response to treatment in patient-derived xenograft mouse models of pancreatic adenocarcinoma. *PLoS ONE*. (2014) 9:e89474. doi: 10.1371/journal.pone.0089474

23. Gast CE, Silk AD, Zarour L, Riegler L, Burkhart JG, Gustafson KT, et al. Cell fusion potentiates tumor heterogeneity and reveals circulating hybrid cells that correlate with stage and survival. *Sci Adv*. (2018) 4:eaat7828. doi: 10.1126/sciadv.aat7828

24. Zhang Y, Zhou N, Yu X, Zhang X, Li S, Lei Z, et al. Tumacrophage: macrophages transformed into tumor stem-like cells by virulent genetic material from tumor cells. *Oncotarget*. (2017) 8:82326–43. doi: 10.18632/oncotarget.19320

25. Hidalgo M, Cascinu S, Kleef J, Labianca R, Lohr JM, Neoptolemos J, et al. Addressing the challenges of pancreatic cancer: Future directions fro improving outcomes. *Pancreatology*. (2015) 15:8–18. doi: 10.1016/j.pan.2014.10.001

26. Oliveira-Cuhna M, Newman WG, Siriwardena AK. Epidermal growth factor receptor in pancreatic cancer. *Cancers*. (2011) 3:1513–6. doi: 10.3390/cancers3021513

27. Khan MA, Azim S, Zubair H, Bhardwaj A, Patel GK, Khushman M, et al. Molecular drivers of pancreatic cancer pathogenesis: looking inward to move forward. *Int J Mol Sci*. (2017) 18:E779. doi: 10.3390/ijms18040779

28. Aras S, Zaidi MR. TAMless traitors: macrophages in cancer progression and metastasis. *Br J Cancer*. (2017) 117:1583–91. doi: 10.1038/bjc.2017.356

29. Ribeiro KB, da Silva Zanetti J, Ribeiro-Silva A, Rapatoni L, de Oliveira HF, da Cunha Tirapelli DP, et al. KRAS mutation associated with CD44/CD166 immuno expression as predictors of worse outcome in metastatic colon cancer. *Cancer Biomark*. (2016) 16:513–21. doi: 10.3233/CBM-160592

30. Sergeant G, van Eijsden R, Roskams T, Van Duppen V, Topal B. Pancreatic cancer circulating tumour cells express a cell motility gene signature that predicts survival after surgery. *BMC Cancer*. (2012) 12:527. doi: 10.1186/1471-2407-12-527

31. Harouaka R, Kang Z, Zheng SY, Cao L. Circulating tumor cells: advances in isolation and analysis, and challenges for clinical applications. *Pharmacol Ther*. (2014) 141:209–21. doi: 10.1016/j.pharmthera.2013.10.004

32. Samain R, Jean C, Bousquet C. Pancreatic cancer cell invasion: mesenchymal switch or just hitchhiking? *Transl Cancer Res*. (2016) 5:S1093–7. doi: 10.21037/tcr.2016.11.09

33. Zhao XH, Wang ZR, Chen CL, Di L, Bi ZF, Li ZH, et al. Molecular detection of epithelial-mesenchymal transition markers in circulating tumor cells from pancreatic cancer patients: potential role in clinical practice. *World J Gastroenterol*. (2019) 25:138–50. doi: 10.3748/wjg.v25.i1.138

34. Satelli A, Mitra A, Brownlee Z, Xia X, Bellister S, Overman MJ, et al. Epithelial-mesenchymal transitioned circulating tumor cells capture for detecting tumor progression. *Clin Cancer Res*. (2015) 21:899–906. doi: 10.1158/1078-0432.CCR-14-0894

35. Nguyen LV, Vanner R, Dirks P, Eaves CJ. Cancer stem cells: an evolving concept. *Nat Rev Cancer*. (2012) 12:133–43. doi: 10.1038/nrc3184

36. Marhaba R, Klingbeil P, Nuebel T, Nazarenko I, Buechler MW, Zoeller M. CD44 and EPCAM: cancer-initiating cell markers. *Curr Mol Med*. (2008) 8:784–804. doi: 10.2174/156652408786733667

37. Deschênes-Simard X, Parisotto M, Rowell MC, Le Calvé B, Igelmann S, Moineau-Vallée K, et al. Circumventing senescence is associated with stem cell properties and metformin sensitivity. *Aging Cell*. (2019) 18:e12889. doi: 10.1111/acel.12889

38. Yang X, Zhang Y, Hosaka K, Andersson P, Wang J, Tholander F, et al. VEGF-B promotes cancer metastasis through a VEGF-A-independent mechanism and serves as a marker of poor prognosis for cancer patients. *Proc Natl Acad Sci USA*. (2015) 112:E2900–9. doi: 10.1073/pnas.1503500112

39. Albrecht I, Kopfstein L, Strittmatter K, Schomber T, Falkevall A, Hagberg CE, et al. Suppressive effects of vascular endothelial growth factor-B on tumor growth in a mouse model of pancreatic neuroendocrine tumorigenesis. *PLoS ONE*. (2010) 5:e14109. doi: 10.1371/journal.pone.0014109

40. Seino S, Shigeishi H, Hashikata M, Higashikawa K, Tobiume K, Uetsuki R, et al. CD44(high) /ALDH1(high) head and neck squamous cell carcinoma cells exhibit mesenchymal characteristics and GSK3 β-dependent cancer stem cell properties. *J Oral Pathol Med*. (2016) 45:180–8. doi: 10.1111/jop.12348

41. Park NR, Cha JH, Jang JW, Bae SH, Jang B, Kim JH, et al. Synergistic effects of CD44 and TGF-β1 through AKT/GSK-3β/β-catenin signaling during epithelial-mesenchymal transition in liver cancer cells. *Biochem Biophys Res Commun*. (2016) 477:568–74. doi: 10.1016/j.bbrc.2016.06.077

42. Wang D, Zhu H, Zhu Y, Liu Y, Shen H, Yin R, et al. Retraction notice to "CD133+/CD44+/Oct4+/Nestin+ stem-like cells isolated from Panc-1 cell line may contribute to multi-resistance and metastasis of pancreatic cancer". *Acta Histochem*. (2018) 120:302. doi: 10.1016/j.acthis.2018.03.005

43. Kahlert C, Weber H, Mogler C, Bergmann F, Schirmacher P, Kenngott HG, et al. Increased expression of ALCAM/CD166 in pancreatic cancer is an independent prognostic marker for poor survival and early tumour relapse. *Br J Cancer*. (2009) 101:457–64. doi: 10.1038/sj.bjc.6605136

44. Hong X, Michalski CW, Kong B, Zhang W, Raggi MC, Sauliunaite D, et al. ALCAM is associated with chemoresistance and tumor cell adhesion in pancreatic cancer. *J Surg Oncol.* (2010) 101:564–9. doi: 10.1002/jso.21538

45. Wang Z, Banerjee S, Li Y, Rahman KM, Zhang Y, Sarkar FH. Down-regulation of notch-1 inhibits invasion by inactivation of nuclear factor-kappaB, vascular endothelial growth factor, and matrix metalloproteinase-9 in pancreatic cancer cells. *Cancer Res.* (2006) 66:2778–84. doi: 10.1158/0008-5472.CAN-05-4281

46. Shah AN, Summy JM, Zhang J, Park SI, Parikh NU, Gallick GE. Development and characterization of gemcitabine-resistant pancreatic tumor cells. *Ann Surg Oncol.* (2007) 14:3629–37. doi: 10.1245/s10434-007-9583-5

47. Mohammed A, Janakiram NB, Brewer M, Ritchie RL, Marya A, Lightfoot S, et al. Antidiabetic drug metformin prevents progression of pancreatic cancer by targeting in part cancer stem cells and mTOR signaling. *Transl Oncol.* (2013) 6:649–59. doi: 10.1593/tlo.13556

48. Satelli A, Li S. Vimentin in cancer and its potential as a molecular target for cancer therapy. *Cell Mol Life Sci.* (2011) 68:3033–46. doi: 10.1007/s00018-011-0735-1

49. Huo Y, Zheng Z, Chen Y, Wang Q, Zhang Z, Deng H. Downregulation of vimentin expression increased drug resistance in ovarian cancer cells. *Oncotarget.* (2016) 7:45876–88. doi: 10.18632/oncotarget.9970

50. Liu LG, Yan XB, Xie RT, Jin ZM, Yang Y. Stromal expression of vimentin predicts the clinical outcome of stage II colorectal cancer for high-risk patients. *Med Sci Monit.* (2017) 23:2897–905. doi: 10.12659/MSM.904486

51. Zou S, Sun H, Fan L, Xiao X, Gong L, Zhu J, et al. Prognostic indicators in patients with early stage endometrioid adenocarcinoma: a retrospective case-control study of 523 patients. *Int J Clin Exp Med.* (2017) 10:3692–8.

52. Szubert S, Koper K, Dutsch-Wicherek MM, Jozwicki W. High tumor cell vimentin expression indicates prolonged survival in patients with ovarian malignant tumors. *Ginekol Pol.* (2019) 90:11–9. doi: 10.5603/GP.2019.0003

53. Avan A, Quint K, Nicolini F, Funel N, Frampton AE, Maftouh M, et al. Enhancement of the antiproliferative activity of gemcitabine by modulation of c-Met pathway in pancreatic cancer. *Curr Pharm Des.* (2013) 19:940–50. doi: 10.2174/138161213804547312

Isofuranodiene synergizes with temozolomide in inducing glioma cells death

Alessandra Brunetti[a,1], Oliviero Marinelli[a,b,1], Maria Beatrice Morelli[a], Romilde Iannarelli[a], Consuelo Amantini[b], Domenico Russotti[a], Giorgio Santoni[a], Filippo Maggi[a,1,*], Massimo Nabissi[a,1,*]

[a] School of Pharmacy, University of Camerino, Camerino 63032, Italy
[b] School of Biosciences and Veterinary Medicine, University of Camerino, Camerino 63032, Italy

ARTICLE INFO

ABSTRACT

Background: Glioblastoma multiforme (GBM) is the most common and deadly brain form of tumor. GBM exhibits high resistance to the standard treatment consisting of temozolomide (TMZ) combined with radiotherapy. Isofuranodiene (IFD) is a bioactive sesquiterpene occurring in the essential oils obtained from Alexanders (*Smyrnium olusatrum* L., Apiaceae). This compound has shown a broad spectrum of antitumoral activities in different human cancer cell lines both *in vitro* and *in vivo*. However, the mechanism of action of IFD on GBM and its potential effects in combination with chemotherapeutic drugs, have not been fully elucidated.
Purpose: The aim of the present study was to evaluate the anticancer effects of IFD itself and in combination with TMZ in GBM.
Methods: Sulforhodamine B-based proliferation assay, cell cycle analysis and Annexin V/PI staining were carried out to determine the IFD effects on three human GBM cell lines, U87, T98, U251 and in normal human astrocyte. Modulation of protein expression levels was determined by western blot analysis. Reactive oxygen species (ROS) production was evaluated by cytofluorimetry. Moreover, the effects on cell viability of the IFD and TMZ co-administration was evaluated through the calculation of combination index (CI).
Results: IFD exerted cytotoxic effects against the GBM cell lines, but not in normal cells (normal human astrocytes). This compound induced a cell cycle blockage and a necrotic cell death depending on the increase of intracellular ROS levels. Furthermore, the synergism between IFD and TMZ was demonstrated in GBM cell lines.
Conclusion: This study demonstrated the glioma selectivity of IFD and its cytotoxic properties suggesting a new strategy for the treatment of GBM in order to overcome the TMZ resistance and to reduce its side effects.

Introduction

Glioblastoma (GBM) represents a group of brain tumors characterized by high morbidity, malignity, proliferating activities and infiltration into adjacent brain structures (Nieder et al., 2006). Currently, the standard procedure to treat GBM consists in a combination of surgery, radiation and chemotherapy with temozolomide (TZM) (Lee, 2017; Irani et al., 2017). TMZ is an alkylating agent, which breaks the DNA double-strand, thus causing cell cycle arrest and, ultimately, cell death. However, due to its short half-life, TMZ is administered at high dose, and prolonged systemic administration leads to a series of systemic side effects (Lee, 2017; Irani et al., 2017). In recent years an increasing interest towards natural compounds as promising adjuvant agents in chemotherapy has emerged (Liu, 2004; Bahmani et al., 2016; Chen and Blumberg, 2008). Phytochemicals present several advantages, such as low-toxicity and potential efficacy (Issa et al., 2006; Aggarwal and Shishodia, 2006). Terpenoids are the biggest group of plant secondary metabolites, with about 20,000 molecular structures known and, many of them, have shown a great potential in cancer prevention (Sharm et al., 2017). The chemical class of sesquiterpenes enjoys a good reputation as an alternative source of anti-inflammatory and anticancer drugs (Sut et al., 2018). Sesquiterpenes are compounds made up of fifteen carbon atoms biosynthetically formed via the mevalonate pathway from farnesyl pyrophosphate (FPP) (Dewick, 2002).

Depending on the specific enzyme catalyzing the molecular rearrangement from FPP, several groups of sesquiterpenes with bisabolane, germacrane, cuparane, cadinane, humulane, elemane, eudesmane and guaiane backbones can be formed (Majdi et al., 2011). Sesquiterpenes are frequently found in essential oil-producing plants, where they play an important role as environmental mediators (Cheng et al., 2007). In the present study, the attention was focused on isofuranodiene (IFD), a sesquiterpene containing a furan ring, firstly isolated and described in rhizoma Curcumae in 1968 (Maggi et al., 2012) and then found in both marine and plant organisms (Giordano et al., 2017). *Curcuma wenyujin* Y.H. Chen & C. Ling, *Commiphora* spp., *Eugenia uniflora* L. and *Smyrnium olusatrum* L. represent the main sources of this compound (Amorim et al., 2009; Maggi et al., 2015; Quassinti et al., 2014). Notably, *S. olusatrum*, currently known under the common name of wild celery or Alexanders, is an overlooked horticultural crop which has been historically used as an edible vegetable in the Roman age, then abandoned because of the changing tastes in the Western world as well as the introduction of the improved form of celery (*Apium graveolens* L.) (Maggi et al., 2015). IFD is a relative molecule of furanogermacrane-type sesquiterpenes and it is abundant in essential oils obtained from various parts of *S. olusatrum* (Maggi et al., 2012; Quassinti et al., 2014). This compound is also considered the precursor of sesquiterpene lactones (Kawabata et al., 1985) which are known to exert an important role in the plant defense. IFD is a thermosensitive molecule, undergoing Cope rearrangement after exposure to high temperatures or oxidative reactions (Maggi et al., 2017). IFD has shown anticancer activity in several human cancer cell lines. Indeed, it was able to inhibit the proliferation of breast cancer cells *in vitro* and *in vivo* and enhanced tamoxifen-induced growth inhibition in MCF-7 breast cancer cells (Zhong et al., 2012a; Mustafa et al., 2016; Buccioni et al., 2014). IFD also increased the anti-proliferative activity of paclitaxel in 95-D lung cancer cells (Xu et al., 2014). Moreover, IFD suppressed the growth of colon carcinoma cell line HCT 116 and hepatocellular carcinoma cell line HepG2 by cell cycle arrest at G2/M and induced apoptosis through MAPK signaling and mitochondria-caspase pathways (Quassinti et al., 2014; Xiao et al., 2007). Additionally, IFD showed anti-proliferative activity against prostate adenocarcinoma (PC3) cell lines with efficacy close to that of cisplatin (Buccioni et al., 2014). More recently, it was found that IFD exerts a potential anti-angiogenic effect through the suppression of endothelial cell growth, invasion, migration, and tube formation through regulation of the PI3K pathway in human umbilical vein endothelial cells (Zhong et al., 2012b). Because of its low-molecular weight and high hydrophobicity, IFD is capable to cross easily the blood-brain barrier (Mustafa et al., 2016). Given this background and the absence of comprehensive studies regarding the activity of IFD on GBM, the aim of this work was to evaluate the anticancer activity of IFD, in terms of cytotoxicity on three human GBM experimental cell line models, namely U87, T98 and U251 cell lines. In addition, the cytotoxicity of IFD and TMZ combination treatments was evaluated with the aim to verify a possible synergism between them. Results of this study shed light into the use of IFD to reduce the dosage and side effects of TMZ therapy.

Materials and methods

Isofuranodiene

Isofuranodiene (IFD), (5E,9E)-3,6,10-trimethyl-4,7,8,11-tetrahydrocyclodeca[b]furan, CAS registry number: 57566-47-9, synonim: furanodiene ($C_{15}H_{20}O$, crystals, purity 99% as determined by HPLC) was obtained by crystallization at -20 °C from the essential oil of *S. olusatrum* according to a previously reported procedure (Maggi et al., 2015). The typical GC–MS chromatogram of this oil is reported in Fig. 1. Purification was achieved by recrystallization in methanol followed by filtration and solvent removal. The chemical structure was confirmed by comparison of NMR data with that of standard available in our laboratory and literature data (Maggi et al., 2017).

Reagents

Temozolomide (TMZ, Temodal) was purchased from Sigma Aldrich, St. Louis, MO. TMZ and IFD were dissolved in DMSO.

Cell lines

U87, T98 and U251 cell lines, obtained from European Collection of Cell Cultures (ECACC, Salisbury, UK), were cultured in Eagle's Minimum Essential Medium (Lonza Bioresearch, Basel, Switzerland) supplemented with 10% (v/v) heat-inactivated fetal bovine serum (FBS), 2 mM L-glutamine and 100 IU/ml of penicillin, 100 µg of streptomycin (Lonza), 1 mM sodium pyruvate (Lonza) and non-essential amino acids (Lonza). Normal human astrocytes (NHA) (Cambrex, Berkshire, UK) were grown in Astrocyte Growth Media System (Cambrex) and used within 10 passages to avoid biological responsiveness and function deterioration. Cell lines were maintained at 37 °C, 5% CO_2 and 95% of humidity.

Sulforhodamine B (SRB) assay

Cells were seeded at the density of 3×10^4 cells/ml in 96-well plates. After 24 h of incubation, IFD or vehicle (DMSO) were added. Given the short half-life of IFD, treatment was performed in single or repeated administration (after 12 h from the first treatment), washing the cells with medium. Six replicates were used for each dose. At 48 h post-treatments, cells were fixed with 10% cold trichloroacetic acid (TCA) and stained with 0.4% SRB in 1% acetic acid solution. Unbound dye was removed by washing with 1% acetic acid. Bound stain was subsequently solubilized with Trizma 10 mM. The absorbance of the samples against a background control (medium alone) was measured at 520 nm using an ELISA reader microliter plate (BioTek Instruments, Winooski, VT, USA). The SRB assay was also performed with the association between IFD (repeated administration) and TMZ in single administration, for synergism analysis. Synergistic activity of the IFD/TMZ combination was calculated by the Chou-Talalay method, which provides the theoretical basis for the combination index (CI)-isobologram equation. This method allows quantitative determination of drug interactions, where CI < 1, =1, and >1 indicates synergism, additive effect and antagonism, respectively. Based on these algorithms, computer software, CompySyn (CompuSyn Software, ComboSyn, Inc. Paramus, NJ 2007) was used for determining automatically synergism and antagonism at all doses or effect levels.

Cell cycle analysis

Cells were starved for 24 h in medium without FBS in order to synchronize the cell population in the G1-phase of cell cycle. Then cells were seeded into 6-well plates (3×10^4 cells/ml) with medium supplemented with FBS and treated with IFD (150 µM) or vehicle for 24 h. The treatment was performed in single or repeated (every 12 h) administration. Cells were fixed by adding ice-cold 70% ethanol for 1 h and then washed with staining buffer (PBS, 2% FBS and 0.01% NaN_3). Next, cells were incubated with 100 µg/ml Ribonuclease A solution (Sigma Aldrich) for 30 min at 37 °C, stained with propidium iodide (PI) 20 µg/ml (Sigma Aldrich) at room temperature for 10 min and analysed on a FACScan flow cytometer using linear amplification and CellQuest software.

Western blot analysis

Twenty micrograms of the glioma cell lines lysates were separated on a SDS-polyacrylamide gel, transferred onto Hybond-C extra membranes (GE Healthcare), blocked with 5% low-fat dry milk in PBS-
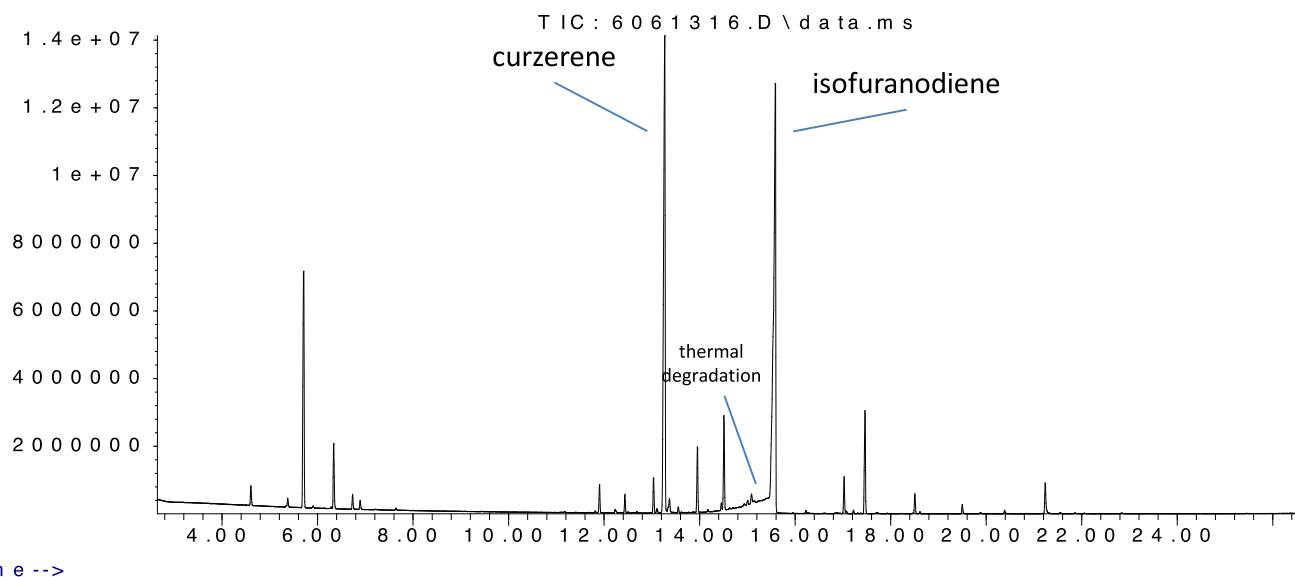
Fig. 1. GC–MS chromatogram of the essential oil from flowers of *Smyrnium olusatrum* from which IFD was isolated. During the GC run IFD undergoes Cope rearrangement (thermal degradation) giving rise to curzerene.

Tween 20, immunoblotted with mouse anti-pERK1/2(Thr202/Tyr204) (1:2000, #9106, Cell Signaling, Danvers, MA, USA), rabbit anti-ERK1/2 (1:1000, #9102, Cell Signaling), rabbit anti-pAKT(Ser473) (1:1000, #9271, Cell Signaling), rabbit anti-AKT (1:1000, #9272, Cell Signaling), rabbit anti-phospho-histone H2AX(Ser139) (1:1000, #9718, Cell Signaling) and rabbit anti-glyceraldehyde-3-phosphate dehydrogenase (GAPDH, 1:3000, #2118, OriGene, Rockville, MD, USA) Abs for 1 h and then incubated with their respective HRP-conjugated anti-mouse or anti-rabbit (1:2000, Cell Signaling) Abs for 1 h. The detection was performed using the LiteAblot ®PLUS or the LiteAblot ®TURBO (EuroClone, Milano, Italy) kits and densitometric analysis was carried out by evaluating three independent experiments by a Chemidoc using the Quantity One software (BioRad, Hercules, USA).

Reactive oxygen species (ROS) production

The fluorescent probe dichlorodihydrofluorescein diacetate (DCFDA, Life Technologies Italia, Italy) was used to assess oxidative stress levels. Briefly, glioma cells (3×10^4 cells/ml) treated with IFD (150 μM) or vehicle for 6 h, were incubated with 20 μM DCFDA 20 min prior to the harvest time point. In some experiments, cells were pre-incubated for 1 h with 10 mM of the oxidative stress inhibitor N-acetylcysteine (NAC). The intensity of the fluorescence was assayed using flow cytometry and CellQuest software.

Apoptosis assay and PI staining

Cell death was evaluated using Annexin V-FITC and PI staining followed by bi-parametric FACS analysis. 3×10^4 glioma cells/ml were seeded into 6-well plates and treated for 24 h with IFD (150 μM) in single or repeated administration, and then incubated with 5 μl Annexin V-FITC (Enzo life sciences, Farmingdale, NY, USA) and 20 μg/ml PI for 10 min at room temperature. In some experiments, cells were pre-incubated for 1 h with NAC 10 mM. The percentage of positive cells determined over 5000 events was analysed on a FACScan cytofluorimeter using the CellQuest software.

Statistical analysis

The data are presented as the mean values ± SE and are representative of the results of at least three independent experiments. The significance of the differences between data ($*^{\#}p < 0.05$) was assessed using Student's *t*-test or a one-way analysis of variance (ANOVA). The statistical analysis of IC$_{50}$ levels was performed using Prism 5.0a (Graph Pad).

Results and discussion

Cytotoxicity of IFD in GBM cell lines

IFD is a molecule possessing interesting activity for human health and can be considered as an effective compound for potential cancer therapy. In fact, IFD has been demonstrated to exert anticancer effects in many cancer cells such as HCT 116 colon carcinoma (Quassinti et al., 2014), MCF-7, MDA-MB 231, BT 474 breast cancer (Buccioni et al., 2014; Zhong et al., 2012a, 2016), PC3 prostate cancer (Buccioni et al., 2014), HepG2 hepatocellular carcinoma (Xiao et al., 2007), and HL-60 leukemia (Ma et al., 2008). To the best of our knowledge, there are not comprehensive studies regarding the activity of IFD *in vitro* model of GBM. In our study we analysed the impact of IFD isolated from the essential oil of Alexanders, in three human GBM cell lines (U87, T98 and U251) and in normal human astrocytes (NHA). The cytotoxic effect of IFD was evaluated by performing a dose-response SRB assay. The cell lines were treated with increasing concentrations of IFD (from 50 μM to 250 μM). Given the short half-life of IFD, cells were treated in single and repeated administration (every 12 h) and cell viability was evaluated at 48 h post-treatments. Results showed that IFD reduced cell viability in all glioma cell lines used, with higher effect in T98 followed by U87 and U251 (Fig. 2). To ascribe a potential glioma-selective toxicity of IFD, we evaluated these treatments also in NHA cells. As shown, no significant cytotoxic effects were observed in NHA (Fig. 2), suggesting that these cells were refractory to IFD activity. On the other hand, the results in GBM cells were consistent with the data demonstrated in other types of tumors (Quassinti et al., 2014; Zhong et al., 2012a, 2016; Xu et al., 2014; Xiao et al., 2007; Ma et al., 2008). It is worth to note that the IFD cytotoxic effect was higher when
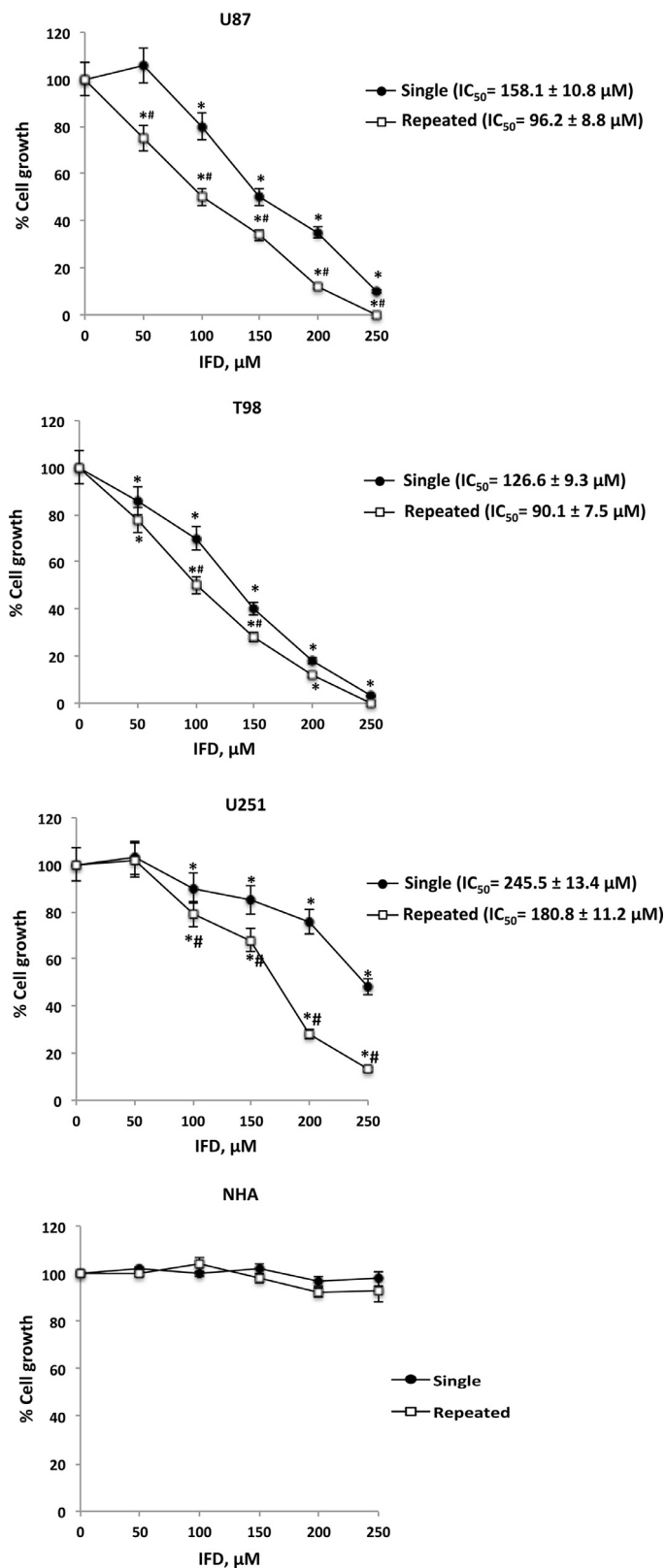
Fig. 2. Cytotoxicity of IFD in glioma cell lines.
Cell viability was determined by SRB assay. U87, T98, U251 and NHA cells were treated for 48 h with different concentrations of IFD (up to 250 μM). Data shown are expressed as mean $\pm$ SE of three separate experiments. $*p < 0.05$ treated vs vehicle, $\#p < 0.05$ repeated vs single administration.
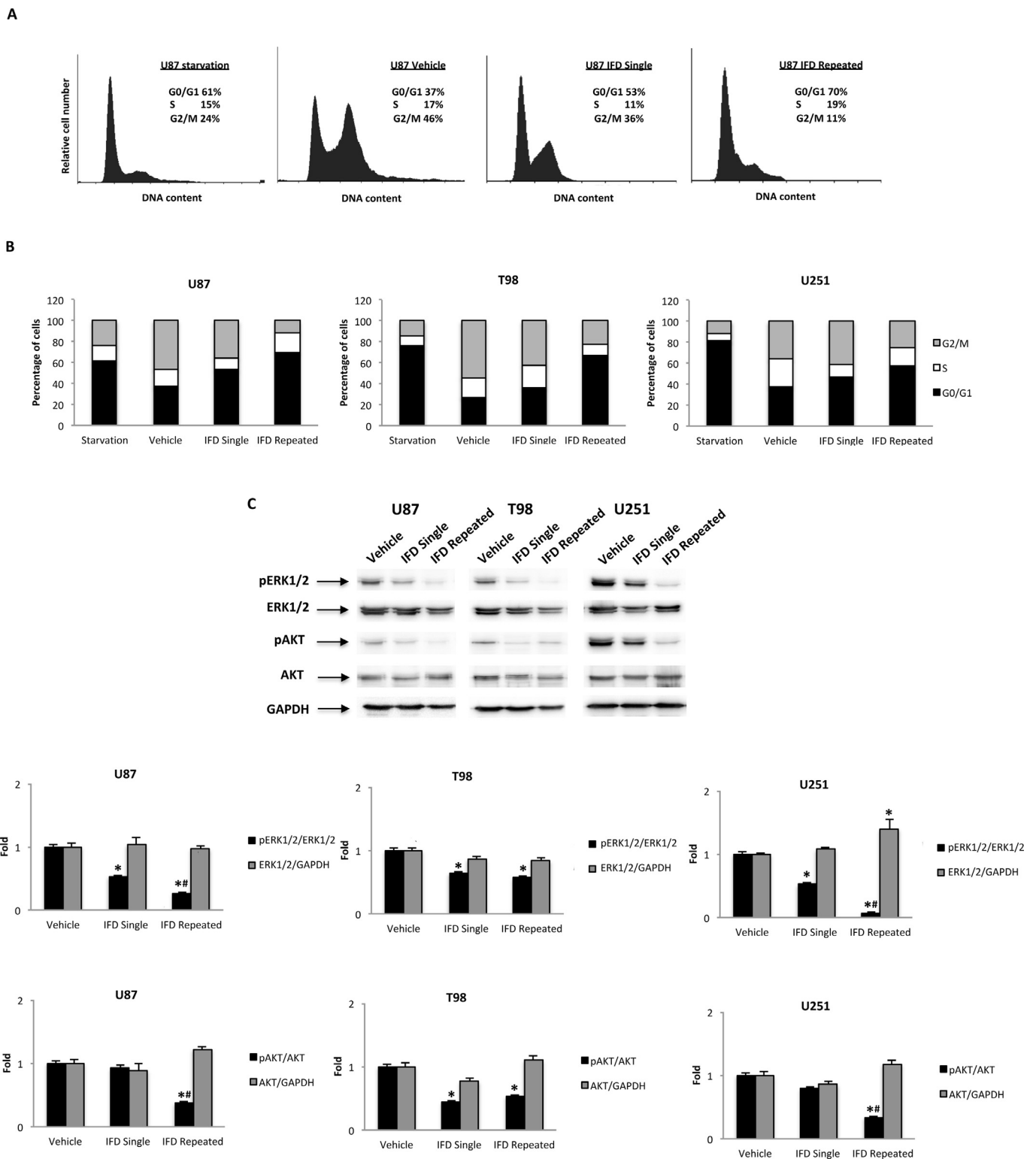
Fig. 3. IFD induces cell cycle arrest in glioma cell lines.
U87, T98 and U251 cell lines were starved and then cultured in the presence of IFD 150 µM (single or repeated administration) for 24 h. (A) Representative cell cycle distribution by FACS analysis. (B) Histograms representation of the cell cycle phases in the three cell lines. (C) Western blot analysis of pERK1/2(Thr202/Tyr204), ERK1/2, pAKT(Ser473), AKT and GAPDH protein levels in glioma cells after treatments. Blots are representative of one of three separate experiments. The pERK1/2(Thr202/Tyr204) and pAKT(Ser473) protein levels were determined with respect to ERK1/2 and AKT levels. ERK1/2 and AKT densitometry values were normalized to GAPDH used as loading control. Densitometric values shown are the mean $\pm$ SE of three separate experiments. $*p < 0.05$ vs vehicle cells, $\#p < 0.05$ repeated vs single administration.
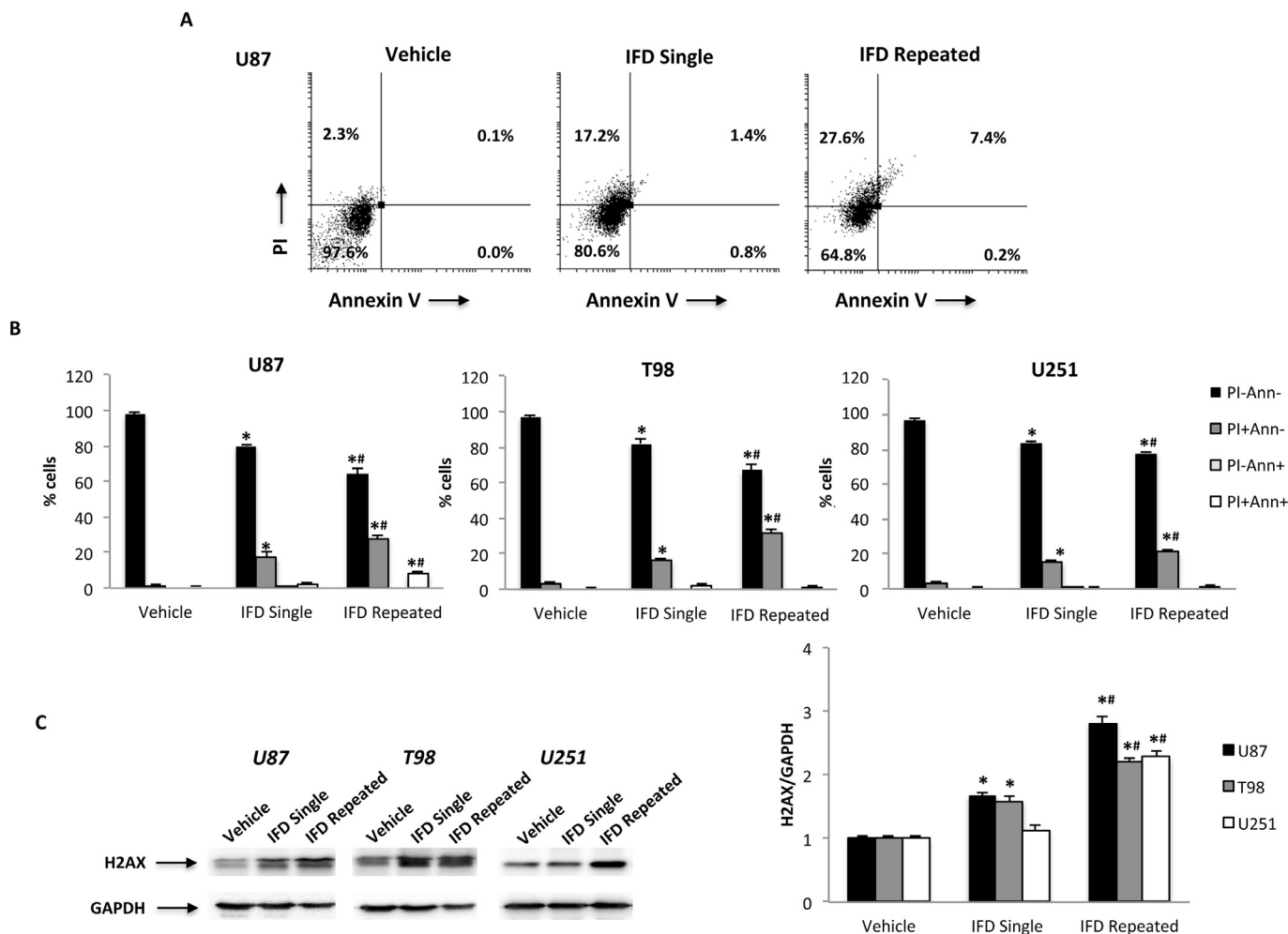
Fig. 4. IFD induces necrotic cell death.
T98, U87 and U251 lines were treated with IFD 150 μM for 24 h. (A) Flow cytometry was performed by Annexin V and PI double-staining. Data represent the percentage of PI and/or Annexin V positive cells and are representative of one of three separate experiments. (B) Graph represents the mean ± SE percentage of PI and/or Annexin V positive cells of at least three separate experiments. *$p < 0.05$ vs vehicle cells, #$p < 0.05$ repeated vs single administration. (C) Representative blots of H2AX and GAPDH protein levels in glioma cells after treatments. H2AX densitometry values were normalized to GAPDH used as loading control. Densitometric values shown are the mean ± SE of three separate experiments. *$p < 0.05$ vs vehicle cells, #$p < 0.05$ repeated vs single administration.

administered twice daily, as evidenced by the IC_{50} values (Fig. 2). A major effect related to the repeated administration was observed in all GBM cell lines, with U251 still remaining the most resistant cells. Given the positive response to the 150 μM dose of IFD in all cell lines, we decided to treat cells with this dose in the subsequent experiments.

IFD induces cell cycle blockage in glioma cell lines

Starved cells were treated with IFD (150 μM) for 24 h to evaluate its influence on the cell cycle phase distribution in glioma cell lines. As shown in Fig. 3A,B, IFD induced an accumulation of cells in G1 phase, mostly after twice daily treatments, in all cell lines. These data evidenced that IFD-reduced cell viability, mainly by repeated administration, was partially due to inhibition of cell cycle and this data was consistent with other works involving breast cancer and leukemia cell lines (Zhong et al., 2012a, 2016; Ma et al., 2008).

To elucidate whether the anti-proliferative activity of IFD is associated with the modulation of ERK and Akt/PKB pathways, a western blot analysis was performed in glioma cells treated for 24 h in single or repeated administration (Fig. 3C). ERK is usually associated with pro-survival signaling through mechanisms involving the activation of the cAMP response element binding protein (CREB) and the regulation of the anti-apoptotic protein Bcl-2 and the pro-apoptotic protein BAD. In

addition to MAPK pathway, the serine/threonine kinase, Akt/PKB, one of the main downstream effectors of PI3K, exerts a pivotal role in cell survival. IFD treatment was able to induce a significant inhibition of both ERK1/2 and AKT signaling. Indeed, the phosphorylated forms decreased after single and mostly after repeated treatment in all glioma cell lines. Data are in accordance with results obtained in HepG2 cells for ERK inhibition signaling (Xiao et al., 2007) and in breast cancer cell lines for AKT inhibition (Zhong et al., 2016).

These findings suggest that IFD might be an anticancer agent for the treatment of glioma and that its anti-proliferative activity was associated with the inhibition of important cell survival pathways.

IFD induces ROS-dependent necrotic cell death

Recently, it has been reported that IFD also induces apoptotic cell death through a mitochondria – caspase pathway in human hepatic cancer cells (Xiao et al., 2007). Apoptotic cell death was although triggered in HL60 leukemia cells via activation of TNF receptor signaling pathway (Ma et al., 2008) and in MCF-7 cell line (Zhong et al., 2016). Therefore, we evaluated the cytotoxic effect of IFD exposure in glioma cells by Annexin V-FITC/PI staining. The cell lines were treated with vehicle or IFD 150 μM in single and repeated administration for 24 h. Then, fluorescence was analysed by flow cytometry. The results
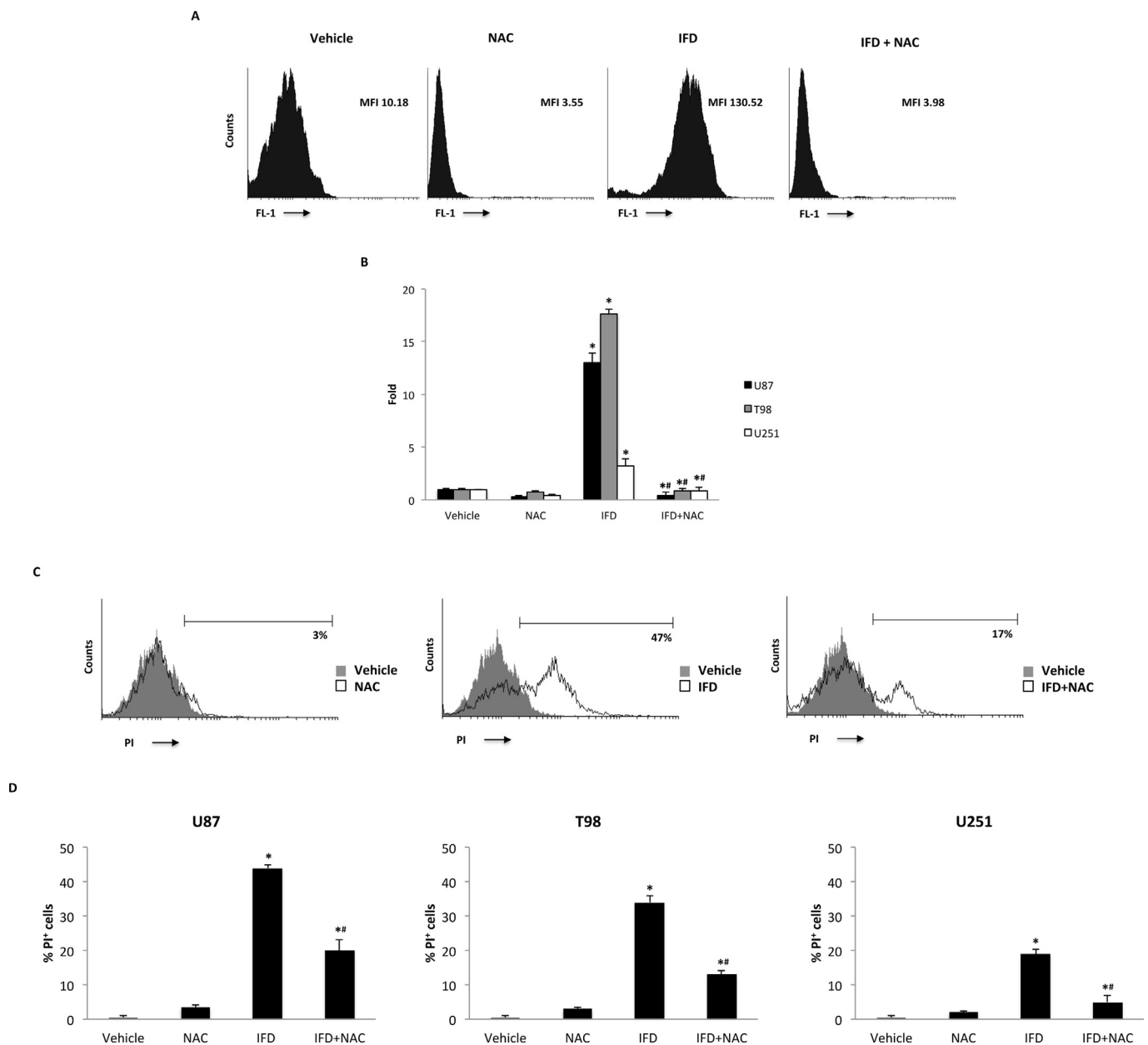
Fig. 5. IFD induces ROS production.
(A,B) T98, U87 and U251 cell lines were pretreated or not with NAC (10 mM) for 1 h and then treated with IFD (150 μM) for 6 h. Cells were stained with DCFDA before flow cytometric analysis. (A) Histograms are representative of one of three separate experiments in U87. MFI = mean fluoresce intensity. (B) Data shown are expressed as fold respect to vehicle treated cells of three separate experiments. *$p < 0.05$ vs vehicle or NAC treated cells, #$p < 0.05$ vs IFD. (C,D) T98, U87 and U251 cell lines were pretreated or not with NAC (10 mM) for 1 h and then treated with IFD (150 μM) for 24 h. Cells were stained with PI to assess cell death. (C) Histograms are representative of one of three separate experiments in U87. Data represent the percentage of positive cells. (D) Data shown represent the percentage of PI$^+$ cells and are representative of three separate experiments. *$p < 0.05$ vs vehicle or NAC treated cells, #$p < 0.05$ vs IFD.

evidenced that IFD treatment did not induce Annexin V$^+$ or Annexin V$^+$PI$^+$ cells, but only PI$^+$ cells in all cell lines, indicating that IFD induced necrotic cell death (Fig. 4A,B). Data confirmed that the effect of IFD was higher in repeated compared to single administration treatments.
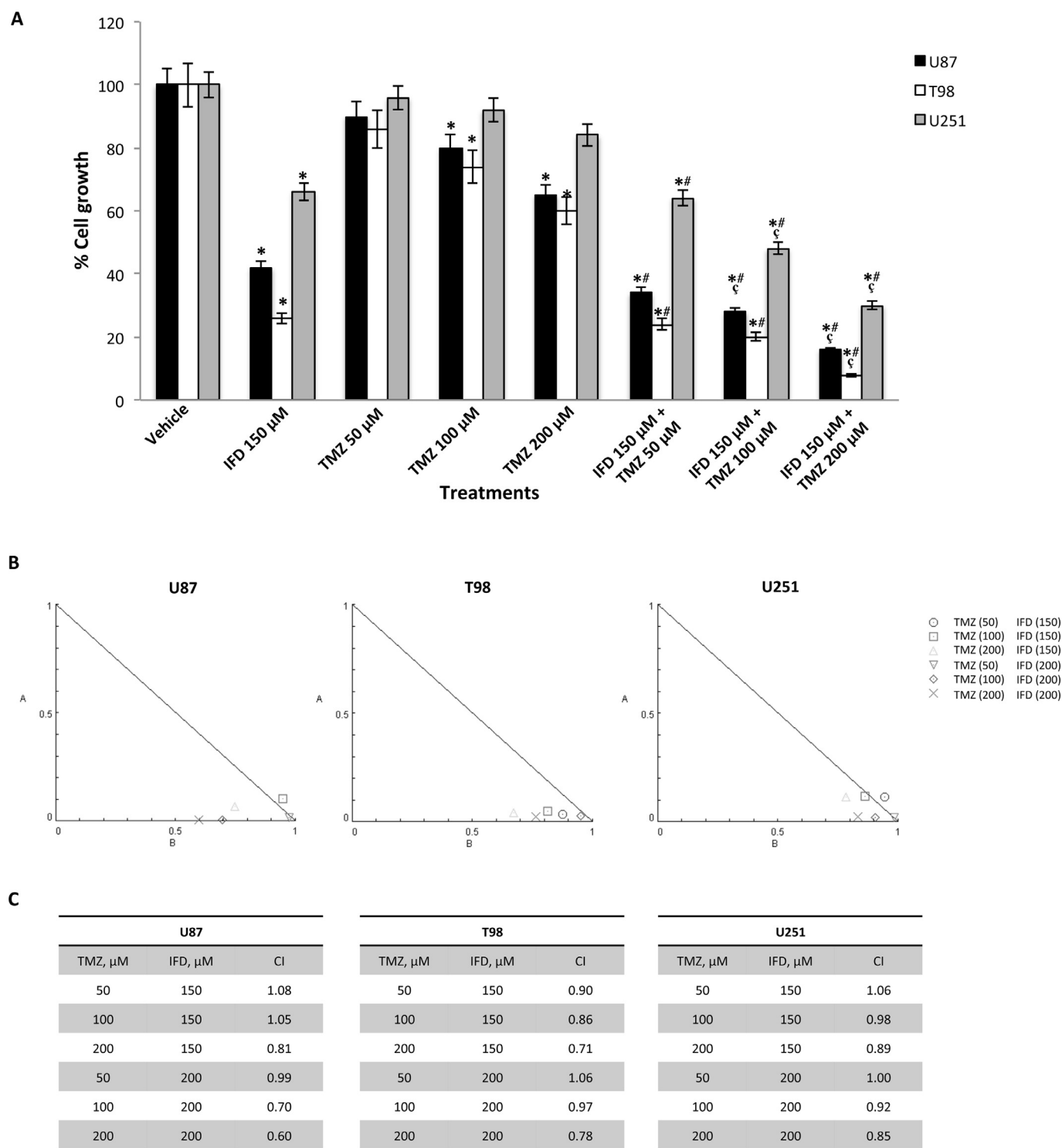
Moreover, we investigated the presence of γ-H2AX (H2AX), a phosphorylated variant of histone 2A that is associated with DNA double-strand breaks. Interestingly, western blot analysis revealed strong induction of the DNA damage marker after 24 h of IFD administration in all glioma cell lines, being more sustained after repeated treatment (Fig. 4C).

Since the presence of H2AX is linked with the production of reactive oxygen species (ROS) inducing a caspase-independent programmed

necrosis (Artus et al., 2010; Suzuki et al., 2015), we also evaluated the production of ROS as a possible mechanism of death induced in GBM cells. At 6 h post-treatment, IFD administration induced an increase in ROS production (Fig. 5A,B). Moreover, to investigate the involvement of ROS in IFD-induced glioma cell death, a PI incorporation assay was performed by pretreating cells with the free radical scavenger NAC (10 mM). The same NAC dose able to abrogate the increase in ROS generation induced by IFD treatment (Fig. 5A,B), partially inhibited the IFD-induced cell death in all cell lines (Fig. 5C,D).

IFD synergizes with TMZ in reducing cell viability in glioma cell lines

Currently, the standard therapies of GBM consist of surgery

A

B

C

U87		
TMZ, µM	IFD, µM	CI
50	150	1.08
100	150	1.05
200	150	0.81
50	200	0.99
100	200	0.70
200	200	0.60

T98		
TMZ, µM	IFD, µM	CI
50	150	0.90
100	150	0.86
200	150	0.71
50	200	1.06
100	200	0.97
200	200	0.78

U251		
TMZ, µM	IFD, µM	CI
50	150	1.06
100	150	0.98
200	150	0.89
50	200	1.00
100	200	0.92
200	200	0.85

Fig. 6. The combination IFD-TMZ exerts a synergistic cytotoxic effect.
(A) Cell viability was determined in U87, T98 and U251 lines by SRB assay. Cells were treated for 48 h with IFD (150 µM), alone and in combination with TMZ (50, 100, 200 µM). Data shown are expressed as mean $\pm$ SE of three separate experiments. *$p < 0.05$ treated vs vehicle, #$p < 0.05$ vs TMZ alone, ç$p < 0.05$ vs IFD. (B) Isobologram plots for combination treatments of IFD and TMZ in U87, T98 and U251 cell lines. On the lower left of the hypotenuse synergism, on the hypotenuse additive effect, and on the upper right of the hypotenuse antagonism. Synergistic activity of IFD-TMZ was assessed by CompuSyn software. (C) CI values for combination treatments of IFD and TMZ in U87, T98 and U251 cell lines. CI = 1, <1 and >1 indicates additive effect, synergism and antagonism, respectively.

followed by radiotherapy and chemotherapy with alkylating agents, including carmustine and TMZ (Lee, 2017). TMZ is a second-generation imidazotetrazine derivative which exerts its cytotoxic effects by methylation of specific DNA sites. Although it is effective in the treatment of GBM, drug resistance limits its successful application (Lee, 2017).

Recently, Zhong et al. (2016) demonstrated that the combination between IFD and the chemotherapeutic agent doxorubicin is more effective than the doxorubicin itself. In our work, the possible synergism between IFD and TMZ in the three GBM cell lines has been evaluated with the aim to reduce the TMZ dosage and toxicity. Cells were exposed

to various concentrations of IFD and TMZ for 48 h. The combined treatment with the two drugs induced increased levels of cytotoxicity, as compared with single treatments with either IFD or TMZ alone (Fig. 6A). In the cells treated with IFD and TMZ concurrently (i.e. IFD 150/200 µM and TMZ 100/200 µM), the CI values were <1 (Fig. 6B,C). These results indicated a synergistic interaction between IFN and TMZ on the GBM growth inhibition, thus supporting the feasible use of IFD as an adjuvant in the treatment of human GBM.

Conclusion

Results of this work justify the recent increase of interest towards the use of phytochemicals in the treatment of human diseases or as adjuvants with the current therapies. This is the first study demonstrating the anticancer activity of IFD against human glioma cells. In particular, IFD exhibited anti-proliferative activity against glioma cells through inhibition of proliferation and induction of necrotic cell death. The mechanism of action of IFD is not completely understood but our results suggest that IFD can cause ROS-dependent DNA damage. Therefore, the synergistic effects of the IFD-TMZ combination could be a consequence of an accumulation of DNA damage causing cell death. Synergism analysis showed that IFD might be an interesting agent for the treatment of GBM in order to overcome the TMZ resistance or to reduce its doses and consequently the TMZ systemic toxicity. It is worth to note that its small size and the extremely high lipophilicity allow it to easily cross the blood-brain barrier, thus making this sesquiterpene a promising therapeutic agent for the treatment of brain tumors.

Conflict of interest

The authors declare that there is no conflict of interest.

Acknowledgment

References

Aggarwal, B.B., Shishodia, S., 2006. Molecular targets of dietary agents for prevention and therapy of cancer. Biochem. Pharmacol. 71, 1397–1421.

Amorim, A.C., Lima, C.K., Hovell, A.M., Miranda, A.L, Rezende, C.M., 2009. Antinociceptive and hypothermic evaluation of the leaf essential oil and isolated terpenoids from *Eugenia uniflora* L. (Brazilian Pitanga). Phytomedicine 16, 923–928.

Artus, C., Boujrad, H., Bouharrour, A., Brunelle, M.N., Hoos, S., Yuste, V.J., Lenormand, P., Rousselle, J.C., Namane, A., England, P., Lorenzo, H.K., Susin, S.A., 2010. AIF promotes chromatinolysis and caspase independent programmed necrosis by interacting with histone H2AX. EMBO J. 29, 1585–1599.

Bahmani, M., Shirzad, H., Shahinfard, N., Sheivandi, L., Rafieian-Kopaei, M., 2016. Cancer phytotherapy: recent views on the role of antioxidant and angiogenesis activities. J. Evid. Based Complement. Altern. Med 2016; pii: 2156587215625157.

Buccioni, M., Dal Ben, D., Lambertucci, C., Maggi, F., Papa, F., Thomas, A., Santinelli, C., Marucci, G., 2014. Antiproliferative evaluation of isofuranodiene on breast and prostate cancer cell lines. Sci. World J. 2014, 264829.

Chen, C.Y., Blumberg, J.B., 2008. Phytochemical composition of nuts. Asia Pac. J. Clin. Nutr. 17, 329–332.

Cheng, A.X., Lou, Y.G., Mao, Y.B., Lu, S., Wang, L.J., Chen, X.Y., 2007. Plant terpenoids: biosynthesis and ecological functions. J. Integr. Plant Biol. 49, 179–186.

Dewick, P.M., 2002. Medicinal Natural Products: A Biosynthetic Approach, 2nd Ed. John Wiley & Sons Ltd, Chichester.

Giordano, G., Carbone, M., Ciavatta, M.L., Silvano, E., Gavagnin, M., Garson, M.J., Cheney, K.L., Mudianta, I.W., Russo, G.F., Villani, G., Magliozzi, L., Polese, G., Zidorn, C., Cutignano, A., Fontana, A., Ghiselin, M.T., Mollo, E., 2017. Volatile secondary metabolites as aposematic olfactory signals and defensive weapons in aquatic environments. Proc. Natl. Acad. Sci. USA 114, 3451–3456.

Irani, M., Sadeghi, G.M.M., Haririan, I., 2017. Gold coated poly (ɛ-caprolactonediol) based polyurethane nanofibers for controlled release of temozolomide. Biomed. Pharmacother. 88, 667–676.

Issa, A.Y., Volate, S.R., Wargovich, M.J., 2006. The role of phytochemicals in inhibition of cancer and inflammation: new directions and perspectives. J. Food Compos. Anal. 19, 405–419.

Kawabata, J., Fukushi, Y., Tahara Mizutani, J., 1985. Isolation and structural elucidation of four sesquiterpenes from *Chloranthus japonicus* (Chloranthaceae). Agric. Biol. Chem. 49, 1479–1486.

Lee, C.Y., 2017. Strategies of temozolomide in future glioblastoma treatment. Onco Targets Ther. 10, 265–270.

Liu, R.H., 2004. Potential synergy of phytochemicals in cancer prevention: mechanism of action. J. Nutr. 134, 3479S–3485S.

Ma, E., Wang, X., Li, Y., Sun, X., Tai, W., Li, T., Guo, T., 2008. Induction of apoptosis by furanodiene in HL60 leukemia cells through activation of TNFR1 signaling pathway. Cancer Lett. 27, 158–166.

Maggi, F., Barboni, L., Papa, F., Caprioli, G., Ricciutelli, M., Sagratini, G., Vittori, S., 2012. A forgotten vegetable (*Smyrnium olusatrum* L., Apiaceae) as a rich source of isofuranodiene. Food Chem. 135, 2852–2862.

Maggi, F., Papa, F., Giuliani, C., Maleci Bini, L., Venditti, A., Bianco, A., Nicoletti, M., Iannarelli, R., Caprioli, G., Sagratini, G., Cortese, M., Ricciutelli, M., Vittori, S., 2015. Essential oil chemotypification and secretory structures of the neglected vegetable *Smyrnium olusatrum* L. (Apiaceae) growing in central Italy. Flavour Fragrance J. 30, 139–159.

Maggi, F., Papa, F., Pucciarelli, S., Bramucci, M., Quassinti, L., Barboni, L., Dal Ben, D., Ramadori, A.T., Graiff, C., Galassi, R., 2017. Stabilization of the cyclodecadiene derivative isofuranodiene by silver (I) coordination. Mechanistic and biological aspects. Fitoterapia 117, 52–60.

Majdi, M., Liu, Q., Karimzadeh, G., Malboobi, M.A., Beekwilder, J., Cankar, K., de Vos, R., Todorovic, S., Simonovic, A., 2011. Bouwmeester H. Biosynthesis and localization of parthenolide in glandular trichomes of feverfew (*Tanacetum parthenium* L. Schulz Bip.). Phytochemistry 72, 1739–1750.

Mustafa, A.M., Maggi, F., Papa, F., Kaya, E., Dikmen, M., Öztürk, Y., 2016. Isofuranodiene: a neuritogenic compound isolated from wild celery (*Smyrnium olusatrum* L., Apiaceae). Food Chem. 192, 782–787.

Nieder, C., Adam, M., Molls, M., Grosu, A.L., 2006. Therapeutic options for recurrent high-grade glioma in adult patients: recent advances. Crit. Rev. Oncol. Hematol. 60, 181–193.

Quassinti, L., Maggi, F., Barboni, L., Ricciutelli, M., Cortese, M., Papa, F., Garulli, C., Kalogris, C., Vittori, S., Bramucci, M., 2014. Wild celery (*Smyrnium olusatrum* L.) oil and isofuranodiene induce apoptosis in human colon carcinoma cells. Fitoterapia 97, 133–141.

Sharma, S.H., Thulasingam, S., Nagarajan, S., 2017. Terpenoids as anti-colon cancer agents - a comprehensive review on its mechanistic perspectives. Eur. J. Pharmacol. 795, 169–178.

Sut, S., Maggi, F., Nicoletti, M., Baldan, V., Dall Acqua, S., 2018. New drugs from old natural compounds: scarcely investigated sesquiterpenes as new possible therapeutic agents. Curr. Med. Chem. 25, 1241–1258.

Suzuki, M., Bandoski, C., Bartlett, J.D., 2015. Fluoride induces oxidative damage and SIRT1/autophagy through ROS-mediated JNK signaling. Free Radic. Biol. Med. 89, 369–378.

Xiao, Y., Feng-Qing, Y., Shao-Ping, L., Jian-Li, G., Guang, H., Sin-Cheng, L., ..., Simon, L.M.Y., 2007. Furanodiene induces G2/M cell cycle arrest and apoptosis through MAPK signaling and mitochondria-caspase pathway in human hepatocellular carcinoma cells. Cancer Biol. Ther. 6, 1044–1050.

Xu, W.S., Dang, Y.Y., Chen, X.P., Lu, J.J., Wang, Y.T., 2014. Furanodiene presents synergistic anti-proliferative activity with paclitaxel via altering cell cycle and integrin signaling in 95-D lung cancer cells. Phytother. Res. 28, 296–299.

Zhong, Z., Dang, Y., Yuan, X., Guo, W., Li, Y., Tan, W., Cui, J., Lu, J., Zhang, Q., Chen, X., Wang, Y., 2012a. Furanodiene, a natural product, inhibits breast cancer growth both *in vitro* and *in vivo*. Cell Physiol. Biochem. 30, 778–790.

Zhong, Z.F., Hoi, P.M., Wu, G.S., Xu, Z.T., Tan, W., Chen, X.P., Cui, L., Wu, T., Wang, Y.T., 2012b. Anti-angiogenic effect of furanodiene on HUVECs *in vitro* and on zebrafish *in vivo*. J. Ethnopharmacol. 141, 721–727.

Zhong, Z.F., Tan, W., Qiang, W.W., Scofield, V.L., Tian, K., Wang, C.M., Qiang, W.A., Wang, Y.T., 2016. Furanodiene alters mitochondrial function in doxorubicin-resistant MCF-7 human breast cancer cells in an AMPK-dependent manner. Mol. Biosyst. 12, 1626–1637.

Thyme extract increases mucociliary-beating frequency in primary cell lines from chronic obstructive pulmonary disease patients

Massimo Nabissi[a],[*], Oliviero Marinelli[a], Maria Beatrice Morelli[a], Giovanna Nicotra[c], Romilde Iannarelli[a], Consuelo Amantini[b], Giorgio Santoni[a], Filippo Maggi[a]

[a] School of Pharmacy, University of Camerino, Camerino, MC, Italy
[b] School of Biosciences and Veterinary Medicine, University of Camerino, Camerino, MC, Italy
[c] E.P.O. s.r.l. Istituto Farmochimico Fitoterapico, Milano, Italy

ARTICLE INFO

ABSTRACT

Chronic obstructive pulmonary disease (COPD) is a respiratory disorder characterized by a progressive and irreversible airflow limitation. COPD is associated to a chronic inflammatory response with infiltration of inflammatory cells in the surface epithelium of large airways and abnormalities in structure and functions of cilia. Thyme (*Thymus vulgaris* L.) is a traditional medicinal plant of the Mediterranean area used to treat respiratory disorders. We previously evidenced that thyme extract reduce IL-1beta and IL-8, by downregulating the activated NF-κB levels, suggesting its potential therapeutically use in COPD. Cilia beating frequency (CBF) is dramatically impaired in COPD and different pharmacological agents can modulate cilia function. Herein we evaluated the effect of a commercial thyme extract in modulating CBF by measuring its activity in stimulating cAMP, Ca^{2+} levels and CBF in a MucilAir 3D human COPD airway epithelia reconstituted *in vitro* system using salmeterol, YM976, isoproterenol and GSK1016790 A as positive controls. Results showed that thyme extract increased cAMP levels starting from 12 h post-treatment, decreased extracellular Ca^{2+} levels and increased the CBF in airway epithelia from COPD donors. Overall, this work demonstrated that thyme extract is effective in stimulating CBF by inducing an increase of cAMP and Ca^{2+} levels, thus supporting its therapeutical use in the treatment of COPD.

1. Introduction

Chronic Obstructive Pulmonary Disease (COPD) is a respiratory disorder characterized by a progressive and irreversible airflow limitation [1]. COPD is associated to a chronic inflammatory response with infiltration of inflammatory cells in the surface epithelium of large airways and abnormalities in structure and functions of cilia [2]. Another striking histological feature in COPD lungs is the expression of mucus in small airways, which increases with disease progression and the extent of mucus expression in the small airways is an important risk factor for mortality in patients with severe COPD [3].

Phytoextracts are natural products obtained from medicinal and aromatic plants (MAPs) that have been widely used for treating acute and chronic inflammation of lung [4,5]. Among them, thyme (*Thymus vulgaris* L.) is one of the most cited herbal remedies for the treatment of respiratory tract inflammations [6]. Thyme is an aromatic shrub of the Lamiaceae family occurring in the Mediterranean area where it is widely used either as flavouring of food and beverages or as herbal

remedy for the treatment of respiratory and digestive disorders, parasitosis and urinary retention [7]. In particular, thyme is indicated, by traditional healers and physicians, as an antitussive, expectorant, antimicrobial and spasmolytic agent [8]. The Committee on Herbal Medicinal Products of the European Medicines Agency (EMA) has approved the use of thyme-based preparations, such as dry and liquid extracts and tinctures, for the treatment of cough associated with cold [9]. Furthermore, the German Commission E indicated thyme for treatments of cough, bronchitis and catarrh [8]. The pharmacological potential of thyme-based products is given by the presence of bioactive compounds such as phenolic monoterpenes (thymol), phenolic acids (rosmarinic and caffeic acid), flavonoids (rutin, luteolin, quercetin and apigenin derivatives), and triterpenes (ursolic and oleanolic acids) [10–12]. In COPD, inflammatory cells as neutrophils, macrophages and lymphocytes are activated to release different cytokines as IL-1beta, IL-6 and IL-8 through the activation of nuclear factor κB (NF-κB), which induces their gene transcription [1,13]. We previously evidenced that thyme extract, used at a concentration of 0.3%, reduced IL-1beta and

IL-8, by down-regulating the activated NF-κB levels, in a model of LPS-induced inflammation in normal human bronchial cells [6]. Moreover, thyme extract as other drugs (ex. guaifenesin) can be effective in reducing cellular content and secretion of MUC5AC, one of the components of mucus, being useful for the treatment of airway mucus hypersecretion [6,14]. However, thyme extract effects in regulating cilia function have been never evaluated. Cilia beating frequency (CBF) is dramatically impaired in COPD and different pharmacological agents can modulate cilia function. Indeed, CBF is dependent on the soluble nucleotides cAMP and cGMP and intracellular calcium concentrations [15,16]. Since the rate of cAMP efflux is proportional to the intracellular levels of cAMP and the process begins within minutes following stimulation of adenylyl cyclase [17]. cAMP can be measured both in intracellular and in extracellular compartments. Salmeterol xynaphoate is a beta-2-receptor agonist that causes an immediate cAMP-dependent increase of CBF, followed by a cAMP-dependent increase in intracellular calcium, which in turn increases CBF. Salmeterol activity depends on beta 2-receptors expressed at the apical membranes of epithelial cells [18]. The effect of salmeterol has been evaluated at 10^{-9} M up to 10^{-6} M and maximum CBF stimulation was observed at 10^{-7} M and 10^{-6} M, in "*ex vivo*" model of human nasal epithelial cells isolated from COPD patients [18]. As a result, salmeterol has been used clinically to treat COPD [19]. YM976 is a novel phosphodiesterase type 4 inhibitor that is able to inhibit (at 100 nM) PDE4 (PDEIV), resulting in increased cAMP and CBF, and PKA activation [20]. The Transient Receptor Potential Vanilloid 4 (TRPV4) is a calcium permeable ion channel expressed in airway epithelial cells and modulates epithelial calcium levels and CBF [21]. It has been demonstrated that the TRPV4 agonist GSK1016790 A produces concentration-dependent calcium responses in TRPV4-expressing HEK293, BEAS2B and 16HBE cells, while the TRPV4 antagonist HC067047 caused a rightward shift of the GSK1016790 A concentration-response curves. Nasal epithelial cells responded to the TRPV4 agonist with increased CBF and also this effect was prevented or inhibited by the TRPV4 antagonist HC067047.

In this work, to further support the use of thyme extract in the treatment of COPD, we evaluated its effects in regulating CBF in a 3D Human Airway Epithelia reconstituted *in vitro* model, using three different bronchial primary cells derived from COPD single donors.

2. Materials and methods

2.1. Cell lines

Three different primary human cell lines (1401, 5401 and 904) obtained from COPD (Chronic Obstructive Pulmonary Disease) patients were purchased from Epithelix Sarl (Geneve, Switzerland). Cell lines were cultured in MucilAir 3D Human Airway Epithelia reconstituted *in vitro* system (Epithelix Sarl), growth in ready to use commercial MucilAir™ culture medium (Epithelix Sarl) and maintained at 37 °C, 5% CO_2 in a cell incubator, as recommended by the manufactory. MucilAir-COPD is an organotypic 3D airway tissue model in which differentiated human epithelial from COPD donor cells are cultured at the air–liquid interface (ALI) and are capable to form a pseudo-stratified cell layer containing mucus-secreting goblet cells and ciliated columnar cells, as reported by manufacturing instruction (http://www.epithelix.com/products/mucilair). The ALI allows a direct administration of an aerosol onto the apical surface, a situation resembling aerosols exposure of the *in vivo* respiratory system. Moreover, the epithelium is nourished by a culture medium from the basolateral surface.

2.2. Chemicals

Salmeterol xinafoate, isoproterenol, GSK1016790A and HC-067047 were purchased from Cayman (MI, USA). YM 976 was purchased from Tocris (UK). Ruthenium Red (RR) was purchased from Sigma Aldrich (MI, USA). All compounds were dissolved in ethanol 70%, except

isoproterenol and RR that were dissolved in water. The compound stock solutions were prepared according to the manufacturing's data sheet. Aliquots were prepared for each compound and stored at −20 °C. Each aliquot was used only once. The commercial standardized thyme hydroalcoholic extract (thymol 0.3% w/w, rosmarinic acid 0.6%, traces of linalool and carvacrol) was kindly provided by EPO s.r.l., Istituto Farmochimico Fitoterapico (Milan, Italy). Thyme extract was prepared in ethanol 70% and water 30%, sonicated and filtered (20 μm filter), as previously described [6]. Aliquots were prepared and stored at −20 °C for single use. For all the experiments the final concentration of Thyme extract in the cell medium was 0.3%. The extract was always added apically in the 3D cell wells.

2.3. cAMP assay

Extracellular cAMP concentration was evaluated in 100 μl of cell culture supernatants, in salmeterol, YM 976 and thyme extract treated-cell lines, using the cyclic AMP ELISA kit (Cayman, MI, USA). Each sample was analysed after 1, 12, 24 h post-treatments. Then the cell cultures were washed with MucilAir culture medium (Wash-out) and cAMP was detected after 30 min. cAMP concentrations were calculated plotting the O.D. values in the equation curve obtained with standard, according to the manufacturer's protocol. Each sample was evaluated in duplicated and in two independent experiments.

2.4. Calcium assay

Extracellular Ca^{2+} concentration was measured with the Fluo-8 No Wash Calcium Assay kit (Abcam, Cambridge, MA) according to the manufacturing instructions. The plates were transferred to a scanning fluorometer chamber (Molecular Devices, Sunnyvale, CA), then the cells were excited at 490 nm and Ca^{2+}-bound fluo-8 emission was recorded at 525 nm. The fluo-8 fluorescence was expressed as $F_{max}/F0$, where F_{max} was the maximum and F_0 was the baseline fluorescence measured. Briefly, cell lines were treated with GSK1016790 A, HC067047, RR, Ionomycin and thyme extract (0.3%) for 1, 3, 5 min and extracellular Ca^{2+} was measured. Then the cells were washed with MucilAir culture medium (Wash-out) and extracellular Ca^{2+} was further detected after 30 min from washing out. Each sample was evaluated in triplicate and in two independent experiments.

2.5. Measurement of the cilia beating frequency (CBF)

Cilia beating frequency was measured by a system consisting of three parts: a camera (Sony XCD V60 Firewire), a PCI card and a specific package of software. The Cilia beating frequency, expressed in Hz, was determined using CiliaFA software; 256 images movies were recorded at 37 °C. Thirty ml of thyme extract (0.3% final concentration) was diluted in saline solution (0.9% NaCl; 1.25 mM $CaCl_2$; 10 mM Hepes + max 1% DMSO) and applied on the apical surface of MucilAir-COPD. The epithelia were incubated for 1 h (37 °C; 5% CO_2) before sequentially measuring CBF. The epithelia were then incubated for further 23 h before sequentially measuring CBF.

2.6. Statistical analysis

The data reported represent the mean with standard deviation (SD) of at least 2 independent experiments. The statistical significance was determined by Student's *t*-test and by one way ANOVA; *$p < 0.05$.

3. Results

3.1. Thyme extract increases extracellular cAMP levels in primary COPD cell lines

Primary COPD cell lines (1401, 5401, 904) were treated at different
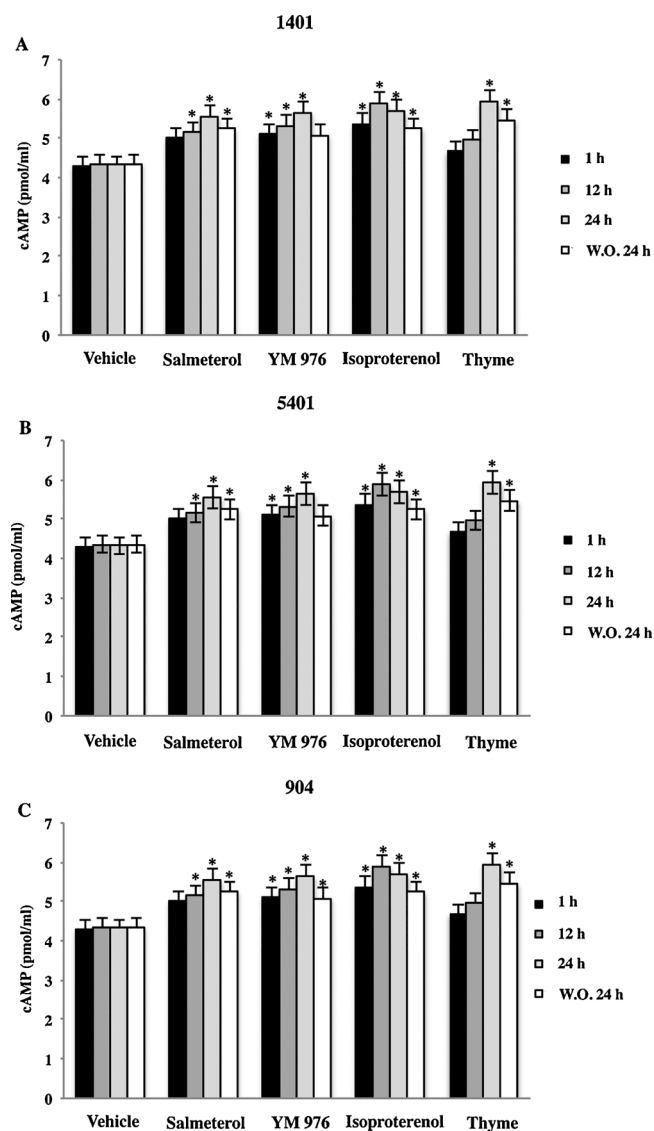
Fig. 1. Thyme extract increases extracellular cAMP-levels in COPD cell lines. Primary COPD cell lines (1401, 5401, 904) were treated with salmeterol (250 nM), YM 976 (2 nM), isoproterenol (50 microMolar) and thyme extract (0.3%). Supernatant cAMP levels were determined at the indicated times and 24 h post washing out (W.O. 24 h) (A, C). Each sample was evaluated in duplicate and in two independent experiments. cAMP levels were calculated from the equation obtained from the standard curve (A) and expressed as pmoles/ml. * $p < 0.05$ vehicle *vs* treatments.

times (1, 12, 24 h) with salmeterol (250 nM), YM 976 (2 nM), isoprotenerol (50 μM) and thyme extract (0.3%) and supernatant cAMP levels were determined at the indicated times and 24 h post washing out (W.O. 24 h). The results showed that thyme extract induced an increase in supernatant cAMP levels starting from 12 h post-treatment in a similar manner to salmeterol, YM976 and isoprotenerol (Fig.1B,D). In addition, we found that a sustained release of cAMP is maintained at 24 h post washing-out too, suggesting that the stimulatory effects of thyme extract and of the others compounds utilized, on cAMP production, were maintained also 24 h post-treatments (Fig. 1B-D). These results evidenced that thyme extract acts in a similar manner to the other treatments in activating a signaling pathway leading to the increase of CBF.

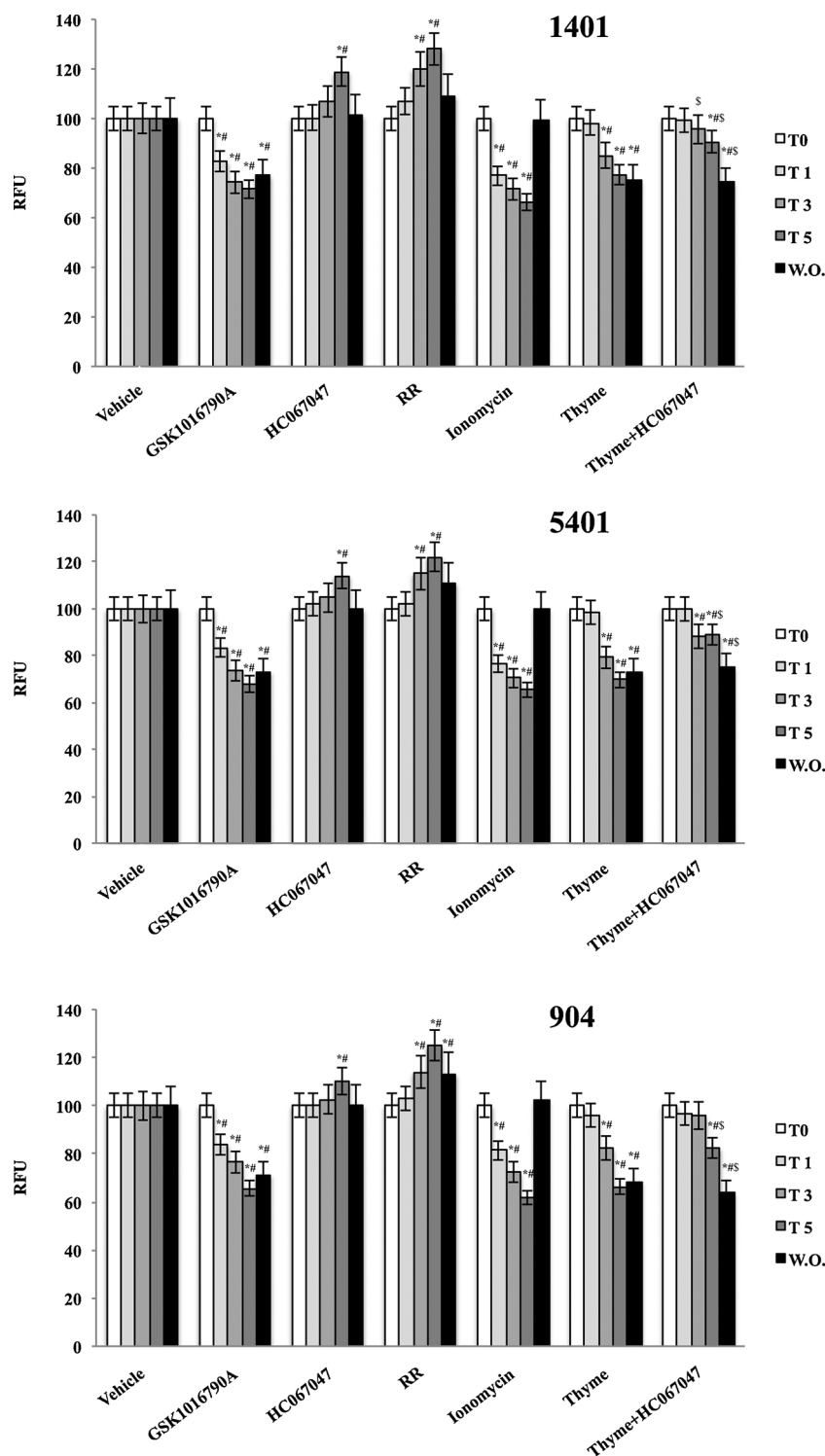### 3.2. Thyme extract reduces extracellular calcium in COPD cell lines

To evaluate the influence of thyme extract in regulating Ca^{2+} levels, primary COPD cell lines (1401, 5401, 904) were treated for different times with thyme extract (0.3%), and supernatant Ca^{2+} levels were determined in culture medium. Since TRPV4 is a cation channel whose activation induces calcium influx and ciliary activity in human airway epithelial cells [19], we used 10 nM GSK1016790A (TRPV4 agonist) as positive control and 1 μM HC067047 (TRPV4 antagonist) as negative control. Moreover, the cell lines were treated with 1 mM ionomycin, which is used to raise the intracellular Ca^{2+} levels. The results showed that GSK1016790A reduced extracellular Ca^{2+} levels (inducing Ca^{2+} influx), while HC067047 increases extra-cellular Ca^{2+} levels compared with vehicle-treated cells (Fig.2A–C). As expected, ionomycin decreased extra-cellular Ca^{2+} levels. To evaluate the thyme extract effect in regulating the extracellular Ca^{2+} levels, we compared its effect with GSK1016790A - and HC067047-treated cell lines. The results evidenced that thyme extract acted in a similar manner to GSK1016790A and its activity is partially reversed by HC067047, suggesting that thyme is able to decrease extracellular Ca^{2+} levels and that its effect is partly due to TRPV4 activation (Fig. 2A–C).

3.3. Thyme extract increases cilia beating frequency (CBF) in COPD cell lines

The aim of the experiments was to evaluate the effect of thyme extract on CBF in fully differentiated airway epithelia from COPD donors. To mimic airborne delivery, thyme extract (0.3%) or isoproterenol (as positive control) have been applied in solution on the apical surface of MucilAir™-COPD. The epithelia have been incubated for 1 h and 24 h before sequentially measuring CBF. The results showed that thyme extract is able to increase CBF at both incubation times compared with vehicle treated-cells (Fig. 3). Moreover, this effect was lower at 1 h but similar at 24 h post-treatment compared with isoproterenol (Fig. 3). These data strongly confirm that thyme extract is active in increasing CBF in airway epithelia from COPD donors.

4. Discussion

Ciliary beating of airway epithelial cells constitutes an important part of the mucociliary transport apparatus, which must exhibit a cohesive beating of all ciliated epithelial cells that line the upper and lower respiratory tract. Impaired mucociliary clearance is seen in patients with COPD and cilia features may contribute to lung disease, including cilia dysfunction (ciliary beat frequency-CBF and wave pattern) due to the susceptibility of the cilia to endogenous and exogenous factors that modify their CBF and quality of motion [2]. Accumulating evidence shows that mammalian CBF changes in response to the phosphorylation state of ciliary targets and to the levels of $[Ca^{2+}]_i$, both events mainly occurring through variation of cAMP levels inside the cells [22]. So, for the regulation of airway cilia, cAMP needs to be made available to the axonemes from within the cell and beta-adrenergic agonists or phosphodiesterase -4 inhibitors are used to increase CBF in a cAMP-dependent manner *via* beta 2- receptors expressed at the apical membrane [23]. Herein, we found that thyme extract is able to increase c-AMP levels at comparable levels with salmeterol or isoproterenol (beta-adrenergic agonists) or YM 976 (phosphodiesterase-4 inhibitor) suggesting its possible involvement in increasing CBF in a cAMP-dependent manner in COPD cell lines. Since the increase of $[Ca^{2+}]_i$ is often associated with an increase of CBF [24], whereas its decrease usually causes a reduction of CBF itself, the understanding of the changes in $[Ca2^{+}]_I$ levels is of key importance to identify the effect of drugs inducing CBF [24]. The source of calcium to mediate an increase in CBF can derive from intracellular stores or from calcium influx through the plasma membrane, an event occurring possibly directly or after receptor-mediated calcium release from intracellular stores [25].

Fig. 2. Thyme extract reduces extracellular calcium in COPD cell lines. Primary COPD cell lines (1401, 5401, 904) were treated at different times with GSK1016790A (10 nM), HC067047 (1 µM), RR (10 µM), ionomycin (1 microMolar) and thyme extract (0.3%), and supernatant Ca^{2+} levels were determined (A–C). Each sample was evaluated in duplicate and in two independent experiments. Ca^{2+} levels were calculated as % of RFU (relative fluorescent units) respect to vehicle. * $p < 0.05$ vehicle *vs.* treatments; # $p < 0.05$ T0 *vs.* T1, T3, T5, W.O. $ p > 0.05$ Thyme *vs.* Thyme + HC.

The transient receptor potential vanilloid 4 (TRPV4) is a calcium permeable ion channel expressed in airway epithelial cells [26]. In particular, the high potent TRPV4 agonist GSK1016790A was found to significantly increase CBF to levels comparable with those seen after addition of the adenylate cyclase activator forskolin, a well-known stimulator of ciliary beating, and the CBF increase was completely inhibited by HC067047 and the aspecific inhibitor ruthenium red [26].

Thus, TRPV4 may participate in mucociliary clearance and airway protection. In addition, evidence from animal studies supports a role of TRPV4 in the auto-regulation of cell volume and CBF in the airway epithelium [26]. However, the role of TRPV4 in CBF regulation in human ciliated epithelial cells remains to be elucidated.

In this study, we explored the effects of TRPV4 activation on calcium influx in human airway epithelial cell lines using the recently

A 1401

B 5401

C 904
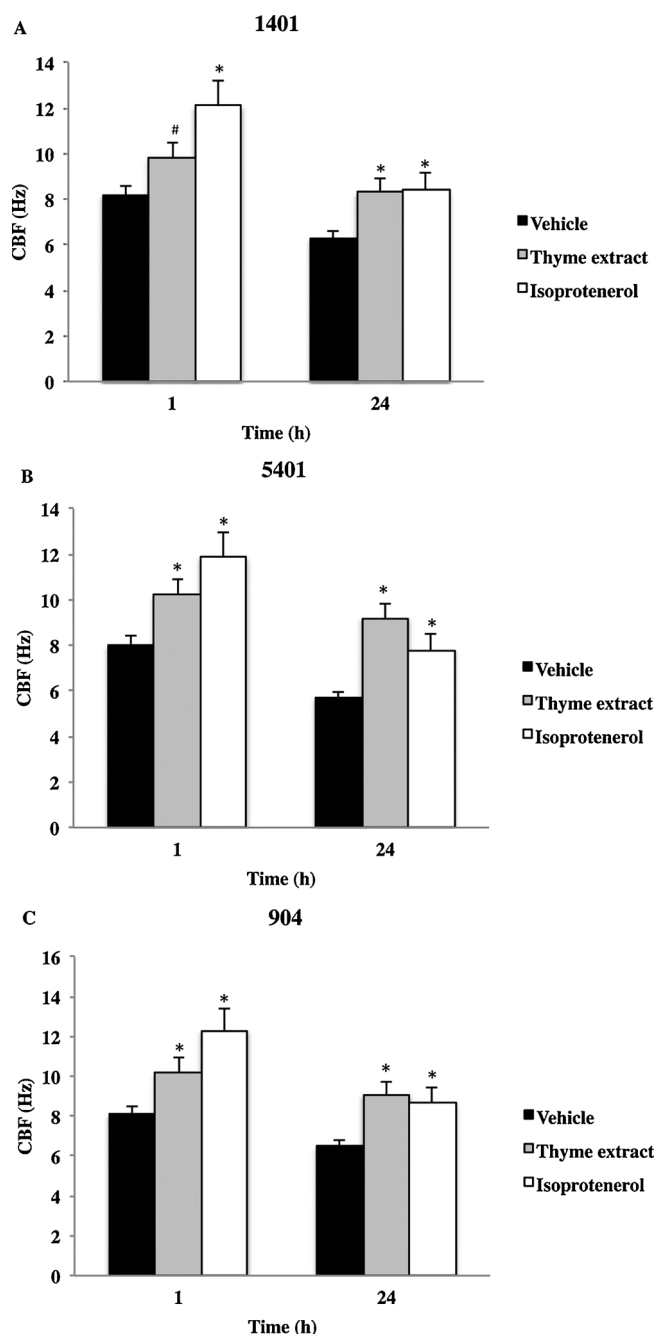
Fig. 3. Thyme extract increases Cilia Beating Frequency (CBF) in COPD cell line. Measurement of the Cilia Beating Frequency (CBF) was evaluated in COPD cell lines treated with isoproterenol or thyme extract (0.3%) for 1 and 24 h (A–C). Each sample was evaluated in triplicate and in two independent experiments. The CBF was expressed as Hz. 256 images movies recorded at 37 °C. * $p < 0.05$ vs vehicle; # $p < 0.05$ vs isoproterenol.

developed highly potent TRPV4 agonist GSK1016790A [26]. As previously demonstrated, GSK1016790A elicited calcium responses that were prevented by the TRPV4 antagonist HC067047. Furthermore, GSK1016790A was found to significantly increase CBF to levels comparable with those seen after addition of the adenylate cyclase activator forskolin, a well-known stimulator of ciliary beating, and the CBF increase was completely inhibited by HC067047 and ruthenium red [26]. Herein, we compared the effects of GSK1016790A and HC067047 with that of thyme extract in human primary COPD cell models. As shown we found that thyme extract was able to act similarly to GSK1016790A and that its effect was reversed by HC067047. This suggests that thyme

extract stimulates the increase of $[Ca_i^{2+}]$ *via* activation of TRPV4. Lastly, to confirm the role of thyme extract in regulating CBF, we measured the changes in CBF respect to isoproterenol used as positive control. The data clearly evidenced that thyme extract increase CBF in COPD cell lines by increasing cAMP levels and $[Ca_i^{2+}]$ levels. In addition, the increase of CBF should include other beneficial effect in COPD patients, since mucociliary clearance (MCC) that is an innate defence mechanism to remove inhaled pathogens from the airways, is frequently impaired in COPD patients. In fact, efficient MCC requires the proper regulation of three major processes: salt and water transport, mucin synthesis and secretion, and CBF coordination [27]. Our results were consistent with literature data where thymol was found to exert antispasmodic activity on rat trachea and ileum and increase the mucociliary transport in mice through a modulatory action on the β2-receptor system [28,29]. However, other compounds occurring in the extract, such as luteolin derivatives, may be involved since thymol-deprived extracts were proven to maintain these therapeutic properties [30]. In conclusion, taken together these data support the historical uses of thyme in the treatment of respiratory disorders and shed light on its possible role as CBF enhancer in COPD.

Conflict of interest

Authors' contribution

Massimo Nabissi conceived the experiments. Massimo Nabissi, Oliviero Marinelli, Maria Beatrice Morelli designed the experiments. Massimo Nabissi, Oliviero Marinelli, Maria Beatrice Morelli, Romilde Iannarelli performed the experiments. Giovanna Nicotra contributed for reagents/materials. Massimo Nabissi, Consuelo Amantini, Filippo Maggi, Giorgio Santoni contributed for the analysis tool and for writing the paper.

Acknowledgment

References

[1] V. Cukic, V. Lovre, D. Dragisic, A. Ustamujic, Asthma and chronic obstructive pulmonary disease (COPD) – differences and similarities, Mater. Soc.-Med. 24 (2012) 100–105 (PMID: 23678316).

[2] A. Yaghi, M.B. Dolovich, Airway epithelial cell cilia and obstructive lung disease, Cells 5 (4) (2016) E40 (PMID: 27845721).

[3] J.C. Hogg, F.S. Chu, W.C. Tan, D.D. Sin, S.A. Patel, P.D. Pare, F.J. Martinez, R.M. Rogers, B.J. Make, G.J. Criner, et al., Survival after lung volume reduction in chronic obstructive pulmonary disease: insights from small airway pathology, Am. J. Respir. Crit. Care Med. 176 (5) (2007) 454 (PMID: 17556723).

[4] M. Asadbeigi, T. Mohammadi, M. Rafieian-Kopaei, K. Saki, M. Bahmani, M. Delfan, Traditional effects of medicinal plants in the treatment of respiratory diseases and disorders: an ethnobotanical study in the Urmia, Asian Pac. J. Trop. Med. 7 (2014) S364–S368 (PMID: 25312151).

[5] A.P. Rogerio, A. Sá-Nunes, L.H. Faccioli, The activity of medicinal plants and secondary metabolites on eosinophilic inflammation, Pharmacol. Res. 62 (4) (2010) 298–307 (PMID: 20450976).

[6] O. Marinelli, R. Iannarelli, M.B. Morelli, M. Valisi, G. Nicotra, C. Amantini, C. Cardinali, G. Santoni, F. Maggi, M. Nabissi, Evaluations of thyme extract effects in human normal bronchial and tracheal epithelial cell lines and in human lung cancer cell line, Chem. Biol. Interact. 256 (2016) 125–133 (PMID: 27369807).

[7] F.A. Al-Bayati, Synergistic antibacterial activity between *Thymus vulgaris* and *Pimpinella anisum* essential oils and methanol extracts, J. Ethnopharmacol. 116 (3) (2008) 403–406 (PMID: 18226481).

[8] E. Basch, C. Ulbricht, P. Hammerness, A. Bevins, D. Sollars, Thyme (*Thymus vulgaris* L.), thymol, J. Herb. Pharmacother. 4 (1) (2004) 49–67 (PMID: 15273078).

[9] European Medicine Agency (EMA), An agency of the European Union, B. Boros, S. Jakabová, Á. Dörnyei, G. Horváth, Z. Pluhár, F. Kilár, A. Felinger, Determination of polyphenolic compounds by liquid chromatography–mass spectrometry in

Thymus species, J. Chromatogr. A 1217 (51) (2010) 7972–7980 (PMID: 20692666), http://www.ema.europa.eu/docs/en_GB/document_library/Herbal_-_Summary_of_assessment_report_for_the_public/2016/10/WC500214266.pdf.

[10] S. Fecka, Turek, Determination of polyphenolic compounds in commercial herbal drugs and spices from Lamiaceae: thyme, wild thyme and sweet marjoram by chromatographic techniques, Food Chem. 108 (3) (2008) 1039–1053 (PMID: 26065769).

[11] L.O. Somova, A. Nadar, P. Rammanan, F.O. Shode, Cardiovascular, antihyperlipidemic and antioxidant effects of oleanolic and ursolic acids in experimental hypertension, Phytomedicine 10 (2-3) (2003) 115–121 (PMID: 12725563).

[12] A.G. Duque, A. Descoteaux, Macrophage Cytokines, Involvement in immunity and infectious diseases, Front. Immunol. 5 (2014) 491 (PMID: 25339958).

[13] T.A. Wyatt, M.A. Forgèt, J.M. Adams, J.H. Sisson, Both cAMP and cGMP are require for maximal ciliary beat stimulation in a cell-free model of bovine ciliary axonemes, Am. J. Physiol. Lung Cell. Mol. Physiol. 288 (3) (2005) L546–551 (PMID: 15542545).

[14] J. Seagrave, H.H. Albrecht, D.B. Hill, D.F. Rogers, G. Solomon, Effects of guaifenesin, N-acetylcysteine, and ambroxol on MUC5AC and mucociliary transport in primary differentiated human tracheal-bronchial cells, Respir. Res. 13 (98) (2012) (PMID: 23113953).

[15] L. Zhang, M.J. Sanderson, The role of cGMP in the regulation of rabbit airway ciliary beat frequency, J. Physiol. 551 (Pt 3) (2003) 765–776 (PMID: 12819300).

[16] E.K. Jackson, R.K. Dubey, Role of the extracellular cyclic AMP-adenosine pathway in renal physiology, Am. J. Physiol. 281 (2001) F597–F612 (PMID: 11553506).

[17] K. Kanthakumar, D.R. Cundell, M. Johnson, P.J. Wills, G.W. Taylor, P.J. Cole, R. Wilson, Effect of salmeterol on human nasal epithelial cell ciliary beating: inhibition of the ciliotoxin: pyocyanin, Br. J. Pharmacol. 112 (2) (1994) 493–498 (PMID: 7915610).

[18] B. Jarvis, A. Markham, Inhaled salmeterol: a review of its efficacy in chronic obstructive pulmonary disease, Drugs Aging 18 (6) (2001) 441–472 (PMID: 11419918).

[19] A. Yaghi, A. Zaman, G. Cox, M.B. Dolovich, Ciliary beating is depressed in nasal cilia from chronic obstructive pulmonary disease subjects, Respir. Med. 106 (8) (2012) 1139–1147 (PMID: 22608352).

[20] L. Alenmyr, L. Uller, L. Greiff, E.D. Högestätt, P.M. Zygmunt, TRPV4-mediated calcium influx and ciliary activity in human native airway epithelial cells, Basic Clin. Pharmacol. Toxicol. 114 (2) (2014) 210–216 (PMID: 24034343).

[21] H. Kogiso, S. Hosogi, Y. Ikeuchi, S. Tanaka, T. Inui, Y. Marunaka, T. Nakahari, [Ca(2+)](i) modulation of cAMP-stimulated ciliary beat frequency via PDE1 in airway ciliary cells of mice, Exp. Physiol. 103 (3) (2018) 381–390 (PMID: 29282782).

[22] M. Salathe, Effects of β-agonists on airway epithelial cells, J. Allergy Clin. Immunol. 110 (6) (2002) S275–S281 (PMID: 12464936).

[23] I. Gertsberg, V. Hellman, M. Fainshtein, S. Weil, S.D. Silberberg, M. Danilenko, Z. Priel, Intracellular Ca2+ regulates the phosphorylation and the dephosphorylation of ciliary proteins via the NO pathway, J. Gen. Physiol. 124 (5) (2004) 527–540 (PMID: 15477378).

[24] L. Zhang, M.J. Sanderson, Oscillations in ciliary beat frequency and intracellular calcium concentration in rabbit tracheal epithelial cells induced by ATP, J. Physiol. 546 (3) (2003) 733–749 (PMID: 12563000).

[25] I.M. Lorenzo, W. Liedtke, M.J. Sanderson, M.A. Valverde, TRPV4 channel participates in receptor-operated calcium entry and ciliary beat frequency regulation in mouse airway epithelial cells, Proc. Natl. Acad. Sci. U. S. A. 105 (34) (2006) 12611–12616 (PMID: 18719094).

[26] Y.A. Alpizar, B. Boonen, A. Sanchez, C. Jung, A. López-Requena, R. Naert, B. Steelant, K. Luyts, C. Plata, V. De Vooght, J.A.J. Vanoirbeek, V.M. Meseguer, T. Voets, J.L. Alvarez, P.W. Hellings, P.H.M. Hoet, B. Nemery, M.A. Valverde, K. Talavera, TRPV4 activation triggers protective responses to bacterial lipopolysaccharides in airway epithelial cells, Nat. Commun. 8 (2017) 1059 (PMID: 29057902).

[27] P.R. Sears, W.N. Yin, L.E. Ostrowski, Continuous mucociliary transport by primary human airway epithelial cells in vitro, Am. J. Physiol. Lung Cell. Mol. Physiol. 309 (2) (2015) L99–108 (PMID: 25979076).

[28] F. Begrow, J. Engelbertz, B. Feistel, R. Lehnfeld, K. Bauer, E.J. Verspohl, Impact of thymol in thyme extracts on their antispasmodic action and ciliary clearance, Planta Med. 76 (04) (2010) 311–318 (PMID: 19809973).

[29] N. Wienkötter, F. Begrow, U. Kinzinger, D. Schierstedt, E.J. Verspohl, The effect of thyme extract on β2-receptors and mucociliary clearance, Planta Med. 73 (07) (2007) 629–635 (PMID: 17564943).

[30] J. Engelbertz, M. Lechtenberg, L. Studt, A. Hensel, E.J. Verspohl, Bioassay-guided fractionation of a thymol-deprived hydrophilic thyme extract and its antispasmodic effect, J. Ethnopharmacol. 14 (141) (2012) 848–853 (PMID: 22465593).

"Immuno-Transient Receptor Potential Ion Channels": The Role in Monocyte- and Macrophage-Mediated Inflammatory Responses

Giorgio Santoni[1]*, Maria Beatrice Morelli[1,2], Consuelo Amantini[3], Matteo Santoni[4], Massimo Nabissi[1], Oliviero Marinelli[1,3] and Angela Santoni[2,5]

[1] *Section of Experimental Medicine, School of Pharmacy, University of Camerino, Camerino, Italy,* [2] *Department of Molecular Medicine, Sapienza University, Rome, Italy,* [3] *School of Biosciences and Veterinary Medicine, University of Camerino, Camerino, Italy,* [4] *Clinical Oncology Unit, Macerata Hospital, Macerata, Italy,* [5] *Neuromed I.R.C.C.S. – Istituto Neurologico Mediterraneo, Pozzilli, Italy*

Monocytes and macrophages play important roles in health and disease. They have a central role in protecting the host, as they clear pathogens and modulate other immune cell functions through the production of regulatory molecules. Their functions include immune surveillance, bacterial killing, tissue remodeling and repair, clearance of cell debris and more. Macrophages can have beneficial and detrimental effects on the outcome of several diseases depending on the microenvironment and the activation state of cells. Over the past few years, there has been an increasing interest in the expression and functions of ion channels, in particular of transient receptor potential (TRP) channel family in immune cells. The 30 members of mammalian TRP channels are subdivided into TRPC, TRPV, TRPM, TRPML, TRPP, and TRPA superfamily, and several members of TRP subfamily have been found to be functionally expressed in monocytes and macrophages. TRP are cation-selective channels that are weakly voltage-sensitive and diversely gated by temperature, mechanical force, electrophiles, ligands, and internal cues, such as membrane composition and pH, contributing to immune and inflammatory responses. The TRP channels play major roles in controlling several monocyte and macrophage functions such as phagocytosis, production of chemokines and cytokines, cell survival, polarization and so forth. In addition, they can also be potential therapeutic targets in a variety of inflammatory diseases. Thus, the goal of this review is to describe the role of TRP channels in the control of monocyte–macrophage functions in inflammatory and immune-mediated diseases.

Keywords: macrophages, transient receptor potential, macrophage polarization, migration, phagocytosis

INTRODUCTION

Macrophages play a crucial role in defense and disease by triggering immune surveillance, bacterial killing, tissue remodeling, and tissue repair (1–4). Macrophages show beneficial or detrimental effects in different diseases depending on their cell activation state and the microenvironment where they are present (5).

In the last years, there has been an increasing interest in the expression and functions of transient receptor potential (TRP) ion channel family in myeloid cells.

On the basis of amino acid sequence homology, TRP channels are grouped into different subfamily, called canonical (TRPC), melastatin (TRPM), vanilloid (TRPV), ankyrin (TRPA), mucolipin (TRPML), and polycystin (TRPP) subfamily (6, 7). Structurally they have six transmembrane spanning domains (S1–S6) with a pore domain between the fifth (S5) and sixth (S6) segment and intracellular C and N termini (8–10). TRP channels conduct cations, are weakly voltage-sensitive and non-selective for calcium, with a permeability ratio to Na (P_{Ca}/P_{Na}) in a range between 0.3 and 10.

At present, TRP channel ligands are only partially known, although they function as multimodal signal integrators for exogenous ligands. The G protein-coupled receptors ($G_{q/11}$; linked to PLCβ) and tyrosine kinase receptors (linked to PLCγ) potentiate the signaling and function of most TRP channels (11). Elements of phosphatidylinositol signaling pathway, in particular, PIP_2, can regulate TRP channels (12). In addition, intracellular Ca^{2+} increases TRP activity and modulates all TRP channels. For detailed description of TRP channels, there are many excellent reviews (13–16).

Several members of TRP subfamily are expressed in monocytes and macrophages (M/MΦ) (17). In these cells, they can recognize exogenous signals, including damage-associated molecular pattern molecules from the environment (heat, acidity, and chemicals) and endogenous danger signals released during trauma/tissue injury (ATP, mechanical, osmotic stress, and uric acid). In addition, they sensitize the pattern recognition receptors expressed in myeloid cells to respond to pathogen-associated molecular patterns (PAMPs) (18).

Aim of this review is to describe the cellular functions mediated by different members of TRP channels in M/MΦ.

EFFECTS OF TRP CHANNELS ON M/MΦ SURVIVAL AND PROLIFERATION

TRPM channels control the survival and proliferation of M/MΦ. In this regard, TRPM2 has been found to inhibit reactive oxygen species (ROS) generation in phagocytic cells and protect the mice from LPS-induced effects. LPS-treated $TRPM2^{(-/-)}$ mice show an increased inflammatory response and reduced cell viability with respect to wild-type mice. In addition, TRPM2 channels damp NADPH oxidase-stimulated ROS generation by phagocytes, through the induction of plasma membrane depolarization (19). The other TRP family member, TRPM4, controls M/MΦ survival in sepsis (20). The knockout of the TRPM4 gene increases the mortality in a murine model of LPS-induced sepsis. The lack of TRPM4 affects peritoneal macrophage infiltrate and increases the monocyte number, and the release of IL-1β and TNFα cytokines. Macrophages from $TRPM4$ knockout mice display reduced Ca^{2+} mobilization that inhibits the Akt pathway, and consequently macrophage survival, phagocytosis of bacteria (20).

TRPC1 plays an important role in the protection from bacterial infection, through TLR4-TRPC1 activation of protein kinase (PK) Cα pathway (**Figure 1**) (21). Ca^{2+} entry, induced by TRPC1 channel, stimulates the production of pro-inflammatory cytokines in murine pneumocytes. The TLR4-dependent TRPC1 activation triggers Ca^{2+} depletion from endoplasmic reticulum
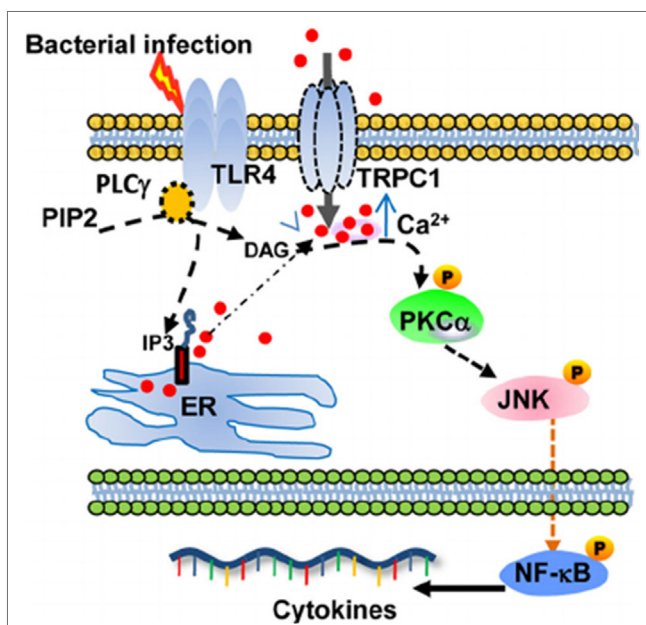
FIGURE 1 | Schematic describing the proposed TRPC1/PKCα/JNK/NF-κB axis involved in the dysregulated pro-inflammatory response during bacterial infection. From Ref. (21) Copyright 2015 Molecular and Cellular Biology.

(ER) store. After activation of PLC-γ, TRPC1 mediates Ca^{2+} entry and stimulates PKCα activity, which results in NF-κB/Jun kinase nuclear translocation and cytokine release leading to tissue destruction (21). The $TRPC1^{(-/-)}$ mice show reduced survival, lung tissue damage, and systemic infection. Moreover, bone-marrow macrophages from $TRPC3^{(-/-)}$ mice show reduction in basal Ca^{2+} influx, impaired TNFα-induced signal as compared to wild-type cells (22).

TRP CHANNELS AND INFLAMMASOME ACTIVATION IN M/MΦ

The inflammasomes are multiprotein platforms that mediate pro-caspase-1 cleavage and promote cytokine maturation (e.g., IL-1β and IL-18), in response to microbial and non-microbial stimuli, by canonical and non-canonical mechanisms. The activation of non-canonical inflammasome is mediated by caspase-11 that triggers IL-1β, IL-18, and IL-1α release in a caspase-1-dependent and -independent manner. Caspase-11 also promotes pyroptosis, a form of genetically programmed cell death (23). TRPC1 represents a substrate for caspase-11. Defects in TRPC1 expression enhance caspase-1-independent IL-1β release or macrophage death. Thus, intraperitoneal LPS injection in $TRPC1^{(-/-)}$ mice induces higher IL-1β secretion (24). Recently, in human U937 monocytes exposed to high glucose (HG) condition that induces the NLRP3-ASC inflammasome stimulation leading to caspase-1 activation and IL-1β and IL-18 secretion, TRPM2 regulates the thioredoxin-interacting protein-mediated triggering of NLRP3 inflammasome *via* interaction with the p47phox protein (25). In particular, TRPM2 activation and TRPM2-mediated Ca^{2+} influx represent the critical steps in NLRP3 activation. In response

to HG, the reduction of TRPM2 expression reduces ROS generation and NADPH oxidase activity (25).

In phagocytes, the formation of crystals also induces oxidative stress that triggers NLRP3-mediated IL-1β secretion. Recently, Zhong et al. have demonstrated that liposomes are required for NLRP3 activation (26) and ROS-dependent TRPM2-mediated calcium influx (27). Infact, in macrophages from TRPM2 knock-out mice, neither NLRP3 activation nor IL-1β production, is evidenced.

The NLRP3 inflammasome senses cell swelling and regulatory volume decrease (RVD), and the TRPV2 channel has been found to control volume regulation (18, 28). The reduction in extracellular osmolarity results in K(+)-dependent conformational change of the inactive NLRP3 inflammasome state followed by its activation, which is controlled by TRPV2 during RVD (28). Moreover, NLRP3-independent activation has been reported in human THP-1 macrophages (29). Apoptosis-associated speck-like protein containing a CARD domain (ASC) is required for the inflammatory processes. ASC bring NLRP proteins near to procaspase-1 into the inflammasome complex. Under hypotonic conditions, in TRPV2-dependent and independently by NLRP3, ASC forms specks that are unable to mediate pro-caspase-1 activation and pyroptosis. However, ASC speck formation leading to inflammasome and pro-caspase-1 cleavage is increased by interaction with NLRP3 (29).

CONTRIBUTION OF TRP CHANNELS TO MΦ POLARIZATION

Similar to the Th1/Th2 nomenclature (30, 31), in response to different cytokines or PAMPs, there are specialized and polarized M1 and M2 macrophages. Activated M1 macrophages are induced by IFNγ alone or by microbial stimuli (e.g., LPS) or cytokines (e.g., TNF and GM-CSF). IL-4 and IL-13 other than to be inhibitors of macrophage activation, can induce the alternative M2 phenotype of macrophages (30). Activated M2 macrophages include cells exposed to IL-4 or IL-13, immune complexes, IL-10, glucocorticoids, or hormones (32). M1 cells secrete high levels of IL-12 and IL-23 and exhibit low IL-10 production; they generate NO and ROS and produce IL-1β, TNF, IL-6; they participate in Th1-polarized responses and mediate increased resistance against intracellular parasites and tumors. In contrast, M2 macrophages secrete low levels of IL-12 and IL-23 and high levels IL-10. Low expression of IL-1β and caspase-1 and high levels of IL-1ra, and decoy type II receptor were found in M2 cells (33). M1 and M2 cells also have distinct chemokine and chemokine receptor repertoire (31). M2 cells cooperate with Th2 cells in promoting the killing of parasites (34); they are present in some tumors and stimulate tissue repair (35). Moreover, recently, the analysis of transcriptomes in human macrophages stimulated with different stimuli has revealed the presence of distinct stimulus-specific macrophage polarization program and a broader spectrum of macrophage activation states, other that M1 and M2 (36).

A number of evidences indicate that the TRP channels regulate macrophage differentiation. Thus, gastric inflammation and reduced bacterial colonization were observed in *Helicobacter pylori*-infected *TRPM2* knockout mice compared to controls (37).
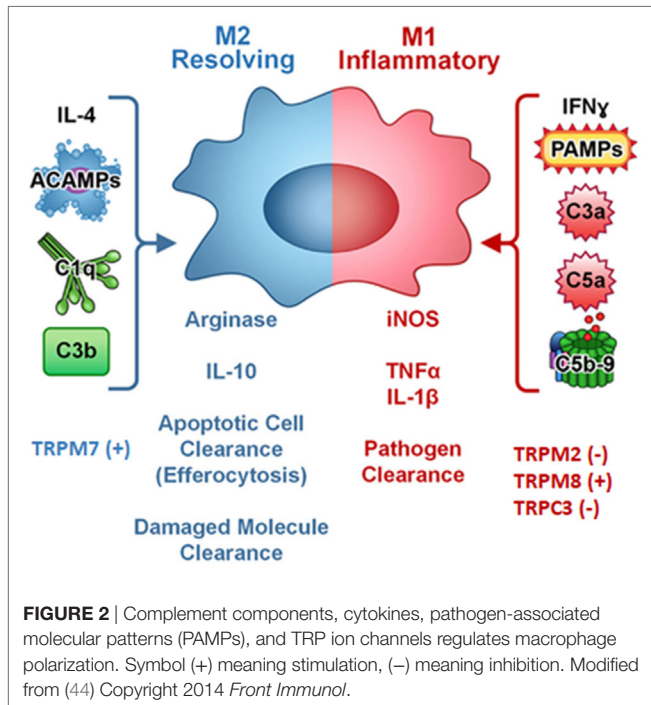
Loss of TRPM2 in *H. pylori*-infected macrophages triggers an increased production of inflammatory mediators and M1 polarization. Stimulation of TRPM2-deficient macrophages with *H. pylori* induces calcium overloading and increase of ERK1/2 and NADPH oxidase activities respect to wild type cells (37).

The expression and activity of TRPM7 are differentially regulated in bone-marrow derived murine M1 and M2 macrophages (38). Unlike M1 macrophages, in IL-4 stimulated M2 macrophages, higher TRPM7 current density (about 4.7-fold) was observed, whereas TRPM7 mRNA levels remain unchanged upon cell polarization. NS8593 and FTY720, two specific TRPM7 inhibitors, block IL-4- and M-CSF-induced macrophage proliferation and prevent M2 polarization. Inhibition of TRPM7 expression diminishes IL-4-induced arginase-1 mRNA levels and activity and completely inhibits the IL-4 or M-CSF mediated effects on TNF production in LPS-stimulated macrophages. In addition, TRPM7 inhibition decreases PI3K and ERK1/ERK2 phosphorylation levels and induces apoptosis in rat hepatic stellate cells (32, 39). In addition, adoptive transfer of macrophages from *TRPM8*-deficient mice, aggravates colitis, and IL-10 overexpression rescues M2 macrophage subpopulation. Thus, TNFα production in TRPM8-positive macrophages promotes the M1 macrophage phenotype and pro-inflammatory activity (40). Consequently, activation of TRPM8 channel in murine peritoneal macrophages triggers calcium transient currents in wild type but not *TRPM8*-deficient mice exhibiting defective phagocytosis and increased motility (40).

In addition, polarized macrophages from mice with specific *TRPC3* deficiency show an increased *in vitro* phagocytic function (22). A crosstalk between TRP channels and unfolded protein response (UPR) system regulating macrophage polarization was also evidenced (41, 42). Thus, in *Apoe*$^{(-/-)}$ *TRPC3*$^{(-/-)}$ mice, M1 but not M2 macrophages show diminished ER stress-mediated apoptosis is reported. The reduced susceptibility of *TRPC3*-deficient M1 macrophages to apoptosis induced by ER stress is associated with impaired UPR and down-regulation of pro-apoptotic molecules as calmodulin-dependent PK II (**Figure 2**) (22, 42–44).

ROLE OF TRP CHANNELS IN ADHESION AND MIGRATION IN M/MΦ

Macrophage migration and infiltration is a multi-step process characterized by cell adhesion to different extracellular matrix (ECM) substrates, degradation of ECM proteins, topology and pericellular sense, intracellular transport, cell protrusion stabilization, and transmigration (45). In this regard, the organelles appointed to mediate these important functions are the podosomes. Recent studies have demonstrated that TRPV2 is localized in the podosome, and stimulation by fMLP further recruits TRPV2 to this compartment (46). Numerous signaling molecules including PI3K, Src, Cas, Pyk2, and Rho GTPases are associated with the podosome. TRPV2 may regulate Pyk2 activation, since *TRPV2* knockdown inhibits the phospho-Pyk2 expression in macrophages. Activation of Pyk2 by ionomycin leads to breakdown of the podosome. On the contrary, increase of podosome numbers upon Pyk2 blocking by using a dominant negative variant of PyK2, PRNK, was observed. Gelsolin-assembled actin filaments and gelsolin activity are required for podosome

FIGURE 2 | Complement components, cytokines, pathogen-associated molecular patterns (PAMPs), and TRP ion channels regulates macrophage polarization. Symbol (+) meaning stimulation, (−) meaning inhibition. Modified from (44) Copyright 2014 *Front Immunol*.

assembly. It can be suggested that TRPV2, by activating gelsolin, promotes the formation of podosome. In murine macrophages, TRPV2 also contributes to fMLP-induced Ca^{2+} entry and migration (47). Notably, translocation of TRPV2 to the membrane induced by fMLP stimulation, is completely abrogated by PI3K inhibition or by Gi/0 trimeric G protein, suggesting that trafficking of TRPV2 channel is PI-(3,4,5)-P3 (PIP3)-dependent (46, 47).

Overexpression of mouse TRPM7 channel results in focal adhesion (FA) formation, spreading, and adhesion by increasing Ca^{2+} levels. The transformation of FA into podosomes depends by a kinase-dependent TRPM7-mediated activation (48). Non-activated TRPM7 channel is not associated with the actomyosin protein in the cytoskeleton. Triggering with PLC agonists induces TRPM7-mediated Ca^{2+} influx and TRPM7 kinase activity. Autophosphorylation of TRPM7 protein promotes a conformational change in the channel structure that allows Ca^{2+}-dependent myosin IIA association, myosin IIA heavy chain phosphorylation leading to myosin dissociation and cytoskeletal remodeling. Finally, silencing of TRPC6 by siRNA or treatment with SKF-96365, a TRP blocker induce cytoskeleton disruption in murine podocytes (49).

Cellular migration and contractility are regulated by cytoskeleton rearrangements, FA turnover and changes in Ca^{2+} flux. In this regard, a role for TRPM4 as regulator of FA/cytoskeleton dynamics, mechanotransduction, and adhesome has been reported (50). The mouse TRPM4 channel localizes at FAs, where it contributes to FA turnover and disassembly of lamellipodial actin cytoskeleton components. Moreover, TRPM4 by regulating FAK and Rac GTPase activities modulates cellular contractility and migration in M/MΦ (51).

TRPM2 is involved in chemokine production from M/MΦ (52). The expression of TRPML2 is negligible in resting macrophages,

but its levels increase in response to TLR4, TRL7, and TLR8 stimulation. In activated macrophages, TRPML2 facilitates the fusion of recycling endosomes or plasma membrane, thus promoting secretion of specific chemokines and cytokines. Recent data (53) demonstrated that CCL2, CCL3, and CCL5 chemokines are reduced in *TRPML2*$^{(-/-)}$ mice. Furthermore, *TRPML2* knockout mice display impaired recruitment of peripheral macrophages in response to intraperitoneal injection of either LPS or live bacteria (53). In human U937 monocyte cell line, CXCL8 production depends on TRPM2-mediated Ca^{2+} influx. Monocytes from *TRPM2* knockout mice exhibit reduced hydrogen peroxide-stimulated CXCL2 production (52). Activation of TRPM2 in human monocytes increases LPS-induced TNFα, IL-6, IL-8, and IL-10 production and phagocytosis *in vitro* (54).

The expression of TRPA1 mRNA in macrophages is upregulated in inflammatory bowel disease patients (55). In colitis, human TRPA1 channel activation exerts a mucosal protective role by reducing the expression of pro-inflammatory neuropeptides (SP, NKA, NKB, and VIP), cytokines (IL-1β, IFN, and TNF α/β), and of MCP-1 chemokine (55). Blocking of TRPA1 increases IL-10 levels and decreases TNF α secretion and TRPA1 siRNA normalizes monocyte IL-10 secretion (56).

CONTRIBUTION OF TRP CHANNELS IN M/MΦ PHAGOCYTOSIS

Macrophage phagocytosis of pathogens is essential function of innate immune responses and depends on a large repertoire of receptors capable to recognize different targets. Phagosome maturation requires endosomal pathway regulators, including the phosphoinositide lipids. Both, PtdIns(3,5)P2 and PIP3, are required for phagosome maturation. Inhibition of the lipid kinase that generates PtdIns(3,5)P2, PIKfyve, and phosphatidylinositol-5-phosphate [PtdIns(5)P] blocks phagosome-lysosome fusion and abrogates the phagosome degradative capability in RAW264.7 macrophages. PIKfyve inactivation disrupts membrane recycling by causing lysosome swelling and blocks phagosome and endosome maturation (57). In this regard, TRPML1 regulates phagosome biogenesis; both particle ingestion and lysosomal exocytosis are inhibited by TRPML1 blockers (56, 58). Instead, TRPML1 overexpression and TRPML1 agonist stimulation trigger lysosomal exocytosis and particle uptake. The particle binding stimulates lysosomal PI(3,5)P2 increase that triggers TRPML1-dependent lysosomal Ca^{2+} release, rapidly delivering TRPML1 translocation from lysosomal membranes to Lamp1$^+$ nascent phagosomes (59, 60). PIKfyve and PtdIns(3,5)P2 trigger the TRPML1 channel to mediate phagosome–lysosome fusion. Genetic deletion of *TRPML1* gene hinders the acquisition of lysosomal markers in the phagosomes and reduces their bactericidal activity. Finally, cytosolic Ca^{2+} level increases during the TRPML1- and PIKfyve-dependent phagocytosis (57).

A role of TRPV2 in early phagocytosis was also demonstrated (61). The chemoattractant-elicited mobility, zymosan or complement-mediated particle binding, and phagocytosis are impaired in macrophages from *TRPV2* knockout mice. The TRPV2 recruitment to the nascent phagosome and plasma membrane depolarization increases PIP2 synthesis that triggers

actin depolymerization indispensable for phagocytic receptor clustering (61). Moreover, recently recruitment of TRPV2 at cell surface, preferential localization in lipid rafts, and calcium influx upon *P. aeruginosa* infection have been reported. Furthermore, deregulated TRPV2-signaling in macrophages from cystic fibrosis is responsible for their defective phagocytosis and consequently chronic infection (62). Moreover, in RAW 264.7 macrophages, the TRPM8 activator icilin stimulates cation currents that result in macrophage membrane depolarization. It is intriguing to hypothesize that TRPM8 alters macrophage efferocytosis by inducing actin depolymerization and indirectly influences Ca^{2+}-dependent macrophage survival or apoptosis by reducing the driving force for Ca^{2+}-mediated positive feedback on other Ca^{2+} permeable channels (63).

Finally, Riazanski et al. have demonstrated that TRPC6 channel translocation into phagosomal membrane increases phagosomal functions. TRPC6 channel restores microbicidal function in compromised alveolar macrophages from cystic fibrosis patients (64).

Collectively, these findings indicate that TRP expression sensitizes M/MΦ to recognize phagocyte bacteria, and defective TRP channel expression and function lead to inefficient bacterial killing. Thus, TRPV4 mediates LPS-stimulated murine macrophage phagocytosis of *Escherichia coli in vitro* and opsonized particles *in vitro* and *in vivo* in mice model (65). Intracellular Ca^{2+} is a second messenger in TLR4-dependent recognition and signaling (65). In this regard, Ca^{2+}-depletion in *TRPV2*-deficient mice challenged with *Listeria monocytogenes* induces accelerated mortality and greater bacterial organ load (61).

TRPM2 is required for bacterial clearance in *E. coli* sepsis. Thus, during polymicrobial sepsis, macrophages from *TRPM2* knockout mice show inefficient bacterial killing and increased infection and death. Disruption of TRPM2 affects phagolysosomal acidification, impairs the phagosome-lysosome fusion, impedes the phagosome maturation, and increases intracellular Ca^{2+}-facilitated phagosome maturation in $TRPM2^{(-/-)}$ macrophages (66). $TRPM2^{(-/-)}$ mice are also extremely susceptible to *Listeria monocytogenes* infection and exhibit a defective innate immune response (19, 67). Similarly, the catalase from *Francinella tularensis* restricts ROS generation by hindering TRPM2-dependent Ca^{2+} entry in murine macrophages (68). In addition, TRPM2 disruption reduces heme oxygenase-1 expression and increases bacterial-induced macrophage infiltration. Pretreatment of

macrophages from *TRPM2* knockout mice, with heme oxygenase-1 inducer, reduces bacterial burden (69). Finally, suppression of macrophage activation through inhibition of the TRPC1 activity has been evidenced in parasites-(helminths) induced diseases (70).

CONCLUSION

Several evidences suggest the involvement of ion channels, in particular of TRP cation channel superfamily, in the pathogenesis of immune-mediated chronic inflammatory diseases. In this regard, the study of TRP channel functional expression in the M1/M2 macrophage polarization is an interesting research field to better understand how ion channels might participate in the generation of endogenous signaling capable of modifying macrophage polarization and differentiation, in the view to maintain health or to induce diseases. Crosstalk between inflammatory receptors and ion channels belonging to the TRP channel superfamily and the specific signaling pathway activated upon protein to protein interaction have been only partially elucidated and the contribution of a single TRP channel in the inflammatory response is still lacking. Further studies, both *in vitro* and *in vivo* aimed at uncovering the direct impact of different members of TRP subfamily in inflammatory processes are required. Thus, there is the need in the next future to explore and fully characterize the monocyte and macrophage expression of specific pattern of TRP channels and their signaling pathways activated in different immune-mediated diseases in order to identify new molecular targets for therapy of these inflammatory conditions.

AUTHOR CONTRIBUTIONS

GS supervised the work and wrote the manuscript. CA and MM contributed to the preparation of the subchapters about TRP channels and macrophage phagocytosis and migration. MN and OM cooperated in the preparation of the subchapters about TRP channels and macrophage survival and polarization. MS collaborated in the drafting of the introduction and conclusion. AS provided critical revision of the manuscript.

FUNDING

REFERENCES

1. Gordon S, Taylor PR. Monocyte and macrophage heterogeneity. *Nat Rev Immunol* (2005) 5(12):953–64. doi:10.1038/nri1733
2. Martinez FO, Helming L, Gordon S. Alternative activation of macrophages: an immunologic functional perspective. *Annu Rev Immunol* (2009) 27:451–83. doi:10.1146/annurev.immunol.021908.132532
3. Pollard JW. Trophic macrophages in development and disease. *Nat Rev Immunol* (2009) 9(4):259–70. doi:10.1038/nri2528
4. Wynn TA, Chawla A, Pollard JW. Origins and hallmarks of macrophages: development, homeostasis, and disease. *Nature* (2013) 496(7446):445–55. doi:10.1038/nature12034
5. Feske S, Wulff H, Skolnik EY. Ion channels in innate and adaptive immunity. *Annu Rev Immunol* (2015) 33:291–353. doi:10.1146/annurev-immunol-032414-112212
6. Clapham DE, Julius D, Montell C, Schultz G. International union of pharmacology. XLIX. Nomenclature and structure-function relationships o transient receptor potential channels. *Pharmacol Rev* (2005) 57(4):427–50. doi:10.1124/pr.57.4.6
7. Wu LJ, Sweet TB, Clapham DE. International union of basic and clinical pharmacology. LXXVI. Current progress in the mammalian TRP ion channel family. *Pharmacol Rev* (2010) 62:381–404. doi:10.1124/pr.110.002725
8. Yu FH, Yarov-Yarovoy V, Gutman GA, Catterall WA. Overview of molecular relationships in the voltage-gated ion channel superfamily. *Pharmacol Rev* (2005) 57(4):387–95. doi:10.1124/pr.57.4.13
9. Clapham DE. TRP channels as cellular sensors. *Nature* (2003) 426(6966):517–24. doi:10.1038/nature02196
10. Ramsey IS, Delling M, Clapham DE. An introduction to TRP channels. *Annu Rev Physiol* (2006) 68:619–47. doi:10.1146/annurev.physiol.68.040204.100431

11. Trebak M, Lemonnier L, Smyth JT, Vazquez G, Putney JW Jr. Phospholipase C-coupled receptors and activation of TRPC channels. *Handb Exp Pharmacol* (2007) 179:593–614. doi:10.1007/978-3-540-34891-7_35

12. Voets T, Nilius B. Modulation of TRPs by PIPs. *J Physiol* (2007) 582 (Pt 3):939–44. doi:10.1113/jphysiol.2007.132522

13. Venkatachalam K, Montell C. TRP channels. *Annu Rev Biochem* (2007) 76:387–417. doi:10.1146/annurev.biochem.75.103004.142819

14. Talavera K, Nilius B, Voets T. Neuronal TRP channels: thermometers, pathfinders and life-savers. *Trends Neurosci* (2008) 31(6):287–95. doi:10.1016/j.tins.2008.03.002

15. Latorre R, Zaelzer C, Brauchi S. Structure-functional intimacies of transient receptor potential channels. *Q Rev Biophys* (2009) 42(3):201–46. doi:10.1017/S0033583509990072

16. Nilius B, Owsianik G. Transient receptor potential channelopathies. *Pflugers Arch* (2010) 460(2):437–50. doi:10.1007/s00424-010-0788-2

17. Parenti A, De Logu F, Geppetti P, Benemei S. What is the evidence for the role of TRP channels in inflammatory and immune cells? *Br J Pharmacol* (2016) 173(6):953–69. doi:10.1111/bph.13392

18. Santoni G, Cardinali C, Morelli MB, Santoni M, Nabissi M, Amantini C. Danger- and pathogen-associated molecular patterns recognition by pattern-recognition receptors and ion channels of the transient receptor potential family triggers the inflammasome activation in immune cells and sensory neurons. *J Neuroinflammation* (2015) 12:21. doi:10.1186/s12974-015-0239-2

19. Di A, Gao XP, Qian F, Kawamura T, Han J, Hecquet C, et al. The redox-sensitive cation channel TRPM2 modulates phagocyte ROS production and inflammation. *Nat Immunol* (2011) 13(1):29–34. doi:10.1038/ni.2171

20. Serafini N, Dahdah A, Barbet G, Demion M, Attout T, Gautier G, et al. The TRPM4 channel controls monocyte and macrophage, but not neutrophil, function for survival in sepsis. *J Immunol* (2012) 189:3689–99. doi:10.4049/jimmunol.1102969

21. Zhou X, Ye Y, Sun Y, Li X, Wang W, Privratsky B, et al. Transient receptor potential channel 1 deficiency impairs host defense and proinflammatory responses to bacterial infection by regulating protein kinase Cα signaling. *Mol Cell Biol* (2015) 35:2729–39. doi:10.1128/MCB.00256-15

22. Tano JY, Solanki S, Lee RH, Smedlund K, Birnbaumer L, Vazquez G. Bone marrow deficiency of TRPC3 channel reduces early lesion burden and necrotic core of advanced plaques in a mouse model of atherosclerosis. *Cardiovasc Res* (2014) 101(1):138–44. doi:10.1093/cvr/cvt231

23. Viganò E, Mortellaro A. Caspase-11: the driving factor for non-canonical inflammasomes. *Eur J Immunol* (2013) 43:2240–5. doi:10.1002/eji.201343800

24. Py BF, Jin M, Desai BN, Penumaka A, Zhu H, Kober M, et al. Caspase-11 controls interleukin-1β release through degradation of TRPC1. *Cell Rep* (2014) 6:1122–8. doi:10.1016/j.celrep.2014.02.015

25. Tseng HH, Vong CT, Kwan YW, Lee SM, Hoi MP. TRPM2 regulates TXNIP-mediated NLRP3 inflammasome activation via interaction with p47 phox under high glucose in human monocytic cells. *Sci Rep* (2016) 6:35016. doi:10.1038/srep35016

26. Zhong Z, Zhai Y, Liang S, Mori Y, Han R, Sutterwala FS, et al. TRPM2 links oxidative stress to NLRP3 inflammasome activation. *Nat Commun* (2013) 4:1611. doi:10.1038/ncomms2608

27. Munoz-Planillo R, Kuffa P, Martinez-Colon G, Smith BL, Rajendiran TM, Nunez G. K+ efflux is the common trigger of NLRP3 inflammasome activation by bacterial toxins and particulate matter. *Immunity* (2013) 38:1142–53. doi:10.1016/j.immuni.2013.05.016

28. Compan V, Baroja-Mazo A, López-Castejón G, Gomez AI, Martínez CM, Angosto D, et al. Cell volume regulation modulates NLRP3 inflammasome activation. *Immunity* (2012) 37:487–500. doi:10.1016/j.immuni.2012.06.013

29. Compan V, Martín-Sánchez F, Baroja-Mazo A, López-Castejón G, Gomez AI, Verkhratsky A, et al. Apoptosis-associated speck-like protein containing a CARD forms specks but does not activate caspase-1 in the absence of NLRP3 during macrophage swelling. *J Immunol* (2015) 194(3):1261–73. doi:10.4049/jimmunol.1301676

30. Gordon S. Alternative activation of macrophages. *Nat Rev Immunol* (2003) 3:23–35. doi:10.1038/nri978

31. Mantovani A, Sica A, Sozzani S, Allavena P, Vecchi A, Locati M. The chemokine system in diverse forms of macrophage activation and polarization. *Trends Immunol* (2004) 25(12):677–86. doi:10.1016/j.it.2004.09.015

32. Fang L, Zhan S, Huang C, Cheng X, Lv X, Si H, et al. TRPM7 channel regulates PDGF-BB-induced proliferation of hepatic stellate cells via PI3K and ERK pathways. *Toxicol Appl Pharmacol* (2013) 272:713–25. doi:10.1016/j.taap.2013.08.009

33. Dinarello CA. Blocking IL-1 in systemic inflammation. *J Exp Med* (2005) 201(9):1355–9. doi:10.1084/jem.20050640

34. Noël W, Raes G, Hassanzadeh Ghassabeh G, De Baetselier P, Beschin A. Alternatively activated macrophages during parasite infections. *Trends Parasitol* (2004) 20(3):126–33. doi:10.1016/j.pt.2004.01.004

35. Wynn TA. Fibrotic disease and the T(H)1/T(H)2 paradigm. *Nat Rev Immunol* (2004) 4:583–94. doi:10.1038/nri1412

36. Xue J, Schimdt SV, Sander J, Draffenhn A, Krebs W, Quester I, et al. Transcriptome-based network analysis reveals a spectrum model of human macrophage activation. *Immunity* (2014) 40(2):274–88. doi:10.1016/j.immuni.2014.01.006

37. Beceiro S, Radin JN, Chatuvedi R, Piazuelo MB, Horvarth DJ, Cortado H, et al. TRPM2 ion channels regulate macrophage polarization and gastric inflammation during *Helicobacter pylori* infection. *Mucosal Immunol* (2017) 10(2):493–507. doi:10.1038/mi.2016.6

38. Schilling T, Miralles F, Eder C. TRPM7 regulates proliferation and polarisation of macrophages. *J Cell Sci* (2014) 127:4561–6. doi:10.1242/jcs.151068

39. Zhu Y, Men R, Wen M, Hu X, Liu X, Yang L. Blockage of TRPM7 channel induces hepatic stellate death through endoplasmic reticulum stress-mediated apoptosis. *Life Sci* (2014) 94(1):37–44. doi:10.1016/j.lfs.2013.10.030

40. Khalil M, Babes A, Lakra R, Försch S, Reeh PW, Wirtz S, et al. Transient receptor potential melastatin 8 ion channel in macrophages modulates colitis through a balance-shift in TNF-alpha and interleukin-10 production. *Mucosal Immunol* (2016) 9(6):1500–13. doi:10.1038/mi.2016.16

41. Solanki S, Dube PR, Tano JY, Birnbaumer L, Vazquez G. Reduced endoplasmic reticulum stress-induced apoptosis and impaired unfolded protein response in TRPC3-deficient M1 macrophages. *Am J Physiol Cell Physiol* (2014) 307:C521–31. doi:10.1152/ajpcell.00369.2013

42. Amantini C, Farfariello V, Cardinali C, Morelli MB, Marinelli O, Nabissi M, et al. The TRPV1 ion channel regulates thymocyte differentiation by modulating autophagy and proteasome activity. *Oncotarget* (2017) 8(53):90766–80. doi:10.18632/oncotarget.21798

43. Vazquez G, Solanki S, Dube P, Smedlund K, Ampem P. On the roles of the transient receptor potential canonical 3 (TRPC3) channel in endothelium and macrophages: implications in atherosclerosis. *Adv Exp Med Biol* (2016) 898:185–99. doi:10.1007/978-3-319-26974-0_9

44. Bohlson SS, O'Conner SD, Hulsebus HJ, Ho MM, Fraser DA. Complement, C1q, and C1q-related molecules regulate macrophage polarization. *Front Immunol* (2014) 5:402. doi:10.3389/fimmu.2014.00402

45. Linder S, Wiesner C. Tools of the trade: podosomes as multipurpose organelles of monocytic cells. *Cell Mol Life Sci* (2015) 72(1):121–35. doi:10.1007/s00018-014-1731-z

46. Nagasawa M, Kojima I. Translocation of calcium-permeable TRPV2 channel to the podosome: its role in the regulation of podosome assembly. *Cell Calcium* (2012) 51(2):186–93. doi:10.1016/j.ceca.2011.12.012

47. Nagasawa M, Nakagawa Y, Tanaka S, Kojima I. Chemotactic peptide fMetLeuPhe induces translocation of the TRPV2 channel in macrophages. *J Cell Physiol* (2007) 210:692–702. doi:10.1002/jcp.20883

48. Clark K, Langeslag M, van Leeuwen B, Ran L, Ryazanov AG, Figdor CG, et al. TRPM7, a novel regulator of actomyosin contractility and cell adhesion. *EMBO J* (2006) 25(2):290–301. doi:10.1038/sj.emboj.7600931

49. Liu Z, Yang J, Zhang X, Xu P, Zhang T, Yang Z. Developmental changes in the expression and function of TRPC6 channels related the F-actin organization during differentiation in podocytes. *Cell Calcium* (2015) 58(6):541–8. doi:10.1016/j.ceca.2015.09.001

50. Barbet G, Demion M, Moura IC, Serafini N, Léger T, Vrtovsnik F, et al. The calcium-activated nonselective cation channel TRPM4 is essential for the migration but not the maturation of dendritic cells. *Nat Immunol* (2008) 9(10):1148–56. doi:10.1038/ni.1648

51. Cáceres M, Ortiz L, Recabarren T, Romero A, Colombo A, Leiva-Salcedo E, et al. TRPM4 is a novel component of the adhesome required for focal adhesion disassembly, migration and contractility. *PLoS One* (2015) 10(6):e0130540. doi:10.1371/journal.pone.0130540

52. Yamamoto S, Shimizu S, Kiyonaka S, Takahashi N, Wajima T, Hara Y, et al. TRPM2-mediated Ca2+influx induces chemokine production in monocytes that aggravates inflammatory neutrophil infiltration. *Nat Med* (2008) 14:738–47. doi:10.1038/nm1758

53. Sun L, Hua Y, Vergarajauregui S, Diab HI, Puertollano R. Novel role of TRPML2 in the regulation of the innate immune response. *J Immunol* (2015) 195:4922–32. doi:10.4049/jimmunol.1500163

54. Wehrhahn J, Kraft R, Harteneck C, Hauschildt S. Transient receptor potential melastatin 2 is required for lipopolysaccharide-induced cytokine production in human monocytes. *J Immunol* (2010) 184(5):2386–93. doi:10.4049/jimmunol.0902474

55. Kun J, Szitter I, Kemény A, Perkecz A, Kereskai L, Pohóczky K, et al. Upregulation of the transient receptor potential ankyrin 1 ion channel in the inflamed human and mouse colon and its protective roles. *PLoS One* (2014) 9(9):e108164. doi:10.1371/journal.pone.0108164

56. Billeter AT, Galbraith N, Walker S, Lawson C, Gardner SA, Sarojini H, et al. TRPA1 mediates the effects of hypothermia on the monocyte inflammatory response. *Surgery* (2015) 158(3):646–51. doi:10.1016/j.surg.2015.03.065

57. Dayam RM, Saric A, Shilliday RE, Botelho RJ. The phosphoinositide-gated lysosomal Ca(2+) channel, TRPML1, is required for phagosome maturation. *Traffic* (2015) 16(9):1010–26. doi:10.1111/tra.12303

58. Samie M, Wang X, Zhang X, Goschka A, Li X, Cheng X, et al. A TRP channel in the lysosome regulates large particle phagocytosis via focal exocytosis. *Dev Cell* (2013) 26:511–24. doi:10.1016/j.devcel.2013.08.003

59. Thompson EG, Schaheen L, Dang H, Fares H. Lysosomal trafficking functions of mucolipin-1 in murine macrophages. *BMC Cell Biol* (2007) 8:54. doi:10.1186/1471-2121-8-54

60. Kim GH, Dayam RM, Prashar A, Terebiznik M, Botelho RJ. PIKfyve inhibition interferes with phagosome and endosome maturation in macrophages. *Traffic* (2014) 15(10):1143–63. doi:10.1111/tra.12199

61. Link TM, Park U, Vonakis BM, Raben DM, Soloski MJ, Caterina MJ. TRPV2 has a pivotal role in macrophage particle binding and phagocytosis. *Nat Immunol* (2010) 11:232–9. doi:10.1038/ni.1842

62. Lévêque M, Penna A, Le Trionnaire S, Belleguic C, Desrues B, Brinchault G, et al. Phagocytosis depends on TRPV2-mediated calcium influx and requires TRPV2 in lipids rafts: alteration in macrophages from patients with cystic fibrosis. *Sci Rep* (2018) 8(1):4310. doi:10.1038/s41598-018-22558-5

63. Wu SN, Wu PY, Tsai ML. Characterization of TRPM8-like channels activated by the cooling agent icilin in the macrophage cell line RAW 264.7. *J Membr Biol* (2011) 241:11–20. doi:10.1007/s00232-011-9358-6

64. Riazanski V, Gabdoulkhakova AG, Boynton LS, Eguchi RR, Deriy LV, Hogarth DK, et al. TRPC6 channel translocation into phagosomal membrane augments phagosomal function. *Proc Natl Acad Sci U S A* (2015) 112(47):E6486–95. doi:10.1073/pnas.1518966112

65. Scheraga RG, Abraham S, Niese KA, Southern BD, Grove LM, Hite RD, et al. TRPV4 mechanosensitive ion channel regulates lipopolysaccharide-stimulated macrophage phagocytosis. *J Immunol* (2016) 196:428–36. doi:10.4049/jimmunol.1501688

66. Zhang ZQ, Cui P, Zhang K, Chen QP, Fang XM. Transient receptor potential melastatin 2 regulates phagosome maturation and is required for bacterial clearance in *Escherichia coli* sepsis. *Anesthesiology* (2017) 126(1):128–39. doi:10.1097/ALN.0000000000001430

67. Knowles H, Heizer JW, Li Y, Chapman K, Ogden CA, Andreasen K, et al. Transient receptor potential melastatin 2 (TRPM2) ion channel is required for innate immunity against *Listeria monocytogenes*. *Proc Natl Acad Sci U S A* (2011) 108:11578–83. doi:10.1073/pnas.1010678108

68. Shakerley NL, Chandrasekaran A, Trebak M, Miller BA, Melendez JA. *Francisella tularensis* catalase restricts immune function by impairing TRPM2 channel activity. *J Biol Chem* (2016) 291(8):3871–81. doi:10.1074/jbc.M115.706879

69. Qian X, Numata T, Zhang K, Li C, Hou J, Mori Y, et al. Transient receptor potential melastatin 2 protects mice against polymicrobial sepsis by enhancing bacterial clearance. *Anesthesiology* (2014) 121:336–51. doi:10.1097/ALN.0000000000000275

70. Chauhan A, Sun Y, Pani B, Quenumzangbe F, Sharma J, Singh BB, et al. Helminth induced suppression of macrophage activation is correlated with inhibition of calcium channel activity. *PLoS One* (2014) 9(7):e101023. doi:10.1371/journal.pone.0101023

Conflict of Interest Statement: The authors declare that the research was conducted in the absence of any commercial or financial relationships that could be construed as a potential conflict of interest.

REVIEW ARTICLE
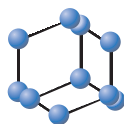
ICOS-L as a Potential Therapeutic Target for Cancer Immunotherapy

Oliviero Marinelli[1,2,#], Massimo Nabissi[1,*,#], Maria Beatrice Morelli[1], Luciana Torquati[3,4], Consuelo Amantini[2] and Giorgio Santoni[1]

[1]*School of Pharmacy, University of Camerino, Camerino (MC), Italy;* [2]*School of Bioscience and Veterinary Medicine, University of Camerino, Camerino (MC), Italy;* [3]*University of Exeter Medical School, Exeter, UK;* [4]*School of Human Movement and Nutrition Sciences, University of Queensland, Queensland, Australia*

Abstract: ***Background***: The co-stimulatory B7 family members are cell-surface protein ligands, binding to receptors on lymphocytes to regulate immune responses. One of them is the inducible co-stimulatory molecule ligand (ICOS-L). This protein is expressed on professional antigen-presenting cells (APCs), including B cells, macrophages, and dendritic cells (DCs), but it can also be expressed by endothelial cells, lung epithelium and in tumour microenvironment cells. ICOS-L is important for memory and effector T cells during the specific humoral immune responses, but its role in cancer is not yet understood.

Objective: To discuss the role of ICOS/ICOS-L in cancer, given importance of identifying selective targets for cancer treatment, and knowing the mechanism of immune evasion by tumour.

Main Findings: ICOS/ICOS-L signal has opposite effects on the T-cell response. ICOS-L is activated in several types of cancers to maintain immunosuppressive CD4^{+} T cell subsets, such as regulatory T cells (Tregs). ICOS-L over-expression is associated with tumour progression and poor overall survival. In colon cancer, activation of this co-stimulatory signal is associated with improved survival suggesting a dualistic effect of the ICOS/ICOs-L signal pathway. Interestingly, following anti-cancer vaccine or anti-CTLA-4 treatment, ICOS^{+} T cells increased significantly in both the CD4^{+} and CD8^{+} population and the ratio Teff/Treg increased in tumour microenvironment. This suggests a potential role of ICOS/ICOS-L in improving effectiveness of cancer therapy.

Conclusion: ICOS/ICOS-L signal pathway has the potential to improve cancer treatment. However, studies in other models are needed to understand whether inhibition of ICOS expression or the blockage of its co-stimulation could be a potential therapeutic target or adjuvant treatment for immunotherapy.

Keywords: ICOS-L, ICOS, CD275, CD278, B7, Tregs, cancer.

1. INTRODUCTION

1.1. ICOS-L, a Member of Co-stimulatory B7 Family

The co-stimulatory B7 family members are cell-surface protein ligands, binding to receptors expressed on lymphocytes and involved in regulating immune responses. This system not only provides positive signals to stimulate T-cell activation, but also it delivers negative signals to inhibit T-cell responses. The inducible co-stimulatory molecule ligand (ICOS-L), also known as B7RP-1, B7-H2, LICOS, GL50, B7h and CD275, is a member of B7 family. It is expressed on professional antigen-presenting cells (APCs), including B cells, macrophages and dendritic cells (DCs), but also in certain endothelial cells and lung epithelium [1-3]. Despite limited evidence, ICOS-L is known to act as a co-stimulatory

signal for T-cell proliferation and cytokines secretion and to induce B-cell proliferation and differentiation into plasma cells. ICOS-L could also play an important role in mediating local tissue responses to inflammatory conditions and in modulating the secondary immune response by co-stimulating memory T-cell function [2, 3].

1.1.1. ICOS-L: Gene, Transcripts and Proteins

The gene encoding the inducible co-stimulator ligand (ICOS-L), is located in the 21q22.3, is 24,477 bases in length and contains 10 exons [4]. At transcriptional level, four transcript variants (Var) have been cloned. Var$_a$ (the canonical form) represents the longest transcript (3320 nts) and encodes the isoform *a*, Var$_b$ (1188 nt) uses an alternative 3' terminal exon and it thus differs in the 3' coding region and 3' UTR, compared to Var$_a$. Var$_c$ (2969 nt) lacks an alternate in-frame exon in the 5' coding region, compared to Var$_a$, resulting in an isoform *c* that is shorter than isoform a. Var$_d$ (3168 nt) uses an alternate splice site in the 5' region, resulting in translation initiation at a downstream in-frame start

[*]Address correspondence to this author at the School of Pharmacy, Department of Experimental Medicine, via Madonna delle Carceri 9, 62032 Camerino (MC), Italy; Tel:+390737403306; Fax:+390737403325;
E-mail: massimo.nabissi@unicam.it
[#]*Both authors contributed equally.*

codon, compared to Var$_a$. The encoded isoform *d* is shorter at the N-terminus, compared to isoform *a* (Supplementary **1**, Fig. **1**). Isoform *a* is widely expressed (brain, heart, kidney, liver, lung, pancreas, placenta, skeletal muscle, bone marrow, colon, ovary, prostate, testis, lymph nodes, leukocytes, spleen, thymus and tonsil), while isoform *b* is detected only in lymph nodes, leukocytes, spleen and it is expressed on activated monocytes and dendritic cells [5]. Tissue and organ expression of Var$_c$ and Var$_d$ are yet to be studied.

2. IMMUNOLOGICAL ROLE OF ICOS-L

ICOS-L specifically binds the T-cell inducible co-stimulatory molecule (ICOS), also named CD278 [3], which is expressed at high levels in germinal centre T cells or TFH (follicular helper) cells. Activation of ICOS receptor induces recruitment of class IA phosphatidylinositol 3-kinase (PI3K), a signaling molecule that leads to the production of membrane-bound phosphatidylinositol 3,4,5-trisphosphate (PIP3). This culminates in the activation of Akt, a kinase that promotes cellular proliferation and survival. ICOS activation also recruits the p50α and p85α regulatory subunits and p110δ catalytic subunit of PI3K. *In vivo* and *in vitro* experiments indicate that ICOS/ICOS-L pathway activation contributes to the production of cytokines, such as IL-5, IL-4, IL-10 and IL-13. ICOS/ICOS-L co-stimulatory signal is important for memory and T helper cell effector functions. This is particularly important for T helper-2 differentiation and antibodies response during the specific humoral immune responses against pathogens such as bacteria, parasites, and viruses [1, 2]. Moreover, ICOS-L seems to alternatively promote or repress T helper-1 responses under different infection conditions and these divergent phenotypes may in part be explained by ICOS-dependent regulatory T cells

(Tregs) induction (Fig. **2**). Thus, the ability of ICOS-L to influence Tregs induction points to a complex role in regulating CD4$^+$ T cell differentiation, and suggests that ICOS-L signalling may be mutually important in preventing immune-mediated pathology, as well as inducing pro-inflammatory CD4$^+$ T cells.

3. ICOS-L IN TUMOUR INFILTRATE LYMPHO-CYTES

Malignant cells may adopt several mechanisms to interfere with the effector immune response or with regulatory cells in tumour microenvironment, in order to escape from immune surveillance. Regulatory T cells (Tregs) constitute 5% to 10% of all peripheral CD4$^+$ T cells and play an important role in maintaining tolerance to both auto-immune and cancer cells. Starting from the identification of Forkhead box protein 3 (Foxp3) as a critical transcriptional factor for Tregs, Foxp3$^+$CD4$^+$ T cells have been regarded as Tregs with immunosuppressive functions and divided in three subpopulations: effector Tregs (eTregs), naive Tregs, and non-Tregs [6]. Tregs, like other T cells, respond to TCR stimulation. They also express co-stimulatory receptors, such as CTLA-4, PD-1, ICOS and CD28 that further promote their activation, proliferation and survival. A large body of evidence confirms that activation of ICOS/ICOS-L pathway is involved in maintenance of this subtype of T cells in tumour microenvironment, which usually is associated with a poor prognosis of patient [6].

3.1. ICOS-L in Cancer

ICOS/ICOS-L pathway was reportedly be activated in melanoma [7], myeloma [8, 9], breast [10], ovarian [11],

```
NP_001269980.1   ------------------------------------------------------------
NP_001269979.1   MRLGSPGLLFLLFSSLRADTQEKEVRAMVGSDVELSCACPEGSRFDLNDVYVYWQTSESK
NP_001269981.1   ------------------------------------------------------------
NP_ 056074.1     MRLGSPGLLFLLFSSLRADTQEKEVRAMVGSDVELSCACPEGSRFDLNDVYVYWQTSESK

NP_001269980.1   ---------------------------------------------------------MRL
NP_001269979.1   TVVTYHIPQNSSLENVDSRYRNRALMSPAGMLRGDFSLRLFNVTPQDEQKFHCLVLSQSL
NP_001269981.1   -------------------MSPAGMLRGDFSLRLFNVTPQDEQKFHCLVLSQSL
NP_ 056074.1     TVVTYHIPQNSSLENVDSRYRNRALMSPAGMLRGDFSLRLFNVTPQDEQKFHCLVLSQSL
                                                                            *

NP_001269980.1   GSPGLLFLLFSSLRAANFSVPVVSAPHSPSQDELTFTCTSINGYPRPNVYWINKTDNSLL
NP_001269979.1   GFQEVLSVEVTLHVAANFSVPVVSAPHSPSQDELTFTCTSINGYPRPNVYWINKTDNSLL
NP_001269981.1   GFQEVLSVEVTLHVAANFSVPVVSAPHSPSQDELTFTCTSINGYPRPNVYWINKTDNSLL
NP_ 056074.1     GFQEVLSVEVTLHVAANFSVPVVSAPHSPSQDELTFTCTSINGYPRPNVYWINKTDNSLL
                 * :*:. .:   *******************************************

NP_001269980.1   DQALQNDTVFLNMRGLYDVVSVLRIARTPSVNIGCCIENVLLQQNLTVGSQTGNDIGERD
NP_001269979.1   DQALQNDTVFLNMRGLYDVVSVLRIARTPSVNIGCCIENVLLQQNLTVGSQTGNDIGERD
NP_001269981.1   DQALQNDTVFLNMRGLYDVVSVLRIARTPSVNIGCCIENVLLQQNLTVGSQTGNDIGERD
NP_ 056074.1     DQALQNDTVFLNMRGLYDVVSVLRIARTPSVNIGCCIENVLLQQNLTVGSQTGNDIGERD
                 ************************************************************

NP_001269980.1   KITENPVSTGEKNAAT**WSILAVLCLLVVVAVAIGWVC**RDRCLQHSYAGAWAVSPETELTG
NP_001269979.1   KITENPVSTGEKNAAT**WSILAVLCLLVVVAVAIGWVC**RDRCLQHSYAGAWAVSPETELTE
NP_001269981.1   KITENPVSTGEKNAAT**WSILAVLCLLVVVAVAIGWVC**RDRCLQHSYAGAWAVSPETELTG
NP_ 056074.1     KITENPVSTGEKNAAT**WSILAVLCLLVVVAVAIGWVC**RDRCLQHSYAGAWAVSPETELTG
                 ***********************************************************

NP_001269980.1   HV-------
NP_001269979.1   SWNLLLLLS
NP_001269981.1   HV-------
NP_ 056074.1     HV-------
```

Fig. (1). Sequence alignment analysis of ICOS-L protein variants. **Vara** (NP_056074.1, 302 aa), **Varb** (NP_001269979.1, 309 aa), **Varc** (NP_001269980.1, 185 aa), **Vard** (NP_001269981.1, 217 aa). * (asterisk) indicates positions, which have a single, fully conserved residue. : (colon) indicates conservation between groups of strongly similar properties. . (period) indicates conservation between groups of weakly similar properties. In Bold: trans-membrane domain, Clear: cytoplasmic domain, Underline and clear: extracellular domain. Alignment analysis was performed by Clustar Omega software.

gastric [6], liver [12] and colorectal cancers [13]. Furthermore, ICOS-L was also found in classical Hodgkin lymphoma [14], B lymphoma [2], leukaemia [15], glioblastoma [16] and rhabdomyosarcoma [17], but its role in these cancers is yet to be completely elucidated. In tumour microenvironment, Treg cells contribute to tumour growth by inhibiting tumour-specific immunity through not yet characterized mechanisms. It is hypothesised that this mechanism may involve FAS-L, CD39/Adenosine, perforins, CTLA-4, or PD-1 and the generation of high levels of IL-10, which mediate a suppressive capability, especially against dendritic cell functions. Finally, it was demonstrated that ICOS/ICOS-L pathway could modulate the efficacy of therapy in patients with prostate cancer [18], pancreatic cancer [19], bladder cancer [20], multiple myeloma [21] and melanoma [22, 23].
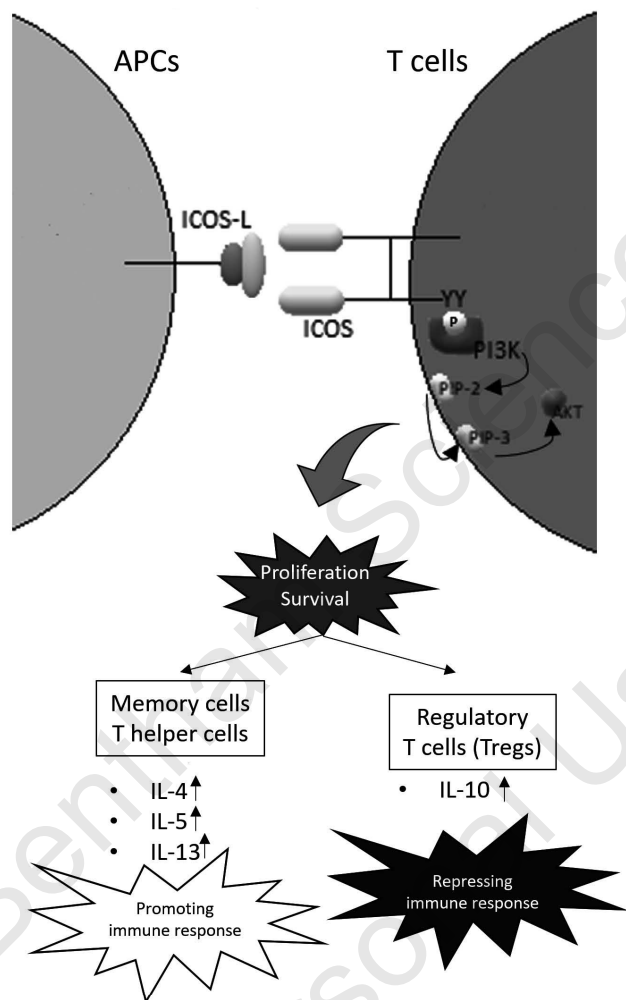
Fig. (2). ICOS-ICOS-L pathway. ICOS-L is a member of B7 family expressed on professional antigen-presenting cells (APCs) and it binds ICOS receptor expressed on T cells. Activation of ICOS receptor induces the recruitment PI3K, a signaling molecule that leads to the activation of Akt, a kinase that promotes cellular proliferation and survival. ICOS/ICOS-L pathway activation contributes to the production of cytokines, such as IL-5, IL-4, IL-13 and IL-10. It is suggested that ICOS/ICOS-L co-stimulatory signal is very important for memory and T helper cell effector functions, but ICOS is seemingly capable of alternatively promoting or repressing T helper-1 responses by ICOS-dependent regulatory T cells (Tregs) induction.

3.2. ICOS-L in Melanoma

Melanoma tumour biopsies analysis showed an estimated 25% of the CD4$^+$ T cells found were Foxp3$^+$, more than 3 times the abundance found in the peripheral blood of the same patients (7%) [7]. This indicates that ICOS-L expressed by melanoma cells could co-stimulate Tregs to induce high levels of Foxp3, CD25, ICOS and also production of IL-10. This evidence suggest that tumour cells may act themselves as direct APC, since they can express HLA class II and provide self-antigen presentation and co-stimulation through ICOS-L, allowing a tumour self-tolerance [7].

3.3. ICOS-L in Haematological Tumours

In several haematological malignancies, ICOS-L was expressed in cancer cells. Malignant Hodgkin Reed Sternberg cells derived from a germinal centre B cells over-expressed different surface molecules, including CD70, CD80/CD86, CD30, CD40, OX40-L/CD252, and ICOS-L [14]. Their respective receptors were often present on typical Hodgkin lymphoma microenvironment immune cells, and were considered to be up-regulated on activated T Helper cells. Evidence suggests that malignant tumours were capable of sequestering a substantial number of activated functional T cells, contributing to a profound systemic immune deficit in advanced disease [14]. Additionally, it was shown that leukemic cells, obtained from patients with acute myeloid leukaemia, express ICOS-L and this it was associated with a poor prognosis [15]. Thus suggesting that expression of ICOS-L in leukemic cells might contribute to their proliferation by helping them to evade antitumor immune responses [15]. Although ICOS-L expression has been evaluated on B lymphoma tissues, its biological functions in regulating anti-cancer immune response is not completely understood [2]. Immunohistochemical staining showed that ICOS-L was expressed in thyroid B-cell lymphoma but not in thyroid adenoma tissue or healthy thyroid tissue, suggesting that ICOS-L molecules may be involved in the development of malignant B lymphoma [2]. In an *in vitro* model of myeloma, tumour cells express ICOS-L [8, 9], which directly induces Tregs expansion and also Treg cells generation in a contact-dependent manner and in absence of APC cells. The induction of Treg cells mediated by cell-to-cell contact with the ICOS/ICOS-L system supports the hypothesis that this pathway may play a central role in the immune suppression response [8].

3.4. ICOS-L in Ovarian and Breast Cancer

While previously described evidence indicated ICOS-L expression in tumour cells, recent investigations in ovarian cancer and breast cancer are in contrast with this theory. In ovarian and breast cancer, ICOS-L was not expressed in cancer cells indicating that Tregs expansion was activated by other cells expressing ICOS [10, 11]. In ovarian cancer, many Foxp3$^+$ Treg cells were found to infiltrate the tumour microenvironment, a phenomenon that strongly predicts disease progression [11]. These Tregs constitutively expressed ICOS and were frequently detected in the tumour of patients with epithelial ovarian cancer. Survival, proliferation and functions of ICOS$^+$Foxp3$^+$Treg cells was strictly dependent to the presence of tumour-infiltrating plasmacytoid dendritic

Table 1. Differential role of ICOS-L/ICOS activation in different tumours. ICOS/ICOS-L pathway is activated in different types of cancer and it plays a central role in immune suppression. ICOS-L is present in tumour microenvironment because it is expressed by cancer cells or tumour-infiltrating plasmacytoid dendritic cells (pDCs).

Tumour	ICOS-L expression in cancer cells	ICOS/ICOS-L activation	References
Melanoma	Yes	Treg costimulation, tumour self-tolerance	[7]
Myeloma	Yes	Treg generation and expansion, immune suppression	[8]
Classical Hodgkin lymphoma	Yes	Sequestering of functional T cells, contributing to a profound immune defect	[14]
Thyroid B-cell lymphoma	Yes	Involvement in malignant B lymphoma development	[2]
Leukaemia	Yes	Proliferation of leukemic cells and immune evasion	[15]
Breast	No	Involvement of tumour-infiltrating pDCs, Treg local accumulation, poor prognosis	[10]
Ovarian	No	Involvement of tumour-infiltrating pDCs, immune suppression	[11]
Gastric	No	Involvement of tumour-infiltrating pDCs, poor prognosis	[6]
Liver	No	Involvement of tumour-infiltrating pDCs, activation of Tr1, immune suppression	[12]
Glioblastoma	Yes	Not investigated	[16]
Rhabdomyosarcoma	Yes	Not investigated	[17]
Colorectal	Yes	Promotion of Th1 effector response, good prognosis	[13]

cells (pDCs) [11]. Human DCs consist of two subsets, myeloid dendritic cells (mDCs) and plasmacytoid dendritic cells (pDCs). The first express TLR2-6, 8 and induce T helper 1 effector cells, while pDCs express TLR7 and 9 and have been reported to exist in most human solid tumours. pDCs are associated with induction and maintenance of immunosuppressive conditions by the secretion of indoleamine 2,3-dioxygenase, IL-3, expression of ICOS-L, CD40-L and through Treg cells activation. There is substantial evidence suggesting that pDCs have a specialized role in the induction of peripheral tolerance by inducing IL-10-production through Tregs-ICOS-L/ICOS signaling [6, 24]. In summary, in epithelial ovarian cancer the ICOS/ICOS-L pathway activation involved a tumour-infiltrating pDCs that express high levels of ICOS-L, while cancer cells did not express significant levels of this protein. This evidence supports the hypothesis that tumour-infiltrating pDCs were directly involved in creating an immunosuppressive tumour microenvironment through the expansion of the ICOS$^+$Foxp3$^+$ Treg cell subset [11].

Likewise, infiltration of pDS indirectly induced by ICOS was associated with poor prognosis of breast cancer patients [10]. While ICOS-L was not expressed in neither primary breast tumour cells or in breast tumour cell lines, ICOS engagement was described as a major contributing pathway to ICOS$^+$Tregs local accumulation. Tumour-associated ICOS$^+$Tregs directly interacted with pDCs *in situ*, as confirmed by immunohistochemistry on primary breast tumour frozen sections. Upstream of this cascade, CCL22 was produced by cancer cells to recruit CCR4$^+$Treg cells from the bloodstream to breast tumour microenvironment. This resulted in CCR4$^+$Treg cells local expansion through ICOS/ICOS-L interaction with pDC in breast tumour environment [10].

3.5. ICOS-L in Gastric and Liver Cancers

In gastric cancer, a high number of ICOS+ cells were found in gastric tissue of late-stage gastric cancer patients. In these patients, the expression level of ICOS-L was high in pDCs while high ICOS expression in Foxp3$^+$ infiltrating T lymphocyte was associated with a poor prognosis. Immunohistochemistry results showed a coexistence of ICOS$^+$Foxp3$^+$ cells and pDCs in gastric cancer tissues suggesting some functional relationship between these cells, as seen in other tumour types [6]. Additionally, this ICOS/ICOS-L pathway was not only involved in regulating the Treg cell subset but also other types of inhibitory T cells potentially involved in local immunosuppression. Among these, T regulatory type 1 cells (Tr1), initially considered important in promoting and maintaining tolerance in autoimmunity, allergy and transplantation, also demonstrated to be involved in promoting tumour escape from immune surveillance [12]. In patients with primary and secondary liver cancer, tumour infiltrating Tr1 cells contributed to local immune suppression via ICOS/ICOS-L signalling and ICOS-L$^+$pDCs stimulated IL-10 production in the tumour microenvironment [12].

3.6. ICOS-L in Others Solid Cancers

ICOS-L is expressed in human glioma cells, but not in normal central nervous system tissues adjacent to the neoplastic cells. Whether ICOS-L plays a role in supporting this

malignancy is yet to be investigated [16]. In rhabdomyosarcoma (RMS), the most common paediatric soft tissue malignancy, ICOS-L is expressed in FLOH1, RH41, RD6, and TE671 RMS cell lines and its expression levels marginally increased in presence of TNFα [17]. Even if the involvement of ICOS/ICOS-L pathway supported cancer progression and worsen prognosis in several cancer models, in colorectal cancer the expression of ICOS was associated with a good prognosis [13]. Although limited data are available on ICOS-L expression in colorectal cancer, ICOS is mainly expressed on CD4$^+$T cells in patients' tumour tissues or peripheral blood cells [13]. Compared to ICOS$^-$T cells, ICOS$^+$T cells produce more INFγ and less IL-4 and show up-regulated expression of transcriptional factor of Th1 cells (T-bet). This suggests that ICOS promotes Th1 effector response in patients with colon cancer. It is known that Th1 cells inhibit tumour cell invasion and metastasis by communicating with tumour-associated myeloid cells (*i.e.* tumour-associated macrophages and myeloid-derived suppressor cells) contributing to an improvement of survival [13]. Studies showed a significant correlation between high ICOS expression and good prognosis, in relation to tumour size, Carcinoembryonic antigen (CEA) levels, tumour staging, lymphatic metastasis and distant metastasis (TNM classifications). Furthermore, ICOS expression correlates with the expression of checkpoint inhibitors CTLA-4 and PD-1 on T cells, indicating that ICOS could also be a useful marker for a selection of anti-CTLA-4 or PD-1 therapy in colorectal cancer [13].

4. ICOS/ICOS-L PATHWAY IN CANCER IMMUNO-THERAPY

The opposite effects of ICOS/ICOS-L pathway on the T-cell response may explain the lack of anti-tumour efficacy of ICOS-L blockade in mono-therapy [25]. Instead, studies blocking the ICOS/ICOS-L pathway in combination with other therapy showed different results. For example**,** therapy with GM-CSF-modified cancer cell vaccine combined with anti-ICOS monoclonal antibody induced more powerful anti-tumour immunity [18]. Indeed, Mo *et al.* demonstrated how in murine models of prostate cancer tumour-infiltrated T lymphocyte increased after treatment with GM-CSF-modified cancer cell vaccine and how combination therapy induced higher infiltration compared with vaccine alone. Furthermore, ICOS$^+$Foxp3$^+$T cells infiltration into tumour tissues were higher after vaccine therapy, while the proportion of these cells decrease in combination treatment compared with control condition. Although the vaccine induced an efficient anti-tumour immunity inhibiting tumour growth, it also induced an increase of Tregs tumour infiltration that could challenge the effectiveness of this therapy. In this case, combination with ICOS blocking could deplete infiltrated Tregs with the possibility to enhance the vaccine-induced immunity [18].

Further supporting this evidence, treatment of pancreatic cancer targeting mesothelin (MSLN), a potential immune-therapeutic target, showed similar results. MSLN-virus-like particles (mMSLN-VLPs) immunization was able to break tolerance to intrinsic MSLN, resulting in reduced frequency of CD4$^+$Foxp3$^+$ICOS$^-$Treg cells and stimulation of cytotoxic CD8$^+$ T cells anti-tumour activity. However, because mMSLN-VLP induces IL-6 production, increasing ICOS-L

expression on pDC-like cells and proliferation of immuno-suppressive CD4$^+$Foxp3$^+$ICOS$^+$Treg cells, combination therapies with ICOS blocking remain necessary [19]. In an *in vitro* model of multiple myeloma, lenalidomide pre-treatment of MM cell lines reduced Treg generation and the Treg/Teff ratio, probably due to a reduced ICOS-L gene transcription. Combined treatment with lenalidomide and dexamethasone significantly reduced both Treg induction and the Treg/Teff cell ratio [21]. Additionally, depletion of Tregs in conjunction with ICOS agonist could remove the potential immunosuppressive effects of ICOS signaling and allow ICOS agonist to act solely in promoting activity of CD4$^+$ Teff. In fact, ICOS is highly expressed in tumour Tregs, and thus a single ICOS agonist with strong Fc engagement may be sufficient to induce a simultaneous ADCC-mediated depletion of Tregs and agonist-based enhancement of anti-tumour responses [25].

Nevertheless, blocking of ICOS/ICOS-L system is not always a good strategy. *In vivo* models of prostate, melanoma [22], and bladder cancer [20], showed anti-CTLA-4 therapy leads to an increase in the frequency of CD4$^+$ICOS$^+$ and CD8$^+$ICOS$^+$ T cells producing IL-2 and IFN-γ. Here, ICOS seems to play an important role in the activation/development of functional antitumor CD8 T cells [23]. In mouse syngeneic tumours, ICOS was found highly expressed by Tregs, but it was also found up-regulated across CD8$^+$ and CD4$^+$ effector populations, suggesting that ICOS expression is associated with opposite functions. According to this evidence, ICOS/ICOS-L pathway could be another therapeutic target and it may have implications in the development of novel combined cancer immunotherapy strategies [22, 23]. Indeed, in murine models of prostate cancer, CTLA-4 blockade enhanced activation of tumour-reactive T cells with concomitant up-regulation of ICOS. In this context, IVAX (vaccine of ICOSL-positive tumour cells) triggered the ICOS pathway, leading to a higher density of Teff cells inside the tumour, as indicated by an increase in the Teff/Treg cell ratio [22]. Likewise, after anti–CTLA-4 treatment ICOS$^+$ T cells increased significantly in both the CD4$^+$ and CD8$^+$ populations. In this case, anti–CTLA-4 therapy increased a population of Foxp3$^-$ cells and then stimulated an expansion of ICOS$^+$ T effector cells over Treg cells. These results suggest that ICOS$^+$ T cells may represent a population of T effector cells that play an important role in anti-tumour immune responses induced by anti–CTLA-4 therapy. Further, ICOS$^+$ T cells produced Th1 cytokine IFN-γ and cytokine IL-2 necessary for effective anti-tumour responses, suggesting that ICOS$^+$ T cells might play a functional role in improving the effectiveness of combinatorial immunotherapy. In a recent clinical trial, treatment of patients with bladder cancer with a blocking anti-CTLA-4 monoclonal antibody resulted in increased percentage of CD4$^+$T cells in peripheral blood and tumour tissues, thus potential higher levels of ICOS. Upon re-stimulation, ICOS$^+$CD4$^+$ T cells produced greater levels of IFN-γ compared to ICOS$^-$CD4$^+$ T cells, suggesting that T cells with higher levels of ICOS, have elevated effector functions in anti-tumour activity, as seen in melanoma models [20].

CONCLUSION

The pathway ICOS/ICOS-L is involved in several processes in cancer, ranging from support of tumour growth to

improvement of immune-stimulating therapy efficacy. Data suggest that inhibition of the ICOS/ICOS-L system alone may not particularly effective in treatment of cancer, because this pathway showed opposing effects in regulating T-cell response. The importance of ICOS/ICOS-L blockade was attributable to its role as adjuvant in combined cancer immunotherapy strategies. ICOS expression was positively correlated with the expression of other important immune checkpoints (CTLA-4 and PD-1 on T cells) in colon cancer patients, with antibodies anti-CTLA-4 and anti PD-1 currently being used for the treatment of several types of cancer. This suggests that ICOS could be a marker in therapy selection, with effectiveness depending on CTLA-4 or PD-1 expression correlated with ICOS expression. While increasing of Tregs in tumour microenvironment could reduce vaccine efficacy, a combination with anti-ICOS antibody might be a more effective therapy. This could increase immune response, as it would reduce the population of tumour infiltrated Tregs. In summary, ICOS/ICOS-L pathway could be considered as a novel immune target and its role should be investigated in other cancers, taking into account that this pathway shows a dualistic behaviour.

CONSENT FOR PUBLICATION

Not applicable.

CONFLICT OF INTEREST

The authors declare no conflict of interest, financial or otherwise.

ACKNOWLEDGEMENTS

REFERENCES

[1] Greaves, P.; Gribben, J.G. The role of B7 family molecules in hematologic malignancy. *Blood*, **2013**, *121*, 734-744.

[2] Wang, F.; Zhu, W.; Liu, T.; Sun, Z.; Ju, S.; Ju, S.; Yu, G.; Xie, W.; Deng, Z.; Lu, B.; Zhang, X. The expression analysis of ICOS-L on activated T cells and immature dendritic cells as well as malignant B cells and Grave's-disease-derived thyroid tissues by two novel mAbs against human ICOS-L. *Tissue Antigens*, **2007**, *69*, 62-72.

[3] Wikenheiser, D.J.; Stumhofer, J.S. ICOS co-stimulation: Friend or foe? *Front. Immunol.,* **2016**, *7*, 304.

[4] Yoshinaga, S.K.; Zhang, M.; Pistillo, J.; Horan, T.; Khare, S.D.; Miner, K.; Sonnenberg, M.; Boone, T.; Brankow, D.; Dai, T.; Delaney, J.; Han, H.; Hui, A.; Kohno, T.; Manoukian, R.; Whoriskey, J.S.; Coccia, M.A. Characterization of a new human B7-related protein: B7RP-1 is the ligand to the co-stimulatory protein ICOS. *Int. Immunol.*, **2000**, *12*(10), 1439-1447.

[5] Aicher, A.; Hayden-Ledbetter, M.; Brady, W.A.; Pezzutto, A.; Richter, G.; Magaletti, D.; Buckwalter, S.; Ledbetter, J.A.; Clark, E.A. Characterization of human inducible costimulator ligand expression and function. *J. Immunol.*, **2000**, *164*(9), 4689-4696.

[6] Nagase, H.; Takeoka, T.; Urakawa, S.; Morimoto-Okazawa, A.; Kawashima, A.; Iwahori, K.; Takiguchi, S.; Nishikawa, H.; Sato, E.; Sakaguchi, S.; Mori, M.; Doki, Y.; Wada, H. ICOS(+) Foxp3(+) TILs in gastric cancer are prognostic markers and effector regulatory T cells associated with *Helicobacter pylori*. *Int. J. Cancer*, **2017**, *140*, 686-695.

[7] Martin-Orozco, N.; Li, Y.; Wang, Y.; Liu, S.; Hwu, P.; Liu, Y.J.; Dong, C.; Radvanyi, L. Melanoma cells express ICOS ligand to promote the activation and expansion of T-regulatory cells. *Cancer Res.*, **2010**, *70*, 9581-9590.

[8] Feyler, S.; Scott, G.B.; Parrish, C.; Jarmin, S.; Evans, P.; Short, M.; McKinley, K.; Selby, P.J.; Cook, G. Tumour cell generation of inducible regulatory T-cells in multiple myeloma is contact-dependent and antigen-presenting cell-independent. *PLoS One*, **2012**, *7*, e35981.

[9] Yamashita, T.; Tamura, H.; Satoh, C.; Shinya, E.; Takahashi, H.; Chen, L.; Kondo, A.; Tsuji, T.; Dan, K.; Ogata, K. Functional B7.2 and B7-H2 molecules on myeloma cells are associated with a growth advantage. *Clin. Cancer Res.,* **2009**, *15*(3), 770-777.

[10] Faget, J.; Bendriss-Vermare, N.; Gobert, M.; Durand, I.; Olive, D.; Biota, C.; Bachelot, T.; Treilleux, I.; Goddard-Leon, S.; Lavergne, E.; Chabaud, S.; Blay, J.Y.; Caux, C.; Ménétrier-Caux, C. ICOS-ligand expression on plasmacytoid dendritic cells support breast cancer progression by promoting the accumulation of immunosuppressive CD4+ T cells. *Cancer Res.*, **2012**, *72*(23), 6130-6141.

[11] Conrad, C.; Gregorio, J.; Wang, Y.H.; Ito, T.; Meller, S.; Hanabuchi, S.; Anderson, S.; Atkinson, N.; Ramirez, P.T.; Liu, Y.J.; Freedman, R.; Gilliet, M. Plasmacytoid dendritic cells promote immunosuppression in ovarian cancer *via* ICOS co-stimulation of Foxp3(+) T-regulatory cells. *Cancer Res.,* **2012**, *72*(20), 5240-5249.

[12] Pedroza-Gonzalez, A.; Zhou, G.; Vargas-Mendez, E.; Boor, P.P.; Mancham, S.; Verhoef, C.; Polak, W.G.; Grünhagen, D.; Pan, Q.; Janssen, H.; Garcia-Romo, G.S.; Biermann, K.; Tjwa, E.T.; IJzermans, J.N.; Kwekkeboom, J.; Sprengers, D. Tumor-infiltrating plasmacytoid dendritic cells promote immunosuppression by Tr1 cells in human liver tumors. *Oncoimmunology,* **2015**, *4*(6), e1008355.

[13] Zhang, Y.; Luo, Y.; Qin, S.L.; Mu, Y.F.; Qi, Y.; Yu, M.H.; Zhong, M. The clinical impact of ICOS signal in colorectal cancer patients. *Oncoimmunology,* **2016**, *5*(5), e1141857.

[14] Greaves, P.; Clear, A.; Owen, A.; Iqbal, S.; Lee, A.; Matthews, J.; Wilson, A.; Calaminici, M.; Gribben, J.G. Defining characteristics of classical Hodgkin lymphoma microenvironment T-helper cells. *Blood*, **2013**, *122*(16), 2856-2863.

[15] Tamura, H.; Dan, K.; Tamada, K.; Nakamura, K.; Shioi, Y.; Hyodo, H.; Wang, S.D.; Dong, H.; Chen, L.; Ogata, K. Expression of functional B7-H2 and B7.2 costimulatory molecules and their prognostic implications in *de novo* acute myeloid leukemia. *Clin. Cancer Res.*, **2005**, *11*(16), 5708-5717.

[16] Schreiner, B.; Wischhusen, J.; Mitsdoerffer, M.; Schneider, D.; Bornemann, A.; Melms, A.; Tolosa, E.; Weller, M.; Wiendl, H. Expression of the B7-related molecule ICOSL by human glioma cells *in vitro* and *in vivo*. *Glia*, **2003**, *44*(3), 296-301.

[17] Simon-Keller, K.; Paschen, A.; Hombach, A.A.; Ströbel, P.; Coindre, J.M.; Eichmüller, S.B.; Vincent, A.; Gattenlöhner, S.; Hoppe, F.; Leuschner, I.; Stegmaier, S.; Koscielniak, E.; Leverkus, M.; Altieri, D.C.; Abken, H.; Marx, A. Survivin blockade sensitizes rhabdomyosarcoma cells for lysis by fetal acetylcholine receptor-redirected T cells. *Am. J. Pathol.*, **2013**, *182*(6), 2121-2131.

[18] Mo, L.; Chen, Q.; Zhang, X.; Shi, X.; Wei, L.; Zheng, D.; Li, H.; Gao, J.; Li, J.; Hu, Z. Depletion of regulatory T cells by anti-ICOS antibody enhances anti-tumor immunity of tumor cell vaccine in prostate cancer. *Vaccine*, **2017**, *35*(43), 5932-5938.

[19] Zhang, S.; Yong, L.K.; Li, D.; Cubas, R.; Chen, C.; Yao, Q. Mesothelin virus-like particle immunization controls pancreatic cancer growth through CD8+ T cell induction and reduction in the frequency of CD4+ foxp3+ ICOS- regulatory T cells. *PLoS One*, **2013**, *8*(7), e68303.

[20] Chen, H.; Liakou, C.I.; Kamat, A.; Pettaway, C.; Ward, J.F.; Tang, D.N.; Sun, J.; Jungbluth, A.A.; Troncoso, P.; Logothetis, C.; Sharma, P. Anti-CTLA-4 therapy results in higher CD4+ICOShi T cell frequency and IFN-gamma levels in both nonmalignant and malignant prostate tissues. *Proc. Natl. Acad. Sci. USA*, **2009**, *106*(8), 2729-2734.

[21] Scott, G.B.; Carter, C.; Parrish, C.; Wood, P.M.; Cook, G. Down-regulation of myeloma-induced ICOS-L and regulatory T cell generation by lenalidomide and dexamethasone therapy. *Cell Immunol.*, **2015**, *297*(1), 1-9.

[22] Fan, X.; Quezada, S.A.; Sepulveda, M.A.; Sharma, P.; Allison, J.P. Engagement of the ICOS pathway markedly enhances efficacy of CTLA-4 blockade in cancer immunotherapy. *J. Exp. Med.*, **2014**, *211*(4), 715-725.

[23] Fu, T.; He, Q.; Sharma, P. The ICOS/ICOSL pathway is required for optimal antitumor responses mediated by anti-CTLA-4 therapy. *Cancer Res.*, **2011**, *71*(16), 5445-5454.

[24]   Ito, T.; Yang, M.; Wang, Y.H.; Lande, R.; Gregorio, J.; Perng, O.A.; Qin, X.F.; Liu, Y.J.; Gilliet, M. Plasmacytoid dendritic cells prime IL-10–producing T regulatory cells by inducible costimulator ligand. *J. Exp. Med.*, **2007,** *204*(1), 105-115.

[25]   Metzger, T.C.; Long, H.; Potluri, S.; Pertel, T.; Bailey-Bucktrout, S.L.; Lin, J.C.; Fu, T.; Sharma, P.; Allison, J.P.; Feldman, R.M.

ICOS promotes the function of CD4+ effector T cells during anti-OX40-mediated tumor rejection. *Cancer Res.*, **2016,** *76*(13), 3684-3689.

Research Paper

High CTLA-4 expression correlates with poor prognosis in thymoma patients

Giorgio Santoni[1], Consuelo Amantini[2], Maria Beatrice Morelli[1,3], Daniele Tomassoni[2], Matteo Santoni[4], Oliviero Marinelli[1,2], Massimo Nabissi[1], Claudio Cardinali[3], Vittorio Paolucci[4], Mariangela Torniai[4], Silvia Rinaldi[4], Francesca Morgese[4], Giovanni Bernardini[3,5] and Rossana Berardi[4]

[1]School of Pharmacy, University of Camerino, Camerino, Italy

[2]School of Biosciences and Veterinary Medicine, University of Camerino, Camerino, Italy

[3]Department of Molecular Medicine, Sapienza University of Rome, Rome, Italy

[4]Medical Oncology Unit, Università Politecnica delle Marche, Azienda Ospedaliero-Universitaria Ospedali Riuniti Umberto I-Lancisi, Salesi di Ancona, Italy

[5]I.N.M. Neuromed, Pozzilli, Isernia (IS), Italy

Correspondence to: Giorgio Santoni, *email:* giorgio.santoni@unicam.it

ABSTRACT

Thymomas, tumors that arise from epithelial cells of the thymus gland, are the most common neoplasms of the anterior mediastinum, with an incidence rate of approximately 2.5 per million/year. Cytotoxic T Lymphocyte Antigen 4 (CTLA-4 or CD152) exerts inhibitory activity on T cells, and since its oncogenic role in the progression of different types of tumors, it has emerged as a potential therapeutic target in cancer patients.

In this study, we assessed the expression of CTLA-4 both at mRNA and protein levels in paraffin embedded-tissues from patients with thymomas. Furthermore, we evaluated the relationship between CTLA-4 expression and the clinical-pathologic characteristics and prognosis in patients with thymomas. Sixty-eight patients with median age corresponding to 62 years were included in this analysis. Thymomas were classified accordingly to the WHO and Masaoka-Koga for histochemical analysis and for prognostic significance.

A statistical difference was found between CTLA-4 mRNA levels in human normal thymus compared with thymoma specimens. CTLA-4 expression was statistically found to progressively increase in A, B1, B2, AB and it was maximal in B3 thymomas. According to Masaoka-Koga pathological classification, CTLA-4 expression was lower in I, IIA and IIB, and higher in invasive III and IV stages. By confocal microscopy analysis we identified the expression of CTLA-4 both in tumor cells and in CD45^{+} tumor-infiltrating leukocytes, mainly in B3 and AB thymomas.

Finally, CTLA-4 overexpression significantly correlates with reduced overall survival in thymoma patients and in atypical thymoma subgroup, suggesting that it represents a negative prognostic factor.

INTRODUCTION

Thymomas, tumors that arise from epithelial cells of the thymus gland, are the most common neoplasms of the anterior mediastinum, with an incidence rate of approximately 2.5 per million/year [1]. Thymomas are rare in patients under 25 years of age and show a wide age distribution, with a mean of incidence around 50–60 years of age, without a major sex predilection [1]. Although thymomas are, in general, indolent neoplasms, they are considered as malignant, irrespective to different subtypes.

Thymic neoplasms are divided according to the WHO classification [1], which is based on the premise that thymoma cells can belong to two histologic types: spindle/oval (designated as type "A") or round/epithelioid (designated as type "B"). The type B were additionally subclassified based on the proportional increase in infiltrating lymphocytes and emergence of atypia of the neoplastic epithelial cells into B1, B2 and B3 subtypes. Finally a C category (thymic carcinoma) displaying cytological features of malignancy, including marked atypia, nuclear pleomorphism and high mitotic activity is accounted [2–5]. The Masaoka-Koga stage classification distinguished thymic malignancies in not-invasive I and IIA and invasive IIB, IIIA, IIIB, IVA and IVB stages [6]. Furtherly, accordingly to Moran and Suster classification, a more simplified approach in classifying the thymic epithelial neoplasms based on the histologic grading in well-differentiated (A, AB, B1 and B2, typical thymoma), moderately differentiated (B3, atypical thymoma) and poorly differentiated (C, thymic carcinoma), has been proposed [6–10]. Type AB thymoma is not considered a mixed tumor of type A and type B thymomas, but a distinct type of thymoma derived from a mixture of type A- and type B-like component positive for E-cadherin and negative for vimentin or a mixture of type B-like components and metaplastic mesenchymal components, positive for vimentin and negative for E-cadherin [11]. Once a tumor has been assigned to a differentiation category of thymic epithelial neoplasms, reliable prognostication can be determined by clinical and pathological Masaoka-Koga staging of the lesions. However, in several cases, histologic classification, according to WHO and/or pathological Masaoka-Koga stage classifications, cannot be completely correlated with clinical outcome [12], so the need to identify new prognostic biomarkers. In addition, an association between myasthenia gravis (MG), a neuromuscular disorder characterized by a defective transmission of nerve impulses to muscles, and thymoma has been reported [13]. About forty percent of the thymoma patients had associated MG, and preoperative absence of MG has been considered an independent predictor of poorer overall survival (OS) [12]. This disease is caused by an autoimmune reaction against components of the neuromuscular junction on the post-synaptic membrane

of the striated skeletal muscles [13] and it is present at first diagnosis in up to a third of thymoma patients [14].

Cytotoxic T lymphocyte antigen-4 (CTLA-4, CD152) is an immune checkpoint molecule and a CD28 homologue that binds the ligands B7-1 (CD80) and B7-2 (CD86) [15]. Human CTLA-4 is present as a full-length membrane-bound receptor and as a secreted soluble molecule [16, 17]. Both the two isoforms reduce T cell activation by forming a negative feedback to maintain immune self-tolerance and homeostasis. CTLA-4 outcompetes CD28 for B7 ligands, attenuating the T cell response through the inhibition of IL-2 and blockage of cell cycle progression [18]. CTLA-4 is constitutively expressed at low levels on the surface of naïve, effector T (Teff) and regulatory T cells (Treg). The expression of CTLA-4 on Tregs reduces the levels of B7 ligands on antigen presenting cells. CTLA-4 has been also implicated in immune dysregulation of B cell chronic lymphocytic leukemia [19] and non Hodking's lymphoma [20].

The CTLA-4 molecule is expressed on normal non-lymphoid cells including placental fibroblasts [21], cultured muscle cells [22], monocytes [23] and mature dendritic cells [24]. In addition, it has been demonstrated that CTLA-4 is constitutively expressed not only in leukemia cells [25], but also in several types of tumor-derived cell lines including breast, colon, renal, lung, ovarian, uterine, bladder carcinoma, osteo/rabdomyosarcoma, neuroblastoma and melanoma [26] and in cancer tissues, such as osteosarcomas [26], non-small cell lung [27] and breast [28], nasopharyngeal [29], gastric [30] and esophageal carcinomas [31] and mesotheliomas [32]. Finally, CTLA-4 gene polymorphisms have been associated to increased susceptibility to multiple types of cancer such as breast [33], melanoma [34] gastric and colon cancers [35] and cervical carcinomas [36].

At present, the expression of CTLA-4 was only taken into account for the MG profiling indicating an association between different CTLA-4 single nucleotide variants and susceptibility to disease [37].

Thus, in this study, we assessed the expression of CTLA-4 both at mRNA and protein levels in fixed paraffin-embedded thymoma tissues. Furthermore, we also evaluated the correlation between CTLA-4 expression and clinico-pathologic characteristics and prognosis of patients with thymomas.

RESULTS

Study population

The complete list of patient characteristics is summarized in Table 1. Clinico-pathologic analyses according to WHO and Masaoka-Koga classifications are reported in Supplementary Tables 1 and 2, respectively. Extra-capsular invasive behavior was evidenced mainly in B2, B3 and C thymoma types (71, 83 and 100%,

Table 1: Patient demographics and clinical features

	PATIENTS N=68 (100%)
GENDER	
M	33 (48.5%)
F	35 (51.5%)
AGE (years)	
Range	21-81
21-45	14 (20.6%)
46-59	19 (27.9%)
>60	35 (51.5%)
Median	62
Myasthenia Gravis	
Yes	22 (32.4%)
No	46 (67.6%)
Tumor Histology	
A	11 (16.2%)
AB	17 (25.0%)
B1	6 (8.8%)
B2	17 (25.0%)
B3	12 (17.6%)
C	5 (7.4%)
TUMOR SIZE	
< 5 cm	28 (41.2%)
> 5 cm	40 (58.8%)
Invasion	
Yes	55 (80.9%)
Capsular	24 (43.6%)
Extracapsular	31 (56.4%)
No	11 (16.2%)
ND	2 (2.9%)

respectively) (Supplementary Table 1). In addition, concomitant MG is present in about 1/3 of thymoma patients, mainly in B2-B3 thymoma types (59 and 50%, respectively). In regard to extra-capsular invasion, it was more evident in IIB, III and IV Masaoka-Koga stages (Supplementary Table 2).

CTLA-4 mRNA expression in thymoma tissues

The CTLA-4 mRNA expression was evaluated in thymoma specimens (n = 63/68), two different batches of RNA from human normal thymus and, as control, peripheral blood mononuclear cells (PBMCs),

from healthy donors, unstimulated and stimulated with phorbol 12-myristate 13-acetate (PMA). Given the small number of thymoma type C samples, the expression of CTLA-4 mRNA was not evaluated in these specimens. CTLA-4 mRNA was expressed at low levels in normal thymus, unstimulated PBMCs, whereas increased CTLA-4 levels (8-fold) were evidenced in PMA-stimulated PBMCs, upon PMA stimulation, as previously described [23, 38] (Figure 1A). Moreover, independently of WHO classification, CTLA-4 mRNA levels were very low in normal thymus respect to thymoma tissues (Figure 1B). Quantitative real time polymerase chain reaction (qRT-PCR) analysis also identified that the CTLA-4 mRNA expression progressively increase from A, B1, B2, AB and B3, with the higher levels in B3 type thymomas, as evaluated by statistical analysis (Figure 1B). Then, analyzing CTLA-4 expression in thymomas according to Masaoka-Koga stage, a significant difference between I vs IIA, IIB, III and IV, IIA and IIB vs III or IV stages was observed. No major differences were found comparing IIA vs IIB or III vs IV grade (Figure 1C). Finally, according to Moran and Suster classification [5, 7, 8, 10] significant difference in CTLA-4 mRNA expression were evidenced comparing typical (A, B1, B2 and AB types) vs atypical (B3 type) thymomas, with the last expressing very higher CTLA-4 mRNA levels respect to typical thymomas (Figure 1D). Finally, we evaluated whether adjuvant chemo-, radio-therapy or MG may affect the expression of CTLA-4 mRNA in thymoma patients (Supplementary Figure 1). We found higher CTLA-4 mRNA levels in thymoma patients undergoing adjuvant radiotherapy compared to untreated patients. No major differences in CTLA-4 expression were observed in untreated vs chemotherapy-administered thymoma patients and in MG vs non-MG thymoma patients.

Expression of CTLA-4 protein in tumor cells and tumor-infiltrating leukocytes (TILs) from thymoma tissues

The results obtained in thymoma tissues by qRT-PCR prompted us to evaluate the expression of CTLA-4 protein in the different histological type of thymomas by immunohistochemistry (IHC) and semi-quantitative analysis. CTLA-4 immunoreactivity was found in all thymoma type sections and the percentage of CTLA-4+ cells progressively increase from A, B1, B2, AB and B3, with the highest levels in B3 type thymomas (Figure 2A and 2B). No reactivity was found in tissue sections used as negative control incubated with the omission of primary Ab (Figure 2A). Moreover, although the number of thymoma type C samples was limited to be included in the statistical analysis, the immunohistochemistry was performed and showed a strong CTLA-4 staining in these specimens (Supplementary Figure 2).

Since B1, B2 and B3 types are characterized by a proportional increase in TILs, the co-expression of CD45 and CTLA-4 antigens was evaluated using the anti-human CD45 and anti-CTLA-4 monoclonal Abs by confocal microscopy. CTLA-4 expression progressively increased in B1, B2, AB and B3 thymomas, whereas negligible CTLA-4 protein expression was found in type A thymoma as demonstrated by the Fluorescence Intensity confirming the IHC data (Figure 3A and 3B). Moreover, in tumor cells, CTLA-4 protein localised in the membrane, cytoplasm or both in a scattered pattern (Figure 3A). In addition, we found in accordance with previous reports [3, 4, 9], that TILs progressively increase from B1 to B3 and AB thymomas with about 20.1% and 14.6% of CTLA-4 positive cells being CD45 positive in B3 and AB thymomas respectively (Figure 3C). Finally, in AB thymomas the expression of vimentin and CTLA-4 in tumor cells was evaluated using an anti-human vimentin and anti-CTLA-4 mAbs. A mixture of less represented CTLA-4$^+$/Vimentin$^+$ tumor cells as well as a more represented CTLA-4$^+$/Vimentin$^-$ tumor cells was observed in AB thymoma sections (Figure 4).

Correlation between clinico-pathologic and prognostic parameters, CTLA-4 tumor expression and overall survival in thymoma patients

Survival curves were calculated according to univariate analysis (Table 2) and the Kaplan–Meier method by evaluating the age (≤ 60 vs > 60 years), sex, MG, invasion phenotype, invasion localization (capsular vs extra-capsular), tumor dimensions ≤ 5 cm or > 5 cm, radicality and CTLA-4 mRNA expression. In regard to CTLA-4 expression, patients were divided into two groups showing low < 0.5 (n = 15 specimens) and high > 0.5 (n = 48 specimens) CTLA-4 level. CTLA-4 mRNA expression reached significance for survival (p = 0.0107) (Figure 5A) with in CTLA-4^{low} OS = 188.31 vs CTLA-4^{high} OS = 119.50 months. In addition, atypical histological type thymoma (OS = 65.73 months) (Figure 5B) showed a significant (p = 0.0055) reduced survival respect to typical thymoma (OS = 188.22 months) confirming that high CTLA-4 expression in atypical thymoma (Figure 1D) is associated with negative prognosis. Age > 60 and tumor dimension > 5 cm were
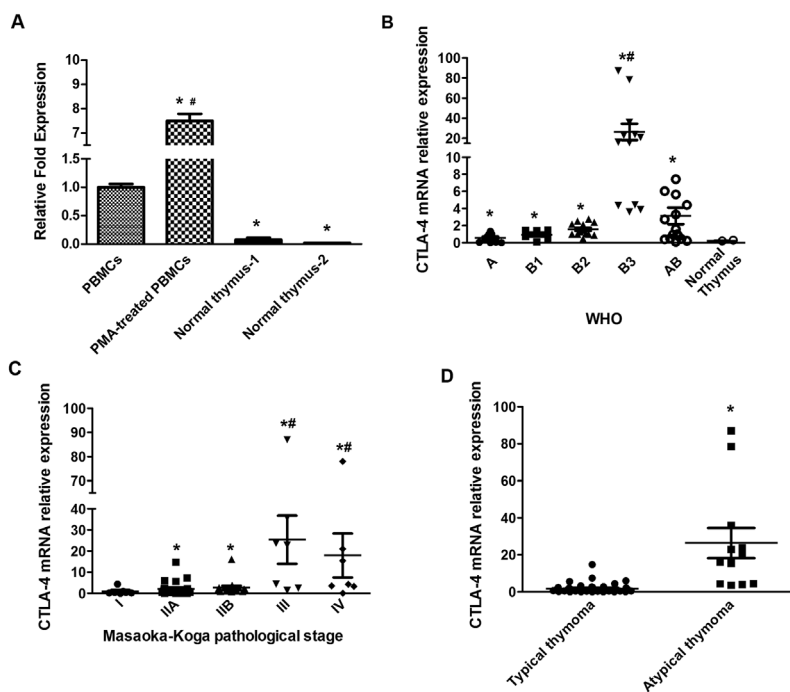
Figure 1: CTLA-4 expression on normal human thymus, lymphocytes and thymoma tissues. (A) CTLA-4 mRNA expression was evaluated by qRT-PCR in normal human thymus and PBMCs treated or not with PMA. CTLA-4 mRNA levels were normalized for GAPDH expression. Data are expressed as fold mean ± SD. *p<0.05 vs PBMCs, #p<0.05 vs PBMC, normal thymus -1 and normal thymus -2. **(B)** CTLA-4 mRNA expression levels distribution according to WHO classification; statistical analysis was performed using non-parametric Kruskal-Wallis with Dunn's multiple comparisons test. Data are expressed as fold mean ± SD, *p<0.05 vs normal thymus-2; #p<0.05 vs A, B1, B2 and AB. **(C)** CTLA-4 mRNA expression levels distribution according to Masaoka-Koga classification; statistical analysis was performed by non-parametric Kruskal-Wallis with Dunn's multiple comparisons test. Data are expressed as fold mean ± SD, *p<0.05 vs I, #p<.0.05 vs IIA or IIB. **(D)** CTLA-4 mRNA expression level distribution according to Moran and Suster classification; statistical analysis was performed using non-parametric Kruskal-Wallis with Dunn's multiple comparisons test. Data are expressed as fold mean ± SD, *p<0.05 typical vs atypical thymomas.

positively correlated (p = 0.0002, with OS ≤ 60 = 196.83 vs > 60 = 119.50 months; p = 0.0429, with OS ≤ 5cm = 209.88 vs > 5cm = 137.72 months, respectively) (Figure 6A and 6B). The presence of concomitant MG in thymoma patients approximates the significance (p = 0.0889, OS = 188.32 vs non MG = 153.66 months) (Figure 6C). No correlation for sex, tumor invasion, extra-capsular tumor invasion (Figure 6D) and radicality (Figure 6E) was evidenced. Thus, the higher CTLA-4 mRNA expression, age > 60 years and tumor dimension > 5 cm strongly correlated with short survival in total thymoma group and in atypical thymoma subgroup. Additionally we performed a multivariate analysis based on the Cox regression model to test the influence of CTLA-4 mRNA expression, age > 60 years and tumor dimensions > 5 cm on the survival of thymoma patients. We found that CTLA-4 overexpression, age > 60 years and typical vs atypical histological subtypes retained their prognostic negative significance in thymoma patients (p = 0.0235, 0.0071 and 0.0041, respectively) (Table 2).

DISCUSSION

Thymic epithelial tumors (TETs) are uncommon neoplasms with a wide range of anatomical, clinical, histological and molecular malignant entities. At present, the management of TETs within clinical practice is based on a multimodal therapeutic strategy including surgery, chemotherapy and radiotherapy with a multidisciplinary approach and prognostic evaluation mainly based on Masaoka-Koga staging and WHO classification [39–41].

Novel strategies are needed, especially for refractory, recurrent thymic tumors after first-line chemotherapy failure. The investigation of molecular profiling and the analyses of immunological markers in thymic tumors could also allow determining potentially new targets.

To our knowledge, this is the first study demonstrating that elevated CTLA-4 tumor expression in thymoma patients correlates with poor prognosis and shorter OS. At present, CTLA-4 association to thymomas has only been taken into account for the MG profiling.
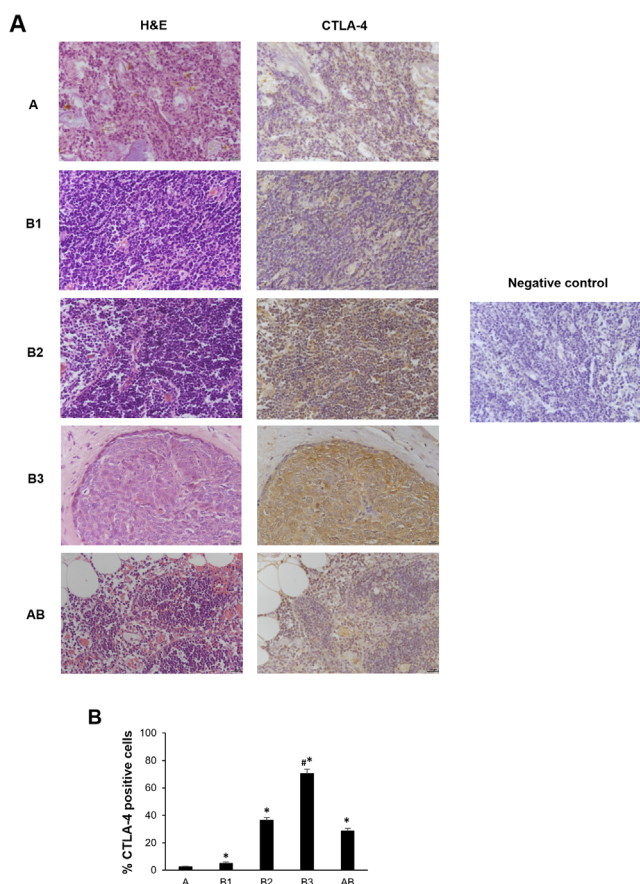
Figure 2: CTLA-4 protein expression in different subtypes of thymoma tissues. (A) Sections of A, B1, B2, B3 and AB thymomas A were processed for hematoxylin and eosin staining (right column) and for CTLA-4 (left column) by immunohistochemistry. Sections of thymoma B1 thymomas processed for immunohistochemistry without incubation of primary antibody, were used as negative control. Calibration bar: 25 μm. **(B)** The percentage of CTLA-4 positively stained cells was determined in all samples according to the staining intensity by the NIS Software. Data represents the mean ± SD. *p<0.05 vs A; #p<0.05 vs B1, B2 and AB.
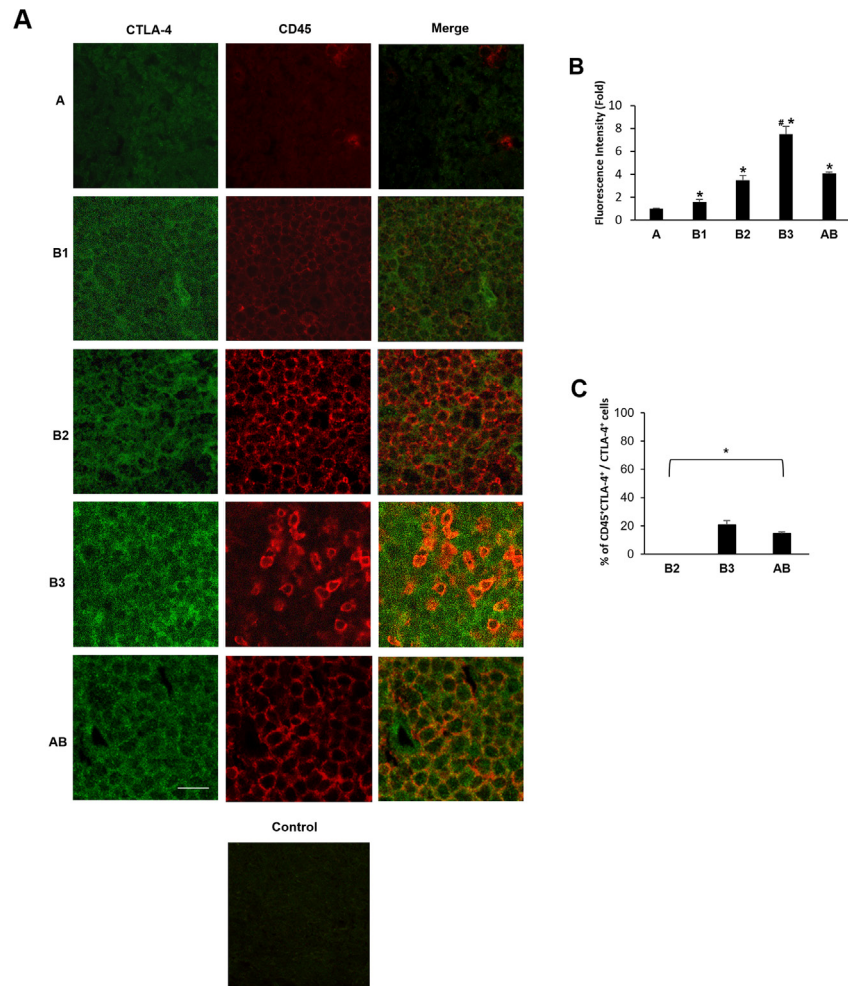
Figure 3: Expression of CTLA-4 in tumor cells and CD45$^+$ TILs from thymoma specimens. Confocal microscopy analysis was performed in thymoma tissues double-stained with anti-CTLA-4 and anti-CD45 mAbs, followed by Alexa Fluor 488- and Alexa Fluor 594-conjugated secondary Abs, respectively. Control = merge of secondary Abs without the incubation of the primary Abs. Data shown are representative of one out of three separate experiments. Calibration bar: 25 μm. **(B)** The CTLA-4 Fluorescence intensity was evaluated in all samples by using the NIS Software. Data represent the mean ± SD. *p<0.05 vs **(A)**; #p<0.05 vs B1, B2 and AB. **(C)** The percentage of CTLA-4$^+$CD45$^+$cells was evaluated in B2, B3 and AB samples according to the double fluorescence intensity by using the NIS Software and considering the total CTLA-4$^+$ cells as 100%. Data represent the mean ± SD. *p<0.05 vs total CTLA-4$^+$ cells.
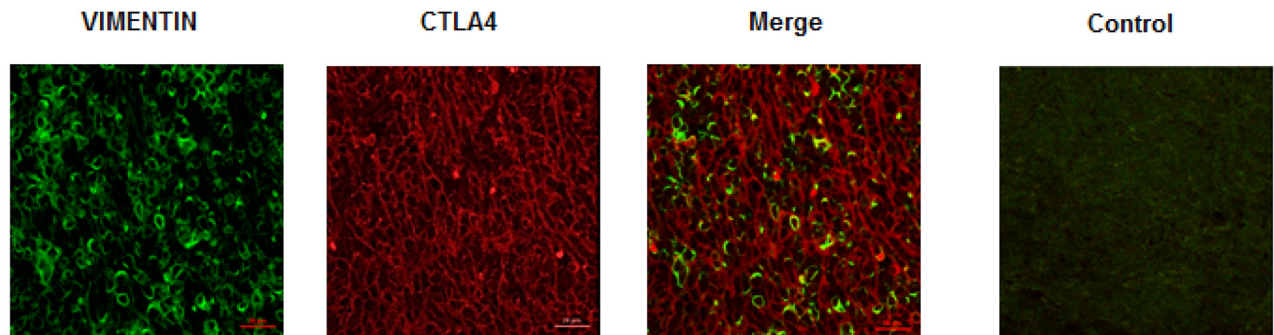
Figure 4: Expression of vimentin and CTLA-4 in AB subtype thymomas. Confocal microscopy analysis was performed in thymoma AB specimens double-stained with anti-vimentin and anti-CTLA-4 mAbs, followed by Alexa Fluor 488- and Alexa Fluor 594-conjugated secondary Abs, respectively. Control = merge of secondary Abs without the incubation of the primary Abs. Data shown are representative of one out of three separate experiments. Calibration bar: 25 μm.

In particular, single nucleotide polymorphisms (SNPs) of CTLA-4 seem to be associated with the manifestation of MG in patients with thymoma. SNPs in position 49 in patients expressing high CTLA-4 levels, in particular SNP +49 A/A and SNP +49 A/G showed a bad prognosis and reduced OS [42–44].

Herein, we analyzed the expression of CTLA-4 in thymoma patients with different WHO histological types and Masaoka-Koga stages. We found that CTLA-4 expression was significantly higher in all thymoma WHO types, compared with healthy thymus. We also stated that CTLA-4 gene expression was lower in A and B1, progressively increased in B2 and AB and was higher in B3 type thymomas, representing this histological type, the atypical thymoma subgroup, according to Moran and Suster classification [5, 7, 8, 10]. Thus, following both the WHO or Moran and Suster classifications the highest CTLA-4 value was evidenced in atypical B3 thymomas.

In parallel, by qRT-PCR, we observed a higher CTLA-4 expression in more advanced Masaoka-Koga grade IIB, III and IV compared to I and IIA, suggesting that CTLA-4 overexpression may be related to tumor aggressiveness. In regard to AB thymomas, a mixture of less represented mesenchymal CTLA-4+/Vimentin+ tumor cells as well as a more represented CTLA-4+/Vimentin- tumor cells was observed in AB thymoma sections. The metaplastic CTLA-4+/Vimentin+ tumor cells likely derived from an epithelial mesenchymal transition process and trans-differentiation of spindle cells that have up-regulated mesenchymal markers [11].

According to previously reported data [12], Kaplan-Mayer and univariate analysis evidenced in thymoma patients with concomitant MG higher OS and good prognosis compared to non-MG patients. Autoimmunity and malignancy frequently coexist and they may share etiological and pathogenic mechanisms [45]. A sort of protective autoimmunity has been reported to improve the survival of cancer patients [46]; however at the other hand, better OS observed in MG patients could also depend to early discovery of MG vs non-MG thymomas, allowing a better survival of thymoma patients [47].

More importantly, our results suggest that in thymoma patients higher CTLA-4 mRNA expression represents a negative prognostic marker. In fact, the increase of CTLA-4 gene expression in total thymoma group and in B3 subgroup was associated with a shorter survival. In a multivariate Cox proportional hazards regression model, high CTLA-4 levels both in total and atypical thymoma, as well as age > 60 and tumor dimension > 5 cm, confirm their significance as negative prognostic factor for survival. Overall, tumor-associated CTLA-4 could promotes tumor progression by inhibiting the anti-tumor T cell immunity, inducing tumor-specific T cell apoptosis or impairing cytokine production and T cell-mediated cytotoxicity [48].

We also found that CTLA-4 is expressed not only in tumor cells, but also in CD45 leukocytes infiltrating the thymomas. In immune cells, CTLA-4 has been found to be expressed in B lymphocytes [17], monocytes [49], and activated effector CD4+ and CD8+ T cells, as well as constitutively expressed on a subset of regulatory Treg [50] participating in the co-stimulatory activation of naïve T cells or depletion of activated T cells [51]. Antigen specific activation of naïve T cells induces the expression of cytokines such as interferon-γ, which in turn triggers CTLA-4 expression in surrounding immune and tumor cells. The presence of Treg in tumor microenvironment has been associated with poor outcomes in patients with cancers [52]. In this regard, confocal microscopy analysis evidenced CTLA-4+CD45+ TILs, likely Treg lymphocytes, in the tumor microenvironment of B3 and AB thymomas, showing reduced OS. Thus the presence of CD45+CTLA-4+ TILs, in tumor environment of B3 and AB thymomas, might contribute to the profile of immunosuppression allowing unrestrained tumor progression due to impaired host immune surveillance.

The clinical implication of CTLA-4 expression in tumors or immune cells in the tumor microenvironment
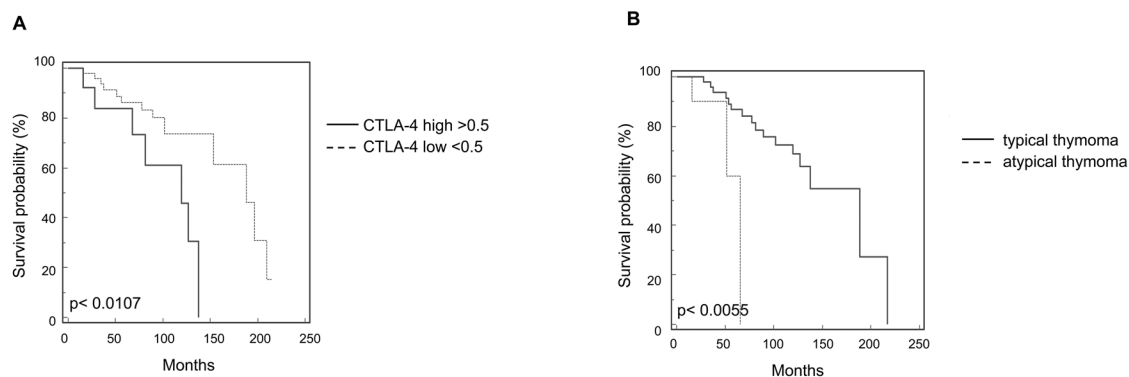
Figure 5: Kaplan-Meier curves of survival according to CTLA-4 expression and histological types. (A) Kaplan-Meier plot was evaluated stratifying patients according to CTLA-4 expression levels. (B) Kaplan-Meier plot was evaluated stratifying patients according to typical vs atypical thymoma subtypes.

Table 2: Univariate and multivariate analysis of overall survival in thymomas (Tumor CTLA-4 expression)

Variable	Univariate analyses			Multivariate analyses		
	HR	95% CI	P-value	HR	95% CI	P-value
-Tumor CTLA-4 expression	2.9987	1.4599	0.0107*	2.9301	1.2351	0.0235*
-Typical/Atypical	0.2170	0.029	0.0055*	0.1490	1.7970	0.0041*
-Myastenia Gravis	0.4874	0.2158	0.0889ns	0.6116	0.7171	0.1919ns
-Age	0.2145	0.0612	0.0002*	0.2971	1.6236	0.0071*
-Sex	1.4669	0.2516	0.4048ns	2.9641	0.4203	0.9807ns
-Tumor invasion	0.4150	0.6388	0.1745ns	0.4390	0.3312	0.5793ns
-Tumor dimension	0.4035	0.1634	0.0429*	0.3240	0.3814	0.6237ns
-Metastatic spread	1.4670	0.5050	0.5145ns	2.0072	0.4367	0.5149ns
-Radicality	1.7180	0.9976	0.0878ns	1.9703	0.9024	0.1531ns

Abbreviations: HR, hazard ratio; CI, confidence interval.
*$p < 0.05$; ns = not significant.

is still controversial, and the potential for CTLA-4 as prognostic and therapeutic marker has been complicated by differences in study population, methods and histological tumor types [53–54]. In agree with our results, univariate analysis demonstrates that higher tumor CTLA-4 expression is associated with shorter OS and poorer prognosis of patients with esophageal cancers [31]. Moreover in human breast cancer, high tumor CTLA-4 expression is associated with shorted OS, disease-free survival and worse prognosis [28]. The OS, failure-free survival and distant failure free survival rate was lower in nasopharyngeal carcinoma (NPC) patients and NPC patients with high tumor CTLA-4 levels [29]. By contrast, the CTLA-4 expression positively correlates with less advanced stage, intestinal type and well/moderately differentiated gastric adenocarcinoma [30] and represents a favorable prognostic factor in mesothelioma tissues, serum and
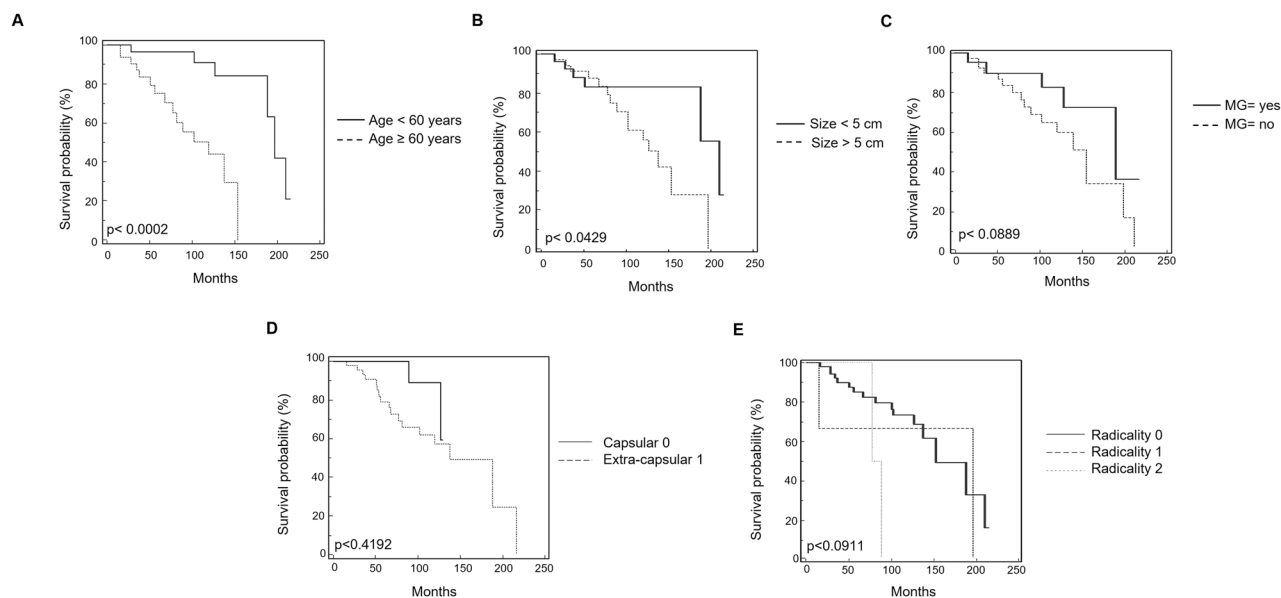
Figure 6: Kaplan-Meier curves of survival according to age, Myasthenia Gravis, tumor size, extra-capsular invasion and radicality. **(A)** Kaplan-Meier plot was evaluated stratifying patients by age. **(B)** Kaplan-Meier plot was evaluated stratifying patients according to the tumor size. **(C)** Kaplan-Meier plot was evaluated stratifying patients according to the presence or not of Miastenia Gravis. **(D)** Kaplan-Meier plot was evaluated stratifying patients according to the presence of extra-capsular invasion or capsular invasion. **(E)** Kaplan-Meier plot was evaluated stratifying patients according to the radicality. R0: complete tumor resection; R1: incomplete microscopic tumor resection; R2: incomplete macroscopic tumor resection.

pleural effusion [32]. Finally, a higher frequency of CTLA-4 overexpression was found in non-squamous as respect to squamous non-small cell lung cancer, and a reduced death rate was found in CTLA-4 overexpressing tumors [27].

Different cellular and murine models have been used to demonstrate that drugs inducing CTLA-4 blockade, used alone or in combination with other therapeutic interventions, improves endogenous responses to several tumor types, leading to tumor cell death when utilized. Treatment of CTLA-4 expressing tumor cell lines with recombinant forms of the CTLA-4 ligands CD80 and CD86 induced caspase-8-dependent apoptosis and the level of apoptotic tumor cells was reduced by soluble CTLA-4 and anti-CTLA-4 single-chain variable fragment antibodies [26]. Preclinical findings have been translated into the clinical development of two different CTLA-4 blocking Ab, ipilimumab (IPI) and tremelimumab [55–56]. Thus, antibody-mediated blockade of CTLA-4 may ultimately prove useful, either alone or in combination with other immune-based manipulations, have been successful employed in patients with metastatic melanoma, advanced prostate and pancreatic carcinomas [57–59], refractory B-cell non-Hodgkin lymphoma [60], early stage breast cancer [61] and we suggested it could be also used to improve the effectiveness of thymoma therapy. Moreover, in the view of increasing numbers of effective drugs available for treatment of thymoma, upfront identification of patients who are more likely to fail or benefit of treatment is the major unmet need. Regarding the use of IPI, thymoma patients showing high CTLA-4 expression could be benefit of immunotherapy with IPI. Thus, the higher CTLA-4 expression not only in Teff and Treg cells, but also in tumor cells, might facilitate tumor cellular lysis through an IPI-dependent cell-mediated cytoxicity by FcRγ expressing immune cells, such as monocytes for Treg [62] or natural killer and lymphocytes Tγδ for tumor cells [63]. In addition, CTLA-4 could also serve as a predictive biomarker for selecting the most appropriate therapy for thymoma patients and maximizing the clinical benefit with minimal toxicity. Other immunosuppressive co-stimulatory molecules, including PD-L1, PD-L2 remain under investigation in the context of thymomas and may similarly facilitate the downregulation of anti-tumor immune responses. In this regard, as demonstrated for PD-L1 immunotherapy, increased CTLA-4 expression where observed in patients undergoing adjuvant radiotherapy [64].

Overall, further clinical studies may be warranted to completely address the meaning of CTLA-4 expression in tumor cells and tumor-infiltrating leukocytes and/or of others co-stimulatory molecules to define the most effective treatment and prognosis in thymoma patients.

MATERIALS AND METHODS

Patients and thymoma specimens

The study population consisted of all consecutive patients aged 18 years or older (n = 68) who underwent surgery for thymomas from 1993 to 2013 at Università Politecnica delle Marche–Azienda Ospedaliero-Universitaria Ospedali Riuniti Umberto I – Lancisi – Salesi, Ancona, Italy. Other inclusion criteria included Eastern Cooperative Oncology Group performance status ≤ 2, adequate organ functions and no serious concomitant disease. All patients gave their consent and the local Ethical Committee approved the study (214439942015 approval number).

Paraffin-embedded tissues were prepared from surgically removed thymomas. Thick sections (5-7 μm) of thymoma tissues were collected and processed. Thymoma sections were stained with hematoxylin and eosin (H&E) and classified according to WHO histologic classification, in type A, AB, B1, B2, B3 and C, as well as Masaoka-Koga classification in I, IIA, IIB, III and IV stages.

Stimulation of PBMCs with PMA

PBMCs were isolated from whole blood of healthy donors (ASUR 9, Macerata) by density gradient centrifugation on a Lympholyte solution (Cederlane, Burlington, Canada). After washing, purified cells were counted and then 10^7 cells (1×10^6/ml) were treated with 5 ng/ml of PMA (Sigma Aldrich, St Louis, MO, USA) for 48 h at 37°C, 5% CO_2 and 95% of humidity in RPMI 1640 (Euroclone Ltd, Devon, UK) supplemented with 10% heat-inactivated fetal calf serum 2mM L-glutamine, 100 IU/ml of penicillin and 100 μg/ml of streptomycin (Euroclone Ltd). Untreated cells were used as control.

Tissues, RNA extraction and reverse transcription

Total RNA from unstimulated and PMA-stimulated PBMCs was extracted by RNeasy Mini Kit (QIAGEN, Milan, Italy) whereas from fixed paraffin-embedded tissue slices by using "RNeasy® FFPE" kit (Qiagen). Two different lots of RNA from human normal thymus were purchased from Zyagen (San Diego, USA) and Clontech (Mountain Valley, CA). All RNA samples were eluted in the appropriate buffer and their concentration and purity evaluated by 260/280nm measurement. Five hundred nanograms of RNA were subjected to reverse transcription in a total volume of 25 μl using the high-capacity cDNA archive kit (PE Applied Biosystems, Foster City, CA, USA) according to the manufacturer's instructions. Five microliters of the resulting cDNA products were pre-amplified for 10 cycles using kit "RT²

PreAMP cDNA Synthesis" (QIAGEN). Two microliters of the resulting preAmp products was used as template for PCR quantification employing "RT^2 qPCR Primer Assay" kit (QIAGEN).

Quantitative real time polymerase chain reaction (qRT-PCR)

qRT-PCR was performed by using IQ5 Multicolor real-time PCR detection system (BioRad, Hercules, CA, USA). The reaction mixture contained the RT^2 SYBR® Green qPCR Mastermix (QIAGEN), human CTLA-4 and GAPDH primers (RT^2 qPCR Primer Assay for Human CTLA-4 and GAPDH, QIAGEN). The PCR parameters were 10 min at 95°C followed by 40 cycles of 95°C for 15 s and 60°C for 40 s. All samples were assayed in triplicate in the same plate. The relative amount of target mRNA was calculated by the $2^{-\Delta\Delta Ct}$ method, using GAPDH as a housekeeping gene.

Immunohistochemistry (IHC)

For IHC, sections were pretreated in microwave for 10 min with Tris-HCl EDTA pH 9. After washes in PBS, sections were treated with 3% H_2O_2 for 20 min, washed, incubated for 1 h at room temperature with 3% bovine serum albumin and 0.3% Triton X-100 in PBS, and then overnight at 4°C with a mouse anti-CTLA-4 mAb (clone BNI3, isotype IgG2a, 1:100) (Novus Biologicals, Littleton, CO, USA). Thereafter, slides were incubated for 30 min at room temperature with a biotinylated secondary antibody, rinsed, and exposed for 30 min to the streptavidin–biotin complex (ABC Elite kit; Vinci Biochem, Vinci, Italy). Immunoreactivity was detected by the addition of diaminobenzidine (Vector, USA) for 5 min, counterstained with hematoxylin for 30 seconds and embedded in mounting medium. Four random fields of each tissue specimen were analyzed under 20X magnification using the Olympus BX51 Microscope and the Image J software (National Institutes of Health, Bethesda, MD, USA). The percentage of CTLA-4 positively stained cells was determined in all samples according to the staining intensity by the NIS Software (Nikon, Otawara, Japan). For each tumor specimens positive cells were counted in 10-fields of 0,5 mm^2.

Confocal microscope analysis

Sections were pre-treated in microwave for 10 min with Tris-HCl EDTA pH 9. After 2 washes in PBS sections were treated with 3% H_2O_2 for 20 min, washed, treated for 6 min with potassium permanganate solution (KMnO4 0.06%) and incubated for 1 h at room temperature with 3% bovine serum albumin and 0.3% Triton X-100 in PBS. After that sections were incubated overnight at 4°C with mouse anti-CTLA-4 mAb (Novus Biologicals, Littleton,

USA, clone BNI3, isotype IgG2a, 1:25) followed by anti-mouse IgG AlexaFluor 488 secondary Ab (Thermo Fisher Scientific corporation, Waltham, USA, 1:100) for 60 min at 37°C, then overnight at 4°C with mouse anti-human CD45 mAb (Dako, Glostrup, Denmark, clone 2B11+PD7/26, isotype IgG1, 1:50) followed by anti-mouse IgG1 AlexaFluor 594 secondary Ab (Thermo Fisher Scientific corporation, 1:100) for 60 min at 37°C. In some experiments sections were incubated overnight at 4°C with mouse anti-CTLA-4 mAb (1:25) followed by anti-mouse IgG2a AlexaFluor 594 secondary Ab (Thermo Fisher Scientific corporation, 1:100) for 60 min at 37°C, then overnight at 4°C with mouse anti-human Vimentin mAb (Sigma, Saint Louis, USA, clone V9, isotype IgG1, 1:50) followed by anti-mouse IgG AlexaFluor 488 secondary Ab (Thermo Fisher Scientific corporation, 1:100) for 60 min at 37°C. Finally sections were embedded in mounting medium. Four random fields of each tissue specimen were analysed under 40X magnification using the Confocal Microscopy Nikon C2plus and the NIS software (Nikon, Otawara, Japan). The CTLA-4 Fluorescence Intensity was evaluated in all samples by using the NIS Software. For each tumor specimens fluorescence intensity was evaluated in 10-fields of 0,5 mm^2. Moreover, to assess the contribution of CD45$^+$ cells and tumor cells in the CTLA-4 expression, the percentage of CD45$^+$CTLA-4$^+$ was evaluated in B2, B3 and AB samples according to the Fluorescence intensity and considering the total CTLA-4$^+$ cells as 100% by the NIS Software.

Statistical analysis

Statistical analysis was perfomed using One Way-Anova and Two Way-Anova with Bonferroni's post-test. In addition, the non-parametric Kruskal-Wallis with Dunn's multiple comparisons was used to analyze CTLA-4 expression between the different WHO thymoma type histological and Masaoka-Koga stages.

The significant contribute of adjuvant chemo- or radiotherapy on the CTLA-4 mRNA expression in thymoma patients was evaluated by unpaired t' test, $p < 0.05$.

OS were estimated using Kaplan-Meier method with Rothman's 95% confidence intervals (CI) and compared across the groups using the log-rank test. We determined by Relative Operating Characteristic (ROC) curve analysis the CTLA-4 mRNA value that best discriminated between good and poor survival. Then, patients were divided for age, sex, invasiveness, extra-capsular or capsular invasion, tumor dimension more or less 5 cm, concomitant myasthenia gravis, WHO histological types and on the basis of CTLA-4 mRNA expression in CTLA-4^{low}≤ 0.5 and High CTLA-4^{high} > 0.5 (evaluated by ROC analysis), and typical and atypical thymomas. Overall survival was defined as the interval between the date of surgery to death or last follow-up visit. These groups were subjected to univariate and multivariate

survival analysis. For survival analysis, the Kaplan-Meier method was used. For univariate analysis of significance, the long-rank test or Cox analysis was used. The Cox proportional hazards model was used for multivariate analysis. p< 0.05 was considered as statistically significant. Statistical analysis was performed with MedCalc package (MedCalc® v16.4.3).

Abbreviations

Cytotoxic T lymphocyte antigen 4 (CTLA-4), Overall Survival (OS), Myasthenia Gravis (MG), effector T cells (Teff), regulatory T cells (Treg), Peripheral Blood Mononuclear Cells (PBMCs), Phorbol 12-Myristate 13-acetate (PMA), Quantitative real time polymerase chain reaction (qRT-PCR), Tumor-infiltrating Leukocytes (TILs), Immunohystochemistry (IHC), Monoclonal Antibody (mAB), Thymic Epithelial Tumors (TETs), Single Nucleotide Polymorphisms (SNPs), Nasopharyngeal Carcinoma (NPC), Ipilimumab (IPI), Hematoxylin Eosin (H&E).

Author contributions

G.S., C.A., M.B.M., C.C., designed the research, performed the experiments, and analyzed the data. G.S. conceived of the research, supervised the work and wrote the paper. D.T. performed the experiments about Immunohistochemistry. C.A., M.B.M., M.N., O.M. contributed to data interpretation and manuscript preparation, and provided critical revisions to the manuscript. M.S., V.P., M.T., S.R., F.M., G.B. and R.B. provided critical revision of the intellectual content and text of the manuscript. All authors provided final approval of the version to be published.

ACKNOWLEDGMENTS

CONFLICTS OF INTEREST

The authors declare no conflicts of interest.

FUNDING

REFERENCES

1. Den Bakker MA, Roden AC, Marx A, Marino M. Histologic classification of thymoma: a practical guide for routine cases. J Thorac Oncol. 2014; 9:125–130.

2. Chen G, Marx A, Chen WH, Yong J, Puppe B, Stroebel P, Mueller-Hermelink HK. New WHO histologic classification predicts prognosis of thymic epithelial tumors: a clinicopathologic study of 200 thymoma cases from China. Cancer. 2002; 95:420–429.

3. Chalabreysse L, Roy P, Cordier JF, Loire R, Gamondes JP, Thivolet-Bejui F. Correlation of the WHO Schema for the Classification of Thymic Epithelial Neoplasms With Prognosis: A Retrospective Study of 90 Tumors. Am J Surg Pathol. 2002; 26:1605–1611.

4. Rieker RJ, Hoegel J, Morresi-Hauf A, Hofmann WJ, Blaeker H, Penzel R, Otto HF. Histologic classification of thymic epithelial tumors: comparison of established classification schemes. Int J Cancer. 2002; 98:900–906.

5. Suster S, Moran CA. Problem areas and inconsistencies in the WHO classification of thymoma. Semin Diagn Pathol. 2005; 22:188–197.

6. Detterbeck FC, Nicholson AG, Kondo K, Van Schil P, Moran C. The Masaoka-Koga stage classification for thymic malignancies: clarification and definition of terms. J Thorac Oncol. 2011; 6:1710–1716.

7. Marchevsky AM, Gupta R, McKenna RJ, Wick M, Moran C, Zakowski MF, Suster S. Evidence-based pathology and the pathologic evaluation of thymomas: the World Health Organization classification can be simplified into only 3 categories other than thymic carcinoma. Cancer. 2008; 112:2780–2788.

8. Moran CA, Suster S. The World Health Organization (WHO) Histologic Classification of Thymomas: a reanalysis. Curr Treat Options Oncol. 2008; 9:288–299.

9. Roden AC, Yi ES, Jenkins SM, Donovan JL, Cassivi SD, Garces YI, Marks RS, Aubry MC. Diagnostic significance of cell kinetic parameters in World Health Organization type A and B3 thymomas and thymic carcinomas. Hum Pathol. 2015; 46:17–25.

10. Moran CA, Weissferdt A, Kalhor N, Solis LM, Behrens C, Wistuba II, Suster S. Thymomas I: a clinicopathologic correlation of 250 cases with emphasis on the World Health Organization schema. Am J Clin Pathol. 2012; 137:444–450.

11. Miki Y, Hamada K, Yoshino T, Miyatani K, Takahashi K. Type AB thymoma is not a mixed tumor of type A and type B thymomas, but a distinct type of thymoma. Virchows Arch. 2014; 464:725–734.

12. Wilkins KB, Sheikh E, Green R, Patel M, George S, Takano M, Diener-West M, Welsh J, Howard H, Askin F, Bulkley GB. Clinical and Pathologic Predictors of Survival in Patients with Thymoma. Ann Surg. 1999; 230:562–574.

13. Desmedt JE. Nature of the defect of neuromuscular transmission in myasthenic patients: post-tetanic exhaustion. Nature. 1957; 179:156–157.

14. Engels EA. Epidemiology of thymoma and associated malignancies. J Thorac Oncol. 2010; 5:S260–265.

15. Salama AK, Hodi FS. Cytotoxic T-lymphocyte-associated antigen-4. Clin Cancer Res. 2011; 17:4622–4628.

16. Magistrelli G, Jeannin P, Herbault N, Benoit De Coignac A, Gauchat JF, Bonnefoy JY, Delneste Y. A soluble form of CTLA-4 generated by alternative splicing is expressed by nonstimulated human T cells. Eur J Immunol. 1999; 29:3596–3602.

17. Oaks MK, Hallett KM, Penwell RT, Stauber EC, Warren SJ, Tector AJ. A native soluble form of CTLA-4. Cell Immunol. 2000; 201:144–153.

18. Sharpe AH, Freeman GJ. The B7–CD28 superfamily. Nat Rev Immunol. 2002; 2:116–126.

19. Suwalska K, Pawlak E, Karabon L, Tomkiewicz A, Dobosz T, Urbaniak-Kujda D, Kuliczkowski K, Wolowiec D, Jedynak A, Frydecka I. Association studies of CTLA-4, CD28, and ICOS gene polymorphisms with B-cell chronic lymphocytic leukemia in the Polish population. Hum Immunol. 2008; 69:193–201.

20. Monne M, Piras G, Palmas A, Arru L, Murineddu M, Latte G, Noli A, Gabbas A. Cytotoxic T-lymphocyte antigen-4 (CTLA-4) gene polymorphism and susceptibility to non-Hodgkin's lymphoma. Am J Hematol. 2004; 76:14–18.

21. Kaufman KA, Bowen JA, Tsai AF, Bluestone JA, Hunt JS, Ober C. The CTLA-4 gene is expressed in placental fibroblasts. Mol Hum Reprod. 1999; 5:84–87.

22. Nagaraju K, Raben N, Villalba ML, Danning C, Loeffler LA, Lee E, Tresser N, Abati A, Fetsch P, Plotz PH. Costimulatory markers in muscle of patients with idiopathic inflammatory myopathies and in cultured muscle cells. Clin Immunol. 1999; 92:161–169.

23. Wang XB, Giscombe R, Yan Z, Heiden T, Xu D, Lefvert AK. Expression of CTLA-4 by human monocytes. Scand J Immunol. 2002; 55:53–60.

24. Wang XB, Fan ZZ, Anton D, Vollenhoven AV, Ni ZH, Chen XF, Lefvert AK. CTLA4 is expressed on mature dendritic cells derived from human monocytes and influences their maturation and antigen presentation. BMC Immunol. 2011; 12:21.

25. Pistillo MP, Tazzari PL, Palmisano GL, Pierri I, Bolognesi A, Ferlito F, Capanni P, Polito L, Ratta M, Pileri S, Piccioli M, Basso G, Rissotto L, et al. CTLA-4 is not restricted to the lymphoid cell lineage and can function as a target molecule for apoptosis induction of leukemic cells. Blood. 2003; 101:202–209.

26. Contardi E, Palmisano GL, Tazzari PL, Martelli AM, Falà F, Fabbi M, Kato T, Lucarelli E, Donati D, Polito L, Bolognesi A, Ricci F, Salvi S, et al. CTLA-4 is constitutively expressed on tumor cells and can trigger apoptosis upon ligand interaction. Int J Cancer. 2005; 117:538–550.

27. Salvi S, Fontana V, Boccardo S, Merlo DF, Margallo E, Laurent S, Morabito A, Rijavec E, Dal Bello MG, Mora M, Ratto GB, Grossi F, Truini M, et al. Evaluation of CTLA-4 expression and relevance as a novel prognostic factor in patients with non-small cell lung cancer. Cancer Immunol Immunother. 2012; 61:1463–1472.

28. Yu H, Yang J, Jiao S, Li Y, Zhang W, Wang J. Cytotoxic T lymphocyte antigen 4 expression in human breast cancer: implications for prognosis. Cancer Immunol Immunother. 2015; 64:853–860.

29. Huang PY, Guo SS, Zhang Y, Lu JB, Chen QY, Tang LQ, Zhang L, Liu LT, Zhang L, Mai HQ. Tumor CTLA-4 overexpression predicts poor survival in patients with nasopharyngeal carcinoma. Oncotarget. 2016; 7:13060–13068. https://doi.org/10.18632/oncotarget.7421.

30. Kim JW, Nam KH, Ahn SH, Park DJ, Kim HH, Kim SH, Chang H, Lee JO, Kim YJ, Lee HS, Kim JH, Bang SM, Lee JS, et al. Prognostic implications of immunosuppressive protein expression in tumors as well as immune cell infiltration within the tumor microenvironment in gastric cancer. Gastric Cancer. 2016; 19:42–52.

31. Zhang XF, Pan K, Weng DS, Chen CL, Wang QJ, Zhao JJ, Pan QZ, Liu Q, Jiang SS, Li YQ, Zhang HX, Xia JC. Cytotoxic T lymphocyte antigen-4 expression in esophageal carcinoma: implications for prognosis. Oncotarget. 2016; 7:26670–26679. https://doi.org/10.18632/oncotarget.8476.

32. Roncella S, Laurent S, Fontana V, Ferro P, Franceschini MC, Salvi S, Varesano S, Boccardo S, Vigani A, Morabito A, Canessa PA, Giannoni U, Rosenberg I, et al. CTLA-4 in mesothelioma patients: tissue expression, body fluid levels and possible relevance as a prognostic factor. Cancer Immunol Immunother. 2016; 65:909–917.

33. Erfani N, Razmkhah M, Talei AR, Pezeshki AM, Doroudchi M, Monabati A, Ghaderi A. Cytotoxic T lymphocyte antigen-4 promoter variants in breast cancer. Cancer Genet Cytogenet. 2006; 165:114–120.

34. Bouwhuis MG, Gast A, Figl A, Eggermont AM, Hemminki K, Schadendorf D, Kumar R. Polymorphisms in the CD28/CTLA4/ICOS genes: role in malignant melanoma susceptibility and prognosis? Cancer Immunol Immunother. 2010; 59:303–312.

35. Hadinia A, Hossieni SV, Erfani N, Saberi-Firozi M, Fattahi MJ, Ghaderi A. CTLA-4 gene promoter and exon 1 polymorphisms in Iranian patients with gastric and colorectal cancers. J Gastroenterol Hepatol. 2007; 22:2283–2287.

36. Ivansson EL, Juko-Pecirep I, Gyllensten UB. Interaction of immunological genes on chromosome 2q33 and IFNG in susceptibility to cervical cancer. Gynecol Oncol. 2010; 116:544–548.

37. Sun L, Meng Y, Xie Y, Zhang H, Zhang Z, Wang X, Jiang B, Li W, Li Y, Yang Z. CTLA4 variants and haplotype contribute genetic susceptibility to myasthenia gravis in northern Chinese population. PLoS One. 2014; 9:e101986.

38. Cilio CM, Daws MR, Malashicheva A, Sentman CL, Holmberg D. Cytotoxic T lymphocyte antigen 4 is induced in the thymus upon *in vivo* activation and its blockade prevents anti-CD3-mediated depletion of thymocytes. J Exp Med. 1998; 188:1239–1246.

39. Berardi R, De Lisa M, Pagliaretta S, Onofri A, Morgese F, Savini A, Ballatore Z, Caramanti M, Santoni M, Mazzanti P, Cascinu S. Thymic neoplasms: an update on the use

of chemotherapy and new targeted therapies. A literature review. Cancer Treat Rev. 2014; 40:495–506.

40. Berardi R, Morgese F, Garassino MC, Cascinu S. New findings on thymic epithelial tumors: something is changing. World J Clin Oncol. 2015; 6:96–98.

41. Berardi R, De Lisa M, Pagliaretta S, Paolucci V, Morgese F, Savini A, Caramanti M, Ballatore Z, Onofri A, Cascinu S. Thymic Malignancies in the Targeted Therapies Era. J Carcinog & Mutagen. 2014; S8:S8.

42. Chuang WY, Ströbel P, Gold R, Nix W, Schalke B, Kiefer R, Opitz A, Klinker E, Müller-Hermelink HK, Marx A. A CTLA4 high genotype is associated with myasthenia gravis in thymoma patients. Ann Neurol. 2005; 58:644–648.

43. Zheng K, Zhang J, Zhang P, Guo Y. PTPN22 and CTLA-4 gene polymorphisms in resected thymomas and thymus for myasthenia gravis. Thorac Cancer. 2012; 3: 307–312.

44. Wang XB, Kakoulidou M, Qiu Q, Giscombe R, Huang D, Pirskanen R, Lefvert AK. CDS1 and promoter single nucleotide polymorphisms of the CTLA-4 gene in human myasthenia gravis. Genes Immun. 2002; 3:46–49.

45. Maverakis E, Goodarzi H, Wehrli LN, Ono Y, Garcia MS. The etiology of paraneoplastic autoimmunity. Clin Rev Allergy Immunol. 2012; 42:135–144.

46. Toubi E, Shoenfeld Y. Protective autoimmunity in cancer (review). Oncol Rep. 2007; 17:245–251.

47. Maggi G, Casadio C, Cavallo A, Cianci R, Molinatti M, Ruffini E. Thymoma: results of 241 operated cases. Ann Thorac Surg. 1991; 51:152–156.

48. Laurent S, Queirolo P, Boero S, Salvi S, Piccioli P, Boccardo S, Minghelli S, Morabito A, Fontana V, Pietra G, Carrega P, Ferrari N, Tosetti F, et al. The engagement of CTLA-4 on primary melanoma cell lines induces antibody-dependent cellular cytotoxicity and TNF-α production. J Transl Med. 2013; 11:108.

49. Laurent S, Carrega P, Saverino D, Piccioli P, Camoriano M, Morabito A, Dozin B, Fontana V, Simone R, Mortara L, Mingari MC, Ferlazzo G, Pistillo MP. CTLA-4 is expressed by human monocyte-derived dendritic cells and regulates their functions. Hum Immunol. 2010; 71:934–941.

50. Bergholdt R, Taxvig C, Eising S, Nerup J, Pociot F. CBLB variants in type 1 diabetes and their genetic interaction with CTLA4. J Leukoc Biol. 2005; 77:579–585.

51. Ward FJ, Dahal LN, Wijesekera SK, Abdul-Jawad SK, Kaewarpai T, Xu H, Vickers MA, Barker RN. The soluble isoform of CTLA-4 as a regulator of T-cell responses. Eur J Immunol. 2013; 43:1274–1285.

52. Callahan MK, Wolchok JD, Allison JP. Anti-CTLA-4 antibody therapy: immune monitoring during clinical development of a novel immunotherapy. Semin Oncol. 2010; 37:473–484.

53. Hu P, Liu Q, Deng G, Zhang J, Liang N, Xie J, Zhang J. The prognostic value of cytotoxic T-lymphocyte antigen 4 in cancers: a systematic review and meta-analysis. Sci Rep. 2017; 7:42913.

54. Scorsetti M, Leo F, Trama A, D'Angelillo R, Serpico D, Macerelli M, Zucali P, Gatta G, Garassino MC. Thymoma and thymic carcinomas. Crit Rev Oncol Hematol. 2016; 99:332–50.

55. Ribas A, Kefford R, Marshall MA, Punt CJ, Haanen JB, Marmol M, Hauschild A. Phase III randomized clinical trial comparing tremelimumab with standard-of-care chemotherapy in patients with advanced melanoma. J Clin Oncol. 2013; 31:616–622.

56. Wolchok JD, Hodi FS, Weber JS, Allison JP, Urba WJ, Robert C. Development of ipilimumab: a novel immunotherapeutic approach for the treatment of advanced melanoma. Ann NY Acad Sci. 2013; 1291:1–13.

57. Hodi FS, O'Day SJ, McDermott DF, Weber RW, Sosman JA, Haanen JB, Gonzalez R, Robert C, Schadendorf D, Hassel JC, Akerley W, van den Eertwegh AJ, Lutzky J, et al. Improved survival with ipilimumab in patients with metastatic melanoma. N Engl J Med. 2010; 363:711–723.

58. Royal RE, Levy C, Turner K, Mathur A, Hughes M, Kammula US, Sherry RM, Topalian SL, Yang JC, Lowy I, Rosenberg SA. Phase 2 trial of single agent Ipilimumab (anti-CTLA-4) for locally advanced or metastatic pancreatic adenocarcinoma. J Immunother. 2010; 33:828–833.

59. Slovin SF, Higano CS, Hamid O, Tejwani S, Harzstark A, Alumkal JJ, Scher HI, Chin K, Gagnier P, McHenry MB, Beer TM. Ipilimumab alone or in combination with radiotherapy in metastatic castration-resistant prostate cancer: results from an open-label, multicenter phase I/II study. Ann Oncol. 2013; 24:1813–1821.

60. Ansell SM, Hurvitz SA, Koenig PA, LaPlant BR, Kabat BF, Fernando D, Habermann TM, Inwards DJ, Verma M, Yamada R, Erlichman C, Lowy I, Timmerman JM. Phase I study of ipilimumab, an anti-CTLA-4 monoclonal antibody, in patients with relapsed and refractory B-cell non-Hodgkin lymphoma. Clin Cancer Res. 2009; 15:6446–6453.

61. McArthur HL, Diab A, Page DB, Yuan J, Solomon SB, Sacchini V, Comstock C, Durack JC, Maybody M, Sung J, Ginsberg A, Wong P, Barlas A, et al. A pilot study of preoperative single-dose ipilimumab and/or cryoablation in women with early-stage breast cancer with comprehensive immune profiling. Clin Cancer Res. 2016; 22:5729–5737.

62. Romano E, Kusio-Kobialka M, Foukas PG, Baumgaertner P, Meyer C, Ballabeni P, Michielin O, Weide B, Romero P, Speiser DE. Ipilimumab-dependent cell-mediated cytotoxicity of regulatory T cells ex vivo by nonclassical monocytes in melanoma patients. Proc Natl Acad Sci U S A. 2015; 112:6140–6145.

63. Rajasekaran N, Chester C, Yonezawa A, Zhao X, Kohrt HE. Enhancement of antibody-dependent cell mediated cytotoxicity: a new era in cancer treatment. Immunotargets and Therapy. 2015; 4:91–100.

64. Formenti SC, Demaria S. Combining Radiotherapy and Cancer Immunotherapy: A Paradigm Shift. J Natl Cancer Inst. 2013; 105:256–265.

Structure−Activity Relationships and Computational Investigations into the Development of Potent and Balanced Dual-Acting Butyrylcholinesterase Inhibitors and Human Cannabinoid Receptor 2 Ligands with Pro-Cognitive in Vivo Profiles

Dominik Dolles,[†] Matthias Hoffmann,[†] Sandra Gunesch,[†] Oliviero Marinelli,[‡] Jan Möller,[§] Giorgio Santoni,[‡] Arnaud Chatonnet,[∥] Martin J. Lohse,[§] Hans-Joachim Wittmann,[⊥] Andrea Strasser,[⊥] Massimo Nabissi,[‡] Tangui Maurice,[#] and Michael Decker*,[†]

[†]Pharmaceutical and Medicinal Chemistry, Institute of Pharmacy and Food Chemistry, Julius Maximilian University of Würzburg, Am Hubland, D-97074 Würzburg, Germany

[‡]School of Pharmacy, Department of Experimental Medicine, University of Camerino, I-62032 Camerino, Italy

[§]Institute of Pharmacology and Toxicology, Julius Maximilian University of Würzburg, Versbacher Strabe 9, D-97078 Würzburg, Germany

[∥]INRA UMR866, University of Montpellier, F-34060 Montpellier, France

[⊥]Pharmaceutical and Medicinal Chemistry II, Institute of Pharmacy, University of Regensburg, D-95053 Regensburg, Germany

[#]INSERM UMR-S1198, University of Montpellier, EPHE, F-34095 Montpellier, France

S *Supporting Information*

ABSTRACT: The enzyme butyrylcholinesterase (BChE) and the human cannabinoid receptor 2 (hCB$_2$R) represent promising targets for pharmacotherapy in the later stages of Alzheimer's disease. We merged pharmacophores for both targets into small benzimidazole-based molecules, investigated SARs, and identified several dual-acting ligands with a balanced affinity/inhibitory activity and an excellent selectivity over both hCB$_1$R and hAChE. A homology model for the hCB$_2$R was developed based on the hCB$_1$R crystal structure and used for molecular dynamics studies to investigate binding modes. In vitro studies proved hCB$_2$R agonism. Unwanted μ-opioid receptor affinity

could be designed out. One well-balanced dual-acting and selective hBChE inhibitor/hCB$_2$R agonist showed superior in vivo activity over the lead CB$_2$ agonist with regards to cognition improvement. The data shows the possibility to combine a small molecule with selective and balanced GPCR-activity/enzyme inhibition and in vivo activity for the therapy of AD and may help to rationalize the development of other dual-acting ligands.
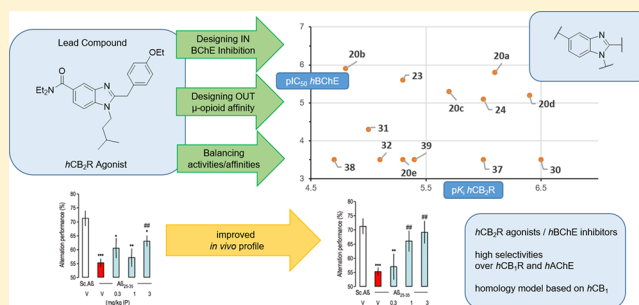
INTRODUCTION

Alzheimer's disease (AD) is the most common form of dementia. According to the annual Word Alzheimer Report, there are more than 47 million people suffering from AD. By 2050, researchers expect this number to climb up to even more than 130 million.[1] Currently, a cure is pending and pharmacotherapy is very limited. Three acetylcholinesterase (AChE) inhibitors (rivastigmine, donepezil, and galantamine) and one *N*-methyl-D-aspartate receptor (NMDA) antagonist (memantine) are currently available as drugs. Unfortunately, these drugs are only effective in early stages of AD, and they only act symptomatically but do not slow down progression or even cure AD.[2]

The reasons for an outbreak of this complex disease still remain unknown. AD is pathobiologically characterized by the presence of senile plaques, which consist of β-amyloid (Aβ). Aβ is an insoluble peptide and is formed by β/γ-secretase-induced cleavage of the amyloid precursor protein (APP). Another hallmark is the

formation of neurofibrillary tangles, which consist of hyperphosphorylated τ-protein aggregates. Once formed, both Aβ and τ-proteins trigger the progressive loss of muscarinergic neurons in the brain and lead to memory deficits and cognitive dysfunction.[3−5] Moreover, Aβ induces activation of neuroinflammatory pathways characterized by activated microglia and astrocytes as observed in the brains of AD patients.[6] Neuroinflammation then leads to the production of pro-inflammatory chemokines, cytokines, and neurotoxins, which speed up AD progression by themselves.[7] The exact sequence of these cascade processes is still under discussion.

In the past years, the human cannabinoid receptors (hCBRs) were identified as targets for drug development concerning neurodegenerative disorders. Currently, there are two known subtypes:

the human cannabinoid receptors 1 (hCB$_1$R) and 2 (hCB$_2$R). hCB$_1$Rs are mainly expressed in the brain;[8] hCB$_2$Rs were first described in the peripheral immune system[9] and then described to occur to a lower extent in the central nervous system (CNS), especially microglia.[10,11] In the course of AD, expression levels of hCB$_1$R do not change, but overexpression of hCB$_2$R is observed in certain brain regions (especially in the hippocampus) of AD patients.[12] Furthermore, CB$_2$R expression is associated with microglia and astrocytes that are surrounded by neuritic plaques.[13] The theory that up-regulation of CB$_2$R signaling leads to reduction of associated inflammatory processes[14] was substantiated in several in vitro studies: hCB$_2$R agonists reduce the production of neurotoxic factors, such as reactive oxygen species (ROS) and pro-inflammatory mediators (TNF-α and cytokines).[15−17] Furthermore, in vivo studies support the therapeutic potential of hCB$_2$R agonists: Wu et al. injected Aβ_{1-40} intracerebrally into rat brains and then treated the animals with MDA7, a known hCB$_2$R agonist. After 14 days, behavioral tests were performed (place learning in the Morris water maze) and the rat brains slices were then examined. MDA7 was found to promote Aβ clearance, to decrease secretion of proinflammatory mediators and ultimately led to restored synaptic plasticity, cognition, and memory.[18] In another study, transgenic Tg2576 mice that overexpress APP were continuously treated with JWH-133, another known hCB$_2$R agonist, at different stages of AD. As a result, Aβ production was lowered, reactive microglia cells were reduced, and a positive cognitive performance was observed.[19] The importance of CB$_2$R in Aβ formation was shown in J20APP mice (overexpression of APP in neocortex and hippocampus). Deletion of CB$_2$R led to an increased formation and deposition of Aβ, which supports CB$_2$R's role as a reducing agent of Aβ.[20] In summary, activation of hCB$_2$R leads to various beneficial effects concerning AD and additionally seems to play a central role in other neurodegenerative diseases such as Parkinson's and Huntington's disease.[21]

The oldest theory regarding AD pathophysiology is the "cholinergic hypothesis", which describes the massive loss of cholinergic neurons in AD.[22] The amount of acetylcholinesterase (AChE), the metabolizing enzyme of the neurotransmitter acetylcholine (ACh), decreases in the course of AD. However, the concentration of its isoenzyme butyrylcholinesterase (BChE) stays unchanged or even increases and is able to compensate for the loss of AChE, since BChE can also hydrolyze ACh into choline and acetate.[23,24] Besides that, it was shown that BChE (over-)expression is associated with senile plaques and the transformation of nonfibrillar to fibrillary Aβ plaques.[25,26] Inhibition of BChE is therefore a promising approach when it comes to combat AD's cognitive deficits, especially in later stages when AChE diminishes.[27] In a very recent in vivo study, BChE knockout mice showed enhanced learning abilities in memory tests as compared to wildtype littermates, and after intercerebroventricular injections of Aβ_{25-35} oligomers, BChE knockout mice appeared less sensitive to the learning and memory deficits, oxidative stress, and decrease in hippocampal ACh, as induced by the amyloid peptide in wildtype animals.[28] In another study, a sulfonamide-based nanomolar BChE inhibitor was investigated. In one of the very few in vivo studies that applied BChE-selective inhibitors, mice treated with this inhibitor showed improved memory and learning abilities in passive avoidance and Morris water maze tests without producing acute cholinergic adverse effects.[29]

Furthermore, it is remarkable that there's a colocalization of BChE and hCB$_2$Rs in microglia cells of the pathophysiologically altered branch. Glia cells play an important role in production of BChE and can be specifically targeted by CB$_2$R agonists.[30,31]

The multifactorial character of AD makes it difficult if not impossible to apply the classical "one target−one disease" for successful drug development.[32] It is therefore advantageous to develop multitarget drugs, which address different targets simultaneously. These drugs consist of two drug entities either as a hybrid linked by a spacer[33] or merged into one single entity;[32,34−36] for the latter case, only a few successful examples have been described. (For a review, see ref 35.) Hybrids addressing CBRs as one of the targets have been developed successfully.[37−39] In a remarkable recent work, Rampa et al. have achieved inhibiting both hBChE and fatty acid amide hydrolase (FAAH) and therefore target both the endocannabinoid and cholinergic system.[40] The main disadvantage of hybrid molecules is their (often) high molecular weight, which goes along with a violation of Lipinski's rule of five.[41] In contrast, merged ligands are still "small molecules" and their molar mass remains often at the same level as the "single compound".[35,36] In return, their development is more laborious. Both drug moieties have to be "fused" into one entity. The problem is that, if affinity is increased at one target, it is very likely decreased at the other one.[36,37] There are three common approaches to obtain such merged/dual-acting compounds: "designing in", "designing out", and "balancing". The most common approach is "designing in", where structural elements of two highly selective ligands are combined in one molecule, and the resulting compound then incorporates activity at the two desired targets. In a second approach, a merged compound not only possesses activity for two desired targets but also shows undesirable activity at a third target. In this case, "designing out" aims for excluding activity at the third, undesired target but keeping activity at the other two desired ones. In the third approach, a compound shows a very high affinity for one target but only moderate activity for the other target. Here, the aim is to balance the affinity at both desired targets.[32,35] Despite these difficulties, there are already several successful examples for merged ligands in the recent literature, such as adenosine A$_{2A}$ receptor/monoamine oxidase B ligands and human histamine H$_3$ receptor antagonists/AChE inhibitors developed in our group; the latter proved successful even in vivo.[42,43]

In our previous work,[36] we applied a novel pharmacophore model for BChE inhibitors to several benzimidazole-based selective hCB$_2$R agonists initially developed by AstraZeneca **A** (Figure 1)[44] in a "designing in" approach. A related merged structure based on indazole had been described before.[45] After the synthesis of various heterocyclic templates and applying various substitution patterns, we had obtained a first substance library and some compounds showed activity in the (sub)micromolar range at both targets and an excellent selectivity over both hCB$_1$R and AChE (Figure 1).[36] Furthermore, we conducted molecular dynamics (MD) simulations in both hCB$_2$R and BChE, which gave the first insights into the binding mode of our lead compounds **A** and **B** and helped the understanding of structure−activity relationships (SARs) at both targets.

In the present study, we developed our compound portfolio further by balancing activities at hCB$_2$R and BChE and by investigating and designing out unwanted interactions with the μ opioid receptor (MOP). We synthesized and characterized in a portfolio of in vitro assays 13 novel dual-acting hCB$_2$R ligands and BChE inhibitors. We furthermore investigated for the first time intrinsic activities at the hCB$_2$R for second and third generation compounds. Finally, we evaluated the ability of our second generation lead compound **B** to fight cognition deficits induced by intracerebroventricular (ICV) Aβ_{25-35} injections in mice, as an in vivo pharmacological model for AD.

K_i (hCB$_2$R) = 36.7 nM
24% displ. (hCB$_1$R) at 10 μM

IC$_{50}$ (eqBChE) = 9.7 μM
28% inhib. @ 100 μM (eeAChE)

K_i (hCB$_2$R) = 1.9 μM
13% displ. (hCB$_1$R) at 10 μM

IC$_{50}$ (eqBChE) = 0.7 μM
4% inhib. @ 100 μM (eeAChE)

K_i (hCB$_2$R) = 426.0 nM
45% displ. (hCB$_1$R) at 10 μM

IC$_{50}$ (eqBChE) = 3.7 μM
2% inhib. @ 100 μM (eeAChE)

K_i (hCB$_2$R) = 188.0 nM
14% displ. (hCB$_1$R) at 10 μM

IC$_{50}$ (eqBChE) = 2.3 μM
48% inhib. @ 100 μM (eeAChE)
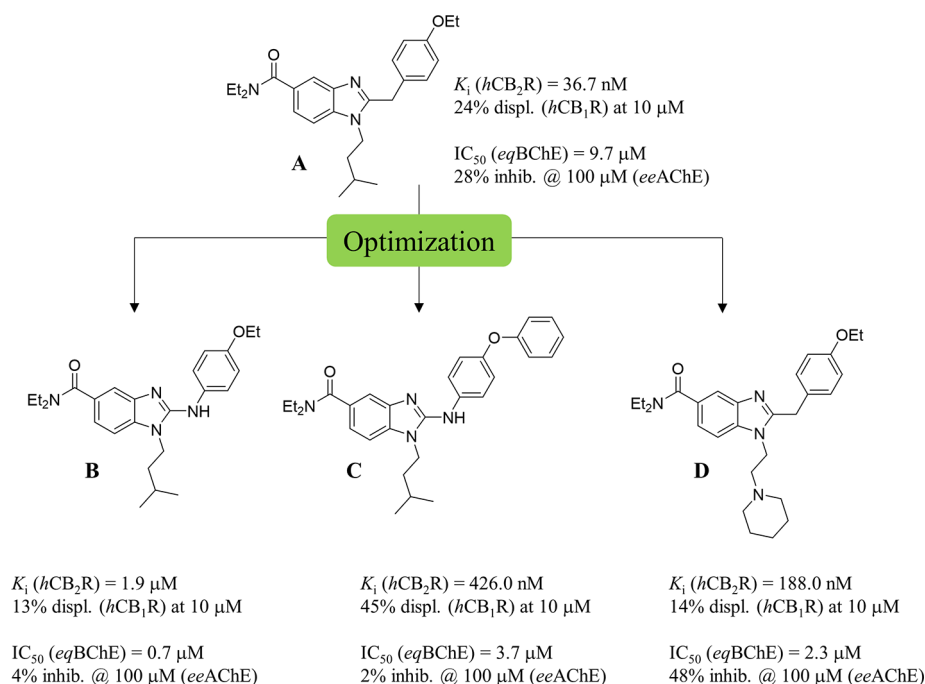
Figure 1. Development of the second generation lead structures **B**, **C**, and **D** starting from AstraZeneca's selective hCB$_2$R agonist **A**, the first generation lead.[36,44]
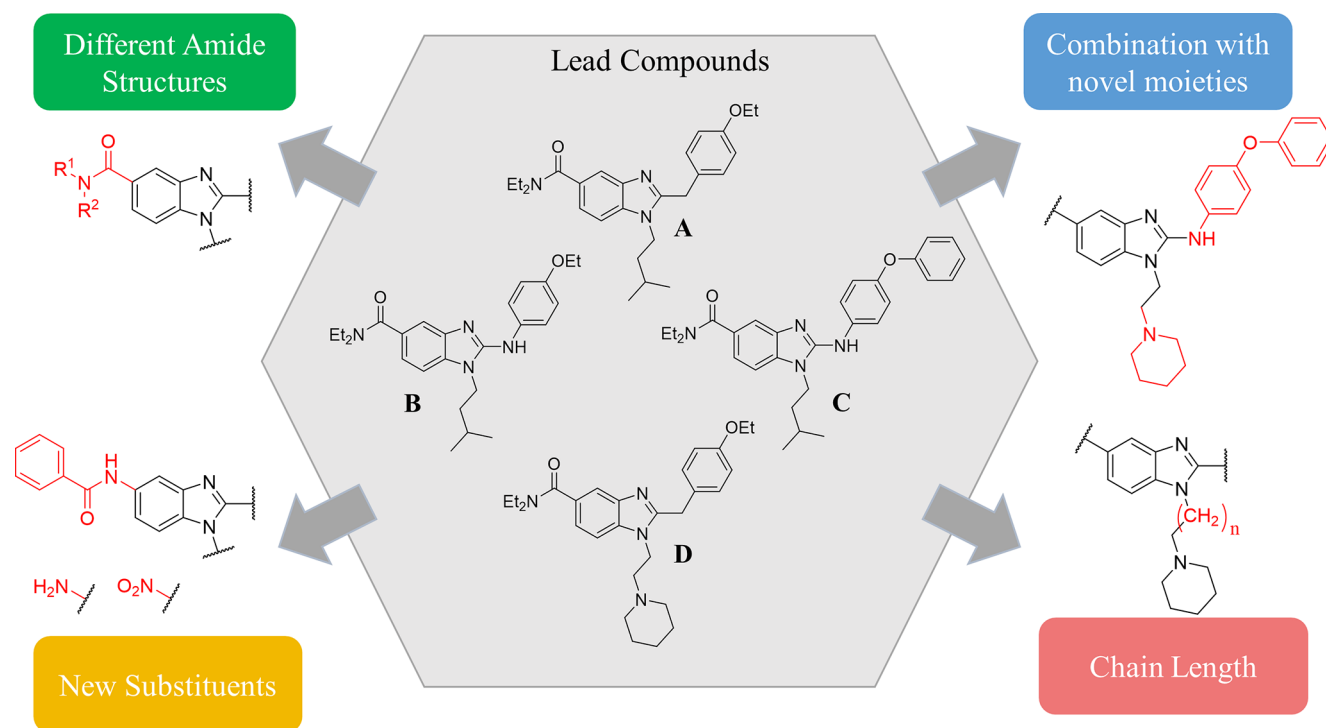
Figure 2. Structural compound design approaches carried out starting from lead compounds **A**−**D**.

RESULTS

Chemistry. The difficulty in designing a multitarget compound is to "fuse" drug entities and at the same time to keep or even improve the activity at both targets. The starting point for advanced synthetic approaches are Astra Zeneca's benzimidazole **A** as well as our second generation lead compounds **B**, **C**, and **D** described very recently (Figures 1 and 2).[36,44] These compounds already showed either a high affinity at one of the two targets or even a balanced micromolar activity profile. From these results, we followed several design approaches (Figure 2): the introduction of different amides (green) and substituents (yellow) at position 5 of the benzimidazole core, alternation of the chain length (red), and a combination of the most promising substitution patterns (blue). Before, we also had synthesized other heterocyclic templates such as amino-indazoles, but the compounds lost affinity at all targets.[36] Therefore, we returned to the initial structural template.

The necessity of a (diethyl)amide for a high hCB$_2$R affinity had been previously demonstrated,[36,44] but data for inhibition of either AChE or BChE of several amides was not available. The

electron-withdrawing character of amides led us using substituents with different electronic effects (e.g., nitro and amino) at position 5 of the benzimidazole core. Ethylenepiperidinyl substitution at the N^1 of the benzimidazole core already caused (sub)micromolar activity at both hCB$_2$R and BChE. The aim was to extend the alkylene chain and to increase lipophilicity and interaction between the side chain and the oxyanion hole of the BChE.[36] Lastly, we combined the most promising substituents in order to increase dual-activity.

Specifically, the synthesis of benzimidazoles and 2-amino benzimidazoles was carried out as previously reported starting from 4-fluoro-3-nitrobenzoic acid **1**.[36] To introduce the different amide moieties in the last step, esterification was performed to obtain ester **2**. For the synthesis of target compounds **23**, **24**, and **30−32**, the diethylamide moiety **3** was formed using HBTU as the coupling agent. In the next step, nucleophilic substitution with various amines afforded compounds **4−8**. Reduction of the nitro group was achieved using tin(II) to obtain o-phenylenediamines **9−13** (Scheme 1).

Scheme 1. Synthesis of o-Phenylene Diamine Precursors 9−13[a]
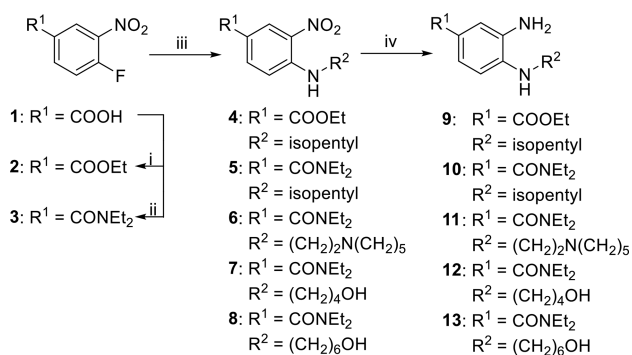
^{a}Conditions: (i) H$_2$SO$_4$, EtOH, reflux, 24 h; (ii) HNEt$_2$, (COCl)$_2$, NEt$_3$, DMF, 0 °C to rt, 5 h; (iii) NHR^2, NEt$_3$, EtOH, rt, 3 h; (iv) SnCl$_2$·2H$_2$O, EtOH, reflux, 6 h.

To obtain benzimidazoles with various amide moieties and spacer lengths, diamines **9**, **12**, and **13** were coupled with 2-(4-ethoxyphenyl)acetic acid to afford compounds **14−16**. Cyclization was achieved in glacial acetic acid, and benzimidazoles **17−19** were obtained in quantitative yields. Ester **17** was hydrolyzed under basic conditions and then coupled with various amines using HBTU as a coupling agent. After purification, amides **20a−e** were obtained in high yields. For various spacer lengths, hydroxy compounds **18** and **19** were treated in an Appel-like reaction with phosphorus tribromide to obtain the bromo compounds **21** and **22**. In the last step, bromine was substituted with piperidine under basic conditions to afford compounds **23** and **24** (Scheme 2).

The synthesis of 2-amino benzimidazoles was performed as previously reported.[36] Upon reaction of benzylic and anilinic amines **25a−c** with carbon disulfide, isothiocyanates **26a−c** were obtained.[46] Thiourea derivatives **27−29** were afforded by reacting the respective isothiocyanates with o-phenylenediamine **10** or **11**. Cyclization was carried out using EDCI as a coupling reagent, and 2-amino benzimidazoles **30−32** were obtained (Scheme 3).

For the introduction of electron-withdrawing/donating functions at position 5 of the benzimidazole core, a different synthetic approach was applied. Starting from 1-chloro-2,4-dinitro benzene **33**, nucleophilic substitution with isopentylamine led to compound **34** in quantitative yields. Selective reduction of the 2-nitro moiety to obtain o-phenylenediamine **35** was carried out according to Freitag et al.[47] using sodium sulfide as a reducing agent. Amide coupling and cyclization were carried out as described above. 5-Nitro benzimidazole **37** was reduced by tin(II) to afford 5-amino benzimidazole **38**. In the final step, HBTU-mediated amide coupling with benzoic acid afforded compound **39** (Scheme 4).
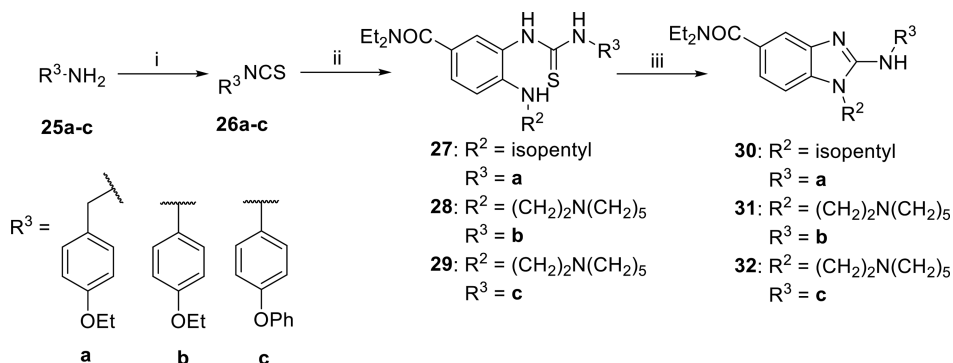
Pharmacological Profile of Dual-Acting Compounds. All target compounds were tested for affinity to hCB$_1$R and hCB$_2$R in radioligand binding studies (HEK cells stably expressing hCB$_2$R; CHO cells stably expressing hCB$_1$R). Inhibition of AChE (eeAChE, E.C.3.1.1.7, from electric eels and hAChE, E.C.3.1.1.7, from humans) and BChE (hBChE, E.C.3.1.1.8, from humans) was evaluated in the colorimetric Ellman's assay (Table 1). Sequence alignment had shown that the isoform eeAChE exhibits a very high sequence homology to the human enzyme (88% sequence identity)[48] (Table 1).

Scheme 2. Synthesis of Benzimidazoles with Different Amide Moieties or Spacer Lengths[a]
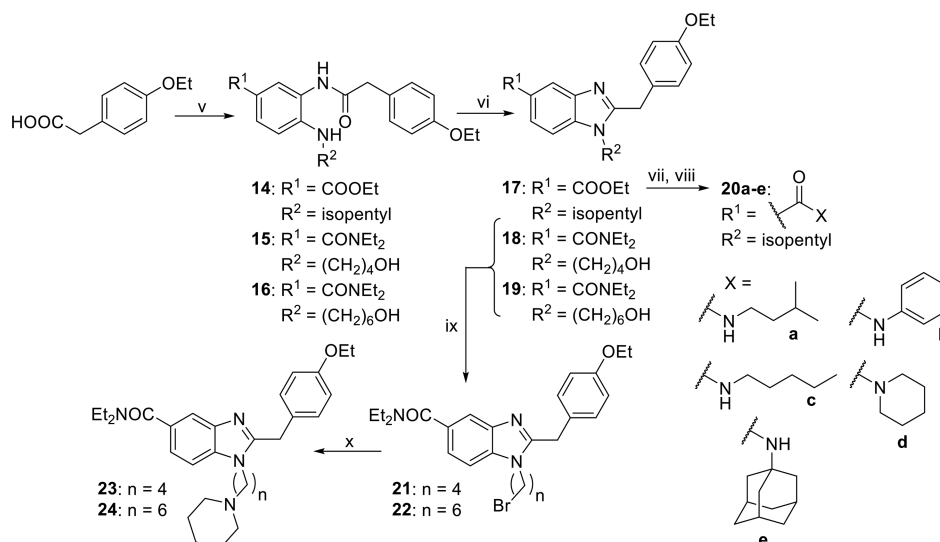
^{a}Conditions: (v) o-phenylene diamine **9**, **12**, or **13**, HBTU, NEt$_3$, DMF, rt, 24 h; (vi) AcOH, reflux, 2 h; (vii) LiOH, THF/H$_2$O, rt, 24 h; (viii) primary and secondary amines **a−e**, HBTU, NEt$_3$, DMF, rt, 24 h; (ix) PBr$_3$, CH$_2$Cl$_2$, 0 °C to rt, 12 h; (x) piperidine, K$_2$CO$_3$, DMF, 70 °C, 12 h.

Scheme 3. Synthesis of 2-Amino Benzimidazoles[a]

27: R^2 = isopentyl R^3 = **a**
28: R^2 = $(CH_2)_2N(CH_2)_5$ R^3 = **b**
29: R^2 = $(CH_2)_2N(CH_2)_5$ R^3 = **c**

30: R^2 = isopentyl R^3 = **a**
31: R^2 = $(CH_2)_2N(CH_2)_5$ R^3 = **b**
32: R^2 = $(CH_2)_2N(CH_2)_5$ R^3 = **c**

[a]Conditions: (i) CS_2, NEt_3, Boc_2O, THF, 0 °C to rt, 12 h; (ii) o-phenylene diamine **10** or **11**, THF, rt, 6 h; (iii) EDCI·HCl, NEt_3, THF, reflux, 5 h.

Scheme 4. Synthesis of Benzimidazoles with Electron-Withdrawing/Donating Substituents at Position 5[a]
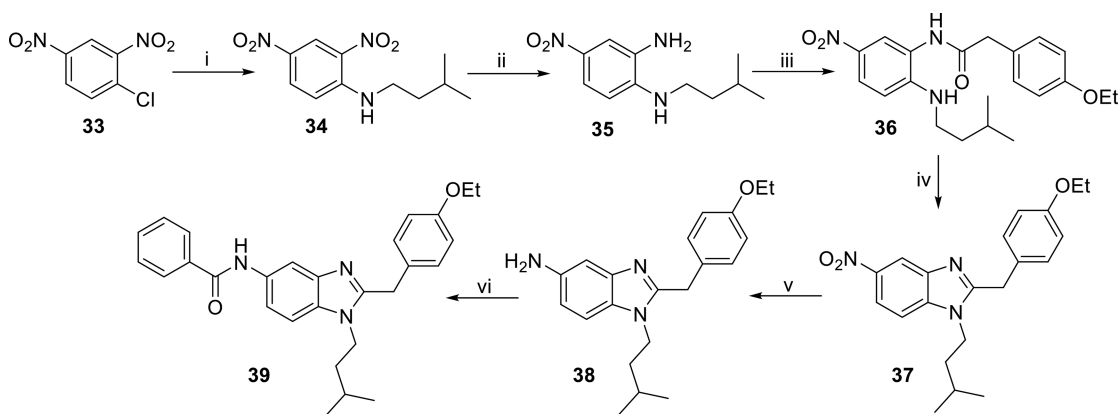
[a]Conditions: (i) isopentylamine, NEt_3, EtOH, rt, 24 h; (ii) $Na_2S \cdot H_2O$, $NaHCO_3$, $MeOH/H_2O$, reflux, 4 h; (iii) 2-(4-ethoxyphenyl)acetic, HBTU, NEt_3, DMF, rt, 12 h; (iv) AcOH, reflux, 6 h; (v) $SnCl_2 \cdot 2H_2O$, EtOH, reflux, 6 h; (vi) benzoic acid, HBTU, NEt_3, DMF, rt, 6 h.

In the first set of compounds, we kept the benzimidazole scaffold of lead compound **A** and introduced different amide moieties at position 5 of the benzimidazole core (**20a−d**). While **20c**, with a straight N-alkyl chain, shows a low micromolar affinity toward hCB_2R and a micromolar inhibition of BChE, compound **20a**, with a branched N-alkyl chain, shows a micromolar inhibition of BChE as well as a submicromolar affinity toward hCB_2R (**20a**, $K_i(hCB_2R)$ = 763.3 nM and $IC_{50}(hBChE)$ = 1.6 μM; **20c**, $K_i(hCB_2R)$ = 1.9 μM and $IC_{50}(hBChE)$ = 5.2 μM; Table 1). When we replaced the straight/branched N-alkyl chains with a 1-piperidinyl amide (**20d**), the activity at BChE did not change, but the affinity for hCB_2R could be increased (**20d**, $K_i(hCB_2R)$ = 384.5 nM and $IC_{50}(hBChE)$ = 5.7 μM; Table 1). It is furthermore remarkable that the introduction of a 1-piperidinyl amide (**20d**), which is similar to AstraZeneca's benzimidazole **A**, resulted in some, albeit moderate, regain in affinity toward hCB_1R ($K_i(hCB_1R)$ = 17.0 μM; Table 1). The introduction of a sterically demanding 1-adamantyl amide scaffold (**20e**), a typical CB pharmacophore, resulted in a complete loss of activity at both ChEs. The affinity at hCB_2R still was in the micromolar range (**20e**, $K_i(hCB_2R)$ = 4.7 μM; Table 1), which suggests a tolerance of hCB_2R concerning bulky and nonpolar substituents at position 5 of the benzimidazole core. Lastly, we introduced an aniline amide (**20b**), which kept micromolar activity at BChE but led to an approximately 10-fold decreased affinity at hCB_2R compared to other investigated amides (**20a−e**) (**20b**, $K_i(hCB_2R)$ = 14.4 μM and $IC_{50}(hBChE)$ = 1.2 μM; Table 1). We also introduced a "flipped" amide, where the amine moiety is directly attached to

the benzimidazole (**39**). Compound **39** is a structural isomer of **20b** and surprisingly shows a different pharmacological profile. While **20b** shows a one-digit micromolar activity at BChE and two-digit affinity at hCB_2R (Table 1), **39** completely lost inhibitory activity at BChE, but the affinity toward hCB_2R is increased compared to compound **20b** (**39**, $K_i(hCB_2R)$ = 4.3 μM; **20b**, $K_i(hCB_2R)$ = 14.4 μM; Table 1).

With another set of compounds, we investigated the influence of electron-withdrawing/donating substituents at position 5 of the benzimidazole core, which was otherwise not altered (**37** and **38**). Our assumption was based on our previous results from computational studies[36] that an electron-withdrawing substituent is crucial for any affinity/activity at both hCB_2R and BChE. We could confirm this by completely losing activity at BChE and dramatically decreasing affinity at hCB_2R when we introduced an amino moiety (**38**). Moreover, an electron-withdrawing nitro substituent (**37**) achieved a submicromolar affinity at hCB_2R, but again it completely lost the ability to inhibit BChE (**37**, $K_i(hCB_2R)$ = 961.8 nM; Table 1).

For a third set, we synthesized a set of "combination" compounds using scaffolds from our lead compounds **B**, **C**, and **D** and combining them in several 2-amino benzimidazoles (**31** and **32**). With this, we obtained **32**, a combination of the para-phenoxy phenyl moiety from **C** and ethylene piperidinyl from **D**, and **31**, which combine the para-ethoxy phenyl moiety of **B** with the ethylene piperidinyl moiety of **D**. Both compounds failed to show the desired pharmacological profile though. While affinity at hCB_2R decreased compared to the lead compounds **B−D**

Table 1. Results of the Biological Evaluation of the Inhibitory Effect of AChE/BChE and Radioligand Binding Studies at hCB$_1$R/hCB$_2$R

No.	X	R^1	R^2	R^3	hBChE IC$_{50}$ (pIC$_{50}$ ± SD) or % Inhibition	AChE[c, d] IC$_{50}$ (pIC$_{50}$ ± SD) or % Inhibition	hCB$_2$R[a] K_i (pIC$_{50}$ ± SD) or [^{3}H]CP55,950 displ. at 10 μM	hCB$_1$R[b] K_i (pIC$_{50}$ ± SD) or [^{3}H]CP55,950 displ. at 10 μM
Tacrine					9.1 nM (8.0 ± 0.0)	18.5 nM[c] (7.7 ± 0.0)	n.d.	n.d.
Rimonabant					n.d.	n.d.	4.0%	143.0 nM (6.8 ± 0.1) 25.0 nM [49]
SR-144,528					n.d.	n.d.	19.7 nM (7.7 ± 0.1) 5.6 nM [50]	687.0 nM (6.1 ± 0.1) 254.0 nM [50]
A	CH$_2$	NEt$_2$	isopentyl	4-OEt phenyl	2 % at 10 μM	6 %[c] at 100 μM	36.7 nM [36] (7.4 ± 0.1)	24 % [36]
B	NH	NEt$_2$	isopentyl	4-OEt phenyl	3 % at 10 μM	13 %[c] at 10 μM	1.9 μM [36] (5.7 ± 0.1)	13 % [36]
C	NH	NEt$_2$	isopentyl	4-OPh phenyl	0 % at 10 μM	3 %[c] at 10 μM	426.0 nM [36] (6.3 ± 0.2)	45 % [36]
D	CH$_2$	NEt$_2$	piperidinyl-propyl	4-OEt phenyl	36.8 μM (4.4 ± 0.1)	12 %[c] at 10 μM	188.0 nM [36] (6.7 ± 0.1)	14 % [36]
20a	CH$_2$	N-isopentyl (NH)	isopentyl	4-OEt phenyl	1.6 μM (5.8 ± 0.1)	3 %[d] at 25 μM / 11 %[c] at 10 μM	763.6 nM (6.1 ± 0.1)	37 %
20b	CH$_2$	NH-Ph	isopentyl	4-OEt phenyl	1.2 μM (5.9 ± 0.1)	2 %[d] at 10 μM / 5 %[c] at 10 μM	14.4 μM (4.8 ± 0.2)	18 %
20c	CH$_2$	N-hexyl (NH)	isopentyl	4-OEt phenyl	5.2 μM (5.3 ± 0.1)	9 %[d] at 10 μM / 6 %[c] at 10 μM	1.9 μM (5.7 ± 0.5)	39 %
20d	CH$_2$	piperidinyl	isopentyl	4-OEt phenyl	5.7 μM (5.2 ± 0.1)	8 %[d] at 10 μM / 2 %[c] at 10 μM	384.5 nM (6.4 ± 0.4)	17.0 μM (4.8 ± 0.2)
20e	CH$_2$	NH-Adamantyl	isopentyl	4-OEt phenyl	1 % at 10 μM	5 %[d] at 10 μM	4.7 μM (5.3 ± 0.4)	31 %
23	CH$_2$	NEt$_2$	piperidinyl-(CH$_2$)$_3$	4-OEt phenyl	2.7 μM (5.6 ± 0.1)	20.5 μM[d] (4.7 ± 0.2) / 60.1 μM[c] (4.2 ± 0.2)	4.8 μM (5.3 ± 0.2)	2 %

(**31**, K_i(hCB$_2$R) = 10.4 μM; **32**, K_i(hCB$_2$R) = 8.9 μM), both compounds completely lost inhibitory activity at BChE. Nevertheless, both compounds are still selective hCB$_2$R ligands. Compound **30** was developed by using the 2-amino benzimidazole scaffold from lead compound **B** and changing the *para*-ethoxy phenyl to a *para*-ethoxy benzyl moiety. With the additional methylene

Table 1. continued

No.	X	R^1	R^2	R^3	hBChE IC$_{50}$ (pIC$_{50}$ ± SD) or % Inhibition	AChE$^{c,\ d}$ IC$_{50}$ (pIC$_{50}$ ± SD) or % Inhibition	hCB$_2$R^a K_i (pIC$_{50}$ ± SD) or [^{3}H]CP55,950 displ. at 10 μM	hCB$_1$R^b K_i (pIC$_{50}$ ± SD) or [^{3}H]CP55,950 displ. at 10 μM
24	CH$_2$	NEt$_2$	(piperidinyl-pentyl chain)	(OEt-phenyl)	8.2 μM (5.1 ± 0.1)	11.9 μM^d (4.9 ± 0.1) / 20.0 μM^c (4.7 ± 0.1)	1.0 μM (5.9 ± 0.1)	4 %
30	NH	NEt$_2$	(isopentyl)	(OEt-phenyl)	4 % at 50 μM	7 %^{d} at 50 μM	353.4 nM (6.4 ± 0.1)	21 %
31	NH	NEt$_2$	(piperidinyl-ethyl)	(OEt-phenyl)	53.4 μM (4.3 ± 0.1)	18 %^{d} at 100 μM / 3 %^{c} at 10 μM	10.4 μM (4.9 ± 0.2)	17 %
32	NH	NEt$_2$	(piperidinyl-ethyl)	(OPh-phenyl)	4 % at 25 μM	3 %^{d} at 25 μM	8.9 μM (5.1 ± 0.2)	37 %
37	CH$_2$	NO$_2$	(isopentyl)	(OEt-phenyl)	12 % at 50 μM	14 %^{d} at 50 μM	961.8 nM (6.0 ± 0.2)	41 %
38	CH$_2$	NH$_2$	(isopentyl)	(OEt-phenyl)	39 % at 100 μM	15 %^{d} at 100 μM	21.0 μM (4.7 ± 0.1)	27 %
39	CH$_2$	Ph-C(O)-NH	(isopentyl)	(OEt-phenyl)	25 % at 10 μM	2 %^{d} at 10 μM	4.3 μM (5.4 ± 0.4)	36 %

(benzimidazole core structure with R^1, R^2, R^3, N, N, X labels)

^{a}Screened on membranes of HEK cells stably expressing hCB$_2$R using 10 μM of the compound; values are mean values from at least 2 independent experiments performed in triplicates. K_i value was determined when displacement of [^{3}H] CP 55,940 was >50%, mean values of at least 2 independent experiments performed in triplicates. ^{b}Screened on membranes of CHO cells stably expressing hCB$_1$R using 10 μM of the compound; values are mean values from at least 2 independent experiments performed in triplicates. K_i value was determined when displacement of [^{3}H] CP 55,940 was >50%, mean values of at least 2 independent experiments. ^{c}Values are means of at least three determinations. AChE from human erythrocytes. n.d. = not determined ^{d}Values are means of at least three determinations. AChE from electric eel. Also included in this table, see references 36, 49, and 50.

group, a higher degree of freedom is achieved and the conjugated system is interrupted, which may increase basicity and thereby interaction with BChE. Compared to lead compound **B**, affinity toward hCB$_2$R increased; selectivity was kept (**30**, K_i(hCB$_2$R) = 353.4 nM), but again inhibition of both ChEs was lost.

On the basis of our previous computational studies, which indicated a binding cavity in the oxyanion hole of the BChE and the N^1-alkyl chain pointing toward it,[36] we changed the length of the ethylene piperidinyl moiety of our lead structure **D**. We synthesized N^1-substituted benzimidazoles with a butylene (**23**) and a hexylene spacer (**24**) with the aim to increase lipophilicity and interactions between the side chain and the oxyanion hole of the BChE. Compared to the structurally similar lead compound **D** with an ethylene spacer, both compounds **23** and **24** show an approximately 10-fold decreased affinity toward hCB$_2$R (**23**, K_i(hCB$_2$R) = 4.8 μM; **24**, K_i(hCB$_2$R) = 1.0 μM; Table 1), with an improved selectivity over hCB$_1$R. Regarding BChE, both compounds indeed showed a low micromolar activity at BChE (**23**, IC$_{50}$(hBChE) = 2.7 μM; **24**, IC$_{50}$(hBChE) = 8.2 μM; Table 1) but lose selectivity over AChE with longer alkylene spacers

(**23**, IC$_{50}$(eeAChE) = 20.5 μM; **24**, IC$_{50}$(eeAChE) = 11.9 μM; Table 1). When tested at the hAChE, both compounds showed a similar inhibitory activity (**23**, IC$_{50}$(hAChE) = 60.1 μM; **24**, IC$_{50}$(hAChE) = 20.0 μM; Table 1).

Since lead compounds **A−D** were previously only tested at the eqBChE and eeAChE (Figure 1), we also investigated activity at both human enzymes, hBChE and hAChE. Surprisingly, lead compounds **A−D**, which showed a (sub)micromolar activity at eqBChE, completely lost significant activity at hBChE. In contrast, values for hAChE were very similar to the eeAChE (Figure 1 and Table 1). We recommend using the human enzyme whenever possible, which is in the literature rarely done in the development of BChE inhibitors, probably due to its high price.[27b] Some heterocyclic templates can show pronounced differences in inhibitory activities between species, so for each template, we recommend at least to test representative compounds at hBChE to check whether interspecies-dependent BChE inhibition occurs.[27c]

We were able to successfully develop a set of second-generation benzimidazole/2-aminobenzimidazole compounds, which nearly all show good selectivity for both hCB$_2$R and hBChE

with affinity/activity in the micromolar to submicromolar range. Furthermore, our best compounds show a well-balanced activity profile at both targets. A balanced profile is one of the main difficulties in designing merged dual-active compounds.

For a better comparison of all compounds and investigating/describing SARs, we correlated pK_i values from hCB$_2$R and pIC_{50} values from hBChE in Figure 3. Interpretation is greatly
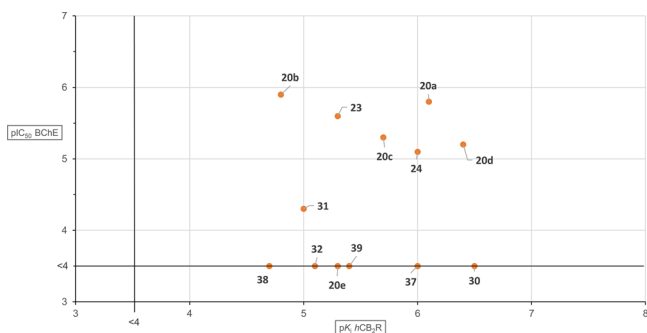
Figure 3. Plot of IC_{50} values for hBChE inhibition against pK_i values of hCB$_2$R affinity. Compounds with no significant affinity for one of the targets are placed on the black lines.

simplified by the fact that the majority of compounds still show a high selectivity over both hCB$_1$R and AChE.

Computational Studies, Construction of the Active-State Model of the hCB$_2$R, and Docking of Compounds

20a and 20d. Computationally driven multitarget drug discovery has emerged recently as a subfield of computational drug design, and it uses fragment-based approaches to identify multitarget hits in silico or deals with optimizing multitarget hits, e.g., by application of molecular dynamics (MD) [ref 51 and references cited herein].

Within a previous study, an active state model of the hCB$_2$R was constructed based on the crystal structure of the active human β_2R adrenergic receptor ($h\beta_2$R).[36] Since a crystal structure of the hCB$_1$R in complex with the agonist AM11542 ((6aR,10aR)-3-(8-bromanyl-2-methyl-octan-2-yl)-6,6,9-trimethyl-6a,7,10,10a-tetrahydrobenzo[c]chromen-1-ol) was published (PDB ID: 5XRA),[52] a new homology model of the hCB$_2$R based on this crystal structure was constructed because the homology between the hCB$_2$R and the hCB$_1$R is considerably higher than between the hCB$_2$R and the $h\beta_2$R. For the alignment of the amino acid sequences between the hCB$_1$R and the hCB$_2$R (Figure 4), the most conserved amino acid of each transmembrane (TM) domain according to Ballesteros and Weinstein[53] (marked by an asterisk) was used as reference.

For homology modeling of the hCB$_2$R, the software package SYBYL 7.0 (Tripos Inc.) was used. The flavodoxin of the hCB$_1$R crystal was deleted. The first 18 amino acids of the N-terminus and the last 44 amino acids of the C-terminus were not included in the hCB$_2$R homology model because these parts are not solved in the crystal structure of the hCB$_1$R. All amino acids that were different between the sequence of the hCB$_1$R (inclusive
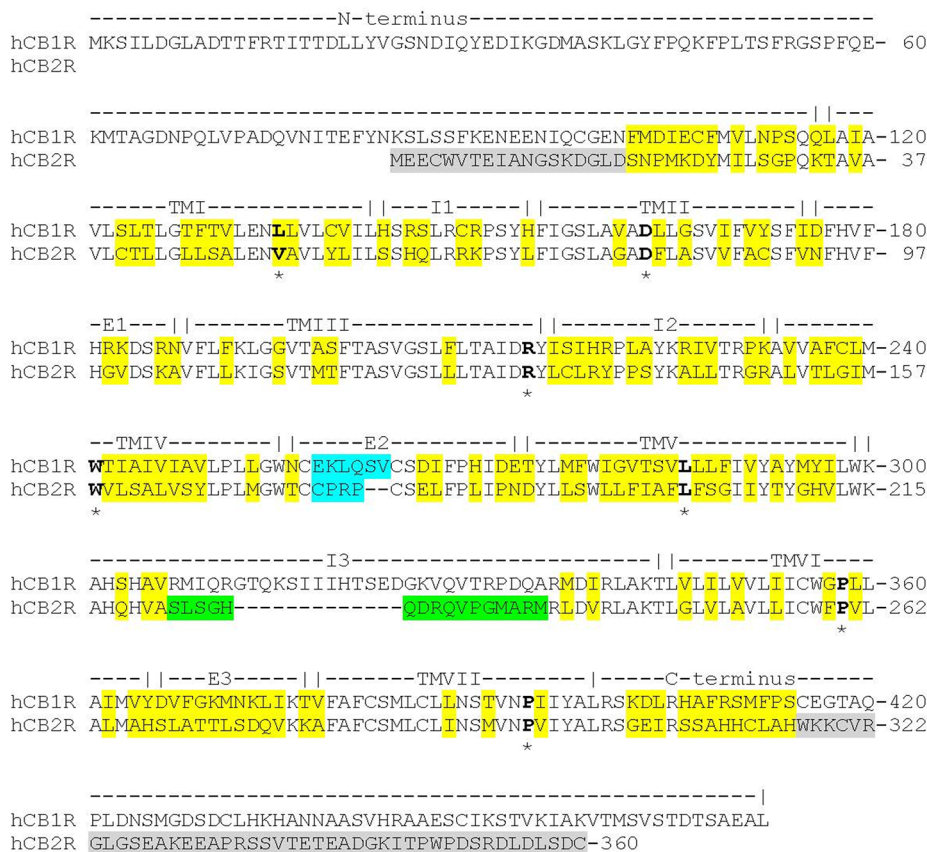
Figure 4. Amino acid sequence alignment of the hCB$_1$R (UniProtKB accession code: P21554) and the hCB$_2$R (UniProtKB accession code: P34972). Asterisk: highly conserved amino acids, according to the Ballesteros and Weinstein nomenclature. Yellow boxes: amino acids, different between hCB$_1$R and hCB$_2$R. Gray boxes: amino acids of the hCB$_2$R, not included in the homology model within the present work. Cyan boxes: part of the E2-loop, deleted in the hCB$_1$R template and inserted by "LoopSearch" according to the amino acid sequence of the hCB$_2$R. Green boxes: part of the I3-loop of the hCB$_2$R, inserted by "LoopSearch".

mutations in the X-ray structure) and the hCB$_2$R were mutated into the corresponding amino acid of the hCB$_2$R, except these parts of the extracellular loop E2 and the intracellular loop I3, marked in Figure 4: To model the E2-loop, the amino acids Glu258 (hCB$_1$R) to Val263 (hCB$_1$R) were deleted and the missing amino acids of the hCB$_2$R Cys175 to Pro178 were inserted, using the "LoopSearch" module of SYBYL 7.0 (Figure 4, cyan boxes). Furthermore, to model the I3-loop, the amino acids Ser222 to Met237 of the hCB$_2$R were inserted, using the "LoopSearch" module of SYBYL 7.0 (Figure 4, green boxes). Compounds **20a** and **20d** were docked manually in two different poses (mode 1 and mode 2), inspired by the AM11542-hCB$_1$R-crystal structure (5XRA), into the binding pocket of the hCB$_2$R (Figure 5).
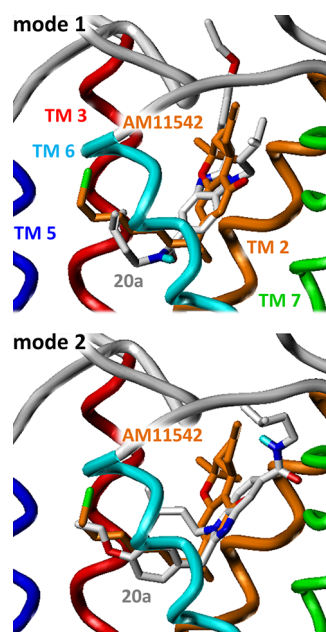
Figure 5. Docking poses (mode 1 and mode 2) of **20a** compared to the pose of compound AM11542 in the hCB$_1$R-crystal structure (5XRA).

Molecular Dynamics Simulations at the hCB$_2$R. The ligand–receptor complex, constructed with SYBYL 7.0, as described above was embedded in a POPC lipid bilayer. The parametrization for the ligands **20a** and **20d** was obtained from the PRODRG server (davapc1.bioch.dundee.ac.uk/prodrg/). For the generation of the complete simulation box (6.9 nm × 6.9 nm × 9.2 nm) and subsequent molecular dynamics simulations, the software package GROMACS 4.0.2 (www.gromacs.org) was used. Intracellular and extracellular water molecules were added using the command "genbox". To achieve electroneutrality, 5 sodium and 17 chloride ions were added using the command "genion". After minimization of the simulation box, MD simulations (10 ns equilibration phase and 10 ns productive phase) were performed for the ligand-free hCB$_2$R and the ligand–hCB$_2$R complexes, as described previously.[54,55]

Binding Mode of Compounds 20a and 20d at the hCB$_2$R. For compounds **20a** and **20d**, MD simulations for both binding modes 1 and 2 were performed. For **20a**, the short-range Coulomb and Lennard-Jones interactions amounted to ca. −19 kJ/mol and ca. −277 kJ/mol for mode 1 and ca. −44 kJ/mol and ca. −290 kJ/mol for mode 2. Similarly, for **20d**, the short-range Coulomb and Lennard-Jones interactions amounted to ca. −25 kJ/mol and ca. −246 kJ/mol for mode 1

and ca. −63 kJ/mol and ca. −260 kJ/mol for mode 2. Because mode 2 is the more stable one in both cases, subsequent data analysis was performed only on this mode. Since the orthosteric binding pocket of the hCB$_2$R is mainly formed by the aromatic amino acids Phe$^{3.36}$, Phe183 (E2-loop), Trp$^{5.43}$, and Trp$^{6.48}$, an aromatic moiety of the ligand in this region of the binding site should be preferred with respect to a more aliphatic one. Thus, for ligands containing an aromatic moiety in side chain R^1 and in side chain R^3, e.g., **20b**, both modes should be considered.

The ligands **20a** and **20d** are stably embedded (mode 2) in the orthosteric binding pocket of the hCB$_2$R (Figure 6).
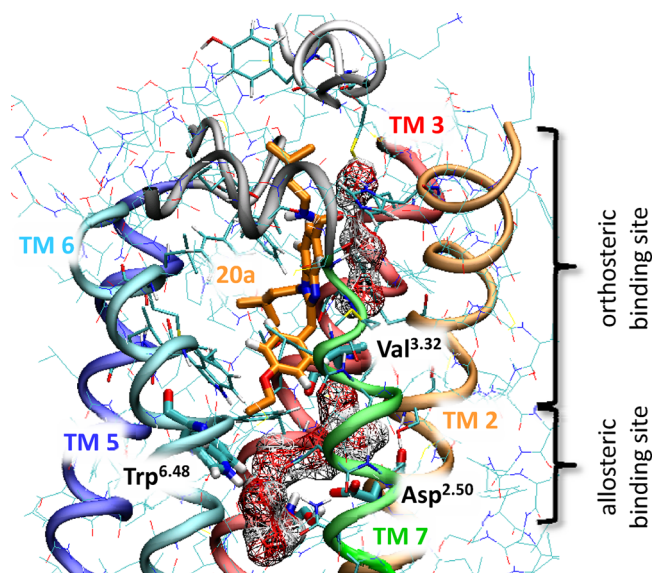

Figure 6. Orthosteric binding pocket of the hCB$_2$R with compound **20a** as well as internal water molecules and the allosteric binding site, as obtained by MD simulations.
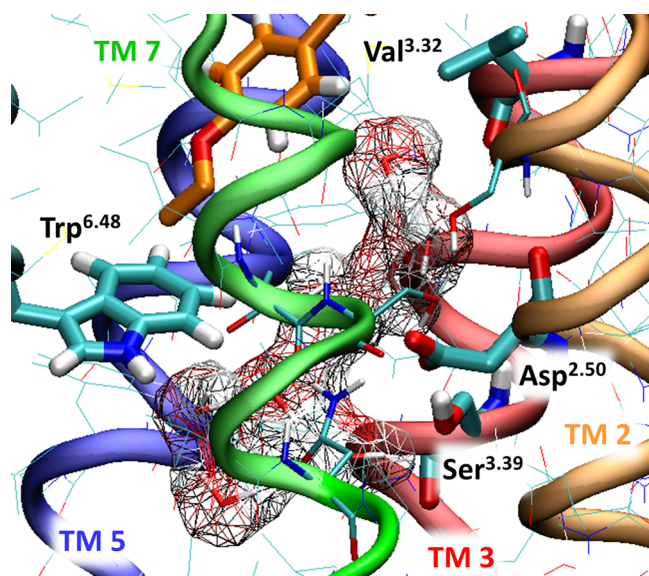
For compound **20a**, the benzimidazole core interacts with Phe$^{2.57}$, Phe183 (E2-loop), and Phe$^{7.35}$ (Figure 7a). The aliphatic side chain R^1 is embedded in a subpocket at the extracellular domains of the hCB$_2$R. The isopentyl moiety (R^2) is well-embedded in a hydrophobic pocket, formed by the amino acids Ile$^{3.29}$, Val$^{3.32}$, Thr$^{3.33}$ (methyl group), Phe$^{3.36}$, Phe183 (E2-loop), Ile186 (E2-loop), Leu$^{5.40}$, Trp$^{5.43}$, Leu$^{5.44}$, Val$^{6.51}$, and Met$^{6.55}$ (Figure 7b). The 4-ethoxybenzyl moiety (R^3) is embedded in a hydrophobic pocket, mainly formed by the amino acids Phe$^{3.36}$, Trp$^{6.48}$, Val$^{6.51}$, Met$^{6.55}$, and Leu$^{7.41}$ (Figure 7c). During ∼33% of the whole productive phase, a direct H-bond between the carbonyl oxygen of **20a** and the OH moiety of Ser$^{7.39}$ was observed. Alternatively, the interaction between **20a** and the hCB$_2$R was stabilized by a water-mediated H-bond interaction between the CO moiety of **20a** and Ser$^{7.39}$ or His$^{2.65}$ (Figure 7d).

Furthermore, the MD simulations of the **20a**−hCB$_2$R complex revealed a well-established interaction network between the highly conserved Asn$^{7.49}$, Asn$^{7.45}$, Trp$^{6.48}$, Ser$^{3.39}$, Asp$^{2.50}$, and internal water molecules (Figure 8). A comparable water chain was also revealed by MD simulations for the histamine H$_3$ and H$_4$ receptor.[56] Thus, at the hCB$_2$R, the allosteric Asp$^{2.50}$ binding site, which is described as the Na$^+$ binding site for several GPCRs[57] is well-connected with the orthosteric ligand binding site. Because the highly conserved amino acids of the allosteric binding site may be involved in receptor activation, it may be speculated that ligands (e.g., agonists), bound to the orthosteric binding site, may transfer information for activation of the receptor
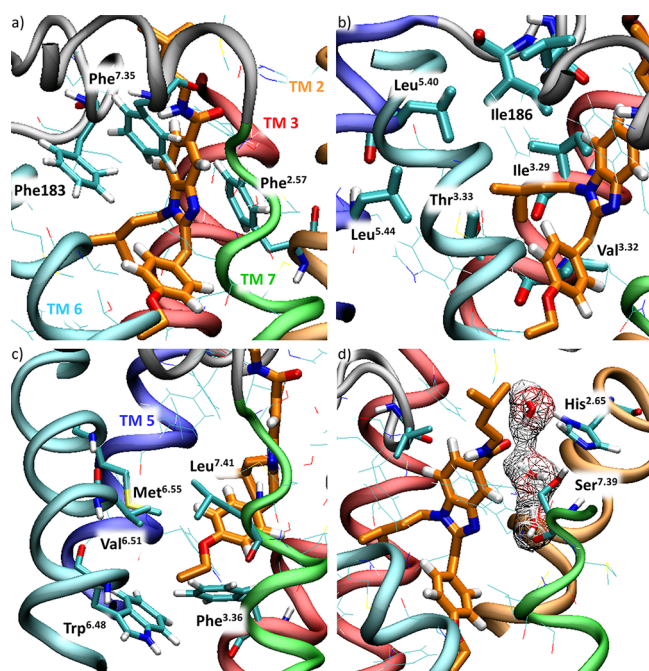
Figure 7. Interaction sites of the hCB$_2$R with (a) the benzimidazole core (R^2), (b) the isopentyl side chain (R^2), (c) the 4-ethoxy phenyl moiety (R^3), and (d) the carbonyl moiety (mediated by water molecules) of compound **20a**.

Figure 8. Interaction network between the hCB$_2$R and internal water molecules between the orthosteric (Val$^{3.32}$) and allosteric (Asp$^{2.50}$) binding site, obtained by MD simulations in the presence of **20a**.

downstream not only by the highly conserved amino acids but also by the internal water molecules located in this region.

Compared to **20a**, the MD simulations revealed different binding modes for **20d** (Figure 9): For compound **20d**, the benzimidazole core interacts with Phe$^{2.57}$, Phe$^{2.61}$, Phe183 (E2-loop), and Phe$^{7.35}$. The piperidine moiety R^1 is embedded in a subpocket at the extracellular domains of the hCB$_2$R, mainly formed by the amino acids Phe$^{2.61}$, Leu182, Leu$^{6.54}$, and Lys$^{7.32}$ (aliphatic part). The isopentyl moiety (R^2) is well-embedded in a hydrophobic pocket, formed by the amino acids Val$^{2.56}$, Phe$^{3.25}$, Lys$^{3.28}$ (aliphatic part), and Ile$^{3.29}$. The 4-ethoxybenzyl moiety (R^3) is
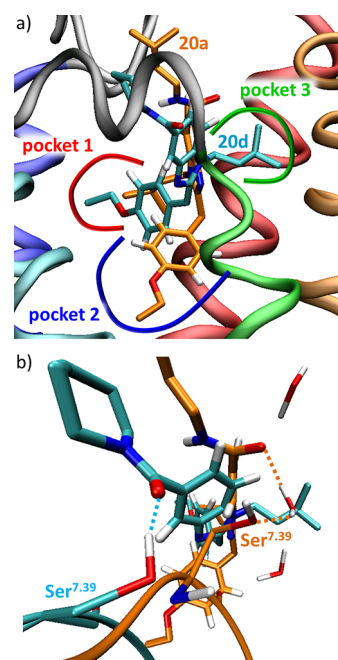
Figure 9. (a) Overlay of **20a** and **20d** in the binding pocket of the hCB$_2$R, obtained by MD simulations. (b) Differences in H-bond interactions between the hCB$_2$R and **20a** or **20d**.

embedded in a hydrophobic pocket, mainly formed by the amino acids Ile$^{3.29}$, Val$^{3.32}$, Thr$^{3.33}$ (methyl group), Phe$^{3.36}$, Phe183 (E2-loop), Ile186 (E2-loop), Leu$^{5.40}$, Trp$^{5.43}$, Leu$^{5.44}$, Val$^{6.51}$, and Met$^{6.55}$ (Figure 9a). During ~95% of the whole productive phase, a direct H-bond between the carbonyl oxygen and the OH moiety of Ser$^{7.39}$ was observed. However, in contrast to **20a**, the H-bond to His$^{2.65}$ was not observed and there was no water-mediated interaction between the ligand and the receptor (Figure 9b). An overlay of **20a** and **20d** in the binding pocket of the hCB$_2$R, obtained by MD simulations, is presented in Figure 9: The moiety R^1 points for both ligands toward the extracellular region of the receptor. The isopentyl moiety (R^2) is located in pocket 1 in the case of **20a** and in pocket 3 in the case of **20d**. The 4-ethoxy phenyl moiety (R^3) is located in pocket 2 in the case of **20a** and in pocket 1 in the case of **20d**. Consequently, the benzimidazole core of **20d** is twisted about 45° with respect to **20a**.

Since pocket 1 (Ile$^{3.29}$, Val$^{3.32}$, Thr$^{3.33}$, Phe$^{3.36}$, Phe183, Ile186, Leu$^{5.40}$, Trp$^{5.43}$, Leu$^{5.44}$, Val$^{6.51}$ and Met$^{6.55}$) is formed by aromatic and aliphatic side chains, ligands comprising of one or more of these moieties may be able to establish more than one binding pose. In this context two orientations of ligand **20a** (R^2 aliphatic) as well as **20d** (R^3 aromatic/aliphatic) are to be considered. Furthermore, it can be speculated that an equilibrium between different binding poses may be established depending on the chemical nature of the moieties R^1, R^2 and R^3. Since the two ligands differ in R^1, which points into the extracellular domain, this group may influence the equilibrium of different binding poses.

Determination of Efficacy at hCB$_2$R. CB$_2$Rs are coupled through G$_{i/o}$ proteins and negatively regulate adenylate cyclase, the enzyme that catalyzes the conversion of adenosine triphosphate (ATP) to cyclic adenosine monophosphate (cAMP).[58] One of the notable CB$_2$R biological responses is the regulation of intracellular cAMP levels. CB$_2$R agonists decrease cAMP levels and revert forskolin-stimulated cAMP production, while CB$_2$R antagonists/reverse agonists increase cAMP levels and enhance forskolin-stimulated cAMP production in cell lines.[59] So the
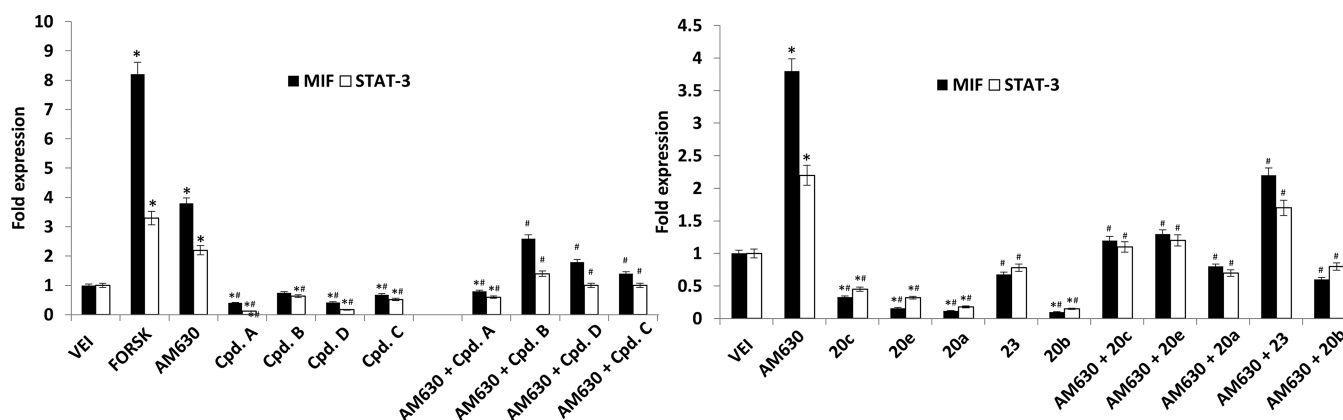
Figure 10. Test compounds (**A−D, 20a−c, 20e,** and **23**) reduce MIF and STAT-3 gene expression. U266 cells were treated with test compounds (50 μM), forskolin (10 μM), or AM630 (25 μM) for 2 h. In combination experiment (AM630 plus test compounds), U266 cells were preincubated with AM630 for 30 min before adding the test compounds. MIF and STAT-3 mRNA levels were determined by qRT-PCR. GAPDH was used for normalization. Data are expressed as relative fold with respect to vehicle-treated cells used as the control. Data are expressed as mean $\pm$ SD *$p < 0.01$ vs untreated; # vs AM630.

detection of the cAMP concentration, for example, by ELISA, is a common method for the identification of CB$_2$R ligand activity. In addition, receptor-mediated changes in the intracellular cAMP concentration can be detected via changes in the expression level of particular genes, which are regulated by the transcription factor cAMP response-element binding (CREB) protein binding to upstream cAMP response elements (CREs).[60] Between potential cAMP-target genes, macrophage migration inhibitory factor (MIF), which is highly expressed in multiple myeloma, is under cAMP-induced expression, since a functional cAMP-responsive element (CRE) in the proximal region of the MIF promoter is detected.[61,62] Signal transducer and activators of transcription (STAT-3) is another gene highly expressed in multiple myeloma cells, and its expression is also under CRE promoter control.[63,64]

Before evaluating the CB$_2$R activity of the compounds, the nontoxic concentration of each compound was evaluated by an MTT assay, and the IC$_{50}$ values were determined. U266 myeloma cells were treated with different concentrations of each compound (up to 100 μM) for 48 h, and the cell viability was calculated. As shown in Figure S1 of the Supporting Information, the compounds show different cytotoxic activity in U266 cells, with each IC$_{50}$ value over 40 μM, calculated at 48 h post-treatment.

To evaluate the biological activity of the compounds (as agonist or antagonist/reverse agonist), a cAMP assay was applied. U266 cell lines were treated for 2 h with forskolin (10 μM) as the cAMP-inducer, AM630 (25 μM) as the CB$_2$R antagonist/reverse agonist or with test compounds (50 μM) alone, and in combination with AM630, respectively. In combination treatment, U266 cells were pretreated with AM630 for 30 min and then treated with the single test compounds. In the cAMP assay, we found that forskolin increased the cAMP levels (as expected) and so did AM630 (by inhibiting CB$_2$R basal activity), compared to vehicle-treated cells (Figure S2 of the Supporting Information).

All of the test compounds decreased cAMP levels compared to vehicle, indicating that they are CB$_2$R agonists. To further confirm this data, test compounds were incubated in competition with AM630, and the results revealed that the compounds were able to revert AM630-increased cAMP levels (Figure S2 of the Supporting Information). By summarizing these results, we confirmed that test compounds **A−D** act, with different potency, as CB$_2$R agonists.

Since changes in the cAMP concentration can be detected via changes in expression level of specific genes regulated by the

CREB binding to upstream cAMP response elements (CREs), we selected two genes that are under cAMP-regulated transcription, the macrophage migration inhibitory factor (MIF) and the signal transducer and activator of transcription 3 (STAT-3). First, U266 cells were treated with forskolin to confirm that MIF and STAT-3 are under cAMP-induced transcription. As shown, both gene levels increase compared with vehicle-treated cells (Figure 10), confirming that this assay can show changes in the cAMP levels. Then, U266 cells were treated with test compounds **A−D** alone and in combination with AM630. The results show that AM630 increases the expression of MIF and STAT-3, confirming that AM630 increases the cAMP levels (Figure 10), as previously evidenced by cAMP ELISA, while all of our test compounds reduced MIF and STAT-3 expression levels compared with vehicle-treated cells and reduced AM630-induced MIF and STAT-3 when coincubating our test compounds and AM630 (Figure 10).

Herein, we confirmed that AM630 was able to increase cAMP production in U266 cells and that all compounds tested were able to reduce basal cAMP levels and to reverse the AM630-induced increase of cAMP concentration. An additional sensitive tool for evaluating variation in intracellular cAMP levels is the detection of CREB-induced gene expression.[65,66] In this context, the transcription of two genes highly expressed in U266 cells, MIF and STAT-3, were found to be under CREB regulation.[62,63] So, we applied a RT/PCR methodology to evaluate the MIF and STAT-3 gene expression levels in U266 cells. This experimental approach confirmed that AM630 as well as forskolin, by increasing the cAMP levels, induced MIF and STAT-3 expression, while test compounds reduced MIF and STAT-3 gene expression levels both when used alone or when combined with AM630. Since all of this data was strongly evidenced by cAMP ELISA and RT/PCR, we were able to characterize the agonist activity of test compounds and this data provides evidence that the entire set of test compounds acts as CB$_2$R agonists, further confirming the data obtained by the cAMP ELISA assay.

***μ*-Opioid Receptor Binding.** As already described above, dual-acting compounds have been developed to be applied for a variety of different targets in various diseases. One example is merged/dual-acting μ-opioid (MOP) receptor agonists/neuronal nitric oxide synthase (*n*NOS) inhibitors for the treatment of pain. Such a set of compounds was designed by Renton et al. on the basis of several NOS inhibitors and etonitazene, a well-known

MOP receptor agonist developed in the 1960s.[67,68] During the development of our own dual-acting compounds, we came across etonitazene, which shows strong structural similarities: an electron-withdrawing substituent at position 5 of the benzimidazole core (red), a 4-ethoxybenzyl moiety at position 2 (green), and a basic amine linked with an ethylene bridge to N^1 (blue), with the latter structural feature only shown by some of our compounds (Figure 11). On the basis of these observations,

Etonitazene **D**

$K_i(MOP) = 0.2$ nM
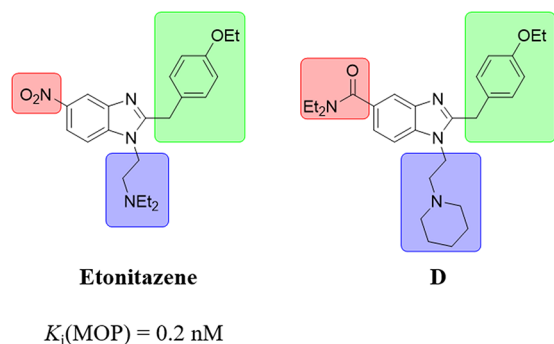
Figure 11. Structural similarities between etonitazene[68] and (exemplary) lead compound **D**: an electron-withdrawing substituent at position 5 of the benzimidazole (red), a 4-ethoxybenzyl moiety at position 2 (green), and a basic amine linked with an ethylene bridge to N^1 (blue).

we tested our lead compounds **A**, **B**, and **D** in a radioligand binding assay at the MOP receptor (HEK cells transient transfected with the hMOP receptor) to evaluate unwanted interactions with the MOP receptor and to avoid them in further compound development (Table 2).

Radioligand binding studies confirmed our assumptions. While compound **D**, with the highest structural analogy, shows a significant, albeit moderate, three-digit nanomolar binding to the MOP receptor (**D**, $K_i(MOP) = 556.0$ nM; Table 2), lead compound **A** only shows a one-digit micromolar affinity (**A**, $K_i(MOP) = 6.7$ μM; Table 2). This is probably due to the lack of a basic amine. Compound **B**, which does lack not only the basic amine but also the methylene unit between the benzimidazole core and the 4-ethoxy phenyl moiety, shows the lowest affinity at the MOP receptor (**B**, $K_i(MOP) = 53.6$ μM; Table 2). Based on these observations for "designing out" the MOP affinity, a basic amine

attached over an alkylene linker to N^1 should advantageously be avoided and the methylene unit should be substituted by a 2-amino moiety. Substitution/removal of the electron-withdrawing amide function at position 5 should be avoided to keep affinity/activity at hCB$_2$R and BChE as discussed above (cf. Table 1 and ref 36).

In Vivo Studies. Lead compounds **A** and **B** and compound **20a** were tested for their neuroprotectant and pro-cognitive effects in the in vivo mouse model of AD, in which neuroinflammation and cognitive deficits are induced by the intracerebroventricular injection of the oligomerized Aβ_{25-35} peptide into the mouse brains.[28,69,70]

Each compound was solubilized in DMSO/saline or DMSO/Tween-80/saline vehicle solutions (cf. Supporting Information for detailed description). Compounds were fully dissolved, and no precipitation was observed. Extended (in vitro) pharmacokinetic studies were not conducted since they are beyond the scope of this work.[71]

The prepared compounds were injected intraperitoneally between day 1 and 7. Animal status and weight were checked daily during the treatments. Vehicle solutions, compounds **A** and **B**, did not affect weight gains (+0.3 g/day on average). Compound **20a** decreased weight gain (+0.2 g/day at 0.3 mg/kg, +0.1 g/day at 1 mg/kg, and 0 g/day at 3 mg/kg) but did not provoke weight loss. No treatment induced behavioral alteration, prostration, signs of abdominal pain, or changes in the fur aspect, suggesting that high DMSO concentrations applied in some groups were well-tolerated. Moreover, since the injection period was limited and animals were used for behavioral observation 24 h after the last injection, vehicle-treated animals showed the performances expected for Sc.Aβ- or Aβ_{25-35}-treated groups.[69,70] The amyloid peptide was injected on day 1 and the behavioral examination performed between day 8 and 10. All animals were then sacrificed on day 11 and their brains stored at −80 °C (Figure 12).

The spontaneous alternation performance, an index of spatial working memory, was tested on day 8 in the Y-maze test. Long-term memory response was measured on days 9 and 10 in a step-through passive avoidance test.

Repeated Treatment with Compounds A, B, and 20a. As described above, none of the treatments (ip for the compounds solubilized in DMSO/water or DMSO/Tween-80/water and ICV for peptides solubilized in water) affected the mouse body

Table 2. Biological Evaluation of Radioligand Binding Studies at the hMOP Receptor

No.	X	R^1	R^2	R^3	K_i(hMOP)^a (pK_i ± SD)
Etonitazene					0.2 nM [68]
A	CH$_2$	CONEt$_2$	(isopentyl)	(4-ethoxyphenyl, OEt)	6.7 μM (5.2 ± 0.1)
B	NH	CONEt$_2$	(isopentyl)	(4-ethoxyphenyl, OEt)	53.6 μM (4.3 ± 0.0)
D	CH$_2$	CONEt$_2$	(piperidinylethyl)	(4-ethoxyphenyl, OEt)	556.0 nM (6.3 ± 0.1)

^{a}Screened on membranes of HEK cells transiently transfected with the hMOP receptor; values are mean values from at least 2 independent experiments performed in triplicates.
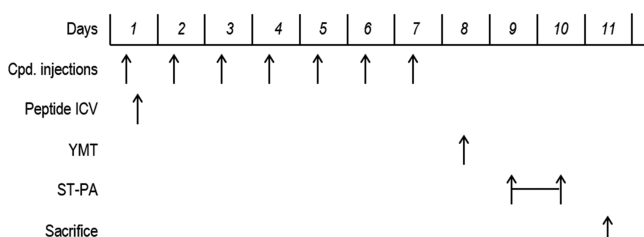
Figure 12. Protocol followed. Abbreviations key: Cpd, compound; ICV, intracerebroventricular injection; YMT, spontaneous alternation test in the Y-maze; ST-PA, step-through passive avoidance test.

weight, suggesting a good tolerability. Animals gained about 2.1 g during the 7 day treatment period.

Spontaneous Alternation Performances. CB_2 agonist **A** attenuated, significantly but partially, the $A\beta_{25-35}$-induced alternation deficit at the highest dose tested, 3 mg/kg (Figure 13a).
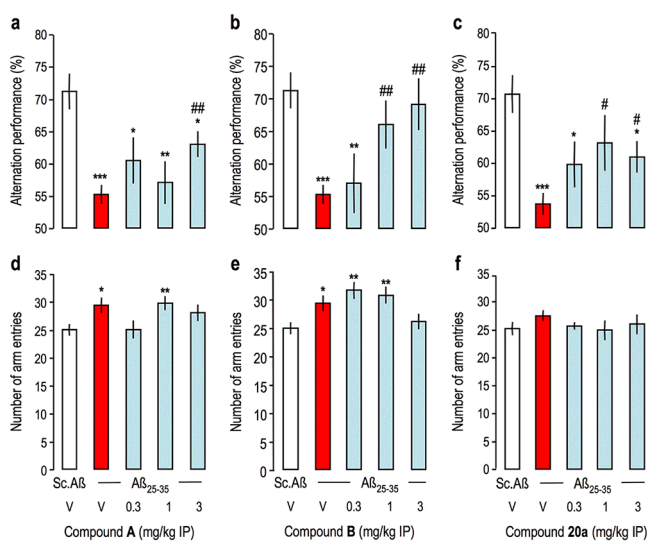
Figure 13. Effect of test compounds **A**, **B**, and **20a** on $A\beta_{25-35}$-induced spontaneous alternation deficits in mice. Animals received $A\beta_{25-35}$ or Sc.Aβ peptide (9 nmol ICV) on day 1 and the test compounds (0.3 mg/kg ip) or vehicle solution (V, DMSO 20% in saline or DMSO 20%, Tween-80 2% in saline) od between days 1–7. Alternation performance was tested on day 8. Data shown mean ± SEM. ANOVA: $F_{(4,54)} = 6.55$, $p < 0.001$, $n = 9$–14 per group in part a; $F_{(4,54)} = 5.43$, $p < 0.001$, $n = 8$–14 per group in part b; $F_{(4,57)} = 4.05$, $p < 0.01$, $n = 9$–14 per group in part c; $F_{(4,54)} = 2.72$, $p < 0.05$ in part d; $F_{(4,54)} = 4.70$, $p < 0.01$ in part e; $F_{(4,57)} = 0.59$, $p > 0.05$ in part f. * $p < 0.05$, ** $p < 0.01$, *** $p < 0.001$ vs (Sc.Aβ+V)-treated group; ## $p < 0.01$, ### $p < 0.001$ vs (Aβ_{25-35}+V)-treated group; Dunnett's test.

Dual-acting compounds **B** and **20a** showed significant preventions at 1 and 3 mg/kg (Figure 13b,c). Note that the $A\beta_{25-35}$ treatment slightly, but significantly for compounds **A** and **B** (Figure 13c,d), increased locomotion, measured in terms of number of arms entered during the session, in these experiments. This is not routinely observed but remains pertinent considering the model. Slight variations with compounds **A** and **B** were noted (Figure 13c,d).

Passive Avoidance Test. For the long-term memory response, CB_2 agonist **A** failed to show any prevention of the step-through latency deficit induced by $A\beta_{25-35}$, at all doses tested (Figure 14a). Dual-acting compound **B** showed significant prevention of the latency diminution at the highest dose tested,
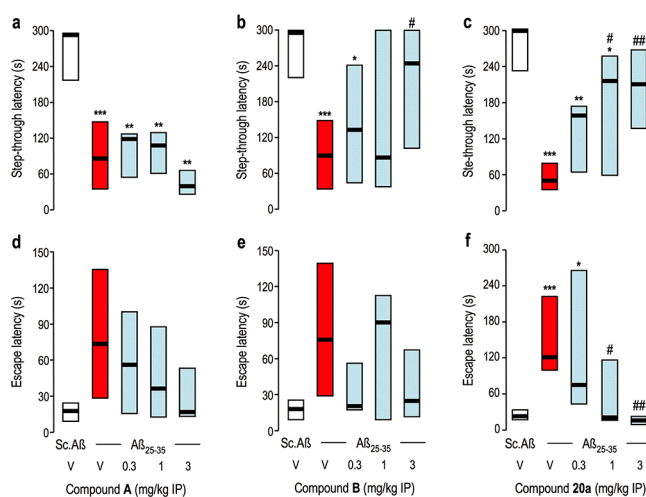
Figure 14. Effect of test compounds **A**, **B**, and **20a** on $A\beta_{25-35}$-induced passive avoidance deficits in mice. Animals received $A\beta_{25-35}$ or Sc.Aβ peptide (9 nmol ICV) on day 1 and the test compounds (0.3 mg/kg ip) or vehicle solution (V, DMSO 20% in saline or DMSO 20%, Tween-80 2% in saline) od between days 1–7. Training was performed on day 9 and retention measured on day 10. Data show median and interquartile range. Kruskal–Wallis ANOVA: $H = 19.0$, $p < 0.001$, $n = 9$–14 per group in part a; $H = 15.0$, $p < 0.01$, $n = 8$–14 per group in part b; $H = 21.1$, $p < 0.001$, $n = 11$–14 in part c; $H = 6.89$, $p > 0.05$ in part d; $H = 6.34$, $p > 0.05$ in part e; $H = 19.7$, $p < 0.001$ in part f. * $p < 0.05$, ** $p < 0.01$, *** $p < 0.001$ vs (Sc.Aβ+V)-treated group; # $p < 0.05$, ## $p < 0.01$ vs (Aβ_{25-35}+V)-treated group; Dunn's test.

3 mg/kg (Figure 14b). Compound **20a** dose-dependently attenuated the step-through latency deficit induced by $A\beta_{25-35}$ with significant effects at 1 and 3 mg/kg (Figure 14c).

Escape latency was also measured. For compounds **A** and **B**, the Kruskal–Wallis ANOVA did not lead to significant effects (Figure 14d,e), but tendencies could be noted. The $A\beta_{25-35}$ treatment led to an increase in escape latency, and several groups treated with the compounds, particularly at the highest doses, showed a trend of a reduction of the latency close to the (Sc.Aβ/V) control group data (Figure 14d,e). For compound **20a**, the ANOVA was significant and the $A\beta_{25-35}$-induced increase was highly significant, while the two highest doses of **20a** significantly prevented the $A\beta_{25-35}$-induced increase (Figure 14f).

A protective activity for dual-acting compounds **B** and **20a** on the two behavioral responses analyzed at doses of 1–3 mg/kg was shown, and compound **20a** appeared as the most active with sustained prevention of $A\beta_{25-35}$-induced learning deficits in both tests at 1 mg/kg. Since compound **A** is a potent hCB_2R agonist, but weakly potent BChE inhibitor and compounds **B** and **20a** show balanced low micromolar activities at both targets, the in vivo studies prove cognition enhancement for such dual-acting compounds and, of course, also prove penetration of the blood–brain barrier. Obviously, the solubilization conditions were not optimized, and the vehicle solutions used here remain first-attempt choices and will be improved in future studies. However, a correct bioavailability was expected for a small dual-acting compound with a much lower molecular weight compared to conventional covalently connected hybrid molecules. The compounds described herein are "true" hybrids in a way that these molecules merge the respective pharmacophores for two targets, whereas compounds termed "hybrid molecules" in the literature in the vast majority of cases covalently connect two distinct molecules that act at two different targets and therefore have a high molecular weight.[34,35]

DISCUSSION AND CONCLUSION

Taken together, a compound library based on benzimidazoles and 2-aminobenzimidazoles was synthesized and SARs were investigated with respect to the hCB_1R and hCB_2R affinity and the AChE and hBChE inhibition, respectively. Generally, the compounds show excellent selectivity over both hCB_1R and AChE, and several compounds show well-balanced affinities at the two desired targets in the low micromolar range. Molecular docking and dynamics studies were performed applying for the first time a homology model of the hCB_2 based on the recently published crystal structure of the hCB_1 receptor bound to an agonist in the orthosteric binding site. While compound **20a** binds, as expected, to the orthosteric binding site, a stable amino acid and water interaction network was observed which extends into the allosteric binding site. Nitro-benzimidazoles can show a significant potency at the MOP receptor, and MOP affinities of dual-acting compounds could be designed out, e.g., by removing the basic nitrogen atom in the alkyl chain. Furthermore, it was proven for the first time by a cAMP assay as well as by two cAMP response elements (MIF and STAT-3) that the compounds act as agonists at the hCB_2R and might therefore exhibit antineuroinflammatory effects in vivo also. In an in vivo study with mice showing neuroinflammation and cognition deficits after $A\beta_{25-35}$ ICV administration, the ability and superiority of a well-balanced dual-acting compound compared to a high-affinity hCB_2R agonist with moderate BChE inhibition in improving cognition at dosages from 1 to 3 mg/kg were demonstrated. This shows that it is possible to design small molecules that act specifically at two very different targets like a GPCR and an enzyme with a high selectivity and a good potency in the same concentration range to yield compounds with a pronounced in vivo activity. The development methods like compound design and application of computational methods shown in this work will hopefully provide support in related drug development efforts for dual-acting compounds.

EXPERIMENTAL SECTION

General Information. All reagents were used without further purification and bought from common commercial suppliers. For anhydrous reaction conditions, THF was dried prior to use by refluxing over sodium slices for at least 2 days under an argon atmosphere. Thin-layer chromatography was performed on silica gel 60 (alumina foils with fluorescent indicator 254 nm). For detection, iodine vapor and UV light (254 and 366 nm) were used. For column chromatography, silica gel 60 (particle size 0.040−0.063 mm) was used. Nuclear magnetic resonance spectra were recorded with a Bruker AV-400 NMR instrument (Bruker, Karlsruhe, Germany) in $CDCl_3$, and chemical shifts are expressed in ppm relative to $CDCl_3$ (7.26 ppm for ^1H and 77.16 ppm for ^{13}C).[72] Purity was determined by HPLC (Shimadzu Products), containing a DGU-20A3R degassing unit, a LC20AB liquid chromatograph, and a SPD-20A UV/vis detector. UV detection was measured at 254 nm. Mass spectra were obtained by a LCMS 2020 (Shimadzu Products). As a stationary phase, a Synergi 4U fusion-RP (150 mm × 4.6 mm) column was used, and as a mobile phase, a gradient of MeOH/water with 0.1% formic acid was used. Parameters: A = water, B = MeOH, V(B)/(V(A) + V(B)) = from 5% to 90% over 10 min, V(B)/(V(A) + V(B)) = 90% for 5 min, V(B)/(V(A) + V(B)) = from 90% to 5% over 3 min. The method was performed with a flow rate of 1.0 mL/min. Compounds were only used for biological evaluation if the purity was ≥95%.

General Procedure for the Synthesis of Target Compounds 20a−e. The respective ester compound **17** (1 equiv) was dissolved in a THF/water mixture (2:1), and LiOH (2 equiv) was added. The mixture was refluxed for 12 h. THF was evaporated, and the aqueous residue was acidified with 2 M aqueous HCl (pH = 4). The organic phase was separated with EtOAc and washed with water and brine. After the residue was dried over Na_2SO_4, the solvent was removed in vacuo and the product was used without further purification. The respective acid (1 equiv) was dissolved in DMF, and NEt_3 (1.5 equiv), HBTU (1.1 equiv), and the appropriate amine (1 equiv) were added in one portion. The mixture was stirred overnight at room temperature. Then, EtOAc and an aqueous saturated $NaHCO_3$ solution were added. The organic layer was washed several times with water and brine and dried over anhydrous Na_2SO_4. The solvent was removed in vacuo, and the product was purified by column chromatography.

2-(4-Ethoxybenzyl)-N,1-diisopentyl-1H-benzo[d]imidazole-5-carboxamide (20a). **20a** was obtained as a light yellow solid (0.26 mmol, 0.11 g, 79%). ^1H NMR(400 MHz, $CDCl_3$): δ = 8.08 (d, J = 1.2 Hz, 1H), 7.76 (dd, J = 8.4, 1.5 Hz, 1H), 7.23 (d, J = 8.5 Hz, 1H), 7.10 (d, J = 8.4 Hz, 2H), 6.78 (d, J = 8.5 Hz, 2H), 6.41 (s, 1H), 4.21 (s, 2H), 3.99−3.90 (m, 4H), 3.46 (dd, J = 13.8, 6.5 Hz, 2H), 1.71−1.61 (m, 1H), 1.56−1.45 (m, 3H), 1.34 (t, J = 7.0 Hz, 5H), 0.92 (d, J = 6.6 Hz, 6H), 0.86 (d, J = 6.6 Hz, 6H) ppm. ^{13}C NMR (101 MHz, $CDCl_3$): δ = 167.96, 158.05, 154.83, 141.97, 137.29, 129.47, 129.05, 127.68, 122.05, 117.78, 114.86, 109.29, 63.46, 42.67, 38.56, 38.43, 38.05, 33.69, 26.11, 25.98, 22.49, 22.31, 14.75 ppm. ESI: m/z calcd for $C_{27}H_{37}N_3O_2$ $[M + H]^+$, 436.29; found, 436.35. HPLC purity: 98% (retention time = 11.03 min).

2-(4-Ethoxybenzyl)-1-isopentyl-N-phenyl-1H-benzo[d]imidazole-5-carboxamide (20b). **20b** was obtained as a light yellow solid (0.21 mmol, 92.0 mg, 64%). ^1H NMR (400 MHz, $CDCl_3$): δ = 8.71−8.75 (m, 1H), 8.23 (s, 1H), 7.79−7.81 (m, 1H), 7.65−7.66 (d, J = 7.7 Hz, 2H), 7.18−7.25 (m, 3H), 6.97−7.03 (m, 3H), 6.68−6.70 (m, 2H), 4.12 (s, 2H), 3.84−3.90 (m, 4H), 1.18−1.30 (m, 6H), 0.79−0.81 (d, J = 6.6 Hz, 6H) ppm. ^{13}C NMR (101 MHz, $CDCl_3$): δ = 166.40, 158.20, 155.00, 141.04, 138.74, 137.33, 129.61, 129.01, 127.31, 124.18, 122.82, 120.36, 118.06, 114.96, 109.78, 63.57, 42.93, 38.06, 33.52, 26.24, 22.40, 14.86 ppm. ESI: m/z calcd for $C_{28}H_{31}N_3O_2$ $[M + H]^+$, 442.24; found, 442.15. HPLC purity: 96% (retention time = 10.69 min).

2-(4-Ethoxybenzyl)-N-hexyl-1-isopentyl-1H-benzo[d]imidazole-5-carboxamide (20c). **20c** was obtained as a light yellow solid (0.15 mmol, 68.0 mg, 45%). ^1H NMR (400 MHz, $CDCl_3$): δ = 8.03 (s, 1H), 7.80−7.82 (m, 1H), 7.30−7.33 (d, J = 8.5 Hz, 1H), 7.08−7.10 (d, J = 8.6 Hz, 2H), 6.75−6.77 (m, 2H), 6.46 (m, 1H), 4.25 (s, 2H), 4.00−4.04 (m, 2H), 3.90−3.96 (q, J = 7.0 Hz, 2H), 3.41−3.46 (m, 2H), 1.36−1.61 (m, 14H), 0.89−0.91 (m, 9H) ppm. ^{13}C NMR (101 MHz, $CDCl_3$): δ = 167.91, 158.46, 154.92, 140.02, 136.83, 130.12, 129.85, 127.02, 122.99, 117.06, 115.18, 110.11, 63.72, 43.25, 40.51, 38.17, 33.40, 31.77, 29.85, 26.93, 26.39, 22.82, 22.54, 14.99, 14.26 ppm. ESI: m/z calcd for $C_{28}H_{39}N_3O_2$ $[M + H]^+$, 450.30; found, 450.25. HPLC purity: 99% (retention time = 11.23 min).

(2-(4-Ethoxybenzyl)-1-isopentyl-1H-benzo[d]imidazol-5-yl)-(piperidin-1-yl)methanone (20d). **20d** was obtained as a light yellow solid (0.15 mmol, 68.0 mg, 45%). ^1H NMR (400 MHz, $CDCl_3$): δ = 7.72 (s, 1H), 7.27−7.30 (m, 1H), 7.20−7.23 (d, J = 9.2 Hz, 1H), 7.07−7.10 (d, J = 8.7, 2H), 6.74−6.76 (m, 2H), 5.95 (s, 1H), 4.22 (s, 2H), 3.91−3.92 (m, 2H), 3.41−3.58 (br, 2H), 1.44−1.61 (m, 7H), 1.29−1.32 (m, 5H), 0.82−0.83 (d, J = 6.6 Hz, 6H) ppm. ^{13}C NMR (101 MHz, $CDCl_3$): δ = 170.73, 158.22, 154.33, 135.65, 130.75, 129.63, 127.52, 122.29, 117.87, 115.02, 109.77, 63.58, 42.85, 38.12, 33.58, 26.21, 24.75, 22.42, 14.87 ppm. ESI: m/z calcd for $C_{27}H_{35}N_3O_2$ $[M + H]^+$, 434.27; found, 434.15. HPLC purity: 98% (retention time = 10.35 min).

N-((3s,5s,7s)-Adamantan-1-yl)-2-(4-ethoxybenzyl)-1-isopentyl-1H-benzo[d]imidazole-5-carboxamide (20e). **20e** was obtained as a light yellow solid (0.23 mmol, 113.0 mg, 70%). ^1H NMR (400 MHz, $CDCl_3$): δ = 7.98 (s, 1H), 7.74−7.76 (d, J = 8.7 Hz, 1H), 7.30−7.33 (d, J = 8.7 Hz, 1H), 7.10−7.12 (m, 2H), 6.77−6.80 (m, 2H), 5.95 (s, 1H), 4.25 (s, 2H), 4.02−4.06 (m, 2H), 3.92−3.98 (d, J = 7.0 Hz, 2H), 2.14 (m, 9H), 1.72 (m, 6H), 1.54−1.61 (m, 1H), 1.35−1.39 (t, J = 7.0 Hz, 3H), 0.89−0.91 (d, J = 7.1 Hz, 6H) ppm. ^{13}C NMR (101 MHz, $CDCl_3$): δ = 167.19, 158.34, 154.87, 140.19, 131.68, 129.76, 127.10, 122.52, 117.11, 115.10, 109.92, 63.64, 52.53, 43.13, 41.83, 38.12, 36.57, 33.37, 29.70, 26.29, 22.48, 14.93 ppm. ESI: m/z calcd for $C_{32}H_{41}N_3O_2$ $[M + H]^+$, 500.32; found, 500.25. HPLC purity: 99% (retention time = 11.77 min).

General Procedure for the Synthesis of Target Compounds 23 and 24. The respective bromine compound **21** or **22** (1 equiv) was

dissolved in DMF, and piperidine (2.5 equiv), Na$_2$CO$_3$ (3 equiv), and a catalytic amount of NaI were added. The mixture was stirred at 70 °C for 12 h. After the reaction has finished, water was added and the organics were extracted with dichloromethane. The organic phase was washed several times with water and afterward dried over Na$_2$SO$_4$. The solvent was removed in vacuo, and the crude product was afterward purified by column chromatography using dichloromethane/methanol/NH$_3$, aq 25% (15:1:0.1), as the eluent system.

2-(4-Ethoxybenzyl)-N,N-diethyl-1-(4-(piperidin-1-yl)butyl)-1H-benzo[d]imidazole-5-carboxamide (23). 23 was obtained as a light yellow oil (0.12 mmol, 58.0 mg, 46%). ^{1}H NMR (400 MHz, CDCl$_3$): δ = 8.00 (s, 1H), 7.74 (t, J = 0.8 Hz, 1H), 7.29 (d, J = 0.8 Hz, 1H), 7.15 (m, 2H), 6.82 (m, 2H), 4.25 (s, 2H), 3.96−4.03 (m, 4H), 3.30−3.61 (m, 4H), 2.52 (s, 3H), 2.36 (t, J = 7.2 Hz, 2H), 1.67−1.73 (m, 2H), 1.48−1.54 (m, 4H), 1.37 (t, J = 7.2 Hz, 3H), 1.13−1.27 (m, 10H) ppm. ^{13}C NMR (101 MHz, CDCl$_3$): δ = 171.90, 158.16, 154.57, 142.17, 135.89, 131.29, 129.66, 128.08, 121.50, 117.70, 115.01, 109.72, 63.62, 57.74, 54.00, 43.88, 33.87, 27.28, 24.62, 23.58, 22.93, 14.94 ppm. ESI: m/z calcd for C$_{30}$H$_{42}$N$_4$O$_2$ [M + H]$^+$, 491.34; found, 491.25. HPLC purity: 97% (retention time = 6.78 min).

2-(4-Ethoxybenzyl)-N,N-diethyl-1-(6-(piperidin-1-yl)hexyl)-1H-benzo[d]imidazole-5-carboxamide (24). 24 was obtained as a light yellow oil (0.26 mmol, 0.13 g, 70%). ^{1}H NMR (400 MHz, CDCl$_3$): δ = 7.98 (s, 1 H), 7.72 (m, 1 H), 7.25−7.26 (m, 1 H), 7.11 (m, 2 H), 6.79 (m, 2 H), 4.22 (s, 4 H), 3.93−3.99 (m, 4 H), 3.27−3.59 (m, 4 H), 2.41 (s, 3 H), 2.28 (t, J = 8 Hz, 2 H), 1.58−1.65 (m, 4 H), 1.50−1.53 (m, 2 H), 1.39−1.47 (m, 3 H), 1.35 (t, J = 7.2 Hz, 3 H), 1.20 (m, 9 H) ppm. ^{13}C NMR (101 MHz, CDCl$_3$): δ = 171.88, 158.09, 154.55, 142.18, 135.98, 131.09, 129.52, 128.05, 121.34, 117.63, 114.91, 109.64, 63.54, 59.02, 54.44, 44.16, 33.87, 29.50, 27.25, 26.83, 26.26, 25.48, 24.15, 14.88 ppm. ESI: m/z calcd for C$_{32}$H$_{46}$N$_4$O$_2$ [M + H]$^+$, 519.37; found, 519.13. HPLC purity: 96% (retention time = 7.06 min).

General Procedure for the Synthesis of Target Compounds 30−32. The respective thiourea compound 27, 28, or 29 (1 equiv) was dissolved in anhydrous THF, and NEt$_3$ (1.5 equiv) and EDCI·HCl (2.5 equiv) were added. The mixture was refluxed for 3−5 h. Afterward, EtOAc was added, and the organic layer was washed with brine. The crude product was purified by column chromatography.

2-((4-Ethoxybenzyl)amino)-N,N-diethyl-1-isopentyl-1H-benzo[d]-imidazole-5-carboxamide (30). The crude product was purified by column chromatography using petroleum ether and EtOAc (1:10) as eluent system. 30 was obtained as a light brown solid (0.71 mmol, 0.31 g, 38%). ^{1}H NMR (400 MHz, CDCl$_3$): δ = 7.42 (d, J = 1.0 Hz, 1H), 7.33−7.28 (m, 2H), 7.04 (dd, J = 8.0, 1.5 Hz, 1H), 6.97 (d, J = 8.0 Hz, 1H), 6.87−6.82 (m, 2H), 4.61 (d, J = 5.3 Hz, 2H), 4.00 (q, J = 7.0 Hz, 2H), 3.79 (dd, J = 16.4, 9.0 Hz, 1H), 3.43 (d, J = 3.8 Hz, 4H), 1.61−1.49 (m, 3H), 1.39 (t, J = 7.0 Hz, 3H), 1.21−1.09 (m, 6H), 0.91 (d, J = 6.2 Hz, 6H) ppm. ^{13}C NMR (101 MHz, CDCl$_3$): δ = 13.79, 15.10, 23.00, 25.79, 37.93, 42.33, 47.91, 64.02, 114.72, 115.46, 119.32, 121.03, 129.99, 133.41, 134.45, 141.67, 151.22, 155.09, 172.78 ppm. ESI: m/z calcd for C$_{26}$H$_{36}$N$_4$O$_2$ [M + H]$^+$, 437.28; found, 437.25. HPLC purity: 97% (retention time = 8.53 min).

2-((4-Ethoxyphenyl)amino)-N,N-diethyl-1-(2-(piperidin-1-yl)-ethyl)-1H-benzo[d]imidazole-5-carboxamide (31). The crude product was purified by column chromatography using dichloromethane/methanol/NH$_3$, aq 25% (50:1:0.1), as the eluent system. 31 was obtained as a light yellow solid (0.56 mmol, 0.26 g, 85%). ^{1}H NMR (400 MHz, CDCl$_3$): δ = 7.52−7.43 (m, 3H), 7.05 (dt, J = 5.9, 3.0 Hz, 1H), 6.96 (d, J = 8.1 Hz, 1H), 6.88−6.81 (m, 2H), 3.97 (dt, J = 14.0, 4.9 Hz, 4H), 3.51−3.32 (m, 4H), 2.67 (dd, J = 5.4, 3.0 Hz, 2H), 2.51 (s, 4H), 1.68−1.59 (m, 4H), 1.54−1.42 (m, 2H), 1.38−1.32 (m, 3H), 1.23−1.02 (m, 6H) ppm. ^{13}C NMR (101 MHz, CDCl$_3$): δ = 172.23, 154.35, 153.75, 142.04, 134.81, 133.71, 130.28, 120.74, 118.80, 115.22, 114.89, 106.63, 63.77, 55.27, 53.48, 43.24, 41.56, 25.84, 23.75, 14.91, 13.85 ppm. ESI: m/z calcd for C$_{27}$H$_{37}$N$_5$O$_2$ [M + H]$^+$, 464.29; found, 464.15. HPLC purity: 96% (retention time = 6.18 min).

N,N-Diethyl-2-((4-phenoxyphenyl)amino)-1-(2-(piperidin-1-yl)-ethyl)-1H-benzo[d] imidazole-5-carboxamide (32). The crude product was purified by column chromatography using dichloromethane/methanol/NH$_3$, aq 25% (50:1:0.1), as the eluent system. 32 was

obtained as a light brown solid (0.82 mmol, 0.42 g, 61%). ^{1}H NMR (400 MHz, CDCl$_3$): δ = 7.59−7.51 (m, 2H), 7.43 (d, J = 1.1 Hz, 1H), 7.25−7.16 (m, 2H), 7.03 (dt, J = 8.7, 4.3 Hz, 1H), 6.99−6.86 (m, 6H), 3.98−3.90 (m, 2H), 3.46−3.22 (m, 4H), 2.67−2.61 (m, 2H), 2.49 (s, 4H), 1.65−1.55 (m, 4H), 1.50−1.41 (m, 2H), 1.14−0.98 (m, 6H) ppm. ^{13}C NMR (101 MHz, CDCl$_3$): δ = 172.22, 158.17, 153.12, 151.41, 141.87, 136.50, 134.66, 130.44, 129.60, 122.61, 120.29, 120.24, 119.07, 118.02, 115.06, 106.84, 59.92, 55.35, 41.60, 31.62, 25.84, 23.73, 13.88 ppm. ESI: m/z calcd for C$_{31}$H$_{37}$N$_5$O$_2$ [M + H]$^+$, 512.29; found, 512.20. HPLC purity: 97% (retention time = 7.79 min).

N-(2-(4-Ethoxybenzyl)-1-isopentyl-1H-benzo[d]imidazol-5-yl)-benzamide (39). Benzoic acid (1 equiv) was dissolved in DMF, and NEt$_3$ (1.5 equiv), HBTU (1.1 equiv), and amine 38 (1 equiv) were added in one portion. The mixture was stirred overnight at room temperature. EtOAc and a saturated aqueous NaHCO$_3$ solution were added. The organic layer was washed several times with water and brine and dried over anhydrous Na$_2$SO$_4$. The solvent was removed in vacuo, and the product was purified by column chromatography using petroleum ether and EtOAc (1:2) as the eluent system. 39 was obtained as a colorless solid (0.42 mmol, 0.19 g, 64%). ^{1}H NMR (400 MHz, CDCl$_3$): δ = 8.08−7.95 (m, 4H), 7.56−7.42 (m, 3H), 7.29 (d, J = 9.3 Hz, 1H), 7.22−7.15 (m, 2H), 6.82 (dd, J = 8.6, 4.4 Hz, 2H), 4.43 (s, 2H), 4.08−4.01 (m, 2H), 4.01−3.93 (m, 2H), 1.62−1.50 (m, 1H), 1.41−1.32 (m, 5H), 0.89 (d, J = 6.6 Hz, 6H) ppm. ^{13}C NMR (101 MHz, CDCl$_3$): δ = 165.98, 158.21, 150.89, 134.89, 131.75, 129.82, 129.61, 128.70, 127.33, 123.31, 114.98, 110.59, 109.88, 63.51, 42.97, 37.93, 33.09, 26.15, 22.33, 14.77 ppm. ESI: m/z calcd for C$_{28}$H$_{31}$N$_3$O$_2$ [M + H]$^+$, 442.24; found, 442.10. HPLC purity: 99% (retention time = 9.27 min).

■ ASSOCIATED CONTENT

Ⓢ Supporting Information

The Supporting Information is available free of charge on the ACS Publications website at DOI: 10.1021/acs.jmedchem.7b01760.

> Experimental and spectral data of compounds, detailed information about the measurement of inhibition of AChE and BChE, radioligand binding studies on the *h*CB$_1$R, *h*CB$_2$R, and *h*MOP receptors, efficacy on *h*CB$_2$R, information on cell culture and cell lines, statistics, animals, biochemical and histological procedures, and statistics of behavioral studies (PDF)
> Molecular formula strings (CSV)
> Crystal structure of the human CB1 receptor (PDB)

Accession Codes

PDB code for the crystal structure of the human CB1 receptor in complex with agonist AM11542 is 5XRA.[52] This crystal structure was used for the generation of the homology model for computational studies of the human CB2 receptor in complex with compound 20a or 20d.

■ AUTHOR INFORMATION

Corresponding Author

*E-mail: michael.decker@uni-wuerzburg.de. Tel: 0049-931-31-89676.

ORCID Ⓞ

Michael Decker: 0000-0002-6773-6245

Author Contributions

The manuscript was written through contributions of all authors. All authors have given approval to the final version of the manuscript.

Notes

The authors declare no competing financial interest.

■ ACKNOWLEDGMENTS

■ ABBREVIATIONS USED

$A\beta$, amyloid β; ACh, acetylcholine; AChE, acetylcholinesterase; AD, Alzheimer's disease; ANOVA, analysis of variance; APP, amyloid precursor protein; ATP, adenosine triphosphate; BChE, butyrylcholinesterase; cAMP, cyclic adenosine monophosphate; CHO, Chinese hamster ovary; CNS, central nervous system; Cpd, compound; CRE, cAMP response element; CREB, cAMP response-element binding protein; EDCI, 1-ethyl-3-(3-(dimethylamino)propyl)carbodiimide; ELISA, enzyme-linked immunosorbent assay; EtOAc, ethyl acetate; GAPDH, glyceraldehyde 3-phosphate dehydrogenase; GPCR, G-protein coupled receptor; HBTU, 2-(1H-benzotriazol-1-yl)-1,1,3,3-tetramethyluronium hexafluorophosphate; $hCB_{1/2}R$, human cannabinoid receptor subtype 1/2; HEK, human embryotic kidney; $h\beta_2R$, human β_2R adrenergic receptor; ICV, intracerebroventricular; ip, intraperitoneal; MD, molecular dynamics; MIF, macrophage migration inhibitory factor; MOP, μ-opioid; MTT, 3-(4,5-dimethylthiazol-2-yl)-2,5-diphenyltetrazolium bromide; n.d., not determined; NMDA, N-methyl-D-aspartate receptor; nNOS, neuronal nitric oxide synthase; od, oculus dextrus; ROS, reactive oxygen species; (q)RT/PCR, (quantitative) reverse transcription polymerase chain reaction; SAR, structure–activity relationship; Sc.Aβ, scrambled amyloid β; STAT-3, signal transducer and activator of transcription; ST-PA, step-through passive avoidance; TM, transmembrane; V or VEI, vehicle; YMT, Y-maze test.

■ REFERENCES

(1) Prince, M.; Comas-Herrera, A.; Knapp, M.; Guerchet, M., Karagiannidou, M. *World Alzheimer Report 2016; Improving healthcare for people living with dementia; Coverage, quality and costs now and in the future*; Alzheimer's Disease International (ADI): London, 2016.

(2) Zemek, F.; Drtinova, L.; Nepovimova, E.; Sepsova, V.; Korabecny, J.; Klimes, J.; Kuca, K. Outcomes of Alzheimer's disease therapy with acetylcholinesterase inhibitors and memantine. *Expert Opin. Drug Saf.* **2014**, *6*, 759–774.

(3) Ballard, C.; Gauthier, S.; Corbett, A.; Brayne, C.; Aarsland, D.; Jones, E. Alzheimer's disease. *Lancet* **2011**, *377*, 1019–1031.

(4) Duyckaerts, C.; Dickson, D. Neuropathology of Alzheimer's disease and its variants. In *Neurodegeneration: The Molecular Pathology of Dementia and Movement Disorders*; Dickson, D., Weller, R., Eds.; Wiley-Blackwell: Oxford, 2011; Vol. 2, pp 62–91.

(5) Ferrer, I. Defining Alzheimer as a common age-related neurodegenerative process not inevitably leading to dementia. *Prog. Neurobiol.* **2012**, *97*, 38–51.

(6) Wyss-Coray, T. Inflammation in Alzheimer disease: driving force, bystander or beneficial response? *Nat. Med.* **2006**, *12*, 1005–1015.

(7) Perry, V. H.; Nicoll, J. A. R.; Holmes, C. Microglia in neurodegenerative disease. *Nat. Rev. Neurol.* **2010**, *6*, 193–201.

(8) Matsuda, L. A.; Lolait, S. J.; Brownstein, M. J.; Young, A. C.; Bonner, T. I. Structure of cannabinoid receptor and functional expression of the cloned cDNA. *Nature* **1990**, *346*, 561–564.

(9) Chiurchiù, V.; Battistini, L.; Maccarone, M. Endocannabinoid signaling in innate and adaptive immunity. *Immunology* **2015**, *144*, 352–364.

(10) Van Sickle, M. D.; Duncan, M.; Kingsley, P. J.; Mouihate, A.; Urbani, P.; Mackie, K.; Stella, N.; Makriyannis, A.; Piomelli, D.; Davison, J. S.; Marnett, L. J.; Di Marzo, V.; Pittman, Q. J.; Patel, K. D.; Sharkey, K. A. Identification and functional characterization of brainstem cannabinoid CB2 receptors. *Science* **2005**, *310*, 329–332.

(11) Núñez, E.; Benito, C.; Pazos, M. R.; Barbachano, A.; Fajardo, O.; González, S.; Tolón, R. M.; Romero, J. Cannabinoid CB2 receptors are expressed by perivascular microglial cells in the human brain: an immunohistochemical study. *Synapse* **2004**, *53*, 208–213.

(12) Grünblatt, E.; Zander, N.; Bartl, J.; Jie, L.; Monoranu, C. M.; Arzberger, T.; Ravid, R.; Roggendorf, W.; Gerlach, M.; Riederer, P. Comparison analysis of gene expression patterns between sporadic Alzheimer's and Parkinson's disease. *J. Alzheimer's Dis.* **2007**, *12*, 291–311.

(13) Solas, M.; Francis, P. T.; Franco, R.; Ramirez, M. J. CB$_2$ receptor and amyloid pathology in frontal cortex of Alzheimer's disease patients. *Neurobiol. Aging* **2013**, *34*, 805–808.

(14) Fernández-Ruiz, J.; Romero, J.; Velasco, G.; Tolón, R. M.; Ramos, J. A.; Guzmán, M. Cannabinoid CB$_2$ receptor: a new target for controlling neural cell survival? *Trends Pharmacol. Sci.* **2007**, *28*, 39–45.

(15) Molina-Holgado, F.; Molina-Holgado, E.; Guaza, C.; Rothwell, N. J. Role of CB$_1$ and CB$_2$ receptors in the inhibitory effects of cannabinoids on liposaccharide-induced nitric oxide release in astrocyte cultures. *J. Neurosci. Res.* **2002**, *67*, 829–836.

(16) Sheng, W. S.; Hu, S.; Min, X.; Cabral, G. A.; Lokensgard, J. R.; Peterson, P. K. Synthetic cannabinoid WIN55,212–2 inhibits generation of inflammatory mediators by IL-1beta-stimulated human astrocytes. *Glia* **2005**, *49*, 211–219.

(17) Ehrhart, J.; Obregon, D.; Mori, T.; Hou, H.; Sun, N.; Bai, Y.; Klein, T.; Fernandez, F.; Tan, J.; Shytle, R. D. Stimulation of cannabinoid receptor 2 (CB$_2$) suppresses microglial activation. *J. Neuroinflammation* **2005**, *2*, 29.

(18) Wu, J.; Bie, B.; Yang, H.; Xu, J. J.; Brown, D. L.; Naguib, M. Activation of the CB$_2$ receptor system reverses amyloid-induced memory deficiency. *Neurobiol. Aging* **2013**, *34*, 791–804.

(19) Martin-Moreno, A. M.; Brera, B.; Spuch, C.; Carro, E.; Garcia-Garcia, L.; Delgado, M.; Pozo, M. A.; Innamorato, N. G.; Cuadrado, A.; de Ceballos, M. L. Prolonged oral cannabinoid administration prevents neuroinflammation, lowers β-amyloid levels and improves cognitive performance in Tg APP 2576 mice. *J. Neuroinflammation* **2012**, *9*, 8–12.

(20) Koppel, J.; Vingtdeux, V.; Marambaud, P.; d'Abramo, C.; Jimenez, H.; Stauber, M.; Friedman, R.; Davies, P. CB$_2$ receptor deficiency increases amyloid pathology and alters tau processing in a transgenic mouse model of Alzheimer's disease. *Mol. Med.* **2014**, *19*, 357–364.

(21) Bisogno, T.; Oddi, S.; Piccoli, A.; Fazio, D.; Maccarone, M. Type-2 cannabinoid receptors in neurodegeneration. *Pharmacol. Res.* **2016**, *111*, 721–730.

(22) Davies, P.; Maloney, A. J. Selective loss of central cholinergic neurons in Alzheimer's disease. *Lancet* **1976**, *308*, 1403.

(23) Nordberg, A.; Ballard, C.; Bullock, R.; Darreh-Shori, T.; Somogyi, M. A Review of butyrylcholinesterase as a therapeutic target in the treatment of Alzheimer's disease. *Prim. Care Companion CNS Disord.* **2013**, *15*, 2.

(24) Darvesh, S.; Hopkins, D. A.; Geula, C. Neurobiology of butyrylcholinesterase. *Nat. Rev. Neurosci.* **2003**, *4*, 131–138.

(25) Mesulam, M. M.; Geula, C. Butyrylcholinesterase reactivity differentiates the amyloid plaques of aging from those of dementia. *Ann. Neurol.* **1994**, *36*, 722−727.

(26) Guillozet, A. L.; Smiley, J. F.; Mash, D. C.; Mesulam, M. M. Butyrylcholinesterase in the life cycle of amyloid plaques. *Ann. Neurol.* **1997**, *42*, 909−918.

(27) (a) Greig, N. H.; Utsuki, T.; Ingram, D. K.; Wang, Y.; Pepeu, G.; Scali, C.; Yu, Q.-S.; Mamczarz, J.; Holloway, H. W.; Giordano, T.; Chen, D.; Furukawa, K.; Sambamurti, K.; Brossi, A.; Lahiri, D. K. Selective butyrylcholinesterase inhibition elevates brain acetylcholine, augments learning and lowers Alzheimer β-amyloid peptide in rodent. *Proc. Natl. Acad. Sci. U. S. A.* **2005**, *102*, 17213−17218. (b) Li, Q.; Yang, H.; Chen, Y.; Sun, H. Recent progress in the identification of selective butyrylcholinesterase inhibitors for Alzheimer's disease. *Eur. J. Med. Chem.* **2017**, *132*, 294−309. (c) Sawatzky, E.; Wehle, S.; Kling, B.; Wendrich, J.; Bringmann, G.; Sotriffer, C. A.; Heilmann, J.; Decker, M. Discovery of highly selective and nanomolar carbamate-based butyrylcholinesterase inhibitors by rational investigation into their inhibition mode. *J. Med. Chem.* **2016**, *59*, 2067−2082.

(28) Maurice, T.; Strehaiano, M.; Siméon, N.; Bertrand, C.; Chatonnet, A. Learning performances and vulnerability to amyloid toxicity in the butyrylcholinesterase knockout mouse. *Behav. Brain Res.* **2016**, *296*, 351−360.

(29) Kosak, U.; Brus, B.; Knez, D.; Sink, R.; Zakelj, S.; Trontelj, J.; Pislar, A.; Slenc, J.; Gobec, M.; Zivin, M.; Tratnjek, L.; Perse, M.; Salat, K.; Podkowa, A.; Filipek, B.; Nachon, F.; Brazzolotto, X.; Wieckowska, A.; Malawska, B.; Stojan, J.; Mlinaric Rascan, I.; Kos, J.; Coquelle, N.; Colletier, J.-P.; Gobec, S. Development of an *in-vivo* active reversible butyrylcholinesterase inhibitor. *Sci. Rep.* **2016**, *6*, 39495−39510.

(30) Darvesh, S.; Hopkins, D. A.; Geula, C. Neurobiology of butyrylcholinesterase. *Nat. Rev. Neurosci.* **2003**, *4*, 131−138.

(31) Wright, C. I.; Geula, C.; Mesulam, M.-M. Neurological cholinesterases in the normal brain and in Alzheimer's disease: relationship to plaques, tangles, and patterns of selective vulnerability. *Ann. Neurol.* **1993**, *34*, 373−384.

(32) Morphy, R.; Rankovic, Z. Designed multiple ligands. An emerging drug discovery paradigm. *J. Med. Chem.* **2005**, *48*, 6523−6543.

(33) (a) Nepovimova, E.; Uliassi, E.; Korabecny, J.; Pena-Altamira, L. E.; Samez, S.; Pesaresi, A.; Garcia, G. E.; Bartolini, M.; Andrisano, V.; Bergamini, C.; Fato, R.; Lamba, D.; Roberti, M.; Kuca, K.; Monti, B.; Bolognesi, M. L. Multitarget drug design strategy: quinone−tacrine hybrids designed To block amyloid-β aggregation and to exert anticholinesterase and antioxidant effects. *J. Med. Chem.* **2014**, *57*, 8576−8589. (b) Nepovimova, E.; Korabecny, J.; Dolezal, R.; Babkova, K.; Ondrejicek, A.; Jun, D.; Sepsova, V.; Horova, A.; Hrabinova, M.; Soukup, O.; Bukum, N.; Jost, P.; Muckova, L.; Kassa, J.; Malinak, D.; Andrs, M.; Kuca, K. Tacrine−Trolox Hybrids: A novel class of centrally active, nonhepatotoxic multi-target-directed ligands exerting anticholinesterase and antioxidant activities with low in vivo toxicity. *J. Med. Chem.* **2015**, *58*, 8985−9003. (c) Spilovska, K.; Korabecny, J.; Nepovimova, E.; Dolezal, R.; Mezeiova, E.; Soukup, O.; Kuca, K. Multitarget tacrine hybrids with neuroprotective properties to confront Alzheimer's disease. *Curr. Top. Med. Chem.* **2017**, *17*, 1006−1026.

(34) Nimczick, M.; Decker, M. New approaches in the design and development of cannabinoid receptor ligands: multifunctional and bivalent compounds. *ChemMedChem* **2015**, *10*, 773−786.

(35) Dolles, D.; Decker, M. Dual-acting compounds acting as receptor ligands and enzyme inhibitors. In *Design of Hybrid Molecules for Drug Development*; Decker, M., Ed.; Elsevier: Oxford, 2017; pp 137−165.

(36) Dolles, D.; Nimczick, M.; Scheiner, M.; Ramler, J.; Stadtmüller, P.; Sawatzky, E.; Drakopoulos, A.; Sotriffer, C.; Wittmann, H.-J.; Strasser, A.; Decker, M. Aminobenzimidazoles and structural isomers as templates for dual-acting butyrylcholinesterase inhibitors and *h*CB₂R ligands to combat neurodegenerative disorders. *ChemMedChem* **2016**, *11*, 1270−1283.

(37) Le Naour, M.; Akgün, E.; Yekkirala, A.; Lunzer, M. M.; Powers, M. D.; Kalyuzhny, A. E.; Portoghese, P. S. Bivalent ligands that target μ opioid (MOP) and cannabinoid 1 (CB₁) receptors are potent analgesics devoid of tolerance. *J. Med. Chem.* **2013**, *56*, 5505−5513.

(38) Perrey, D. A.; Gilmour, B. P.; Thomas, B. F.; Zhang, Y. Toward the development of bivalent ligand probes of cannabinoid CB1 and orexin OX1 receptor heterodimers. *ACS Med. Chem. Lett.* **2014**, *5*, 634−638.

(39) Lange, J. H. M.; Coolen, H. K. A.; Van der Neut, M. A. W.; Borst, A. J. M.; Stork, B.; Verveer, P. C.; Kruse, C. G. Design, synthesis, biological properties, and molecular modeling investigations of novel tacrine derivatives with a combination of acetylcholinesterase inhibition and cannabinoid CB1 receptor antagonism. *J. Med. Chem.* **2010**, *53*, 1338−1346.

(40) Montanari, S.; Scalvini, L.; Bartolini, M.; Belluti, F.; Gobbi, S.; Andrisano, V.; Ligresti, A.; Di Marzo, V.; Rivara, S.; Mor, M.; Bisi, A.; Rampa, A. Fatty acid amide hydrolase (FAAH), acetylcholinesterase (AChE), and butyrylcholinesterase (BuChE): networked targets for the development of carbamates as potential anti-Alzheimer's disease agents. *J. Med. Chem.* **2016**, *59*, 6387−6406.

(41) Lipinski, C. A.; Lombardo, F.; Dominy, B. W.; Feeney, P. J. Experimental and computational approaches to estimate solubility and permeability in drug discovery and development settings. *Adv. Drug Delivery Rev.* **1997**, *23*, 3−25.

(42) Stößel, A.; Schlenk, M.; Hinz, S.; Küppers, P.; Heer, J.; Gütschow, M.; Müller, C. E. Dual Targeting of adenosine A₂ₐ receptors and monoamine oxidase B by 4H-3,1-benzothiazin-4-ones. *J. Med. Chem.* **2013**, *56*, 4580−4596.

(43) (a) Darras, F. H.; Pockes, S.; Huang, G.; Wehle, S.; Strasser, A.; Wittmann, H.-J.; Nimczick, M.; Sotriffer, C. A.; Decker, M. Synthesis, biological evaluation, and computational studies of tri- and tetracyclic nitrogen-bridgehead compounds as potent dual-acting AChE inhibitors and *h*H₃ receptor antagonists. *ACS Chem. Neurosci.* **2014**, *5*, 225−242. (b) Khan, N.; Saad, A.; Nurulain, S. M.; Darras, F. H.; Decker, M.; Sadek, B. The dual-acting H3 receptor antagonist and AChE inhibitor UW-MD-71 dose-dependently enhances memory retrieval and reverses dizocilpine-induced memory impairments in Rats. *Behav. Brain Res.* **2016**, *297*, 155−164. (c) Sadek, B.; Khan, N.; Darras, F. H.; Pockes, S.; Decker, M. The dual-acting AChE inhibitor and H₃ receptor antagonist UW-MD-72 reverses amnesia induced by scopolamine or dizocilpine in passive avoidance paradigm in rats. *Physiol. Behav.* **2016**, *165*, 383−391.

(44) (a) Pagé, D.; Balaux, E.; Boisvert, L.; Liu, Z.; Milburn, C.; Tremblay, M.; Wei, Z.; Woo, S.; Luo, X.; Cheng, Y.-X.; Yang, H.; Srivastava, S.; Zhou, F.; Brown, W.; Tomaszewski, M.; Walpole, C.; Hodzic, L.; St-Onge, S.; Godbout, C.; Salois, D.; Payza, K. Novel benzimidazole derivatives as selective CB2 agonists. *Bioorg. Med. Chem. Lett.* **2008**, *18*, 3695−3700. (b) Cheng, Y.-X.; Tomaszewski, M.; Walpole, C.; Yang, H. Novel Compounds. WO 02/085866 A1, October 31, 2002.

(45) González-Naranjo, P.; Pérez-Macias, N.; Campillo, N. E.; Pérez, C.; Arán, V. J.; Girón, R.; Sánchez-Robles, E.; Martín, M. I.; Gómez-Canas, M.; García-Arencibia, M.; Fernández-Ruiz, J.; Páez, J. A. Cannabinoid agonists showing BuChE inhibition as potential therapeutic agents for Alzheimer's disease. *Eur. J. Med. Chem.* **2014**, *73*, 56−72.

(46) Munch, H.; Hansen, J. S.; Pittelkow, M.; Christensen, J. B.; Boas, U. A new efficient synthesis of isothiocyanates from amines using di-*tert*-butyl dicarbonate. *Tetrahedron Lett.* **2008**, *49*, 3117−3119.

(47) Freitag, M.; Schemies, J.; Larsen, T.; El Gaghlab, K.; Schulz, F.; Rumpf, T.; Jung, M.; Link, A. Synthesis and biological activity of splitomicin analogs targeted at human NAD⁺-dependent histone deacetylases (sirtuins). *Bioorg. Med. Chem.* **2011**, *19*, 3669−3677.

(48) Darras, F. H.; Wehle, S.; Huang, G.; Sotriffer, C. A.; Decker, M. Amine substitution of quinazolinones leads to selective nanomolar AChE inhibitors with 'inverted' binding mode. *Bioorg. Med. Chem.* **2014**, *22*, 4867−4881.

(49) Lange, J. H. M.; van Stuivenberg, H. H.; Coolen, H. K. A. C.; Adolfs, T. J. P.; McCreary, A. C.; Keizer, H. G.; Wals, H. C.; Veerman, W.; Borst, A. J. M.; de Looff, W.; Verveer, C.; Kruse, C. G. Bioisosteric replacements of the pyrazole moiety of rimonabant: synthesis, biological properties, and molecular modeling investigations of thiazoles, triazoles, and imidazoles as potent and selective CB1 cannabinoid receptor antagonists. *J. Med. Chem.* **2005**, *48*, 1823−1838.

(50) Yao, B. B.; Hsieh, G. C.; Frost, J. M.; Fan, Y.; Garrison, T. R.; Daza, A. V.; Grayson, G. K.; Zhu, C. Z.; Pai, M.; Chandran, P.; Salyers, A. K.; Wensink, E. J.; Honore, P.; Sullivan, J. P.; Dart, M. J.; Meyer, M. D. *In vitro* and in vivo characterization of A-796260: a selective cannabinoid CB$_2$ receptor agonist exhibiting analgesic activity in rodent pain models. *Br. J. Pharmacol.* **2008**, *153*, 390−401.

(51) Bottegoni, G.; Cavalli, A. Computational Methods in Multitarget Drug Discovery. In *Design of Hybrid Molecules for Drug Development*; Decker, M., Ed.; Elsevier: Oxford, 2017; pp 239−258.

(52) Hua, T.; Vemuri, K.; Nikas, S. P.; Laprairie, R. B.; Wu, Y.; Qu, L.; Pu, M.; Korde, A.; Jiang, S.; Ho, J. H.; Han, G. W.; Ding, K.; Li, X.; Liu, H.; Hanson, M. A.; Zhao, S.; Bohn, L. M.; Makriyannis, A.; Stevens, R. C.; Liu, Z. J. Crystal structures of agonist-bound human cannabinoid receptor CB1. *Nature* **2017**, *547*, 468−471.

(53) Ballesteros, J. A.; Weinstein, H. Integrated methods for the construction of three-dimensional models and computational probing of structure-function relations in G protein-coupled receptors. *Methods Neurosci.* **1995**, *25*, 366−428.

(54) Igel, P.; Geyer, R.; Strasser, A.; Dove, S.; Seifert, R.; Buschauer, A. Synthesis and structure-activity relationships of cyanoguanidine-type and structurally related histamine H4 receptor agonists. *J. Med. Chem.* **2009**, *52*, 6297−6313.

(55) Strasser, A.; Striegl, B.; Wittmann, H.-J.; Seifert, R. Pharmacological profile of histaprodifens at four recombinant H1-receptor species isoforms. *J. Pharmacol. Exp. Ther.* **2007**, *324*, 60−71.

(56) Wittmann, H.-J.; Seifert, R.; Strasser, A. Sodium binding to hH3R and hH4R - a molecular modeling study. *J. Mol. Model.* **2014**, *20*, 2394−2404.

(57) Strasser, A.; Wittmann, H.-J.; Schneider, E. H.; Seifert, R. Modulation of GPCRs by monovalent cations and anions. *Naunyn-Schmiedeberg's Arch. Pharmacol.* **2015**, *388*, 363−380.

(58) Howlett, A. C.; Barth, F.; Bonner, T. I.; Cabral, G.; Casellas, P.; Devane, W. A.; Felder, C. C.; Herkenham, M.; Mackie, K.; Martin, B. R.; Mechoulam, R.; Pertwee, R. G. International Union of Pharmacology. XXVII. Classification of cannabinoid receptors. *Pharmacol. Rev.* **2002**, *54*, 161−202.

(59) Ross, R. A.; Brockie, H. C.; Stevenson, L. A.; Murphy, V. L.; Templeton, F.; Makriyannis, A.; Pertwee, R. G. Agonist-inverse agonist characterization at CB$_1$ and CB$_2$ cannabinoid receptors of L759633, L759656 and AM630. *Br. J. Pharmacol.* **1999**, *126*, 665−672.

(60) Williams, C. cAMP detection methods in HTS: selecting the best from the rest. *Nat. Rev. Drug Discovery* **2004**, *3*, 125−135.

(61) Zheng, Y.; Wang, Q.; Li, T.; Qian, J.; Lu, Y.; Li, Y.; Bi, E.; Reu, F.; Qin, Y.; Drazba, J.; Hsi, E.; Yang, J.; Cai, Z.; Yi, Q. Role of myeloma-derived MIF in myeloma cell adhesion to bone marrow and chemotherapy response. *J. Natl. Cancer Inst.* **2016**, *108* (11), djw131.

(62) Waeber, G.; Thompson, N.; Chautard, T.; Steinmann, M.; Nicod, P.; Pralong, F. P.; Calandra, T.; Gaillard, R. C. Transcriptional activation of the macrophage migration-inhibitory factor gene by the corticotropin-releasing factor is mediated by the cyclic adenosine 3′,5′-monophosphate responsive element-binding protein CREB in pituitary cells. *Mol. Endocrinol.* **1998**, *12*, 698−705.

(63) Alas, S.; Bonavida, B. Inhibition of constitutive STAT3 activity sensitizes resistant non-Hodgkin's lymphoma and multiple myeloma to chemotherapeutic drug-mediated apoptosis. *Clin. Cancer Res.* **2003**, *9*, 316−326.

(64) Kato, K.; Nomoto, M.; Izumi, H.; Ise, T.; Nakano, S.; Niho, Y.; Kohno, K. Structure and functional analysis of the human STAT3 gene promoter: alteration of chromatin structure as a possible mechanism for the upregulation in cisplatin-resistant cells. *Biochim. Biophys. Acta, Gene Struct. Expression* **2000**, *1493*, 91−100.

(65) Hill, S. J.; Baker, J. G.; Rees, S. Reporter-gene systems for the study of G-protein-coupled receptors. *Curr. Opin. Pharmacol.* **2001**, *1*, 526−532.

(66) Wood, K. V. Marker proteins for gene expression. *Curr. Opin. Biotechnol.* **1995**, *6*, 50−58.

(67) Renton, P.; Green, B.; Maddaford, S.; Rakhit, S.; Andrews, J. S. NOpiates: Novel dual action neuronal nitric oxide synthase inhibitors with μ-opioid agonist activity. *ACS Med. Chem. Lett.* **2012**, *3*, 227−231.

(68) Hunger, A.; Kebrle, J.; Rossi, A.; Hoffmann, K. Benzimidazol-Derivate und verwandte Heterocyclen III. Synthese von 1-Aminoalkyl-2-benzyl-nitro-benzimidazolen. *Helv. Chim. Acta* **1960**, *43*, 1032−1046.

(69) Maurice, T.; Lockhart, B. P.; Privat, A. Amnesia induced in mice by centrally administered β-amyloid peptides involves cholinergic dysfunction. *Brain Res.* **1996**, *706*, 181−193.

(70) Lahmy, V.; Meunier, J.; Malmström, S.; Naert, G.; Givalois, L.; Kim, S. H.; Villard, V.; Vamvakides, A.; Maurice, T. Blockade of Tau hyperphosphorylation and Aβ1−42 generation by the aminotetrahydrofuran derivative ANAVEX2−73, a mixed muscarinic and σ1 receptor agonist, in a nontransgenic mouse model of Alzheimer's disease. *Neuropsychopharmacology* **2013**, *38*, 1706−1723.

(71) Huang, G.; Drakopoulos, A.; Saedtler, M.; Zou, H.; Meinel, L.; Heilmann, J.; Decker, M. Cytotoxic properties of the alkaloid rutaecarpine and its oligocyclic derivatives and chemical modifications to enhance water-solubility. *Bioorg. Med. Chem. Lett.* **2017**, *27*, 4937−4941.

(72) Gottlieb, H. E.; Kotlyar, V.; Nudelman, A. NMR chemical shifts of common laboratory solvents as trace impurities. *J. Org. Chem.* **1997**, *62*, 7512−7515.

The TRPV1 ion channel regulates thymocyte differentiation by modulating autophagy and proteasome activity

Consuelo Amantini[1,*], Valerio Farfariello[2,*], Claudio Cardinali[3,4], Maria Beatrice Morelli[3,4], Oliviero Marinelli[1], Massimo Nabissi[3], Matteo Santoni[3], Laura Bonfili[1], Valentina Cecarini[1], Anna Maria Eleuteri[1] and Giorgio Santoni[3]

[1] School of Biosciences and Veterinary Medicine, University of Camerino, Camerino, Italy

[2] University of Lille, INSERM U1003 - PHYCEL - Physiologie Cellulaire, Lille, France

[3] School of Pharmacy, Experimental Medicine Section, University of Camerino, Camerino, Italy

[4] Department of Molecular Medicine, Sapienza University, Rome, Italy

[*] These authors have contributed equally to this work

Correspondence to: Consuelo Amantini, **email**: consuelo.amantini@unicam.it

ABSTRACT

Autophagy and the ubiquitin-proteasome system (UPS) control thymus cell homeostasis under resting and endoplasmic reticulum (ER) stress conditions. Several evidence support a cross-talk between UPS and autophagy; abrogation of UPS responses stimulates autophagy, and vice versa the inhibition of autophagy alters the UPS functions.

Herein, we found that TRPV1 activation induces ER stress, proteasome dysfunction and autophagy in thymocytes by modulating the expression of UPR–related genes. The TRPV1-mediated autophagy prevents the UPR activation by inhibiting BiP, Grp94 and ERp57 chaperone protein expression.

Thymocytes from TRPV1 KO mice display both autophagy and proteasome dysfunctions, resulting in increased apoptotic cells and reduced total DP thymocyte number.

In addition, positive selection of thymocytes triggered by anti-TCRβ/CD2 Ab-mediated costimulation induces apoptosis in thymocytes from TRPV1 KO as compared with WT mice. Stimulation of TRPV1 KO thymocytes with anti-TCRβ/CD2 mAbs modulates the expression of CD4 antigen on purified DP thymocytes, with reduced number of mature, single positive (SP) CD4 and increased number of immature SP CD4^{low} and DP CD4^{low}CD8$^+$ thymocytes, further supporting the intrinsic role of TRPV1 in T cell maturation. Finally, a reduction in CD8$^+$ and CD4$^+$ T cells is evidenced in the peripheral blood and spleen of TRPV1 KO, as compared with WT mice. Therapeutic strategy by restraining or stimulating the TRPV1 expression and functions in thymocytes might represent a new pharmacological tool in the regulation of different inflammatory T cell responses.

INTRODUCTION

Autophagy and the ubiquitin-proteasome system (UPS) constitute the major intracellular degradation pathways controlling cellular homeostasis under normal conditions and cellular stress [1]. Autophagy is a cellular adaptive response to stress conditions, such as nutrient, growth factor deprivation or oxidative stress. This process is mainly involved in the degradation of long-lived proteins and excess/damaged organelles [2]. The UPS represents the principal degradation mechanism for short-lived proteins labeled with ubiquitin [3]. Unfolded or misfolded proteins are tagged for degradation *via* endoplasmic reticulum-associated degradation (ERAD).

Continued accumulation of incorrectly folded proteins triggers the unfolded protein response (UPR) in the attempt to resolve ER stress and reestablish the folding homeostasis [4-6]. Mild to moderate ER stress induces autophagy as a compensatory cell survival mechanism by relieving proteasome inhibitor-induced ER stress, whereas severe or chronically prolonged ER stress deteriorates cellular functions with a switch from an adaption program to apoptotic cell death [7, 8]. In cases in which mild ER stress activates all UPR sensors, survival is favored as a consequence of increased instability of the mRNAs and proteins that promote apoptosis compared to those that facilitate adaptation and autophagic survival [8]. Several evidence support the existence of an interplay between the UPS and autophagy [9]: inhibition of UPS often induces autophagy whilst inhibition of autophagy alters the UPS function [1].

Autophagy is vital for thymocytes during stress conditions such as starvation, activation, growth and proliferation to provide cells with essential metabolic intermediates. This process is involved in T cell thymic development and the thymus exhibits a considerable high amount of constitutive basal autophagy compared to other tissues. In thymic antigen presenting cells (APCs), intracellular peptides can be presented on MHC class II through autophagy [10].

Members of the transient receptor potential (TRP) ion channel family have been shown to mediate cellular Ca^{2+} homeostasis, initiate ER stress and stimulate UPR and apoptosis, or autophagic survival in normal and neoplastic cells [11]. In this regard, TRPV1 is a cation channels expressed on thymocytes as well as on naïve and effector CD4^{+} T lymphocytes and Jurkat T cell leukemia [12, 13], and a contribute of TRPV1 in TCR-induced Ca^{2+} influx and proper downstream TCR signaling leading to T cell activation has been recently reported [14]. Previously, we have reported that the TRPV1 agonist, capsaicin (CPS) modulates T cell differentiation and functions by regulating the apoptosis of distinct thymocyte subpopulations in rats [12]. Moreover, the presence of an interplay between autophagic survival and apoptotic cell death in response to stress signals has been demonstrated in the mouse thymus [15, 16]. Triggering of TRPV1 by the specific agonist CPS, induces autophagic survival in mouse DP[dull] thymocytes. TRPV1-induced autophagy is Atg4C- and Atg6-dependent and, requires $[Ca^{2+}]_i$ increase and reactive oxygen species (ROS) generation that induces Atg4C protein oxidation resulting in AMPK activation. In addition, the inhibition of TRPV1-mediated autophagy by the 3-MA autophagic inhibitor decreases Atg4C, Bcl-XL, Irgm1 and Beclin-1 expression and induces caspase-3-dependent apoptosis of DP[dull] thymocytes [15].

At present, the molecular mechanism involved in thymus maturation by regulating thymocyte fate has been only partially investigated. Thus, the aim of the present work was to evaluate the role of TRPV1 in the cross-talk between ER stress, proteasome and autophagy responses, resulting in thymocyte survival or death in steady state and during thymic maturation.

RESULTS

## CPS inhibits cellular proteasome function in a TRPV1-dependent manner

Lysates from CPS-treated thymocytes were analyzed for proteasome activity. As shown in Figure 1A, exposure of thymocytes to the TRPV1 agonist, CPS resulted in a time-dependent decrease of ChT-L, T-L, PGPH and 26S proteasome ChT-L activities. To further confirm the effect of CPS on cellular proteasome, the expression level of the proteasome target protein p27 was measured by immunoblot analysis. Figure 1B demonstrates that TRPV1-mediated proteasome inhibition correlates with increased levels of p27 in thymocytes. Then, the involvement of ROS generation and the increase of $[Ca^{2+}]_i$ in TRPV1-mediated inhibition of the proteasome activity was evaluated by using the ROS scavenger NAC, the Ca^{2+} blocker EDTA and the specific TRPV1 antagonist, capsazepine (CPZ). NAC, EDTA and CPZ completely reverted the inhibition of proteasome functionality (Figure 2A) and the p27 accumulation (Figure 2B) induced by CPS in a TRPV1-mediated manner after 2 hours of treatment.

The ER stress inhibitor 4-PBA abrogates the CPS-induced autophagy promoting thymocyte apoptosis

Previously, it has been demonstrated that proteasome inhibition activates autophagy to purge polyubiquitinated protein aggregates with the aim to alleviate ER stress and the UPR [17]. Starting from these results and taking into account our recent data demonstrating that TRPV1 activation by CPS triggers autophagy counteracting apoptotic cell death of DP[dull] thymocytes [15], we decided to evaluate whether autophagy could occur as a consequence of CPS-induced proteasome inhibition and ER stress. To this aim, thymocytes were treated with CPS in combination with 4-PBA, a small chemical chaperone that interacts with the hydrophobic domains of misfolded proteins, preventing their aggregation and supporting the correct protein folding [18]. The autophagy pathway was evaluated by immunoblotting using specific anti-LC3 and -p62 antibodies. In fact, during autophagy, the cytosolic form of LC3 (LC3I) binds phosphatidylethanolamine to form LC3-phosphatidylethanolamine conjugate (LC3II),
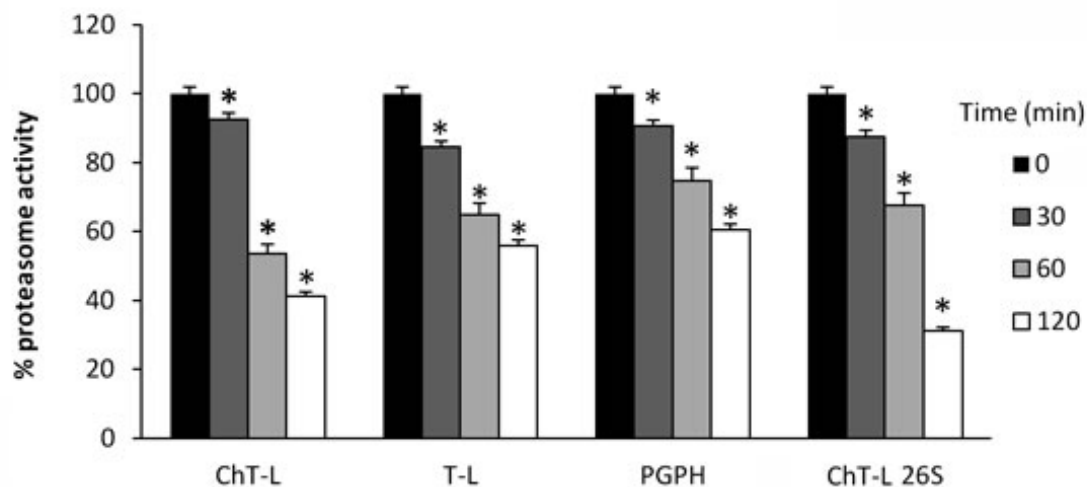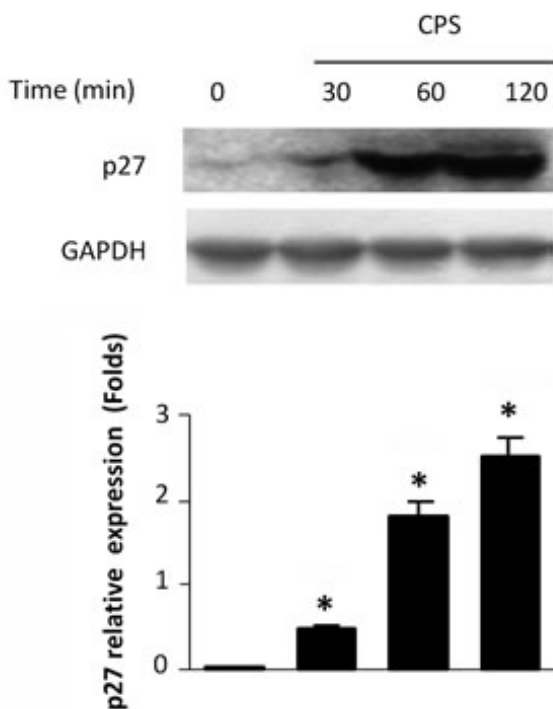
Figure 1: CPS inhibits cellular proteasome activity. A. WT thymocytes were subjected to enzymatic proteasome activity assay after 30, 60 and 120 minutes of CPS treatment. Data, shown as percentage of proteasome activity, are from one representative experiment out of three separate experiments. Error bars are relative to three replicates. *$p < 0.01$ *vs* untreated cells. **B.** Western blot analysis and densitometric quantification of p27 protein levels in thymocytes treated for up to 120 minutes with CPS. p27 densitometry values were normalized to GAPDH used as loading control. Blots are representative of one of three separate experiments. *$p < 0.01$ treated *vs* untreated cells.
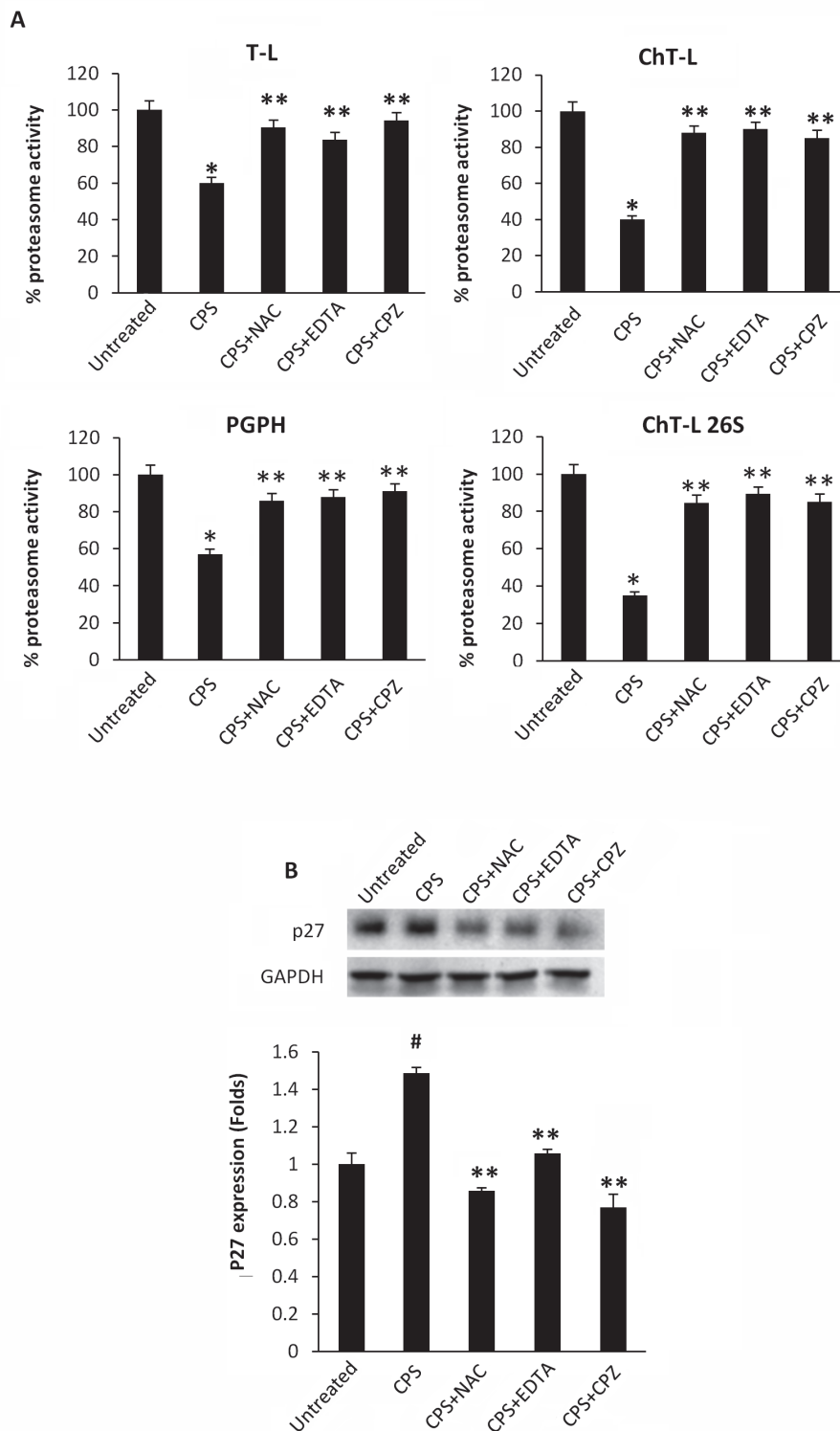
Figure 2: CPS-mediated inhibition of enzymatic proteasome activity is ROS-, Ca²⁺- and TRPV1- dependent. A. Enzymatic proteasome activities were assessed in WT thymocytes pre-treated with NAC, EDTA and CPZ for 60 minutes and then treated with CPS for 120 minutes. Data, shown as percentage of proteasome activity, are from one representative experiment out of three separate experiments. Error bars are relative to three replicates. *$p < 0.01$ *vs* untreated cells; **$p < 0.01$ *vs* CPS-treated cells. **B.** Western blot analysis and densitometric quantification of p27 protein levels in thymocytes treated as above described. p27 densitometric values were normalized to GAPDH used as loading control. Blots are representative of one of three separate experiments. #$p < 0.01$ *vs* untreated; **$p < 0.01$ *vs* CPS-treated cells.

which is recruited to autophagosomal membranes [19], whereas the receptor for cargo p62 is degraded [20]. Our results demonstrated that TRPV1-induced autophagy depends on ER stress, as 4-PBA completely inhibited LC3II formation and p62 degradation (Figure 3A).

In addition, Annexin V/PI or CD4/CD8α staining followed by FACS analysis revealed that 4-PBA in combination with CPS increases the percentage of Annexin V$^+$PI$^-$ early (21.33%) and Annexin V$^+$PI$^+$ late (3.93%) thymocytes (Figure 3B), and reduces the TRPV1-dependent increase of DP^{dull} thymocytes (Figure 3C). Similar results were obtained in CPS-treated thymocytes pretreated with the autophagic inhibitor CQ or with the ROS scavenger NAC (Figure 3C). In addition, no major
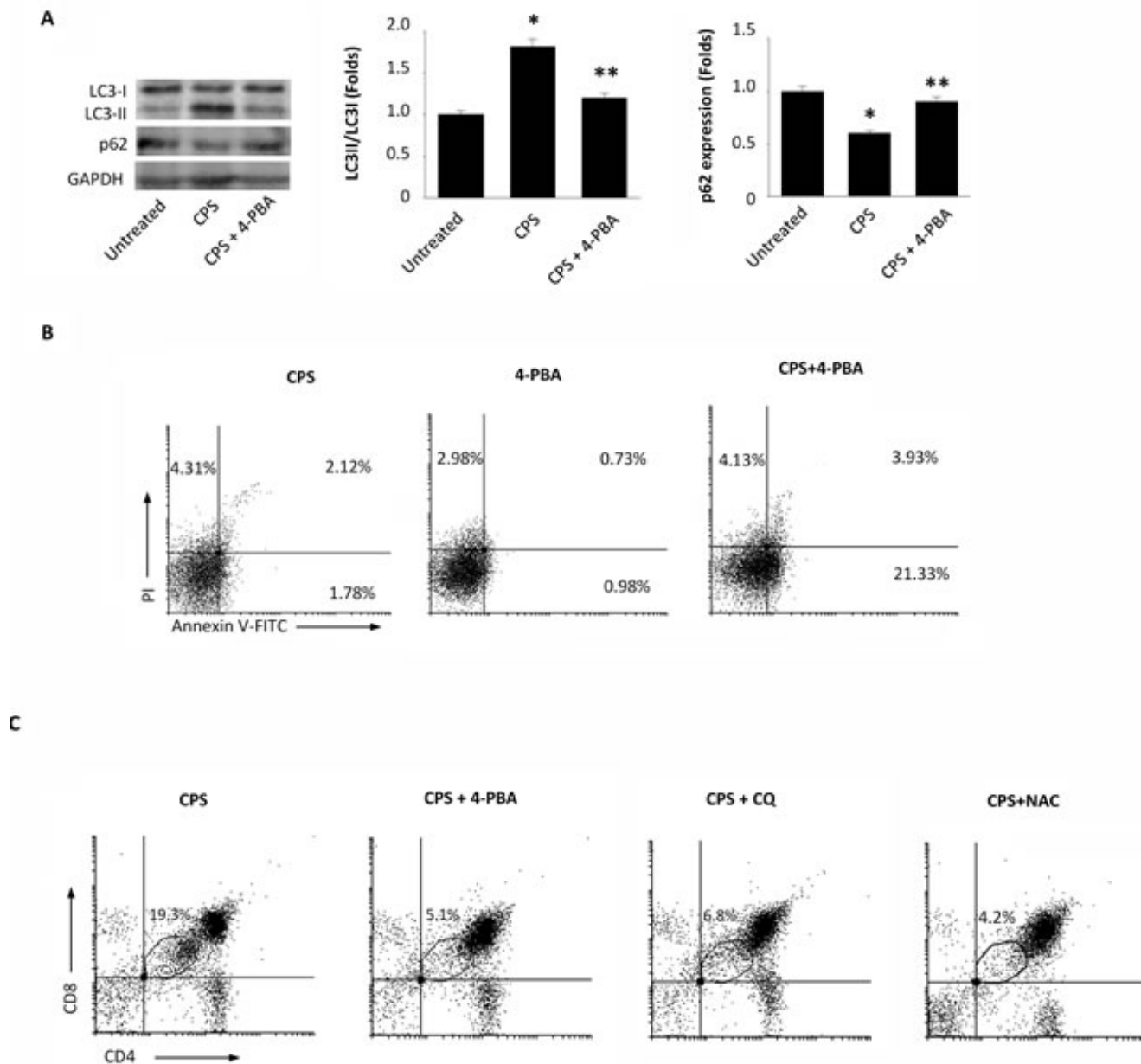
Figure 3: The 4-PBA abrogates the CPS-induced autophagy and reduces the DP^{dull} thymocyte subpopulation. A. Western blot analysis of LC3 and p62 protein in WT thymocytes pre-treated with 4-PBA for 60 minutes and then treated for 120 minutes with CPS. The ratio of LC3 II/I was calculated from densitometric data. p62 densitometric values were normalized to GAPDH used as loading control. Blots are representative of one of three separate experiments. *$p < 0.01$ *vs* untreated cells, **$p < 0.01$ *vs* CPS-treated cells. **B.** Flow cytometric analysis was performed by Annexin V-FITC and PI double-staining of WT thymocytes, pre-treated with 4-PBA for 60 minutes and then treated for 120 minutes with CPS. Data represent the percentage of PI and/or Annexin V positive cells. One representative out of three independent experiments is shown. **C.** Thymocytes, pre-treated with 4-PBA, CQ or NAC for 60 minutes and then treated for 120 minutes with CPS, were stained with anti-CD4-PE and anti-CD8-Cy5 mAbs and analyzed by FACS. The black gate indicates the DP^{dull} subpopulation. One representative out of three independent experiments is shown.

changes in the expression levels of the activation markers CD25 and CD69 were found on CPS-treated as compared with untreated thymocytes (Supplementary Figure 1).

TRPV1 activation modulates the expression of UPR-related genes

UPR activation, upon proteasome dysfunction and ER stress, is a well-documented process [21-23]. Based on these observations, we investigated the effect of the TRPV1 agonist CPS on the expression of UPR components in thymocytes at 1 hour after treatment by RT-PCR array. In particular, the comparison of gene expression levels of CPS-treated with untreated thymocytes (Table 1), demonstrates that Hspa5 (Bip) and Hspa1 (heat shock proteins involved in protein folding), Dnajb9 (regulator of the ATPase activity of 70 kDa heat shock proteins), Bax (pro-apoptotic protein), Xbp1 (transcription factor promoting the expression of genes involved in protein degradation), Insig1 (involved in cell growth) Mbtps2 (regulators of oxidative stress susceptibility) and the Rpn1 (part of the subunit of the 26S proteasome) are down-regulated, whereas Derlin-1 (functional component of ERAD and autophagy), Derlin-2 (functional component of ERAD) and Ero1lb (oxidoreductase involved in protein folding) are up-regulated. Overall, these findings demonstrate that CPS inhibits the expression of UPR and apoptosis genes and enhances that involved in modulation of ERAD and autophagy processes.

The autophagy and ER stress inhibitors revert the TRPV1-mediated UPR down-regulation in CPS-treated thymocytes

The TRPV1-induced changes in the UPR gene expression (Table 1) prompted us to investigate by western blot analysis, the expression of UPR proteins such as BiP, Grp94 and ERp57 chaperones, in thymocytes treated for different times (1, 2 and 4h) with CPS. We found that CPS decreases in a time-dependent manner, BiP, Grp94 and ERp57 protein expression (Figure 4A, 4B). Pretreatment of thymocytes with CQ or 4-PBA, before CPS exposure, completely reverted the CPS-induced UPR protein reduction, in a time-dependent manner, allowing their accumulation (Figure 4A, 4C), suggesting that CPS-stimulated autophagy prevents the ER stress-induced UPR.
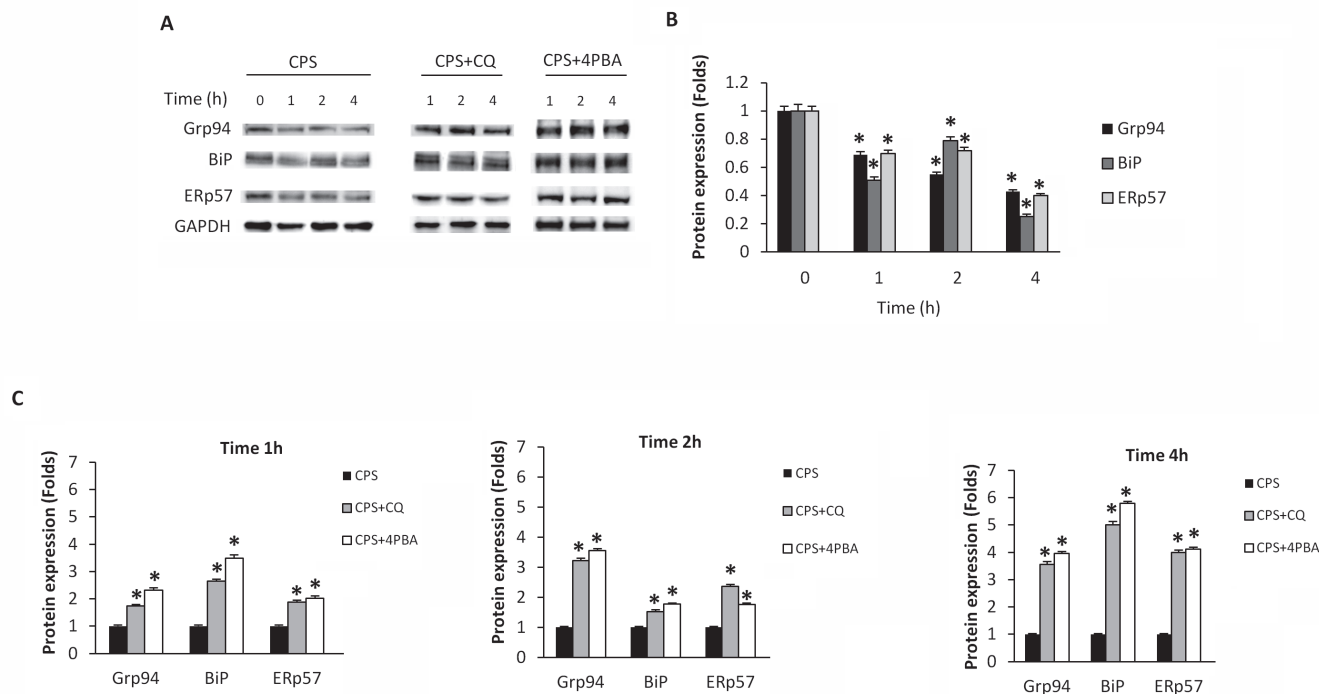

Figure 4: CPS reduces UPR protein levels, and autophagy reverts CPS-induced inhibitory effects. A. Western blot analysis and densitometric quantification of Grp94, BiP and ERp57 protein levels in WT thymocytes pre-treated with CQ and 4PBA for 1h and then treated for up to 4h with CPS. Blots are representative of one of three separate experiments. **B.** Densitometric quantification of Grp94, BiP and ERp57 protein levels in WT thymocytes treated with CPS for different times. Densitometric values were normalized to GAPDH used as loading control and represent the mean ± SEM of three separate experiments. *$p < 0.01$ *vs* untreated cells. **C.** Densitometric quantification of Grp94, BiP and ERp57 protein levels in thymocytes pre-treated with CQ and 4PBA and then treated with CPS. *$p < 0.01$ *vs* CPS-treated cells. Densitometric values were normalized to GAPDH used as loading control and represent the mean ± SEM of three separate experiments.

Thymocytes from TRPV1 KO mice display both autophagy and proteasome dysfunctions

Since a role for TRPV1 in CPS-induced autophagy in thymocytes was found [15], we evaluated the consequence of TRPV1 genetic deletion on thymic autophagy. Our results showed that TRPV1 KO thymocytes express higher basal levels of p62 protein compared with WT cells (Figure 5A). Moreover, differently from WT thymocytes [15], TRPV1 KO thymocytes failed to activate the autophagy when stimulated with the autophagy inducer rapamycin (Figure 5B). Since the increase of p62 protein levels and the autophagic dysfunction result in the inhibition of proteasome [24, 25], the proteasome function was evaluated in TRPV1 KO and WT thymocytes. A decrease in the ChT-L, T-L, PGPH and 26S proteasome ChT-L activities (Figure 5C), a reduction of p27 protein and AMPK phosphorylation levels (Figure 5D and 5E) were found in TRPV1 KO thymocytes compared with WT cells. In addition, the apoptotic regulator Atf4 transcription factor (Figure 5F) and ERp57 (Figure 5G) protein levels were up regulated whereas BiP (Figure 5H) and Grp94 (Figure 5I) UPR proteins were reduced in TRPV1 KO compared with WT thymocytes. Overall, these findings demonstrate that the expression of TRPV1 in thymocytes
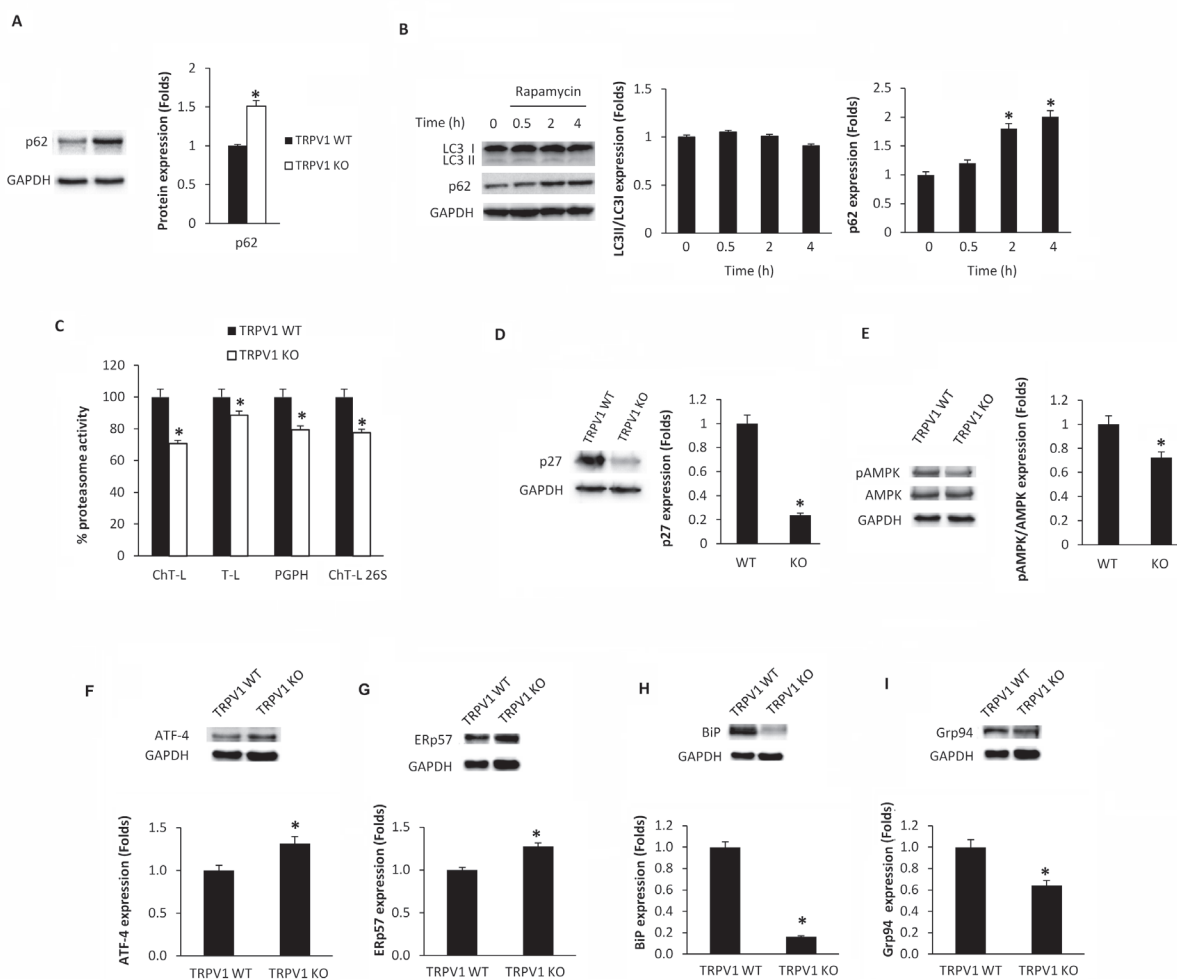
Figure 5: Knock-out of TRPV1 gene affects autophagy, proteasome and UPR protein expression in thymocytes. A. Western blot analysis and densitometric quantification of basal p62 protein levels in WT and TRPV1 KO thymocytes. Densitometric values were normalized to GAPDH used as loading control. Blots are representative of one of three separate experiments, *$p < 0.01$ *vs* WT thymocytes. **B.** Western blot analysis and densitometric quantification of LC3 and p62 protein levels in TRPV1 KO thymocytes treated for up to 4 h with rapamycin. Densitometric values were normalized to GAPDH used as loading control. Blots are representative of one of three separate experiments, *$p < 0.01$ *vs* CPS-treated cells for 0.5h or untreated cells. **C.** Thymocytes from WT and TRPV1 KO mice were subjected to enzymatic proteasome activity assay. Data shown as percentage of inhibition are representative of one of three separate experiments, *$p < 0.01$ TRPV1 KO *vs* WT thymocytes. D-I. Western blot analysis and densitometric quantification of p27 **D.**, pAMPK/AMPK **E.**, ATF-4 **F.**, ERp57 **G.**, Bip **H.** and Grp94 **I.** protein levels in WT and TRPV1 KO thymocytes. Densitometric values were normalized to GAPDH used as loading control. Blots are representative of one of three separate experiments, *$p < 0.01$ *vs* WT thymocytes.

is crucial in regulating autophagy, apoptosis and UPR activity.

Loss of TRPV1 increases the apoptosis, reduces the total thymocyte number and affectes thymocyte distribution

Then we evaluated whether knockout of TRPV1 gene could affect thymocyte number and distribution. To this purpose, freshly isolated thymocytes from TRPV1 KO and WT mice were counted and then labeled with Annexin V. Our findings show a reduction in total thymocyte count (Figure 6A), that is associated with a parallel increase in the percentage of Annexin V+ thymocytes (Figure 6B). In addition, knockout of TRPV1 affected thymocyte cell distribution. Thus, a marked reduction of total DP thymocyte number (Figure 6C) was observed in the thymus from TRPV1 KO respect to WT mice.

## Positive selection is impaired in TRPV1 KO thymocytes

We have previously reported the role of TRPV1 in thymocyte differentiation by regulating the crosstalk between autophagic survival and apoptotic cell death [15]. To understand the contribution of TRPV1 in thymocyte maturation, we mimicked positive selection by stimulating TRPV1 KO and WT thymocytes for 18h with anti-TCRβ plus anti-CD2 mAbs and allowing recovery for 12h [26]. Since positive selection is an essential step for thymocyte survival and TCRβ/CD2 coengagment promotes anti-apoptotic signals [27], we evaluated the extent of apoptotic cell death in un-stimulated and stimulated TRPV1 KO and WT thymocytes by cytofluorimetric analysis. As expected, positive selection promotes cell survival in WT thymocytes, as indicated by the reduced percentage of Annexin V+ cells. On the contrary, an impairment of positive selection was observed in TRPV1 KO thymocytes as shown by the increased frequency of apoptotic cells (Figure 7A). These results prompted us to evaluate the outcome of positive selection, in highly purified (> 97%) TRPV1 KO and WT CD4+CD8+ DP thymocytes, in response to TCRβ plus CD2 stimulation. Since previous results showed that the positive selection of DP cells promotes the maturation of CD4+ thymocytes [26], we performed cytofluorimetric analysis to assess the expression of CD4 and CD8 co-receptors. We found that the maturation process is promoted in both TRPV1 KO and WT thymocytes, as revealed by the modulation of CD4 expression; however, in stimulated TRPV1 KO DP thymocytes, a reduced number of total SP CD4 thymocytes (44.8%) was observed with respect to WT thymocytes (53.6%) (Figure 7B). In addition, CD4 expression levels on mature SP cells was lower in TRPV1 KO (CD4high 13.2% and CD4low 31.6%) with respect to WT thymocytes (CD4high 28.7% and CD4low 24.9%) (Figure 7B). Finally, stimulation of positive selection also induced a marked increase in the percentage of immature CD4lowCD8+ DP subpopulation in TRPV1 KO (32.7%) as compared with WT thymocytes (13.3%) (Figure 7B).

Based on these findings, demonstrating that the absence of TRPV1 increases the basal level of apoptotic thymocytes and impairs thymic positive selection, we finally evaluated the distribution of T lymphocytes in the peripheral blood and spleen. PBMC and splenic lymphocytes from TRPV1 KO and WT control mice were purified by Lympholyte density gradient, stained with anti-mouse CD4 and CD8 mAbs and evaluated by cytofluorimetric and FACS analysis. We observed that the percentage of mature CD8+ and CD4+ T cells in the peripheral blood and spleen was significantly lower in TRPV1 KO vs WT mice (Figure 7C) suggesting that the defect in T cell numbers in the periphery of TRPV1 deficient mice may be the result of the impairment of their maturation in the thymus.
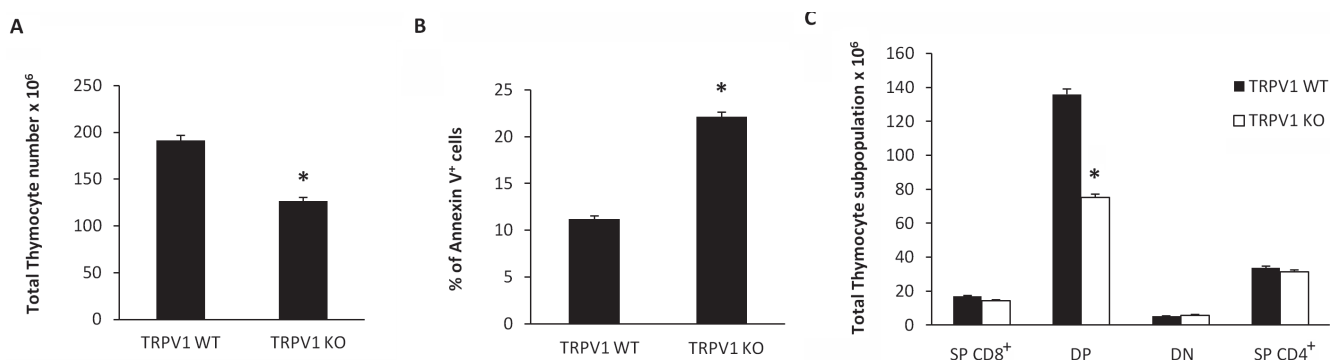
Figure 6: Increased basal levels of apoptotic thymocytes and reduced total thymocyte number in TRPV1 KO mice. Freshly purified thymocytes from WT and KO mice were counted using trypan blue solution **A.**, or stained with Annexin-V FITC and analyzed by FACS analysis **B.** Data are the mean ± SEM of three separate experiments, *$p < 0.01$ vs WT thymocytes. **C.** From the total number of cells per thymus, the relative number of cells in each CD4/CD8 subset was determined staining TRPV1 KO and WT thymocytes with anti-CD4-PE and anti-CD8-Cy5 mAbs and using FACS analysis. Data are the mean ± SEM of three separate experiments *$p < 0.01$ TRPV1 KO vs WT thymocytes.
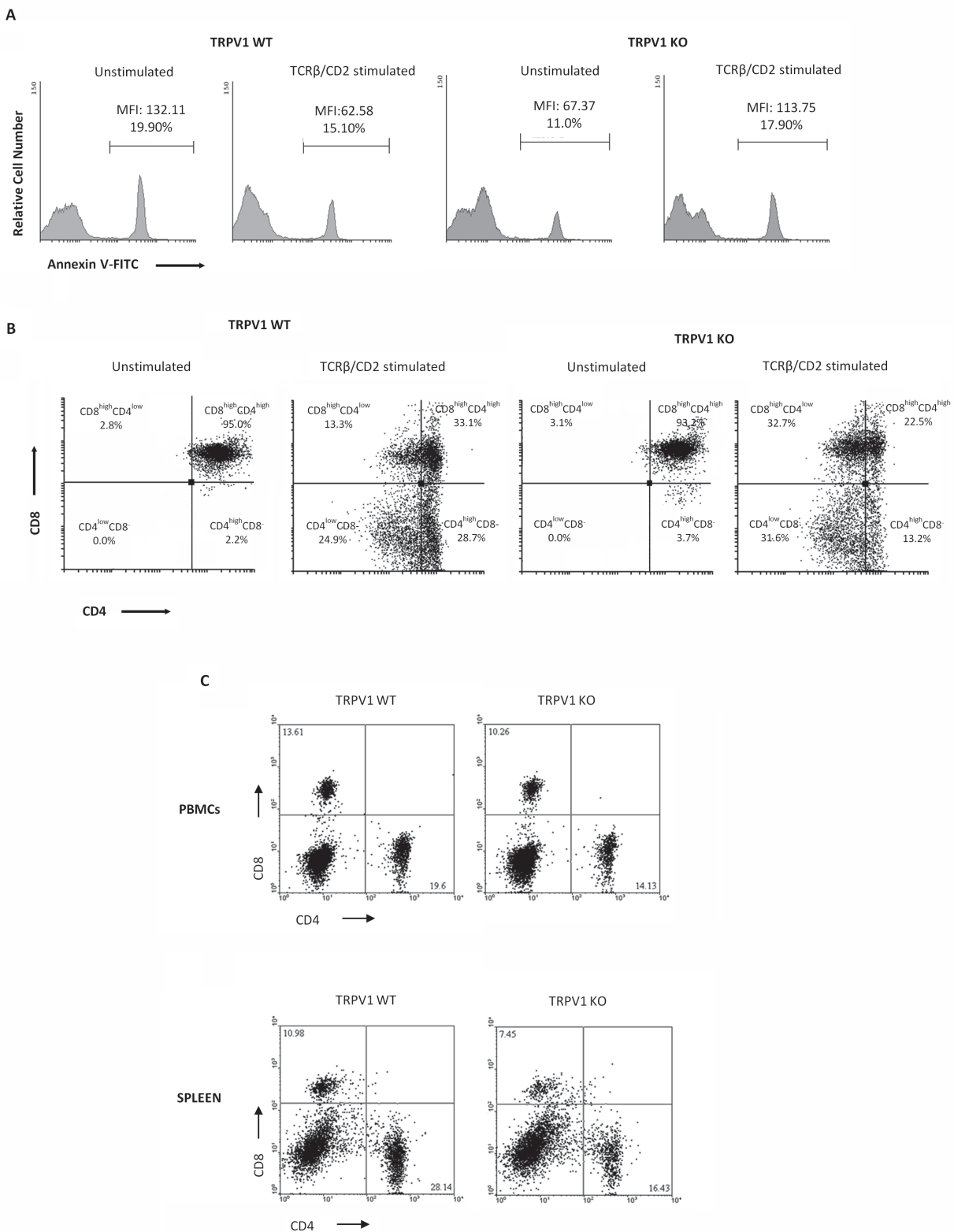
Figure 7: Knock-out of TRPV1 gene impairs positive thymic selection and affects peripheral blood and spleen CD4+ and CD8+ T cell numbers. A. Thymocytes from WT and KO mice, stimulated with anti-TCRβ plus anti-CD2 mAbs after 18h of culture and 12h of recovery, were analyzed by FACS analysis. One representative out of three independent experiments is shown. **B.** Purified DP thymocytes from TRPV1 KO and WT mice stimulated with TCRβ plus CD2 mAbs for 18h, followed by 12h recovery, were stained with anti-CD4-PE and anti-CD8-Cy5 mAbs and analyzed by FACS. One representative out of three independent experiments is shown. **C.** Blood and spleen PBMC from WT and KO thymocytes were stained with anti-CD4-PE and anti-CD8-Cy5 mAbs and analyzed by FACS. One representative out of three independent experiments is shown in each panel.

Table 1: CPS induces UPS gene expression changes.

Ref Seq	Symbol	Description	Fold change CPS-treated vs untreated
NM_007527	Bax	Bcl2-associated X protein	-2.04±0.03*
NM_013760	Dnajb9	Dnaj (Hsp40) homolog, subfamily B, member 9	-2.09±0.08*
NM_022310	Hspa5	Heat shock protein 5	-2.79±0.02*
NM_153526	Insig1	Insulin induced gene 1	-3.31±0.02*
NM_172307	Mbtps2	Membrane-bound transcription factor peptidase, site 2	-2.10±0.02*
NM_133933	Rpn1	Ribophorin 1	-2.40±0.04*
NM_013842	Xbp1	X-box binding protein 1	-2.67±0.05*
NM_013558	Hspa1l	Heat shock protein 1-like	-2.27±0.43*
NM_024207	Derl1	Der1-like domain family, member 1	+2.65±0.03*
NM_033562	Derl2	Der1-like domain family, member 2	+2.09±0.02*
NM_026184	Ero1lb	ERO1-like beta (S.Cerevisiae)	+2.10±0.04*

RT-PCR array in mRNA samples from thymocytes untreated and treated with CPS for 60 min. The expression levels were normalized using the housekeeping gene GAPDH and calculated by the ΔΔCt method. Data, shown as fold change, represent the mean ± SD of three experiments. Untreated thymocyte mRNA was used as calibrator. *$p < 0.01$ vs untreated cells.

DISCUSSION

Several evidence support the existence of a cross-talk between UPS and autophagy [9, 28]. Proteasome inhibitors induce autophagy by triggering ER stress [17]; conversely, suppression of both proteasome and autophagy has been shown to enhance apoptotic cell death [29].

The specific TRPV1 agonist CPS has been found to inhibit the proteasome [30, 31] and trigger autophagy [15, 32, 33], however, the relationship between these degradation systems in thymocytes and the role of TRPV1 have not been addressed so far.

Herein, we found that TRPV1-dependent autophagy occurs as a consequence of proteasome inhibition and ER stress triggered by TRPV1. Reduced 20 and 26S proteasome activities and increased p27 expression were found in CPS-treated thymocytes, and this effect was TRPV1-, ROS- and $[Ca^{2+}]_i$ rise-dependent.

In fact, pretreatment of thymocytes with the 4-PBA that reduces ER stress [18, 34, 35] before the addition of CPS, inhibited LC3II generation and p62 degradation, increased the percentage of AnnexinV⁺ apoptotic cells and completely reverted the CPS-induced increase of DP^dull thymocytes, similarly to the autophagic inhibitor CQ. TRPV1 triggering by CPS resulted in inhibition of UPR and apoptosis as well as increase of ERAD and autophagic gene expression. Since a role of Ero1lb in setting ER redox potential and proper ER folding activity [36] and CPS in disrupting redox state by promoting ROS generation [37], the increased Ero1lb mRNA levels we found in CPS treated thymocytes could be the result of CPS-induced TRPV1-mediated ROS generation [15] altering ER redox homeostasis. In addition, CPS exposure triggers derlin-1 mRNA overexpression; although the role of derlin-1 in the protection of thymocytes from apoptosis is still unknown, knock-down of derlin-1 by abrogating p62 degradation, results in blockage of autophagy flux [38].

In CPS-treated thymocytes, reduction of BiP, Grp94 UPR protein levels, as results of UPR inhibition, was completely reverted by pretreatment with 4-PBA or CQ treatment, ER stress and autophagy inhibitors, respectively, strongly suggesting that CPS-induced autophagy is a TRPV1-dependent ER-stress-stimulated process.

The contribution of TRPV1 in the autophagy and proteasome cross-talk was also evaluated in thymocytes from TRPV1 KO mice. Genetic deletion of TRPV1 results in increased basal levels of p62 and in a defective autophagic response to the mTOR inhibitor and autophagy inducer rapamycin. The p62/SQSTM1 is a multifunctional protein selectively degraded by autophagy but not by UPS [20, 38] that accumulates when autophagy function is inhibited [39, 40]. The p62 accumulation during autophagy inhibition appears to be responsible for the defective UPS function, as p62 silencing attenuates the accumulation of proteasome substrates caused by autophagy inhibition, and the pharmacological inhibition of the proteasome increases p62 expression [41, 42]. In this view, impaired autophagy due to TRPV1 genetic deletion by inducing p62 accumulation reduces proteasome functions. The decreased proteasome activity observed in TRPV1 KO thymocytes was associated with loss of AMPK activity and a decreased p27 expression compared with WT thymocytes [15]. Inhibition of AMPK by compound C or by shRNA-mediated depletion of LKB reduces activation of autophagy by rapamycin, and shRNA-mediated depletion of p27 inhibits rapamycin-induced autophagy [43]. Thus, the AMPK/p27 pathway deregulation observed in TRPV1 KO thymocytes, exacerbates the severity of the autophagy/proteasome defects, further promoting the

reduction of DP thymocyte number.

Our results in TRPV1 KO thymocytes, also provide evidence of a reduction of BiP and Grp94 UPR proteins and increase of ERp57 levels. Knock-down or inhibition of ERp57 resulted in decreased death-inducing signaling complex and caspase activity [44]. On the contrary, autophagy failure, induced by compromised UPR, has been found to increase the ERp57 expression in beta cell islets from Atg7-deficient mice [45]. Thus, the reduction of ERp57 in CPS-treated WT thymocytes may be the result of enhanced autophagic survival, as well as the increase of ERp57 level in TRPV1 KO thymocytes could promote apoptotic death caused by autophagic failure.

In the same view, Atf4 induction by prolonged stress exposure triggers apoptosis in cancer cells [46]; so, the enhancement of Atf4 protein expression evidenced in TRPV1 KO thymocytes, may lead to increased susceptibility of thymocytes to apoptotic stimuli.

In addition, as result of double defects in autophagic and proteasome degradation systems, increased levels of apoptotic thymocytes associated with a reduction of total and DP thymocyte number was found in TRPV1 KO mice. Accordingly, the proteasome inhibitor Bortezomib, results in a dramatic decrease of thymocytes by inducing ER stress-apoptosis [47].

Proteasome inhibition has been also found to interfere with thymic selection, and thereby to influence the survival of DP and SP thymocytes [48, 49]. Differentiation of immature DP thymocytes into mature SP CD4$^+$ and CD8$^+$ T cells is referred as positive selection [26, 50], and requires physical contact with thymic cortical epithelium. Indeed, TCRβ and CD2 co-engagement by increasing survival signals [27] promotes a differentiation pathway resulting in generation of SP CD4$^+$ T cells from DP thymocytes [26]. This pathway requires two distinct steps in which expression of both co-receptors CD4 and CD8 is reduced (CD4^{low}CD8^{low}, DP^{dull}), followed by selective re-expression of CD4 with the CD4^{low} cells representing the immediate precursor of mature CD4$^+$ cells. In this regard, our findings add new straightforward data on the role of TRPV1 in thymocyte maturation. In fact, its absence is responsible for the increased percentage of apoptotic cells after TCR engagement, likely due to the loss of the survival signals that normally characterize the positive selection. The positive selection stimulates the maturation of DP thymocytes in SP CD4$^+$ cells both in TRPV1 KO and WT cells; whereas, the impaired TRPV1 signaling in TCRβ/CD2-stimulated thymocytes markedly reduced the percentage of mature SP CD4$^+$ thymocytes and increased that of immature DP CD4^{low}CD8$^+$ and SP CD4^{low} cells, compared to WT thymocytes. Therefore, the absence of TRPV1 impairs positive selection by reducing/delaying CD4$^+$ thymocyte maturation. Moreover, a reduced percentage of mature CD8$^+$ and CD4$^+$ T cells was observed in PBMC and spleen from TRPV1 deficient mice. These findings are in agreement with previous reports demonstrating that an impaired thymic autophagy affects the distribution of mature SP CD4 and CD8 T cells in the periphery [51].

TRPV1, constitutively expressed in mouse and human CD4$^+$ T cells, is a component of the TCR signaling complex. It is rapidly recruited to TCR clusters upon TCR stimulation in a Src-dependent manner, and contributes to CD4$^+$ T cell activation. In response to TCR stimulation TRPV1 is rapidly tyrosine phosphorylated by the Lck kinase that regulates TRPV1 activity in CD4$^+$ T cells [14]. Analysis of TCR signaling evidenced a diminished p38 and Jnk activation and NF-kB and NFAT-1 translocation to the nucleus in TRPV1 KO CD4$^+$ T respect to WT cells [14]. Thus, the loss of TRPV1 resulted in a reduction of SP CD4 thymocytes, further supporting the recent findings on the intrinsic role of TRPV1 in the activation of and acquisition of pro-inflammatory properties by CD4$^+$ T cells [14]. Thus, in WT thymocytes, TRPV1 activation, by inducing ER stress and proteasome dysfunction, triggers a compensatory autophagy that inhibits the UPR response and rescues DP^{dull} thymocytes from apoptosis. On the contrary, in TRPV1 KO thymocytes, characterized by defects in autophagy and proteasome system, the impaired TRPV1 signalling, stimulates the apoptosis of DP thymocytes and impairs thymocyte maturation induced by TCRβ/CD2 stimulation, leading to a decrease in the percentage of mature SP CD4$^+$.

Thus, pharmacological modulation of TRPV1 expression and functions could represent a new therapeutic strategy for restraining or stimulating different inflammatory T cell responses.

MATERIALS AND METHODS

Animals

C57BL/6 (WT) and B6.129X1-Trpv1tm1Jul/J (TRPV1 KO) male mice were purchased from Harlan (Udine, Italy) and Jackson Laboratory (Bar Harbor, ME, USA), respectively, and housed as described previously [12]. Five TRPV1 KO and five WT animals (6-10 week-old) were sacrificed for each experiment in accordance with the U.S. National Institutes of Health's "Guidelines for the Care and Use of Laboratory Animals". Before and after sacrifice respectively, mice were weighted and thymi were measured by caliper without significant differences between WT and TRPV1 deficient mice.

Cell preparation and culture conditions

Thymi were teased, and cellular debris were removed by washing. Thymocytes were isolated by centrifugation on a Lympholyte-M (Cederlane, Burlington, Canada) gradient and washed in RPMI 1640 medium

supplemented with 5x 10^{-5} M β-mercaptoethanol, 2 mM glutamin, 100 U/ml penicillin, 100 µg/ml streptomycin, and 10% fetal calf serum (FCS). Cell purity (99%) was assessed by FACS analysis using anti-CD3 monoclonal antibody (mAb) (clone KT3) (10 µg/mL, Novus Biologicals, Littleton, CO, USA). Briefly, double positive (DP) CD4/CD8 cells were purified from 1×10^8/ml total thymocytes by using the EasySep CD4 and CD8 purification kits (Stem Cell Technologies, Vancouver, Canada) according to the manufacturer's instructions. The resultant cell population was enriched for CD4$^+$CD8$^+$ DP cells (approximately 97% of purified thymocytes).

To mimic positive selection, thymocytes were stimulated by anti-TCRβ mAb (clone: H57-597) plus anti-CD2 mAb (clone: 12-15) (10 µg/mL, Novus Biologicals) cross-linking. Briefly, thymocytes were cultured *in vitro* for 18 h in mAb-coated (stimulated thymocytes) or uncoated (non-stimulated thymocytes) Petri dishes (day 1) and then incubated for additional 12 h (day 2) in the absence of mAbs.

Compounds

Rapamycin (an autophagy inducer inhibiting the mammalian target of rapamycin mTOR, 10 ng/ml), chloroquine (CQ, an autophagy inhibitor preventing the fusion between the autophagosome and lysosomes, 100 µM), capsaicin (CPS, TRPV1 agonist, 10 µM), capsazepine (CPZ, a synthetic, competitive and selective antagonist of TRPV1, 1 µM), 4-phenylbutyric acid (4-PBA, ER stress inhibitor, 5 mM), Ethylenediaminutesetetraacetic acid (EDTA), a calcium chelating agent, 5 mM), N-acetyl-L-cysteine (NAC, a free radical scavenger, 10 mM), trypan blue, dimethyl sulfoxide (DMSO) as well as the substrates for assaying the chymotrypsin-like (ChT-L), trypsin-like (T-L), peptidylglutamyl-peptide hydrolyzing (PGPH) and proteasome inhibitors, Z-Gly-Pro-Phe-Leu-CHO and lactacystin, were purchased from Sigma-Aldrich (St. Louis, MO, USA).

Measurement of proteasome activity in cell lysates

Cells were washed in PBS and centrifuged at 1,600 g for 5 minutes. The pellet was resuspended in lysis buffer (20 mM Tris, pH 7.4, 250 mM sucrose, 1 mM EDTA and 5 mM β-mercaptoethanol) and passed through a 29-gauge needle at least ten times. Lysates were centrifuged at 12,000 x g for 15 minutes and the supernatants were stored at -80°C. Protein concentration was determined by the method of Bradford using bovine serum albumin (BSA) as standard.

Proteasome peptidase activity in cell lysates was determined with fluorogenic peptides: Suc-Leu-Leu-Val-Tyr-AMC was used for the chymotrypsin-like (ChT-L) activity, Z-Leu-Ser-Thr-Arg-AMC for the trypsin-

like (T-L) activity and Z-Leu-Leu-Glu-AMC for the peptidylglutamyl-peptide hydrolyzing (PGPH) activity. The incubation mixture contained 1 µg of cell lysate, the appropriate substrate and 50 mM Tris-HCl pH 8.0, up to a final volume of 100 µL. Incubation was performed at 37 °C and after 60 minutes the fluorescence of the hydrolysed 7-amino-4-methyl-coumarin (AMC) was detected on a SpectraMax Gemini XPS microplate reader (λexc = 365 nm, λem = 449 nm). The 26S proteasome ChT-L activity was tested using Suc-Leu-Leu-Val-Tyr-AMC as substrate and a 50 mM Tris-HCl pH 8.0 buffer containing 10 mM MgCl$_2$, 1 mM dithiothreitol, and 2 mM ATP. The effective 20S proteasome contribution to short peptide cleavage was evaluated performing control experiments using the specific proteasome inhibitors Z-Gly-Pro-Phe-Leu-CHO and lactacystin (5 µM in the reaction mixture) and then subtracting the obtained fluorescence values from the values obtained in cell lysates.

Immunofluorescence and flow cytometry

Thymocytes from WT or TRPV1 KO mice were stained with anti-CD4-PE (clone: RM4-5) and/or anti-CD8-Cy5 (clone 53-6.7) mAb (1µl/1×10^6 cells; BD Biosciences, Milan, Italy) and analyzed by a FACScan cytofluorimeter (BD Biosciences) using the CellQuest software. In some experiments, double immunofluorescence for CD4 and CD8 was performed on thymocyte from WT mice pre-treated for 1h with 4-PBA (5 mM), CQ (100 µM) or NAC (10 mM) and then treated with CPS (10 µM) for 2h. Moreover, the percentage of CD4 and CD8 positive cells was evaluated on thymocytes from WT or KO mice, un-stimulated or stimulated to mimic thymic positive selection. To investigate the role of TRPV1 in the activation of thymocytes, cells from WT mice were treated or not with CPS for 2 h, and then stained with anti-CD25-FITC (clone PC61) (1µl/1×10^6 cells, Biolegend, San Diego, USA) or anti CD69-PE (clone H1.2F3) mAb (1µl/1×10^6 cells, Biolegend).

Western blot

Thymocytes from WT and KO mice were lysed as described previously [12]. Samples were separated on SDS-PAGE and transferred onto Hybond-C extra membranes (GE Healthcare, Milan, Italy). Membranes were incubated in 5% low-fat dry milk for 1 h and then overnight at 4°C in the primary antibodies solution: rabbit anti-p27 Kip1, anti-p62, anti-Grp94/gp96, anti-BiP/Grp78, anti-ERp57/Grp58, anti-Atf-4, anti-AMPK and anti-pAMPK (1:1000; Cell Signaling Technology, Danvers, MA, USA); rabbit anti-LC3 (2 µg/mL; Novus Biologicals); mouse anti-GAPDH (1:5000; Sigma-Aldrich). Thereafter, membranes were blotted with the respective horseradish peroxidase-conjugated anti-rabbit

(1:2000; Cell Signaling Technology), anti-mouse (1:2000; Cell Signaling Technology) for 1 h. The detection was performed using the LiteAblot Plus or the LiteAblot Turbo (EuroClone, Milano, Italy) kits and densitometric analysis was carried out by evaluating three independent experiments by a ChemiDoc using Quantity One software (Bio-Rad, Hercules, CA, USA). Each sample was compared with its loading control (GAPDH) for quantification. In some experiments, thymocytes from WT mice were treated or not with CPS for different times. Moreover, thymocytes were pre-treated for 1 h with NAC, EDTA, CPZ, 4-PBA or CQ, before the addition of CPS for 2 h. In addition, TRPV1 KO thymocytes were treated for different times with Rapamycin.

Annexin V and PI staining

Cell death was evaluated using Annexin V-fluorescein isothiocyanate (Annexin-FITC, BD Biosciences) and propidium iodide (PI, 2 μg/ ml, Sigma-Aldrich) followed by biparametric FACS analysis. Cells were stained with 5 μl of Annexin V-FITC and/or PI for 10 minutes at room temperature and washed once with binding buffer (10mM Hepes/NaOH pH 7.4, 140 mM NaCl, 2.5 mM $CaCl_2$). The percentage of positive cells determined over 10,000 events was analyzed by a FACScan cytofluorimeter using the CellQuest software.

RNA isolation, reverse transcription, and RT-PCR profiler array

Total RNA was extracted from thymocytes with the RNeasy mini kit (Qiagen, Valencia, CA, USA). Total RNA (1 μg) was subjected to reverse transcription using the ReactionReady first-strand cDNA kit (SuperArray Bioscience, Frederick, MD, USA). qRT-PCR was performed using the iQ5 Multicolor RT-PCR detection system (Bio-Rad), the RT2 real-time SYBR Green PCR mix, and the mouse Unfolded Protein Response PCR Array (SuperArray Bioscience), according to the manufacturer's instructions.

Statistical analysis

The statistical significance was determined by Student's t test and by ANOVA with Bonferroni post-test. No statistically significant difference was found between untreated and vehicle (DMSO)-treated thymocytes (data not shown).

Abbreviations

ChT-L, chymotrypsin-like; CPS, capsaicin; CPZ, capsazepine; CQ, chloroquine; DMSO, dimethyl sulfoxide; DP, double positive; EDTA, Ethylenediaminetetraacetic acid; ER, endoplasmic reticulum; ERAD, endoplasmic reticulum-associated degradation; NAC, N-acetyl-L-cysteine; PGPH, peptidylglutamyl-peptide hydrolyzing; PI, propidium iodide; ROS, reactive oxygen species; SP, single positive; T-L, trypsin-like; TRPV1, transient receptor potential vanilloid channel 1; UPR, unfolded protein response; UPS, ubiquitin-proteasome system; 4-PBA, 4-Phenylbutyric acid.

Authorship contributions

C.A. and V.F. designed the research, performed the experiments, and analyzed the data. G.S. conceived of the research, supervised the work and wrote the paper. V.C. and L.B. performed the experiments about proteasome activity. C.A., V.F., C.C., M.B.M., O.M. and M.N. contributed to data interpretation and manuscript preparation. M.S. and A.M.E. provided critical revision of the intellectual content and text of the manuscript. All authors provided final approval of the manuscript.

CONFLICTS OF INTEREST

The authors declare no conflicts of interest.

REFERENCES

1. Michalak M, Robert Parker JM, Opas M. Ca2+ signaling and calcium binding chaperones of the endoplasmic reticulum. Cell Calcium. 2002; 32: 269-278.

2. Klionsky DJ, Abdelmohsen K, Abe A, Abedin MJ, Abeliovich H, Acevedo Arozena A, Adachi H, Adams CM, Adams PD, Adeli K, Adhihetty PJ, Adler SG, Agam G, et al. Guidelines for the use and interpretation of assays for monitoring autophagy (3rd edition). Autophagy. 2016; 12: 1-222.

3. Hershko A, Ciechanover A. The ubiquitin system. Annu Rev Biochem. 1998; 67: 425-479.

4. Moretti L, Cha YI, Niermann KJ, Lu B. Switch between apoptosis and autophagy: radiation-induced endoplasmic reticulum stress? Cell Cycle. 2007; 6: 793-798.

5. Chakrabarti A, Chen AW, Varner JD. A review of the mammalian unfolded protein response. Biotechnol Bioeng. 2011; 108: 2777-2793.

6. Jäger R, Bertrand MJ, Gorman AM, Vandenabeele P, Samali A. The unfolded protein response at the crossroads of cellular life and death during endoplasmic reticulum stress. Biol Cell. 2012; 104: 259-270.

7. Rutkowski DT, Arnold SM, Miller CN, Wu J, Li J, Gunnison KM, Mori K, Sadigh Akha AA, Raden D, Kaufman RJ. Adaptation to ER stress is mediated by differential stabilities of pro-survival and pro-apoptotic mRNAs and proteins. PLoS Biol. 2006; 4:e374.

8. Rashid HO, Yadav RK, Kim KR, Chae HJ. ER stress: Autophagy induction, inhibition and selection. Autophagy. 2015; 11: 1956-1977.

9. Cecarini V, Bonfili L, Cuccioloni M, Mozzicafreddo M, Rossi G, Buizza L, Uberti D, Angeletti M, Eleuteri AM. Crosstalk between the ubiquitin-proteasome sysstem and autophagy in a human cellular model of Alzheimer's disease. Biochim Biophys Acta. 2012; 1822: 1741-1751.

10. Nedjic J, Aichinger M, Emmerich J, Mizushima N, Klein L. Autophagy in thymic epithelium shapes the T-cell repertoire and is essential for tolerance. Nature. 2008; 455: 396-400.

11. Sukumaran P, Schaar A, Sun Y, Singh BB. Functional role of TRP channels in modulating ER stress and Autophagy. Cell Calcium. 2016; 60: 123-132.

12. Amantini C, Mosca M, Lucciarini R, Perfumi M, Morrone S, Piccoli M, Santoni G. Distinct thymocyte subsets express the vanilloid receptor VR1 that mediates capsaicin-induced apoptotic cell death. Cell Death Differ. 2004; 11: 1342-1356.

13. Wenning AS, Neblung K, Strauss B, Wolfs MJ, Sappok A, Hoth M, Schwarz EC. TRP expression pattern and the functional importance of TRPC3 in primary human T-cells. Biochim Biophys Acta. 2011; 1813: 412-423.

14. Bertin S, Aoki-Nonaka Y, de Jong PR, Nohara LL, Xu H, Stanwood SR, Srikanth S, Lee J, To K, Abramson L, Yu T, Han T, Touma R, et al. The ion channel TRPV1 regulates the activation and proinflammatory properties of CD4+ T cells. Nat Immunol. 2014; 15:1055–63.

15. Farfariello V, Amantini C, Santoni G. Transient receptor potential vanilloid 1 activation induces autophagy in thymocytes through ROS-regulated AMPK and Atg4C pathways. J Leukoc Biol. 2012; 92: 421-431.

16. McLeod IX, He YW. Editorial: TRPV1: how thymocytes sense stress and respond with autophagy. J Leukoc Biol. 2012; 92: 409-411.

17. Ding WX, Ni HM, Gao W, Yoshimori T, Stolz DB, Ron D, Yin XM. Linking of autophagy to ubiquitin-proteasome system is important for the regulation of endoplasmic reticulum stress and cell viability. Am J Pathol. 2007; 171: 513-524.

18. Jiang H, Xiong S, Xia X. Chemical chaperone 4-phenylbutyrate prevents endoplasmic reticulum stress induced by T17M rhodopsin. Cell Biosci. 2014; 4: 75.

19. Tanida I, Ueno T, Kominami E. LC3 and Autophagy. Methods Mol Biol. 2008; 445: 77-88.

20. Bjørkøy G, Lamark T, Brech A, Outzen H, Perander M, Overvatn A, Stenmark H, Johansen T. p62/SQSTM1 forms protein aggregates degraded by autophagy and has a protective effect on huntingtin-induced cell death. J Cell Biol. 2005; 171: 603-614.

21. Obeng EA, Carlson LM, Gutman DM, Harrington WJ Jr, Lee KP, Boise LH. Proteasome inhibitors induce a terminal unfolded protein response in multiple myeloma cells. Blood. 2006; 107: 4907-4916.

22. Nakajima S, Kato H, Takahashi S, Johno H, Kitamura M. Inhibition of NF-κB by MG132 through ER stress-mediated induction of LAP and LIP. FEBS Lett. 2011; 585: 2249-2254.

23. Wickner S, Maurizi MR, Gottesman S. Posttranslational quality control: folding, refolding, and degrading proteins. Science. 1999; 286: 1888-1893.

24. Korolchuk VI, Mansilla A, Menzies FM, Rubinsztein DC. Autophagy inhibition compromises degradation of ubiquitin-proteasome pathway substrates. Mol Cell. 2009; 33: 517-527.

25. Tian Z, Wang C, Hu C, Tian Y, Liu J, Wang X. Autophagic-lysosomal inhibition compromises ubiquitin-proteasome system performance in a p62 dependent manner in cardiomyocytes. PLoS One. 2014; 9:e100715.

26. Cibotti R, Punt JA, Dash KS, Sharrow SO, Singer A. Surface molecules that drive T cell development *in vitro* in the absence of thymic epithelium and in the absence of lineage-specific signals. Immunity. 1997; 6: 245-255.

27. McKean DJ, Huntoon CJ, Bell MP, Tai X, Sharrow S, Hedin KE, Conley A, Singer A. Maturation *versus* death of developing double-positive thymocytes reflects competing effects on Bcl-2 expression and can be regulated by the intensity of CD28 costimulation. J Immunol. 2001; 166: 3468-3475.

28. Lilienbaum A. Relationship between the proteasomal system and autophagy. Int J Biochem Mol Biol. 2013; 4:1–26.

29. Zhu K, Dunner K Jr, McConkey DJ. Proteasome inhibitors activate autophagy as a cytoprotective response in human prostate cancer cells. Oncogene. 2010; 29: 451-462.

30. Mori A, Lehmann S, O'Kelly J, Kumagai T, Desmond JC, Pervan M, McBride WH, Kizaki M, Koeffler HP. Capsaicin, a component of red peppers, inhibits the growth of androgen-independent, p53 mutant prostate cancer cells. Cancer Res. 2006; 66: 3222-3229.

31. Maity R, Sharma J, Jana NR. Capsaicin induces apoptosis through ubiquitin-proteasome system dysfunction. J Cell Biochem. 2010; 109: 933-942.

32. Choi CH, Jung YK, Oh SH. Autophagy induction by capsaicin in malignant human breast cells is modulated by p38 and extracellular signal-regulated mitogen-activated protein kinases and retards cell death by suppressing endoplasmic reticulum stress-mediated apoptosis. Mol Pharmacol. 2010; 78: 114-125.

33. Amantini C, Morelli MB, Nabissi M, Cardinali C, Santoni M, Gismondi A, Santoni G. Capsaicin triggers autophagic cell survival which drives epithelial mesenchymal transition and chemoresistance in bladder cancer cells in an

Hedgehog-dependent manner. Oncotarget. 2016; 7:50180–94. https://doi.org/10.18632/oncotarget.10326.

34. Ozcan U, Yilmaz E, Ozcan L, Furuhashi M, Vaillancourt E, Smith RO, Görgün CZ, Hotamisligil GS. Chemical chaperones reduce ER stress and restore glucose homeostasis in a mouse model of type 2 diabetes. Science. 2006; 313: 1137-1140.

35. Zode GS, Kuehn MH, Nishimura DY, Searby CC, Mohan K, Grozdanic SD, Bugge K, Anderson MG, Clark AF, Stone EM, Sheffield VC. Reduction of ER stress *via* a chemical chaperone prevents disease phenotypes in a mouse model of primary open angle glaucoma. J Clin Invest. 2015; 125: 3303.

36. Sevier CS, Kaiser CA. Ero1 and redox homeostasis in the endoplasmic reticulum. Biochim Biophys Acta. 2008; 1783: 549-556.

37. Hail N Jr. Mechanisms of vanilloid-induced apoptosis. Apoptosis. 2003; 8: 251-262.

38. Moscat J, Diaz-Meco MT. p62 at the crossroads of autophagy, apoptosis, and cancer. Cell. 2009; 137: 1001-1004.

39. Nakai A, Yamaguchi O, Takeda T, Higuchi Y, Hikoso S, Taniike M, Omiya S, Mizote I, Matsumura Y, Asahi M, Nishida K, Hori M, Mizushima N, Otsu K. The role of autophagy in cardiomyocytes in the basal state and in response to hemodynamic stress. Nat Med. 2007; 13: 619-624.

40. Su H, Wang X. p62 Stages an interplay between the ubiquitin-proteasome system and autophagy in the heart of defense against proteotoxic stress. Trends Cardiovasc Med. 2011; 21: 224-228.

41. Kuusisto E, Suuronen T, Salminen A. Ubiquitin-binding protein p62 expression is induced during apoptosis and proteasomal inhibition in neuronal cells. Biochem Biophys Res Commun. 2001; 280: 223-228.

42. Nakaso K, Yoshimoto Y, Nakano T, Takeshima T, Fukuhara Y, Yasui K, Araga S, Yanagawa T, Ishii T, Nakashima K. Transcriptional activation of p62/A170/ZIP during the formation of the aggregates. possible mechanisms and the role in Lewy body formation in Parkinson's disease. Brain Res. 2004; 1012: 42-51.

43. Campos T, Ziehe J, Fuentes-Villalobos F, Riquelme O, Peña D, Troncoso R, Lavandero S, Morin V, Pincheira R, Castro AF. Rapamycin requires AMPK activity and p27 expression for promoting autophagy-dependent Tsc2-null cell survival. Biochim Biophys Acta. 2016; 1863: 1200-1207.

44. Anathy V, Roberson E, Cunniff B, Nolin JD, Hoffman S, Spiess P, Guala AS, Lahue KG, Goldman D, Flemer S, van der Vliet A, Heintz NH, Budd RC, et al. Oxidative processing of latent Fas in the endoplasmic reticulum controls the strength of apoptosis. Mol Cell Biol. 2012; 32:3464–78.

45. Yamamoto E, Uchida T, Abe H, Taka H, Fujimura T, Komiya K, Hara A, Ogihara T, Fujitani Y, Ueno T, Takeda S, Watada H. Increased expression of ERp57/Grp58 is protective against pancreatic beta cell death caused by autophagic failure. Biochem Biophys Res Commun. 2014; 453: 19-24.

46. Ishizawa J, Kojima K, Chachad D, Ruvolo P, Ruvolo V, Jacamo RO, Borthakur G, Mu H, Zeng Z, Tabe Y, Allen JE, Wang Z, Ma W, et al. ATF4 induction through an atypical integrated stress response to ONC201 triggers p53-independent apoptosis in hematological malignancies. Sci Signal. 2016; 9:ra17.

47. Maseda D, Meister S, Neubert K, Herrmann M, Voll RE. Proteasome inhibition drastically but reversibly impairs murine lymphocyte development. Cell Death Differ. 2008; 15: 600-612.

48. Kloetzel PM, Ossendorp F. Proteasome and peptidase function in MHC-class-I-mediated antigen presentation. Curr Opin Immunol. 2004; 16: 76-81.

49. Callahan MK, Wohlfert EA, Menoret A, Srivastava PK. Heat shock up-regulates lmp2 and lmp7 and enhances presentation of immunoproteasome-dependent epitopes. J Immunol. 2006; 177: 8393-8399.

50. Lucas B, Marodon G, Penit C. CD4low TCRint thymocytes do not belong to the CD8 lineage maturation pathway. J Immunol. 1996; 156: 1743-1747.

51. Bronietzki AW, Schuster M, Schmitz I. Autophagy in T-cell development, activation and differentiation. Immunol Cell Biol. 2015; 93: 25-34.